

# THEORETICA CHIMICA ACTA

edenda curat

**Hermann Hartmann**

adiuvantibus

**C. J. Ballhausen, København**

**R. D. Brown, Clayton**

**E. Hellbronner, Basel**

**J. Jortner, Tel-Aviv**

**M. Kotani, Tokyo**

**J. Koutecký, Praha**

**J. W. Linnett, Cambridge**

**E. E. Nikitin, Moskva**

**R. G. Pearson, Evanston**

**B. Pullman, Paris**

**K. Ruedenberg, Ames**

**C. Sandorfy, Montreal**

**M. Simonetta, Milano**

**O. Sinanoğlu, New Haven**



**Vol. 30, 1973**

**Springer-Verlag • Berlin • Heidelberg • New York**

The exclusive copyright for all languages and countries, including the right for photomechanical and any other reproductions, also in microform, is transferred to the publisher.

The use of registered names, trademarks, etc. in this publication does not imply, even in the absence of a specific statement, that such names are exempt from the relevant protective laws and regulations and therefore free for general use.

Alle Rechte, einschließlich das der Übersetzung in fremde Sprachen und das der fotomechanischen Wiedergabe oder einer sonstigen Vervielfältigung, auch in Mikroform, vorbehalten. Jedoch wird gewerblichen Unternehmen für den innerbetrieblichen Gebrauch nach Maßgabe des zwischen dem Börsenverein des Deutschen Buchhandels e. V. und dem Bundesverband der Deutschen Industrie abgeschlossenen Rahmenabkommens die Aufertigung einer fotomechanischen Vervielfältigung gestattet. Wenn für diese Zeitschrift kein Pauschalabkommen mit dem Verlag vereinbart worden ist, ist eine Wertmarke im Betrage von DM 0,40 pro Seite zu verwenden. *Der Verlag läßt diese Beträge den Autorenverbänden zufließen.*

Die Wiedergabe von Gebrauchsnamen, Handelsnamen, Warenbezeichnungen usw. in dieser Zeitschrift berechtigt auch ohne besondere Kennzeichnung nicht zu der Annahme, daß solche Namen im Sinne der Warenzeichen- und Markenschutz-Gesetzgebung als frei betrachtet wären und daher von jedermann benutzt werden dürfen.

Springer-Verlag Berlin Heidelberg New York  
Printed in Germany by Brühlche Universitätsdruckerel, Gießen  
© by Springer-Verlag Berlin Heidelberg 1973

38968  
29.4.80 hyd

# Index

## Commentationes et Relationes

Ahlrichs, R., s. Driessler, F., <i>et al.</i> . . . . .	315
Ajò, D., Bossa, M., Fidenzi, R., Gigli, S., Jeronimidis, G., Damiani, A., Lapicciarella, A.: An EHT Re-Examination of Acetylcholine . . . . .	275
Andreev, E. A.: Exchange Interaction between Two Different Atoms at Large Distances . . . . .	191
Annino, T.: Convenient Formulas for Evaluation of the Hybridized Valence States Involving $s-p$ Hybrid Orbitals and Their Applications to the Atoms and the Ions of Carbon, Nitrogen and Oxygen . . . . .	129
Ballhausen, C. J., s. Král, M., <i>et al.</i> . . . . .	339
Bossa, M., s. Ajò, D., <i>et al.</i> . . . . .	275
Boyd, D. B.: Electron Redistribution in Disulfido Bonds under Torsion . . . . .	137
Ching, C., s. Warren, C. H. . . . .	1
Chuvylkin, N. D., s. Zhidomirov, G. M. . . . .	197
Csizmadia, I. G., s. Houlden, S. A. . . . .	209
Damiani, A., s. Ajò, D., <i>et al.</i> . . . . .	275
Davidson, E. R., s. Schaffer, A. M., <i>et al.</i> . . . . .	9
Davidson, E. R., s. Zeller Stenkamp, L. . . . .	283
Degand, P., Leroy, G., Peeters, D.: L'utilisation d'orbitales localisées dans l'étude théorique des molécules. I. Les hydrocarbures saturés . . . . .	243
Driessler, F., Ahlrichs, R., Staemmler, V., Kutzelnigg, W.: <i>Ab-initio</i> Calculations on Small Hydrides Including Electron Correlation. XI. Equilibrium Geometries and Other Properties of $\text{CH}_3$ , $\text{CH}_3^+$ , and $\text{CH}_3^-$ , and Inversion Barrier of $\text{CH}_3^-$ . . . . .	315
Duben, A. J., Goodman, L., Pamuk, H. Ö., Sinanoğlu, O.: Correlation Effects in the Neutral and Ionized Ground States of Acetylene . . . . .	177
Edwards, T. G.: Calculations on the $\pi \rightarrow {}^1\pi^*$ Transitions in Large Conjugated Carbonyl Compounds Using the Molecules-in-Molecules Method . . . . .	267
Fidenzi, R., s. Ajò, D., <i>et al.</i> . . . . .	275
Fujimoto, H., s. Yamabe, S., <i>et al.</i> . . . . .	327
Fukui, K., s. Yamabe, S., <i>et al.</i> . . . . .	327
Ghio, C., Tomasi, J.: The Protonation of Three-Membered Ring Molecules: The <i>ab initio</i> SCF versus the Electrostatic Picture of the Proton Approach . . . . .	151
Ghirvu, C. I.: CNDO Calculation of the $\pi$ -Electronic Structure and Barrier to Internal Rotation in Benzenesulphonic Acid . . . . .	115
Gigli, S., s. Ajò, D., <i>et al.</i> . . . . .	275
Goodman, L., s. Duben, A. J., <i>et al.</i> . . . . .	177
Gouterman, M., s. Schaffer, A. M., <i>et al.</i> . . . . .	9
Harris, F. E., s. Trautwein, A. . . . .	45
Helfrich, K.: Natural Spin Orbital Analysis of Diatomic Molecular Wave Functions in Terms of Generalized Diatomic Orbitals I. Outline of the Method. Results for the Ground State of $\text{H}_2$ . . . . .	169

Houlden, S. A., Csizmadia, I. G.: The Use of Average Natural Orbitals for Configuration Interaction Calculations on the Boron Hydride Molecule . . . . .	209
Jaszúnski, M., Sadlej, A. J.: Proton Magnetic Shielding in $H_2O$ and $(H_2O)_2$ . . . . .	257
Jeronimidis, G., s. Ajò, D., <i>et al.</i> . . . . .	275
Jortner, J., s. Nitzan, A. . . . .	217
Jug, K.: Semiempirical Extended Hartree-Fock Theory . . . . .	231
Kato, S., s. Yamabe, S., <i>et al.</i> . . . . .	327
König, E., Schnakig, R.: Theory of Spin Triplet Ground States in $d^4$ Transition Metal Compounds and the Effect of High-Energy States on the Nature of the Ground State . . . . .	205
Král, M., Moscovitz, A., Bullhausen, C. J.: A Calculation of the Rotatory Strengths of the Electron-Transfer Transitions of the <i>Tris</i> -(1,10-phenanthroline)iron(II) Ion . . . . .	339
Kutzelnigg, W., s. Driessler, F., <i>et al.</i> . . . . .	315
Langlet, J., Malrieu, J. P.: PCILO Method for Excited States II. 2 <sup>nd</sup> Order Corrected Transition Energies . . . . .	59
Lapicciolla, A., s. Ajò, D., <i>et al.</i> . . . . .	275
Leroy, G., s. Degand, P., <i>et al.</i> . . . . .	243
Mackrodt, W. C.: A Note on an Aspect of Pseudopotential Theory . . . . .	119
Malrieu, J. P., s. Langlet, J. . . . .	59
Moscovitz, A., s. Král, M., <i>et al.</i> . . . . .	339
Naloway, C. A., Schwartz, M. E.: Examination of Charge Alternation in $CH_4$ and $CH_3F$ from <i>ab initio</i> LCAO SCF MO Wavefunctions and Their Localized Bond Orbitals . . . . .	347
Newman, F. T.: Formal Solution for the Three Body Problem in Helium Theoretical Chemistry . . . . .	95
Nitzan, A., Jortner, J.: Non Radiative Transition Probabilities in the Statistical Limit . . . . .	217
Pamuk, H. Ö., s. Duben, A. J., <i>et al.</i> . . . . .	177
Pecters, D., s. Degand, P., <i>et al.</i> . . . . .	243
Peralia, D., s. Saran, A., <i>et al.</i> . . . . .	31
Pullman, B., s. Saran, A., <i>et al.</i> . . . . .	31
Sadlej, A. J., s. Jaszúnski, M. . . . .	257
Sakaki, S.: Electronic Structures of Organo-Transition-Metal Complexes I. Silver(I)-Olefin Complexes . . . . .	159
Saran, A., Peralia, D., Pullman, B.: Molecular Orbital Calculations on the Conformation of Nucleic Acids and Their Constituents VII. Conformation of the Sugar Ring in $\beta$ -Nucleosides: The Pseudorotational Representation . . . . .	31
Schaffer, A. M., Gouterman, M., Davidson, E. R.: Porphyrins XXVIII. Extended Hückel Calculations on Metal Phthalocyanines and Tetrazaporphins . . . . .	9
Schnakig, R., s. König, G. . . . .	205
Schwartz, M. E., s. Naloway, C. A. . . . .	347
Sinanoglu, O., s. Duben, A. J., <i>et al.</i> . . . . .	177
Staemmler, V., s. Driessler, F., <i>et al.</i> . . . . .	315
Tanaka, J., s. Tanaka, M. . . . .	81
Tanaka, M., Tanaka, J.: RPA Method Applied to Molecular Crystals . . . . .	81
Tomasi, J., s. Ghio, C. . . . .	151
Trautwein, A., Harris, F. E.: Molecular Orbital Structure, Mössbauer Isomer Shift, and Quadrupole Splitting in Iron Complexes . . . . .	45



Warren, C.H., Ching, C.: Theoretical Study of the Electronic Spectrum of Carbonyl Cyanide . . . . .	1
Yamabe, S., Kato, S., Fujimoto, H., Fukui, K.: An MO-Theoretical Calculation of Solvent Effect upon the $\text{NH}_3 + \text{HF} = \text{NH}_4\text{F}$ Reaction . . . . .	327
Zeller Stenkamp, L., Davidson, E.R.: An ICSCF Investigation of Walsh's Rules . . . . .	283
Zhidomirov, G.M., Chuvylkin, N.D.: Calculations of the Isotropic Hyperfine Coupling Constants in Free Radicals. . . . .	197

### Recensiones

Avery, J.: The Quantum Theory of Atoms, Molecules and Photons (Ref. E.A.Reinsch)	127
Chemieunterricht heute (Chemistry today). OECD (Hrsg.) (Ref. H. Heydtmann) . . . .	353
Cotton, F.A., Wilkinson, G.: Advanced Inorganic Chemistry. (Ref. K. Hensen) . . . .	282
Löwdin, P.O.: Advances in Quantum Chemistry 6. (Ref. K.Jug) . . . . .	128

Indexed in Current Contents

### Subiecta

Acetylcholine, electronic structure of . . . . .	275
Acetylene . . . . .	177
Ag <sup>+</sup> -olefin complexes. . . . .	159
Atomic charge . . . . .	347
Average natural orbitals . . . . .	209
Benzenesulphonic acid, rotational barrier of . . . .	115
Carbonyl cyanide, calculation of the spectrum of . .	1
Charge density . . . . .	347
Configuration interaction . . . . .	177
Configuration interaction, perturbative . . . . .	59
Conjugated carbonyl compounds. . . . .	267
Correlation energy . . . . .	315
d <sup>6</sup> configuration . . . . .	205
Desoxyribose . . . . .	31
Disulfides, conformation of . . . . .	137
Electron affinity. . . . .	315
Electron-atom interaction . . . . .	191
Electron spin resonance . . . . .	197
Electron-transfer transitions . . . . .	339
Electronic relaxation. . . . .	217
Energy transfer . . . . .	217
Exchange interaction . . . . .	191
Excitation energies of BH . . . . .	209
Generalized diatomic orbitals . . . . .	169
Glycose bond . . . . .	31
Helium type atoms . . . . .	95
Hybridized valence state energy formulas . . . . .	129

Hydrogen bond NMR shift of water molecules and dimer . . . .	257
Hydrogen persulfide . . . . .	137
Hyperfine coupling constants . . . . .	197, 315
Inductive effect . . . . .	347
Inorganic chelates . . . . .	339
Inorganic complexes . . . . .	339
Inversion barrier . . . . .	315
Ionic states . . . . .	177
Iron complexes . . . . .	45
LCDO and LAGDO methods . . . . .	169
Ligand field theory . . . . .	205
Localized orbitals . . . . .	243, 347
Metal phthalocyanines . . . . .	9
Mößbauer isomer shift . . . . .	45
Molecular crystals . . . . .	81
Molecules-in-molecules methods . . . . .	267
Multiconfiguration SCF formalism . . . . .	231
Natural spin orbitals . . . . .	169
Negative Ions . . . . .	191, 315
Orbital energies . . . . .	283
Pair correlation . . . . .	177
PCILO method . . . . .	59
$\pi \rightarrow {}^1\pi^*$ transitions . . . . .	267
Proton magnetic shielding . . . . .	257
Protonation process . . . . .	151
Pseudopotential theory . . . . .	119
Pseudorotation . . . . .	31
Quadrupole splitting . . . . .	45
Radiationless transitions . . . . .	217
Radicals . . . . .	197
Random phase approximation . . . . .	81
Reactivity . . . . .	327
Ribose . . . . .	41
Rotary strengths of inorganic complexes . . . . .	339
Saturated hydrocarbons . . . . .	243
Semiempirical MO theory . . . . .	231
Solvent effect . . . . .	327
Spin-density distribution . . . . .	197
Tetrazaporphyrins . . . . .	9
Three-membered ring . . . . .	151
Tris-(1,10-phenantroline)iron(II) ion . . . . .	339
Walsh's rules . . . . .	283

# Theoretical Study of the Electronic Spectrum of Carbonyl Cyanide

Charles H. Warren and Chorman Ching

Department of Chemistry, Dalhousie University, Halifax, Nova Scotia, Canada

Received October 13, 1972/ February 5, 1973

The ground state properties of carbonyl cyanide and the energies of the electronic transitions are determined by means of the CNDO/2 and CNDO/CI methods respectively. The calculated results are correlated with the observed electronic spectra and assignments are suggested for some previously unassigned transitions. The bonding and delocalization of the  $\pi$  electrons of the ground and excited states of the molecule are discussed through an analysis of the molecular orbitals and charge density distributions.

Die Eigenschaften des Grundzustandes von Carbonylcyanide und die Energie von elektronischen Übergängen werden mit Hilfe der Methoden CNDO/2 und CNDO/CI bestimmt. Die berechneten Ergebnisse werden mit dem beobachteten Elektronenspektrum korreliert; für einige bisher nicht klassifizierte Übergänge werden Zuordnungen vorgeschlagen. Die Bindung und Delokalisierung der  $\pi$ -Elektronen des Grundzustandes und der angeregten Zustände werden mit Hilfe einer Analyse der MO's und der Ladungsverteilung diskutiert.

## Introduction

The absorption spectrum of carbonyl cyanide,  $(\text{CN})_2\text{CO}$ , has been the subject of a number of recent investigations. The spectrum was first studied by Kemula and Wierzchowski [1] and more recently by Wierzchowski *et al.* [2] who examined the absorption and fluorescence spectrum of the  $n \rightarrow \pi^*$  ( $^1A_2 \leftarrow \tilde{X}^1A_2$ ) transition at high and intermediate dispersion. The spectrum in the vacuum ultraviolet region has just been reported by Duncan and Whittock [3]. Only one resolved transition was observed between 46900 and 78100  $\text{cm}^{-1}$ . Since their experimental data was not sufficient to make an assignment for the above transition, we decided that a theoretical treatment might aid the interpretation of the electronic spectrum. As far as we can ascertain, no detailed theoretical study has been previously carried out for carbonyl cyanide. The two cyanogen groups attached symmetrically to a carbonyl group should provide an interesting study of the mixing of the  $\pi$  orbitals of the CO and CN groups as well as the mixing of the  $n$  orbitals of the atoms.

In this paper, we report the application of the CNDO method [4-7] to the study of the ground state and electronic spectrum of carbonyl cyanide. This method should be quite suitable since it treats all valence electrons.

Table 1. Bond distance and angles used for carbonyl cyanide

Bond	Distance, Å	Angle	Size, deg
C=O	1.220*	C C C	115 19
C≡N	1.165*	C C N*	0
C C	1.450		

\* Assumed

### Method of Calculation

For the calculation of the ground state properties of carbonyl cyanide, the CNDO/2 method [6] was adopted without modification. The parameters used were those developed by Pople and Segal [5,6]. In this form, the method has been successfully applied to ground state calculations of many small molecules.

Since the CNDO/2 method gives very poor results when applied to the treatment of excited state properties, the electronic spectrum of carbonyl cyanide was computed using the modification of the CNDO/2 method proposed by Del Bene and Jaffé [8]. This method has been satisfactorily applied in the prediction of both  $\pi \rightarrow \pi^*$  and  $n \rightarrow \pi^*$  transitions. The parameters  $\beta_A^0$  used in the program to estimate the resonance integrals between carbon, oxygen and nitrogen were taken to be the same as those suggested by Jaffé [8]. In the Jaffé modification, the two-centre Coulomb integrals were evaluated by the extrapolation technique proposed by Pariser [9]. However, in our calculations, we have used a modified Mataga-Nishimoto approximation [10] for these integrals since we feel that this method leads to slightly better results [11].

The bond distances and angles of carbonyl cyanide chosen for the calculations are given in Table 1. These values were obtained from a recent analysis of the microwave spectrum by Lees [12]. In their determination of the molecular parameters, they assumed that the CCN chain was linear. Since their data were consistent with a planar structure, we assumed in our work that carbonyl cyanide was planar with  $C_{2v}$  symmetry. By convention [13], we have chosen the  $C_2$  axis as the  $z$ -axis and the  $x$ -axis as perpendicular to the molecular plane.

### Results of the Calculations

#### a) Ground State Properties

The ground state properties of carbonyl cyanide were obtained by the original CNDO/2 method and also by the Jaffé modification. The charge density distributions on the nuclei are given in Fig. 1. These represent the flow of charge in the molecule from the neutral atoms. One can see that the Jaffé method leads to a greater total net charge on the nuclei. Both schemes lead to a polarization of the  $\pi$  electrons (formed from the  $2p_z$  orbitals of the nuclei) on the carbonyl group. The  $\pi$  bond can be designated  $C^+ - O^-$  and is quite polar in contrast to the analogous bond in formaldehyde. The  $\pi$  electrons of the remaining nuclei are polarized only slightly.

Berthier, Pullman, and Pontis [14] have found that the characteristic carbonyl stretching frequency of aldehydes and ketones gives an excellent

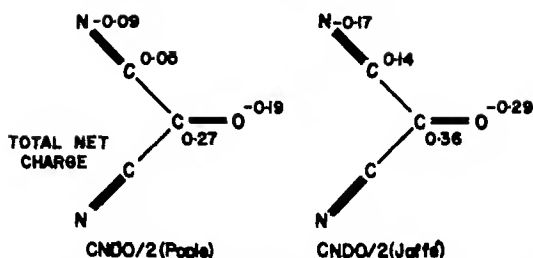


Fig. 1. Charge density distributions for the  $\tilde{X}^1A_1$  ground state of carbonyl cyanide as calculated by a) CNDO/2 (Pople) and b) CNDO/2 (Jaffé)

correlation with the  $\pi$ -bond order of the carbonyl group. In order to assess our calculations, we have determined the carbonyl frequency with this correlation using our values of 0.913 (CNDO/2) and 0.914 (Jaffé) for the  $\pi$ -bond order between carbon and oxygen. We obtained 1710 and 1711  $\text{cm}^{-1}$  respectively. Experimentally the carbonyl frequency is observed at 1712  $\text{cm}^{-1}$  [15].

Our results also show that the oxygen  $2p_y$  orbital (the  $n$ -orbital) is not completely full. There is a "back-donation" effect present in which electrons in orbitals of this symmetry ( $b_2$ ) are transferred into the antisymmetric  $\text{C}(\text{CN})_2$ -orbitals forming a partial pseudo- $\pi$  bond or  $\pi_y$  bond. Similarly as with formaldehyde, there is a concentration of oxygen lone pair electrons on the  $z$ -axis on the side away from the rest of the molecule.

The bond order defined as

$$P_{\mu\nu} = 2 \sum_{i=1}^{\text{occ}} C_{i\mu} C_{i\nu}$$

where the sum is over all the occupied orbitals and  $C_{i\mu}$  are the coefficients of the LCAO SCF molecular orbitals gives a measure of the bonding due to contributions by the atomic orbitals  $i$  and  $j$ . The out-of-plane  $\pi$  bond orders were determined to be 0.96, 0.27 and 0.91 between nitrogen and carbon; carbon and carbon; and carbon and oxygen respectively. There is some delocalization of the  $\pi$ -electrons into the CCC skeleton but it is not extensive. One can regard the C-C bond as essentially a single bond. This is also demonstrated by a comparison of the "bond indices" which appear to be closely related to the bond character [16]. This quantity is given by the sum of the squares of the bond orders to an atom and corresponds to the number of covalent bonds formed by that atom, corrected for the ionic character in each bond. The bond indices determined were 2.88, 1.02 and 1.84 for  $\text{C}\equiv\text{N}$ , C-C, and C=O respectively. Since these will be later compared with the values obtained for the first excited state, we have reported only the results for the Jaffé calculation. In any case, the values obtained by the CNDO/2 method are quite similar. The value 1.02 shows that delocalization across the CCC skeleton is small and there does not appear to be a great loss in the triple bond character of  $\text{C}\equiv\text{N}$ . This loss and subsequent delocalization was predicted to occur in carbonyl cyanide by Bates [15] who analysed the vibrational frequencies of a number of compounds containing the carbonyl and nitrile groups.

Both methods yield a dipole moment [0.12 D and 0.14 D (Jaffé)] which is much smaller than the experimental value of 0.70 D [12]. The energies of the

Table 2. Energies and classification of the molecular orbitals of carbonyl cyanide

Symmetry	Energy (a.u.)	Symmetry	Energy (a.u.)
$8a_1$	-0.69519	$3b_1$	-0.04237
$1b_1$	-0.63299	$11a_1$	0.02049
$5b_2$	0.59823	$2a_2$	0.03566
$9a_1$	-0.58883	$8b_2$	0.05076
$10a_1$	-0.51399	$4b_1$	0.08000
$1a_2$	0.50916	$12a_1$	0.11889
$6b_1$	-0.49199		
$2b_1$	-0.48688		
$7b_2$	-0.44392		

molecular orbitals as calculated by the Jaffé version of the CNDO/2 method and their group theoretical classification are given in Table 2.

### b) Excited State Properties and Spectra

The electronic spectrum of carbonyl cyanide was calculated with and without the inclusion of configuration interaction (C.I.). When it was included, thirty singly excited configurations were employed. These comprised all the configurations arising from the promotion of an electron from the occupied orbitals  $10a_1 - 5b_2$  to the unoccupied orbitals  $3b_1 - 12a_1$  inclusive. The results of the calculations when C.I. was included are given in Table 3. The correlation with the experimental results is displayed in Fig. 2.

Table 3. Calculated electronic transitions in carbonyl cyanide

Transition	Vertical transition energy (cm <sup>-1</sup> )	Oscillator strength	Configuration mixing
$\tilde{1}^1A_2 - \tilde{X}^1A_1$ ( $n \rightarrow \pi^*$ )	24168	0	$7b_2 \rightarrow 3b_1$ (91%) $7b_2 \rightarrow 4b_1$ (8%) $6b_2 \rightarrow 3b_1$ (1%)
$^1A_2 - \tilde{X}^1A_1$ ( $\pi \rightarrow \pi^*$ )	39434	0	$6b_2 \rightarrow 3b_1$ (62%) $10a_1 \rightarrow 2a_2$ (26%)
$^1B_1 - \tilde{X}^1A_1$ ( $\pi \rightarrow \pi^*$ )	40777	$10^{-4}$	$10a_1 \rightarrow 3b_1$ (50%) $6b_2 \rightarrow 2a_2$ (41%)
$^1B_2 - \tilde{X}^1A_1$ ( $\pi \rightarrow \pi^*$ )	43578	0.006	$1a_2 \rightarrow 3b_1$ (31%) $4b_2 \rightarrow 7a_1$ (30%) $2b_1 \rightarrow 7a_1$ (18%)
$^1A_1 - \tilde{X}^1A_1$ ( $\pi \rightarrow \pi^*$ )	44040	0.05	$10a_1 \rightarrow 8b_2$ (15%) $2b_1 \rightarrow 3b_1$ (34%) $10a_1 \rightarrow 11a_1$ (22%) $6b_2 \rightarrow 8b_2$ (20%) $1a_2 \rightarrow 2a_2$ (19%)
$^1A_2 - \tilde{X}^1A_1$ ( $\pi \rightarrow \pi^*$ )	47023	0	$1a_2 \rightarrow 11a_1$ (60%) $2b_1 \rightarrow 8b_2$ (40%)
$^1B_1 - \tilde{X}^1A_1$ ( $\pi \rightarrow \pi^*$ )	47034	0	$2b_1 \rightarrow 11a_1$ (60%) $1a_2 \rightarrow 8b_2$ (40%)
$^1B_2 - \tilde{X}^1A_1$ ( $n \rightarrow \pi^*$ )	54780	0.008	$7b_2 \rightarrow 11a_1$ (99%)

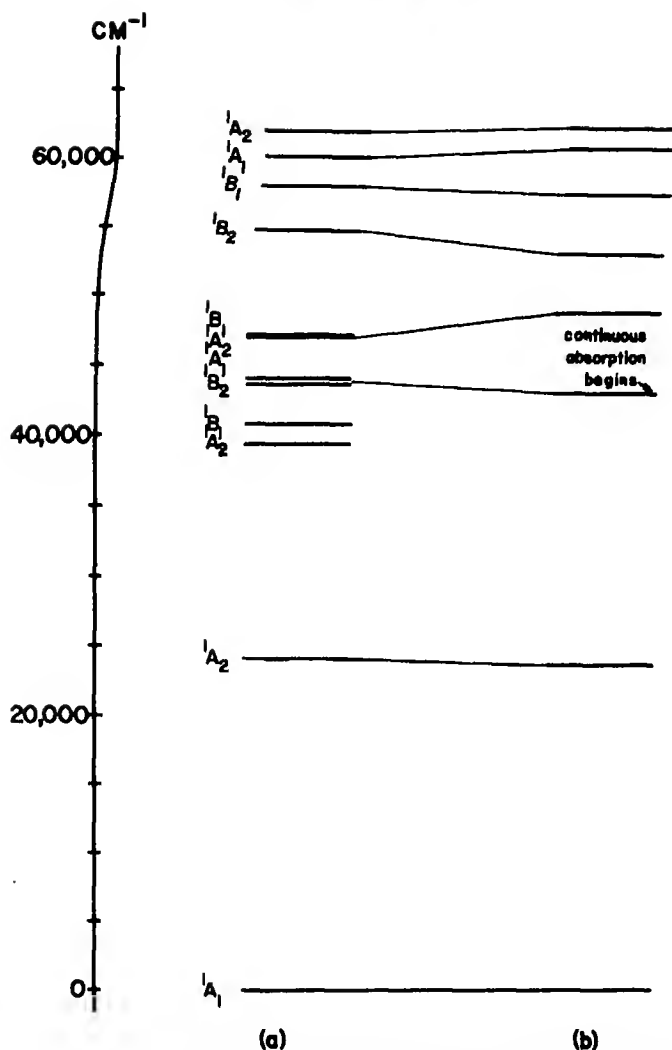


Fig. 2. Electronic states of carbonyl cyanide a calculated results with C.I. and b experimental results

The lowest electronic transition was calculated to be the  $A^1\tilde{A}_2 - \tilde{X}^1A_1$  forbidden electric dipole transition ( $n \rightarrow \pi^*$ ) characteristic of carbonyl compounds. The inclusion of configuration interaction modifies the energy of the  $\tilde{A}^1A_2$  state only slightly. Hence, this state can be described fairly accurately in terms of a single configuration ( $\sim 91\%$ ) – the one arising from the promotion of an electron from the  $7b_2$  orbital to the unoccupied  $3b_1$  orbital. The remaining contribution to this state is made up of the configurations arising from the promotions  $7b_2 \rightarrow 4b_1$  and  $6b_2 \rightarrow 3b_1$ . The  $7b_2$  molecular orbital is essentially the oxygen  $2p_y$  lone pair orbital (65%). The remaining contribution to this molecular orbital is from  $\sigma$  type atomic orbitals of the  $(\text{CN})_2\text{C}$  framework. The  $3b_1$  and  $4b_1$  orbitals are antibonding out-of-plane  $\pi^*$  orbitals composed of the  $2p_x$  atomic orbitals on

each nucleus. The  $3b_1$  orbital is antibonding w.r.t. the  $C=O$  and  $C\equiv N$  chromophores but slightly bonding w.r.t. the  $CCC$  skeleton.  $4b_1$  is the highest unoccupied out-of-plane  $\pi^*$  orbital and is antibonding w.r.t. all adjacent nuclei. The bond indices calculated for the  $\tilde{A}^1A_2$  state are 2.70, 0.98 and 1.52 for the  $C\equiv N$ ,  $C-C$  and  $C=O$  bonds which represents a decrease of 6.3%, 3.9% and 17.4% respectively from the ground state values. Hence, the result of an excitation to this state would be a pronounced weakening of the  $C=O$  bond and an increase in its bond length. Experimentally, this increase is manifested in the appearance of a long progression of the carbonyl stretch in the  $n \rightarrow \pi^*$  transition observed between 24390 and 38461  $\text{cm}^{-1}$ . This stretching frequency has decreased to 1250  $\text{cm}^{-1}$ . The oscillator strength for this transition was reported as  $0.85 \times 10^{-4}$ .

The next two lowest transitions are classified as  $^1A_2 - \tilde{X}^1A_1$  and  $^1B_1 - \tilde{X}^1A_1$  respectively. The  $^1A_2$  state is a linear combination of the configurations arising from the promotions  $6b_2 \rightarrow 3b_1$  and  $10a_1 \rightarrow 2a_2$ . The  $6b_2$  and  $10a_1$  orbitals are best described as in-plane  $\pi$  bonding orbitals localized on the  $C\equiv N$  group.  $2a_2$  is an antibonding  $\pi^*$  out-of-plane orbital localized on the  $C\equiv N$  group. The  $^1B_1$  state is quite similar to the above  $^1A_2$  state.

No transitions are experimentally observed in this region. The transitions are either too weak to be observed which agrees with the low value of the calculated oscillation strengths or they may form part of the continuous absorption beginning at 43000  $\text{cm}^{-1}$ . Wierzchowski *et al.* have reported predissociation in the lowest  $n \rightarrow \pi^*$  transition  $\tilde{A}^1A_2 - \tilde{X}^1A_1$ . They postulate that this is caused by a dissociative state lying close to the  $\tilde{A}^1A_2$  state. The state causing this predissociation is perhaps the second  $^1A_2$  state at 39434  $\text{cm}^{-1}$ .

The strong quasi-continuous absorption beginning at 43000  $\text{cm}^{-1}$  has previously been assigned to either a  $^1A_1 - \tilde{X}^1A_1(\pi \rightarrow \pi^*)$  or a  $^1B_2 - \tilde{X}^1A_1(n \rightarrow \sigma^*)$  transition. Our calculations give two transitions in this region; one at 43578  $\text{cm}^{-1}$ ,  $^1B_2 - \tilde{X}^1A_1(\pi \rightarrow \pi^*)$ ; and the other at 44040  $\text{cm}^{-1}$ ,  $^1A_1 - \tilde{X}^1A_1(\pi \rightarrow \pi^*)$ . The latter transition has an oscillator strength approximately ten times that of the former. Our calculations tend to rule out the assignment of the transition as  $n \rightarrow \sigma^*$ ; our calculated values for transitions of this type are all too high in energy. Since the observed transition is strong, we prefer to assign it as  $^1A_1 - \tilde{X}^1A_1(\pi \rightarrow \pi^*)$ , a transition localized on the  $C\equiv N$  chromophore. The  $^1A_1$  and  $^1B_2$  states are a mixture of configurations (see Table 3).  $11a_1$  and  $2a_2$  are antibonding  $\pi^*$  orbitals localized on the  $C\equiv N$  group. The latter consists of the out-of-plane  $2p_x$  orbitals while the former uses the in-plane  $2p_y$  and  $2p_z$  orbitals.  $1a_2$  is an out-of-plane bonding  $\pi$  orbital localized on the  $C\equiv N$  group. The  $2b_1$  is an in-plane bonding  $\pi$  orbital bonding w.r.t. C and N; slightly bonding w.r.t. C and O; and antibonding w.r.t. the carbon nuclei.

The next two calculated transitions fall at 47023  $\text{cm}^{-1}$ ,  $^1A_2 - \tilde{X}^1A_1$ , and at 47034  $\text{cm}^{-1}$ ,  $^1B_1 - \tilde{X}^1A_1$ . Both are  $\pi \rightarrow \pi^*$  transitions localized on the  $C\equiv N$  chromophore and both have oscillator strengths of zero. One would predict that they might be too weak to be observed but perhaps could be correlated with the weak bands reported at 48656, 48749 and 48831  $\text{cm}^{-1}$ .

The resolved transition between 46900 and 63000  $\text{cm}^{-1}$  has an oscillator strength of approximately 0.07. This transition could possibly be correlated with the transition calculated at 54780  $\text{cm}^{-1}$ ,  $^1B_2 - \tilde{X}^1A_1(\pi \rightarrow \pi^*)$ . Experimentally,



tally, maximum absorption occurs around  $53\,000\text{ cm}^{-1}$ . By the Franck-Condon principle, this would correspond to the vertical transition – the transition which is calculated. The computed oscillator strength of 0.008 agrees with the experimental findings that the transition is weak. The  ${}^1B_2$  state is mainly composed of the single configuration corresponding to  $7b_2 \rightarrow 11a_1$ .  $11a_1$  is an in-plane  $\pi^*$  orbital localized on the CN group.

Duncan and Whitlock [3] observe a prominent transition at  $57\,600\text{ cm}^{-1}$  which cannot be fitted into their vibrational analysis. Our calculations suggest that this band may be caused by another electronic transition as well as the two weak shoulders just above  $60\,000\text{ cm}^{-1}$ . We calculate transitions at  $58\,183$ ,  $60\,260$ , and  $62\,240\text{ cm}^{-1}$  corresponding to the transitions  ${}^1B_1 - \tilde{X}^1A_1$ ,  ${}^1A_1 - \tilde{X}^1A_1$  and  ${}^1A_2 - \tilde{X}^1A_1$  respectively. These are all  $n \rightarrow \pi^*$  and arise chiefly from the configurations  $7b_2 \rightarrow 2a_2$ ,  $7b_2 \rightarrow 8b_2$  and  $7b_2 \rightarrow 4b_1$  respectively.

Beyond this point, a large number of electronic transitions are calculated to be present and probably correspond to the continuous absorption observed between  $63\,000$  and  $78\,100\text{ cm}^{-1}$ , the limit of the experimental data to date.

Triplet spectra have also been calculated but are not reported here for two reasons. The first is that a number of the singlet and triplet transitions are calculated to have the same energy. The cause for this is that the singlet-triplet separation is directly related to the value of an exchange integral which for  $n \rightarrow \pi^*$  transitions vanishes identically within the CNDO approximation causing the singlet and triplet states arising from such a transition to be degenerate. The second reason is that no singlet-triplet spectra have been reported and we have no data with which to correlate our results.

### Discussion

In general, the agreement with the experimental results is good and the calculations should serve as a guide to further work. One should keep in mind, however, that the method is an approximate one and more experimental work is required to verify the results, especially, in the higher energy regions where a large number of transitions occur. The ground state equilibrium geometry was the only geometry used in the calculations. Further work is in progress on the study of the electronic structure of the molecule as a function of the molecular geometry in various states.

*Acknowledgements.* This work was financially supported by the National Research Council of Canada.

### References

1. Kemula, W., Wierzchowski, K. L.: *Roczniki Chem.* **27**, 524 (1953).
2. Prochorow, J., Tramer, A., Wierzchowski, K. L.: *J. molecular Spectroscopy* **19**, 45 (1966).
3. Duncan, A. B. F., Whitlock, R. F.: *Spectrochim. Acta* [London] **27 A**, 2539 (1971).
4. Pople, J. A., Santry, D. P., Segal, G. A.: *J. chem. Physics* **43**, S 29 (1965).
5. Pople, J. A., Segal, G. A.: *J. chem. Physics* **43**, S 136 (1965).
6. Pople, J. A., Segal, G. A.: *J. chem. Physics* **44**, 3289 (1966).
7. Santry, D. P., Segal, G. A.: *J. chem. Physics* **47**, 158 (1967).

8. Del Bene, J., Jaffé, H. H.: J. chem. Physics **48**, 1807 (1968); **48**, 4050 (1968); **49**, 1221 (1968); **50**, 1126 (1969).
9. Pariser, R., Paar, R. G.: J. chem. Physics **21**, 466; **21**, 767 (1953).
10. Mataga, N., Nishimoto, K.: Z. physik. Chem. **13**, 140 (1957).
11. King, G. W., van Putten, A. A. G.: J. molecular Spectroscopy **42**, 514 (1972).
12. Lees, R. M.: Canad. J. Physics **49**, 367 (1970).
13. Mulliken, R. S.: J. chem. Physics **23**, 1997 (1955).
14. Berthier, G., Pullman, B., Pontis, J.: J. Chim. physique **49**, 367 (1952).
15. Bates, J. B., Smith, W. H.: Spectrochim. Acta **26 A**, 455 (1970).
16. Wiberg, K. B.: Tetrahedron **24**, 1083 (1968).

Dr. C. H. Warren  
Department of Chemistry  
Dalhousie University  
Halifax, Nova Scotia, Canada

## Porphyrins XXVIII.\* Extended Hückel Calculations on Metal Phthalocyanines and Tetrazaporphins

Arnold M. Schaffer, Martin Gouterman, and Ernest R. Davidson

Department of Chemistry, University of Washington, Seattle, Washington 98195

Received December 27, 1972

Extended Hückel (EH) calculations on Mg, Zn, Cu, Ni, Fe, Mn, and VO complexes of phthalocyanine and tetrazaporphin are reported and the results compared to similar calculations on porphyrins. The smaller ring size of phthalocyanine gives rise to a larger ligand field. The bridge nitrogen atoms give rise to  $n-\pi^*$  transitions, which are probably in the region of the Soret band. In Ni, Co, Fe, and Mn there is strong mixing of the bridge  $N(2p_z)$  and metal  $b_{2g}(d_{xy})$ , which should affect the ligand field. Extra absorption bands observed in the near uv of NiPc and CoPc are attributed to  $d_{\pi} \rightarrow \pi^*$  transitions. A general symmetrized EH program is reported that speeds calculations on large systems.

Für die Komplexverbindungen von Mg, Zn, Cu, Ni, Fe, Mn und Vo mit Phthalocyanin und Tetrazaporphin werden erweiterte Hückelrechnungen (EH) durchgeführt und die Ergebnisse mit ähnlichen Berechnungen an Porphyrinen verglichen. Die geringere Ringgröße des Phthalocyanins gibt Anlaß zu einem größeren Ligandenfeld. Das Brücken-Stickstoffatom gibt Anlaß zu  $n-\pi^*$ -Übergängen, die wahrscheinlich im Gebiet der Soret-Bande liegen. Beim Ni, Co, Fe und Mn tritt eine starke Mischung der Orbitale des Brückenstickstoff-Atoms  $N(2p_z)$  und  $b_{2g}(d_{xy})$  auf, die das Ligandenfeld beeinflussen sollte. Die zusätzlichen Absorptionsbanden, die im nahen UV bei NiPc und CoPc beobachtet werden, werden  $d_{\pi} \rightarrow \pi^*$ -Übergängen zugeordnet. Ein allgemeines, symmetrisiertes EH-Programm wird mitgeteilt, das die Berechnung großer Systeme beschleunigt.

### Introduction

Previous papers in this series have reported extended Hückel (EH) calculations on a variety of porphyrins and related systems. Studies have been reported for porphyrin complexes with various first row transition metals [1–4], with alkali earth metals [5], and with Group IV metals [6], as well as EH calculations on free bases of porphin (P), tetrazaporphin (TAP), tetrabenzporphin (TBP), and phthalocyanine (Pc) [7]. This paper reports EH calculations on Mg and various first row transition metal complexes of phthalocyanine and tetrazaporphin. In tetrazaporphin the four methine bridge carbon atoms of porphin are replaced by nitrogen atoms. In phthalocyanine there is an additional perturbation of four benzo rings fused onto exo pyrole carbon atoms. The larger size of phthalocyanine required considerable computation time using the original EH programs, and a newer program was developed that is reported here. It allows for more atoms and up to three planes of symmetry – in contrast to the original program that allows only two planes [1, 4]. This paper focuses attention

\* Paper XXVII. M. Gouterman, F. P. Schwarz, P. D. Smith, and D. Dolphin, J. chem. Physics, in press (1973).

on the similarities and contrasts among the porphyrin, tetrazaporphin, and phthalocyanine ring systems as shown by the EH calculations. In particular we consider effects on the ligand field and on electron densities.

Phthalocyanine molecules are similar in many ways but differ significantly from porphyrins. Although they do not occur naturally, since they were first synthesized and characterized by Linstead and co-workers [8,9] they have found many scientific and commercial applications. Over 40 different metal complexes have been prepared, and phthalocyanines have found uses as dyes, catalysts, insulators, and passive Q-switches for lasers [10]. Their vapor properties have been studied [11,12] as well as their photoconductive, semiconductive, and magnetic properties as solids [13]. The tetrazaporphins have not been widely studied since the early reports on their spectra [14] and methods of synthesis [15].

The early calculations on phthalocyanines used one of two approaches: the free electron gas model developed by Kuhn and co-workers [16] or simple molecular orbital theory [17]. The former has been extended by the "projected electron density method" to predict bond lengths as well as spectra [18]. SCMO-PPP theory was applied to phthalocyanine and tetrazaporphin some-time ago [19] and difficulties with the larger phthalocyanine system have been resolved more recently [20]. Linder and Rowlands [21] have correlated SCMO-Cl calculations on the excited states of Mg phthalocyanine negative ions with MCD spectra.

While all the above calculations have only included  $\pi$  electrons, there have been a few attempts made to investigate the interaction of the metal with the Pc ring. Ponomarev and Kubarev [23] empirically treated the effects of the metal in a simple Hückel MO calculation. As an aid in analyzing the ESR spectrum of CuPc, Chen *et al.* [24] used a limited EH model to consider the interaction of Cu with the inner 16-membered ring of phthalocyanine. Kramer and Klein [25] used the EH method to correlate the calculated charge density of Fe in FePc with X-ray photoelectron spectra. Recently Mathur and Singh [26] have carried out a limited EH treatment of several metal phthalocyanines, but their unreasonable results suggest some type of error. Recently Henriksson, Roos, and Sundbom [27] treated CuPc by the "peel" electron method. This takes account of the  $40\pi$  electrons, metal  $3d$ ,  $4s$ ,  $4p$  electrons, and the  $8\sigma$  orbitals of the inner and bridge nitrogens. Unlike the other calculations that include the metal electrons, the peel method takes explicit account of two-electron interactions. The calculations reported here are the only ones that include all valence electrons of the whole molecule, but unlike the peel calculations, two electron interactions are not explicitly included.

### Symmetrized Extended Hückel Program

While some of the calculations reported here were done with a symmetrized EH program originally written by Zerner [1,4], most were performed by a revised more efficient computational method. While the Zerner program can handle up to two planes of symmetry, the present program can handle up to three. Written

for the CDC 6400, the present program will handle many more orbitals. It would, however, require modification before it could be used on any other computer. In this section we review the approximations of the EH method and how they were incorporated into the present program.

In this version of self-consistent extended Hückel theory the basis set is assumed to be the minimum set of SCF atomic orbitals. The overlap between these orbitals,  $\langle \phi_i | \phi_j \rangle$ , is approximated by  $\langle \varphi_i | \varphi_j \rangle$  where  $\varphi_i$  is a Slater-type orbital

$$\varphi_i = N r^{n-l-1} e^{-\zeta r} \times \text{spherical polynomial} \quad (1)$$

with  $\zeta$  chosen so that  $\varphi_i$  and  $\phi_i$  give about the same overlap integrals at normal bond lengths. The Hückel operator is approximated by

$$\begin{aligned} \langle \phi_i | H | \phi_j \rangle &= \frac{1}{4}(\alpha_i + \alpha_j) (K_i + K_j) \langle \varphi_i | \varphi_j \rangle \quad i \neq j \\ \langle \phi_i | H | \phi_i \rangle &= \alpha_i. \end{aligned} \quad (2)$$

The diagonal elements  $\alpha_i$  are approximated by

$$\alpha_i = \alpha_i^0 (1 - |q_v|) + |q_v| \alpha_i^\pm \quad (3)$$

where  $\alpha^+$  or  $\alpha^-$  is used as  $q_v \geq 0$  and where  $q_v$  is the net charge from the Mulliken population on atom  $v$  associated with orbital  $i$ . The free atom valence state ionization potential is used for the  $\alpha_i^0$  of C, N, O, H while atomic orbital ionization potentials are used for the metals [4]; the corresponding ionic ionization potentials are used for  $\alpha_i^\pm$ . The empirical interaction constants  $K_i$  were all chosen to be 1.89 in these calculations although the program allows different  $K_i$  for each electron shell in each atom (but not for different azimuthal quantum numbers within a shell).

The actual calculations are carried out with some symmetry factorization. The program can handle up to three mirror planes at right angles. If  $\phi_i$  is an atomic orbital, then a symmetry adapted group orbital  $\phi_{i,r}$  may be defined as

$$\phi_{i,r} = 2^{-N_i} \prod_{\text{all mirror}} (1 + \chi_r(\sigma) \sigma) \phi_i \quad (4)$$

where  $N_i$  is the number of mirror planes containing  $\phi_i$  and  $\chi_r(\sigma) = \pm 1$  is the character of reflection  $\sigma$  in the irreducible representation  $\Gamma$ . With this normalization, the non-vanishing  $\phi_{i,r}$  reduce to

$$\phi_{i,r} = \Pi' (1 + \chi_r(\sigma) \sigma) \phi_i \quad (5)$$

where the prime indicates that the product is over all planes not containing the atomic center associated with  $\phi_i$ .

The overlap matrix between group orbitals is approximated by

$$\begin{aligned} \langle \phi_{i,r} | \phi_{j,r} \rangle &= \langle \Pi' (1 + \chi_r(\sigma) \sigma) \phi_i | \Pi'' (1 + \chi_r(\sigma) \sigma) \phi_j \rangle \\ &= 2^q \langle \varphi_i | \Pi''' (1 + \chi_r(\sigma) \sigma) \varphi_j \rangle \end{aligned} \quad (6)$$

where  $q$  is the number of planes in  $\prod'$  containing the atomic center of  $\varphi_j$  plus the number of planes in  $\prod''$  containing the atomic center of  $\varphi_i$  and  $\prod'''$  is a product over mirror planes not containing the atomic center of  $\varphi_i$  or  $\varphi_j$ . This

reduces the formula for the overlap to the minimum number of unique integrals  $\langle \phi_i | \sigma \phi_j \rangle$ .

The Hückel matrix may be similarly simplified since

$$\langle \phi_i | H | \sigma \phi_j \rangle = \frac{1}{2}(\alpha_i + \alpha_j) (K_i + K_j) \langle \phi_i | \sigma \phi_j \rangle \quad (7)$$

(i.e.  $K_i$  and  $K_{\sigma(i)}$  are chosen equal as are  $\alpha_j^0$  and  $\alpha_{\sigma(j)}^0$ , and  $q_v$  and  $q_{\sigma(v)}$ ). With this assumption,

$$\langle \phi_{i,l} | H | \phi_{j,l} \rangle = \frac{1}{2}(\alpha_i + \alpha_j) (K_i + K_j) \langle \phi_{i,l} | \phi_{j,l} \rangle \quad i \neq j \quad (8)$$

and

$$\langle \phi_{i,l} | H | \phi_{i,l} \rangle = \alpha_i K_i \langle \phi_{i,l} | \phi_{i,l} \rangle + \alpha_i (1 - K_i) 2^{N_\sigma - N_i} \quad (9)$$

where  $N_\sigma$  is the total number of mirror planes.

The charges  $q_v$  are defined for the molecular orbitals  $\psi_{i,l}$  and the orbital occupation numbers  $n_i$  by the equations:

$$\begin{aligned} \psi_{i,l} &= \sum_j C_{i,l}^j \phi_{j,l} \equiv \sum_j Y_{j,l} \phi_j \\ q_v &= Z_v - \sum_{i \text{ on } v} \left| \sum_j \varrho_{i,j} \langle \phi_j | \phi_j \rangle \right| \end{aligned} \quad (10)$$

where  $Z_v$  is the core charge of atom  $v$  and

$$\varrho_{i,j} = \sum_k n_k Y_{ik} Y_{jk} \quad (11)$$

This can be rearranged to

$$\begin{aligned} q_v &= Z_v - \sum_{i \text{ on } v} \left| \sum_j \sum_l \varrho_{i,j}^l \langle \phi_{i,l} | \phi_{j,l} \rangle \right| \\ \varrho_{i,j}^l &= \sum_k n_k^l C_{i,k}^l C_{j,k}^l \end{aligned}$$

Hence the Hückel matrix elements are computable from  $\langle \phi_{i,l} | \phi_{j,l} \rangle$ , and the individual overlap integrals  $\langle \phi_i | \phi_j \rangle$  do not need to be retained after the reduced overlap elements are formed.

The program operates in a standard fashion with the Givens procedure as modified by Householder and Wilkinson [28] used to find the eigenvectors of the Hückel matrix after it is transformed to an orthogonal basis by a Schmidt transformation. The only non-standard algorithm is that involved in the evaluation of  $\langle \phi_i | \phi_j \rangle$ . Rather than use the formulae for each different overlap of STO's, an exact numerical integration is used [29]. This algorithm is based on the fact that the overlap integrals are separable in elliptical coordinates and the points and weights for each of the three one-dimensional integrals in that coordinate system are easily computed and rotated back into cartesian coordinates. Further efficiency is gained since the same set of points will work with all azimuthal quantum numbers. The overlap routine will handle principle quantum numbers up to 6 and angular momentum up to  $l = 3$ .

## Geometry

Although there have been several recent reviews on the X-ray structures of porphyrins [30,31], there has been no similar recent review on the X-ray structures of phthalocyanine. Very little was done following the original

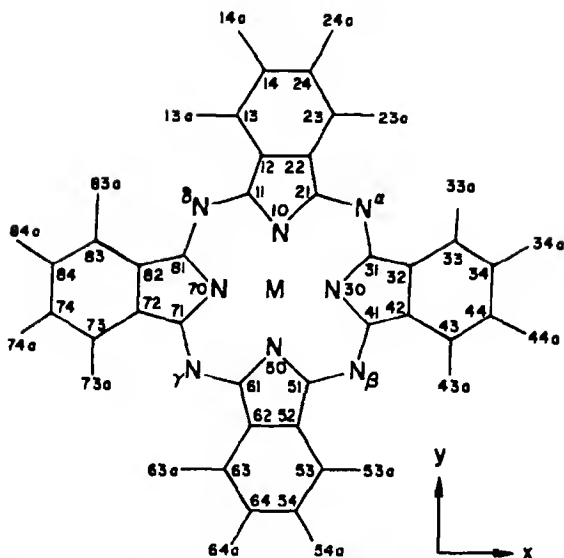


Fig. 1. Numbering scheme for phthalocyanine. The same numbers are used for TAP with the H atoms attached to 12, 22, 32, ... called 12a, 22a, 32a, ...

pioneering studies of Robertson and co-workers [32–34] until recently. In the last few years additional structures of phthalocyanines have been reported: the two polymorphs of  $\text{PtPc}$  [35], a neutron diffraction study of  $\text{H}_2\text{Pc}$  [36],  $\text{MgPc} \cdot \text{H}_2\text{O} \cdot (\text{pyridine})_2$  [37],  $\beta\text{-CuPc}$  [38],  $(\text{Mn(III)Pc Pyridine})_2\text{O}$  [39],  $\text{Sn(II)Pc}$  [40],  $\text{Sn(IV)Cl}_2\text{Pc}$  [41], a 4:1 amine complex between  $\text{FePc}$  and 4-methylpyridine [42], a 2:3 complex between  $\text{ZnPc}$  and *n*-hexylamine [43], and  $\text{Si}[\text{CH}_3][\text{OSi}(\text{C}_2\text{H}_5)_3]\text{Pc}$  [44]. Only the structures of the Mg, Cu, and Sn(IV) compounds have been solved with an estimated standard deviation of less than  $0.01 \text{ \AA}$ . An analysis of these structures leads to several general conclusions about the relation of phthalocyanine and porphyrin geometries, which we shall discuss in terms of the numbering scheme given in Fig. 1. We shall assume  $D_{4h}$  symmetry.

(1) If the hole size is taken as the distance from the center to  $\text{N}_x$ , phthalocyanines are on the average  $0.065 \text{ \AA}$  smaller than the corresponding porphyrins.

(2) Concomitant with point (1) we find that for a given metal, the center to  $\text{N}_{10}$  distance is  $0.05 \text{ \AA}$  smaller in phthalocyanine than in porphyrin. (However for nickel this distance is  $0.13 \text{ \AA}$  shorter, which may be exaggerated by experimental error.)

(3) The  $\text{C}_{21}\text{--N}_x\text{--C}_{31}$  bond angle is about  $3^\circ$  less in phthalocyanine, presumably a consequence of electron repulsion involving the lone pair on the trigonally hybridized nitrogen atom.

(4) The  $\text{C}_{11}\text{--C}_{12}$  bond length in phthalocyanine is larger than in porphyrin, indicating less interaction between the inner 16-membered ring and the remaining electrons.

There are a number of structural reasons why the properties of metallo-phthalocyanines may differ from the corresponding porphyrins. These may

Table 1. Coordinates (x, y) of tetrazaporphin and phthalocyanine in Å

Atom	CuPc	CuTAP
Cu	(0, 0)	(0, 0)
N <sub>10</sub>	(0, 1.935)	(0, 1.935)
C <sub>21</sub>	(1.100, 2.745)	(1.100, 2.745)
C <sub>22</sub>	(0.701, 4.142)	(0.681, 4.142)
C <sub>23</sub> , H <sub>22a</sub>	(1.407, 5.337)	(1.321, 5.002)
H <sub>23a</sub>	(2.487, 5.337)	-
C <sub>24</sub>	(0.709, 6.523)	-
H <sub>24a</sub>	(1.249, 7.458)	-
N <sub>9</sub>	(2.376, 2.376)	(2.376, 2.376)

Table 2. Distance (in Å) from plane of metal (M) and any fifth coordinating atom (L); distance from center of N<sub>10</sub>

	M(z)	L(z)	N <sub>10</sub> (z)
Mg <sup>a</sup>	0.45		1.99
V(1)	0.48	2.11 (0)	1.99
Mn	0		1.99
Fe	0	[1.95 (N <sub>pyr</sub> )] <sup>b</sup>	1.99
Co	0	[1.95 (N <sub>pyr</sub> )]	1.90
Ni	0	[1.95 (N <sub>pyr</sub> )]	1.90
Cu	0		1.935
ZnPc	0.448		1.99
ZnTAP	0		2.00

<sup>a</sup> Geometry of remaining atoms taken from X-ray structure [37], not from Table 1.

<sup>b</sup> Indicates the geometry used for the mono and bispyridine complexes of Fe and Ni and the monopyridimate complex of Co, which were calculated as discussed in the text.

include (i) presence of benzo groups, (ii) aza nitrogens at the bridge positions, (iii) different skeletal geometry, and (iv) different metal-nitrogen bond distances. In order to determine the influence of these last two factors, EH calculations were performed on various skeletal geometries for a given metal phthalocyanine. These calculations are discussed in more detail elsewhere [45]. In this paper, except for MgPc where we used a recent X-ray structure [37], we used the geometry of CuPc [38] as standard with the inner nitrogens moved out from the center to distances appropriate for the given metal. The structures used are given in Tables 1 and 2. For Fe, Co, and Ni, calculations were also done with pyridine as a ligand with geometry given in Table 2.

## Results

### A. Mg and Zn

Fig. 2 compares the MO energy levels of ZnP, ZnTBP, ZnTAP, and ZnPc. The effect on the  $\pi$  MO's is as expected:  $a_{2u}(\pi)$ ,  $a_{1u}(\pi)$  and  $e_g(\pi^*)$  of phthalocyanine are lowered by about 0.6, 0.3, and 0.5 eV respectively relative to



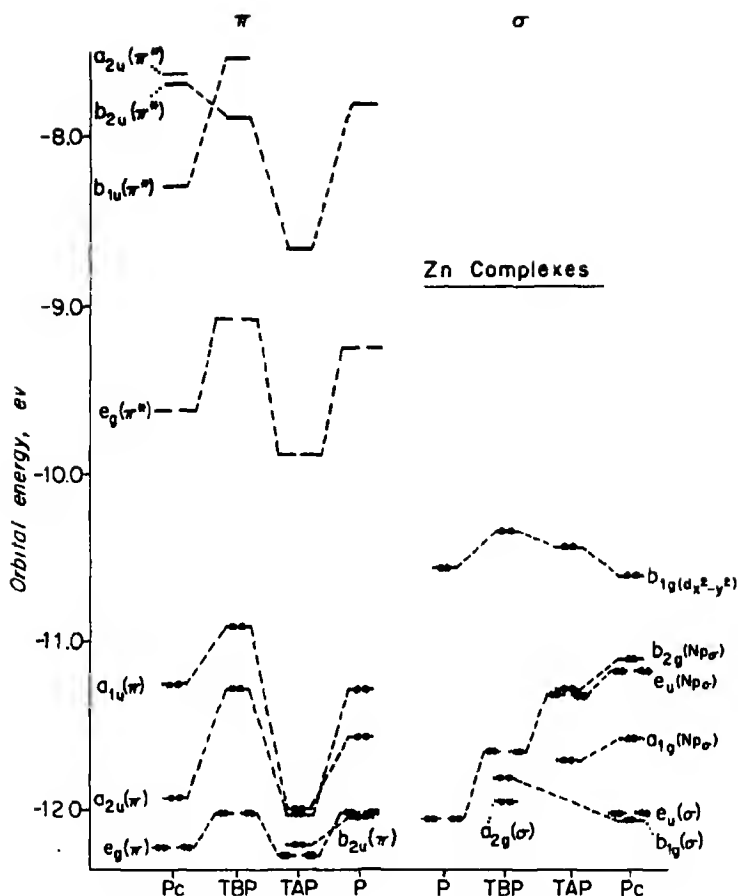


Fig. 2. Top filled and lowest empty  $\pi$  and  $\sigma$  MO's of ZnPc, ZnTBP, ZnTAP, and ZnP

tetrabenzporphyrin, while  $a_{2u}(\pi)$ ,  $a_{1u}(\pi)$ , and  $e_g(\pi^*)$  of tetrazaporphyrin are lowered by about 0.7, 0.4, and 0.6 eV respectively relative to porphyrin. More low energy  $\pi^*$  orbitals appear in ZnPc and ZnTBP as compared to ZnTAP and ZnP. Also low energy filled  $Np_\sigma$  orbitals, due to the bridge nitrogens appear in ZnTAP and ZnPc. Fig. 3 shows the orbitals of MgPc and MgTAP, which are essentially the same as the Zn complexes, except for a low energy empty  $a_1(3p_z)$  at  $\sim -7$  eV, slightly above the range of the diagram.

Are there any spectral effects due to these orbitals? Although there have been many studies of film and crystal spectra [46–48] as well as photoconductivity responses [49, 50], solution or vapor spectra are more useful for comparison with our calculations. Edwards' [12, 51] studies of phthalocyanine show for Mg and Zn five absorption bands assigned as  $\pi\pi^*$ : Q, B, N, L, and C, whose maxima are approximately 15200, 31300, 36400, 40800, and 47600  $\text{cm}^{-1}$  respectively. The spectra of tetrazaporphyrin have been less extensively studied [15, 52]. There are visible and Soret peaks at 17000 and 29500  $\text{cm}^{-1}$  with little study of the higher energy region. The  $\pi\pi^*$  spectra are well accounted for

by SCMO-PPP calculations [19, 20]. The  $Q$  band is relatively pure  $a_{1u}(\pi) \rightarrow e_g(\pi^*)$ , so there is some point to compare our EH calculated energy to the average of the lowest singlet and triplet transition in Pc, where the triplet is known [53]. Our calculated result ranges from 12800 to 13400  $\text{cm}^{-1}$  while the experimental range is 11800 to 12500  $\text{cm}^{-1}$ . We predict the blue shift of the band in TAP.

The top filled  $Np_\sigma$  orbitals in TAP and Pc may be expected to give rise to transitions, with  $e_u(Np_\sigma) \rightarrow e_g(\pi^*)$  being allowed,  $z$  polarized. The energy diagram of Fig. 2 suggests these transitions are at lower energy than the  $Q$  bands, and in fact near *ir* absorption is observed in solid phase [48]. However, the fact that the  $Q$  band fluoresces [11] is very strong evidence that it is the lowest excited singlet state in Mg and Zn complexes. The calculations of Henriksson and Sundbom [54] on free base phthalocyanine put the lowest energy  $Np_\sigma \rightarrow e_g(\pi^*)$  in the Soret region. The EH calculations, while calibrated to fit  $\pi\pi^*$  transitions, seem to generally underestimate transitions involving transfer of charge. We believe that underlying  $Np_\sigma \rightarrow e_g(\pi^*)$  transitions are responsible for the broadening of the Soret region absorption observed in TAP and Pc as compared to P and TBP, in accord with the observations of Hochstrasser and Marzocco [55] that underlying  $n\pi^*$  transitions cause diffuseness in  $\pi\pi^*$  bands.

There is other experimental evidence for the existence of at least one  $n\pi^*$  transition between 15000 and 30000  $\text{cm}^{-1}$ . In Mg triazatetrabenzporphyrin there is a weak but distinct band at  $\sim 22000 \text{ cm}^{-1}$  [56]. This band could be very well due to a  $n\pi^*$  transition, forbidden in a  $D_{4h}$  molecule.

### B. Cu

Fig. 3 gives the MO diagram for CuPc and CuTAP. While the diagram shows  $b_{1g}(d_{x^2-y^2})$  above  $e_g(\pi^*)$ , it is the former that contains the odd electron as shown by ESR [24, 57, 58]. If the odd electron is placed in  $e_g(\pi^*)$ , the EH calculation shows a strong reversal of their relative energies. While the diagram suggests that  $b_{1g}(d_{x^2-y^2}) + e_g(\pi^*)$  should be low in energy, the observation of phosphorescence [53] shows this is not the case as does the peel calculation of Henriksson *et al.* [27].

From the ESR and magnetic properties [59, 60] the ligand field order has been established:  $(d_{xy})^2 < (d_x)^4 < (d_{z^2})^2 \ll (d_{x^2-y^2})^1$ , which exactly matches calculated results. (The four lower energy  $d$  orbitals are not shown in Fig. 3.) Because the  $d_x$  energy is so low, it mixes little with  $e_g(\pi^*)$  as shown in Table 3.

Using certain approximations, one can use the ESR [57, 58] and the magnetic susceptibility results [60] to calculate both the amount of metal delocalization and the ligand field splitting. Due to experimental uncertainty and the approximations involved, a range of values for these properties are obtained. The "experimental"  $d_{xy} \rightarrow d_{x^2-y^2}$  energy separation varies from 26000 to 31000  $\text{cm}^{-1}$  while the  $d_x \rightarrow d_{x^2-y^2}$  gap varies from 17000 to 29000  $\text{cm}^{-1}$ . This compares to our calculated values of 33400 and 32500  $\text{cm}^{-1}$  respectively. We find (see Table 3) that the  $b_{1g}(d_{x^2-y^2})$  orbital is only 28% localized on Cu while ESR results lead to a value  $\sim 70\%$  [57, 58]. From the ESR experiments  $d_{xy}$  and  $d_x$  are found to be  $\sim 100\%$  [57, 58] and  $\sim 55\%$  [58] localized which may be

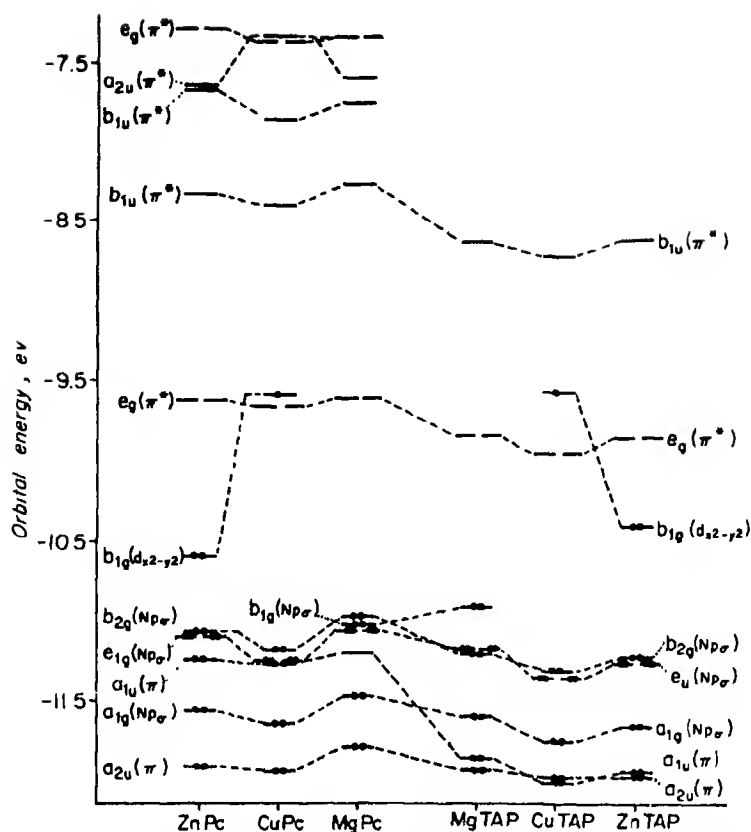


Fig. 3. Top filled and lowest empty MO's of ZnPc, CuPc, MgPc, ZnTAP, CuTAP, and ZnTAP

compared to our values of 92% and 40% respectively. Again our values are too low, but it should be noted that in the interpretation of the experimental ESR spectra, only interaction with the central nitrogens was considered. Henriksson *et al.* [27] found  $b_{1g}(d_{x^2-y^2})$  to be 71% localized on the Cu.

The crystal structure of CuPc [38] indicates that the molecule is not perfectly  $D_{4h}$ . It is almost surely  $D_{4h}$  in solution and vapor, but it is possible that crystal packing forces perturb the molecule slightly away from fourfold symmetry. To determine the effect of such a slight perturbation on the ligand field splitting, we used the geometry of Brown [38] directly; consequently, the angles between the pyrrole nitrogens and Cu are no longer 90°. In this configuration the  $b_{1g}(d_{x^2-y^2})$  orbital is no longer pointing directly at the four pyrrole nitrogens. It thus has less antibonding character and as a result its energy is lowered  $\sim 1.1$  eV and its metal composition increases to 60%. The effect on the  $\pi$  orbitals is small although  $e_g(\pi^*)$  is now split by 0.1 eV. This calculation indicates that even small distortions away from fourfold symmetry will have a large effect on ligand field splittings.

Table 3 Percent composition of top filled and lowest empty orbitals in phthalocyanines<sup>a</sup>

	$a_{1g}(\pi)$					
	C <sub>11</sub>	C <sub>12</sub>	C <sub>13</sub>	C <sub>14</sub>		
Mg	61.6	2.7	23.4	12.8		
Zn	60.4	2.8	23.4	13.4		
Cu	57.4	2.6	25.5	14.5		
Ni	60.4	2.8	23.4	13.4		
Co	60.5	2.8	23.3	13.4		
Fe	59.9	2.5	24.0	13.6		
Mn	59.3	2.3	24.7	13.7		

	$a_{1g}(\pi)$					
	N <sub>10</sub>	C <sub>11</sub>	C <sub>12</sub>	C <sub>13</sub>	C <sub>14</sub>	N <sub>2</sub>
Mg <sup>b</sup>	32.6	1.6	2.4	0.1	1.6	54.9
Zn	26.5	1.9	5.3	0.1	3.8	56.4
Cu	33.8	1.5	3.9	0.1	2.8	55.5
Ni	31.3	1.8	5.8	0.1	4.3	54.5
Co	26.9	2.1	7.8	0.2	6.0	54.6
Fe	33.2	1.3	3.3	0.1	2.2	58.2
Mn	35.6	0.9	2.5	0.1	1.8	57.9

	$e_g(\pi^*)$					
	N <sub>10</sub>	C <sub>11</sub>	C <sub>12</sub>	C <sub>13</sub>	C <sub>14</sub>	N <sub>2</sub>
Mg	15.9	31.8	10.7	6.0	8.8	26.5
Zn	14.2	31.6	11.3	5.8	9.5	27.0
Cu	14.5	31.2	11.2	6.6	10.2	25.9
Ni	15.6	31.0	10.8	5.9	9.2	24.6
Co	15.6	29.8	10.7	5.6	9.0	24.6
Fe	13.9	30.3	11.2	5.5	9.2	27.3
Mn	13.5	30.1	10.9	5.4	9.1	26.9

	$e_g(Np_a)$		$a_{1g}(Np_a)$			
	N <sub>1</sub> (2p <sub>a</sub> )	N <sub>10</sub> (2p <sub>a</sub> )	N <sub>2</sub> (2g)	N <sub>7</sub> (2p <sub>a</sub> )	N <sub>10</sub> (2p <sub>a</sub> )	
Mg	60.0	21.2	7.3	68.1	9.3	
Zn	59.3	18.8	8.0	68.6	7.5	
Cu	59.0	20.6	7.7	67.8	8.9	
Ni	60.5	19.8	8.1	69.2	8.4	
Co	61.3	20.1	7.8	68.4	9.1	
Fe	62.5	21.0	7.1	66.2	8.5	
Mn	64.1	19.7	8.2	64.5	7.7	

	$b_{2g}(Np_a)$ or $b_{2g}^*(d_{xy})^c$		
	N <sub>1</sub> (2p <sub>a</sub> )	N <sub>10</sub> (2p <sub>a</sub> )	3d <sub>xy</sub>
Mg	71.8	15.7	
Zn	72.7	14.2	0.1
Cu	71.0	15.4	1.6
Ni	40.3	10.9	41.5
Co	30.2	8.7	54.8
Fe	38.6	9.9	42.5
Mn	26.1	7.9	60.1

Table 3 (Continued)

	$b_{1g}(d_{x^2-y^2})$ $N_2(2p_\sigma)$	$N_{10}(2s)$	$N_{10}(2p_\sigma)$	$3d_{x^2-y^2}$
Mg <sup>d</sup>	3.9	2.5	65.6	—
Zn	3.6	4.6	68.0	3.6
Cu	1.7	5.1	58.4	28.1
Ni	0.7	4.8	40.9	50.4
Co	0.6	4.8	39.8	53.2
Fe	1.0	3.5	41.8	49.7
Mn	0.9	3.6	41.0	51.1

	$a_{1g}(d_{z^2})$ $N_2(2p_\sigma)$	$4s$	$3d_{z^2}$	$e_g(\pi)$ $3d_\pi$
Ni	4.4	3.5	83.0	83.5
Co	3.8	4.2	87.0	83.9
Fe	8.3	4.4	73.1	85.1
Mn	6.3	5.8	81.8	84.1

	$b_{2g}(d_{xy})$ $N_2(2p_\sigma)$	$N_{10}(2p_\sigma)$	$3d_{xy}$
Ni	34.0	5.9	55.4
Co	44.9	8.1	40.9
Fe	36.0	5.1	55.3
Mn	47.2	7.4	36.4

<sup>a</sup> The total electron density for all  $D_{4h}$  related atoms. For  $\sigma$  orbitals and non-planar Mg and Zn  $\pi$  orbitals, not all atomic orbitals with density are listed.

<sup>b</sup>  $3p_z$  of MgPc.

<sup>c</sup> The  $b_{2g}(Np_\sigma)$  orbital for Mg, Zn, and CuPc, otherwise  $b_{2g}^*(d_{xy})$ .

<sup>d</sup> The  $b_{1g}(Np_\sigma)$  of MgPc.

### C. Ni

Fig. 4 gives the MO diagram for NiPc and NiTAP. The  $b_{2g}(d_{xy})$  shows a curious behavior, which also occurs in Co, Fe, and Mn. It can be seen in the figures and in Tables 3 and 4. The  $d_{xy}$  orbital, which is 96% pure in porphyrins, combines with the  $b_{2g}(Np_\sigma)$  of the bridge nitrogens to give two orbitals. We call the higher energy orbital  $b_{2g}^*(d_{xy})$  and the lower energy orbital  $b_{2g}(d_{xy})$ . Although our EH calculations usually overestimate delocalization of  $d$  orbitals, we believe the different behavior of the  $d_{xy}$  in TAP and Pc as compared to P and TBP due to the bridge nitrogens is real. As discussed below this delocalization may have effects on the magnetic properties and may also influence the absorption spectra.

There are two spectral phenomena in Ni complexes that should be noted.

(i) There is no luminescence of Ni complexes of porphyrins [61] or phthalocyanines [53]. (ii) NiPc shows unusual absorption bands in the near UV at 35200, 42600, and 45900  $\text{cm}^{-1}$  [12]. The lack of luminescence suggests that the partly filled  $d$  shell gives rise to transitions at lower energy than  $\pi\pi^*$ . Fielding

Table 4 Percent composition of the ligand field orbitals of tetrazaporphins<sup>a</sup>

	$b_{1g}(d_{xy}, d_{z^2})$ $N_x(2p_x)$	$N_{10}(2s)$	$N_{10}(2p_x)$	$3d_{xy}, d_{z^2}$
Mg <sup>b</sup>	3.3	4.3	75.4	
Zn	2.8	2.8	76.1	3.0
Cu	1.3	3.2	59.9	28.2
Ni	0.6	4.8	41.6	50.2
Co	0.6	4.8	40.4	51.6
Fe	0.9	3.5	42.4	49.5
VO	0.7	4.5	24.9	35.7

	$b_{2g}^*(d_{xy})$ $N_x(2p_x)$	$N_{10}(2p_x)$	$3d_{xy}$
Ni	33.9	9.8	50.3
Co	26.8	8.2	59.7
Fe	34.8	9.4	48.6

	$b_{2g}(d_{xy})$ $N_x(2p_x)$	$N_{10}(2p_x)$	$3d_{xy}$
Ni	41.8	8.0	45.8
Co	49.6	9.5	35.8
Fe	14.5	6.3	47.5
VO <sup>c</sup>	6.2	3.2	86.8

	$a_{1g}(d_{xy})$ $N_{10}(2p_x)$	4s	$3d_{xy}$	$e_g(d_{xy})$ $3d_x$
Ni	3.8	3.6	86.6	84.5
Co	3.7	4.3	88.0	82.0
Fe	8.3	4.8	78.3	84.9
VO	2.1	3.2	54.8	62.8

<sup>a</sup> The total electron density for all  $D_{4h}$  related atoms.<sup>b</sup> The  $b_{1g}(Np_x)$  of MgTAP.<sup>c</sup> No  $b_{2g}^*(d_{xy})$  orbital for VOTAP.

and MacKay [46] observe bands at  $\sim 6400\text{ cm}^{-1}$  in NiPc that they assign to  $d-d$  transitions that would provide a radiationless path to the ground state. Our energy gap for  $dd$  transitions in Ni is very large, which would suggest that any low energy  $d-d$  transition must be a triplet. If there is no singlet below the singlet  $\pi\pi^*$  then Ni complexes may show a weak fluorescence, as do Pd complexes [53, 62], a point that may have escaped experimental notice.

It has previously been suggested that the unusual absorption bands of NiPc in the UV region are  $d\pi^*$  in origin [12]. There are two reasons why phthalocyanines have many more metal dependent bands than porphyrins: (1) additional delocalization of metal orbitals in phthalocyanines to give greater intensity to  $d\pi^*$  transitions; (2) additional number of low lying empty  $\pi^*$  orbitals to give a

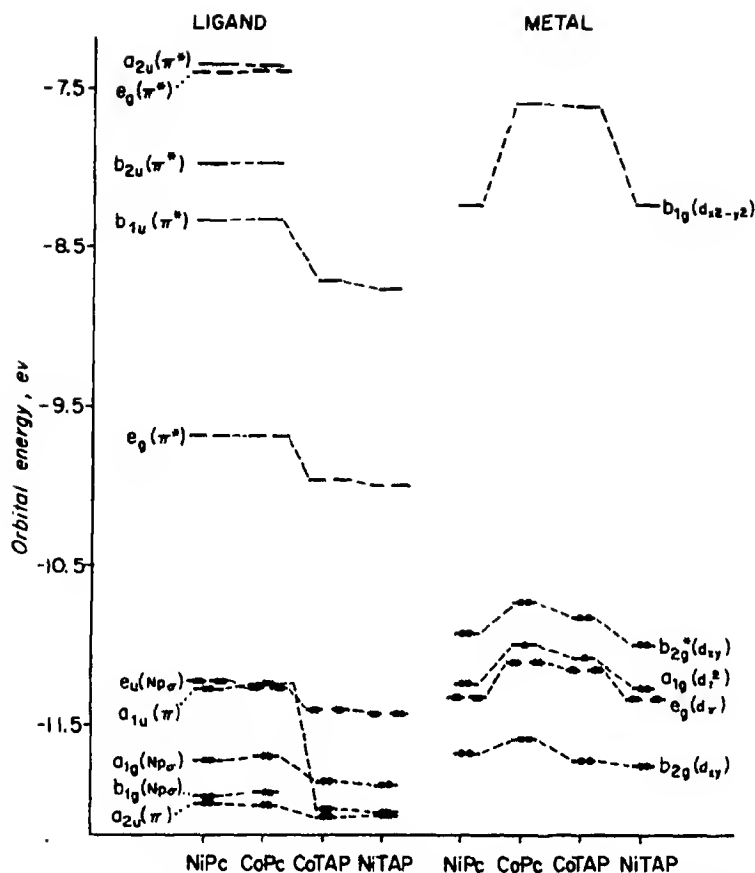


Fig. 4. Top filled and lowest empty MO's of NiPc, CoPc, NiTAP, and CoTAP. The ligand and metal orbitals are indicated separately. No fifth or sixth ligand on metal

greater number of allowed transitions. Table 5 lists the allowed  $d\pi^*$  transitions with orbital energy differences of less than  $45000\text{ cm}^{-1}$  for Ni porphyrins [1] and phthalocyanines. Originally Edwards and Gouterman [12] assigned the NiPc near UV bands to  $b_{2g}(d_{xy}) \rightarrow b_{1u}(\pi^*)$ , since  $d_{xy}$  is now considerably delocalized. However, this transition is  $z$  polarized and even with the increased delocalization is probably too weak to explain the high intensity of these bands. Therefore, we propose that the three metal dependent bands of NiPc correspond to the three  $d_\pi \rightarrow \pi^*$  transitions listed in Table 5. The fairly high intensity of these metal to phthalocyanine transitions is partly a consequence of the increased delocalization of the  $d_\pi$  orbital in phthalocyanines compared to porphyrins. This in turn is a result of the decreased metal-nitrogen bond distance in phthalocyanines. For example,  $d_\pi$  is an 83.5% metal orbital in NiPc with a Ni-N bond distance of  $1.90\text{ \AA}$  (Table 3), while in NiP  $d_\pi$  is 90.0% localized for a Ni-N distance of  $1.96\text{ \AA}$  [1].

Table 5 Calculated energies ( $\text{cm}^{-1}$ ) of allowed  $d \rightarrow \pi^*$  transitions in NiP, NiPc, CoP, and CoPc<sup>a</sup>

Transition	Polarization	NiP	NiPc(X)	CoP	CoPc(XII)
$b_{2g}^*(d_{xy}) \rightarrow b_{1u}(\pi^*)$	$z$		20 800		19 500
$b_{2g}(d_{xy}) \rightarrow b_{1u}(\pi^*)$	$z$	25 000	27 000	23 400	26 500
$a_{1g}(d_{z^2}) \rightarrow a_{2u}(\pi^*)$	$z$		31 200		29 300
$e_g(d_{xz}) \rightarrow b_{1u}(\pi^*)$	$(x, y)$	24 900	24 100	25 200	22 500
$e_g(d_{yz}) \rightarrow b_{2u}(\pi^*)$	$(x, y)$	35 600	27 000	36 000	25 300
$e_g(d_{xy}) \rightarrow a_{2u}(\pi^*)$	$(x, y)$		31 900		30 100

<sup>a</sup> Only allowed transitions with orbital energy differences of less than  $45000 \text{ cm}^{-1}$  were included in the table

Table 5 indicates that the  $e_g(d_{xz}) \rightarrow b_{1u}(\pi^*)$  transition could possibly also be observed in Ni and Co porphyrins, although with a decreased intensity. The experimental vapor spectra of Co and Ni octaethyl [63] and tetraphenyl [64] porphins do not preclude this possibility. In the  $30000$  to  $40000 \text{ cm}^{-1}$  region of the Co and Ni TPP's there seems to be an underlying band which is not present in Cu, Zn, and MgTPP.

The energy of NiPc and NiTAP were calculated for a wide range of skeletal geometries and Ni-N<sub>10</sub> bond distances [45]. The results demonstrate that TAP is a good model for Pc since geometry changes have similar effects on the  $d$  orbitals. The  $b_{1g}(d_{xz-yz})$  orbital energy is very geometry dependent. A point of interest is that for equal Ni-N bond distances, NiTBP and NiP have a higher calculated  $b_{1g}(d_{xz-yz})$  energy than NiPc and NiTAP. Therefore, the increased ligand field splitting of phthalocyanines relative to porphyrins is not due to substitution of C-H by nitrogens at the bridge positions, but to a decrease in the metal-nitrogen bond distance.

The energy of the  $Np_\sigma$  and  $\pi$  orbitals is essentially unaffected by changes in the Ni-N distance but is dependent on skeletal geometry. For example,  $e_g(\pi^*)$  decreases by  $\sim 0.2 \text{ eV}$  when the TBP geometry is used for NiPc.

As expected, the amount of metal orbital delocalization increases as the Ni-N distance decreases. The composition of  $b_{2g}(d_{xy})$  and  $b_{2g}^*(d_{xy})$  is especially susceptible to geometry changes. The composition of these orbitals would be very sensitive to ring substituents rather than to axial ligands.

Our calculations clearly indicate NiPc and NiTAP to be diamagnetic with  $b_{2g}(d_{xy}) < e_g(d_{xz}) < a_{1g}(d_{z^2}) < b_{2g}^*(d_{xy}) \ll b_{1g}(d_{xz-yz})$  (see Fig. 4). The calculated energy gap between  $a_{1g}(d_{z^2})$  and  $b_{1g}(d_{xz-yz})$  is strongly dependent on the Ni-N distance; e.g., it decreases from  $3.84$  to  $2.52 \text{ eV}$  as the Ni-N distance increases from  $1.83$  to  $1.96 \text{ \AA}$ .

One would like to use this result to explain why NiPc shows no tendency to form paramagnetic six coordinate derivatives [13] while nickel porphyrins do form high spin complexes with nitrogen bases [65]. To test this point a calculation was made on a NiTAP dipyrindine octahedral complex. The two pyridines raise the energy of  $d_{z^2}$  by  $2.75 \text{ eV}$  and  $d_{xz-yz}$  by  $\sim 0.13 \text{ eV}$ . This result does suggest that NiTAP (and NiPc) would be paramagnetic in the presence of fifth and sixth ligands. That such octahedral coordination is not formed may be due to the small size of the Pc and TAP rings. It is well known that high spin Ni(II)



complexes normally have Ni-N bond distances greater than 2.0 Å. In order to accommodate a high spin Ni(II), the porphyrin ligand can expand its hole size, while for phthalocyanine, such an expansion is impossible. The geometric explanation for lack of formation of pyridine complexes is further supported by the higher positive charge in NiPc compared to NiP - which would tend to favor complex formation.

#### D. Co

Fig. 4 shows the MO energy levels of Co in comparison with Ni. The major differences from Ni are the shift of the *d* levels to somewhat higher energy - particularly  $b_{1g}(d_{x^2-y^2})$  - and the unpaired electron in orbital  $a_{1g}(d_{z^2})$ . However, our results for CoPc (Co-N distance = 1.90 Å) clearly indicate that the odd electron should go in the  $b_{2g}(d_{xy})$  orbital. Unfortunately, this does not agree with the conclusion drawn from studies on the magnetic properties [59,66] and ESR [67,68] of CoPc. All studies seem to agree that the odd electron is in  $d_{z^2}$ , in accord with the observation that the ESR of CoPc is solvent dependent while CuPc is not [59,67]. The abnormal temperature dependence of the magnetic susceptibility of CoPc [59] suggests that  ${}^2E_g$  and  ${}^2B_{2g}$  mix in with the  ${}^2A_{1g}$  ground state.

The calculated  $b_{2g}(d_{xy}) - a_{1g}(d_{z^2})$  energy gap is not very sensitive to changes in the Co-N distance. Increasing this distance from 1.87 to 1.96 Å does not change the energy separation by more than 0.04 eV. In the crystal, however, one has *N* atoms of parallel molecules lying above and below the molecular plane ~3.4 Å from the metal atom [34]. This will tend to raise the energy of  $d_{z^2}$  relative to  $d_{xy}$ , thus approaching the experimental result. The energy of the  $d_{z^2}$  orbital is very sensitive to the presence of ligands; e.g., placing one pyridine 2.0 Å above the plane of CoTAP raises the  $d_{z^2}$  energy by ~1.5 eV. However, the odd electron in  $d_{z^2}$  actually prevents the close association of any ligands [13].

As for allowed bands in the near UV, CoPc has the same possibilities as NiPc, as shown in Table 5. One extra band is observed [12]. Since the CoPc transitions are generally calculated to be red shifted with respect to NiPc, it may be that some are buried under the Soret band. The hole in  $a_{1g}(d_{z^2})$  allows for low energy *z* polarized transitions  $a_{2u}(\pi) \rightarrow a_{1g}(d_{z^2})$ . This may be observable in solid near *ir* absorption. Also low energy *dd* transitions are possible and would provide pathways for radiationless decay.

#### E. Fe

The MO diagram for FePc and FeTAP is given in Fig. 5. For FeTAP Fig. 5 also shows a calculation with a shortened Fe-N<sub>10</sub> distance, the only effect being to raise  $b_{1g}(d_{x^2-y^2})$ . Consistent with the high energy of this orbital, all investigators save one [69] conclude the spin is *S* = 1. This can be compared to Fe(II) TPP with no ligands, which is clearly high spin [70]. High spin requires a substantial lowering of  $b_{1g}(d_{x^2-y^2})$  in porphyrin. We believe the principal cause of this difference is the larger size of the Fe-N<sub>10</sub> distance. In Fe(II) porphyrin the energy of  $b_{1g}(d_{x^2-y^2})$  is ~ -8.4 eV for a planar Fe N distance of 2.05 Å while in Pc and TAP the energy of this orbital goes from -8.0 to -7.7 eV as the Fe-N distance decreases from 1.99 to 1.95 Å (Fig. 5).

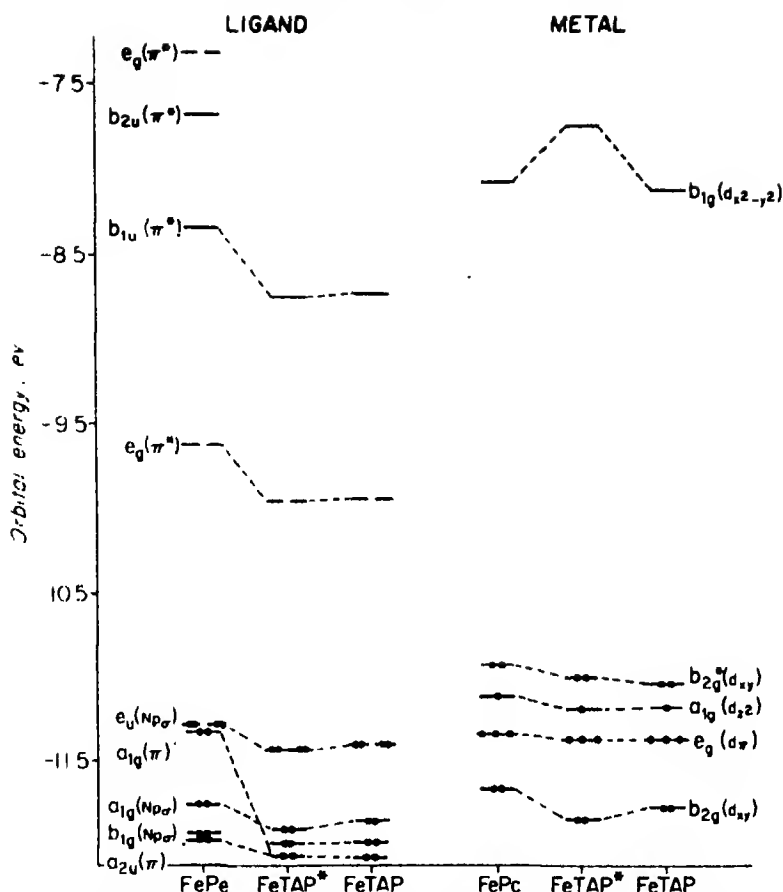


Fig. 5 Top filled and lowest empty ligand and metal MO's of FePc and FeTAP. For FeTAP\* the Fe-N<sub>10</sub> distance was decreased to 1.95 Å. No fifth or sixth ligand on metal

There is some disagreement over the FePc ground state configuration. Dale *et al.* [71] claim a  ${}^3E_g$  ground state while Barraclough *et al.* [72] interpret the magnetic susceptibility and anisotropy data as implying a  ${}^3B_{2g}$  ground state. We predict one odd electron in  $a_{1g}(d_{z^2})$  and one in  $b_{2g}^*(d_{xy})$ , although in Fig. 5 we show one odd electron in  $e_g(d_x)$  and one in  $a_g(d_{z^2})$ .

From results of Paper VIII [3] it is clear that raising Fe(II) out of the plane by  $\sim 0.49$  Å will make Fe(II) porphyrin high spin. Since the radius of the phthalocyanine ring is at least  $0.05$  Å smaller than the corresponding porphyrin, in order to make FePc high spin, the Fe will have to be brought out considerably farther than  $0.49$  Å. This will weaken the Fe-N bonds considerably, thus making high spin FePc energetically unfavorable. We did calculations on FeTAP-dipyridine which clearly indicate this molecule to be diamagnetic in agreement with experimental measurements [59, 72].

The opening of a hole in  $e_g(d_x)$  in Fe (and similarly for Mn) opens the possibility for low energy charge transfer transitions  $a_{1g}(\pi)$  or  $a_{2g}(\pi) \rightarrow e_g(d_x)$ . These

are (x, y) polarized and may possibly be easily observed in the near IR. Finally we note that with a pyridine ligand we find a possible  $b_{2g}(d_x) \rightarrow b_{3u}(2p_x^*)$  [ $D_{2h}$  notation] charge transfer transition. The  $b_{2g}(d_x)$  is  $\sim 80\%$  localized on the metal while  $b_{3u}(2p_x^*)$  is  $\sim 98\%$  localized on pyridine. The orbital energy difference is about  $22500\text{ cm}^{-1}$  which agrees amazingly well with the charge transfer transition found by Dale [73] in FePc (pyridine)<sub>2</sub> at  $24100\text{ cm}^{-1}$ . Kobayashi and Yanagawa [70] assigned the band at  $21000\text{ cm}^{-1}$  in Fe(II)TPP (pyridine)<sub>2</sub> to charge transfer from iron to pyridine. As a result of our calculation this assignment seems entirely reasonable.

### F. Mn

MnPc again demonstrates the difference between porphyrins and phthalocyanines. MnPc forms an intermediate-spin,  $S=3/2$ , four coordinate complex [59, 72], while Mn porphyrins form a high-spin complex that is most likely five-coordinate and non-planar [74]. Our calculated results for MnPc (Fig. 6) are

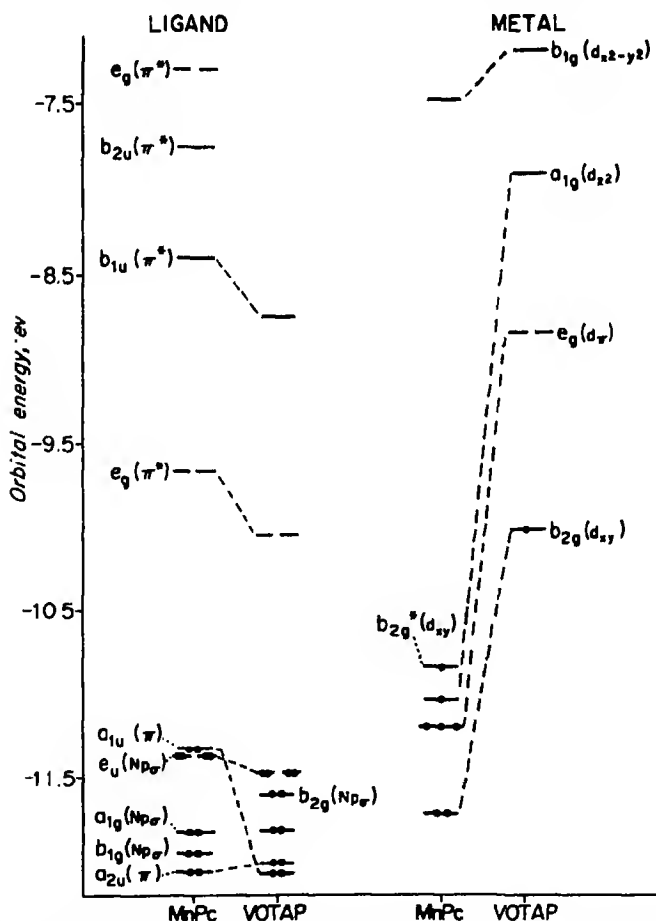


Fig. 6. Top filled and lowest empty ligand and metal MO's of MnPc and VOTAP

again unambiguous. An  $e_g(d_{xz})^3 a_{1g}(d_{zz}) b_{2g}^*(d_{xy})$  ground state is indicated. The magnetic moment of MnPc being larger than the spin only value implies that there is a mixing of the ground and excited spin states [72]. Barraclough *et al.* [72] prefer a  $d_{xy}^2 d_{xz}^2 d_{zz}^1$  ground state with mixing coming from the  $d_{xz}^3 d_{xy} d_{zz}^1$  state.

### G. VO

The MO diagram for VOTAP is given in Fig. 6. We find the odd electron in  $d_{xy}$ . Because of its relatively high energy, this orbital does not interact with the ring  $b_{2g}(Np_x)$  to give  $b_{2g}^*(d_{xy})$  and  $b_{2g}(d_{xz})$ , and we calculate it to be 87%  $d_{xy}$  in characters. (See Table 4.) There is some disagreement among the experimentalists as to how pure it is. Assour, Goldmacher, and Harrison [75] concluded it was relatively pure  $d_{xy}$  on the basis of lack of nitrogen hyperfine splitting. A similar conclusion had been reached by Kivelson and Lee [76] for VO tetraphenylporphyrin. More recently Sato and Kwan [77] report nitrogen superhyperfine structure in VOpc and Guzy *et al.* [78] deduce only 73% occupancy.

Zerner and Gouterman [2] identified the 42000 to 50000  $\text{cm}^{-1}$  bands observed in vanadyl compounds with a charge transfer transition from oxygen to the unfilled metal orbitals ( $d_x$  or  $d_{z^2}$ ). In VOTAP we also have the possibility of such transitions. We thus identify the extra band observed by Edwards in VOpc at 48100  $\text{cm}^{-1}$  with these charge transitions.

### H. Electronic Populations

Tables 6 and 7 present the results of a Mulliken population analysis for various metal complexes of Pc and TAP. It would be useful to compare these results with those obtained by Zerner and Gouterman for porphyrins [1-5]. Except for Mn, all metals have a greater net positive charge in phthalocyanines. This result is also found if equal bond lengths are used for the phthalocyanine and porphyrin calculations. Except for the reversal of Ni and Cu our metal net charges,  $\text{Mg} > \text{Zn} > \text{Co} > \text{Cu} > \text{Ni} > \text{Fe} > \text{Mn}$ , follow those in porphyrin.

Charge densities can be somewhat related to stability. The stability of porphyrin derived from consideration of displacement reactions, dissociation reactions, and electronic spectral data is  $\text{Ni} > \text{Co} > \text{Cu} > \text{Zn} > \text{Mg}$  [79]. Thus, the order of increased stability corresponds to a decrease in the ionic character of the metal-nitrogen bond [1]. However, metal phthalocyanines are considerably more stable than the corresponding porphyrin, yet the ionic character of the metal-nitrogen bond is greater in phthalocyanines. Thus predictions about stability involve geometric as well as electronic consideration.

Table 6 shows a slightly greater negative charge on the bridged compared to the central nitrogens. However, their difference is rather small. This contrasts to the far larger difference in charge we have calculated for the three types of nitrogen atoms in  $\text{H}_2\text{Pc}$  with a bonded structure [7]. Zeller and Hayes [80] have recently reported on the X-ray photoelectron spectra of the N 1s electron in  $\text{H}_2\text{Pc}$  and CuPc. The broad line observed for  $\text{H}_2\text{Pc}$  and sharp line observed for CuPc agree qualitatively with our calculated charge densities.

Finally we should note that the charge density on any atom does not change more than 0.01 as the geometry is varied.

Table 6. Electronic population of phthalocyanines\*

A. Total ligand population								
Atom	Mg	Zn	Cu	Ni	Co	Fe	Mn	SCF <sup>a</sup>
N <sub>10</sub>	5.169	5.149	5.151	5.141	5.148	5.120	5.126	1.605
C <sub>11</sub>	3.932	3.924	3.918	3.926	3.927	3.924	3.918	0.834
C <sub>12</sub>	4.006	4.001	3.999	3.996	3.997	3.995	3.993	1.016
C <sub>13</sub>	4.029	4.035	4.032	4.031	4.031	4.031	4.026	0.981
C <sub>14</sub>	4.042	4.042	4.041	4.039	4.041	4.039	4.039	0.998
N <sub>2</sub>	5.196	5.188	5.196	5.184	5.179	5.198	5.178	1.238
H <sub>15</sub> <sup>d</sup>	0.941	0.940	0.938	0.939	0.940	0.939	0.939	
H <sub>14</sub> <sup>d</sup>	0.946	0.946	0.941	0.945	0.945	0.945	0.944	
PC <sup>b</sup>	-0.630	0.452	-0.334	-0.315	-0.359	-0.249	-0.101	
B. Metal population								
	3d	4s	4p	Total	Net	Porphin <sup>c</sup>		
Mg <sup>d</sup>		0.517	0.853	1.370	+0.630	+0.572		
Zn	9.986	0.648	0.914	11.548	+0.452	+0.401		
Cu	9.669	0.466	0.531	10.666	+0.334	+0.281		
Ni	8.739	0.439	0.507	9.685	+0.315	+0.301		
Co	7.718	0.381	0.542	8.641	+0.359	+0.342		
Fe	7.136	0.301	0.314	7.751	+0.249	+0.226		
Mn	6.357	0.352	0.190	6.899	+0.101	+0.111		

<sup>a</sup> SC MO-PPP  $\pi$  electron results, Refs. [19, 20].<sup>b</sup> Net charge on ligand given.<sup>c</sup> See Refs. [1-5].<sup>d</sup> Population of 3s and 3p given.

Table 7. Electronic population of tetrazaporphins\*

A. Total ligand population								
Atom	Mg	Zn	Cu	Ni	Co	Fe	VO	SCF
N <sub>10</sub>	5.173	5.164	5.164	5.147	5.152	5.135	5.133	1.603
C <sub>11</sub>	3.929	3.914	3.906	3.925	3.927	3.921	3.916	0.844
C <sub>12</sub>	4.041	4.035	4.037	4.027	4.029	4.026	4.025	1.003
N <sub>2</sub>	5.180	5.179	5.178	5.171	5.168	5.174	5.169	1.200
H <sub>15</sub> <sup>d</sup>	0.936	0.936	0.927	0.929	0.930	0.930	0.930	
1AP	-0.657	-0.454	-0.332	-0.315	0.366	0.259	-0.489	
B. Metal population								
	3d	4s	4p	Total	Net			
Mg		0.511	0.832	1.343	+0.657			
Zn	9.987	0.911	0.648	11.546	+0.454			
Cu	9.664	0.469	0.535	10.668	+0.332			
Ni	8.725	0.443	0.517	9.685	+0.315			
Co	7.691	0.386	0.557	8.634	+0.366			
Fe	7.113	0.303	0.324	7.741	+0.259			
VO	3.720	0.288	0.503	4.511	+0.484			

<sup>a</sup> For additional detail see footnotes to Table 6.

### Summary

These calculations were undertaken with the hope of elucidating some of the differences between porphyrins and phthalocyanines. We discussed the following points:

(1) A detailed literature investigation into phthalocyanine crystal structure indicates that the radius of the metal phthalocyanine ring is on the average 0.065 Å smaller than the corresponding porphyrin.

(2) The extra UV bands in NiPc and CoPc are suggested to be due to  $d_{\pi} \rightarrow \pi^*$  transitions. One of these transitions is also expected to be observed in Ni and Co porphyrin.

(3) Phthalocyanines and tetrazaporphin are found to have low lying  $n \rightarrow \pi^*$  transitions which are probably responsible for the diffuseness of the Soret band.

(4) The  $b_{2g}(Np_{\pi})$  orbital of the phthalocyanine and tetrazaporphin ligand mixes with  $b_{2g}(d_{xy})$  of Ni, Co, Fe, and Mn to form a lower energy  $b_{2g}(d_{xy})$  and a higher energy  $b_{2g}^*(d_{xy})$ .

(5) The ordering of the  $d$  orbitals derived from these calculations differ somewhat from those obtained from ESR and magnetic measurements. The  $b_{2g}(d_{xy})$  orbital is usually higher than  $a_g(d_{z^2})$ .

(6) The larger ligand field splitting of phthalocyanines compared to porphyrins is mainly due to the smaller ring size. The inability of the Pc ring to expand as much as porphyrin is used to explain why FePc is of intermediate spin and a high spin NiPc (pyridine)<sub>2</sub> complex does not form.

(7) FePc (pyridine)<sub>2</sub> is clearly diamagnetic with a  $d_{\pi} \rightarrow$  pyridine charge transfer transition around 24000 cm<sup>-1</sup>.

(8) The skeletal geometry is more important in determining the energy of  $Np_{\pi}$  and  $\pi$  orbitals while the Ni-N bond distance is crucial in determining the ligand field splitting.

*Acknowledgements* This research was supported in part by Public Health Services Grant GM 14292 from the Division of General Medical Sciences

### References

1. Paper IV: Zerner, M., Gouterman, M.: *Theoret. chim. Acta (Berl.)* **4**, 44 (1966).
2. Paper V and VI: Zerner, M., Gouterman, M.: *Inorg. Chemistry* **5**, 1699, 1707 (1966).
3. Paper VIII: Zerner, M., Gouterman, M., Kobayashi, H.: *Theoret. chim. Acta (Berl.)* **6**, 363 (1966).
4. Zerner, M.: Ph. D. Thesis, Dept. of Chemistry, Harvard University (1966).
5. Paper X: Zerner, M., Gouterman, M.: *Theoret. chim. Acta (Berl.)* **8**, 26 (1967).
6. Paper XXI: Schaffer, A. M., Gouterman, M.: *Theoret. chim. Acta (Berl.)* **18**, 1 (1970).
7. Paper XXV: Schaffer, A. M., Gouterman, M.: *Theoret. chim. Acta (Berl.)* **25**, 62 (1972).
8. Linstead, R. P.: *Brit. Assoc. Advancement Sci., Rep. annu. Meeting* 465 (1933).
9. Dent, C. E., Linstead, R. P., Lowe, A. R.: *J. chem. Soc. (London)*, (1934), 1027, 1033.
10. Moser, F. H., Thomas, A. I.: *Phthalocyanine compounds*. New York: Reinhold Publishing Corporation 1963.
11. Paper VII: Eastwood, D., Edwards, L., Gouterman, M., Steinfeld, J.: *J. molecular Spectroscopy* **20**, 381 (1966).
12. Paper XV: Edwards, L., Gouterman, M.: *J. molecular Spectroscopy* **33**, 292 (1970).
13. Lever, A. P.: *Advances inorg. Chem. Radiochem.* **7**, 27 (1965), and references therein.
14. Stern, A., Pruckner, F.: *Z. physik. Chem.* **178A**, 420 (1937).
15. Linstead, R. P., Whalley, M.: *J. chem. Soc. [London]*, 4839 (1952).

- 6 Kuhn, H.: *J. chem. Physics* **17**, 1198 (1949); *Fortschr. Chem. org. Naturstoffe* [Wien], **17**, 404 (1959); *Angew. Chem.* **71**, 93 (1959); *Chimia* [Aarau, Schweiz], **15**, 53 (1961).
- 7 Basu, S.: *Indian J. Physics Proc. Indian Assoc. Cultivat. Sci.* **28**, 511 (1954).
- 8 Forsterling, H. D., Kuhn, H.: *Int. J. quant. Chemistry* **2**, 413 (1968).
- 9 Paper III: Weiss, C., Kobayashi, H., Gouterman, M.: *J. molecular Spectroscopy* **16**, 415 (1965).
- 10 Paper XXIV: McHugh, A., Gouterman, M., Weiss, C.: *Theoret. chim. Acta* (Berl.) **24**, 346 (1972).
- 11 Linder, R. E., Rowlands, J. R.: *Molecular Physics* **21**, 417 (1971).
- 12 Taube, R.: *Z. Chem.* **6**, 8 (1966).
- 13 Ponomarev, D. A., Kubarev, S. I.: *Theoret. Exp. Chem.* **4**, 318 (1968).
- 14 Chen, I., Abkowitz, M., Sharp, J. H.: *J. chem. Physics* **50**, 2237 (1969).
- 15 Kramer, I. N., Klein, M. P.: *Chem. Physics Letters* **8**, 183 (1971).
- 16 Mathur, S. C., Singh, J.: *Int. J. quant. Chemistry* **6**, 57 (1972).
- 17 Henriksson, A., Roos, B., Sundbom, M.: *Theoret. chim. Acta* (Berl.) **27**, 303 (1972).
- 18 Wilkinson, J. H.: *The algebraic eigenvalue problem*. Oxford: Oxford University Press 1965.
- 19 Davidson, E. R.: unpublished.
- 20 Fleischer, E. B.: *Chem. Comm.* **105** (1970).
- 21 Hoard, J. L.: *Sciences* **174**, 1295 (1971).
- 22 Robertson, J. M.: *J. chem. Soc. [London]* **615** (1935); **1195** (1936).
- 23 Linstead, R. P., Robertson, J. M.: *J. chem. Soc. [London]* 1736 (1936).
- 24 Robertson, J. M., Woodward, L.: *J. chem. Soc. [London]* 219 (1937); 36 (1940).
- 25 Brown, C. J.: *J. chem. Soc. (A) [London]* 2494 (1968).
- 26 Hoskins, B. F., Mason, S. A., White, J. C. B.: *Chem. Comm.*, 554 (1969).
- 27 Fischer, M., Templeton, D. H., Zalkin, A., Calvin, M.: *J. Amer. chem. Soc.* **93**, 2622 (1971).
- 28 Brown, C. J.: *J. chem. Soc. (A) [London]*, 2488 (1968).
- 29 Vogt, L. H. Jr., Zalkin, A., Templeton, D. H.: *Inorg. Chemistry* **6**, 1725 (1967).
- 30 Friedel, M. K., Hoskins, B. F., Martin, R. L., Mason, S. A.: *Chem. Comm.*, 400 (1970).
- 31 Rogers, D., Osborn, R. S.: *Chem. Comm.*, 840 (1971).
- 32 Kobayashi, T., Kurokawa, F., Ashida, T., Uyeda, N., Suito, E.: *Chem. Comm.*, 1631 (1971).
- 33 Kobayashi, T., Ashida, T., Natsu, N., Suito, E., Kakudo, M.: *Bull. chem. Soc. Japan* **44**, 2095 (1971).
- 34 D'Addario, A. D.: *Diss. Abst. Int.* **B32**, 1423 (1971).
- 35 Schaffer, A. M.: Ph. D. Thesis. Chemistry Department, University of Washington, Seattle (1972).
- 36 Fielding, P. E., MacKay, A. G.: *J. chem. Physics* **38**, 2777 (1963).
- 37 Fielding, P. E., MacKay, A. G.: *Austral. J. Chem.* **17**, 750 (1964).
- 38 Schechtman, B. H., Spicer, W. E.: *J. molecular Spectroscopy* **33**, 28 (1970).
- 39 Day, P., Williams, R. J. P.: *J. chem. Physics* **42**, 4049 (1965).
- 40 Day, P., Price, M. G.: *J. chem. Soc. (A) [London]*, 236 (1969).
- 41 Edwards, L.: Ph. D. Thesis, Committee on Chemical Physics, Harvard University (1969).
- 42 Baguley, M. E., France, H., Linstead, R. P., Whalley, M.: *J. chem. Soc. [London]*, 3521 (1955).
- 43 Vincett, P. S., Voigt, E. M., Rieckhoff, K. E.: *J. chem. Physics* **55**, 4131 (1971).
- 44 Henriksson, A., Sundbom, M.: *Theoret. chim. Acta* (Berl.) **27**, 213 (1972).
- 45 Hockstrasser, R. M., Marzzacco, C.: *J. chem. Physics* **49**, 971 (1968).
- 46 Sevchenko, A. N., Shkirman, S. F., Mashenkov, V. A., Solov'ev, K. N.: *Soviet Phys. Dokl.* **12**, 710 (1968).
- 47 Harrison, S. E., Assour, J. M.: *J. chem. Physics* **40**, 365 (1964).
- 48 Guzy, C. M., Raynor, J. B., Symons, M. C. K.: *J. chem. Soc. (A) [London]*, 2299 (1969).
- 49 Lever, A. B. P.: *J. chem. Soc. [London]*, 1821 (1965).
- 50 Martin, R. L., Mitra, S.: *Inorg. Chemistry* **9**, 182 (1970).
- 51 Paper XVIII: Eastwood, D., Gouterman, M.: *J. molecular Spectroscopy* **35**, 359 (1970).
- 52 Paper XXI: Callis, J. B., Gouterman, M., Jones, Y. M., Henderson, B. H.: *J. molecular Spectroscopy* **39**, 410 (1971).
- 53 Paper XVI: Edwards, L., Gouterman, M., Dolphin, D. H.: *J. molecular Spectroscopy* **35**, 90 (1970).
- 54 Paper XVII: Edwards, L., Dolphin, D. H., Gouterman, M., Adler, A. D.: *J. molecular Spectroscopy* **38**, 16 (1971).
- 55 McLees, B. D., Coughy, W. S.: *Biochemistry* **7**, 642 (1968).
- 56 Martin, R. L., Mitra, S.: *Chem. Physics Letters* **3**, 183 (1969).
- 57 Assour, J. M., Kahn, W. K.: *J. Amer. chem. Soc.* **87**, 207 (1965).

- 68 Rollman, L.D., Chan, S.L.: *Inorg. Chemistry* **10**, 1972 (1971).
- 69 Dizsi, I., Balázs, A., Molnár, B., Gorobshenko, V.D., Lukashevich, I.I.: *J. inorg. nuclear Chem* **31**, 1661 (1969)
- 70 Kobayashi, T., Yanagawa, Y.: *Bull. chem. Soc. Japan* **45**, 450 (1972).
- 71 Dale, B.W., Williams, R.J.P., Johnson, C.E., Thorp, T.L.: *J. chem. Physics* **49**, 3441 (1965).
- 72 Barraclough, C.G., Martin, R.L., Mitra, S., Sherwood, R.C.: *J. chem. Physics* **53**, 1638, 1643 (1970).
- 73 Dale, B.W.: *Trans. Faraday Soc.* **65**, 331 (1969).
- 74 Boucher, L.: *Coord. Chem. Rev.* **7**, 289 (1972)
- 75 Assour, I.M., Goldmacher, J., Harrison, S.L.: *J. chem. Physics* **43**, 159 (1965).
- 76 Kivelson, D., Lee, S.-K.: *J. chem. Physics* **41**, 1896 (1964).
- 77 Sato, M., Kwan, T.: *J. chem. Physics* **50**, 558 (1969).
- 78 Guzy, C.M., Raynor, J.B., Stodulski, L.P., Symons, M.C.R.: *J. chem. Soc. (A) [London]*, 997 (1969)
- 79 Boucher, L.J., Katz, J.J.: *J. Amer. chem. Soc.* **89**, 1340 (1967).
- 80 Zeller, M.V., Hayes, R.G.: submitted for publication

Dr. Arnold M. Schaffer  
Department of Chemistry  
University of Houston  
Houston, Texas 77004, USA



## Molecular Orbital Calculations on the Conformation of Nucleic Acids and Their Constituents

### VII. Conformation of the Sugar Ring in $\beta$ -Nucleosides: The Pseudorotational Representation\*

Anil Saran, David Perahia, and Bernard Pullman

Institut de Biologie Physico-Chimique, Laboratoire de Biochimie Théorique associé au C.N.R.S.,  
13, rue P. et M. Curie, Paris 5<sup>e</sup>

Received January 22, 1973

The conformational properties of the furanose ring of purine- and pyrimidine- $\beta$ -nucleosides and -nucleotides are studied quantum-mechanically with the help of the PCILO method, using the pseudorotational concept. The computations point to the existence of two stable conformational zones centered around the C(3')-endo and C(2')-endo conformations which in the isolated furanose ring are separated by barriers of the order of 4 kcal/mole. In nucleosides one of the barriers (the one running through the O(1')-exo-C(2')-exo path) becomes very high. A detailed study is made of the relation between the phase angle of pseudorotation,  $P$ , and the torsion angle about the glycosyl bond,  $\chi_{CN}$ . A very satisfactory agreement with the available experimental data is observed.

Die Konformationseigenschaften des Furanoserings in  $\beta$ -Nucleosiden und Nucleotiden von Purin und Pyrimidin werden nach der PCILO-Methode unter Berücksichtigung der pseudorotationen Betrachtungsweise studiert. Die Rechnung läßt auf die Existenz zweier stabiler Konformationszonen schließen, die in der Umgebung der C(2')-endo und der C(3')-endo Konformationen liegen, und die im isolierten Furanosering durch Energiebarrieren der Größenordnung von 4 kcal/mol voneinander getrennt sind. In Nucleosiden wird eine der Barrieren (die durch den Weg O(1')-exo-C(2')-exo gekennzeichnete) sehr hoch. Die Relation zwischen dem Phasenwinkel der Pseudorotation,  $P$ , und dem Drehwinkel um die Glycosylbindung,  $\chi_{CN}$ , wird einer eingehenden Untersuchung unterworfen. Man beobachtet eine sehr zufriedenstellende Übereinstimmung mit den verfügbaren experimentellen Daten.

Les propriétés conformationnelles du noyau furanose des  $\beta$ -nucleosides et nucleotides des purines et pyrimidines sont étudiées par la méthode PCILO en faisant appel au concept de la pseudorotation. Les calculs indiquent l'existence de deux zones de conformations stables, centrées autour des conformations C(2')-endo et C(3')-endo, qui sont dans le sucre isolé séparées par des barrières de l'ordre de 4 kcal/mole. Dans les nucleosides, l'une de ces barrières (celle qui passe par le chemin O(1')-exo-C(2')-exo) devient très élevée. Une étude détaillée est effectuée sur la relation entre l'angle de phase de la pseudorotation  $P$  et l'angle de torsion autour de la liaison glycosylique,  $\chi_{CN}$ . Un excellent accord avec les données expérimentales disponibles est observé.

### Introduction

In continuation of our studies by the quantum mechanical PCILO (Perturbative Configuration Interaction using Localized Orbitals) method on the conformation of nucleic acids and their constituents [1–6], we present in this paper the results of computations carried out on the conformation of the sugar

\* This research was supported by the R.C.P. 173 and the A.T.P. A 655-2303 of the C.N.R.S.

ring in  $\beta$ -nucleosides. In the previous publications of this series fixed conformations have been adopted for the furanose rings, corresponding generally to the most frequently encountered ones in the X-ray studies of nucleosides, nucleotides and polynucleotides, namely C(2')-*endo* and C(3')-*endo* [7, 8].

The present study has been carried out using the concept of pseudorotation which seems the most suitable one for a complete exploration of the conformational characteristics of the five membered sugar ring. It was first introduced in 1947 by Kilpatrick, Pitzer, and Spitzer [9] in the description of the conformation of cyclopentane. Their results showed an „indefiniteness” of the cyclopentane conformation, the angle of maximum puckering rotating around the ring without any substantial change in the potential energy. Later, in 1959, Pitzer and Donath [10] refining the earlier calculations, showed that the presence of substituents in cyclopentane induces potential energy barriers which restrict the free pseudorotation. Altona and co-workers [11–16] have explored the consequences of this limited pseudorotation for the conformation of ring D in steroids and of several other five-membered ring systems. Recently, Altona and Sundaralingam [17] have shown the usefulness of the pseudorotational concept in a slightly modified form for the description of the conformation of the sugar rings in  $\beta$ -nucleosides and  $\beta$ -nucleotides. In their study, each conformation of the furanose ring is unequivocally determined in terms of two parameters: the phase angle of pseudorotation,  $P$  and the degree of pucker,  $\tau_M$ . The authors have evaluated these two parameters for a large number of  $\beta$ -nucleosides and nucleotides for which X-ray crystal data were available. Another useful utilization of the concept of pseudorotation in connection with NMR studies of the conformation of ribosides and arabinosides in solution is due to Hruska, Wood, and Dalton [18] and Hall, Steiner, and Pedersen [19].

From the theoretical point of view a few studies on the conformation of the sugar rings in  $\beta$ -nucleosides have also appeared recently [20–23], employing both classical and quantum mechanical approaches. Sasisekharan [20], working within the scheme of the empirical partitioned potential energy functions [24, 25], used four parameters to describe the pseudorotation in ribose and deoxyribose and then applied the pseudorotational concept to  $\beta$ -pyrimidine and  $\beta$ -purine nucleosides. Similarly, Lugovskoi and Dashevskii [21], also utilizing classical partitioned potential energy functions, have chosen two parameters to describe the pseudorotation in  $\beta$ -D-ribose and in a somewhat restricted fashion have extended their work to  $\beta$ -pyrimidine nucleosides [22], and very recently to  $\beta$ -purine nucleosides [22a].

In the field of the quantum mechanical methods, Govil and Saran [23] have utilized the EHT and CNDO procedures to describe, with the help of two parameters, the conformations of  $\beta$ -D-ribose. These authors did not call, however, upon the pseudorotational concept but used the more common representations of the conformations.

Finally in connection with the forthcoming discussion, we must indicate that a number of related theoretical studies, both by the classical [24–28] and quantum-mechanical methods [1, 2, 5, 29, 30] are available dealing with the relation between the furanose ring conformations and the glycosyl torsion angle  $\chi_{CN}$ . In all these studies, however, fixed sugar ring conformations, whether

C(3')-endo, C(2')-endo, C(3')-exo or C(2')-exo have been selected and  $\chi_{CN}$  was varied to establish the dependence between the sugar pucker and  $\chi_{CN}$ .

## The Procedure

### A) The Method

The method employed for the calculation of the conformational energies is the PCILO method, as used in the previous papers of this series, the details of which may be found in original papers [31–33]. The computational program may be obtained from Q.C.P.E. (Quantum Chemistry Program Exchange) at the Chemistry Department of Indiana University, Bloomington, Ind., USA.

### B) Definitions and Conventions

A schematic diagram of  $\beta$ -D-ribose is shown in Fig. 1. The conventions and notations of the torsion angles are essentially those of Sundaralingam [7]. The different torsion angles are defined as:

$$\tau_0 = C4' - O1' - C1' - C2'$$

$$\tau_1 = O1' - C1' - C2' - C3'$$

$$\tau_2 = C1' - C2' - C3' - C4'$$

$$\tau_3 = C2' - C3' - C4' - O1'$$

$$\tau_4 = C3' - C4' - O1' - C1'$$

$$\chi_{CN} = O1' - C1' - N1 - C2 \quad (\text{for pyrimidine nucleosides})$$

$$\chi_{CN} = O1' - C1' - N9 - C8 \quad (\text{for purine nucleosides})$$

$$\phi_{C(2')-O(2')} = C1' - C2' - O2' - H(O2')$$

$$\phi_{C(3')-O(3')} = C2' - C3' - O3' - H(O3')$$

$$\phi_{C(4')-O(5')} = C3' - C4' - C5' - O5'$$

$$\phi_{C(5')-O(5')} = C4' - C5' - O5' - H(O5').$$

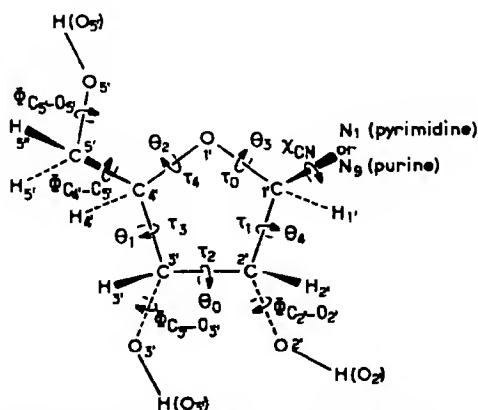


Fig. 1. Numbering of atoms and designation of torsion angles in the furanose ring

We remind that the torsion angle  $\phi_{B-C}$  of the bonded atoms A-B-C-D is the angle between the planes formed by atoms A, B, C and B, C, D.  $\phi_{B-C}$  is considered positive for a right-handed rotation: when looking along the bond B-C, the far bond C-D rotates in the clockwise direction with the respect to the near bond A-B. The zero value of the torsion angle corresponds to the *cis-planar* arrangement of the bonds A-B and C-D.

### C) Pseudorotational Parameters, $P$ and $\tau_M$

In this paper we have adopted the description of pseudorotation of Altona and Sundaralingam [17] so as to have an easy comparison with the experimental data which they have collected. Following these authors, the five torsional angles ( $\theta_0, \theta_1, \theta_2, \theta_3, \theta_4$ ) of cyclopentane along the pseudorotational pathway are described by

$$\theta_j = \theta_m \cos(P + j\delta) \quad (1)$$

where  $j = 0, 1, 2, 3, 4$  and  $\delta = 144^\circ$ .

For  $j = 0$ , Eq. (1) becomes:

$$\theta_0 = \theta_m \cos P. \quad (2)$$

It is evident from Eq. (2), that  $\theta_0$  passes through the values of  $\theta_m, 0, -\theta_m, 0$  and  $\theta_m$ , when  $P$  goes through a full pseudorotational cycle ( $0 - 360^\circ$ ), and so a pseudorotation over  $P = 180^\circ$  produces the mirror image of the original ring. From Eq. (1), one gets:

$$\tan P = \frac{(\theta_2 + \theta_4) - (\theta_1 + \theta_3)}{2\theta_0(\sin 36^\circ + \sin 72^\circ)} \quad (3)$$

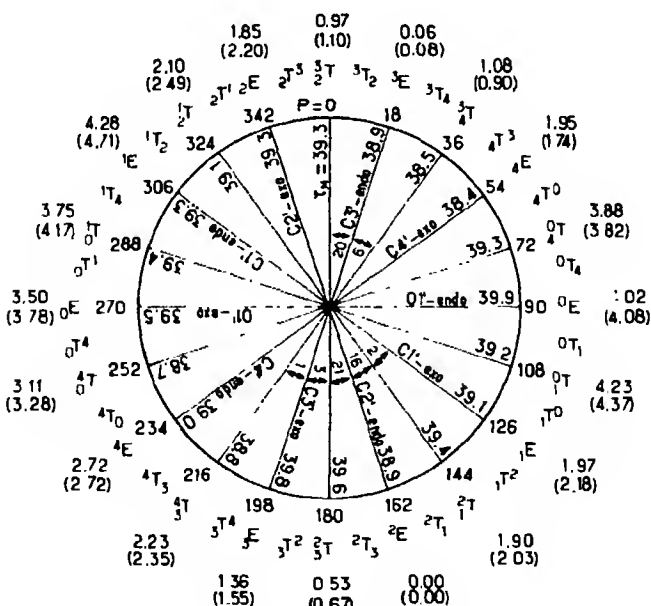


Fig. 2. The conformational wheel, in the pseudorotational representation, for D-ribose and deoxyribose (see text for details)

Knowing the five torsion angles about the sugar ring bonds, one can easily evaluate  $P$  from Eq. (3). For negative values of  $\theta_0$ ,  $180^\circ$  should be added to the calculated value of  $P$  from Eq. (3). A standard conformation is chosen for  $P = 0^\circ$  which corresponds to the maximum value of  $C1'-C2'-C3'-C4'$  ( $=\tau_2$ ) torsion angle. It represents the  $C(3')$ -endo- $C(2')$ -exo ( $^3T_2$ ) conformation of the sugar. The simple relationships between  $\theta$ 's and  $\tau$ 's are:

$$\theta_0 = \tau_2, \quad \theta_1 = \tau_3, \quad \theta_2 = \tau_4, \quad \theta_3 = \tau_0, \quad \theta_4 = \tau_1 \quad \text{and} \quad \theta_m = \tau_m.$$

Figure 2 shows the continuously varying  $P$  values from  $0-360^\circ$ . The symmetrical twist ( $T$ ) and envelope ( $E$ ) conformations occur, respectively, at even and odd multiples of  $18^\circ$  in  $P$ , and are also indicated in the figure. The  $C(3')$ -endo and  $C(2')$  endo conformations occur, respectively, at  $P$  equal to  $18^\circ$  and  $162^\circ$ .

#### D) Geometrical Input Data

Sundaralingam [8] has obtained average geometries for the  $C(3')$ -endo and  $C(2')$  endo sugars from the known crystal structure studies on  $\beta$ -nucleosides and nucleotides. The five bond lengths of the sugar ring are exactly the same in these two fundamental conformations; however three out of five valence angles of the ring differ in the two conformations; the maximum difference being  $1.7^\circ$ . We adopted the bond lengths and valence angles of the  $C(3')$ -endo geometry for all the different forms of the sugar with only a slight variation of  $\pm 1.9^\circ$  permitted for the valence angles. These geometrical parameters have been kept constant to get all the sugar forms corresponding to the different  $P$  and  $\tau_M$  values.

We have not attempted to vary  $\tau_M$  for each value of  $P$  but instead have adopted the mean value of  $39^\circ$  obtained for  $\beta$ -pyrimidine and  $\beta$ -purine nucleosides from the X-ray crystal structure studies of nucleosides and nucleotides [17].  $P$  has been varied from  $0-360^\circ$  in  $18^\circ$  increments corresponding to the ten twist ( $T$ ) and ten envelope ( $E$ ) conformations of the sugar ring.

A computer program for the ring closure of the five membered cycle was developed, which for given bond lengths and valence angles and given  $P$  and  $\tau_M$  values, provides the cartesian and internal coordinates of the ring with an accuracy of  $P$  within  $\pm 0.5^\circ$  and of  $\tau_M = 39^\circ \pm 1^\circ$ . The method employed for the minimization procedure used in this program is the Simplex method [34] which minimizes a function the value of which defines the magnitude of the closure on the stereochemical basis discussed above, by varying the valence and dihedral angles in conformity with the desired values of  $\tau_M$  and  $P$ . In a practical way the dihedral angles are calculated from Eq. (1) for given  $P$  and  $\tau_M$  values and used as initial values for the minimization procedure. The above mentioned function is designed in the following way: The torsion angles for the five atoms 1-5 of the sugar are kept initially at their respective values of  $P$  and  $\tau_m$ . Three complementary fictitious atoms 6, 7 and 8 are considered such that the bond lengths  $5-6 = 5-1$ ,  $6-7 = 1-2$  and  $7-8 = 2-3$ , that the valence angles  $5-6-7 = 5-1-2$  and  $6-7-8 = 1-2-3$  and that the torsion angles  $3-4-5-6 = 3-4-5-1$ ,  $4-5-6-7 = 4-5-1-2$  and  $5-6-7-8 = 5-1-2-3$ . The function is defined as the sum of the distance between atoms  $6-1$ ,  $7-2$  and  $8-3$ . These three

pairs of atoms are superimposed when the function is equal to zero and the ring is then fully closed.

For energy calculations, the ribose and deoxyribose have been constructed with the particular geometry of the sugar ring associated with the corresponding values of  $P$  and  $\tau_M$ . All the constituents of ribose and deoxyribose have been taken into consideration. All hydrogens have been included. The bond lengths and the valence angles of other atoms have been taken following the proposal for a C(3')-endo sugar given in Ref. [8].

For the energy calculations for the nucleosides, we have chosen adenosine and deoxyadenosine for the  $\beta$ -purine nucleosides and uridine and deoxyuridine for  $\beta$ -pyrimidine nucleosides. The geometry of adenine has been taken from the recent X-ray crystal structure study of adenosine by Lai and Marsh [35], and that of uracil from the recent experimental study of  $\beta$ -deoxyuridine by Rahman and Wilson [36].

#### *E) Construction of the Conformational Energy Maps $\chi_{CN}$ vs. $P$*

Conformational energy maps have been constructed as a function of the pseudorotational parameter  $P$  and the torsion angle  $\chi_{CN}$  about the glycosyl bond in  $\beta$ -purine and  $\beta$ -pyrimidine nucleosides. The computations have been carried out in 20 increments of the torsion angle  $\chi_{CN}$  for twenty values of  $P$ , from 0–360°, at an increment of 18°. The presentation of the results on the conformational energy maps has been confined to the 6 kcal/mole above the global minimum isoenergy curve.

### **Results and Discussion**

#### *A) Conformational Properties of Ribose and Deoxyribose*

The conformational energies obtained by the PCILO computations for the ribose and deoxyribose rings as a function of the pseudorotation parameter  $P$  are presented in Fig. 2. The outermost numbers on the conformational wheel represent the values of the energy of the ribose (in kcal/mole) with respect to the global minimum taken as energy zero. The energies of the deoxyribose are given in parentheses. In the calculations of these energies for both ribose and deoxyribose, we have adopted the values of  $\Phi_{C(4')-C(5')} = 60^\circ$  (*gg*) and  $\Phi_{C(5')-O(5')} = 180^\circ$ . The choice of these values results from our previous study [4] and also from experimental evidence [8]. The values of  $\Phi_{C(3')-O(3')}$  for both ribose and deoxyribose and of  $\Phi_{C(2')-O(2')}$  for ribose have been fixed at 60°. Figure 2 shows also the conformations of the sugar ring in terms of the envelope (*E*) and twist (*T*) forms as defined by Sundaralingam [37]. The values of  $\tau_M$  associated in the computations with each  $P$  are also indicated in Fig. 2 along the corresponding radii of the conformational wheel. Finally the distribution of the observed experimental compounds from X-ray crystal structure studies is shown by numbers placed along the arrows in the populated  $P$  values. We have taken account in this distribution of a number of new compounds whose crystal structures have been determined [35, 36, 38–42] since the publication of Altona and Sundaralingam's compilation [17].

The results of Fig. 2, show the existence of two nearly equivalent global energy minima occurring at  $P$  equal to  $18^\circ$  and  $162^\circ$  and corresponding to the  $C(3')\text{-endo}$  and  $C(2')\text{-endo}$  conformations, respectively; the energy associated with the later being slightly lower than that of the former. The experimental data cluster around these selected conformations in very good agreement with the theoretical values. The areas of higher energies are unoccupied, with one exception, an  $O(1')\text{-endo}$  conformation found in the crystal structure of dihydrothymidine (*vide infra*).

The two populated conformational zones may in fact be considered as separated by energy barriers on both sides, which in the isolated furanose ring are nearly equivalent and of the order of 4 kcal/mole. This order of magnitude seems to be confirmed by experiment [17, 18].

In a recent elegant analysis of the general aspects of the conformational wheel for ribose and deoxyribose Hruska, Wood and Dalton [18] have shown that the preference for the  $C(2')\text{-}$  and  $C(3')\text{-endo}$  conformations arises from the fact that these puckerings involve bond rotations which stagger all substituents on the furanose ring. They have also pointed out that interconversions *within* the two stable zones centered around the  $C(2')\text{-endo}$  and  $C(3')\text{-endo}$  conformations require a sign change for  $\tau_0$  and  $\tau_4$  but not for  $\tau_1$ ,  $\tau_2$  and  $\tau_3$ . This situation accounts for the fact that the experimental values of  $\tau_0$  and  $\tau_4$  as found in crystals of nucleosides and nucleotides when presented in the form of conformational wheels [7] display a continuous range of values centered approximately at  $0^\circ$  (and ranging approximately from  $-30^\circ$  to  $30^\circ$ ), while  $\tau_1$ ,  $\tau_2$  and  $\tau_3$  manifest a forbidden range around  $0^\circ$ . These observations substantiate the validity of the division of the conformational wheel of the sugar into two stable pseudorotational zones separated by two barrier zones. It may be remarked that although the two zones appear theoretically as energetically nearly equivalent, the zone centered around  $C(2')\text{-endo}$  is both more populated and occupies a larger portion (in fact extends over  $C(3')\text{-exo}$ ) on the conformational wheel than the zone centered around  $C(3')\text{-endo}$ .

Our results can now be compared with the results obtained for  $\beta\text{-D-ribose}$  by other theoretical studies. Sasisekharan [20], using classical partitioned potential energy functions, found also that there are two equally stable conformational zones around the  $C(2')\text{-endo}$  and  $C(3')\text{-endo}$  conformations, and that the barrier between the two minima along the pseudorotational path is about 2.5–3.0 kcal/mole for the ribose and about 2 kcal/mole for deoxyribose. Lugovskoi and Dashevskii, in a similar study using also partitioned potential functions, have calculated the energy of  $\beta\text{-D-ribose}$  as function of  $\Phi_5$  and  $\Phi_4$ . (Their  $\Phi$ 's are related to our  $\tau$ 's or  $\theta$ 's (see Fig. 1) by the simple relations:  $\Phi_1 = \tau_1 = \theta_4$ ,  $\Phi_2 = \tau_2 = \theta_0$ ,  $\Phi_3 = \tau_3 = \theta_1$ ,  $\Phi_4 = \tau_4 = \theta_2$  and  $\Phi_5 = \tau_0 = \theta_3$ ). Their computations have been carried out in two distinct approximations. When the electrostatic interactions are completely neglected, the results show two energy minima corresponding to the  $C(2')\text{-endo}$  and  $C(3')\text{-endo}$  conformations, the former being more restricted than the later. The transition from one stable conformation to the other along the pseudorotational pathway is through a barrier of the order of 2.5 kcal/mole. However, when the electrostatic interactions are included, a step which in principle represents a refinement, the minimum at the  $C(2')\text{-endo}$

conformation is strikingly destabilized, hardly representing even a local minimum, about 4 kcal/mole above the C(3')-*endo* conformation which represents now the unique stable arrangement. The transition between C(3')-*endo* and C(2')-*endo* which could occur both ways around the pseudorotational pathway becomes now forbidden along the C(2')-*exo*-C(3')-*exo* road (barriers of about 13 kcal/mole) and remains possible only through the alternant C(1')-*exo*-C(4')-*exo* road with a barrier of 5 kcal/mole. This example shows the difficulties connected with the utilization of the empirical partitioned potential function procedures.

The only previous quantum-mechanical computation on the structure of D-ribose is due, as quoted above, to Govil and Saran [23] and was made through the use of the E11T and CNDO methods but did not involve the pseudorotational approach. These authors also found the C(2')-*endo* and C(3')-*endo* conformations to represent the stable arrangements of the ring system.

### B) Relation Between $P$ and $\chi_{CN}$

#### 1) $\beta$ -Purine Ribosides

Adenosine and deoxyadenosine have been chosen for the study of the relation between the glycosyl torsion angle  $\chi_{CN}$  and the pseudorotation parameter  $P$  in the series of  $\beta$ -purine ribosides. For each value of  $P$ , the geometry of the sugar was taken from the study of D-ribose described above. The torsion angles  $\Phi_{C(4)-C(5)}$  and  $\Phi_{C(5)-O(5)}$  have been kept the same as in the study of the ribose and deoxyribose moieties. The torsion angle  $\Phi_{C(3')-O(3')}$  for both adenosine and deoxyadenosine has been fixed at  $180^\circ$  and the torsion angle  $\Phi_{C(2')-O(2')}$  for adenosine was kept at  $180^\circ$ .

The results of the calculations on  $\beta$ -adenosine are shown in Fig. 3. The global minimum occurs at  $P = 162$  (i.e. C(2')-*endo* conformation) for  $\chi_{CN}$  varying from  $70^\circ$  to  $100^\circ$ . There is a large area included within the 1 kcal/mole isoenergy curve associated with this global minimum. There are also three local minima about 1 kcal/mole higher than the global one. Two of them are associated with the same value of  $P$ , and correspond to  $\chi_{CN} = 240^\circ$ ,  $260^\circ$  and  $300^\circ$ ,  $320^\circ$ . The third local minimum also 1 kcal/mole above the global one occurs for  $P = 18^\circ$ , corresponding to the C(3')-*endo* conformation, with  $\chi_{CN}$  varying from  $70^\circ$  to  $125^\circ$ .

Figure 3 contains also the representation of all the presently known experimental results from X-ray crystal studies on  $\beta$ -purine ribonucleosides and nucleotides. It is easily seen that all the representative points are concentrated around or in the vicinity of the above mentioned calculated global and the lowest local energy minima. Remembering that following Sundaralingam's convention [7] the *anti* conformations are defined by  $\chi_{CN} = 0^\circ \pm 90^\circ$  and the *syn* conformations by  $\chi_{CN} = 180^\circ \pm 90^\circ$ , the results of Fig. 3 account satisfactorily for the fact that while both *anti* and *syn* conformation are found for the C(2')-*endo* derivatives only *anti* conformations are observed in the case of the C(3')-*endo* purine nucleosides.

Moreover, the conformational energy map of Fig. 3 also indicates that the possible transition between the C(3')-*endo* and C(2')-*endo* conformations of the sugar, if occurring, should do so through the C(4')-*exo*-C(1')-*exo* pathway. The energy barrier is about 5 kcal/mole. The transition through the



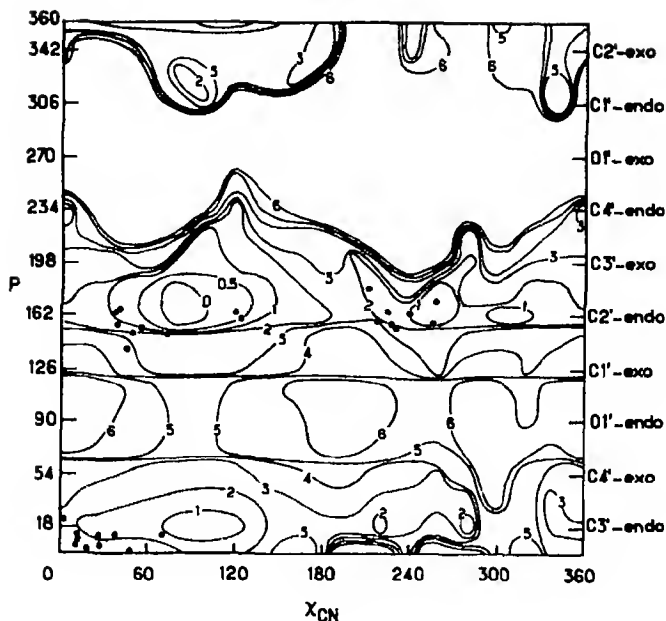


Fig. 3. Conformational energy map,  $P$  vs.  $\chi_{CN}$  in  $\beta$ -purine ribosides. Isoenergy curves in kcal/mole with respect to the global minimum taken as energy zero. ● Experimental X-ray results

$C(3')\text{-}exo$ – $C(2')\text{-}exo$  pathway is practically forbidden as it would involve a large energy barrier.

Figure 4 shows the conformational energy map obtained for  $\beta$ -deoxyadenosine. It is quite similar to that of Fig. 3, with some small variations: the local minimum at  $P = 162$ ,  $\chi_{CN} = 240^\circ$  is only 0.5 kcal/mole above the global minimum, which remains at the same place as in Fig. 3 and the minimum at  $P = 18^\circ$ ,  $\chi_{CN} = 90^\circ$  although also 1 kcal/mole above the global minimum occupies a much smaller area.

Only two experimental results are known for  $\beta$ -deoxyribosides of purines. These are deoxyadenosine monohydrate [43] and 2'-deoxyguanosine in complex with 5-bromo-2'-deoxycytidine [44]. They are indicated by dots in Fig. 4. The first corresponds to a  $C(3')\text{-}exo$  conformation of the sugar ( $P = 198^\circ$ ) and an *anti* value for  $\chi_{CN}$  at about 2 kcal/mole above the global minimum, the second to a  $C(2')\text{-}endo$  conformation of the sugar at  $P = 162^\circ$  and a *syn* value for  $\chi_{CN}$ , also at about 2 kcal/mole above the global minimum.

The results of the maps of Figs. 3 and 4 may be compared to the results of Sasisekharan [20] obtained with the use of partitioned potential energy functions. Broadly speaking they are similar, showing comparable energy minima and energy barriers. The partitioned potential energy functions put, however, all the energy minima at the same level and appear thus unable to distinguish between them and in particular to pick up the global minimum. They remain therefore from this quantitative point of view behind the performance of the quantum-mechanical computations. This point has already been discussed in a related context in Ref. [3].

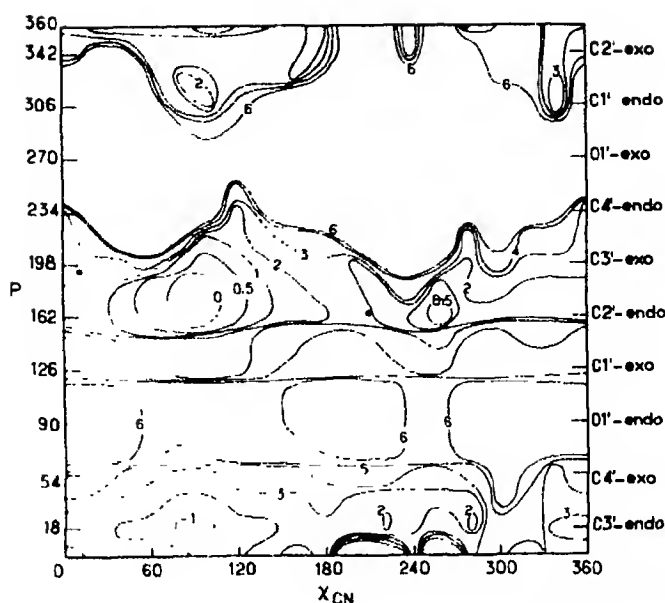


Fig. 4 Conformational energy map,  $P$  vs  $\chi_{CN}$  in  $\beta$ -purine deoxyribosides. Isoenergy curves in kcal/mole with respect to the global minimum taken as energy zero. ● Experimental X-ray results

## 2) $\beta$ -Pyrimidine Ribosides

The compounds utilized in this research were uridine and deoxyuridine. The values of the torsion angles  $\Phi_{C(4')-C(5')}$ ,  $\Phi_{C(5')-O(5')}$ ,  $\Phi_{C(3')-O(3')}$  and  $\Phi_{C(2')-O(2')}$  were kept the same as in the study of the purines.

Figure 5 shows the results of the computations carried out for  $\beta$ -uridine. This map shows a global minimum for  $P=18^\circ$ , corresponding thus to the  $C(3')$ -endo conformation with  $\chi_{CN}$  in the *anti* region, varying from  $0-45^\circ$ . There is a large area within 1 kcal/mole associated with this global minimum. Then, there is a local minimum at  $P=162^\circ$ , corresponding to the  $C(2')$ -endo conformation only 1 kcal/mole above the global one, also in the *anti* region ( $\chi_{CN}$  varying from  $50-85^\circ$ ) and another local minimum, also 1 kcal/mole above the global one, associated with  $P=18^\circ$  in the *syn* region ( $\chi_{CN}$  around  $260^\circ$ ). There are also other local minima in the *syn* region associated with  $P=18^\circ$  and  $162^\circ$  but situated 2-3 kcal/mole above the global minimum.

All the experimental results obtained through X-ray crystallography for  $\beta$ -ribonucleosides of pyrimidines are indicated in Fig. 5. It is clearly seen that the great majority of the experimental conformations cluster around the two fundamental *anti* energy minima at  $P=18^\circ$  and  $162^\circ$ . Three representative points are found in the *syn* region: 4-thiouridine [45] with a  $C(3')$ -endo conformation of the sugar and 6-methyluridine [39] with a  $C(2')$ -endo conformation which has two molecules in the asymmetric crystallographic unit. They occupy the secondary energy minima predicted for this region.

It may be worth stressing that while the theoretical global energy minimum of adenosine was found for the  $C(2')$ -endo conformation, the global energy

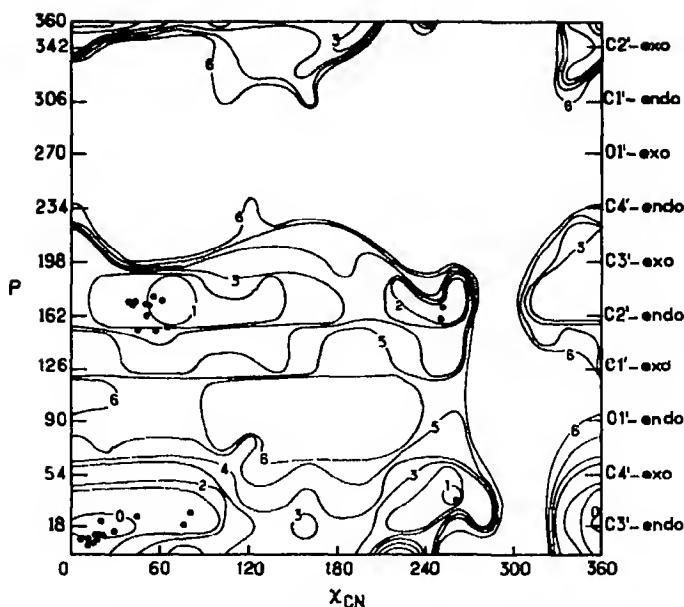


Fig. 5. Conformational energy map,  $P$  vs.  $\chi_{CN}$  in  $\beta$ -pyrimidine ribosides. Isoenergy curves in kcal/mole with respect to the global minimum taken as energy zero. ● Experimental X-ray results

minimum of uridine is associated with the  $C(3')\text{-endo}$  conformation. The direction of the easiest transition between the two minima remains, however, the same for the pyrimidines as for the purines, namely *via* the  $C(4')\text{-exo}$ – $C(1')\text{-exo}$  path. The barrier is about 6 kcal/mole as compared to 5 kcal/mole found for adenosine.

The results of the computations carried out for  $\beta$ -deoxyuridine are shown in Fig. 6. The map shows two global minima of almost similar depth associated with  $P = 18^\circ$  and  $P = 162^\circ$  and for  $\chi_{CN}$  in the *anti* region. There is a particularly large area within the 0.5 kcal/mole isoenergy curve around the global minimum at  $P = 162^\circ$ . The *syn* regions associated with both  $P = 18^\circ$  and  $P = 160^\circ$  present local energy minima but at 2 kcal/mole above the global ones.

The experimentally observed conformations in compounds of this category cluster practically exclusively around the large global minimum at  $P = 162^\circ$  ( $C(2')\text{-endo}$  and *anti*). One compound dihydrothymidine [46], the only known compound with a  $O(1')\text{-endo}$  conformation of the sugar ( $P = 84.4^\circ$ ) lies in a relatively high energy region, at 5 kcal/mole above the global minimum. Possibly the map of Fig. 6 is not well representative of this particular compound. Deoxycytidine 5'-phosphate monohydrate [47], which has a  $C(3')\text{-exo}$  sugar pucker lies close to the 2 kcal/mole isoenergy curve, not far from the global minimum associated with  $P = 162^\circ$ . There is only one compound, deoxycytidine hydrochloride [48], associated with the global minimum at  $P = 18^\circ$ , corresponding to the  $C(3')\text{-endo}$  conformation of the sugar ring.

The barrier for transition from  $C(3')\text{-endo}$  to  $C(2')\text{-endo}$  conformation is 5 kcal/mole, as compared to 6 kcal/mole in the case of uridine and this transition is possible only through the  $C(4')\text{-exo}$ – $C(1')\text{-exo}$  pathway.

38968...

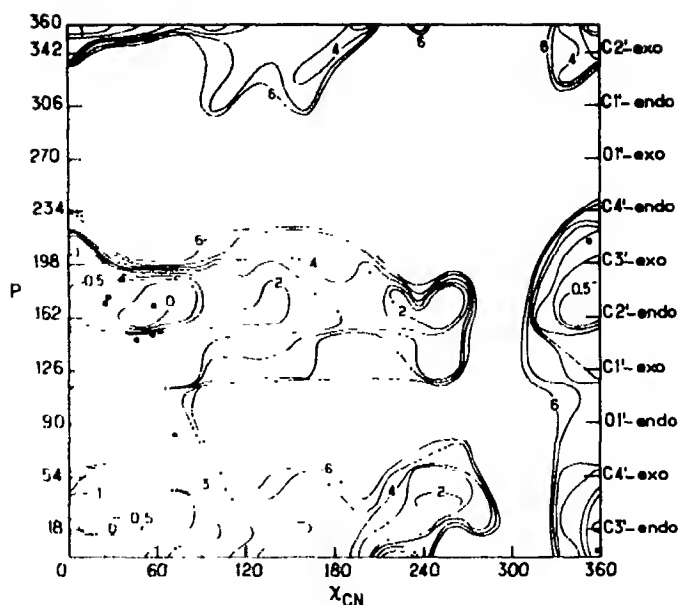


Fig. 6. Conformational energy map,  $P$  vs  $\chi_{CN}$  in  $\beta$ -pyrimidine deoxyribosides. Isoenergy curves kcal/mole with respect to the global minimum taken as energy zero. ● Experimental X-ray results.

The results of the maps in Figs. 5 and 6 can also be compared with the results obtained from the computations done by using partitioned potential energy functions [20]. Again these last computations fail to distinguish the global minimum among the three minima obtained, one in the *anti* region for the C(3') *endo* conformation and two in the *anti* and *syn* regions for the C(2') *endo* conformation. 4-thiouridine lies in Sasisekharan's map [20] in high energy zone devoid of a local minimum. However, the transition from the C(2') *endo* to the C(3') *endo* conformation through the C(3') *exo* C(2') *exo* direction is forbidden as in the PCILO calculations. The energy barrier for the transition through the C(4') *exo* C(1') *exo* path is of the order of 3 kcal/mole as compared to 5–6 kcal/mole in PCILO computations.

### Conclusions

The principal conclusions which can be drawn from this study seem to be twofold. In the first place we continue to observe the extremely satisfactory agreement between the results of the quantum-mechanical PCILO computations and the experimental data shown to exist for the other aspects of the conformations of nucleic acid and their constituents in the previous papers of this series. This satisfactory agreement, in particular with the data from X-ray crystallography, is worth stressing as the calculations are performed for isolated molecules. It indicates the general significance of the global and local energy minima put into evidence by the calculations. Secondly, the results point to the usefulness of the pseudorotational concept in its applications to the conformational analysis of nucleic acid and their constituents.

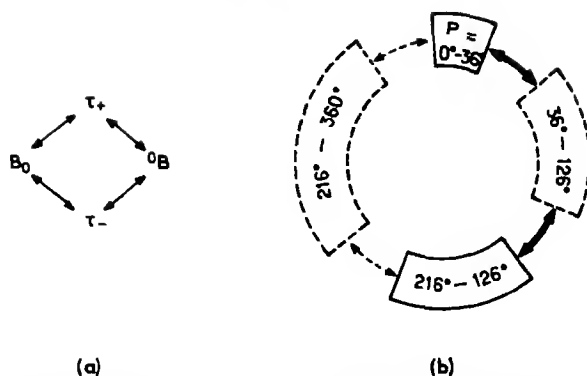


Fig. 7. Classes of states of the pseudorotational itinerary of the sugar ring in nucleosides. a Following Hruska *et al.* [18]. b Proposed here.

mations of the furanose ring. It shows simultaneously the continuity of the deformability of the ring along the pseudorotational pathway and the existence of two zones of stable conformations separated by large zones of relatively unstable ones. This result is particularly important for the comprehension of the conformational equilibrium of nucleosides in solution. Hruska and coworkers [18], in particular, have deduced from their abundant studies of vicinal proton-proton couplings in the sugar rings of nucleosides that the furanose rings exist in dynamic equilibria involving well-defined states corresponding to the two stable conformational zones, centered around the C(3') *endo* and C(2')-*endo* conformations, which they denote by the symbols  $\tau_+$  and  $\tau_-$ , respectively, separated by two barrier zones, corresponding to the two pathways C(1')-*exo*-C(4') *exo* (which they denote by the symbol  ${}^0B$ ) and C(3') *exo*-C(2')-*exo* (which they denote by the symbol  $B_0$ ). These authors give, however, a symmetrical representation of the overall situation (Fig. 7a). An unsymmetrical representation such as given in Fig. 7b seems to describe more adequately the real situation in nucleosides.

**Acknowledgement.** The authors thank Drs. Hruska, Sasisekharan, Saenger and Sundaralingam for communication of data prior to publication.

## References

1. Berthod, H., Pullman, B.: *Biochim. Biophysica Acta* **232**, 595 (1971).
2. Berthod, H., Pullman, B.: *Biochim. Biophysica Acta* **246**, 359 (1971).
3. Pullman, B., Perahia, D., Saran, A.: *Biochim. Biophysica Acta* **269**, 1 (1972).
4. Saran, A., Pullman, B., Perahia, D.: *Biochim. Biophysica Acta* **287**, 211 (1972).
5. Pullman, B., Berthod, H.: In: *Conformations of biological molecules and polymers. Proceedings of the 5th Jerusalem Symposium*, ed. by Bergmann, E. D., Pullman, B., p. 209. New York: Academic Press 1973.
6. Saran, A., Pullman, B., Perahia, D.: *Biochim. Biophysica Acta* **299**, 497 (1973).
7. Sundaralingam, M.: *Biopolymers* **7**, 821 (1969) and references quoted therein.
8. Sundaralingam, M.: In: *Conformations of biological molecules and polymers. Proceedings of the 5th Jerusalem Symposium*, ed. by Bergmann, E. D., Pullman, B., p. 417. New York: Academic Press 1973.

9. Kilpatrick, J. E., Pitzer, K. S., Spitzer, R.: *J. Amer. chem. Soc.* **69**, 2483 (1947).
10. Pitzer, K. S., Donath, W. E.: *J. Amer. chem. Soc.* **81**, 3213 (1959).
11. Altona, C., Buys, H. R., Havinga, E.: *Rech. Trav. Chim.* **85**, 973 (1966).
12. Geise, H. J., Altona, C., Romers, C.: *Tetrahedron Letters* 1383 (1967).
13. Altona, C., Geise, H. J., Romers, C.: *Tetrahedron* **24**, 13 (1968).
14. Altona, C., VandDer Veek, A. P. M.: *Tetrahedron* **24**, 4377 (1968).
15. Romers, C., Altona, C., Buys, H. R., Havinga, E.: *Topics in stereochemistry*, ed. by Eliel, E. L., Allinger, N. L., Vol. 4, p. 39. New York: Wiley Interscience 1969.
16. Altona, C.: In: *Conformational analysis*, ed. by Chirndoglu, G., p. 1. New York: Academic Press 1971.
17. Altona, C., Sundaralingam, M.: *J. Amer. chem. Soc.* **94**, 8205 (1972).
18. Hruska, I. L., Wood, D. J., Dalton, J. G.: *J. Amer. chem. Soc.*, in press.
19. Hall, I. D., Steiner, P. R., Pedersen, C.: *Canad. J. Chem.* **48**, 1155 (1970).
20. Sasisekharan, V.: In: *Conformations of biological molecules and polymers*. Proceedings of the 5<sup>th</sup> Jerusalem Symposium, ed. by Bergmann, I. D., Pullman, B., p. 247. New York: Academic Press 1973.
21. Ingoskov, A. A., Dashevskii, V. G.: *Molecular Biology USSR (Engl. Ed.)* **6**, 354 (1972).
22. Ingoskov, A., Dashevskii, V. G., Kitagorodskii, A. I.: *Molecular Biology, USSR (Engl. Ed.)* **6**, 361 (1972).
- 22a. Ingoskov, A. A., Dashevskii, V. G., Kitagorodskii, A. I.: *Molekulyarnaya Biologiya* **6**, 614 (1972).
23. Govil, G., Saran, A.: *J. Theoret. Biology* **33**, 399 (1971).
24. Lakshminarayanan, A. V., Sasisekharan, V.: *Biochim. Biophysica Acta* **204**, 49 (1970).
25. Lakshminarayanan, A. V., Sasisekharan, V.: *Biopolymers* **8**, 475 (1969).
26. Haschemeyer, A. F. V., Rich, A.: *J. molecular Biol.* **27**, 369 (1967).
27. Wilson, H. R., Rahman, A., Tollin, P.: *J. molecular Biol.* **46**, 585 (1969).
28. Wilson, H. R., Rahman, A.: *J. molecular Biol.* **56**, 129 (1971).
29. Kang, S.: *J. molecular Biol.* **58**, 297 (1971).
30. Berthod, H., Pullman, B.: *J. BS Letters*, **30**, 231 (1973).
31. Diner, S., Malrieu, J. P., Claverie, P.: *Theoret. chim. Acta (Berl.)* **13**, 1 (1969).
32. Malrieu, J. P., Claverie, P., Diner, S.: *Theoret. chim. Acta (Berl.)* **13**, 18 (1969).
33. Diner, S., Malrieu, J. P., Jordan, F., Gilbert, M.: *Theoret. chim. Acta (Berl.)* **15**, 100 (1969).
34. Nelder, J. A., Mead, R.: *Comp. J.* **7**, 308 (1965).
35. Lai, T. F., Marsh, R. E.: *Acta crystallogr. B* **28**, 1982 (1972).
36. Rahman, A., Wilson, H. R.: *Acta crystallogr. B* **28**, 2260 (1972).
37. Sundaralingam, M.: In: *The purines: theory and experiment*. Proceedings of the 4<sup>th</sup> Jerusalem Symposium, ed. by Pullman, B., Bergmann, I. D., Vol. IV, p. 73. New York: Academic Press 1972.
38. Voet, D., Rich, A.: *Proc. nat. Acad. Sci. USA* **68**, 1151 (1971).
39. Suck, D., Saenger, W.: *J. Amer. chem. Soc.* **94**, 6520 (1972).
40. Kennard, O., Isaacs, N. W., Motherwell, W. D. S., Coppola, J. C., Wampler, D. L., Larson, A. C., Watson, D. G.: *Proc. Royal Soc. (London)* **A 325**, 401 (1971).
41. Vishwamitra, M. A., Reddy, B. S., James, M. N. G., Williams, G. J. B.: *Acta crystallogr. B* **28**, 1108 (1972).
42. Schwalbe, C. H., Saenger, W.: Private communication.
43. Watson, D. G., Sutor, D. J., Tollin, P.: *Acta crystallogr.* **19**, 111 (1965).
44. Haschemeyer, A. F. V., Sobell, H. M.: *Acta crystallogr.* **19**, 125 (1965).
45. Saenger, W., Scheit, K. H.: *J. molecular Biol.* **50**, 153 (1970).
46. Konert, J., Karle, I. L., Karle, J.: *Acta crystallogr. B* **26**, 1089 (1970).
47. Vishwamitra, M. A., Reddy, B. S., Lin, G. H. Y., Sundaralingam, M.: *J. Amer. chem. Soc.* **93**, 4565 (1971).
48. Subramanian, E., Hunt, D. J.: *Acta crystallogr. B* **26**, 303 (1970).

Prof. Dr. B. Pullman  
 Institut de Biologie Physico-Chimique  
 Laboratoire de Biochimie Théorique  
 associé au C.N.R.S.  
 13, rue P. et M. Curie  
 Paris 5<sup>e</sup>, France

# Molecular Orbital Structure, Mössbauer Isomer Shift, and Quadrupole Splitting in Iron Complexes\*

Alfred Trautwein\*\*

Institut für Metallphysik, Universität des Saarlandes, 6600 Saarbrücken, West Germany

Frank E. Harris

Department of Physics, University of Utah, Salt Lake City, Utah 84112

Received January 18, 1973

Molecular orbital calculations are made on six iron complexes, using iterative Hückel methods and, where required for proper description of spin states, a spin-projected semi-empirical configuration interaction (CI). Many integrals are avoided in the CI studies by making direct calculation of energy differences between states. From the calculations are obtained charge and spin bond order matrices, dipole moments, and atomic orbital charges. These quantities are used to calculate charge densities at the Fe nucleus, nuclear quadrupole splittings, and spin populations. From calculations of all six complexes we estimate an  $\text{Fe}^{57}$  Mössbauer isomer-shift calibration  $\alpha \equiv \Delta\delta/\Delta\rho(0) \approx -0.31$  to  $-0.38 a_0^3$  mm/sec.

Mit Hilfe iterativer Hückel-Methoden werden MO-Rechnungen für sechs Eisenkomplexe durchgeführt. Wo es für die Beschreibung der Spinzustände notwendig ist, wird nach einem CI-Verfahren mit Spinprojektion gearbeitet. Durch direkte Berechnung von Energiedifferenzen zwischen den einzelnen Zuständen werden viele Integrale in den CI-Berechnungen vermieden. Aus den Rechnungen erhält man die Matrizen der Ladungs- und Spin-Bindungsordnungen, Dipolmomente und AO-Ladungsverteilungen. Diese Größen werden zur Berechnung der Ladungsdichte am Fe-Kern, der Kernquadrupolaufspaltung und der Spinpopulation verwendet. Aufgrund der Berechnungen aller sechs Komplexe wird die  $\text{Fe}^{57}$ -Mößbauer-Isomerieverschiebung auf  $\alpha \equiv \Delta\delta/\Delta\rho(0) = -0.31$  bis  $-0.38 a_0^3$  mm/sec geschätzt.

## Introduction

The essential role of iron complexes in biological processes makes particularly interesting and important a good understanding of the electronic structures of such complexes. This understanding can to some extent be obtained experimentally, but there remain many questions which theoretical studies might resolve. Since the complexes involve to varying extents covalent binding between iron and ligands and charge rearrangements within the ligand structure, a theoretical description cannot justifiably be limited to an iron atom and its

\* Supported in part by U.S. National Science Foundation Grant GP-31373X, in part by an award from the Biomedical Sciences Support Grant at the University of Utah (U.S. Public Health Service Grant RR 07092), and in part by the Centre Européen de Calcul Atomique et Moléculaire, Orsay, France.

\*\* Supported at the Centre Européen de Calcul Atomique et Moléculaire, Orsay, France by a fellowship (No. 531) of the European Molecular Biology Organization and by the French Government through Monsieur le Ministre des Affaires Etrangères, de la République Française (No. 12778 CT/b/1).

immediate neighbors. Moreover, the three-dimensional structure of the complexes contraindicates approximations which do not include all relevant valence electrons.

Rigorous all-valence-electron treatments of systems as large as typical iron complexes are prohibitive in cost, even at the self-consistent-field (SCF) level of approximation. It is even extremely costly to pursue semi-empirical antisymmetrized molecular orbital theory or approximations based on neglect of differential overlap, such as the CNDO/2 method. The key simplification appearing to permit calculation at reasonable cost is the avoidance of constructing an explicit antisymmetrized many-electron wavefunction; methods in this category include those of the Hückel type and the "multiple-scattering  $X\alpha$  method" of Johnson *et al.* [1]. The present paper describes theoretical studies based on an iterative extended Hückel method previously described by one of the authors [2]. The iterative feature gives the method SCF character, and "extended" indicates the application to all valence electrons.

The Hückel model is inadequate to distinguish spin eigenstates and to calculate energy differences between them, and many iron complexes exist in "high-spin" states necessitating the use of singly-occupied molecular orbitals (MO's). For such problems we supplemented the Hückel calculations by proceeding to a limited configuration interaction (CI), simplifying the computations by using the Hückel SCF MO's to construct configurations, by calculating only energy differences, and by using approximate integrals.

In semi-empirical studies such as that reported here, the success of the description should rest on the capability for inter-relating a variety of data on a variety of systems. We show here the extent to which our studies agree with conventional spectral data, such as ligand field splittings, and also with Mössbauer data, such as isomer shifts and quadrupole splittings. By comparing calculations for six different complexes, we are able to obtain information regarding the calibration constant relating the Mössbauer isomer shift to the charge density at the iron nucleus.

### Hückel Calculations

Iterative extended Hückel calculations were carried out by methods described in detail previously [2]. The Hückel one-electron Hamiltonian  $H$  was assumed to have diagonal elements  $H_{aa} = \alpha_a - q_a \Delta\alpha_a$ , where  $\alpha_a$  is the " $\alpha$ " parameter for atomic orbital  $a$  (of real form) in a neutral atom,  $q_a$  is the net charge of the atom at which orbital  $a$  is centered, and  $\Delta\alpha_a$  is an additional parameter controlling the variation of  $H_{aa}$  with net atomic charge. The off-diagonal elements  $H_{ab}$  were determined from  $H_{aa}$  and  $H_{bb}$  by the Cusachs approximation [3]  $H_{ab} = S_{ab}(1 - \frac{1}{2}|S_{ab}|)(H_{aa} + H_{bb})$ . Here  $S_{ab}$  is the overlap integral of atomic orbitals  $a$  and  $b$ , calculated assuming Slater-type orbitals (STO's). In evaluating  $H_{ab}$ , all operations are performed in a coordinate system passing through the orbital centers so as to retain full invariance with respect to rotation of the molecule in the coordinate system.

Iterations were carried out until the occupied-orbital solutions of the matrix equation  $(H - E_i S) c_i = 0$  were consistent with the net atomic charges used in calculating  $H$ . Here  $E_i$  is the orbital energy of the molecular orbital whose



atomic-orbital coefficients are represented by the vector  $c_i$ . The overlap matrix  $S$  is built from the  $S_{ab}$  as already defined. The iterative process must be sophisticated enough to overcome the strong nonlinearity of the theory; we use a combination of damping and second-order extrapolations and thereby ordinarily achieve convergence to  $\pm 0.01$  units in atomic charge in five to ten iterations. The net atomic charges are obtained by apportioning exactly-computed overlap charges among the atoms involved, in a fashion which preserves the projection of the charge centroid on the intercenter line. This causes the atomic charges to be approximately consistent with computed dipole moments and to reflect the actual charge distribution far better than would an equal division of overlap charge.

The Hückel-method output includes orbital energies and corresponding MO's, the bond-order matrix, net atomic and orbital charges, and the molecular dipole moment. All programming is in FORTRAN, and is set up for a Univac 1108 system. The Hückel program, the CI program described in the next section, and all data storage for calculations involving a maximum of 60 atomic orbitals fit into approximately 50,000 words of core and run without the use of peripheral equipment for intermediate storage. Typical SCF computation times for the iron

Table 1. Approximate molecular-orbital calculations of small fluorine compounds

Molecule <sup>a</sup>	Method <sup>b</sup>	Energy sequence <sup>c</sup> (valence orbitals)	Dipole moment (D) <sup>d</sup>	Ionization potential (eV)
HF	CNDO/2	$\sigma^2 \sigma^2 \pi^4$	1.86	15.77
	INDO		1.98	21.14
	IEHT		2.36	14.61
	expt.		1.82	19.96
F <sub>2</sub>	CNDO/2	$\sigma_u^2 \sigma_u^2 \pi_u^4 \pi_g^4$	0	15.7
	INDO		0	19.19
	IEHT		0	17.68
	expt.		0	18.32
CF <sub>2</sub>	CNDO/2	$a_1^2 b_2^2 a_1^2 b_2^2 a_1^2 b_1^2 a_1^2 b_2^2 a_1^2$	0.53	
	INDO	$b_2^2 a_1^2 b_1^2$	0.26	
	IEHT	$b_1^2 a_1^2 b_2^2$	0.75	14.21
NF <sub>2</sub>	CNDO/2	$a_1^2 b_2^2 a_1^2 b_1^2 a_1^2 b_2^2 a_2^2 b_2^2 a_1^2 b_1$	-0.12	
	INDO	$b_1^2 a_1^2 b_2^2$	-0.38	
	IEHT	$b_2^2 b_1^2 a_1^2$	-0.21	13.03
OF <sub>2</sub>	CNDO 2	$a_1^2 b_2^2 a_1^2 b_1^2 a_1^2 b_2^2 a_2^2 b_2^2 a_1^2 b_1^2$	-0.21	
	INDO	$b_1^2 a_1^2 b_2^2$	-0.40	
	IEHT	$b_2^2 a_1^2 b_1^2$	-0.61	15.32
	expt.		$\pm 0.30$	
FH <sub>2</sub>	CNDO	$\sigma_u^2 \sigma_u^2 \pi_u^2 \sigma_g$	0	
	INDO		0	
	IEHT		0	1.89

<sup>a</sup> Geometries: HF,  $R = 0.917$  Å; F<sub>2</sub>,  $R = 1.435$  Å; CF<sub>2</sub>,  $R_{CF} = 1.32$  Å,  $\angle_{FCF} = 104^\circ$ ; NF<sub>2</sub>,  $R_{NF} = 1.35$  Å,  $\angle_{FNF} = 104^\circ$ ; OF<sub>2</sub>,  $R_{OF} = 1.41$  Å,  $\angle_{FOF} = 104^\circ$ ; FH<sub>2</sub>,  $R = 0.92$  Å,  $\angle_{HHF} = 180^\circ$ .

<sup>b</sup> CNDO/2 and INDO calculations and experimental data as reported by Pople and Beveridge (Ref. [4]); IEHT are iterative extended Hückel calculations of this work.

<sup>c</sup> Energy sequences agree for all methods except where underlined portions are repeated.

<sup>d</sup> Dipole moment of AB or AB<sub>2</sub> molecules is + in the direction A<sup>+</sup>B<sup>-</sup> or A<sup>-</sup>B<sub>2</sub><sup>+</sup>.

Table 2. Orbital parameters for Hückel and CI calculations:  $\zeta$  = STO screening parameters;  $\alpha$ ,  $\Delta\alpha$  = Hückel energy parameters,  $h$  = atomic core energy;  $\gamma$  = single-center repulsion energy

		$\zeta$	$\alpha$	$\Delta\alpha$	$h$	$\gamma$
1s	3d	2.87	7.0	8	135	23.5
	4s	1.40	7.5	8	56	6.0
	4p	1.40	6.5	8	64	8.0
1	2s	2.60	34.0	18	130	16.0
	2p	2.60	18.5	15	115	14.0
O	2s	2.275	33.0	15		
	2p	2.275	14.0	15		
N	2s	1.95	30.0	12		
	2p	1.95	11.5	12		
C	2s	1.625	25.0	11		
	2p	1.625	10.0	11		
H	1s	1.20	11.6	14		

Table 3. Geometries used for iron complexes. Principal symmetry axis taken in  $z$  direction, octahedral ligands also in  $\pm z$  and  $\pm y$  directions

$\text{Fe}(\text{C}(\text{N})_3)_2\text{NO}^{2-}$	Symmetry $C_{4v}$ , data based on $\text{Na}_2\text{Fe}(\text{CN})_5\text{NO} \cdot 2\text{H}_2\text{O}^a$ Cartesian coordinates (Å): Fe(0, 0, 0), N <sub>1</sub> (0, 0, 1.63), O(0, 0, 2.76), C <sub>1</sub> (0, 0, -1.91), N(0, 0, -3.07), C'(±1.90, 0, -0.20), C'(0, ±1.90, -0.20), N(±3.05, 0, -0.32), N(0, ±3.05, -0.32)
$\text{Fe}(\text{C}'\text{O})_5^b$	Symmetry $D_{3h}$ $R_{\text{Fe}-\text{C}} = 1.84 \pm 0.03$ Å; $R_{\text{C}-\text{O}} = 1.15 \pm 0.04$ Å All $R_{\text{Fe}-\text{C}}$ equal; all $R_{\text{C}-\text{O}}$ equal. Trigonal bipyramid; C <sub>1</sub> , C <sub>2</sub> , C <sub>3</sub> equatorial, C <sub>4</sub> , C <sub>5</sub> polar
$\text{Fe}(\text{C}'\text{N})_6^{4-}$	Symmetry $O_h$ , data based on $\text{K}_4\text{Fe}(\text{C}'\text{N})_6^c$ $R_{\text{Fe}-\text{C}} = 1.89$ ; $R_{\text{C}-\text{N}} = 2.157$
$\text{Fe}(\text{C}'\text{N})_6^{4-}$	Symmetry $O_h$ , data based on $\text{K}_4\text{Fe}(\text{C}'\text{N})_6 \cdot 311_2\text{O}^d$ $R_{\text{Fe}-\text{C}} = 1.91$ , $R_{\text{C}-\text{N}} = 2.157$
$\text{Fe}(\text{C}'\text{N})_5^e$	Symmetry $O_h$ , data based on $\text{Fe}(\text{C}'\text{N})_5^e$ $R_{\text{Fe}-\text{C}} = 1.92$ Å
$\text{Fe}(\text{C}'\text{N})_6^{4-}$	Symmetry $O_h$ , data based on $\text{KFeF}_6^f$ $R_{\text{Fe}-\text{F}} = 2.06$ Å

<sup>a</sup> Wyckoff, R. W. G.: Crystal structures, second ed., Vol. 3, p. 623. New York: Interscience 1965.<sup>b</sup> Tables of interatomic distances and configurations in molecules and ions, ed. L. E. Sutton. London: Chemical Society 1958.<sup>c</sup> Kohn, J. W., Townes, W. D.: Acta crystallogr. **14**, 617 (1961).<sup>d</sup> Wyckoff, R. W. G.: Crystal structures, second ed., Vol. 3, p. 687. New York: Interscience 1965.<sup>e</sup> Tables of interatomic distances and configurations in molecules and ions, ed. L. E. Sutton. London: Chemical Society 1965.<sup>f</sup> Wells, A. F.: Structural inorganic chemistry. Oxford: Oxford University Press 1962.

complexes reported here are 1–2 min. A Hückel program version handling up to 140 atomic orbitals and using intermediate drum storage and approximately 50000 words of core has also been implemented; a typical 130-orbital, 138-electron SCF calculation requiring 8 iterations ran in 12 min.

The calculations in this paper include all valence orbitals, i.e.  $1s$  for H;  $2s$  and  $2p$  for C, N, O, and F; and  $3d$ ,  $4s$ , and  $4p$  for Fe. For H, C, N, and O, the orbital parameters  $\alpha_a$ ,  $\Delta\alpha_a$ , and  $\zeta_a$  (the STO screening parameters) were taken from previous iterative Hückel calculations [2].

For fluorine, we used values of  $\zeta_{2s}$  and  $\zeta_{2p}$  calculated by Slater's rules, and chose  $\alpha_a$  and  $\Delta\alpha_a$  values after study of a set of six molecules: HF, F<sub>2</sub>, CF<sub>2</sub>, NF<sub>2</sub>, F<sub>2</sub>O, and H<sub>2</sub>F. Starting from  $\alpha_a$  and  $\Delta\alpha_a$  values as reported in the literature [4], we made adjustments to optimize the consistency with the parameters already adopted for H, C, N, and O. Our criteria included the energy sequences of the MO's, the ionization potentials, and the dipole moments. Our calculations for the fluorine compounds, previous calculations, and experimental data are summarized in Table 1.

For iron, we used values of  $\zeta_{4s}$  and  $\zeta_{4p}$  as given for the neutral atom by Clementi and Raimondi [5]. Starting from  $\zeta_{3d}$ ,  $\alpha_a$  and  $\Delta\alpha_a$  values given by Zerner *et al.* [6], we made slight adjustments to fit the ligand field splittings for Fe(CN)<sub>6</sub><sup>4-</sup> and Fe(CN)<sub>6</sub><sup>3-</sup>, and to have the Fe  $3d$ , orbitals as major components of the highest occupied MO's for both compounds.

The orbital parameters for all atoms entering the Hückel calculations are listed in Table 2. The molecular geometries used for the iron complexes are given in Table 3.

### CI Calculations

As even a limited CI study is expensive for large systems, and since our present needs were to characterize the MO structure and to intercompare different spin states, we confine attention to the calculation of energies relative to that of a "reference configuration". If the reference configuration has energy  $E_0$ , energies relative thereto can be obtained as eigenvalues of  $H - E_0 S$ , where  $H$  and  $S$  now refer to many-electron space-spin states of appropriate symmetries. As  $E_0$  can be written in terms of the integrals occurring in the elements of  $H$ , the elements of  $H - E_0 S$  will depend only upon the orbitals affected by passage from the reference configuration to the configurations actually used in  $H$  and  $S$ . The foregoing statements have been written carefully to avoid the implication that the reference configuration necessarily refers to a specific spin state; on the contrary, if different spin states are to be compared, it must be the same for all states and should be chosen to cause a maximum degree of integral cancellation.

The definition we have found most satisfactory for a reference configuration is that which results if we assume its singly-occupied orbitals are averaged over spin orientations. Letting  $\langle ij|h|j \rangle$  refer to a matrix element of the one-electron part of the Hamiltonian between MO's  $i$  and  $j$ , letting  $\langle ij \rangle$  stand for a MO overlap integral, and letting  $[ij|mn]$  stand for an MO electron repulsion integral in Mulliken notation

$$[ij|mn] = \int \phi_i^*(1) \phi_j(1) r_{12}^{-1} \phi_m^*(2) \phi_n(2) d\tau_1 d\tau_2,$$

we have

$$E_0 = \sum_{i_0} \langle i_0|h|i_0 \rangle + \sum_{i_0 < j_0} ([i_0 i_0 | j_0 j_0] - \frac{1}{2}(1 - \langle i_0 | j_0 \rangle) [i_0 j_0 | j_0 i_0]),$$

where the summations are over all electrons and  $i_0(j_0)$  refers to the MO of the  $i^{\text{th}}(j^{\text{th}})$  electron before antisymmetrization. The MO's may be doubly occupied, but distinct MO's are assumed orthogonal.

The many-electron states used in  $H$  and  $S$  are constructed by antisymmetrization and spin projection [7] of spinorbital products. As in the preceding paragraph, we assume the spatial orbitals to be chosen from a set of orthogonal MO's. The matrix elements of  $H$  and  $S$  can then be written in terms of spatial integrals and spin projection (Sanibel) coefficients [8]. If two configurations  $\mu$  and  $\nu$  have different MO occupancies,  $S_{\mu\nu}$  will vanish,  $(H - E_0 S)_{\mu\nu}$  will be identical with  $H_{\mu\nu}$ , which may be evaluated by existing formulas. The important point here is that  $H_{\mu\nu}$  will depend only upon two-electron integrals containing MO's whose occupancy differs in configurations  $\mu$  and  $\nu$ , and therefore will at worst involve a number of integrals comparable to the number of electrons.

When  $\mu$  and  $\nu$  refer to configurations with the same spatial MO occupancy ( $\mu$  and  $\nu$  may differ in spin assignment), then  $E_0 S_{\mu\nu}$  does not vanish and  $(H - E_0 S)_{\mu\nu}$  can be simplified. Using the expression already given for  $E_0$  and the published expressions for  $H_{\mu\nu}$  and  $S_{\mu\nu}$ , one may derive

$$\begin{aligned} (H - E_0 S)_{\mu\nu} = & C_k \left\{ \sum_i (i|h|i) - \sum_p (p|h|p) + \sum_{rr'} \{ [ii|rr] - \frac{1}{2} [ir|ri] \} \right. \\ & - \sum_{pp'} \{ [pp|rr] - \frac{1}{2} [pr|rp] \} + \sum_{ij} \{ [ii|jj] - \frac{1}{2} [ij|ji] \} \\ & \left. - \sum_{p,q} \{ [pp|qq] - \frac{1}{2} [pq|qp] \} \right\} + \sum_{l,m} (\frac{1}{2} C_k - C_k) [lm|ml] \end{aligned}$$

In this equation, summations of  $i$  and  $j$  range over electrons in MO's of  $\mu$  which are unoccupied in the reference configuration;  $p$  and  $q$  summations are over electrons in reference MO's not occupied in  $\mu$ ;  $r$  ranges over electrons in MO's common to  $\mu$  and the reference configuration; and  $l$  and  $m$  range over electrons in singly-occupied MO's of  $\mu$ . The symbol  $C_k$  stands for the Sanibel coefficient appropriate to the spin state and the relative spin assignments of the MO's in  $\mu$  and  $\nu$ ; when  $C_k$  occurs within a summation over  $l$  and  $m$ , it denotes the Sanibel coefficient which is appropriate after the spin assignments of electrons  $l$  and  $m$  are interchanged in configuration  $\mu$ . The key feature of this equation for  $(H - E_0 S)_{\mu\nu}$  is that very few integrals are needed for configurations differing little from the reference configuration in MO occupancy.

The integrals needed for the CI calculations were calculated using approximations of types common in semi-empirical MO theory. However, the large size of the molecules involved made it necessary to use relatively simple approximations and to be careful to obtain proper cancellation of long-range opposing electrostatic forces. Expanding each MO into atomic orbitals, the atomic-orbital integral  $(a|h|b)$  is related to "core energies"  $h_a$ ,  $h_b$  and to point charge nuclear-attraction energies  $e_a$ ,  $e_b$ :

$$(a|h|b) = S_{ab} (1 - \frac{1}{2} |S_{ab}|) (h_a + h_b) - \frac{1}{2} S_{ab} (e_a + e_b)$$

Here  $h_a$ ,  $h_b$  are input parameters, and  $e_a = \sum_{b \neq a} Z_b / R_{ab}$ , where the sum is over all atoms except that on which orbital  $a$  is centered,  $Z_b$  is the core charge of

atom  $b$ , and  $R_{ab}$  is the distance between the center of orbital  $a$  and atom  $b$ . Note that the Cusachs approximation is used for the two-center contributions for the core energies, but that a normal Mulliken approximation [10], is used for the two-center nuclear attraction energies. The evaluation of  $(a|h|b)$  must be carried out in a rotationally invariant manner.

Atomic-orbital electron repulsion integrals are also evaluated using a Mulliken approximation:

$$[ab|cd] = \frac{1}{2} S_{ab} S_{cd} \{ [aa|cc] + [bb|cc] + [aa|dd] + [bb|dd] \},$$

and  $[aa|bb]$  are evaluated by the modified point-charge formula of Mataga and Nishimoto [11]:

$$[aa|bb] = (R_{ab} + [2/(\gamma_a + \gamma_b)])^{-1},$$

where  $\gamma_a$  and  $\gamma_b$  are empirical parameters describing single-center electron repulsions for orbitals  $a$  and  $b$ .

After obtaining CI wavefunctions, charge and spin (i.e., first-order density) matrices were obtained for states of interest. The charge bond order matrix  $P$  is first generated in the MO basis. For a state formed from configurations  $\Psi_\mu$  by  $\sum_\mu c_\mu \Psi_\mu$ , the element  $P_{ij}$  is simply

$$P_{ij} = \sum_{\mu\nu} c_\mu^* c_\nu \langle \Psi_\mu | B | \Psi_\nu \rangle,$$

where  $B$  is the one-electron operator built from  $|j\rangle\langle i|$ . These one-electron matrix elements can be calculated from published spin-projection formulas [9]. After finding  $P$  in the MO basis, it is transformed to the atomic-orbital basis and presented as output.

Similar methods yield the spin bond-order matrix  $Q$ , with the exception that the one-electron operator  $B$  is now spin-dependent, being built from  $|j\rangle s_z \langle i|$ , where  $s_z$  is the operator for the  $z$  component of the electron spin. Convenient formulas for spin-projected matrix elements of spin-dependent operators for wavefunctions built from orthogonal MO's had not been published, and we therefore had to derive such formulas by specialization of more general relationships [12]. These formulas will be reported elsewhere.

The CI calculations described here were carried out for the fluoride complexes  $\text{FeF}_6^{3-}$  and  $\text{FeF}_4^{4-}$ , and we therefore needed  $h_a$  and  $\gamma_a$  parameters for Fe and F. Using ionization potentials, atomic energy levels, and STO atomic electron-repulsion integrals as a guide, we adjusted the parameter values for maximum consistency with experimental data. The parameters as finally adopted are included in Table 2.

### Isomer Shifts

The isomer shift in Mössbauer spectroscopy,  $\delta$ , depends upon the electron density at the nucleus under study,  $\rho(0)$ . Values of  $\delta$  are proportional to changes in  $\rho(0)$  from a reference compound:  $\delta = \alpha \Delta \rho(0)$ , where  $\alpha$  is known as the calibration constant. We are concerned here with application to  $\text{Fe}^{57}$ . We may estimate isomer shifts from our MO calculations, using the approximation that atomic orbitals on other centers have no density at the Fe nucleus. As the

Fe 3d and 4p orbitals also vanish at the Fe nucleus, the only contributing atomic orbital in our calculations is Fe 4s. However, the Fe inner-shell densities are also affected by the molecular structure and at least the Fe 3s contribution cannot be neglected. Following ideas developed by Flygare and Hafemeister [13], we estimate the Fe 3s contribution by considering its lack of orthogonality to the valence orbitals of neighboring ligands. This nonorthogonality can be interpreted as requiring a renormalization of the wavefunction, with a consequent change in the Fe 3s orbital density. We also consider differences in shielding associated with changes in the Fe 3d orbital occupancy.

The Fe 4s density at the nucleus is obtained by multiplying  $|\psi_{4s}(0)|^2$  by  $P_{4s,4s}$ , its coefficient as given in the bond-order matrix. There is some uncertainty as to the optimum value of  $|\psi_{4s}(0)|^2$ . Walker *et al.* [14] give the value  $2|\psi_{4s}(0)|^2 = 15 a_0^{-3}$  calculated using the (nonrelativistic) Fermi-Segré-Goudsmit formula and a relativistic correction term  $S'(Z)$  which is about 1.3 for iron [15]. This method of calculation assumes no screening of inner s electrons by an additional 4s electron. However, Blomquist *et al.* [16] report the smaller value  $|\psi_{4s}(0)|^2 = 6.7 a_0^{-3}$  for the electron density produced at the nucleus of an iron atom by a single 4s electron of configuration  $3d^6 4s^1$ , based on nonrelativistic Hartree-Fock calculations with the  $S'(Z)$  correction. In the present work we use both values for comparison.

The Fe 3s density at the nucleus, including 3d shielding effects but before the nonorthogonality correction, is taken as

$$2|\psi_{3s}(0)|^2 = 138.2 - 1.762(\sum_{3d} P_{3d,3d} - 5).$$

This formula is based on Hartree-Fock atomic-orbital values for various electronic configurations of Fe and its ions [17].

The nonorthogonality of Fe 3s to other orbitals has the effect of changing the coefficient of  $|\psi_{3s}(0)|^2$  away from 2, even though the Fe 3s orbital is assumed to remain fully occupied. The effect can be calculated by orthogonalizing the Fe 3s orbital to the other occupied MO's. The results are invariant with respect to the orthogonalization procedure chosen, and we therefore found it simplest to achieve orthogonality through changes of the Fe 3s orbital only, leaving all other MO's unaltered. This approach eliminates approximations attendant upon the use of the symmetric orthogonalization procedures, and which are only marginally justified for the degree of overlap encountered in the complexes presently under study. We therefore write

$$\phi_{3s} = N \left[ \psi_{3s} - \sum_{i \neq 3s} \langle \phi_i | \psi_{3s} \rangle \phi_i \right],$$

where

$$N = \left( 1 - \sum_{i \neq 3s} |\langle \phi_i | \psi_{3s} \rangle|^2 \right)^{-\frac{1}{2}},$$

the  $\phi_i$  are occupied MO's and  $\psi_{3s}$  is the 3s Hartree-Fock atomic orbital.

Now the density at the Fe nucleus may be written

$$\begin{aligned} \rho(0) &= P_{4s,4s} |\psi_{4s}(0)|^2 + 2N^2 |\phi_{3s}(0)|^2 \\ &= P_{4s,4s} |\psi_{4s}(0)|^2 + \frac{2}{1-A} |\psi_{3s}(0) - B\psi_{4s}(0)|^2 \end{aligned}$$

where  $A = \frac{1}{4} \sum_{ab} P_{ab} S_{a,3s} S_{3s,b}$  and  $B = \frac{1}{2} \sum_a P_{4s,a} S_{a,3s}$ . In using this expression for  $\varrho(0)$ , we assume that the overlap integrals are to be evaluated using Hartree-Fock atomic orbitals, as STO's give a qualitatively incorrect overlap with Fe 3s. We may then omit Fe 4s from the summations in  $A$  and  $B$ , as  $S_{3s,4s} = 0$ . We have omitted the 1s and 2s contributions to  $\varrho(0)$  because they are assumed to be constant for all the complexes under study.

### Quadrupole Splitting

The Mössbauer quadrupole splitting  $\Delta E_Q$  is proportional to the electric quadrupole moment  $Q$  of the Mössbauer nucleus and to the electric field gradient (there,  $q$ ):  $\Delta E_Q = \frac{1}{2} e^2 q Q$ . The field gradient is calculated here from contributions of the Fe 3d and Fe 4p orbitals, plus contributions from ligand orbitals estimated from the distribution of net atomic charge.

Complexes of symmetry  $O_h$  have no quadrupole splittings, while those of symmetry  $C_4$ , or  $D_{3h}$  have splittings given in the above-described approximation by

$$\Delta E_Q = \frac{1}{2} e^2 Q \left\{ (1-R) \langle r^{-3} \rangle \left( \sum_{3d} P_{3d,3d} f_{3d} + \sum_{4p} P_{4p,4p} f_{4p} \right) + (1-\gamma_\tau) \sum_a q_a (3z_a^2 - r_a^2) / r_a^5 \right\}.$$

The 3d and 4p summations are over the appropriate sets of Fe orbitals, the  $a$  summation is over all atoms other than Fe; and  $q_a$ ,  $z_a$ ,  $r_a$  are the net charge,  $z$  coordinate and distance (from Fe) of atom  $a$ . We actually limited the sum over  $a$  to the nearest neighbors of the Fe atom. The quantity  $\langle r^{-3} \rangle$  is the common radial factor resulting from taking the expectation value of  $(3z^2 - r^2)/r^5$ ; angular factors needed for individual 3d and 4p orbitals of varying magnetic quantum number are indicated as  $f_{3d}$ ,  $f_{4p}$ . These factors are  $f_{3d\pm 2} = 4/7$ ,  $f_{3d\pm 1} = -2/7$ ,  $f_{3d0} = -4/7$ ,  $f_{4p\pm 1} = 2/5$ ,  $f_{4p0} = -4/5$ . The quantities  $(1-R)$  and  $(1-\gamma_\tau)$  are Sternheimer shielding corrections [19];  $1-R$  represents the shielding effect experienced by charge on the Fe atom, while  $1-\gamma_\tau$  gives the antishielding factor to be applied to charge far removed from the Fe atom. In this work  $1-\gamma_\tau$  was assigned the value 10.1.

The major uncertainties in the calculation of  $\Delta E_Q$  are the assignments of values to  $Q$  and  $(1-R) \langle r^{-3} \rangle$ . The value of  $\langle r^{-3} \rangle$  should be expected to depend upon the electronic configuration of the Fe atom. The quantity  $\Delta E_Q^0 = \frac{1}{2} e^2 Q (1-R) \langle r^{-3} \rangle$  has been measured by McNab *et al.* [20] in an Fe dimer, with the result  $\Delta E_Q^0 = 4.05$  mm/sec. This dimer is interpreted as having Fe electronic configuration  $3d^6$ , for which  $(1-R) \langle r^{-3} \rangle$  has been calculated to have the value 3.3 a.u. [21]. These data yield for the relevant state of  $\text{Fe}^{57}$  the value  $Q = 0.21$  barn, which was the value adopted in the present work. The literature, however, contains other estimates of  $Q$  ranging from 0.17 barn [22] to 1.41 barn [23].

The compound  $\text{Fe}(\text{CO})_5$  has a calculated Fe electronic configuration  $1d^6 4s^{0.08} 4p^{0.43}$ , and we have assumed the 4s and 4p occupancy to have little effect on the value of  $\langle r^{-3} \rangle$ . We have consequently assumed that for  $\text{Fe}(\text{CO})_5$

we may use  $\Delta E_Q^0 = 4$  mm/sec, essentially the same value measured for a  $3d^6$  configuration. However, our other compound with quadrupole splitting,  $\text{Fe}(\text{CN})_5\text{NO}^{2-}$ , has a calculated Fe electronic configuration with a higher  $3d$  occupancy, and this will lead to a reduction in  $\langle r^{-3} \rangle$  [22] which we have accounted for by reducing  $\Delta E_Q^0$  by 10%.

### Results and Discussion

In Table 4 we present calculated data indicating some features of the charge distributions in the six iron complexes under study. Two of these complexes,  $\text{FeF}_6^{4-}$  and  $\text{FeF}_6^{3-}$ , are largely ionic, while the remaining four complexes have considerably more covalent character. The fluoride complexes are "high-spin" compounds, and were studied by the CI method; for the other complexes only Hückel calculations were made. As is generally true of well-calibrated semi-empirical studies, the methods used here probably suffice to give qualitatively reasonable charge distributions in the occupied MO's. In Table 5 we give experimental and calculated values of quantities related to spectroscopic observations.

Let us start by considering the Mössbauer isomer shifts  $\delta$ . Considerable previous work has dealt with the evaluation of isomer shifts and their relation to calculated charge densities  $\rho(0)$  at the  $^{57}\text{Fe}$  nucleus [24-35]. However, some of these studies differ from the present work in that they have not fully included the effect of changes in the Fe electronic configuration from one compound to another. Examining first the two fluoride complexes, we note that the  $\delta$  and  $\rho(0)$  values correspond to a calibration constant  $\alpha = \Delta\delta/\Delta\rho(0) = -0.38 \text{ a.u.}^3 \text{ mm/sec}$ , in qualitative agreement with the values  $-0.4$  of Ingalls *et al.* [24] and  $-0.34$  of Chappert *et al.* [25]. This  $\alpha$  value differs substantially, however, from the

Table 4 Diagonal bond-order matrix elements  $P_{aa}$  and atomic charges of iron complexes. Data calculated by Hückel method except for the fluoride complexes, for which spin-projected CI was used. Atomic charges obtained using centroid projection method described in the text. Orientation of complexes in the coordinate system is specified in Table 3

$P_{aa}$	$\text{Fe}(\text{CN})_5\text{NO}^{2-}$	$\text{Fe}(\text{CO})_5$	$\text{Fe}(\text{CN})_6^{3-}$	$\text{Fe}(\text{CN})_6^{4-}$	$\text{FeF}_6^{3-}$	$\text{FeF}_6^{4-}$
$a - d_{x^2-y^2}$	1.10	1.30	1.05	0.95	1.33	1.23
$d_{x^2-y^2}$	0.90	0.82	1.05	0.95	1.33	1.23
$d_{xz}, d_{yz}$	1.33	1.31	1.53	1.69	1.23	1.08
$d_{xy}$	1.83	1.30	1.53	1.69	1.23	2.00
$s$	0.10	0.08	0.11	0.15	0.15	0.14
$p_z$	0.22	0.17	0.23	0.24	0.15	0.13
$p_x, p_y$	0.20	0.26	0.23	0.24	0.15	0.13
Atomic charges						
Fe:	0.27	Fe: 0.40	Fe: 0.14	Fe: -0.03	Fe: 0.52	Fe: 0.40
N <sub>1</sub> :	-0.06	C <sub>1-3</sub> : 0.07	C: -0.31	C: -0.38	F: -0.59	F: -0.72
C <sub>1</sub> :	-0.16	C <sub>4-5</sub> : 0.08				
C <sub>2-5</sub> :	-0.14					



Table 5 Isomer shifts  $\delta$ , charge densities at Fe nucleus  $\rho(0)^a$ , quadrupole splittings  $1E_Q$ , ligand field splittings  $10Dq$ , and spin populations at Fe  $n_i$ . Calculated data by Hückel method except for the fluoride complexes, for which spin-projected CI was used, with  $S = 5/2$  for  $FeF_6^{3-}$ ,  $S = 2$  for  $FeF_6^{4-}$

Compound	$Fe(CN)_5NO^{-2}$	$Fe(CO)_5$	$Fe(CN)_6^{3-}$	$Fe(CN)_6^{4-}$	$FeF_6^{3-}$	$FeF_6^{4-}$
$\delta$ , exptl. (mm sec)	$-0.560 \pm 0.003^d$	$-0.44 \pm 0.01^e$	$-0.413 \pm 0.003^d$	$-0.333 \pm 0.005^d$	$0.687^f$	$1.59 \pm 0.011^f$
$\rho(0)$ , calc. ( $a_0^{-3}$ ) <sup>a</sup>	141.3	$140.7 \pm 0.2$	141	140.7	143.1	140.7
					144.8 <sup>b</sup>	142.2 <sup>b</sup>
$\Delta E_Q$ , exptl. (mm sec)		$140.3 \pm 0.2^a$			143.4 <sup>c</sup>	139.9 <sup>c</sup>
		$1.73^d, 1.85^e, 2^b$	140.5 <sup>a</sup>	140.2 <sup>a</sup>	142.4 <sup>a</sup>	140.0 <sup>a</sup>
		2.3				
Sign of $q$ , exptl.	Positive <sup>b</sup>	Positive <sup>1</sup>				
calc.	Positive	Positive				
$10Dq$ , exptl. ( $cm^{-1}$ )						
calc.						
$n_i$ , calc. ( $a_0^{-3}$ )	0	0	35000 <sup>m</sup> 36000 0	31000 <sup>a</sup> 30000 0	14000 <sup>o</sup> 1.80	7600 – 10000 <sup>o</sup> 22000 <sup>p</sup> 1.67

<sup>a</sup> Not including  $1s$  and  $2s$  contributions.

<sup>b</sup> Using Fe  $4s$  orbital charge rather than  $P_{4s,4s}$ ; see text

<sup>c</sup> Neglecting  $3d_{xy} - 2d_{xy}$  overlap integrals; see text.

<sup>d</sup> Kerler, W., Neuwirth, W., Fluck, E.: Z. Physik 175, 200 (1963). Values of  $\delta$  obtained with  $Co^{57}$  Pt source at 300 K, absorber temperature 143 K.

<sup>e</sup> Kerler, W., Neuwirth, W., Fluck, E., Kuhn, P., Zimmermann, B.: Z. Physik 173, 321 (1963). Values of  $\delta$  obtained with  $Co^{57}$  Pt source at 300 K, absorber temperature 158 K.

<sup>f</sup> Perkins, H. K., Hazony, Y.: Physic. Rev. B 5, 7 (1972). Values of  $\delta$  obtained with  $Co^{57}$  Pd source at 300 K, absorber temperature and  $\delta$  values extrapolated to 0 K.

<sup>g</sup> Costa, N. L., Danon, J., Zavier, R. M.: Physic. chem. Solids 23, 1783 (1962).

<sup>h</sup> Osterhuis, W. T., Lang, G.: J. chem. Physics 50, 4381 (1969); Absorber temperature 77 K.

<sup>i</sup> Ref. [d]: absorber temperature 201 K, absorber material:  $Fe(CO)_5$  in frozen solution.

<sup>j</sup> Ref. [28].

<sup>k</sup> Kienle, P.: Phys. Verh. 3, 33 (1963).

<sup>l</sup> Naiman, C. S.: J. chem. Physics 35, 323 (1961).

<sup>m</sup> Klück-Jørgensen, C.: Absorption spectra and chemical bonding in complexes, p. 110. London: Pergamon Press, Ltd. 1962.

<sup>n</sup> Oelkrug, D.: In: Structure and bonding, Vol. 9, Berlin: Springer-Verlag 1971.

<sup>o</sup> Shulman and Sugano (Ref. [32]) reported a value of about  $20,000\text{ cm}^{-1}$ .

<sup>p</sup> Individual entries marked "q" are calculated using the Blomquist value for  $|v_{4s}(0)|^2$  (see text). All other  $\rho(0)$  entries are based on the Walker value of  $|v_{4s}(0)|^2$ .

value  $-0.15$  obtained by Šimaňek and Šroubek [26] through consideration of  $\text{FeO}$  and  $\text{Fe}_2\text{O}_3$ , and a similar value obtained by Šimaňek and Wong [27] on  $\text{FeF}_2$  and  $\text{FeF}_3$ .

Upon examining the work of Šimaňek *et al.*, we note that they made several different approximations than were used in our work. In including the correction for orbital nonorthogonality in the fluorides, they neglected the overlap of  $\text{Fe } 3s$  and  $\text{F } 2s$  orbitals, retaining only the  $\text{Fe } 3s - \text{F } 2p\sigma$  overlap. They also assumed the fluorine  $2s$  orbitals to be fully occupied, whereas we took the fluorine orbital occupancies from our MO calculations. To determine more fully the results of these approximations, we repeated our calculations of  $q(0)$  neglecting the  $\text{Fe } 3s - \text{F } 2p\sigma$  overlap, but retaining our charge distributions as calculated. The result, shown in Table 5, leads to a reduction of the calibration constant to  $\alpha = 0.26 a_0^3 \text{ mm/sec}$ , halfway to the value of Šimaňek *et al.*

Šimaňek and Šroubek observed that the large change in  $\delta$  on going from  $\text{Fe}^{2+}$  to  $\text{Fe}^{3+}$  salts could be consistent with their calibration if the  $\text{Fe } 4s$  occupancy were considerably higher in the trivalent salts. However, this hypothesis does not agree with our MO calculations; we find very little increase, from  $P_{4s,4s} = 0.142$  in  $\text{Fe}^{2+}$  to  $P_{4s,4s} = 0.145$  in  $\text{Fe}^{3+}$ . If we look at the  $4s$  orbital charge as obtained from a Mulliken population analysis, the corresponding numbers are  $0.37$  and  $0.33$ . The value  $0.33$  for trivalent  $\text{Fe}$  is in good agreement with an earlier estimate of  $0.32$  made by Danon [28] and by Viste and Gray [29]. Our work suggests a  $\Delta q(0)$  between divalent and trivalent fluorides somewhat smaller than postulated by Šimaňek and Šroubek, and mainly due to changes in overlap integrals with internuclear distance and to changes in  $3d$  shielding. In summary, even for these relatively ionic compounds it may be a serious oversimplification to approach too closely descriptions such as  $\text{Fe}^{2+}$  and  $\text{F}^-$ .

To assess further the reliability of our calibration, we made one additional auxiliary calculation in which we used the Mulliken-population orbital charge instead of  $P_{4s,4s}$  as a measure of the  $\text{Fe } 4s$  orbital occupancy. This is probably a poorer measure of the  $4s$  contribution to  $q(0)$ , as the overlap charge causing an occupancy difference from  $P_{4s,4s}$  is for the most part not near the  $\text{Fe}$  nucleus. Even so, the calibration was only altered slightly, from  $-0.38$  to  $-0.35 a_0^3 \text{ mm/sec}$ .

We now turn to the more covalent compounds. Attempts to relate these to the fluorides fail, most probably because small inconsistencies in the parametrization of  $\text{F}$  in relation to  $\text{C}$ ,  $\text{N}$ , and  $\text{O}$  can produce systematic changes in charge distribution of a magnitude sufficient to obscure the tiny effect under study. However, meaningful comparisons can be made within the group of more covalent compounds.

Our first observation in these compounds is that their differences in  $q(0)$  are small, in agreement with the narrow range of observed  $\delta$ . If we allow for the uncertainty in the calculated  $q(0)$  for  $\text{Fe}(\text{CO})_5$  (this uncertainty comes from that in the  $\text{Fe}-\text{C}$  bond length) and if we use the Blomquist value for  $|\psi_{4s}(0)|^2$ , we find that the  $q(0)$  values are consistent with a calibration in the range  $\alpha = -0.31$  to  $-0.38 a_0^3 \text{ mm/sec}$ , in agreement with our analysis of the fluorides, and in agreement with our recent isomer shift calibration using multivalent states of  $^{57}\text{Fe}$  in  $\text{KMgF}_3$  [30]. Furthermore our molecular orbital study of Mössbauer

results on iron dissolved in solid noble gases [31] supports the choice of  $6.7 a_0^{-3}$  for the electron density produced at the nucleus of an iron atom by a single  $4s$  electron of configuration  $3d^6 4s^1$ .

The cyanide complexes have previously been studied by Shulman and Sugano [32], who attributed the small  $\Delta\delta$  between  $\text{Fe}(\text{CN})_6^{4-}$  and  $\text{Fe}(\text{CN})_6^{3-}$  to nearly unchanged  $P_{4s,4s}$  and  $\Sigma_{3d} P_{3d,3d}$  in both compounds. We find this to be nearly consistent with our MO studies, which show that a small change in  $q(0)$  due to change in  $P_{4s,4s}$  is nearly exactly compensated by a small change in  $\Sigma_{3d} P_{3d,3d}$ . In contrast to the fluoride compounds, the Fe-C bond distances remain almost unchanged on going from  $\text{Fe}(\text{CN})_6^{4-}$  to  $\text{Fe}(\text{CN})_6^{3-}$ , so that changes in overlap integrals are unimportant.

Thus far, we have not emphasized the fact that all our nonorthogonality corrections in  $q(0)$  have been based on Hartree-Fock atomic orbitals rather than STO's. The STO's seriously underestimate the overlaps and cannot realistically be used in this context. Moreover, the nonorthogonality of Fe  $3s$  and  $4s$  STO's would introduce a correction of questionable value.

To summarize, our study of both ionic and covalent iron complexes leads to an  $\text{Fe}^{57}$  Mössbauer calibration value in the range  $\alpha = -0.31$  to  $-0.38 a_0^3 \text{ mm/sec}$ .

The reliability of the MO studies can also be studied by examining other calculated quantities. In the present work, these include quadrupole splittings  $1E_Q$ , ligand field splittings  $10Dq$ , and atomic spin populations at  $\text{Fe } n_s$ . Two of the compounds under study have nonvanishing  $\Delta E_Q$ ; both calculated values are in qualitative accord with experiment. The  $10Dq$  values are also satisfactory, and the spin densities (only applicable to the high-spin compounds) look reasonable.

## References

1. Johnson, K. H., Smith, F. C.: *Chem. Physics Letters* **7**, 541 (1970).
2. Rein, R., Fukuda, N., Win, H., Clarke, G. A., Harris, F. E.: *J. chem. Physics* **45**, 4743 (1966).  
Rein, R., Clarke, G. A., Harris, F. E.: *Quantum aspects of heterocyclic compounds in chemistry and biochemistry*, II. Jerusalem: Israel Academy of Sciences and Humanities, 1970.
3. Cusachs, L. C.: *J. chem. Physics* **43**, S157 (1965).  
Cusachs, L. C., Reynolds, J. W.: *J. chem. Physics* **43**, S160 (1965).
4. Pople, J. A., Beveridge, D. L.: *Approximate molecular orbital theory*. New York: McGraw-Hill Book Co. 1970.
5. Clementi, E., Raimondi, D. L.: *J. chem. Physics* **38**, 2686 (1963).
6. Zerner, M., Gouterman, M., Kobayashi, H.: *Theoret. chim. Acta (Berl.)* **6**, 363 (1966).
7. Löwdin, P. O.: *Physic. Rev.* **97**, 1509 (1955).
8. So-called because many of the relationships satisfied by these coefficients were developed at the International Symposium on Quantum Chemistry and Solid State Physics sponsored by the University of Florida at Sanibel Island. A review of the mathematical properties of the coefficients is given by: Smith, V. H., Harris, F. E.: *J. math. Physics* **10**, 771 (1969).
9. Harris, F. E.: *J. chem. Physics* **46**, 2769 (1967).
10. Mulliken, R. S.: *J. Chim. physique* **46**, 497, 675 (1949).
11. Malaga, N., Nishimoto, K.: *J. phys. Chem.* **13**, 140 (1954).
12. Harris, F. E.: *Molecular Physics* **11**, 243 (1966); *Advances in quant. Chemistry* **3**, 61 (1966).
13. Flygare, W. H., Hafemeister, D. W.: *J. chem. Physics* **43**, 789 (1965).
14. Walker, L. R., Wertheim, G. K., Jaccarino, V.: *Physic. Rev. Letters* **6**, 98 (1961).
15. Shirley, D. A.: *Rev. mod. Physics* **36**, 339 (1964).

16. Blomquist, J., Roos, B., Sandboin, M.: *J. chem. Physics* **55**, 141 (1971).
17. Watson, R. E.: Solid state and molecular theory group, Technical Report No. 12, MIT, 1959 (unpublished).
18. Clementi, E.: Supplement to IBM, *J. Res. Dev.* **9**, 2 (1956).
19. Sternheimer, R. M.: *Physic. Rev.* **130**, 1423 (1963).
20. McNah, T. K., Micklitz, H., Barrett, P. H.: *Physic. Rev. B* **4**, 3787 (1971).
21. Ingalls, R.: *Physic. Rev.* **128**, 1155 (1962).
22. Freeman, A. J., Watson, R. L.: *Physic. Rev.* **131**, 2566 (1963).
23. Weissbluth, M., Maling, J. E.: Conference on the physical properties of iron proteins, J. E. Maling and M. Weissbluth, Eds., p. 171. Stanford, California: 1967.
24. Artman, J. O.: *Physic. Rev.* **133**, 541 (1966).
25. Ingalls, R., Drickamer, H. G., De Pasquah, G.: *Physic. Rev.* **155**, 165 (1967).
26. Ingalls, R.: *Physic. Rev.* **155**, 157 (1967).
27. Chappert, J., Regnard, J. R., Danon, J. R.: *C. R. Acad. Sci. Paris* **272**, 1070 (1971).
28. Šimaňek, I., Šroubek, Z.: *Physic. Rev.* **163**, 275 (1967).
29. Šimaňek, I., Wong, A. Y. C.: *Physic. Rev.* **166**, 348 (1968).
30. Danon, J.: In: Applications of the Mossbauer effect (International Atomic Energy Agency, Vienna, Austria, 1966), Series No. 50, p. 89.
31. Viste, A., Gray, H. B.: *J. inorg. Chem.* **3**, 1113 (1964).
32. Trautwein, A., Regnard, J. R., Harris, F. E., Maeda, Y.: *Physic. Rev. B* **7**, 947 (1973).
33. Trautwein, A., Harris, F. E.: *Physic. Rev. B* (1973).
34. Shulman, R. G., Sugano, S.: *J. chem. Physics* **42**, 39 (1965).
35. Kalvins, G. M.: Hyperfine interactions in excited nuclei. Goldring and Kalish, Eds., p. 523. New York: Gordon and Breach 1971.
36. Keune, W.: *Ann. Univ. Saraviensis* **8**, 93 (1970).
37. Pletner, I., Kolk, B.: *Physic. Letters* **34B**, 296 (1971).

Prof. Dr. F. E. Harris  
Department of Physics  
University of Utah  
Salt Lake City, Utah 84112  
USA

# PCILO Method for Excited States

## II. 2<sup>nd</sup> Order Corrected Transition Energies

J. Langlet and J. P. Malrieu

Institut de Biologie Physico-Chimique, Laboratoire de Biochimie Théorique associé au C.N.R.S.  
13, rue P. et M. Curie, Paris 5<sup>e</sup>

Received December 27, 1972

The zeroth order excitonic wave-function built previously is considered as a zeroth order wave-function for the excited state. The interaction with other singly, doubly and triply excited determinants is taken into account through a 2<sup>nd</sup> order perturbation process. A proper definition of the unperturbed Hamiltonian allows cancellation between the ground state and excited state series, and thus the direct calculation of transition energies. The complete localization of MO's in the CNDO approximation makes the calculation very rapid. The method is applied to the series of linear polyenes  $H-(CH=CH)_N-H$  ( $2 \leq N \leq 7$ ) with the CNDO-2 parametrization. The evolution of the excitonic wave-function is analyzed.

Die zuvor konstruierte excitonische Wellenfunktion nullter Ordnung wird als Wellenfunktion nullter Ordnung für den angeregten Zustand verwendet. Die Wechselwirkung mit anderen einfach, doppelt und dreifach angeregten Determinanten wird mittels Störungsrechnung 2. Ordnung berücksichtigt. Bei geeigneter Wahl des ungestörten Hamiltonoperators hebt sich der Grundzustand bei Berechnung der Übergangsenergien heraus, was auf ihre direkte Bestimmung hinausläuft. Die vollständige Lokalisierung der MO's hat zur Folge, daß bei Anwendung des CNDO-Verfahrens die Berechnung sehr schnell vonstatten geht. Die Methode wird auf die Reihe linearer Polyene des Typs  $H-(CH=CH)_N-H$  ( $2 \leq N \leq 7$ ) angewendet (CNDO/2-Parametrisierung). Die excitonische Wellenfunktion wird bezüglich der Zellenpopulation und deren Schwankungen untersucht.

On prend la fonction d'onde excitonique déjà construite comme fonction d'onde d'ordre zéro pour l'état excité. L'interaction avec les autres déterminants monoexcités, les déterminants di- et tri-excités est prise en considération par une perturbation au 2<sup>e</sup> ordre. Un choix judicieux de l'Hamiltonien non perturbé met en évidence d'importantes suppressions entre les séries de l'état excité et de l'état fondamental, et par conséquent le calcul direct des énergies de transition. Malgré le caractère multiconfigurationnel de  $\Psi_0$ , la localisation complète des OM rend le calcul extrêmement rapide dans les hypothèses CNDO. La méthode est appliquée à la série des polyènes linéaires  $H-(CH=CH)_N-H$  ( $N = 2 \text{ à } 7$ ). Analyse de la fonction d'onde excitonique en terme de populations de loge et de leur fluctuations.

The use of fully localized Molecular Orbitals (MO's) for the ground state energy calculation appeared to be very interesting from both computational and interpretative points of view [1]. The PCILO (Perturbative Configuration Interaction from Localized Orbitals) method [2] built along this scheme has been widely used for conformational studies. This method, at least with the CNDO [3] approximations on the atomic integrals, is much more rapid than the usual variational methods. The use of localized MO's for the excited states representations generally requires multiconfigurational wave functions. The well-known excitonic methods [4] use fully localized MO's and represent the excited

state as a linear combination of local single excitations. The linear combination results from the solution of the Configuration Interaction (CI) problem between the singly excited determinants. In the preceding paper of this series [5], the construction of such wave-functions have been analyzed for conjugated systems, and it has been proved that the  $\pi\pi^*$  transitions might be treated as linear combinations of  $\pi\pi^*$  local single excitations, the  $(\sigma - \pi)$  coupling which mixes the  $\pi\pi^*$  and  $\sigma\sigma^*$  excitations being treated by perturbational methods with a sufficient accuracy.

But such excitonic wave functions may only be considered as zeroth-order wave-functions. When one treats the ground state problem one takes into account all the singly and doubly excited determinants which interact with the zeroth-order ground state determinant, and which introduce respectively delocalization and correlation effects [2]. The linear combination of singly excited determinants will interact with the ground state determinant, and with numerous doubly and triply excited determinants. In order to calculate a reasonable transition energy, one must take into account in a coherent way both the interactions with the ground state determinant and with the excited state zeroth order wave-function. The present paper proposes a method which calculates second order corrected transition energies: the second order energy corrections are calculated from both the fully localized single determinant for the ground state and the excitonic multiconfigurational wave-function for the excited state. A convenient definition of the unperturbed Hamiltonian  $H^0$  allows important cancellations between the two series. Due to these cancellations, the computational time of the transition energy is analogous to that of the ground state energy calculations, despite the multiconfigurational character of the excited state and the very great number of doubly and triply excited configurations included in the process.

## 1. Method

The zeroth order wave-function  $\Psi_m^0$  is a linear combination of certain number of determinants, defining a subspace  $S$

$$\Psi_m^0 = \sum_{I \in S} c_{mI} \Phi_I, \quad (1)$$

For the  $\pi\pi^*$  transitions, the states  $\Phi_I$  will be the singly excited  $\pi\pi^*$  determinants

$$\Phi \begin{pmatrix} j^* \\ i \end{pmatrix} = a_j^\dagger a_i \Phi_0 \quad \Psi_m^0 = \sum_i \sum_{j \in \pi^*} c_{mij} \Phi \begin{pmatrix} j^* \\ i \end{pmatrix}. \quad (2)$$

The coefficients  $c_{mij}$  are obtained from the diagonalization of the CI matrix restricted to the  $S$  subspace, i.e. the  $\pi$  excitonic matrix. Therefore the interaction matrix elements between the zeroth wave functions of two  $\pi\pi^*$  excited states  $\Psi_m^0$  and  $\Psi_n^0$  are zero.

$$\langle \Psi_m^0 | H | \Psi_n^0 \rangle = 0.$$

The CI matrix restricted to subspace  $S$  is diagonal in the basis of the function  $\Psi_m^0$ .

Now one performs a change of the basis set of the CI in the subspace  $S$ ; the determinants outside of  $S$  are kept unchanged. Therefore the new basis is now

	$\phi_0$	$\psi_m^0$	other singly exc. deter.	doubly exc. deter.	triply exc. deter.	quadruply exc. deter.
$\phi_0$					0	0
$\psi_m^0$						0

Fig. 1. Structure of the interactions between the excitonic wave-functions  $\psi_m^0$  with the various functions of the new basis set of the CI matrix.  $\phi_0$  is the ground state single determinant

- the multiconfigurational wave functions  $\psi_m^0$  in the subspace  $S$ ,
- the single determinants  $\phi_j$  outside of  $S_0$ .

Since the singly excited determinants  $\phi_i^{(j*)}$  belonging to  $S$  interact with other singly excited determinants outside of  $S$  and some doubly and triply excited determinants, the states  $\psi_m^0$  also interact with these determinants, as illustrated in Fig. 1.

We shall take into account through a second order perturbation process the interactions of the excitonic wave-function  $\psi_m^0$  for the state  $m$  with the ground state determinant on one hand and with the various excited determinants outside of  $S$  on the other hand.

In the second order energy, the summation is restricted to the determinants outside of  $S$ :

$$c_m^2 = \sum_{I \notin S} \frac{\langle \psi_m^0 | H | \phi_I \rangle^2}{E_m^0 - E_I^0} \quad (3)$$

where  $E_m^0$  and  $E_I^0$  are the zeroth order energies associated with the state  $m$  and the determinant  $\phi_I$

$$H^0 \psi_m^0 = E_m^0 \psi_m^0 \quad (4)$$

$$H^0 \phi_I = E_I^0 \phi_I; \quad \text{for } I \notin S. \quad (5)$$

$H^0$  will be defined by these relations, and by a proper choice of  $E_m^0$  and  $E_I^0$ .

$E_I^0$  will be taken as the mean value of the exact Hamiltonian for the state  $\phi_I$ , according the Epstein-Nesbet partition of the total Hamiltonian [6].

$$E_I^0 = \langle \phi_I | H | \phi_I \rangle. \quad (6)$$

$E_m^0$  will not be taken according to the same definition which would lead to absurd dependencies of the transitions energies to the number of particles [7]. We use a "barycentric" definition of  $H^0$  for the state  $m$

$$E_m^0 = \sum_{I \in S} c_{mI}^2 \langle \phi_I | H | \phi_I \rangle \quad (7)$$

$E_m^0$  differs from the eigenvalue  $E'_m$  of the excitonic matrix. If  $P_S$  is the projector on the subspace  $S$ ,

$$P_S H P_S \psi_m^0 = E'_m \psi_m^0 \quad (8)$$

$$E'_m = \langle \psi_m | H | \psi_m \rangle = \sum_I \sum_{J \in S} c_{mI} c_{mJ} \langle \phi_I | H | \phi_J \rangle. \quad (9)$$

As will be shown further on, this definition of  $E_m^0$  will lead to important cancellations in the calculation of the transition energy.

The second order energy may be developed.

$$\begin{aligned}
 \epsilon_m^2 = & \sum_{I \notin S} \sum_{J \in S} \epsilon_{mJ}^2 \frac{\langle \Phi_J | H | \Phi_I \rangle^2}{E_m^0 - E_I^0} \\
 + & \sum_{I \notin S} \sum_{J \in S} \sum_{K \in S} \epsilon_{mJ} \epsilon_{mK} \frac{\langle \Phi_J | H | \Phi_I \rangle \langle \Phi_J | H | \Phi_K \rangle}{E_m^0 - E_I^0}
 \end{aligned} \quad (10)$$

In this expression, the first terms will be called diagonal terms, and the second ones will be called cross-terms. Since one is supposed to work on a given excited state, the subscript  $m$  will be omitted here after.

Among the configurations  $I$  outside of  $S$ , one finds first the ground state configuration, which leads to the correction

$$a = \underbrace{\sum_I \sum_K \sum_{I'} \sum_{K'}}_{\pi} 2c_{I'K'} c_{IK} \frac{F_{I'K'} F_{IK}}{E_{I'}^0 - E_I^0} \quad (11)$$

where in  $F_{IJ} = \langle i | F | j \rangle^*$ ,  $F$  is the Fock operator. This Fock operator reduces to its mono-electric part if  $i$  and  $j$  are different when the MO's are fully localized in the C'NDO hypotheses

The subspace outside of  $S$  also includes singly excited configurations.

If  $S$  is built of singly excited  $\left(\pi^*\right)$  configurations, the singly excited configurations outside of  $S$  belong to two groups:

the  $\left(\sigma^*\right)$  singly excited configurations, which reduce to the "polarization"  $\left(\sigma^*\right)$  configurations in the PCIL O-C'NDO hypotheses,

the  $\left(\pi^*\right)$  and  $\left(\pi\right)$  configurations, which only play a role in non-planar systems. The second order effect of the singly-excited configurations is given in Appendix.

According to the Slater's rules, a singly excited configuration  $\Phi\left(i^*\right)$  only interacts with the doubly excited determinants which involve either  $i$  or  $i^*$  in their excitation process, i.e.  $\Phi\left(\begin{smallmatrix} i^* & q^* \\ i & p \end{smallmatrix}\right)$  or  $\Phi\left(\begin{smallmatrix} j^* & q^* \\ i & p \end{smallmatrix}\right)$ . But in the C'NDO hypotheses, the full localization implies

$$i^* = j^* \quad \text{to get a non zero } \left\langle \Phi\left(\begin{smallmatrix} j^* \\ i \end{smallmatrix}\right) \middle| H \middle| \Phi\left(\begin{smallmatrix} i^* & q^* \\ i & p \end{smallmatrix}\right) \right\rangle \text{ matrix element,}$$

or

$$i = i \quad \text{to get a non zero } \left\langle \Phi\left(\begin{smallmatrix} j^* \\ i \end{smallmatrix}\right) \middle| H \middle| \Phi\left(\begin{smallmatrix} j^* & q^* \\ i & p \end{smallmatrix}\right) \right\rangle \text{ matrix element.}$$



The doubly excited determinants which belong to the summation over  $l$  in Eq. (3), actually involve one  $\begin{pmatrix} \pi^* \\ \pi \end{pmatrix}$  excitation and one  $\begin{pmatrix} q^* \\ p \end{pmatrix}$  excitation, where  $p$  and  $q$  may be  $\sigma$  or  $\pi$  MO's. If  $n_\pi$  is the number of  $\pi$  bonds, and  $n$  the total number of bonds, the number of doubly excited determinants involved in the 2nd order correction of the excited state is proportional to  $n_\pi^2 \times n^2$ .

The triply excited determinants which interact with a given  $\Phi \begin{pmatrix} i^* \\ i \end{pmatrix}$  singly excited determinant may be written as  $\Phi \begin{pmatrix} j^* & q^* & s^* \\ i & p & r \end{pmatrix}$  according to the Slater's rules.

But the CNDO hypotheses and the full localization of the MO's implicate

$$p = q \quad \text{and} \quad r = s \quad (\text{or } p = s \text{ and } r = q)$$

since

$$\left\langle \Phi \begin{pmatrix} j^* & q^* & s^* \\ i & p & r \end{pmatrix} \middle| H \middle| \Phi \begin{pmatrix} i^* \\ i \end{pmatrix} \right\rangle = \langle pr | q^* s^* \rangle - \langle pr | s^* q^* \rangle.$$

(Once more the number of triply excited determinants interacting with the zeroth order description of the excited state is proportional to  $n_\pi^2 \times n^2$ .)

One may already notice at this stage the benefit of the localized model; in a delocalized framework, there would be  $n^3$  triply excited configurations  $\Phi \begin{pmatrix} j^* & q^* & s^* \\ i & p & r \end{pmatrix}$  interacting with a given singly excited determinant  $\Phi \begin{pmatrix} i^* \\ i \end{pmatrix}$ , even in the CNDO hypotheses. This feature already balance the disadvantage of having a multiconfigurational zeroth order wave-function for the excited state.

## 2. Cancellations between the Ground State and Excited States 2<sup>nd</sup> Order Corrections

One knows that if one uses the same set of MO's for the ground state the excited state, and if the excited state zeroth order wave-function is a single configuration, important cancellations occur between the perturbation series of the ground state and of the excited state [8]; for instance in the second order energies, the effect of most of the triply excited determinants upon the excited configuration are equal to the effect of most of the doubly excited determinants upon the ground state determinant.

We shall demonstrate that this phenomenon, which may be called "cancellation of common diagrams in transition energies", also occurs in the excitonic treatment as long as a correct definition of  $H^0$  has been chosen.

Let us consider for instance the effect of the delocalization single excitations  $p \rightarrow q^*$  ( $p \neq q$ ) on the ground and excited states. On the ground state these excitations lead to the so called delocalization 2<sup>nd</sup> order energy [2]

$$e_0^2 \text{ del} = \sum_{p \neq q} \sum_q 2F_{pq^*}^2 / \left( E_0^0 - E^0 \begin{pmatrix} q^* \\ p \end{pmatrix} \right).$$

On the excited state, such excitations are also possible. They will lead to some cross terms which will be analyzed in the Appendix and diagonal terms

$$e_1^2 \text{ del} = \sum_i \sum_j c_{ij}^2 \sum_{p \neq q} 2 \left\langle \Phi \left( \begin{smallmatrix} j^* \\ i \end{smallmatrix} \right) \middle| H \middle| \Phi \left( \begin{smallmatrix} j^* & q^* \\ i & p \end{smallmatrix} \right) \right\rangle^2 / (E' - E^0 \left( \begin{smallmatrix} j^* & q^* \\ i & p \end{smallmatrix} \right)) - R \quad (12)$$

where  $R$  is a remainder triple summations where  $p$  or  $q = i$  or  $j$ ; this term occurs because when  $p$  or  $q$  is equal to  $i$  or  $j$ , there is only one excitation instead of two.

$$e_1^2 \text{ del} + R = \sum_i \sum_j c_{ij}^2 \sum_{p \neq q} 2 F_{pq}^2 / (E' - E^0 \left( \begin{smallmatrix} j^* & q^* \\ i & p \end{smallmatrix} \right))$$

Let us assume

$$E^0 \left( \begin{smallmatrix} j^* & q^* \\ i & p \end{smallmatrix} \right) - E_0^0 = E^0 \left( \begin{smallmatrix} j^* \\ i \end{smallmatrix} \right) - E_0^0 + E \left( \begin{smallmatrix} q^* \\ p \end{smallmatrix} \right) - E_0^0. \quad (13)$$

Then

$$E' - E^0 \left( \begin{smallmatrix} j^* & q^* \\ i & p \end{smallmatrix} \right) = E' - E^0 \left( \begin{smallmatrix} j^* \\ i \end{smallmatrix} \right) - E^0 \left( \begin{smallmatrix} q^* \\ p \end{smallmatrix} \right) + E_0^0$$

$$\left| E' - E^0 \left( \begin{smallmatrix} j^* & q^* \\ i & p \end{smallmatrix} \right) \right| \left[ 1 - \frac{E' - E^0 \left( \begin{smallmatrix} j^* \\ i \end{smallmatrix} \right)}{E_0^0 - E^0 \left( \begin{smallmatrix} q^* \\ p \end{smallmatrix} \right)} \right]. \quad (14)$$

Since  $E'$  is the barycenter of the  $\left( \begin{smallmatrix} j^* \\ i \end{smallmatrix} \right)$  single excitations, the quantity  $E' - E^0 \left( \begin{smallmatrix} j^* \\ i \end{smallmatrix} \right)$  is small with respect to the denominator  $E_0^0 - E^0 \left( \begin{smallmatrix} q^* \\ p \end{smallmatrix} \right)$  which represents a single excitation energy. Therefore, a limited development gives

$$\left| E' - E^0 \left( \begin{smallmatrix} j^* & q^* \\ i & p \end{smallmatrix} \right) \right|^{-1} \simeq \left| E_0^0 - E^0 \left( \begin{smallmatrix} q^* \\ p \end{smallmatrix} \right) \right|^{-1} \left[ 1 + \frac{E' - E^0 \left( \begin{smallmatrix} j^* \\ i \end{smallmatrix} \right)}{E_0^0 - E^0 \left( \begin{smallmatrix} q^* \\ p \end{smallmatrix} \right)} \right] \quad (15)$$

Thus

$$e_1^2 \text{ del} + R = \sum_i \sum_j c_{ij}^2 \sum_{p \neq q} \frac{2 F_{pq}^2}{E_0^0 - E^0 \left( \begin{smallmatrix} q^* \\ p \end{smallmatrix} \right)} \left[ 1 - \frac{E' - E^0 \left( \begin{smallmatrix} j^* \\ i \end{smallmatrix} \right)}{E_0^0 - E^0 \left( \begin{smallmatrix} q^* \\ p \end{smallmatrix} \right)} \right] \quad (16)$$

$$= \sum_{p \neq q} \sum_j \frac{2 F_{pq}^2}{E_0^0 - E^0 \left( \begin{smallmatrix} q^* \\ p \end{smallmatrix} \right)} \sum_i c_{ij}^2$$

$$+ \sum_{p \neq q} \sum_j \frac{2 F_{pq}^2}{E_0^0 - E^0 \left( \begin{smallmatrix} q^* \\ p \end{smallmatrix} \right)} \sum_i c_{ij}^2 \left[ E' - E^0 \left( \begin{smallmatrix} j^* \\ i \end{smallmatrix} \right) \right]. \quad (17)$$

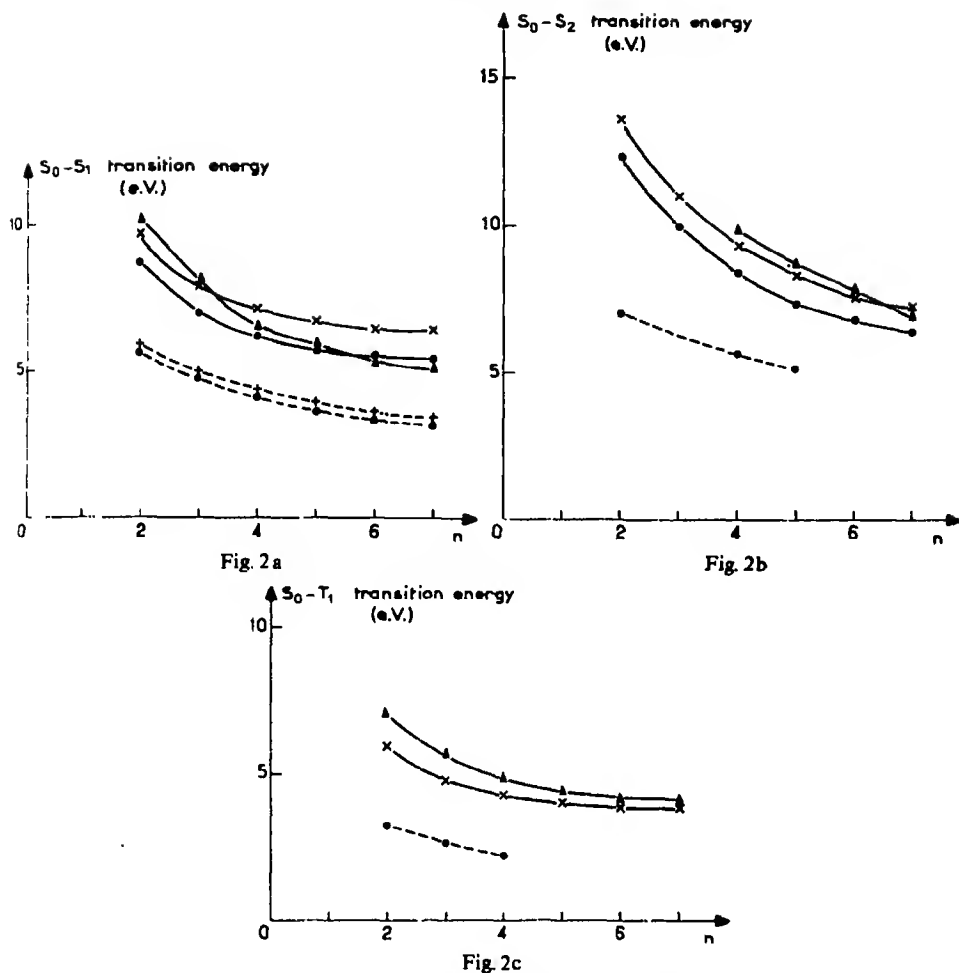


Fig. 2. Evolution of the experimental and calculated transition energies  $S_0-S_1$  towards the first singlet excited state (2a),  $S_0-S_2$  towards the second singlet excited state (2b),  $S_0-T_1$  towards the first triplet excited state (2c). + ... + experimental values in vapor state, . . . experimental values in solution,  $\times$  —  $\times$   $E_i^0$  zeroth order transition energies,  $\bigcirc$  —  $E_i^{2,\sigma}$  zeroth order transition energies corrected by the  $\binom{\sigma^*}{\sigma}$  singly excited determinants,  $\Delta$  —  $\Delta E_i^2$  calculated transition energies after the full second order correction

The normalization condition and the definition of  $E'$  [Eq. (8)] imply  $\sum_i \sum_j c_{ij}^2 = 1$  and  $E' = \sum_i \sum_j c_{ij}^2 E^0 \binom{j^*}{i}$ . Therefore  $\varepsilon_1^2 \text{ del} + R = \varepsilon_0^2 \text{ del}$ .

This demonstration requires Eq. (13) to be valid. This is verified if  $H^0$  for the ground state is the sum of mono-electronic hamiltonians, for instance in the Moller-Plesset definition of  $H^0$  [9]; with such a definition the transition energies are simply differences between mono-electronic energies, and are therefore additive. With the Epstein-Nesbet definition of  $H^0$  [6], Eq. (13) is only approximate.

The practical consequence of this cancellation is that if  $\epsilon_0^2$  del has been already calculated for the second order ground state energy, through an  $n^2$  summation, the calculation of the delocalization effects on the transition energy only requires the calculation of  $R$ , through a  $n_\pi^2 \times n$  summation and of the cross terms. The number of cross terms contributions is demonstrated in the Appendix to increase like  $n_\pi^3 \times n$  at most. The cancellation of common diagrams reduces the computation time from  $n_\pi^2 n^2$  to  $n_\pi^3 n$ . The same considerations might be developed for the 2<sup>nd</sup> order correlation effects on ground state, resulting from the interaction with the doubly excited determinants, and on the excited state, resulting from its interaction with the triply excited determinants.

### 3. Calculated Transition Energies

We have studied the all-trans linear polyenes  $C_{2N}H_{2N+2}$  from  $N = 2$  to  $N = 7$ . Most of experimental spectra have been obtained in liquid phase in solvents such as hexane or isooctane [10]. But for butadiene, hexatriene and octatetraene, spectra in gaseous phase have been given [11] showing a bathochromic solvent effect of 0.2–0.3 eV.

In our calculations, all bond angles are taken equal to 120° and the bond lengths are those calculated by Julg [12].

#### a) $S_0 - S_1$ Transitions Energies

Table I gives the zeroth order transition energies  $E_i^0$ , i.e. the transition energies calculated after the diagonalization of the  $(\pi)$  excitonic matrix,  $E_i^{2,m}$  the transition energies including the second order correction of the  $\sigma$  monoexcited configurations  $\Phi\left(\begin{smallmatrix} \sigma^* \\ \sigma \end{smallmatrix}\right)$  on the excited state,  $E_i^2$  the transition energies obtained after the full second order correction on both states, and  $E_i$  the experimental transition energies ( $E_{i,v}$ ,  $E_{i,s}$  are obtained respectively in vapor phase and in solution).

Figure 2a shows the evolutions of  $E_i^0$ ,  $E_i^{2,m}$ ,  $E_i^2$  and the experimental ( $E_{i,v}$  and  $E_{i,s}$ ) transition energies with  $N$ , the number of double bonds.

The curve  $E_i^0$  parallels the experimental one, but lies several electronvolts too high.

The curve  $E_i^{2,m}$  runs also quite parallel to the experimental curves, the calculated transition energies are always lower than the calculated  $(\pi)$  excitonic transition energies  $E_i^0$ , due to the negative effect of the  $(\sigma)$  singly excited configurations.

The effect of the singly excited configurations  $\Phi\left(\begin{smallmatrix} \sigma^* \\ \sigma \end{smallmatrix}\right)$  is rather important in small polyenes as noticed by Herzberg *et al.* [12], Dunning and Mc Koy [14] and Giessner and Pullman [15]. Denis and Malrieu [16] had demonstrated that this effect decreases as  $N^{-1}$  when using the usual delocalized description. In our model, one notices only a small decrease of this correction (1.05–0.95) when  $N$  varies from 2–7 (Table I). The value of this correction tends towards a *non-zero* constant. This difference between the delocalized and excitonic models is due to

Table 1. Experimental and calculated transition energies for  $H-(CH=CH)_N-H$  polyenes from  $N = 2$  to  $N = 7$ 

<i>N</i>	State	Experimental values	$E_i^0$	$E_i^{2,m}$	$E_i^2$	<i>s</i> 1	<i>s</i> 2	<i>d</i> 1	<i>d</i> 2	<i>cs</i>	<i>cd</i>
2	S1	5.9 (5.7)	9.69	8.65	10.09	+0.39	-1.38	+0.40	+0.57	+1.23	+0.23
	S2		13.69	12.34							
	T1	3.20	5.99	5.99	6.98	+0.66	-0.65	+0.96	+0.48	-0.47	0
3	S1	5 (4.75)	7.94	6.96	7.95	+0.75	-1.76	+0.49	+0.60	+0.64	+0.27
	S2		10.99	9.99							
	T1	2.60	4.81	4.81	5.65	+1.12	-0.97	+1.05	+0.52	-0.97	0
4	S1	4.45 (4.20)	7.15	6.18	6.59	+0.92	-2.05	+0.54	+0.62	+0.12	+0.29
	S2	(5.84)	9.38	8.36	9.86	+0.70	-2.07	+0.55	+0.62	+1.48	+0.10
	T1	2.20	4.30	4.30	4.84	+1.27	-1.20	+1.09	+0.53	-1.16	0
5	S1	(3.75)	6.75	5.80	5.83	+0.99	-2.22	+0.57	+0.63	-0.25	+0.31
	S2	(5.27)	8.39	7.40	8.72	+0.84	-2.15	+0.56	+0.63	+1.20	+0.17
	T1		4.06	4.06	4.40	+1.33	-1.31	+1.10	-1.54	-1.32	0
6	S1	(3.45)	6.63	5.58	5.36	+1.03	-2.29	+0.58	+0.63	-0.49	+0.31
	S2		7.77	6.81	7.79	+0.92	-2.24	+0.57	+0.63	+0.85	+0.22
	T1		3.93	3.93	4.15	+1.35	-1.37	+1.11	+0.55	-1.42	0
7	S1	(3.18)	6.40	5.45	5.04	+1.05	-2.33	+0.59	+0.63	-0.66	+0.31
	S2		7.35	6.40	7.08	+0.97	-2.30	+0.59	+0.63	+0.52	+0.25
	T1		3.86	3.86	4.00	+1.37	-1.41	+1.11	+0.56	-1.48	0

The experimental transition energies as those obtained in solution (values between brackets) and in vapor phase.

$E_i^0$  = Zeroth order transition energies.

$E_i^{2,m}$  = Zeroth order transition energies corrected to the 2<sup>nd</sup> order by the  $\left(\frac{\sigma^*}{\sigma}\right)$  singly excited configurations.

$E_i^2$  = 2<sup>nd</sup> order corrected transition energies.

*s*1 = diagonal 2<sup>nd</sup> order correction due to the  $u_p^+ u_p$  delocalization single excitations.

*s*2 = diagonal 2<sup>nd</sup> order correction due to the  $u_p^+ u_p$  polarization single excitations.

*d*1 = diagonal 2<sup>nd</sup> order correction due to the  $u_p^+ u_q u_p^+ u_p$  double excitations.

*d*2 = diagonal 2<sup>nd</sup> order correction due to the  $u_p^+ u_p u_p^+ u_p$  double excitations.

*cs* and *cd* are the cross terms for the single and double excitations.

the non vanishing weight of the polarization local excitation  $\left(\frac{\pi_i^*}{\pi_i}\right)$  in the excitonic model and will be discussed in details in a further publication [17].

Figure 3 gives the evolution of the second order correction due to the single excitations, the double excitations and the full second order correction.

The effect of the single excitations on the transition energies decreases from a positive value for  $N = 2$  (+0.23) to a negative value which tends to a constant for  $N > 7$ . This effect can be analyzed as follows:

- The delocalization excitations  $u_q^+ u_p$  ( $p \neq q$ ) are all possible on the ground state determinant, while some of them are impossible when acting on the excited determinants. Since in the CNDO-PCILO hypotheses, the matrix elements are the same, the final diagonal correction is positive (see 1<sup>st</sup> term of B 1/*a* and B 3/*a* of the Appendix). This correction tends to a nearly constant value for  $N > 5$  (see Table 1).

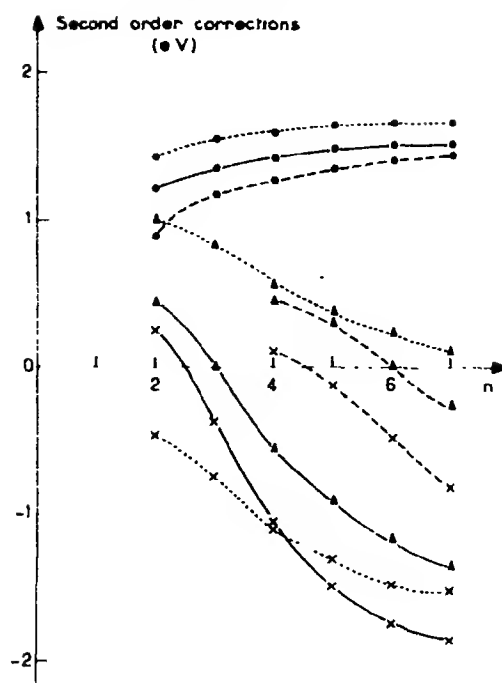


Fig. 3 Evolution with  $N$  of the various second order corrections upon the transition energy. Correction due to the single excitations upon the first singlet  $S_1$   $\times$   $\times$ , the second singlet  $S_2$   $\times$   $\times$ , the first triplet  $T_1$   $\times$   $\times$ . Correction due to the double excitations upon the first singlet  $S_1$   $\bullet$   $\bullet$ , the second singlet  $S_2$   $\bullet$   $\bullet$ , the first triplet  $T_1$   $\bullet$   $\bullet$ . Total second order correction upon the first singlet  $\blacktriangle$   $\blacktriangle$ , the second singlet  $\blacktriangle$   $\blacktriangle$ , the first triplet  $\blacktriangle$   $\cdots$   $\blacktriangle$ .

The polarization excitations  $a_p^\dagger a_p$  give stronger interactions with the excited determinants  $\binom{q^*}{q}$  than with the ground-state determinant (2<sup>nd</sup> term of the contribution B 3/a of Appendix) and their diagonal element is therefore negative. The variation of this correction is rather important but tends to a constant.

The non-diagonal corrections (due to the interaction of the same doubly excited determinants with two singly excited determinants) are more difficult to analyze, and depend on the sign changes of the excitonic wave function.

The double excitations increase the transition energy by a quantity (curve C) which increases slightly from  $N=2$  to  $N=4$ , and remains constant for  $N \geq 4$ . This effect is mainly due to impossibility of making an excitation  $a_q^\dagger a_q a_p^\dagger a_p$  on a determinant  $\Phi \binom{j^*}{i}$  if  $p$  or  $q$  are equal to  $i$  or  $j$ .

The final full second order effect is positive for  $N < 3$  then it becomes negative and tends to a constant value which is not yet obtained for  $N=7$ . This correction

decreases the parallelism of the calculated and experimental transition energies curves, at least for the small values of  $N^1$ .

One may compare  $E_t^2$ , including the full 2<sup>nd</sup> order correction, with  $E_t^{2,m}$  which represents the usual CI of singly excited states. One notices on Fig. 2a that for  $N=2$  to  $N=4$ ,  $E_t^2 > E_t^{2,m}$ , while for  $N > 5$ ,  $E_t^2 < E_t^{2,m}$ . In the region  $3 < N < 6$  (usual conjugated systems) the difference between the full 2<sup>nd</sup> order corrected transition energy and the usual singly excited states CI is rather small, which may explain the success of this approximation.

### b) $S_0 - S_2$ Transition Energy

The transition  $S_0 - S_2$  toward the 2<sup>nd</sup> singlet state is reported in Fig. 2b and Table 1. The results  $E_t^2$  are not reported for  $N=2$  and 3 since a near degeneracy occurs between the excitonic wave function  $\Psi_m^0$  and the doubly excited determinants of the type  $\begin{pmatrix} j^* & i^* \\ i & j \end{pmatrix}$ . For larger polyenes the degeneracy occurs with higher excited states.

The calculated transition energies are too high, worse than for the  $S_0 - S_1$  transition, but the various effects are rather similar, except that the fully 2<sup>nd</sup> order corrected transition energy  $E_t^2$  is always close to  $E_t^0$ , the excitonic transition energy, and larger than  $E_t^{2,m}$ , the singly excited CI result.

As concerns the effect of the singly excited determinants  $\begin{pmatrix} \sigma^* \\ \sigma \end{pmatrix}$ , two factors compete: the second excited state is more polar than the first one, and thus interacts less with the  $\begin{pmatrix} \sigma^* \\ \sigma \end{pmatrix}$  determinants, but it lies higher in energy, and the denominator energies are smaller.

The single excitations lower more the  $S_0 - S_1$  transition energy than the  $S_0 - S_2$  transition energy. A detailed analysis shows that this is predominantly due to the cross terms and is difficult to analyze. The double excitations have a very small ( $\sim 0.1$  eV) and decreasing effect on the spacing between the two lowest singlet excited states. The full 2<sup>nd</sup> order correction increases the spacing between these excited states.

### c) $S_1 - T_1$ Energy Difference

Figure 2c gives to evolution with  $N$  of the zeroth order and the second order transition energy is  $S_0 - T_1$ .

The singlet-triplet spacing is known experimentally for  $N=2$  to 4. The  $\pi$  excitonic treatment gives too large a spacing. This spacing is diminished under the influence of the  $\begin{pmatrix} \sigma^* \\ \sigma \end{pmatrix}$  monoexcited states by an almost constant quantity

<sup>1</sup> All the results given here take into account the cancellation of common diagrams demonstrated in Section 2. This cancellation is only approximate (especially in the Epstein-Nesbet definition of  $H^0$ ). Calculations performed without taking benefit of these cancellations show that they are well satisfied for double excitations, but the "common" single excitations may introduce a correction up to 0.5 eV.

					4	0.22	1.80	5.76	(12.53)		
					3	1.44	11.97	(10.82)	(14.06)		
					2	4.58	20.25	(1.80)	(2.86)		
					1	3.96	(7.62)	(0)	(0.26)		
					1	2	3	4			
20.98	(24.90)	1	2	10	11	83	(22.28)				
					2	10.37	(0.0)	(23.33)			
29.05	(25.00)	1	9	61	(1.49)	(2.89)					
1	2	1	2	3							
58	10	(49.80)				51	36	(44.56)			
41	90	(50.20)				48	64	(55.44)			
					6	0	0.02	0.17	0.74	1.77	(4.04)
0.02	0.23	1.16	3.03	(6.92)	5	0.02	0.23	1.51	6.05	(14.90)	(4.80)
0.18	1.80	8.88	(16.40)	(8.06)	4	0.11	1.30	7.84	(4.08)	(7.90)	(1.44)
0.79	8.00	(0.0)	(6.55)	(2.10)	3	0.46	5.11	14.82	(0.30)	(1.12)	(0.25)
2.28	12.04	(1.44)	(0.50)	(0.30)	2	1.27	7.40	(4.84)	(0.03)	(0.08)	(0.03)
1.99	(7.12)	(0.61)	(0.01)	(0.03)	1	1.12	(5.15)	(1.00)	(0.03)	(0.0)	(0.0)
1	2	3	4	5	1	2	3	4	5	6	



Table 2. Mean  $\pi$  population, ( $\bar{n}$ ) and  $\pi$  charges fluctuations ( $\sigma$ ) in the double bonds loges for the excitonic description of the two first singlet excited states

N	State	Loge 1		Loge 2		Loge 3		Loge 4	
		$\bar{n}$	$\sigma$	$\bar{n}$	$\sigma$	$\bar{n}$	$\sigma$	$\bar{n}$	$\sigma$
2	$S_1$	2	0.65						
	$S_2$	2	0.71						
3	$S_1$	1.99	0.51	2.02	0.67				
	$S_2$	2.22	0.51	1.57	0.51				
4	$S_1$	1.98	0.38	2.01	0.61				
	$S_2$	2.10	0.49	1.90	0.52				
5	$S_1$	1.99	0.19	2	0.50	2.02	0.60		
	$S_2$	2.03	0.43	2.04	0.49	1.87	0.44		
6	$S_1$	1.99	0.21	1.99	0.42	2.02	0.56		
	$S_2$	2.01	0.36	2.04	0.49	1.95	0.41		
7	$S_1$	1.99	0.17	1.99	0.34	2.00	0.30	2.05	0.54
	$S_2$	2.00	0.21	2.02	0.45	2.00	0.43	1.95	0.32

( $\sim 1$  eV) since in the CNDO approximations, the triplet  $\pi$  and triplet  $\sigma$  configurations do not interact [16]. The single excitations stabilize more the triplet excited state  $T_1$  than the ground state  $S^0$ , but this stabilization varies more slowly than the corresponding stabilization for the singlet excited state  $S_1$ , so that the  $S_1 - T_1$  distance is reduced. The double excitations only give a small decrease ( $\approx 0.2$  eV) in the  $S_1 - T_1$  spacing.

#### 4. Analysis of the Wave Functions

##### a) Ionic versus Neutral Structures

One may analyse the evolution of the relative weight of ionic (delocalization) versus neutral (polarization) structures in the zeroth-order excitonic wavefunction. It appears from Fig. 4 that the first singlet is more neutral than the second one, but the difference decreases when  $N$  increases. One may notice that the weight of neutral structures in the first singlet excited state tends towards a constant about 46%. This fact is very important because it introduces a qualitative difference with the usual delocalized MO descriptions of excited states and will be demonstrated and discussed in detail elsewhere [17].

In the triplet states, the neutral structures have larger weight. This is mainly due to the fact that the triplet  ${}^3\binom{i^*}{i}$  polarization configurations have lower energies than the singlet  ${}^1\binom{i^*}{i}$  polarization configurations, while the  ${}^3\binom{j^*}{i}$  and  ${}^1\binom{j^*}{i}$  have the same energy in the CNDO approximations.

##### b) Localization of the Excitation on the Nuclear Skeleton

Qualitatively, from Fig. 4, the first singlet excitations appears to be located on the center of the molecule (bond  $N/2$  and  $N/2 + 1$  if  $N$  is even ( $N + 1/2$  if  $N$  is

odd), the second excitations being more probable on the neighbour bonds (bonds number  $N/2 - 1$  and  $N/2 + 2$  when  $N$  is even  $(N - 1)/2$  and  $(N + 3)/2$  when  $N$  is odd).

*c) The Populations in the Bond-Loges and their Fluctuations*

Table 2 gives the  $\pi$  bond charges, i.e. the mean  $\pi$  populations or mean numbers of  $\pi$  electrons per double bond in the two lowest singlet excited states. The lowest singlet state appears to be almost neutral, in agreement with the pairing theorem in the delocalized description. The fact that the mean population is almost 2.0 does not mean that the polar charge transfer structures play no role. It simply means that the  $i \rightarrow j^*$  and  $j \rightarrow i^*$  excitations have almost equal weights.

(On the contrary the second singlet state implies significant displacement of the mean charges. The central bond(s) is (are) positive, the other bonds are negative.

We also have reported in Table 2 the fluctuations of the number of  $\pi$  electrons per double-bond. For a wave-function

$$\Psi = \sum_{ij^*} c_{ij^*} \Phi_i^{(j^*)}$$

one may define the number of electrons in bond  $k$  for  $\Phi_i^{(j^*)}$

$$n_{ij^*}^k = \left\langle \Phi_i^{(j^*)} \left| \pi^k \right| \Phi_i^{(j^*)} \right\rangle$$

using the operator  $\pi^k$ , number of particles in loge  $k$  [19].

Then if  $\bar{n}^k$  is the mean number of electrons in bond  $k$

$$\bar{n}^k = \sum_{ij^*} c_{ij^*}^2 n_{ij^*}^k$$

The fluctuation of the number of electrons in bond  $k$  is given by

$$\sigma_k = \sqrt{\sum_{ij^*} (n_{ij^*}^k - \bar{n}^k)^2 c_{ij^*}^2}$$

Since the  $n_{ij^*}^k$  differs from 2 only when  $i$  or  $j^* = k$ , this fluctuation decreases for this type of wave function, as may be seen from Table 2 but they are larger than for the ground state.

### Conclusions

We have considered the classical  $\pi$  excitonic wave function

$$\Psi = \sum_{ij^*} c_{ij^*} \Phi_i^{(j^*)}$$

as a multiconfigurational zeroth order wave-function. This wave function has been perturbed under the influence of i) the other singly excited determinants (the  $^1(\sigma^*)$  configurations coupled with the  $^1(\pi^*)$  configurations through dipole-

dipole interactions), ii) the doubly excited determinants, which introduce polarization effects on the excited state, iii) the triply excited determinants, which introduce bond and interbond correlation effects on the excited state.

A correct definition of  $H^0$  allows, through an algebraic derivation of the various 2<sup>nd</sup> order corrections, to calculate only the *changes* of polarization, delocalization and correlation energies in the excited state with respect to the ground state, despite the multiconfigurational form of the zeroth order wave-function for the excited state, we have been able therefore to get the "cancellation of common diagrams in excitation energies" well established when the zeroth order wave-function for the excited state is the single determinantal Virtual Orbital approximation. Although a very large number of determinants are taken into account, the calculation of 2<sup>nd</sup> order corrected transition energies is very short, much shorter than when one perturbs a single configuration using delocalized MO's. For instance the calculation of 10 transition energies in  $C_{14}H_{16}$  requires 6m 3seconds on an IBM 360-75 computer. This speed is obtained through both the complete localization of the MO's reducing the number and calculation time of non zero molecular integrals, and a careful choice of the perturbation procedure. It appears therefore that the use of localized MO's is very useful not only for the ground state energy and ground state properties calculation, but also for the excited states and excitation properties, for which the canonical delocalized MO's are often presented as necessary.

This PCILO method for excited states will be applied to some conceptual and numerical problems. In further publications [17], it will be shown that the single determinantal description of the excited state overestimates the delocalization of the excitation with respect to the excitonic treatment. The method will be applied to some conformational problems involving the excited states.

## Appendix

Detailed 2<sup>nd</sup> order energy corrections on the excited state.

This Appendix gives the various types of interactions which appear in the 2<sup>nd</sup> order energy correction on the excitonic wave-function

$$\Psi^0 = \sum_i \sum_{j \in \{\pi\}} c_{ij} \Phi \begin{pmatrix} j^* \\ i \end{pmatrix}$$

We report successively the 2<sup>nd</sup> order effects of the triply, doubly, singly, excited determinants and of the ground state determinant  $\Phi_0^0$ . The following notations are used

$a_{pq^*} = (pp^*, q^*q^*)$ ,  $a_{pq} = (pp^*, qq)$  are charge-dipole interaction matrix elements.

$b_{pq} = (pp^*, qq^*)$ , is a dipole-dipole interaction matrix element

$\Delta \begin{pmatrix} q^* \dots \\ p \dots \end{pmatrix} = E' - E^0 \begin{pmatrix} q^* \dots \\ p \dots \end{pmatrix}$  is a typical energy denominator.

$i, j, k$  and  $l$  belong to the subspace  $\{\pi\}$  of the  $\pi$  MO's,

$\sigma$  belong to the complementary subspace,

$p$  and  $q$  are any MO's, belonging to  $\{\pi\}$  or not.

$s = 0$  or  $1$  according to the singlet or triplet character of the excited state.

In the typical 2<sup>nd</sup> order energy correction [Eq. (3)] we shall distinguish the cases where  $\Phi_i$  and  $\Phi_j$  are 1) both ionic, 2) ionic and neutral and 3) both neutral. In the following paragraphs we give in Table form the various non-zero interactions which occur under the CNDO-hypotheses when the MO's are fully localized, and the corresponding energy corrections, in a form which makes the programming straightforward. In the Tables the doubly bordered columns represent diagonal interactions.

### A) Effect of the Triply Excited Determinants

#### 1) $\Phi_i$ and $\Phi_j$ both ionic

$\Phi_j$					
$\Phi_i$		$\begin{pmatrix} i^* \\ k \end{pmatrix}$			
		$\begin{pmatrix} i^* \\ i \end{pmatrix}$	$\begin{pmatrix} k^* \\ i \end{pmatrix}$	$\begin{pmatrix} i^* \\ k \end{pmatrix}$	$\begin{pmatrix} k^* \\ i \end{pmatrix}$
	$\begin{pmatrix} i^* \\ i \end{pmatrix}$	$\boxed{\begin{pmatrix} i^* & p^* & q^* \\ i & p & q \end{pmatrix}_a}$	0	0	0

Due to the CNDO-PCILO hypothesis we only have diagonal terms:

$$a = \sum_i \sum_j c_{ij}^2 \left[ \sum_{p,q} b_{pq}^2 (2 - \delta_{pi} - \delta_{pj} - \delta_{qi} - \delta_{qj} + \delta_{pi}\delta_{qj}) / A \right] \begin{pmatrix} j^* & p^* & q^* \\ i & p & q \end{pmatrix} \\ + \sum_p b_{ip}^2 (1 - \delta_{ip} - \delta_{jp}) / A \begin{pmatrix} j^* & p^* & \bar{p}^* \\ i & p & \bar{p} \end{pmatrix}$$

The  $\delta$ 's take into account the possible spin restrictions.

#### 2) $\Phi_i$ ionic and $\Phi_j$ neutral

No triply excited determinant interact with  $\Phi_i$  and  $\Phi_j$  in a such a case, due to the CNDO-PCILO hypothesis.

#### 3) $\Phi_i$ and $\Phi_j$ both neutral

$\Phi_j$			
$\Phi_i$		$\begin{pmatrix} i^* \\ i \end{pmatrix}$	$\begin{pmatrix} i^* \\ j \end{pmatrix}_{s,i}$
		$\begin{pmatrix} i^* \\ i \end{pmatrix}$	$\begin{pmatrix} i^* \\ j \end{pmatrix}_{s,i}$
	$\begin{pmatrix} i^* \\ i \end{pmatrix}$	$\boxed{\begin{pmatrix} i^* & p^* & q^* \\ i & p & q \end{pmatrix}_a}$	$\begin{pmatrix} i^* & i^* & p^* \\ i & i & p \end{pmatrix}_b$

$$a = \sum_i c_{ii}^2 \left[ \sum_p' \left( \sum_q'' 2b_{pq}^2 / \Delta \begin{pmatrix} i^* & p^* & q^* \\ i & p & q \end{pmatrix} + 4(1-s) b_{ip}^2 / \Delta \begin{pmatrix} i^* & i^* & p^* \\ i & i & p \end{pmatrix} + b_{pp}^2 / \Delta \begin{pmatrix} i^* & p^* & p^* \\ i & p & p \end{pmatrix} \right) \right],$$

$$b = \sum_i \sum_j' c_{ii} c_{jj} \sum_p'' (2 - \delta_{pi} - \delta_{pj}) (1-s) b_{ip} b_{pj} / \Delta \begin{pmatrix} i^* & j^* & p^* \\ i & j & p \end{pmatrix}.$$

Combining the corrections 1a and 3a, and using the demonstration given in Part II, one might introduce explicitly the 2<sup>nd</sup> order correlation effects on the ground state minus some specific terms.

### B) Effect of the Doubly Excited Determinants

#### 1) $\Phi_I$ and $\Phi_J$ both ionic

$\Phi_I \backslash \Phi_J$	$\begin{pmatrix} l^* \\ k \end{pmatrix} \quad k \neq l$	-----		
	$\begin{pmatrix} l^* \\ i \end{pmatrix}$	$\begin{pmatrix} k^* \\ i \end{pmatrix} \quad k \neq j$	$\begin{pmatrix} j^* \\ k \end{pmatrix} \quad k \neq i$	$\begin{pmatrix} l^* \\ k \end{pmatrix} \quad l \neq j$
$\begin{pmatrix} j^* \\ i \end{pmatrix} \quad i \neq j$	$\boxed{\begin{pmatrix} l^* & q^* \\ i & p \end{pmatrix}_a}$	$\begin{pmatrix} l^* & k^* \\ i & p \end{pmatrix}_b$	$\begin{pmatrix} j^* & p^* \\ i & k \end{pmatrix}_c$	$\begin{pmatrix} j^* & l^* \\ i & k \end{pmatrix}_d$

$$a = \sum_i \sum_j' c_{ij}^2 \left[ \sum_{p \neq q}'' (2 - \delta_{pi} - \delta_{qj} + 2\delta_{pi}\delta_{qj}(1-s)) F_{pq}^2 / \Delta \begin{pmatrix} j^* & q^* \\ i & p \end{pmatrix} + \sum_p (2 - \delta_{pi} - \delta_{pj}) (F_{pp} + a_{pj} - a_{pi})^2 / \Delta \begin{pmatrix} j^* & p^* \\ i & p \end{pmatrix} \right],$$

$$b = \sum_i \sum_j' \sum_k'' c_{ij} c_{ik} \left[ \sum_{p \neq q, j} (-1)^{(1 + \delta_{pi}(1-s))} F_{pk} F_{pj} / \Delta \begin{pmatrix} j^* & k^* \\ i & p \end{pmatrix} - (F_{kk} + a_{kj} - a_{ki}) F_{kj} / \Delta \begin{pmatrix} j^* & k^* \\ i & k \end{pmatrix} - (F_{jj} + a_{jk} - a_{ji}) F_{jk} / \Delta \begin{pmatrix} j^* & k^* \\ i & j \end{pmatrix} \right],$$

$$c = \sum_i \sum_j' \sum_k'' c_{ij} c_{kj} \left[ \sum_{p \neq i, k} (-1)^{(1 + \delta_{pj}(1-s))} F_{kp} F_{ip} / \Delta \begin{pmatrix} j^* & p^* \\ i & k \end{pmatrix} + F_{ki} (F_{ii} + a_{ip} - a_{ik}) / \Delta \begin{pmatrix} j^* & l^* \\ i & k \end{pmatrix} + F_{ik} (F_{kk} + a_{kj} - a_{ki}) / \Delta \begin{pmatrix} j^* & k^* \\ i & k \end{pmatrix} \right],$$

$$d = \sum_i \sum_j' \sum_k'' \sum_l''' c_{ij} c_{kl} 2(1-s) F_{ip} F_{kl} / \Delta \begin{pmatrix} j^* & l^* \\ i & k \end{pmatrix}.$$

2)  $\Phi_I$  ionic,  $\Phi_J$  neutral

$\Phi_I$	$\Phi_J$	$\begin{pmatrix} k^* \\ k \end{pmatrix}$		
		$\begin{pmatrix} i^* \\ i \end{pmatrix}$	$\begin{pmatrix} i^* \\ i \end{pmatrix}$	$\begin{pmatrix} k^* \\ k \end{pmatrix}_{k \neq i, l}$
	$\begin{pmatrix} i^* \\ i \end{pmatrix}_{i \neq l}$	$\begin{pmatrix} i^* & i^* \\ i & p \end{pmatrix}_b$	$\begin{pmatrix} i^* & p^* \\ i & i \end{pmatrix}_c$	$\begin{pmatrix} i^* & k^* \\ i & k \end{pmatrix}_d$

$$b = \sum_i \sum_i' c_{i,p} c_{i,p^*} \left[ \sum_p'' 2F_{pp^*} F_{pp^*} A \begin{pmatrix} i^* & i^* \\ i & p \end{pmatrix} + (-1)^p F_{ip^*} (F_{ii^*} + a_{ip^*} - a_{ii}) / A \begin{pmatrix} i^* & i^* \\ i & i \end{pmatrix} \right. \\ \left. + F_{ii^*} (F_{jp^*} + a_{jp^*} - a_{ji}) / A \begin{pmatrix} i^* & j^* \\ i & i \end{pmatrix} \right],$$

$$c = \sum_i \sum_i' c_{i,p} c_{i,p^*} \left[ \sum_p'' 2F_{jp^*} F_{ip^*} A \begin{pmatrix} i^* & p^* \\ i & j \end{pmatrix} + (-1)^p F_{ip^*} (F_{jp^*} + a_{jp^*} - a_{ji}) / A \begin{pmatrix} i^* & j^* \\ i & j \end{pmatrix} \right. \\ \left. + F_{ii^*} (F_{ii^*} + a_{ip^*} - a_{ij}) / A \begin{pmatrix} i^* & i^* \\ i & j \end{pmatrix} \right],$$

$$d = \sum_i \sum_j \sum_k c_{i,p} c_{k,k^*} 2(1-s) F_{ip^*} (F_{kk^*} + a_{kp^*} - a_{ki}) / A \begin{pmatrix} i^* & k^* \\ i & k \end{pmatrix}.$$

3)  $\Phi_I$  and  $\Phi_J$  both neutral

$\Phi_I$	$\Phi_J$	$\begin{pmatrix} i^* \\ i \end{pmatrix}$		
		$\begin{pmatrix} i^* \\ i \end{pmatrix}$	$\begin{pmatrix} i^* \\ i \end{pmatrix}_{i \neq l}$	
	$\begin{pmatrix} i^* \\ i \end{pmatrix}$	$\begin{pmatrix} i^* & q^* \\ i & p \end{pmatrix}_a$	$\begin{pmatrix} i^* & i^* \\ i & i \end{pmatrix}_b$	

$$a = \sum_i c_{ii^*}^2 \left[ \sum_{p^* q^*} (2 - \delta_{pi} - \delta_{qi}) F_{pq^*}^2 / A \begin{pmatrix} i^* & q^* \\ i & p \end{pmatrix} \right. \\ \left. + \sum_p 2(1-s) \delta_{pi} (F_{pp^*} + a_{pi^*} - a_{pi})^2 / A \begin{pmatrix} i^* & p^* \\ i & p \end{pmatrix} \right],$$

$$b = \sum_i \sum_j c_{ii^*} c_{jp^*} 2(1-s) (F_{ii^*} + a_{ip^*} - a_{ij}) (F_{jp^*} + a_{jp^*} - a_{ji}) / A \begin{pmatrix} i^* & j^* \\ i & j \end{pmatrix}.$$

## C) Effect of the Singly Excited Determinants which do Not Belong to S

1)  $\Phi_I$  and  $\Phi_J$  both ionic

$\Phi_j \backslash \Phi_i$	$\begin{pmatrix} j^* \\ k \end{pmatrix} \quad k \neq l$			
	$\begin{pmatrix} j^* \\ i \end{pmatrix}$	$\begin{pmatrix} k^* \\ i \end{pmatrix} \quad k \neq j$	$\begin{pmatrix} j^* \\ k \end{pmatrix} \quad k \neq i$	$j^* \quad k$
$\begin{pmatrix} j^* \\ i \end{pmatrix} \quad i \neq j$	<div><math>\begin{pmatrix} j^* \\ \sigma \end{pmatrix}</math> <math>\begin{pmatrix} \sigma^* \\ i \end{pmatrix}_a</math></div>	$\begin{pmatrix} \sigma^* \\ i \end{pmatrix}$	$\begin{pmatrix} j^* \\ \sigma \end{pmatrix}$	0
		b	c	

$$a = \sum_i \sum_j' c_{ij}^2 \sum_{\sigma} \left( F_{i\sigma}^2 / \Delta \binom{j^*}{\sigma} + F_{j\sigma}^2 / \Delta \binom{\sigma^*}{i} \right),$$

$$b = \sum_i \sum_j' \sum_k'' \sum_{\sigma} \left( c_{ij} c_{ik} F_{j\sigma} F_{\sigma k} / \Delta \binom{\sigma^*}{i} + c_{ij} c_{kj} F_{i\sigma} F_{k\sigma} / \Delta \binom{j^*}{\sigma} \right).$$

2)  $\Phi_I$  ionic,  $\Phi_J$  neutral

$\Phi_j \backslash \Phi_i$	$(k^*)$ $(k)$		
	$(i^*)$ $(i)$	$(j^*)$ $(j)$	$(k^*)$ $(k) \quad k \neq i, j$
$(i^*)$ $(i) \quad i \neq j$	$(\sigma^*)$ $(i)_a$	$(j^*)$ $(\sigma)_b$	0

$$a = \sum_i \sum_j' 2c_{ij} c_{i\sigma} \sum_{\sigma} F_{j\sigma} F_{\sigma i} / \Delta \binom{\sigma^*}{i}$$

$$b = \sum_i \sum_j' 2c_{ij} c_{j\sigma} \sum_{\sigma} F_{i\sigma} F_{\sigma j} / \Delta \binom{j^*}{\sigma}$$

3)  $\Phi_I$  and  $\Phi_J$  both neutral

$\Phi_i \backslash \Phi_j$	$i^*$ $j^*$	
	$\begin{pmatrix} i^* \\ i \end{pmatrix}$	$\begin{pmatrix} j^* \\ j \end{pmatrix} \quad j \neq i$
$\begin{pmatrix} i^* \\ i \end{pmatrix}$	<div> <math>\begin{pmatrix} i^* \\ \sigma \end{pmatrix}</math>  <math>\begin{pmatrix} \sigma^* \\ i \end{pmatrix}</math>  <math>\begin{pmatrix} \sigma^* \\ \sigma \end{pmatrix}_a</math> </div>	$\begin{pmatrix} \sigma^* \\ \sigma \end{pmatrix}$  <

$$a = \sum_i c_{ii}^2 \sum_{\sigma} F_{i\sigma}^2 / \Delta \left( \begin{smallmatrix} i^* \\ \sigma \end{smallmatrix} \right) + F_{\sigma^*i}^2 / \Delta \left( \begin{smallmatrix} \sigma^* \\ i \end{smallmatrix} \right) + 4(1-s) b_{i\sigma} / \Delta \left( \begin{smallmatrix} \sigma^* \\ \sigma \end{smallmatrix} \right),$$

$$b = \sum_i \sum_j c_{ii} c_{jj} \sum_{\sigma} 4(1-s) b_{i\sigma} b_{j\sigma} / \Delta_{\sigma\sigma^*}.$$

#### D) Effect of the Ground State Determinant

$$a = \sum_i \sum_j \sum_k \sum_l c_{i,j} c_{k,l} F_{i,j} F_{k,l} / \Delta(0).$$

One may see from these formulae that

i) the diagonal corrections  $a$  should imply two summations over the  $\pi$  MO's and two summations over all MO's (i.e. a time proportional to  $n_\pi^2 n^2$ ), but the introduction of the ground state corrections reduce them to summations of the type  $\sum_i \sum_j \sum_k \sum_p$  involving  $n_\pi^4 n$  elements.

ii) The cross-terms  $(\Phi_i \neq \Phi_j)$   $b, c, d$  only involve  $\sum_i \sum_j \sum_k \sum_p$  summations of the type  $\sum_i \sum_j \sum_k \sum_p$  involving  $n_\pi^4 n$  matrix elements.

The total computation time of a 2<sup>nd</sup> order corrected transition energy is therefore proportional to  $n_\pi^4 n$ , while the 2<sup>nd</sup> order corrected ground-state energy required a time proportional to  $n^2$ . One may distinguish two cases:

i) The conjugated system involved in the zeroth order description of the excitation is kept constant ( $n_\pi$  constant),  $n$  increasing with the number of substituents. Then the computation time of the transition energy only increases like  $n$ .

ii) The dimension of the conjugated system increases like  $n(n_\pi = n/5$  in conjugated hydrocarbons), and the computation time of the transition energy varies as  $n^4/(5)^3$ .

#### References

1. See for instance Sinanoglu, O. *Advances chem. Physics*, Vol 6, Prigogine Ed., Interscience, New York (1964), p. 315.
2. Diner, S., Malrieu, J. P., Claverie, P. *Theoret. chim. Acta (Berl.)* **13**, 1 (1969). Diner, S., Malrieu, J. P., Jordan, L., Gilbert, M. *Theoret. chim. Acta (Berl.)* **15**, 100 (1969). Gilbert, M., Pincelli, U. *Theoret. chim. Acta (Berl.)* **15**, 211 (1969).
3. Pople, J. A., Segal, G. A. *J. chem. Physics* **43**, S136 (1965); **44**, 3289 (1966).
4. Simpson, W. F. *J. Amer. chem. Soc.* **73**, 5363 (1951); **77**, 6164 (1955).
5. Langlet, J. *Theoret. chim. Acta (Berl.)* **27**, 223 (1972).
6. Epstein, P. S. *Physic. Rev.* **28**, 695 (1926). Nesbet, R. K.; *Proc. Royal Soc. A* **230**, 312, 322 (1955).
7. Huron, B., Malrieu, J. P., Rancurel, P. *J. chem. Physics* (in press).
8. Malrieu, J. P., Claverie, P., Diner, S. *Theoret. chim. Acta (Berl.)* **8**, 404 (1967). Malrieu, J. P. *J. chem. Physics* **47**, 4555 (1967).
9. Møller, C., Plesset, M. S., *Physic. Rev.* **46**, 618 (1934).
10. Woods, F. C., Schwartzman, I. M.; *J. Amer. chem. Soc.* **83**, 404 (1966). Sondheimer, E., Ben-Efraim, D., Wolowsky, R. *J. Amer. chem. Soc.* **83**, 1675 (1961).
11. Schuler, H., Lutz, F., Arnold, G. *Spectrochim. Acta* **17**, 1043 (1961). American Petroleum Research Project **44**, Serial number 39, 65, 91, 92.
12. Jug, A., Benard, M.; *Tetrahedron* **24**, 5575 (1968).
13. Herzberg, A., Sherrington, A., Sweges, M.; *Proc. phys. Soc. (London)* **84**, 465 (1964).



14. Dunning, T. H., McKoy, V.: *J. chem. Physics* **47**, 1735 (1967).
15. Giessner, C., Pullman, A.: *Theoret. chim. Acta (Berl.)* **13**, 265 (1965).
16. Denis, A., Malrieu, J. P.: *J. chem. Physics* **52**, 4769 (1970).
17. Denis, A., Langlet, J., Malrieu, J. P.: *Theoret. chim. Acta (Berl.)* **29**, 117 (1973).
18. Evans, D. F.: *J. chem. Soc.* 2566 (1961).
19. Diner, S., Claverie, P., Malrieu, J. P.: To be published.

Dr. J. P. Malrieu  
Institut de Biologie Physico-Chimique  
Laboratoire de Biochimie Théorique  
Associé au C.N.R.S.  
13, rue P. et M. Curie  
F-75 Paris 5è, France



# RPA Method Applied to Molecular Crystals

Masashi Tanaka and Jiro Tanaka

Department of Chemistry, Faculty of Science, Nagoya University, Chikusa, 464, Nagoya, Japan

Received December 19, 1972

A new theory is presented on the excited states of molecular crystals by using the random phase approximation (RPA). The method is applied to the analysis of the absorption spectrum of anthracene crystal. The Davydov splitting for the long axis polarized band is calculated as about  $9200\text{ cm}^{-1}$  while the observed value is  $9000 \sim 12000\text{ cm}^{-1}$ . In the earlier theories, much larger values are reported and a simple dipole-dipole approximation gives the value of  $32000\text{ cm}^{-1}$ . The general feature of the crystalline spectra is well predicted.

Es wird eine neue Theorie der angeregten Zustände von Molekulkristallen vorgelegt, die mit Hilfe des RPA-Verfahrens gewonnen wurde. Die Methode wird zur Interpretation des Absorptionsspektrums von Anthracenkristallen verwendet. Die Davydow-Aufspaltung des polarisierten Bandes (lange Achse) wird mit  $9200\text{ cm}^{-1}$  berechnet (der beobachtete Wert beträgt  $9000 \sim 12000\text{ cm}^{-1}$ ). Nach den älteren Theorien erhält man viel größere Werte, und eine einfache Dipol-Dipol-Approximation liefert  $32000\text{ cm}^{-1}$ . Das charakteristische Bild des kristallinen Spektrums wird gut wiedergegeben.

## 1. Introduction

The theory of the random-phase (RPA) approximation widely used in nuclear and solid state physics has been applied to the study of electronic correlation in molecules [1–2]. The method uses the Bose second quantization for the electron-hole pair to describe the excited state and the excitation energy is given by diagonalizing the Hamiltonian matrix for these sets. It covers the effect of electron correlation than earlier theories and gives better results in the calculation of energy and oscillator strength of complex molecules.

In the study of the molecular exciton states, Agranovitch [3–4] was the first who used the second quantized version of the electron-hole pair Hamiltonian. Although a formal theoretical treatment has been published, actual calculations by this method has not been appeared as yet. Philpott [5] derived a similar equation as Agranovitch [3] starting from a classical theory of light and investigated the contribution of dipole-dipole interactions to the Davydov splitting of anthracene, tetracene, naphthalene and phenanthrene crystals.

In our previous paper [6] an alternative new approach was presented to the analysis of the electronic absorption spectra of molecular crystal, in which the crystal exciton configuration is constructed from the one-electron excited configurations of the SCF molecular orbitals in the constituent molecules and the mixing between the different exciton configurations has been taken into account using the complete Hamiltonian of the crystal. In the present paper, we consider

the effect of electron correlation by using the RPA method and derive the equation which is non-Hermitian. The equation is applied to the calculation of excited states of anthracene molecule and crystal [7].

## 2. Theory

The Hamiltonian for a crystal containing  $N$  unit cells and  $\sigma$  identical molecules per unit cell may be written by

$$\mathcal{H} = \sum_{\mu} \left\{ -\frac{\hbar^2}{2m} \nabla_{\mu}^2 + \sum_{p\alpha a} V(R_{p\alpha a} - r_{\mu}) \right\} + \frac{1}{2} \sum'_{\mu\nu} \frac{e^2}{r_{\mu\nu}} \quad (1)$$

where the summation is taken over all  $\pi$ -electrons in the  $\sigma$   $N$  molecules of the crystal and the prime in the third summation indicates that the terms for which  $\mu = \nu$  is omitted.  $V(R_{p\alpha a} - r_{\mu})$  is the attraction potential energy between the  $\mu$ -th electron and the  $a$ -th core atom at the  $\alpha$ -th site of the  $p$ -th unit cell and  $e^2/r_{\mu\nu}$  is the electrostatic repulsion between  $\pi$ -electrons  $\mu$  and  $\nu$ . Then, the Hamiltonian of electron field in the second quantized form is:

$$\begin{aligned} \mathcal{H} = & \int \psi^*(\mu) \left\{ -\frac{\hbar^2}{2m} \nabla_{\mu}^2 + \sum_{p\alpha a} V(R_{p\alpha a} - r_{\mu}) \right\} \psi(\mu) d\tau_{\mu} \\ & + \frac{1}{2} \iint \psi^*(\mu) \psi^*(\nu) \frac{e^2}{r_{\mu\nu}} \psi(\nu) \psi(\mu) d\tau_{\mu} d\tau_{\nu} \end{aligned} \quad (2)$$

where  $\psi^*(\mu)$  and  $\psi(\mu)$  are the creation and annihilation operators of the electron field which will be given by the one-electron molecular orbital as shown below, the argument denotes both of the space coordinates and the spin of the electron, and  $d\tau$  is the volume element including spin.

Let  $\varphi_{pai}$  be the  $i$ -th SCF-MO of the  $p\alpha$ -th molecule written as linear combinations of Löwdin's orthogonalized atomic orbitals [8]:

$$\varphi_{pai} = \sum_{a=1}^m X'_{p\alpha a} C_{ai} \quad (3)$$

where

$$X'_{q\beta b} = \sum_{q=1}^N \sum_{\beta=1}^n \sum_{a=1}^m (1+S)^{-1/2}_{p\alpha a, q\beta b} X_{q\beta b}.$$

$X_{q\beta b}$  is the  $2p\pi$  atomic orbital on the atom  $b$  in the molecule  $q\beta$  and  $(1+S)$  is the overlap matrix with elements:

$$S_{p\alpha a, q\beta b} = -\delta_{p\alpha a, q\beta b} + \int X^*_{p\alpha a}(\mu) X_{q\beta b}(\mu) dv_{\mu}. \quad (4)$$

Then, all the MO's in the crystal are orthonormalized to each other:

$$(\varphi_{pai} | \varphi_{q\beta j}) = \int \varphi^*_{pai}(\mu) \varphi_{q\beta j}(\mu) dv_{\mu}. \quad (5)$$

These MO's satisfy the Hartree-Fock equations as follows:

$$\left\{ -\frac{\hbar^2}{2m} \Delta_\mu + \sum_a V(\mathbf{R}_{pa\mu} - \mathbf{r}_\mu) + \sum_h^{\text{occ}} (2J_{pah}(\mu) - K_{pah}(\mu)) \right\} \phi_{pai}(\mu) = \varepsilon_i \phi_{pai}(\mu). \quad (6)$$

Here,  $\varepsilon_i$  is the orbital energy and  $J_{pah}(\mu)$  and  $K_{pah}(\mu)$  are the Coulomb and the exchange operators defined by Roothaan [9]:

$$J_{pah}(\mu) \phi_{pai}(\mu) = e^2 \int \frac{\phi_{pah}^*(v) \phi_{pai}(v)}{r_{\mu v}} \phi_{pai}(\mu) dv_v$$

and

$$K_{pah}(\mu) \phi_{pai}(\mu) = e^2 \int \frac{\phi_{pah}^*(v) \phi_{pai}(v)}{r_{\mu v}} \phi_{pah}(\mu) dv_v. \quad (7)$$

Now, the field operator  $\psi(\mu)$  can be expanded as linear combinations of spin-orbitals  $\phi_{pai}(\mu) = \phi_{pai}(\mu) \eta(\mu)$  where  $\eta(\mu)$  is the spin function:

$$\psi(\mu) = \sum_{pai} a_{pai} \phi_{pai}(\mu). \quad (8)$$

The operators  $a_{pai}^+$  and  $a_{pai}$  are the creation and annihilation operators of the electron which satisfy the following Fermi commutation relations:

$$\begin{aligned} a_{pai}^+ a_{q\beta j}^+ + a_{q\beta j}^+ a_{pai}^+ &= 0 \\ a_{pai} a_{q\beta j} + a_{q\beta j} a_{pai} &= 0 \\ a_{pai}^+ a_{q\beta j} + a_{q\beta j} a_{pai}^+ &= \delta_{pai, q\beta j}. \end{aligned} \quad (9)$$

Substituting Eq. (8) into Eq. (2), the Hamiltonian becomes:

$$\begin{aligned} \mathcal{H} &= \sum_{pai} \varepsilon_i a_{pai}^+ a_{pai} \\ &+ \sum_{pai} \sum_{q\beta j} \left( \phi_{pai} \left| \sum_{s\gamma \neq pa} \sum_a V(\mathbf{R}_{s\gamma a} - \mathbf{r}_\mu) \right| \phi_{q\beta j} \right) a_{pai}^+ a_{q\beta j} \\ &- \sum_{pai} \sum_{q\beta j} \left( \phi_{pai} \left| \sum_h^{\text{occ}} (2J_{pah}(\mu) - K_{pah}(\mu)) \right| \phi_{q\beta j} \right) a_{pai}^+ a_{q\beta j} \\ &+ 1/2 \sum_{pai} \sum_{q\beta j} \sum_{s\gamma k} \sum_{t\delta l} (\phi_{pai} \phi_{q\beta j} | \phi_{s\gamma k} \phi_{t\delta l}) a_{pai}^+ a_{s\gamma k}^+ a_{t\delta l} a_{q\beta j} \end{aligned} \quad (10)$$

where

$$(\phi_{pai} | V(\mathbf{R}_{s\gamma a} - \mathbf{r}_\mu) | \phi_{q\beta j}) = \int \phi_{pai}^*(\mu) V(\mathbf{R}_{s\gamma a} - \mathbf{r}_\mu) \phi_{q\beta j}(\mu) d\tau_\mu$$

and

$$(\phi_{pai} \phi_{q\beta j} | \phi_{s\gamma k} \phi_{t\delta l}) = \iint \phi_{pai}^*(\mu) \phi_{q\beta j}(\mu) \frac{e^2}{r_{\mu\nu}} \phi_{s\gamma k}^*(\nu) \phi_{t\delta l}(\nu) d\tau_\mu d\tau_\nu. \quad (11)$$

Denoting the ground and excited states of the Hamiltonian  $\mathcal{H}$  by  $|0\rangle$  and  $|E\rangle$ , the excitation operator  $A^+(E)$  and the Hermitian conjugate operator  $A(E)$  are defined as follows:

$$\begin{aligned} A^+(E)|0\rangle &= |E\rangle \\ A(E)|0\rangle &= 0. \end{aligned} \quad (12)$$

Then, the operators  $A^+(E)$  and  $A(E)$  satisfy the Bose commutation relation [Eq. (13)] and the equation of motion [Eq. (14)].

$$\begin{aligned} \langle 0| [A(E), A^+(E')] |0\rangle &= \langle 0| A(E) A^+(E') - A^+(E') A(E) |0\rangle \\ &= \langle E|E'\rangle \\ &= \delta_{E,E'} \end{aligned} \quad (13)$$

and

$$[\mathcal{H}, A^+(E)] |0\rangle = \Delta E A^+(E) |0\rangle \quad (14)$$

where  $\Delta E$  is the energy difference ( $E - E_0$ ) between the excited state and ground state and is usually called as the elementary excitation energy. The Hamiltonian can be diagonalized by using the operator  $A^+(E)$  and  $A(E)$  as follows:

$$\mathcal{H} = E_0 + \sum_E \Delta E A^+(E) A(E). \quad (15)$$

This may be easily proved by substituting Eq. (15) into Eq. (14).

In molecular crystals, the exciton states can be characterized by three indices  $f, \mu, k$  [6] and the operator  $A(E)$  is rewritten as  $A(E) = A_{f\mu}(k)$  where  $k$  is the wave vector,  $\mu$  characterizes the exciton state and  $f$  numbers the excited states of molecules in the crystal. Then, the exciton state function  $\Psi_{f\mu}(k)$  and the locally excited configuration  $\theta_{pa}^{i \rightarrow j}$  can be expressed in terms of the operator representation:

$$\begin{aligned} \Psi_{f\mu}(k) &= A_{f\mu}^+(k) |0\rangle, \\ \theta_{pa}^{i \rightarrow j} &= a_{pa}^+ a_{pai} |0\rangle. \end{aligned} \quad (16)$$

It was shown in our previous paper [6] that the wave function  $\Psi_{f\mu}(k)$  can be approximated by the linear combinations of the configuration  $\theta_{pa}^{i \rightarrow j}$ :

$$\Psi_{f\mu}(k) = (N\sigma)^{-1/2} \sum_{ij} \sum_{pa} e^{ik \cdot R_p} C_{ij}^{f\mu}(k) B_{a\mu}(k) \theta_{pa}^{i \rightarrow j}. \quad (17)$$

Comparing Eqs. (16) and (17), the operator  $A_{f\mu}^+(k)$  can be given by the unitary transformation of creation operator  $a_{pa}^+ a_{pai}$  for the electron-hole pair as follows:

$$\begin{aligned} A_{f\mu}^+(k) &= (N\sigma)^{-1/2} \sum_{ij} \sum_{pa} e^{ik \cdot R_p} C_{ij}^{f\mu}(k) B_{a\mu}(k) a_{pa}^+ a_{pai} \\ &= \sum_{ij} \sum_{pa} e^{ik \cdot R_p} u_{aij, f\mu k} a_{pa}^+ a_{pai}. \end{aligned} \quad (18)$$

However, Dunning and McKoy [2] has shown that the operators  $A_{f\mu}^+(k)$  and  $A_{f\mu}(k)$  are defined as linear combinations of the electron-hole creation and

annihilation operators  $a_{pa}^+ a_{pi}$  and  $a_{pi}^+ a_{pa}$  in order to take into account the effect of electron correlation. The ground state wave function to first order is represented by the expansion:

$$|0\rangle = C_0 |HF\rangle + \sum_{paj} \sum_{q\beta kl} C_{paj, q\beta kl} a_{pa}^+ a_{pi} a_{q\beta}^+ a_{q\beta k} |HF\rangle. \quad (19)$$

Now,  $|HF\rangle$  is the Hartree-Fock ground state. The subscripts  $i$  and  $k$  are used to denote the occupied molecular orbitals, and  $j$  and  $l$  are employed to label the vacant MO's and  $m, n$  and  $h$  describe all MO's without differentiation. The second term implies a double excitation. Then, the single excited state is expressed as a linear combination of wave function obtained in two ways: (1) by exciting from the HF ground state or (2) by de-exciting from one of the doubly excited components. Then, the excitation operator  $A_{f\mu}^+(k)$  is given by the following equation:

$$A_{f\mu}^+(k) = \sum_{ij} \sum_{pa} e^{ik \cdot R_p} \{u_{aij, f\mu k} a_{pa}^+ a_{pi} - v_{aij, f\mu k} a_{pi}^+ a_{pa}\} \quad (20)$$

and its Hermitian conjugate  $A_{f\mu}(k)$  becomes as follows:

$$A_{f\mu}(k) = \sum_{ij} \sum_{pa} e^{-ik \cdot R_p} \{u_{f\mu k, aij}^* a_{pi}^+ a_{pa} - v_{f\mu k, aij}^* a_{pa}^+ a_{pi}\}. \quad (21)$$

The pair operators are shown to satisfy the following commutation relations by using the Fermi commutation relations (9):

$$\begin{aligned} [a_{pa}^+ a_{pi}, a_{q\beta}^+ a_{q\beta k}] &= [a_{pi}^+ a_{pa}, a_{q\beta k}^+ a_{q\beta}] = 0 \\ [a_{pi}^+ a_{pa}, a_{q\beta}^+ a_{q\beta k}] &= \delta_{pai, q\beta k} \delta_{pa, q\beta} - \delta_{pai, q\beta k} a_{q\beta}^+ a_{pa} - \delta_{q\beta l, pa} a_{q\beta k}^+ a_{pi}^+ \\ [a_{pa}^+ a_{pi}, a_{q\beta k}^+ a_{q\beta}] &= -\delta_{pai, q\beta k} \delta_{pa, q\beta} + \delta_{pai, q\beta k} a_{pa}^+ a_{q\beta} + \delta_{pa, q\beta} a_{pi}^+ a_{q\beta k}. \end{aligned} \quad (22)$$

If the strict Bose commutation relation is used instead of the commutation relations (22), the transformation of Eqs. (20) and (21) becomes unitary and the coefficients are orthonormalized as follows:

$$\begin{aligned} \sum_{f\mu k} \{U_{f\mu k, pa}^* U_{q\beta kl, f\mu k} - V_{f\mu k, q\beta kl}^* V_{pa, f\mu k}\} &= \delta_{pai, q\beta kl} \\ \sum_{pa} \sum_{ij} \{U_{f\mu k, pa}^* U_{paij, f'\mu'k'} - V_{f\mu k, pa}^* V_{paij, f'\mu'k'}\} &= \delta_{f\mu k, f'\mu'k'} \end{aligned} \quad (23)$$

where  $U_{paij, f\mu k} = e^{ik \cdot R_p} u_{aij, f\mu k}$  and  $V_{paij, f\mu k} = e^{ik \cdot R_p} v_{aij, f\mu k}$ .

This approximation is strict if the excitation density of the system is small, i.e. if the expectation values of the number of the electron-hole pair for the states under consideration are much smaller than the total number of electrons in the system. Then,  $a_{pa}^+ a_{pi}$  and  $a_{pi}^+ a_{pa}$  can be expressed by the operators  $A_{f\mu}^+(k)$  and  $A_{f\mu}(k)$  as

$$\begin{aligned} a_{pa}^+ a_{pi} &= \sum_{f\mu k} \{u_{f\mu k, aij}^* e^{-ik \cdot R_p} A_{f\mu}^+(k) + v_{aij, f\mu k} e^{ik \cdot R_p} A_{f\mu}(k)\} \\ a_{pi}^+ a_{pa} &= \sum_{f\mu k} \{v_{f\mu k, aij}^* e^{-ik \cdot R_p} A_{f\mu}^+(k) + u_{aij, f\mu k} e^{ik \cdot R_p} A_{f\mu}(k)\} \end{aligned} \quad (24)$$

and the Hamiltonian becomes as follows:

$$\mathcal{H} = E_0 + \sum_{f\mu k} E_{f\mu}(k) A_{f\mu}^{\dagger}(k) A_{f\mu}(k). \quad (25)$$

By using the Hamiltonian (10) and the Fermi commutation relation (9), the commutator  $[\mathcal{H}, u_{p\alpha j}^{\dagger} u_{p\alpha i}]$  becomes as follows:

$$\begin{aligned} [\mathcal{H}, u_{p\alpha j}^{\dagger} u_{p\alpha i}] &= (e_j - e_i) u_{p\alpha j}^{\dagger} u_{p\alpha i} \\ &+ \sum_{q\beta m} \sum_{s, \gamma \neq q\beta} \{ (\phi_{q\beta m} | U_{s\gamma} | \phi_{p\alpha j}) a_{q\beta m}^{\dagger} u_{p\alpha i} - (\phi_{p\alpha i} | U_{s\gamma} | \phi_{q\beta m}) a_{p\alpha j}^{\dagger} a_{q\beta m} \} \\ &+ \sum_{q\beta m} \sum_{s, \gamma n} \{ (\phi_{q\beta m} \phi_{s\gamma n} | \phi_{p\alpha i} \phi_{p\alpha j}) - (\phi_{q\beta m} \phi_{p\alpha j} | \phi_{p\alpha i} \phi_{s\gamma n}) \} a_{q\beta m}^{\dagger} a_{s\gamma n} \\ &+ \sum_{q\beta m} \sum_{s, \gamma} \left\{ \left( \phi_{p\alpha i} \left| \sum_h^{\text{occ}} (2J_{s\gamma h} - K_{s\gamma h}) \right| \phi_{q\beta m} \right) a_{p\alpha j}^{\dagger} u_{q\beta m} \right. \\ &\quad \left. - \left( \phi_{q\beta m} \left| \sum_h^{\text{occ}} (2J_{s\gamma h} - K_{s\gamma h}) \right| \phi_{p\alpha j} \right) a_{q\beta m}^{\dagger} u_{p\alpha i} \right\} \\ &- 1/2 \sum_{q\beta m} \sum_{s, \gamma n} \sum_{i\delta h} \{ (\phi_{q\beta m} \phi_{p\alpha j} | \phi_{i\delta h} \phi_{s\gamma n}) \\ &\quad - (\phi_{q\beta m} \phi_{s\gamma n} | \phi_{i\delta h} \phi_{p\alpha j}) \} a_{p\alpha i} a_{q\beta m}^{\dagger} a_{i\delta h}^{\dagger} a_{s\gamma n} \\ &- 1/2 \sum_{q\beta m} \sum_{s, \gamma n} \sum_{i\delta h} \{ (\phi_{p\alpha i} \phi_{s\gamma n} | \phi_{q\beta m} \phi_{i\delta h}) \\ &\quad - (\phi_{q\beta m} \phi_{s\gamma n} | \phi_{p\alpha i} \phi_{i\delta h}) \} a_{p\alpha j}^{\dagger} a_{q\beta m}^{\dagger} a_{i\delta h} a_{s\gamma n} \end{aligned} \quad (26)$$

$$\text{where } U_{s\gamma}(\mu) = \sum_{\mu} V(R_{p\alpha\mu} - r_{\mu}) + \sum_h^{\text{occ}} (2J_{p\alpha h}(\mu) - K_{p\alpha h}(\mu)).$$

Neglecting the interactions of the hole-hole, electron-electron, multiple electron-hole and retaining the first term and part of the second and third terms, Eq. (26) reduces to a simple form:

$$\begin{aligned} [\mathcal{H}, u_{p\alpha j}^{\dagger} u_{p\alpha i}] &= \sum_{kl} (A_{ij,kl} + D_{ij,kl}) a_{p\alpha l}^{\dagger} u_{p\alpha k} \\ &+ \sum_{kl} \sum_{q\beta} \{ I_{p\alpha ij, q\beta kl} a_{q\beta l}^{\dagger} a_{q\beta k} + J_{p\alpha ij, q\beta kl} a_{q\beta k}^{\dagger} a_{q\beta l} \}. \end{aligned} \quad (27)$$

The symbols  $A_{ij,kl}$ ,  $D_{ij,kl}$ ,  $I_{p\alpha ij, q\beta kl}$  and  $J_{p\alpha ij, q\beta kl}$  are defined as follows:

$$A_{ij,kl} = \delta_{i,k} \delta_{j,l} (e_j - e_i)$$

$$D_{ij,kl} = \sum_{q\beta \neq p\alpha} \{ \delta_{i,k} (\phi_{p\alpha i} | U_{q\beta} | \phi_{p\alpha j}) - \delta_{l,j} (\phi_{p\alpha l} | U_{q\beta} | \phi_{p\alpha k}) \}$$

$$I_{p\alpha ij, q\beta kl} = 2\delta_S (\phi_{q\beta l} \phi_{q\beta k} | \phi_{p\alpha i} \phi_{p\alpha j}) - (\phi_{q\beta l} \phi_{p\alpha j} | \phi_{p\alpha i} \phi_{q\beta k})$$

and

$$J_{p\alpha ij, q\beta kl} = 2\delta_S (\phi_{q\beta k} \phi_{q\beta l} | \phi_{p\alpha i} \phi_{p\alpha j}) - (\phi_{q\beta k} \phi_{p\alpha j} | \phi_{p\alpha i} \phi_{q\beta l}) \quad (28)$$



where  $\delta_s = 1$  for the singlet state and  $\delta_s = 0$  for the triplet,

$$(\varphi_{\alpha i} | U_{q\beta} | \varphi_{\alpha j}) = \int \varphi_{\alpha i}^*(\mu) U_{q\beta}(\mu) \varphi_{\alpha j}(\mu) d\mu$$

and

$$(\varphi_{q\beta k} \varphi_{q\beta l} | \varphi_{\alpha i} \varphi_{\alpha j}) = \iint \varphi_{q\beta k}^*(\mu) \varphi_{q\beta l}(\mu) \frac{e^2}{r_{\mu\nu}} \varphi_{\alpha i}^*(\nu) \varphi_{\alpha j}(\nu) d\mu d\nu.$$

Substituting Eq. (24) into Eq. (27), Eq. (27) can be expressed in terms of the operators  $A_{f\mu}^+(k)$  and  $A_{f\mu}(k)$ :

$$\begin{aligned} [\mathcal{H}, a_{\alpha i}^+ a_{\alpha i}] &= \sum_{f\mu k} \left\{ e^{-ik \cdot R_p} A_{f\mu}^+(k) \sum_{kl} \sum_{\beta} [G_{\beta kl, \alpha ij}^*(k) u_{f\mu k, \beta kl}^* + H_{\beta kl, \alpha ij}^*(k) v_{f\mu k, \beta kl}^*] \right. \\ &\quad \left. + e^{ik \cdot R_p} A_{f\mu}(k) \sum_{kl} \sum_{\beta} [G_{\alpha ij, \beta kl}(k) v_{\beta kl, f\mu k} + H_{\alpha ij, \beta kl}(k) u_{\beta kl, f\mu k}] \right\} \quad (29) \end{aligned}$$

where

$$G_{\alpha ij, \beta kl}(k) = \delta_{\alpha, \beta} (A \varepsilon_{ij, kl} + D_{ij, kl}) + \sum_q I_{\alpha ij, q\beta kl} e^{-ik \cdot (R_p - R_q)}$$

and

$$H_{\alpha ij, \beta kl}(k) = \sum_q J_{\alpha ij, q\beta kl} e^{-ik \cdot (R_p - R_q)}. \quad (30)$$

On the other hand, by using Eqs. (24) and (25) and the Bose commutation relation of the operators  $A_{f\mu}^+(k)$  and  $A_{f\mu}(k)$ , the commutator becomes as follows:

$$\begin{aligned} [\mathcal{H}, a_{\alpha i}^+ a_{\alpha i}] &= \sum_{f\mu k} E_{f\mu}(k) \{ u_{f\mu k, \alpha ij}^* e^{-ik \cdot R_p} A_{f\mu}^+(k) - v_{f\mu k, \alpha ij} e^{ik \cdot R_p} A_{f\mu}(k) \}. \quad (31) \end{aligned}$$

By comparing Eqs. (29) and (31), the eigenvalue equation can be obtained and written in matrix notation as:

$$\begin{aligned} UE &= GU + HV \\ -VE &= GV + HU \end{aligned} \quad (32)$$

where the amplitudes  $U$  and  $V$  are normalized to an indefinite matrix as shown in Eq. (23):

$$U^+ U - V^+ V = 1. \quad (33)$$

Comparing the above equations to the equations used in our previous theory [6], the earlier formula corresponds to the equation  $UE = GU$  by neglecting the vector  $V$ . The  $H$  matrix takes into account the effect of the doubly excited configuration and allows for the contribution of the  $\pi$  electron correlation to the single excited state.

The excitation energies are the eigenvalues of a non-Hermitian matrix and can be obtained by transforming Eqs. (32) into a single equation:

$$(U + V) E^2 = (G - H)(G + H)(U + V). \quad (34)$$

Putting the vectors  $U$  and  $V$  in the following forms:

$$\begin{aligned} U &= \frac{1}{2} \{ (G-H)^{1/2} w E^{-1/2} + (G-H)^{-1/2} w E^{1/2} \} \\ V &= \frac{1}{2} \{ (G-H)^{1/2} w E^{-1/2} - (G-H)^{-1/2} w E^{1/2} \}, \end{aligned} \quad (35)$$

the new vector satisfies the orthonormalization condition by Eq. (33) as

$$w^\dagger w = 1. \quad (36)$$

Namely,  $w$  is unitary and Eq. (34) reduces to an equation for  $w$ :

$$w E^2 = (G-H)^{1/2} (G+H) (G-H)^{1/2} w. \quad (37)$$

This is a usual eigenvalue equation for a Hermitian matrix.

Defining the eigenvector  $x$  and eigenvalue  $\lambda$ :

$$\begin{aligned} (G-H) x &= x \lambda \\ x^\dagger x &= 1 \\ (G-H)^n &= x \lambda^n x^\dagger, \end{aligned} \quad (38)$$

Eqs. (36) and (37) can be expressed by using the new vector  $y = x w$  as follows:

$$\begin{aligned} y E^2 &= (\lambda^2 + 2 \lambda^{1/2} x^\dagger H x \lambda^{1/2}) y \\ y^\dagger y &= 1 \end{aligned} \quad (39)$$

and

$$\begin{aligned} U + V &= x \lambda^{1/2} y E^{-1/2} \\ U - V &= x \lambda^{-1/2} y E^{1/2}. \end{aligned} \quad (40)$$

In order to reduce the above matrix elements to those of the integrals over the atomic orbitals, it has been shown [6] that the following approximations are valid:

$$(\varphi_{pai} \varphi_{q\beta j} | \varphi_{x\gamma h} \varphi_{t\delta l}) = \delta_{pa, q\beta} \delta_{x\gamma, t\delta} \sum_a \sum_b C'_{ai} C'_{aj} C'_{bk} C'_{bl} e^2 |R_{paa} - R_{x\gamma b}|. \quad (41)$$

Then, the elements  $G_{xij, \beta kl}$  and  $H_{xij, \beta kl}$  can be approximated as follows:

$$\begin{aligned} G_{xij, \beta kl} - H_{xij, \beta kl} &= \delta_{x, \beta} \{ (A_{ij, kl} + D_{ij, kl}) + (\varphi_{pak} \varphi_{paj} | \varphi_{pai} \varphi_{pai}) - (\varphi_{pai} \varphi_{paj} | \varphi_{pai} \varphi_{pak}) \} \\ H_{xij, \beta kl} &= \delta_{x, \beta} \{ 2 \delta_S (\varphi_{pak} \varphi_{pai} | \varphi_{pai} \varphi_{paj}) - (\varphi_{pak} \varphi_{paj} | \varphi_{pai} \varphi_{pai}) \} \\ &\quad + 2 \delta_S \sum_{q \neq p} e^{-ik \cdot (R_q - R_p)} (\varphi_{q\beta h} \varphi_{q\beta l} | \varphi_{pai} \varphi_{paj}). \end{aligned} \quad (42)$$

Using the above approximation, Eqs. (38), (39) and (40) are reduced to the simple equations:

$$\begin{aligned} (\varepsilon_j - \varepsilon_i - \lambda_q) x_{ij, qa} &+ \sum_{kl} \{ D_{ij, kl} + (\varphi_{pak} \varphi_{paj} | \varphi_{pai} \varphi_{pai}) - (\varphi_{pai} \varphi_{paj} | \varphi_{pai} \varphi_{pak}) \} x_{kl, qa} = 0 \\ (\lambda_q^2 - E_{f\mu}(k)^2) y_{qa, f\mu k} &+ \sum_{\eta\beta} V_{qa, \eta\beta} y_{\eta\beta, f\mu k} = 0 \\ V_{qa, \eta\beta} &= 2 \lambda_q^{1/2} \sum_{ij} \sum_{kl} x_{qa, ij}^\dagger H_{xij, \beta kl} x_{kl, \eta\beta} \lambda_\eta^{1/2} \end{aligned} \quad (43)$$

and

$$\begin{aligned}(U + V)_{aij, f\mu k} &= \sum_q x_{ij, q\alpha} \lambda_q^{1/2} y_{q\alpha, f\mu k} E_{f\mu}(k)^{-1/2} \\ (U - V)_{aij, f\mu k} &= \sum_q x_{ij, q\alpha} \lambda_q^{-1/2} y_{q\alpha, f\mu k} E_{f\mu}(k)^{1/2}.\end{aligned}\quad (44)$$

The dipole moment operator is given in the second quantization formalism:

$$r = \sum_{pam} \sum_{q\beta n} d_{q\beta n, pam} a_{q\beta n}^+ a_{pam} \quad (45)$$

where

$$d_{q\beta n, pam} = \int \varphi_{q\beta n}^*(\mu) r_\mu \varphi_{pam}(\mu) d\mu.$$

Again, retaining only the electron-hole interactions, this is reduced to

$$r = \sum_{pa} \sum_{ij} d_{pai, pai} (a_{pai}^+ a_{pai} + a_{pai}^+ a_{pai}). \quad (46)$$

The dipole transition moment to the singlet state  $f\mu k$  is defined as:

$$M_{f\mu k} = (N\sigma)^{-1/2} \langle 0 | r | f\mu k \rangle \quad (47)$$

or, by using Eqs. (12) and taking into account the spin,

$$\begin{aligned}M_{f\mu k} &= -(N\sigma)^{-1/2} \langle 0 | [A_{f\mu}^+(k), r] | 0 \rangle \\ &= (2N/\sigma)^{1/2} \delta_k \sum_{aij} (u + v)_{aij, f\mu k} d_{pai, pai}\end{aligned}\quad (48)$$

where  $\delta_k = 1$  for  $k = 0$  and  $\delta_k = 0$  for  $k \neq 0$ . The vectors  $u$  and  $v$  may be expressed as products of two coefficients as is seen in Eq. (18):

$$u_{aij, f\mu k} = (N\sigma)^{-1/2} P_{i \rightarrow j}^{f\mu}(k) B_{\alpha\mu}(k)$$

and

$$v_{aij, f\mu k} = (N\sigma)^{-1/2} Q_{i \rightarrow j}^{f\mu}(k) B_{\alpha\mu}(k) \quad (49)$$

where  $P_{i \rightarrow j}^{f\mu}(k)$  and  $Q_{i \rightarrow j}^{f\mu}(k)$  can be determined by solving Eqs. (43) and (44) and  $B_{\alpha\mu}(k)$ 's is found by the symmetry operation of the factor group of the crystal. Then, the transition moments are defined as follows:

$$M_{f\mu k} = \frac{1}{\alpha} \sum_{ij} (P_{i \rightarrow j}^{f\mu}(k) + Q_{i \rightarrow j}^{f\mu}(k)) \left( \sum_x B_{\alpha\mu}(k) d_{pai, pai} \right). \quad (50)$$

The oscillator strength  $f$  is given by:

$$f = 3 \times 0.08753 E_{f\mu}(k) |M_{f\mu k}|^2 \quad (51)$$

where the excitation energy  $E_{f\mu k}$  is given in eV and  $M_{f\mu k}$  is in Å.

The similar equation of molecule has been given by Dunning and McKoy [2] and is reduced to the equations suitable for numerical calculations by the same procedure as above-mentioned:

$$\begin{aligned}(\varepsilon_j - \varepsilon_i - \lambda_q) x_{ij, q} + \sum_{kl} \{(\varphi_k \varphi_j | \varphi_i \varphi_l) - (\varphi_l \varphi_j | \varphi_i \varphi_k)\} x_{kl, q} &= 0 \\ (\lambda_q^2 - E_j^2) y_{q, f} + \sum_{\eta} V_{q, \eta} y_{\eta, f} &= 0 \\ V_{q, \eta} = 2\lambda_q^{1/2} \sum_{ij} \sum_{kl} x_{q, ij}^* \{2\delta_S(\varphi_k \varphi_l | \varphi_i \varphi_j) - (\varphi_k \varphi_j | \varphi_i \varphi_l)\} x_{\eta, kl} \lambda_{\eta}^{1/2}\end{aligned}\quad (52)$$

and

$$M_f = \sqrt{2} \sum_{ij} (U + V)_{ij,f} d_{j,i} \quad (53)$$

$$f = 0.08753 E_f |M_f|^2.$$

The correlation effect is shown by examining the excitation energy  $E$  and transition moment  $M$  of only single electron-hole pair operator  $a_j^\dagger a_i$ . That is, Eq. (37) gives the following eigenvalue and moment:

$$E = (A - \Gamma)^{1/2}$$

$$\cong A - \frac{\Gamma^2}{2A}$$

$$M = \sqrt{2} d_{j,i} \left( \frac{A - \Gamma}{A + \Gamma} \right)^{1/4}, \quad (54)$$

where  $A = G_{ij,ij}$  is the excitation energy of the single configuration and  $\Gamma = H_{ij,ij}$  is the correlation term. Equations (54) show that the correlation term gives an improvement on the excitation energies and oscillator strengths. The triplet state becomes unstable when  $A < \Gamma$ . This problem may be solved by applying the higher random phase approximation [10].

### 3. Results and Discussions

The electronic spectra and structure of anthracene crystal is a problem of wide interest. The present theory will be applied to its analysis.

The SCF-MO's of the anthracene molecule were calculated by solving Fock's equation (6) with an approximation of the neglect of differential overlap [11-12]:

$$X'_a(\mu) X'_b(\mu) = 0 \quad \text{for } a \neq b$$

and of two center Coulomb integrals evaluated by Nishimoto-Mataga's method [13]. The excitation energies and oscillator strengths of anthracene molecule were obtained by employing Eqs. (52) and (53) and considering thirteen electron-hole pairs. The results are shown in Table I. Comparing the observed values

Table I. Comparison between the calculated and observed values of transition energies ( $E_f$  in eV) and oscillator strengths of the anthracene molecule

		The present method		The usual CI method		Observed values	
		$E_f$	$f$	$E_f$	$f$	$E_f$	$f$
I	$B_{1u}$	3.692	0.238	3.812	0.307	3.301	0.11
II	$B_{2u}$	4.849	2.026	5.050	2.805	4.921	1.56
III	$B_{1u}$	5.826	0.353	5.968	0.478	5.603	0.21
IV	$B_{1u}$	6.088	0.135	6.235	0.189	6.52	0.41
V	$B_{1u}$	7.162	0.444	7.255	0.787		

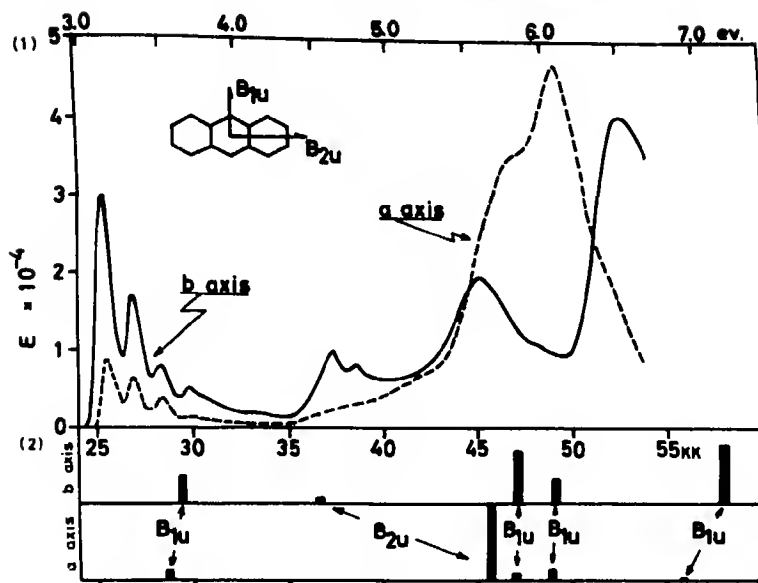


Fig. 1. Observed absorption spectra of anthracene crystal taken by Clark and Philpott with our assignment. 1 the crystalline spectra determined from reflection data [15]. 2 the calculated values by the present theory

with calculated ones, the excited states are assigned to the  $B_{1u}$ ,  $B_{2u}$ ,  $B_{1u}$ ,  $B_{1u}$  and  $B_{1u}$  states in the region of from 4000 Å down to about 1700 Å. The  $B_{1u}$  state is polarized to the short molecular axis and the  $B_{2u}$  state to the long axis. In Table 1, the calculated values obtained by the present theory are compared with those by the usual CI method. The present theory gives better results in the calculation of excitation energies and oscillator strengths than the usual ASMO-SCF-CI method. Presumably, this improvement will be caused by the effect of electron correlation which will be efficient in decreasing the excitation energies and oscillator strengths of intense bands.

Anthracene crystallizes in the monoclinic system with the space group  $C_{2h}^5 - P2_1/a$  and has two molecules per unit cell [7]. In this crystalline lattice, molecule 1 may be transformed into molecule 2 by reflection in the  $ac$  plane

Table 2. Character table for the group  $C_{2h}$  and the selection rule of the exciton states

	$E$	$C_2$	$i$	$\sigma$	Transition moment*	
$A_g$	1	1	1	1	$d_1^S + d_2^S$	
$A_u$	1	1	-1	-1	$d_1^A - d_2^A$	$b$
$B_g$	1	-1	1	-1	$d_1^S - d_2^S$	
$B_u$	1	-1	-1	1	$d_1^A + d_2^A$	$a, c$

\* The lower subscript numbers the site in an unit cell and the upper subscripts  $S$  and  $A$  mean the symmetric ( $A_g$  and  $B_{1u}$ ) and antisymmetric ( $B_{1u}$  and  $B_{2u}$ ) electron-hole pairs with respect to inversion of the anthracene molecule.

Table 3. Comparison between the calculated and observed values of transition energies ( $E_f$  in eV) and oscillator strengths of the anthracene crystal

		The present theory					Observed values [15]			
		$A_u$ state		$B_u$ state			$A_u$ state		$B_u$ state	
		$E_f$	$f^b$	$E_f$	$f^a$	$f^c$	$E_f$	$f^b$	$E_f$	$f^a$
I	$B_{1u}$	3.627	0.508	3.531	0.152	0.010	3.137	0.248	3.161	0.076
II	$B_{2u}$	4.512	0.123	5.656	1.305	3.442	4.623	0.16	5.776	0.7
III	$B_{1u}$	5.801	0.741	5.810	0.146	2.167	5.566	0.6		
IV	$B_{1u}$	6.069	0.428	6.043	0.175	0.229	5.975	0.06	6.52	
V	$B_{1u}$	7.166	1.090	7.077	0.057	0.066	6.508	0.8		

followed by a glide at  $\frac{1}{2}a$ . The coefficients  $B_{\mu}(k)$ 's are determined from the character table of the group  $C_{2h}$  of the wave vector  $k=0$  as displayed in Table 2. It shows that the crystal field mixing arises only between  $A_g$  and  $B_{3g}$ ,  $B_{1u}$  and  $B_{2u}$  of the anthracene molecule and the allowed exciton states are  $A_u$  (polarized parallel to  $b$  axis) and  $B_u$  (polarized perpendicular to  $b$  axis) states. Table 3 gives the exciton state energies and oscillator strengths when the interactions for the inner zone were calculated to 50 Å. The absorption spectra of the anthracene crystal are reported by many workers [14, 15]. The crystalline spectra determined from reflectivity data by Clark and Philpott [15] are shown in the figure together with our assignment.

The calculated Davydov splitting ( $E_{B_u} - E_{A_u}$ ) of the band I is  $-780 \text{ cm}^{-1}$  while the observed value is  $360 \text{ cm}^{-1}$ . This result will be improved when the long range terms are included as is shown in our previous paper [6]. The intensity ratio ( $f^b/f^a = 3.5$ ) is in good agreement with the observed values (3.3) [15]. The Davydov splitting of the long axis polarized band II is a matter of controversial discussion, and the spectra [15] shown in the figure gives a value of  $9300 \text{ cm}^{-1}$ . The earlier transmission measurement by Lyons and Morris [14] gives a value of  $10000 \text{ cm}^{-1}$  for this splitting. Although a correct order of magnitude for this splitting was obtained in the earlier theories, but the agreement with the observed value was not so sufficient. Our calculated value in the present theory is  $9200 \text{ cm}^{-1}$ . The coincidence between the experiment and calculated value is quite satisfactory and it may be due to the correlation effect of  $\pi$ -electrons in high density solid state. Oscillator strengths are evaluated to be about 0.123 for the  $A_u$  state and 1.305 for the  $B_u$  state.

The bands III, IV and V at the higher energy region are originally derived from the molecular  $B_{1u}$  states polarized to the short axis. These bands are at 5.80, 6.07 and 7.12 eV for the  $A_u$  states and the oscillator strengths are 0.74, 0.43 and 1.09, respectively. The  $b$ -axis polarized spectrum has a peak at 5.57 eV, a weak shoulder at 5.98 eV and an intense peak at 6.51 eV and these are satisfactorily correlated with the calculated values. For the  $B_u$  exciton states, the corresponding levels are calculated at 5.81, 6.04 and 7.08 eV with  $f$  values of 0.146, 0.176 and 0.006. The shoulder at the vicinity of 6.5 eV may be assigned to the overlapped band of lower two transitions and the last band may not be observed because of its weak intensity.

### References

1. Fukutome, H.: Progr. theoret. Physics **33**, 380 (1965).
2. Dunning, T.H., McKoy, V.: J. chem. Physics **47**, 1735 (1967).
3. Agranovitch, V. M.: Sov. Physics, J.E.T.P. **10**, 307 (1960).
4. Agranovitch, V. M.: Sov. Physics, Solid State **3**, 592 (1961).
5. Philpott, M.R.: J. chem. Physics **50**, 5177 (1969).
6. Tanaka, M., Tanaka, J.: Molecular Physics **16**, 1 (1969).
7. Cruickshank, D.W.J.: Acta Crystallogr. **9**, 915 (1956).
8. Löwdin, P.O.: J. chem. Physics **18**, 365 (1950).
9. Roothaan, C.C.J.: Rev. mod. Physics **23**, 69 (1951).
10. Shibuya, T., McKoy, V.: J. chem. Physics **54**, 1738 (1971); J. chem. Physics **53**, 1308 (1970); Phys. Rev. A **2**, 2208 (1970).
11. Pariser, R., Parr, R.G.: J. chem. Physics **21**, 466 (1953).
12. Tanaka, M., Nagakura, S.: Theoret. chim. Acta (Berl.) **6**, 320 (1966).
13. Nishimoto, K., Mataga, N.: Z. physik. Chem. (N.F) **12**, 335 (1957).
14. Lyons, L. E., Morris, G.C.: J. chem. Soc. **1959**, 1551.
15. Clark, L. B., Philpott, M. R.: J. chem. Physics **53**, 3790 (1970).

Dr. M. Tanaka  
Department of Chemistry  
Faculty of Science  
Nagoya University  
Chikusa, 464, Nagoya, Japan





# Formal Solution for the Three Body Problem in Helium Theoretical Chemistry

F.T. Newman

Computing Centre, Trent Polytechnic, Nottingham, England

Received September 9, 1971/January 18, 1973

The theory of co-ordinates  $r_a, r_b$ , with  $r_b = \max(r_1, r_2)$  and  $r_a = \min(r_1, r_2)$  is developed to yield formal solutions for Schroedinger equations of helium theoretical chemistry. The correction for nuclear motion is included. Four most significant sets of terms in the ground state for the radial equation give a good approximation for the radial limit independently of the variation theorem. Thirteen most significant terms from the four sets are the basis for accurate variation calculations. A new radial limit is obtained.

Es wird eine Theorie für die Koordinaten  $r_a$  und  $r_b$  ( $r_b = \max(r_1, r_2)$ ,  $r_a = \min(r_1, r_2)$ ) entwickelt, um formale Lösungen der Schrödingergleichung von heliumartigen Systemen zu erhalten. Die Kernbewegung wird durch eine Korrektur berücksichtigt. Vier sehr wichtige Termgruppen des Grundzustandes ergeben im Falle der Radialgleichung eine gute Näherung für das Grenzverhalten, und zwar unabhängig vom Variationstheorem. Dreizehn sehr wichtige Terme aus den erwähnten vier Termgruppen bilden die Grundlage für exakte Variationsrechnungen.

## 1. Introduction

We develop the theory of co-ordinates  $r_a, r_b$  with  $r_b = \max(r_1, r_2)$  and  $r_a = \min(r_1, r_2)$ . This is done to yield formal solutions for Schroedinger equations of helium theoretical chemistry.

An atomic model is introduced in Section 2. This treats electron correlation and by inspection has advantages over more conventional treatments. The work described in this paper is the simplest application of the model. The model is fundamental enough to produce series solutions for radial and angular correlation.

The difficulties of using co-ordinates  $r_a, r_b$ , have been mentioned in the literature [1–3]. The behaviour of functions in  $r_a, r_b$ , to operators  $\partial/\partial r_i$ ,  $\partial^2/\partial r_i^2$ , ( $i = 1, 2$ ), operating in singular space defined by  $r = r_1 = r_2$ , is of special interest. This is because of the possible discontinuity in the first derivatives of such functions. In the general case the first and second derivatives of  $f(r_a, r_b)$  are undefined in singular space. Because the Hamiltonian operator contains  $\Sigma \partial^2/\partial r_i^2$ , ( $i = 1, 2$ ), the basis for treatment of such functions becomes important.

In Section 4 we derive expansions in  $r_1, r_2$ , for functions  $f(r_a, r_b)$ . We compare the operand behaviour of functions  $f(r_a, r_b)$  and their expansions in  $r_1, r_2$ . It is demonstrated that the discontinuities in the first derivatives of  $f(r_a, r_b)$  exist in the first derivatives of the expansions. The second derivatives of  $f(r_a, r_b)$  in singular space are infinite and undefinable. It is shown that the second derivatives of the corresponding expansions gives a divergent series for singular space. Therefore  $f(r_a, r_b)$  is not analytically equivalent to its expansion in  $r_1, r_2$ .  $\partial^2/\partial r_i^2 \cdot f(r_a, r_b)$

is undefined in singular space and is to be correlated with a divergent expansion in  $r_1, r_2$ .

The idea of variation calculations for the radial limit is considered in Sections 5, 6. Simulation functions  $\psi_0 f(r_a, r_b)$  are defined where  $\psi_0$  is the Kellner function from (7). These functions are outside the Domain of  $H$ . Nevertheless they can be used successfully in variation calculations. This is because functions  $\psi_0 f(r_a, r_b)$  can be expanded in  $r_1, r_2$ . Every term in the expansion is in the Domain of  $H$ . Despite the analytical differences between  $\psi_0 f(r_a, r_b)$  and the expansions, the former can be used for the latter in the calculation of matrix elements provided delta functions are used. More general simulation functions are derived.

A further boundary condition is developed in Section 7. This is that the discontinuities in the first derivatives of all terms  $\psi_0 C_{p,q} r_a^p / r_b^q$  in a function should cancel. The constants  $C_{p,q}$  may be adjusted for this condition. These functions are no longer simulation functions. They come into the Domain of  $H$ .

The coefficients  $C_{p,q}$  can be sorted into sets according to the value of  $p - q$ . The four most significant sets correspond to values 0, 1, 2, 3. A recursion formula is developed in Section 8 for these four most significant sets of coefficients in the series solution of the ground state for the radial Schroedinger equation. The estimate of the eigenvalue obtained from these coefficients is  $-2.8788 H$ . This result is accurate to 9 parts in  $10^5$  and is independent of the variation theorem.

The series from the recursion formula and boundary conditions fails to continue to the fifth most significant set of coefficients while remaining in the Domain of  $H$ . The unique way out of this difficulty is to make the series more general with a typical term  $\psi_0 C_{p,q,j} r_a^p / r_b^q \cdot (\log r_b)^j$ ,  $j \geq 0$ ,  $C_{p,q,j} = 0$  when  $p - q < 4j$ .

In Section 9 Kato's cusp theorems are discussed. The cusp relation at the nucleus is shown to follow from the recursion formulae in Section 8. Some difficulty arises when  $H$  is defined in  $r_1, r_2, \cos \theta$ , and  $0.5 \psi_0 r_{12}$  is regarded as part of the solution to helium when  $r_{12} = 0$ .  $r_{12}$  is better replaced by its expansion in  $r_a, r_b, P_1(\cos \theta)$ .

In Section 10 terms are obtained for the ground state of the SP and Complete Schroedinger equations. The latter shows the correct cusp behaviour when  $r_{12}$  tends to zero. From a consideration of the need for logarithmic terms similar to that in Section 8 an analytical form is produced for angular as well as radial correlation. Recursion formulae are produced for the formal solutions to the SP, SPD and Complete Schroedinger equations defined in Section 3. Coefficients from the Complete equation are corrected for the motion of the nucleus in Section 12. The correction though a small one does enable the series solution for the helium three body problem.

Successful and economic variation results are described in Section 11. The thirteen most significant terms of the solution to the radial Schroedinger equation are implemented variationally. This calculation produces a new radial limit of  $-2.879,028,59 H$ .

## 2. An Atomic Model

Instead of a conventional model wave function:

$$\psi_0^{\text{det}} \{1 + \sigma g(r_1, r_2, r_3 \dots \cos \theta_{12}, \cos \theta_{13} \dots)\} \quad (1)$$

we propose:

$$\psi_0^{\text{det}} \{1 + f(r_a, r_b, r_c, \dots \cos \theta_{ab}, \cos \theta_{ac}, \dots)\} \quad (2)$$

with  $r_a \leq r_b \leq r_c, \dots$  and  $\theta_{ij}$  the angle between  $r_i$  and  $r_j$ .  $\psi_0^{\text{det}}$  is a variational form of the determinantal solution from the appropriate zero order problem. This problem is that of non-interacting electrons moving in a central field. A single variation constant is envisaged which is the single exponential constant.  $f$  and  $g$  are functions not usually symmetrical to the interchange of subscripts.  $\sigma$  is the corresponding symmetrising operator.  $f$  is a more flexible form than  $\sigma g$ . If a particular case of  $f$  is symmetrical to the interchange of subscripts it is identical to a particular case  $\sigma g$ . More generally the symmetrising operator must not be included in (2). This is because any  $f$  is intrinsically symmetrical in  $r_1, r_2$ .  $f$  has the advantage of yielding functions which are shown to require an infinite series of functions  $\sigma g$ .

Electron zoning has been introduced in (2) precisely and compactly by using co-ordinates which are useful for the expression of the interelectron potential operator. Our present concern is with the small set of co-ordinates  $r_a, r_b, \theta_{ab}$ . These are co-ordinates for the helium problem.

### 3. Basic Definitions and Results in the Helium Problem

The Hamiltonian operator in the zero order helium problem is:

$$H^0 = -1/2 \cdot \nabla_1^2 - 1/2 \cdot \nabla_2^2 - 2/r_1 - 2/r_2 \quad (3)$$

if operands to  $H^0$  are expressed in the form  $\Sigma C_l$  (radial part)  $\cdot P_l(\cos \theta)$  with  $\theta = \theta_{12} = \theta_{ab}$  in (1), (2) then  $\nabla_i^2$  is conveniently replaced by:

$$\partial^2 / \partial r_i^2 + 2/r_i \cdot \partial / \partial r_i - l(l+1)/r_i^2 \quad (4)$$

$H'$  the interelectron potential operator is usually taken as first order to  $H^0$ . This is here defined as:

$$H' = \sum_i^{0, \infty} r_a^l / r_b^{l+1} \cdot P_l(\cos \theta); \quad r_a = \min(r_1, r_2); \quad r_b = \max(r_1, r_2); \quad (5)$$

The series in (5) has the following properties:

- i) absolute convergence for all parts of space  $r_b > r_a$ .
- ii) uniform convergence for any closed part of space with  $r_b > r_a$ .
- iii) convergence for any part of space with  $r_b = r_a$ ,  $|\cos \theta| < 1$ .

We are to use the series in (5) to form the Hamiltonian operator  $H = H^0 + H'$ . The resulting Schroedinger equation is to be solved formally. Intermediate Schroedinger equations are defined for formal solution. These are the S, SP, SPD, ..., Schroedinger equations as  $H'$  in  $H$  is expanded to the first, second, third, ..., term. The Schroedinger equation for the complete expansion of  $H'$  is called the Complete Schroedinger equation.

$H'$  fails to converge when  $r_a = r_b = r$ ,  $\cos \theta = -1$ . The series oscillates between 0 and  $1/r$  instead of giving  $1/(2r)$ . If this difficulty prevents the numerical processing for any series solution for helium, (5) could be replaced by (5a).

$$H' = \sum_i^{0, \infty} r_a^l / r_b^{l+1} \cdot P_l(\cos \theta) + 1/2 \cdot r_a^{n+1} / r_b^{n+2} \cdot P_{n+1}(\cos \theta) \quad (5a)$$

$n \rightarrow \infty$

As  $n$  increases from zero to infinity  $H'$  is always  $1/(2r)$  when  $r_a = r_b$ ,  $\cos\theta = -1$ . It will be shown in Section 10 that one important series of terms in the helium eigenfunction is given correctly when (5) is used. This is true when  $r_a = r_b$ ,  $\cos\theta = -1$ . It seems probable therefore that (5a) will never need to be substituted for (5).

As the electrons approach the same point  $H'$  tends to infinity. When the electrons occupy the same point the series for  $H'$  diverges. This divergence may be associated with the natural infinity of  $1/r_{12}$ . If  $\Psi$  is a series solution such that  $(H^0 + H')\Psi = E\Psi$ , then the result of  $(H^0 + H')\Psi$  leads to a cancellation of the terms of  $H'\Psi$ . This is true when the separation of the electrons is infinitesimal. When the separation is zero  $H'\Psi$  becomes undefined but  $(H^0 + H')\Psi$  may be defined by a continuity argument.

No practical difficulty appears to arise from the use of  $H'$  if  $\Psi$  can be deduced.

The solutions to the zero order problem defined in (3) form an incomplete set of square integrable orthonormal functions, the  $p$ th element of which is  $\psi_p^0$ . The inclusion of the functions from the continuum makes the set complete. The configuration interaction method for helium uses trial wave functions:

$$\sum C_p \psi_p^0 \quad (6)$$

For the singlet ground state of helium the space spin Kellner variation form is used for  $\psi_0^{\text{det}}$  with the space part given in (7).

$$\psi_0 = \exp\{-\zeta(r_1 + r_2)\} \quad (7)$$

Because of the interelectron energy the average potential energy for helium is less negative than in the zero order problem. It follows from the virial theorem that the average kinetic energy of the former is less positive. If we regard  $\zeta$  as a variation constant in the context of (7), (1) or (2), the average kinetic energy is reduced by reducing  $\zeta$  from 2. Further it is often convenient to give  $\zeta$  the value of minus the square root of the eigenvalue. Under this condition the functions in (7), (1), and (2) have the proper operand behaviour to  $H(=H^0 + H')$  when both electrons are at infinity.  $\psi_0$  is an eigenfunction of  $H^0$  only if  $\zeta = 2$ .

A set of square integrable functions with the  $i$ th element  $\psi_i$  is said to be in the Domain of  $H$  if all  $H\psi_i$  are square integrable and the relationship between matrix elements in (8) is satisfied.

$$\int \psi_i H \psi_j d\tau = \int \psi_j H \psi_i d\tau \quad (8)$$

$\psi_i$  and  $H\psi_i$  are well formed in Hilbert space. The Ritz variation principle may be applied to functions in the Domain of  $H$ . It follows that:

$$\int \left( \sum_n c_n \psi_n \right) H \left( \sum_n c_n \psi_n \right) d\tau / \int \left( \sum_n c_n \psi_n \right)^2 d\tau \geq E_0 \quad (9)$$

where  $E_0$  is the ground state eigenvalue of the system defined in  $H$ . The constants  $c_i$  can be varied to produce a minimum value for the left hand side of (9). If the functions  $\psi_i$  form a complete set then the left hand side of (9) tends to  $E_0$  if the constants  $c_i$  are optimised and  $n$  tends to infinity.

It is noteworthy that  $\psi_0$  is in the Domain of  $H$  but  $H\psi_0$  is not. It is not unexpected therefore that  $\int (H\psi_0) H(H\psi_0) d\tau$  is indeterminately large and negative.

#### 4. The Operand Behaviour of $f(r_a, r_b)$

Let us consider the simple cases of  $f_1 = r_a^2$ ,  $f_2 = 1/r_b$ :

$$\begin{aligned} \partial f_1 / \partial r_{1, r_1 < r_2} &= 2r_a; & \partial f_1 / \partial r_{1, r_1 > r_2} &= 0; \\ \partial f_2 / \partial r_{1, r_1 < r_2} &= 0; & \partial f_2 / \partial r_{1, r_1 > r_2} &= -1/r_b^2; \end{aligned} \quad (10)$$

We see that the first derivatives of  $f_1$ ,  $f_2$ , are discontinuous when  $r_1 = r_2$ . Further differentiation at the discontinuity is undefined. Because first and second derivatives of  $r_a^2$  and  $1/r_b$  are not analytic in the space  $r_1 = r_2$  we call this space singular space.

Three results are stated and then demonstrated.

i) Any continuous function  $f_j(r_a, r_b)$  in (2) may in general be expanded as an infinite series of terms. These terms are symmetrical in  $r_1, r_2$ . Further the first and second derivatives of these terms with respect to  $r_1, r_2$ , are analytic. So we write:

$$f_j(r_a, r_b) = \sum_k C_{k,j} \chi_{k,j}(r_1, r_2) \quad (11a)$$

ii) The equality:

$$\partial / \partial r_i \cdot f_j(r_a, r_b) = \partial / \partial r_i \cdot \sum_k C_{k,j} \chi_{k,j}(r_1, r_2) \quad (11b)$$

with  $i = 1$  or  $2$ , holds for all functions  $f_j$  and  $\chi_{k,j}$  from (11a). This is so for all of space including what is singular space when  $r_1 = r_2$ . If the left hand side of (11b) is discontinuous when  $r_1 = r_2$  then also is the right hand side.

(iii) The inequality:

$$\partial^2 / \partial r_i^2 \cdot f_j(r_a, r_b) \neq \partial^2 / \partial r_i^2 \cdot \sum_k C_{k,j} \chi_{k,j}(r_1, r_2) \quad (11c)$$

holds where the left hand and right hand sides of (11b) are discontinuous. At any discontinuity from (11b), the right hand of (11c) diverges while the left hand side of (11c) cannot be formed.

The results in (11) are demonstrated by comparing two expansions for  $1/r_{12}$ , (5) and (12).

$$\begin{aligned} 1/r_{12} &= (1 + 1/2 \cdot \xi \cos \theta + 1/2 \cdot 3/4 \cdot \xi^2 \cos^2 \theta \dots) (r_1^2 + r_2^2)^{-1/2} \\ \xi &= 2r_1 r_2 / (r_1^2 + r_2^2) \end{aligned} \quad (12)$$

Our interest is to rewrite (12) in Legendre harmonics. To do this we expand  $\cos^m \theta$  in Legendre harmonics. By comparing the  $l$ th harmonic parts of (5) and the re-expansion of (12), we obtain a series for  $r_a^l / r_b^{l+1}$  in  $r_1, r_2, \xi$ . For  $l = 0$  we have (13).

$$1/r_b = (1 + 1/2 \cdot 3/4 \cdot 1/3 \cdot \xi^2 + 1/2 \cdot 3/4 \cdot 5/6 \cdot 7/8 \cdot 1/5 \cdot \xi^4 + \dots) (r_1^2 + r_2^2)^{-1/2} \quad (13)$$

Fortunately the series in (13) converges absolutely for all  $\xi$ ;  $\xi \leq 1$ . Thus the result in (11a) is proved for the particular case:  $f(r_a, r_b) = 1/r_b$ .

We compare the operand behaviour of the two sides of (13) to  $\partial / \partial r_i$  with  $i = 1$  or  $2$ . We obtain (14) from the right hand side of (13) by operating with  $\partial / \partial r_1$ .

$$\begin{aligned} -\{1 + 1/2 \cdot 3/4 \cdot 1/3 \cdot \xi^2 + 1/2 \cdot 3/4 \cdot 5/6 \cdot 7/8 \cdot 1/5 \cdot \xi^4 + \dots\} r_1 (r_1^2 + r_2^2)^{-3/2} \\ + 2\{1/2 \cdot 3/4 \cdot 2/3 \cdot \xi + 1/2 \cdot 3/4 \cdot 5/6 \cdot 7/8 \cdot 4/5 \cdot \xi^3 + \dots\} r_2 (r_2 - r_1) (r_1 + r_2) \\ \cdot (r_1^2 + r_2^2)^{-5/2} \end{aligned} \quad (14)$$

The series factor of the second term in (14) tends to infinity as  $\xi$  approaches 1. The binomial expansion of  $1/2 \cdot (1 - \xi)^{-1/2} - 1/2 \cdot (1 + \xi)^{-1/2}$  tends to infinity in the same way. In the limit the series factor can be replaced by  $1/2(1 - \xi)^{-1/2}$ . Let us consider an interval  $\Delta r = r_2 - r_1$  which is very small so that  $r_2$  and  $r_1$  are considered to approach  $r$ . In the limit (14) converges to (15).

$$-1/2 \cdot 1/r^2 + 1/2 \cdot 1/r^2 \cdot \Delta r / |\Delta r| \quad (15)$$

(15) shows just the discontinuous behaviour shown by  $\partial/\partial r_1(1/r_b)$  in (10). Thus the result in (11b) is justified for the particular case:  $f(r_a, r_b) = 1/r_b$ .

We may repeat the analysis for  $l > 0$  in any  $r_a^l/r_b^{l+1}$  from before (13). More generally series may be obtained for  $f(r_a, r_b)$ . This justifies the results in (11a) and (11b). For example the series for  $r_a$  may be obtained by multiplying the right hand side of (13) by  $r_1 r_2$  and that for  $r_b$  may be obtained by using:

$$r_b = r_1 + r_2 - r_a.$$

The second derivative of (13) with respect to  $r_1$  is the first derivative of (14). The factor  $(r_2 - r_1)$  in the second term of (14) prevents the series from diverging when  $r_1 = r_2$ . The differentiation of the factor  $(r_2 - r_1)$  will cause the second derivative of (13) to diverge when  $r_1 = r_2$ . This divergence in general is to be correlated with the undefined first derivative of a discontinuity. The result in (11c) is justified.

### 5. Variation Calculations, Dirac Delta Functions, The Finite Contribution to Matrix Elements from Singular Space of Zero Volume and Simulation

We consider the terms of the series in (15) as a basis for variation calculations.

$$\psi_0 \sum_p^{0, \infty} \sum_q^{l, p} \sum_i^{0, \infty} C_{p,q,i} r_a^p / r_b^q \cdot P_i(\cos \theta) \quad (16)$$

The Hylleraas expansion can be re-expanded in terms which are a subset of those in (16). The functions in the Hylleraas expansion have been shown to be complete [4]. Therefore the functions in (16) are complete. So are the functions in (17).

$$\psi_0 \sum_p^{0, \infty} \sum_q^{l, p} C_{p,q} r_a^p / r_b^q. \quad (17)$$

Our interest is firstly to implement (17) variationally to estimate the radial limit and secondly to find the series solution for the  $S$ -equation defined after (5). There are two difficulties however.

i) Because of (11c) and the second derivative in (4) the functions  $\psi_0 r_a^p / r_b^q$  are not the same operators to  $H$  as their expansions in (18).

$$\psi_0 r_a^p / r_b^q = \psi_0 \sum_k C_{k,j} \chi_{k,j}(r_1, r_2). \quad (18)$$

The calculation of the left hand side of (19) presents difficulties.

$$\int \psi_0 r_a^p / r_b^q \cdot H \psi_0 r_a^p / r_b^q \cdot d\tau = \sum_k \sum_j C_{k,j} C_{k',j'} \int \psi_0 \chi_{k,j} H \psi_0 \chi_{k',j'} d\tau. \quad (19)$$

The evaluation of the right hand side of (19) presents no such difficulties.

ii) We shall see that functions  $\psi_0 r_a^p / r_b^q$  are not in the Domain of  $H$ .

However if we find some way of evaluating matrix elements such that the matrix relationships in (20) and (21) are satisfied we conclude that functions  $\psi_0 r_a^p / r_b^q$  simulate functions  $\psi_0 \sum_k C_{k,j} \chi_{k,j}(r_1, r_2)$  for the evaluation of matrix elements provided that the functions  $\psi_0 \chi_{k,j}$  are in the Domain of  $H$ .

$$\int \psi_0 H \psi_0 r_a^p / r_b^q d\tau = \int \psi_0 r_a^p / r_b^q H \psi_0 d\tau. \quad (20)$$

$$\int \psi_0 r_a^{p'} / r_b^{q'} \cdot H \psi_0 r_a^p / r_b^q d\tau = \int \psi_0 r_a^p / r_b^q \cdot H \psi_0 r_a^{p'} / r_b^{q'} d\tau. \quad (21)$$

If all relevant cases of (20) and (21) hold and all corresponding functions  $\psi_0 \chi_{k,j}$  are in the Domain of  $H$  it follows from after (9) that the Ritz variation method can be used with (17).

Dirac  $\delta$ -functions [5] are used for the evaluation of the unexpanded matrix elements in (20), (21). From (3), (4) we consider

$$1/2 \cdot \psi_0 \partial / \partial r_1 (r_a^p / r_b^q), 1/2 \cdot \psi_0 \partial^2 / \partial r_1^2 (r_a^p / r_b^q)$$

for a fixed value of  $r_2$ . The first derivative term shows the discontinuity in (22) when  $r_1 = r_2$ .

$$A_1 = -1/2 \cdot (p+q) r_2^{p+q-1} [\psi_0]_{r_1=r_2}. \quad (22)$$

Therefore over this singular space of zero volume the second derivative is infinite. The integration of the second derivative term over singular space can be redistributed over  $r_1$  space. The result is given in (23).

$$\int_0^\infty \psi_0 r_a^{p'} / r_b^{q'} r_1^2 A_1 \delta(r_1 - r_2) dr_1 = [\psi_0]_{r_1=r_2} r_2^{p'+q'+2} A_1 \quad (23)$$

$\delta(r_1 - r_2)$  is a  $\delta$ -function. It has the value zero for all values of  $r_1$  except where  $r_1 = r_2$ .  $\delta(r_1 - r_2)$  then becomes indeterminately large. We integrate the right hand side of (23) for all values of  $r_2$ . The contribution to the left hand side of (21) from the total singular space is:

$$(p+q) \int_0^\infty [\psi_0^2]_{r_1=r_2} r_2^{p+q-1} dr_2. \quad (24)$$

With the aid of  $\delta$ -functions we can evaluate the integrals in (20), (21). However there is no way of evaluating (25). From this follows (ii) after (19).

$$\int [H \psi_0 r_a^p / r_b^q]^2 d\tau \quad (25)$$

## 6. Acceptable Terms $\psi_0 r_a^p / r_b^q$ for the Ritz Variation Method and Successful Simulation

From Section 5 we require the ranges for integers  $p$  and  $q$  for which the matrix relations in (20), (21) hold and all corresponding functions  $\psi_0 \chi_{k,j}$  are in the Domain of  $H$ . The contributions to matrix elements from singular space are calculated according to Section 5. We now state the result for a basis set from (17)

to form a valid wave function. The sufficient conditions for all  $p$  and  $q$  are:

$$q - p \leq 0; \quad p \geq 0; \quad (26)$$

Given (26) we draw conclusions.

(i) With "simulation" defined before (20), the series in (17) successfully "simulates" its expansion according to (18) for the evaluation of matrix elements. This expansion is the proper wave function. The terms of (17) are simulation functions.

(ii) The treatment of singularities in Section 5 is successful and effectively treats the divergence from the right hand side of (11c).

We now sketch the derivation of (26). From (13) it follows that infinitely many functions  $\psi_0 \chi_{k,j}$  for any value  $j$  in (11a) are of the form  $\psi_0(r_1 r_2)^m / (r_1^2 + r_2^2)^{n/2}$ . For these functions to be in the Domain of  $H$  it is necessary and sufficient for  $m - n \geq 0$ . It follows that:

$$p - q \geq 0. \quad (27)$$

A generalisation of (27) is that  $\psi_0 / (r_a, r_b)$  must not tend to infinity near  $r_1 = r_2 = 0$ . The second consideration is the effect of the indices  $p, q, p', q'$ , on the matrix relations (20), (21). We need only consider the Laplacian parts of  $H$  in (28).

$$-1/2 \cdot \int r_a^p / r_b^{q'} \cdot \psi_0 (V_1^2 + V_2^2) \psi_0 r_a^{p'} / r_b^{q'} d\tau. \quad (28)$$

All contributions to (28) are first considered excluding those from singular space examined in Section 5. From (7), (3) and (4) with  $l = 0$ , we represent (28) as:

$$\begin{aligned} & \int_0^{\infty} \exp(-2\zeta r_2) r_2^{p'+p'-2} dr_2 \int_0^{r_1} \exp(-\zeta r_1) / r_1^{q'-1} \cdot \partial^2 / \partial r_1^2 \{ \exp(-\zeta r_1) / r_1^{q'-1} \} dr_1 \\ & + \int_0^{\infty} \exp(-2\zeta r_1) / r_1^{q'+q'-2} dr_1 \int_0^{r_1} \exp(-\zeta r_2) r_2^{p'+1} \cdot \partial^2 / \partial r_2^2 \{ \exp(-\zeta r_2) r_2^{p'+1} \} dr_2. \end{aligned} \quad (29)$$

The integration of (29) by parts gives:

$$\begin{aligned} & - \int_0^{\infty} \exp(-2\zeta r_2) r_2^{p'+p'-2} dr_2 \left[ r_1 \exp(-\zeta r_1) / r_1^{q'-1} \cdot \partial / \partial r_1 \{ \exp(-\zeta r_1) / r_1^{q'-1} \} \right] \\ & + \int_0^{\infty} \exp(-2\zeta r_2) r_2^{p'+p'-2} dr_2 \int_{r_2}^{r_1} \partial / \partial r_1 \{ \exp(-\zeta r_1) / r_1^{q'-1} \} \cdot \partial / \partial r_1 \{ \exp(-\zeta r_1) / r_1^{q'-1} \} dr_1 \\ & - \int_0^{\infty} \exp(-2\zeta r_1) / r_1^{q'+q'-2} dr_1 \left[ r_2 \exp(-\zeta r_2) r_2^{p'+1} \cdot \partial / \partial r_2 \{ \exp(-\zeta r_2) r_2^{p'+1} \} \right] \\ & + \int_0^{\infty} \exp(-2\zeta r_1) / r_1^{q'+q'-2} dr_1 \int_0^{r_1} \partial / \partial r_2 \{ \exp(-\zeta r_2) r_2^{p'+1} \} \cdot \partial / \partial r_2 \{ \exp(-\zeta r_2) r_2^{p'+1} \} dr_2. \end{aligned} \quad (30)$$

We consider the single integral terms in (30) which are unsymmetrical in index pairs  $pp'$  and  $qq'$ . If and only if  $p + p' \geq 0$ , these unsymmetrical terms can be combined together to give:

$$-(p+q) \int_0^{\infty} \exp(-4\zeta r_1) r_1^{p'+p'-q-q'+3} dr_1, \quad (31)$$

$$p + p' \geq 0 \quad (32)$$



We add the remaining contribution to (28) which is (24). This if (32) holds, the result from (28) is symmetrical in  $pp'$  and  $qq'$ . In the evaluation of all matrix elements for a variation calculation using (17), the same values occur for  $p$  as for  $p'$ .  $p$  and  $p'$  must have the same minimum value. Therefore  $p \geq 0$ . (26) is derived. From (26) it follows that the integrands in (30) tend to zero near  $r_1 = r_2 = 0$ . Because of (26) all terms in (17) are simulation functions. These make a complete set.

It is of interest to compare the expansions of  $\psi_0 r_a / r_b$  and  $\psi_0 r_b / r_a$  according to (18). From (26)  $\psi_0 r_a / r_b$  is a simulation function and must yield terms all in the Domain of  $H$ .  $\psi_0 r_b / r_a$  is not a simulation function and must yield at least one term not in the Domain of  $H$ . The condition that the matrix relation in (8) is satisfied with  $\psi_j = \psi_a$  is:

$$\psi_0 r_k \partial / \partial r_k (\psi_i r_k) |_{r_k=0, \infty} = \psi_i r_k \partial / \partial r_k (\psi_0 r_k) |_{r_k=0, \infty} = 0 \quad (33)$$

with  $k = 1, 2$ .

Squaring the series in (13) and multiplying each term by  $\psi_0 r_1 r_2$  we obtain the expansion of  $\psi_0 r_a / r_b$ . All terms satisfy  $\psi_i$  in (33). Now considering  $\psi_0 r_a / r_b$  we have (34).

$$\psi_0 r_b / r_a = \psi_0 r_1 / r_2 + \psi_0 r_2 / r_1 - (\text{the terms for } \psi_0 r_a / r_b). \quad (34)$$

According to (33) the first two terms on the right hand side of (34) are not in the Domain of  $H$ .

Finally we consider just what functions  $\psi(r_a, r_b)$  are valid simulation functions. By arguments similar to those used for the condition for  $p$  in (26) we obtain an analogue to (33) for functions  $\psi(r_a, r_b)$  which are continuous and square integrable. This analogue is (35).

$$\psi_0 r_a \partial / \partial r_a \{r_a \psi(r_a, r_b)\} |_{r_a=0} = \psi(r_a, r_b) r_a \partial / \partial r_a \{\psi_0 r_a\} |_{r_a=0} = 0, \quad (35a)$$

$$\psi_0 r_b \partial / \partial r_b \{r_b \psi(r_a, r_b)\} |_{r_b=0} = \psi(r_a, r_b) r_b \partial / \partial r_b \{\psi_0 r_b\} |_{r_b=0} = 0. \quad (35b)$$

The similarity between (33) and (35) means that simulation functions can be generated by taking any unsymmetrical function in  $r_1, r_2$ , which is in the Domain of  $H$  and substituting  $r_a, r_b$  for  $r_1, r_2$  or  $r_2, r_1$ .

A second sort of simulation function can be formed from (35). This is of the general type  $f(r_a, r_b) \exp(-\zeta r_b)$ . The simplest example is  $\exp(-\zeta r_b)$ . We note that  $\exp(-\zeta r_a)$  is not acceptable according to (35). This function is not even square integrable.

## 7. Two Different Types of Model Wave Functions

The first derivatives of the terms in (17) have discontinuities in singular space. These discontinuities have been characterised in Section 4, 5. It is critical to distinguish two types of functions (17) for which the conditions in (26) hold. This is done according to the sum of the discontinuities. The two different types of functions are referred to as functions of the First Type and functions of the Second Type.

(i) We define a function of the First Type. For such a function the discontinuities from the operation of  $\partial/\partial r_i$ , ( $i = 1, 2$ ), on all terms sum to zero in all singular space.

(ii) For a function of the Second Type the discontinuities do not sum to zero in all singular space.

Because of (26) we write (17) in the form:

$$\psi_0 \sum_n^{0, \infty} \sum_m^{0, \infty} C_{m, m-n} r_a^m / r_b^{m-n} \quad (36)$$

The condition for (36) to represent a general form of the First Type is (37) for all the values of  $n$  in (36).

$$\sum_m^{0, \infty} (2m - n) C_{m, m-n} = 0 \quad (37)$$

There are three results for functions of the First Type which do not extend to functions of the Second Type.

$$(i) \quad \psi_0 \partial^2 / \partial r_i^2 \cdot f_j(r_a, r_b) = \psi_0 \partial^2 / \partial r_i^2 \cdot \sum_k C_{k,j} \chi_{k,j}(r_1, r_2); \quad \text{c.f. (11c)} \quad (38)$$

The result in (38) holds even for singular space. The first derivatives of  $f(r_a, r_b)$  are no longer discontinuous. If both sides of (38) are undefined because of discontinuities they contain what is the same discontinuity. This occurs in a similar way to the result in (15).

(ii)  $\psi_0 f(r_a, r_b)$  is now in the Domain of  $H$  [c.f. (25)]. Matrix elements are evaluated without the use of  $\delta$ -functions. From the definition of simulation functions after (26),  $\psi_0 f(r_a, r_b)$  is no longer merely a simulation function. In general it may be assumed to be analytically equivalent to  $\psi_0 \sum_k C_{k,j} \chi_{k,j}(r_1, r_2)$  for the evaluation of matrix elements.

(iii)  $\psi_0 \sum_i \partial^2 / \partial r_i^2 \cdot f(r_a, r_b)$ , ( $i = 1, 2$ ), is analytically defined for a function of the First Type. This is because any undefined part is proportional to  $\Delta r / |\Delta r| - \Delta r / |\Delta r| = 0$ ; c.f. (15).

It follows from the discussion in this section that any formal solution to a Schroedinger equation will be a function of the First Type. This is because the eigenfunctions of  $H$  are in the Domain of  $H$ . Similarly any complete model wave function of the Second Type will tend towards a function of the First Type.

## 8. The Series Solution for the Ground State of the Radial Helium Schroedinger Equation

We consider the radial helium Schroedinger equation and derive early sets of terms in the series solution for the ground state. These are processed to give an estimate of the eigenvalue. This estimate for what is the radial limit is independent of the variation theorem. From (3), (4) and after (5) the equation is:

$$(H^0 + 1/r_b - E_0) \Psi_0 = 0 \quad (39)$$

We obtain a recursion formula. From this and boundary conditions we produce the four most significant sets of terms in the series solution. This approach fails to produce later sets of terms. From this failure we are able to deduce the general form of the formal solution. This includes logarithmic terms.

The recursion formula used for the partial solution of (39) is simple. To obtain it we take  $\Psi_0$  from the complete expansion in (17). The corresponding recursion formula is:

$$\begin{aligned} p(p+1) C_{p,q} + (q-2)(q-3) C_{p-2,q-2} \\ = -2\{1+\zeta(q-2)\} C_{p-2,q-1} + 2\{p\zeta-2\} C_{p-1,q} \\ - 2(\zeta^2 + E_0) C_{p-2,q} \end{aligned} \quad (40)$$

Suppose  $p-q=n$ . For smaller values of  $p-q$  all  $C_{p,q}$  have been determined. We are to use (40) to determine all  $C_{p,q}$  with the same value of  $n$ . When  $p=n+2$ ,  $n+3$ , then  $C_{p,q}$  is obtained in terms of already determined coefficients with  $p-q=n-1$  and  $n-2$ . When  $p>n+3$  then a non zero already determined term  $(q-2)(q-3) C_{p-2,q-2}$ , with  $p-q=n$ , contributes to the left hand side of (40). From (26) we have the result:

$$C_{p,q} = 0 \quad \text{for } p < 0 \quad \text{or } q > p \quad (41)$$

When  $p=0$  both sides of (40) are zero. When  $p<n+2$  and odd  $C_{p,q}$  can be determined in a similar way to terms  $p \geq n+2$ . For  $p < n+2$  and even there results a set of  $m$  consistent simultaneous equations.  $m$  is given in (42):

$$m = \text{integer part } \{(n+1)/2\} \quad (42)$$

The simultaneous equations have  $m+1$  coefficients  $C_{p,q}$  with  $p-q=n$ , to be determined. Therefore an extra equation is needed. This derives from Section 7. The series solution must be a function of the First Type in the Domain of  $H$ . So from (37) we obtain:

$$\begin{aligned} \sum_p^{0,m} (4p-n) C_{2p,2p-n} = - \sum_p^{0,m} (4p+2-n) C_{2p+1,2p+1-n} \\ - \sum_p^{2m+2,\infty} (2p-n) C_{p,p-n}; \quad n \neq 0 \end{aligned} \quad (43)$$

From (40) the evaluation of  $E_0$  is necessary for the solution of  $\Psi_0$  in (39). The consideration is of an approximation to  $\Psi_0$  made from a series of most significant sets of terms. Each set corresponds to a particular value of  $n$ . An approximation to the eigenvalue is  $E'_0$ . The corresponding approximate eigenfunction is  $\Psi'_0$ .  $E'_0$  is obtained by successive approximations in (44).

$$E'_0 = \int \Psi'_0 (H^0 + 1/r_b) \psi_0 d\tau / \int \Psi'_0 \psi_0 d\tau \quad (44)$$

We indicate the determination of the four most significant sets of coefficients in (40) and (43). These correspond to  $n=0, 1, 2, 3$ .

$C_{p,p} = 0$  for  $p > 0$ .  $C_{0,0}$  is undetermined in (43) and is arbitrarily given the value unity:  $C_{0,0} = 1$ .

From all  $C_{p,p-1}$  we obtain just three non-zero coefficients:

$$C_{2,1} = 1/6, C_{1,0} = \zeta - 2, C_{0,-1} = \zeta - 1.5 \quad (45)$$

From all  $C_{p,p-2}$  we obtain an infinite set of non-zero coefficients. We obtain:  $C_{p,p-2} = 0$  for  $p \geq 5$ ,  $p = \text{odd}$ , otherwise  $C_{p,p-2} \neq 0$  for  $p \geq 0$ .  $C_{p,p-3} \neq 0$  for all values of  $p \geq 0$ .

Values for  $E'_0$  in (44) will depend on the selected value for  $\zeta$  in (7) and (40). We take  $\zeta = (-E'_0)^{1/2}$ . The result is an approximate eigenvalue of  $-2.8788 H$ . This result shows an error of 9 parts in  $10^5$ . This value can be obtained with as few as 29 terms from (36) in (44). All matrix elements in (44) are simple off-diagonal matrix elements. The Ritz variation method requires diagonal matrix elements. The variational method favours the eigenvalue for a comparable eigenfunction. Nevertheless the 29 terms in (44) yield a comparable eigenvalue to a 15-term Ritz variation calculation [6]. The latter employs terms from a complete set of square integrable functions closely related to the functions in (6). The series calculation is shorter and simpler.

Four approximations to the eigenvalue can be obtained usefully from (36) and (44). These correspond to  $n = 0$ ;  $n = 0, 1$ ;  $n = 0, 1, 2$ ;  $n = 0, 1, 2, 3$ . The approximations are:

$$-2.8477, -2.8689, -2.8777, -2.8788 H \quad (46)$$

The eigenvalue to five figures is  $-2.8790 H$ . These results improve in the ratios of 1:3:24:156.

The simple method of series solution becomes more complex for  $n \geq 4$ . Whenever  $n$  is a multiple of 4 the  $m$  equations before (42) can be combined together to give the left hand side of (43). This makes the  $m+1$  equations needed for the simple solution inconsistent. The  $m$  equations give an infinite set of solutions.

(43) can no longer be used to select the set which puts the terms  $\psi_0 \sum_p^{0,\infty} C_{p,p-n} r_a^p / r_b^{p-n}$  in the Domain of  $H$ . Despite the completeness of (17) it becomes necessary to introduce logarithmic terms.

We require an auxiliary series to (36) to be able to remove the discontinuity in first derivatives when  $n = 4$ . Such a series must differ in form from (36) and yet give terms of the sort in (36) on differentiating with respect to  $r_i$  ( $i = 1$  or  $2$ ). The form must be logarithmic and is:

$$\psi_0 \sum_n^{4,\infty} \sum_p^{0,\infty} C_{p,p-n,1} r_a^p / r_b^{p-n} \cdot \log r_b \quad (47)$$

From (47) and considerations similar to those which lead to (26), we obtain (48) with  $j = 1$ . (40) is replaced by (49).

$$C_{p,p-n,j} = 0 \quad \text{for } p < 0 \quad \text{or } n < 4j. \quad (48)$$

$$\begin{aligned} p(p+1) C_{p,p-n,j} + (p-n-2)(p-n-3) C_{p-2,p-n-2,j} \\ = -2\{1 + \zeta(p-n-2)\} C_{p-2,p-n-1,j} + 2(p^2-2) C_{p-1,p-n,j} \\ - 2(\zeta^2 + E_0) C_{p-2,p-n,j} + 2\zeta(j+1) C_{p-2,p-n-1,j+1} \\ + (j+1)(2p-2n-5) C_{p-2,p-n-2,j+1} \\ - (j+1)(j+2) C_{p-2,p-n-2,j+1} \end{aligned} \quad (49)$$

$C_{p,q}$  from (40) corresponds to  $C_{p,q,0}$  in (48), (49), (50). (43) is replaced by (50).

$$\sum_p^{0,m} (4p-n) C_{2p,2p-n,j} = - \sum_p^{0,m} (4p+2-n) C_{2p+1,2p+1-n,j} - \sum_p^{2m+2,\alpha} (2p-n) C_{p,p-n,j} + (j+1) \sum_p^{0,\infty} C_{p,p-n,j+1} \quad (50)$$

When  $j=1$  and  $n=4$  the right hand sides of (49) and (50) are zero. This means that (49) and (50) are interdependent but consistent. Both equations are satisfied by whatever value may be chosen for say  $C_{0,-4,1}$ . When  $j=0$ ,  $n=4$ , (49) and (50) can be made consistent by adjusting the value of  $C_{0,-4,1}$ . (49), (50) become inconsistent when  $n$  is a multiple of 4 ( $n \geq 8$ ) and  $j=0$  unless  $C_{0,-n,1}$  is adjusted to make these consistent. When  $n=8$ ,  $j=1$  (49), (50) are again inconsistent unless an auxiliary series from  $n=8$  with  $j=2$  is started. The total requirement is for the triple series in (51).

$$\psi_0 \sum_j^{0,\infty} \sum_n^{4j,\infty} \sum_p^{0,\infty} C_{p,p-n,j} r_a^p / r_b^{p-n} \cdot (\log r_b)^j \quad (51)$$

There is a remaining problem.  $C_{2,-2,0}$ ,  $C_{2,-6,0}$ ,  $C_{2,-10,0}$ , etc. for example remain undetermined. This will be treated in a subsequent paper. The functions in (17) are in fact overcomplete. The terms corresponding to the undetermined coefficients can be removed from (17). The resultant functions still form an overcomplete set.

### 9. Cusp Behaviour in the Ground State Solutions of Helium Schroedinger Equations

The cusp behaviour of  $\psi_0$  from (39) in the limit of  $r_a$  tending to zero is known to be:

$$1/\psi_0 \cdot (\partial \psi_0 / \partial r_a) = -2; \quad r_a \rightarrow 0; \quad (52)$$

From (17) and (52) we obtain the following recursion formula:

$$(2-\zeta) C_{0,q} + C_{1,q} = 0 \quad (53)$$

The relationship in (53) is also obtained from (40), (41). This proves (52) for any series from (40), (41). (48), (49) produce the analogous result. The correct cusp behaviour at the origin can be shown similarly for the series generated in Section 10.

We now consider the ground state solution  $\Psi$  of the Complete Schroedinger equation for helium defined after (5). We have:

$$(H^0 + H' - E_0) \Psi = 0; \quad \text{c.f. (39)} \quad (54)$$

In particular we consider the cusp behaviour of  $\Psi$  as  $r_{12}$  tends to zero. The cusp theorem first formally stated by Kato can be written:

$$\Psi^{-1} (\partial \Psi / \partial r_{12}) = 0.5; \quad r_{12} \rightarrow 0; \quad (55)$$

From (55) it follows [7] that when  $r_{12}$  tends to zero  $\Psi$  contains  $r_{12}$  in the forms:

$$\exp(0.5 r_{12}) = 1 + 0.5 r_{12} + \dots \quad (56)$$

The result in (56) confirms the use of  $r_{12}$  as a useful co-ordinate for the helium problem. There is a difficulty however. It is that both sides of (56) do not show all the correct properties when  $r_{12} = 0$ . From the right hand side of (56) when  $\cos \theta = 1$ ,  $\Psi$  will contain  $r_b - r_a$ .  $\Psi$  becomes a radial function of the Second Type in Section 7. This is not acceptable. Let us consider the expansion of  $r_{12}$ .

$$u = \sum_l^{0, \infty} [1/(2l+3) \cdot r_a^{l+2}/r_b^{l+1} - 1/(2l+1) \cdot r_a^l/r_b^{l+1}] P_l(\cos \theta) \quad (57)$$

Summing the first  $l+1$  terms of (57) we obtain (58) when  $\cos \theta = 1$ .

$$r_b - r_a + 1/(2l+3) \cdot r_a^{l+2}/r_b^{l+1} + 1/(2l+1) \cdot r_a^{l+1}/r_b^l \quad (58)$$

As  $l$  tends to infinity the terms in  $l$  become zero.  $u$  is identical to  $r_{12}$ . On taking radial derivatives however the terms in  $l$  contribute to  $\partial/\partial r_i$  ( $i = 1, 2$ ), when  $r_1 = r_2$  and  $l$  tends to infinity. The radial derivatives of the expansion are non-uniformly convergent near  $r_1 = r_2$  when  $\cos \theta = 1$ . Because of this  $\Psi$  contains  $0.5 u$  and is still a radial function of the First Type when  $\cos \theta = 1$ .  $\Psi$  will then have the correct cusp behaviour as  $r_{12}$  approaches zero.

Let us consider the operation  $\partial/\partial r_1$  on  $0.5 r_{12}$  and  $0.5 u$  as these functions tend to zero and actually equal zero.

$$0.5(\partial r_{12}/\partial r_1)_{r_1=r_2} = -0.5; \quad 0.5(\partial r_{12}/\partial r_1)_{r_1=r_2} = \text{undefined}; \quad (59)$$

$$0.5(\partial r_{12}/\partial r_1)_{r_1=r_2} = 0.5$$

$$0.5(\partial u/\partial r_1)_{r_1=r_2} = -0.5; \quad 0.5(\partial u/\partial r_1)_{r_1=r_2} = 0; \quad (60)$$

$$0.5(\partial u/\partial r_1)_{r_1=r_2} = 0.5$$

When describing the properties of  $\Psi$  for  $r_1 = r_2$ ,  $\cos \theta = 1$ , it is better to use  $0.5 u$  rather than  $0.5 r_{12}$ .

Given the importance of  $0.5 u$  we expect to find terms from  $0.5 u$  in any series obtained from  $\Psi$ . This expectation is confirmed in Section 10. However we obtain from (45) and before (45) the most significant terms in the solution of (39):

$$\psi_0 \{1 + (\zeta - 2)(r_a + r_b) + 0.5(r_b + 1/3 \cdot r_a^2/r_b)\} \quad (61)$$

The third term of the right hand factor in (61) corresponds to the term in (57) with  $l = 0$ . The constant  $0.5$  is confirmed.

## 10. The Formal Solutions for the Ground States of the SP, SPD, etc. and Complete Helium Schroedinger Equations

The SP helium Schroedinger equation is defined after (5). For this we use an analogous expression to (17). This is:

$$\Psi_1 = \psi_0 \sum_i^{0, \infty} \sum_p^{0, \infty} \sum_q^{-\infty, \infty} C_{p,q,i} r_a^p/r_b^q \cdot P_l(\cos \theta) \quad (62)$$

The recursion formula analogous to (40) is:

$$\begin{aligned}
 -(l-p)(l+p+1) C_{p,q,l} = & -2\{1+\zeta(q-2)\} C_{p-2,q-1,l} \\
 & + 2(p\zeta-2) C_{p-1,q,l} - 2(E_1+\zeta^2) C_{p-2,q,l} \\
 & + (l+q-2)(l-q+3) C_{p-2,q-2,l} \\
 & + 2l/(2l-1) \cdot C_{p-3,q-2,l-1} \\
 & + 2(l+1)/(2l+3) \cdot C_{p-3,q-2,l+1}
 \end{aligned} \quad (63)$$

From (26) and (63) we have:

$$C_{p,q,l} = 0 \quad \text{for } p < l \quad \text{or } q > p-l \quad (64)$$

The analogue to (43) is:

$$C_{l,l-n,l} = -1/(2l-n) \cdot \sum_p^{l+1, \infty} (2p-n) C_{p,p-n,l}; \quad n \neq 2l \quad (65)$$

Using (63), (64) and (65) subsets of coefficients may be extracted. These correspond to the following values for  $l$  and  $n$ :

$$l=0, n=0, 1, 2; l=1, n=1; l \geq 2, n=l \quad (66)$$

There are an infinite number of subsets in (66). There are however significant gaps because of difficulties similar to those which lead to (47).

We concern ourselves with the three most significant subsets in (66). With these are no gaps. The subsets correspond to  $l=0, n=0, 1; l=1, n=1$ . We obtain the following non-zero terms:

$$\psi_0 \{ 1 + (\zeta-2)(r_a+r_b) + 0.5 \sum_l^{0,k} [1/(2l+3) \cdot r_a^{l+2}/r_b^{l+1} - 1/(2l-1) \cdot r_a^l/r_b^{l-1}] \cdot P_l(\cos \theta) \} \quad (67)$$

with  $k=1$ . In the case of  $\Psi$  from (54) which is  $\Psi_u$  in the notation of (62) we obtain (67) with  $k=\infty$ . From (57) this proves the cusp condition in (55) and (56) with the special singular properties in (60).

Fock [8] has shown that the terms of (67) for  $\Psi$  up to the linear terms are:

$$1 - 2(r_1 + r_2) + 0.5 r_{12} \quad (68)$$

These terms can be obtained from (67) by expanding  $\psi_0$  from (7). This shows how the terms in (68) belong to a square integrable series.

It is clear that the form in (62) is inadequate for the complete evaluation of  $\Psi_1, \Psi_2, \dots, \Psi_\infty$ . When  $n=2l$  ( $l \neq 0$ ),  $2l+4$ ,  $2l+8$ ,  $2l+12$  etc. the combination of (63), (64), (65), gives sets of inconsistent simultaneous equations. It is necessary to find the analogue to (51) for total correlation including angular correlation. From arguments similar to those for (51) this is:

$$\psi_0 \sum_l^{0, \infty} \sum_j^{0, \infty} \sum_n^{2j, \infty} \sum_p^{l, \infty} C_{p,p-n,j,l} r_a^p/r_b^{p-n} \cdot (\log r_b)^j P_l(\cos \theta) \quad (69)$$

The analogue to (49) for the SP problem is:

$$\begin{aligned}
 -(l-p)(l+p+1)C_{p,p-n,j,l} = & -2\{1+\zeta(p-n-2)\}C_{p-2,p-n-1,j,l} \\
 & + 2(p\zeta-2)C_{p-1,p-n,j,l} - 2(E_1+\zeta^2)C_{p-2,p-n,j,l} \\
 & + (l+p-n-2)(l-p+n+3)C_{p-2,p-n-2,j,l} \\
 & + 2l(2l-1)C_{p-3,p-n-2,j,l-1} \\
 & + 2(l+1)(2l+3)C_{p-3,p-n-2,j,l+1} \\
 & + 2\zeta(j+1)C_{p-2,p-n-1,j+1,l} \\
 & + (j+1)(2p-2n-5)C_{p-2,p-n-2,j+1,l} \\
 & - (j+1)(j+2)C_{p-2,p-n-2,j+2,l}
 \end{aligned} \quad (70)$$

The analogue to (49) for the SPD problem is:

$$\begin{aligned}
 (l-p)(l+p+1)C_{p,p-n,j,l} = & \{\text{terms on the right hand side of (70)}\} \\
 & + 3(l-1)(2l-3)l(2l-1)C_{p-4,p-n-3,j,l-2} \\
 & + 3\{(l+1)(2l+1) \cdot (l+1)/(2l+3)\} \\
 & + l(2l+1) \cdot l(2l-1) \cdot 1/3\}C_{p-4,p-n-3,j,l} \\
 & + 3(l+2)(2l+5) \cdot (l+1)/(2l+3) \cdot C_{p-4,p-n-3,j,l+2}
 \end{aligned} \quad (71)$$

Recursion formulae like (71) can be built up for the evaluation of  $\Psi_3, \Psi_4$  etc. For  $\Psi_u$  ( $u \geq 3$ ), we obtain (72):

$$\begin{aligned}
 -(l-p)(l+p+1)C_{p,p-n,j,l} = & \{\text{terms on the right hand side of (71)}\} \\
 & + (2l+1) \sum_{i=1}^{3,u-1} \sum_{w=0}^l l_{i-1+2w,i,l} C_{p-i,p-n-i-1,j,l-i+2w}
 \end{aligned} \quad (72)$$

where

$$l_{a,b,i} = \int_1^1 P_a(x) P_b(x) P_i(x) dx$$

When  $u = \infty$  (72) yields the recursion formula for the complete Schrodinger equation. (69) can be used to solve any of this infinite sequence of Schrodinger equations. This confirms Fock's general conclusion [8, 9] that the formal solution of (54) contains logarithmic terms.

The analogue to (50) for  $\Psi_1, \Psi_2$  etc. is:

$$\sum_p^{l,j} (2p-n)C_{p,p-n,j,l} - (j+1) \sum_p^{l,j} C_{p,p-n,j+1,l} = 0 \quad (73)$$

The operation of (73) is similar to that of (50). It is used to ensure that the sets of terms with different values of  $p$  and  $j$  but with the same values of  $l$  and  $n$  are kept within the Domain of  $H$ .

There is the difficulty of undetermined coefficients similar to that mentioned after (51). These coefficients are for example:

- (i) for  $l > 0$ ,  $C_{l,-l-s,0,l}$  where  $s = 0, 4, 8, \dots$
- (ii) for  $l = 0$ ,  $C_{2,-2-s,0,0}$  where  $s = 0, 4, 8, \dots$



The terms corresponding to these coefficients can be removed from (69) without the loss of completeness for the functions in (69).

### 11. Variational Estimates for the Radial Limit

The variational calculations so far undertaken have been small but accurate. These take the expansion in (17) to no more than thirteen terms. Following the series solution in Section 8 the general form (74) was used:

$$\psi_0(1 + d_1 r_b + d_2 r_a + d_3 r_b^2 + d_4 r_a^2 + d_5 r_a r_b + d_6 r_a^2/r_b + d_7 r_a^3/r_b + d_8 r_a^4/r_b^2 + d_9 r_b^3 + d_{10} r_a^3 + d_{11} r_b^2 r_a + d_{12} r_a^2 r_b) \quad (74)$$

For the variation of thirteen independent parameters including  $\zeta$  from (7) an eigenvalue of  $-2.879028589$  H was obtained. This compares with  $-2.8790248$  H obtained by Davis [10] from the variation of 66 independent parameters in a configurational interaction calculation of the sort mentioned before (46). Our value also provides a more precise upper bound than was obtained by Davis from the implementation of up to 66 terms and extrapolating for infinite terms. Not only is the eigenvalue from (74) the best estimate of the radial limit ever obtained but it also represents the most successful eigenvalue obtained in thirteen or so terms for an electron correlation problem. The error from (74) is probably less than 2 parts in  $10^7$ . The result from 14 terms [11, 12] in the Hylleraas expansion for the Complete helium problem shows an error of 2 parts in  $10^5$ . The high accuracy of the present calculation is due partly to the simplicity of the problem and partly to the technique of choosing terms which are important in a series solution.

We obtain the six most interesting trial wave functions from (74) each characterised by a vector of coefficients which are a subset of  $d$ . Optimum results are tabulated below. These are the relevant  $d$ -subscripts; optimum  $\zeta$  values;  $m$ , the number of terms implemented by Davis which give a comparable eigenvalue.

Table 1

$m$	$\zeta$	Subscripts for $d_i$	$E_{\min}$
55	1.598	1, 2, 3...7	$-2.879,023,10$ H
55	1.5941	1, 2, 3...8	$-2.879,023,47$ H
55	1.5132	1, 2, 3...9	$-2.879,025,55$ H
66	1.4842	1, 2, 3... 10	$-2.879,025,93$ H
$\epsilon$	1.4419	1, 2, 3 ...11	$-2.879,027,31$ H
$\epsilon$	1.5899	1, 2, 3... 12	$-2.879,028,59$ H

The coefficients  $d_1$  to  $d_{12}$  for the most accurate function are: 0.0918435727;  $-0.4126805604$ ; 0.0269466033; 0.0046643072;  $-0.0354601186$ ; 0.1679732815; 0.0182867438;  $-0.0038330449$ ; 0.0013156847;  $-0.0111772241$ ;  $-0.0122628367$ ; 0.0218323572.

The accuracy of these results and those in (46) reflect favourably the convergence characteristics of (17) and (51). More extensive calculations need to be carried out. These should be well ordered so as to be extensible by extrapolation procedures.

## 12. The Motion of the Nucleus

The helium three body problem has a feature resulting from the finite mass of the nucleus. (54) is replaced by:

$$(H^0 + H' + H'' - E_0) \Psi = 0 \quad (75)$$

where:

$$H'' = -\mu/M \cdot (\partial^2/\partial x_1 \partial x_2 + \partial^2/\partial y_1 \partial y_2 + \partial^2/\partial z_1 \partial z_2) \quad (76)$$

$\mu$  is the reduced mass of the electron.  $M$  is the mass of the nucleus. The atomic units of length and energy in (75), (76) are defined using the reduced mass of the electron [13].

The recursion formula for the helium three body problem is given in (77), (78).

$$(l-p)(l+p+1)C_{p+1,p-n-1,j,l+1} = \{\text{terms on the right hand side of (72)}\} - 2\mu/M \cdot \{\text{terms in (78)}\} \quad (77)$$

$$\begin{aligned} C_{p+1,p-n-1,j,l+1} & \cdot (l+1)/(2l+3) \cdot (l^2 + 6l + nl + 3n + 9 + pn - p^2) \\ & - C_{p+1,p-n-1,j,l-1} \cdot l/(2l-1) \cdot (-l^2 + 4l + p^2 - pn + ln - 2n - 4) \\ & - C_{p,p-n-1,j,l+1} \cdot (l+1)/(2l+3) \cdot \zeta(l-p+n+3) \\ & + C_{p,p-n-1,j,l-1} \cdot l\zeta/(2l-1) \cdot (l+p-n-2) \\ & - C_{p+1,p-n,j,l+1} \cdot (l+1)\zeta/(2l+3) \cdot (l+p+3) \\ & + C_{p+1,p-n,j,l-1} \cdot l\zeta/(2l-1) \cdot (l-p-2) \\ & + C_{p+1,p-n-1,j+1,l+1} \cdot (l+1)(j+1)/(2l+3) \cdot (l+p+3) \\ & + C_{p+1,p-n-1,j-1,l-1} \cdot l(j+1)/(2l-1) \cdot (-l+p+2) \\ & + l/(2l-1) \cdot \zeta^2 C_{p,p-n,j,l-1} + (l+1)/(2l+3) \cdot \zeta^2 C_{p,p-n,j,l+1} \\ & - l/(2l-1) \cdot \zeta(j+1) C_{p,p-n-1,j+1,l-1} \\ & - (l+1)/(2l+3) \cdot \zeta(j+1) C_{p,p-n-1,j+1,l+1} \end{aligned} \quad (78)$$

An approximation for the two body helium problem may be obtained using (72). The expectation is that this may be refined by successive approximations in (77). Limiting values for  $E_0$  from (72) and (77) will be the eigenvalues for the helium two body and three body problems.

## 13. Conclusions

i) A method has been developed for the series solution of the two and three body problems in helium theoretical chemistry. The analytical form for the problems of radial and angular correlation has been derived. The convergence

of the solution to the radial Schroedinger equation seems satisfactory. More of this series solution remains to be investigated numerically. The series solutions for the SP, SPD, etc. and Complete equations require processing.

(ii) This work requires extension to those excited states of helium in which electrons are described in different orbitals. In these cases the space part of  $\psi_0^{\text{det}}$  from (2) is more complicated than for the ground state and other states in which electrons are paired in the same orbitals. Such work is to be carried out to facilitate the extension of present techniques to lithium for which  $\psi_0^{\text{det}}$  is still more complicated.

(ii) Another problem should be tackled as a prelude to lithium. This is the problem of three negatively charged bosons in the same  $1s$  orbital centred on the nucleus.

(iv) We have made some progress with problems of series solution for Schroedinger equations. The corresponding Rayleigh-Schroedinger perturbation equations appear a parallel field of investigation.

*Acknowledgements.* We gratefully thank Professor G. G. Hall and Professor J. W. Linnett for continuous encouragement without which this work would not have been completed. We thankfully acknowledge detailed criticisms of the final draft from Professor C. A. Coulson.

### References

1. Snyder, L. C., Parr, R. G.: J. chem. Physics **34**, 1661 (1961).
2. Schwartz, C.: Physic. Rev. **126**, 1015 (1962).
3. Hirschfelder, J. O., Nazarov, G. V.: J. chem. Physics **34**, 1666 (1961).
4. Coolidge, A. S., James, H. M.: Physic. Rev. **51**, 855 (1937).
5. Dirac, P. A. M.: The principles of quantum mechanics, 4th. Ed. p. 58 Oxford: Clarendon Press 1958.
6. Shull, H., Löwdin, P.-O.: Physic. Rev. **30**, (1959).
7. Slater, J. C.: Quantum theory of atomic structure, Volume II, 1st. Ed., p. 39. New York: Mc Graw-Hill Book Company, 1960.
8. Fock, V. A.: Izvest. Akad. Nauk. S.S.S.R. Ser. Fiz. **18**, 161 (1954).
9. Fock, V. A.: Kgl. Norske Videnskabs Selskabs. Forh. **31** (22), 23 (1958).
10. Davis, H. L.: J. chem. Physics **39**, 1827 (1963).
11. Chandreskhari, S., Herzberg, G.: Physic. Rev. **98**, 1050 (1955).
12. Schwartz, C.: Physic. Rev. **128**, 1146 (1962).
13. Bethe, H. A., Salpeter, E. E.: Quantum mechanics of one- and two-electron atoms, p. 166, Springer-Verlag 1957.

Dr. F. T. Newman  
Computing Centre  
Trent Polytechnic  
Nottingham, England



## Relationes

# CNDO Calculation of the $\pi$ -Electronic Structure and Barrier to Internal Rotation in Benzenesulphonic Acid

C. I. Ghirvu

The "Al. I. Cuza" University of Jassy, Faculty of Chemistry, Calea 23 August 11, Jassy, Romania

Received June 6, 1972

The CNDO calculation of the charge densities and bond orders show a distinction between two extreme geometrical configurations of the benzenesulphonic acid, but the barrier to internal rotation of the sulphonic group about the C-S bond, calculated by the same method, has revealed that they are energetically equivalent.

## 1. Introduction

Some years ago we put forward a model of interaction between the sulphonic group and the benzene ring [1]. This model has been considered in the simple LCAO-MO method [1], as well as in the Pariser-Parr approximation [2-4]. In this model the conjugation between the sulphonic group and the  $\pi$ -electrons of the benzene ring is considered to be due to the presence of a vacant orbital centered on the sulphur atom in the sulphonic group. However, this model, which is similar to the Crawford's hyperconjugation model of toluene, might be valid only in the case the sulphonic group rotates freely about the C-S bond. Such barriers to internal rotation are in general small quantities, and their physical origin is not entirely known [5].

In this paper the charge densities and the bond orders for benzenesulphonic acid (anion) as well as the barrier to internal rotation of the sulphonic group about the C-S bond, were calculated by using the CNDO/2 variant of the CNDO method [6-9].

## 2. Results and Discussions

For practical calculation the two extreme geometrical configurations of the benzenesulphonic acid with we are concerning with are given in Fig. 1.

In the case of the configuration *A* the projection of one of the S-O bonds lies along the *x*-axis, while this is rotated an angle of 30° about the C-S bond in the case of the configuration *B*. The Broomhead and Nicol's data [10] were used as starting geometrical parameters. For C-H bond length the standard distance of 1.08 Å was used.

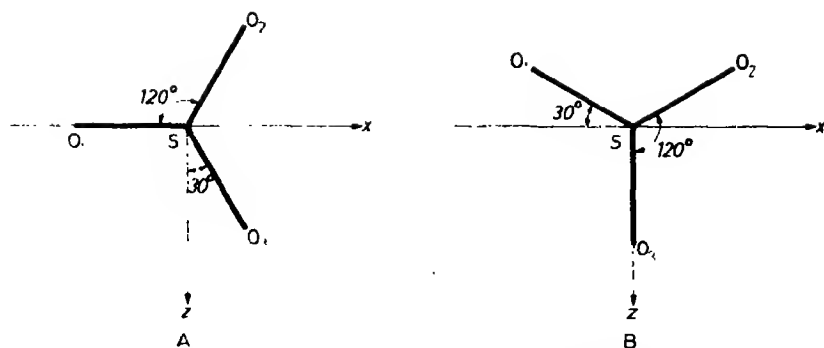


Fig. 1 Configurations A and B of benzenesulphonic acid (anion)

#### a) Charge Densities and Bond Orders

From the analysis of the charge distribution we observed that these are slightly different in the ring, but significantly modified in the substituent.

The  $\pi$ -electron distribution in the ring was different compared to that obtained in a Hückel MO type treatment [1], but in both cases the meta charge is greater than that located in the ortho position which is in agreement with the chemical nature of the sulphonic group.

From the  $\pi$ -bond order analysis the following conclusions were drawn.

1) The modifications of the bond orders in the ring under the rotation of the sulphonic group were insignificant.

2) The C-S bond has a very weak  $\pi$ -character and a small contribution of the sulphur 3d atomic orbitals to this.

3) In the case of the S-O bonds, which are of primarily interest for the present discussion, their physical nature appears to be different both from bond to bond and from configuration A to the configuration B.

#### b) Barrier to Internal Rotation

The experimental data [10] show that the three S-O bonds of the sulphonic group are identically, which seems to be contradictory to the above picture of the chemical bonds. But the above CNDO type description of the chemical bonds of the sulphonic group can be brought into the comparison with the experimental evidences if a free rotation of this group about the C-S bond is admitted. This fact suggested us the calculation of the barrier to internal rotation of the sulphonic group about the C-S bond from the configuration A to the configuration B. The energy difference between the configurations A and B was calculated as indicated by Pople and its coworkers [6], the calculated barrier being approximately 0.038 kcal/mol. As we know, this barrier has never been measured experimentally. Nevertheless, the magnitude of this barrier is of considerable theoretical importance for the understanding of the physical nature of the chemical bonds in the sulphonic group. So, the smallness of this barrier

indicates a free rotation of the sulphonic group about the C—S bond. In view of this remark the three S—O bonds appear as equivalent. This remark is in agreement both with experimental observation and with the interpretation of the interaction between the sulphonic group and the benzene ring [1] in the same manner as in the case of toluene [11].

### References

- 1 Sahini, V.Em., Ghirvu, C.I., Macovei, V. P.: *Rev. Roumaine Chim.* **12**, 237 (1967).
- 2 Sahini, V.Em., Ghirvu, C.I.: *Rev. Roumaine Chim.* **14**, 275 (1969).
- 3 Sahini, V.Em., Ghirvu, C.I.: *Rev. Roumaine Chim.* **15**, 11 (1970).
- 4 Sahini, V.Em., Ghirvu, C.I.: *Rev. Roumaine Chim.* **16**, 149 (1971).
- 5 Lowe, J. P.: *Progress in Phys. Org. Chem.* **6**, 1 (1968).
- 6 Pople, J. A., Santry, D. P., Segal, G. A.: *J. chem. Physics* **43**, S 129 (1965).
- 7 Pople, J. A., Segal, G. A.: *J. chem. Physics* **44**, S 136 (1965).
- 8 Pople, J. A., Segal, G. A.: *J. chem. Physics* **44**, 3289 (1966).
- 9 Santry, D. P., Segal, G. A.: *J. chem. Physics* **47**, 158 (1967).
- 10 Broomhead, J. M., Nicol, A. D. I.: *Acta crystallogr.* **1**, 88 (1948).
- 11 Crawford, V. A.: *Quart. Rev.* **3**, 226 (1949).

Dr. C. Ghirvu  
The "Al. I. Cuza" University of Jassy  
Faculty of Chemistry  
Calca 23 August 11  
Jassy, Romania





# A Note on an Aspect of Pseudopotential Theory

W. C. Mackrodt\*

Department of Theoretical Chemistry, Lensfield Road, Cambridge CB2 1EW, England

Received October 16, 1972

The variational approach of Rice and Weeks [J. chem. physics **49**, 2741 (1968)] is used to derive the pseudopotential equation for the  $T$ -matrix, via a discussion of normal perturbation theory.

## 1. Introduction

It has long been recognized that for atoms, molecules and solids, the rather complicated situation wherein all particles move under the mutual influence of all others, can be approximated, quite accurately, by reasonably simple descriptions. The hartree-fock method, for example, is just such a description, and many useful observations have been derived from it. In particular, it has been found that for a valence electron inside the core of an atom, there is almost complete cancellation between its kinetic and potential energies [1–4]. This suggests that the original equation may be replaced by an alternative which illustrates, in a somewhat more obvious way, the effect of this cancellation, and the mathematical procedure for implementing this alternative formulation is known as the method of pseudopotentials.

What Phillips and Kleinmann [1] first showed, was that the eigenvalue equation,

$$H \Psi_i = E_i \Psi_i \quad (1.1)$$

where

$$\langle \Psi_i | \Psi_j \rangle = \delta_{ij}, \quad \text{and} \quad \Psi_i \in \{ \Psi_c \}, \quad (1.2)$$

for all valence electrons, could be transformed to,

$$(H + \Omega_i) \Phi_i = T_i \Phi_i \quad (1.3)$$

without the orthogonality constraint. The non-local pseudopotentials  $\Omega_i$ , are defined by,

$$\Omega_i \Phi = \sum_c \langle \Psi_c | \Phi \rangle [E_i - E_c] | \Psi_c \rangle$$

and the summation is over the core orbitals  $\{ \Psi_c \}$ . Subsequently, Austin, Heine, and Sham [5], following earlier work by Cohen and Heine [4], showed that the general form of the pseudopotential could be written as,

$$\Omega \Phi = \sum_c \langle \vartheta_c | \Phi \rangle | \Psi_c \rangle$$

\* Present address and for correspondence: I.C.I., Central Instrument Research Laboratory, Bozdown House, Whitechurch Hill, Reading, Berkshire, England.

in which  $g_c$  are arbitrary functions. Weeks and Rice [6] have, in a very elegant way, derived the most general form in terms of any hermitian operator  $\hat{\Theta}$ , and an arbitrary set of functions which define the projection operator  $P$ , thus

$$\Omega = P\hat{\Theta} + \hat{\Theta}P - P\hat{\Theta}P - \lambda P$$

where  $\lambda$  is a lagrange multiplier.

As they stand, pseudopotentials are of no advantage from a computational point of view, although the insight they afford into a given problem may often be valuable. Rather, their importance lies in the model potentials they suggest -- an aspect which has been exploited with success by Heine and his co-workers [8, 9], and Rice and his co-workers [6, 7] -- and in this note, Rice's method is extended to the scattering problem via an examination of the effect of introducing pseudopotentials in perturbation theory.

## 2. Variation Principles and Pseudopotentials

Rice and Weeks [6] have pointed the way in terms of the general discussion of pseudopotential theory and its relation to variation principles. Consider a hermitian operator  $\hat{\Theta}$ , and some arbitrary subset  $\{\phi_c\}$  of the complete set of orthogonal functions that span its function space. The projection operator  $P$  defined in terms of the subset  $\{\phi_c\}$  by,

$$P = \sum_c |\phi_c\rangle \langle \phi_c|, \quad (2.1)$$

may be used to define further a functional  $\omega$  in terms of the operator  $\hat{\Theta}$ , a function  $\phi$  and the subset, thus

$$\omega = \langle (1 - P)\phi | \hat{\Theta} | (1 - P)\phi \rangle. \quad (2.2)$$

An arbitrary variation of  $\phi^*$ , without any constraint, leads to

$$\delta\omega = \langle \delta\phi | (1 - P)\hat{\Theta}(1 - P) | \phi \rangle, \quad (2.3)$$

since the complement of  $P$  is hermitian, so that requiring  $\delta\omega = 0$  leads to

$$\Omega\phi = [P\hat{\Theta} + \hat{\Theta}P - P\hat{\Theta}P]\phi, \quad (2.4)$$

which is the general unconstrained pseudopotential equation. Substitution of (2.1), together with  $[P, \hat{\Theta}] = 0$ , leads to

$$\Omega\phi = \sum_c \langle g_c | \phi \rangle |\phi_c\rangle, \quad (2.5)$$

where

$$\langle g_c | = \langle \phi_c | \hat{\Theta}. \quad (2.6)$$

(2.6) is the equation suggested by Austin, Heine and Sham [5] as defining the general pseudopotential. If the variation of  $\omega$  with respect to arbitrary  $\phi$  ( $\phi^*$ ) is required subject to the normalization condition,

$$\langle (1 - P)\phi | (1 - P)\phi \rangle = 1, \quad (2.7)$$

then the resulting pseudopotential equation is easily seen to reduce to,

$$\Omega\phi = \sum_c \{ \langle g_c | \phi \rangle - \lambda \langle \phi_c | \phi \rangle \} | \phi_c \rangle, \quad (2.8)$$

where  $\lambda$  is the appropriate lagrange multiplier. Eq. (2.8) is the generalized pseudopotential equation first derived by Rice and Weeks [6]. Setting  $\hat{\Theta} = \hat{H}$ , the hartree-fock hamiltonian leads to the Phillips-Kleinman equation [1], and  $\hat{\Theta} = \hat{T}$  to that of Cohen and Heine [4]. Any number of  $\hat{\Theta}$ 's can thus be chosen to suit a variety of situations.

There has been widespread use of these equations and their modifications [4, 5, 8, 9] in many bound-state calculations for atoms [6], molecules and solids [10-12] and more recently attention is being focused on similiar problems involving scattering [13]. Now it is well known that the transition from bound-state to unbound-state problems requires a modification of the formalism to account for the somewhat different physical situation, in which for example, the energy of the system is no longer an observable but simply a parameter. However, before considering the scattering problem in the light of Eqs. (2.5) and (2.8), it may be worthwhile to see what influence the introduction of a pseudopotential has in, say, the hartree-fock perturbation problem. At first sight the introduction of a pseudopotential in hartree-fock perturbation calculations may well seem an expedient measure, for one of the difficulties in such calculations is implementing the requirement that the perturbation equations for the different orbitals be solved subject to the overall orthogonality of the perturbed wavefunctions. Thus to second order, for example, the requirement

$$\langle \psi_i | \psi_j \rangle = \delta_{ij}, \quad (2.9)$$

for the perturbed orbitals  $\psi_i$  and  $\psi_j$  leads to subsidiary conditions such as

$$\langle \psi_i^{(0)} | \psi_j^{(0)} \rangle = \delta_{ij}, \quad (2.10)$$

$$\langle \psi_i^{(0)} | \psi_i^{(1)} \rangle = 0, \quad (2.11)$$

$$\langle \psi_i^{(0)} | \psi_j^{(1)} \rangle = - \langle \psi_i^{(1)} | \psi_j^{(0)} \rangle, \quad (2.12)$$

$$2 \langle \psi_i^{(0)} | \psi_i^{(2)} \rangle = - \langle \psi_i^{(1)} | \psi_i^{(1)} \rangle, \quad (2.13)$$

$$\langle \psi_i^{(2)} | \psi_j^{(0)} \rangle + \langle \psi_i^{(0)} | \psi_j^{(2)} \rangle = - \langle \psi_i^{(1)} | \psi_j^{(1)} \rangle \quad (2.14)$$

for the zero, first and second-order functions. Now the introduction of a pseudopotential transforms the equations,

$$H\psi_i = \epsilon_i\psi_i, \quad (2.15)$$

subject to

$$\langle \psi_i | \psi_j \rangle = \delta_{ij},$$

to

$$(H + \Omega_i) \phi_i = \epsilon_i \phi_i, \quad (2.16)$$

without the subsidiary conditions (2.12) and (2.14) in the perturbation problem.

Suppose, therefore, that a perturbation solution is sought to the equations,

$$(H + V) \psi_i = E_i \psi_i, \quad (2.17)$$

for the perturbed hartree-fock orbitals  $\psi_i$ . The equations for the perturbed wavefunctions are to successive order given by,

$$(H - \epsilon_i^{(0)}) \psi_i^{(0)} = 0, \quad (2.18)$$

$$(H - \epsilon_i^{(0)}) \psi_i^{(1)} = [\epsilon_i^{(1)} - (V + \delta_1 V)] \psi_i^{(0)}, \quad (2.19)$$

$$(H - \epsilon_i^{(0)}) \psi_i^{(2)} = \epsilon_i^{(2)} \psi_i^{(0)} + [\epsilon_i^{(1)} - (V + \delta_2 V)] \psi_i^{(1)}, \quad (2.20)$$

etc. subject to Eqs. (2.10) to (2.14), and in which

$$\epsilon_i^{(1)} = \langle \psi_i^{(0)} | V + \delta_1 V | \psi_i^{(0)} \rangle, \quad (2.21)$$

$$\epsilon_i^{(2)} = \langle \psi_i^{(1)} | V + \delta_1 V | \psi_i^{(0)} \rangle, \quad (2.22)$$

and further

$$\epsilon_i^{(3)} = \langle \psi_i^{(1)} | V + \delta_1 V | \psi_i^{(1)} \rangle. \quad (2.23)$$

$\delta_n V$  is the  $n^{\text{th}}$  order induced perturbation which results from the form of the hartree-fock potential. Now (2.15) may be changed to

$$(H + V + \Omega_i) \phi_i = \eta_i \phi_i, \quad (2.24)$$

in which  $\Omega_i$  is any pseudopotential, and  $E_i = \eta_i$  from the basic theorem. Eq. (2.24) may be grouped in two ways, either

$$[(H + \Omega_i) + V] \phi_i = \eta_i \phi_i, \quad (2.25)$$

or

$$[H + (V + \Omega_i)] \phi_i = \eta_i \phi_i, \quad (2.26)$$

in which the pseudopotential is grouped either with  $H$ , or the perturbation  $V$ . Let the perturbed pseudofunctions be denoted by  $\phi_i^{(k)}$  and the corresponding energies by  $\eta_i^{(k)}$ , and consider first the perturbed functions which follow from the partition (2.25).

$$(H + \Omega_i) \phi_i^{(0)} = \eta_i^{(0)} \phi_i^{(0)}, \quad (2.27)$$

with  $\epsilon_i^{(0)} = \eta_i^{(0)}$ . However,  $\phi_i^{(0)} \neq \psi_i^{(0)}$ , so that in general

$$\phi_i^{(k)} \neq \psi_i^{(k)}, \quad \text{for all } k,$$

and

$$\eta_i^{(k)} \neq \epsilon_i^{(k)}, \quad \text{for all } k > 0.$$

The first partition, therefore, whilst giving the same total and zero-order energies as the usual theory, gives no other correspondence between the perturbed functions and energies. Partition (2.26) on the otherhand, results in the following equations.

$$H \phi_i^{(0)} = \eta_i^{(0)} \phi_i^{(0)}, \quad (2.28)$$

so that  $\phi_i^{(0)} = \psi_i^{(0)}$ , and  $\eta_i^{(0)} = \epsilon_i^{(0)}$ .

Further

$$\eta_i^{(1)} = \varepsilon_i^{(1)}.$$

However, the first-order equation is

$$(H - \varepsilon_i^{(0)}) \phi_i^{(1)} = [\varepsilon_i^{(1)} - (V + \delta_1 V + \Omega_i)] \psi_i^{(0)}, \quad (2.29)$$

and similarly for higher orders. Thus, in general,

$$\phi_i^{(k)} \neq \psi_i^{(k)}, \quad \text{for } k > 0$$

and

$$\eta_i^{(k)} \neq \varepsilon_i^{(k)}, \quad \text{for } k > 1.$$

For the special case of the Phillips-Kleinman potential,

$$\Omega_i \psi_i^{(0)} = 0, \quad (2.30)$$

the  $k^{\text{th}}$  order inequalities, therefore, now become,

$$\phi_i^{(k)} \neq \psi_i^{(k)}, \quad \text{for } k > 1$$

and

$$\eta_i^{(k)} \neq \varepsilon_i^{(k)}, \quad \text{for } k > 3.$$

A lack of correspondence between the actual and the pseudofunctions clearly exists, and could lead to serious discrepancies in the calculation of certain properties - a situation which is likely to be reflected in scattering problems with their formal resemblance to the usual perturbation theory.

Turning now to the formulation in scattering processes, a natural choice for the invariants around which to construct the pseudopotential theory, are the elements of the  $T$ -matrix. Such a choice is rationalized in terms of the central role played by the  $T$ -matrix in scattering, its connection with the  $S$ - and  $K$ -matrices, and its relation to the important observables in the phase-shift analysis.

Equations are sought, therefore, which leave invariant the elements  $T_{ba}$  which in the notation of Lippmann and Schwinger [14] are defined by

$$T_{ba} = \langle \phi_b, V \phi_a^+ \rangle = \langle \phi_b^-, V \phi_a \rangle. \quad (2.31)$$

The incoming and outgoing waves  $\phi_a^\pm$  are defined in terms of the hamiltonian,  $H_0$ , and eigenfunctions  $\{\phi_a\}$  of the initial and final states, and  $V$  the interaction operator, thus [14],

$$\phi_a^\pm = \phi_a + \frac{1}{E_a \pm i\varepsilon - H_0} V \phi_a^\pm, \quad (2.32)$$

The functional corresponding to  $\omega$  for bound states, cf. Eq. (2.2), is now the Lippman-Schwinger functional  $\tau_{ba}$ , defined in the present context by,

$$\begin{aligned} \tau_{ba} = & \left\{ \langle (1-P) \phi_b^-, V \phi_a \rangle + \langle \phi_b, V (1-P) \phi_a^+ \rangle - \langle (1-P) \phi_b^-, V (1-P) \phi_a^+ \rangle \right. \\ & \left. + \left\langle (1-P) \phi_b^-, V \frac{1}{E + i\varepsilon - H_0} V (1-P) \phi_a^+ \right\rangle \right\} \end{aligned} \quad (2.33)$$

in which the projection operator  $P$  is defined with respect to a given subset  $\{\phi_c\}$  of  $H_0$ . Arbitrary variations of  $\phi_a^+$  and  $\phi_b^-$  lead to,

$$\begin{aligned} \delta\tau_{ba} = & \left\{ \langle \delta\phi_b^-, (1-P)V\phi_a^+ \rangle + \langle \phi_b^-, V(1-P)\delta\phi_a^+ \rangle - \langle \delta\phi_b^-, (1-P)V(1-P)\phi_a^+ \rangle \right. \\ & - \left. \langle \phi_b^-, (1-P)V(1-P)\delta\phi_a^+ \rangle \right. \\ & + \left\langle \delta\phi_b^-, (1-P)V \frac{1}{E+i\varepsilon-H_0} V(1-P)\phi_a^+ \right\rangle \\ & + \left\langle \phi_b^-, (1-P)V \frac{1}{E+i\varepsilon-H_0} V(1-P)\delta\phi_a^+ \right\rangle \end{aligned} \quad (2.34)$$

The condition  $\delta\tau_{ba} = 0$  leads to equations of the form,

$$\phi_a^+ = \phi_a + P\phi_a^+ + \frac{1}{E+i\varepsilon-H_0} V(1-P)\phi_a^+, \quad (2.35)$$

which may be written as,

$$\phi_a^+ = \phi_a + \left[ \frac{1}{E+i\varepsilon-H_0} (V + \Omega_a) \right] \phi_a^+, \quad (2.36)$$

from which,

$$\Omega_a \phi_a^+ = [(E+i\varepsilon-H_0) - V] P \phi_a^+. \quad (2.37)$$

Writing  $P = \sum_c |\phi_c\rangle \langle \phi_c|$ , and setting  $\varepsilon$  to zero, Eq. (2.37) reduces to,

$$\Omega \phi_a^+ = \sum_c \{ (E - E_c) (\phi_c | \phi_a^+) - \langle \phi_c, V \phi_a^+ \rangle \} |\phi_c\rangle \quad (2.38)$$

an equation which bears an obvious resemblance to the corresponding Eqs. (2.5) and (2.8). Operators defined by (2.38) clearly leave the elements of the  $T$ -matrix invariant when added to the potential  $V$ , and are therefore genuine pseudopotentials.

The approach to pseudopotentials outlined above is strictly valid for one-electron operators and wavefunctions only, and needs modification when considering the many-electron analogue. Thus the general  $n$ -electron trial function takes the form,

$$\psi(1, \dots, N) = \prod_{i=1}^N (1 - P_i) \phi(1, \dots, N), \quad (2.39)$$

with  $P_i$  defined in the usual way by,

$$P_i = \sum_c |\phi_c(i)\rangle \langle \phi_c(i)|. \quad (2.40)$$

Eq. (2.39) may be written as,

$$\psi(1, \dots, N) = (1 - Q) \phi(1, \dots, N),$$

in which  $(1 - Q)$  is idempotent, so that for the hermitian operator  $\hat{\Theta}$ , the  $n$ -electron pseudopotential equation is given by,

$$\Omega \phi(1, \dots, N) = \{Q \hat{\Theta} + \hat{\Theta} Q - Q \hat{\Theta} Q - \lambda Q\} \phi(1, \dots, N). \quad (2.42)$$

Product functions  $\phi_1(1), \dots, \phi_N(N)$ , whether antisymmetrized or not, reduce Eq. (2.42) to the usual form when  $\hat{\Theta}$  is a one-electron operator, but for two-electron operators the situation is slightly more complicated. A simple product variation function of the form,

$$\psi(1, 2) = (1 - Q) \phi(1) \psi(2), \quad (2.43)$$

in which

$$Q = P_1 + P_2 - P_1 P_2, \quad (2.44)$$

leads to the following two-electron pseudopotential equation,

$$\Omega(1, 2) \phi(1) = [\langle \psi(2) | Q \hat{\Theta} | \psi(2) \rangle - \lambda \langle \psi(2) | Q | \psi(2) \rangle] | \phi(1) \rangle. \quad (2.45)$$

which may be expanded to,

$$\begin{aligned} \Omega(1, 2) \phi(1) = & \sum_c [\langle \phi_c(1) | \psi(2) | \hat{\Theta}(1, 2) | \phi(1) \psi(2) \rangle - \lambda \langle \phi_c(1) | \phi_c(1) \rangle] | \phi_c(1) \rangle \\ & + \sum_d \langle \phi_d(2) | \psi(2) \rangle [\langle \phi_d(2) | \hat{\Theta}(1, 2) | \psi(2) \rangle \\ & - \lambda \langle \phi_d(2) | \psi(2) \rangle] | \phi(1) \rangle \\ & + \sum_{c,d} \langle \phi_d(2) | \psi(2) \rangle \langle \phi_c(1) | \phi(1) \rangle [\langle \phi_c(1) | \phi_d(2) | \hat{\Theta}(1, 2) | \phi(1) \psi(2) \rangle \\ & - \lambda \langle \phi_d(2) | \psi(2) \rangle \langle \phi_c(1) | \phi(1) \rangle] | \phi_c(1) \rangle, \end{aligned} \quad (2.46)$$

and similarly for  $\psi(2)$ . In the calculation of the matrix elements of  $\Omega$ , expansions in terms of orthogonal functions greatly simplify (2.46), and the only non-vanishing elements derive from the first summation.

For antisymmetrized products of the form,

$$\psi(1, 2) = 2^{-1/2} (1 - P_1) (1 - P_2) (\phi(1) \psi(2) - \psi(1) \phi(2)), \quad (2.47)$$

Eq. (2.45) is modified to include exchange, and is now given by,

$$\begin{aligned} \Omega \phi(1) = & [\langle \psi(2) | Q \hat{\Theta} | \psi(2) \rangle - \lambda \langle \psi(2) | Q | \psi(2) \rangle] | \phi(1) \rangle \\ & - [\langle \psi(2) | Q \hat{\Theta} | \phi(2) \rangle - \lambda \langle \psi(2) | Q | \phi(2) \rangle] | \psi(1) \rangle \end{aligned} \quad (2.48)$$

Once again, the only non-vanishing matrix elements of involving exchange, are obtained from the expansion,

$$- \sum [\langle \phi_c(1) | \psi(2) | \hat{\Theta} | \psi(1) \phi(2) \rangle - \lambda \langle \psi(2) | \phi_c(2) \rangle] | \phi_c(1) \rangle.$$

## References

1. Phillips, J. C., Kleinman, L.: *Physic. Rev.* **116**, 287 (1959).
2. Antoncik, E.: *J. Phys. Chem. Solids* **10**, 314 (1959).
3. Kleinman, L., Phillips, J. C.: *Physic. Rev.* **118**, 1153 (1960).
4. Cohen, M. H., Heine, V.: *Physic. Rev.* **122**, 1821 (1961).
5. Austin, B. J., Heine, V., Sham, L. J.: *Physic. Rev.* **127**, 276 (1962).

6. Weeks, J. D., Rice, S. A.: J. chem. Physics **49**, 2741 (1968).
7. Hazi, A. U., Rice, S. A.: J. chem. Physics **48**, 495 (1967).
8. Abarenkov, I. V., Heine, V.: Philos. Mag. **12**, 529 (1965).
9. Animalu, A. O., Heine, V.: Philos. Mag. **12**, 1249 (1965).
10. Kahn, L. R., Goddard, W. A.: Chem. Physics Letters **2**, 667 (1968).
11. Anderson, P. W.: Physic. Rev. Letters **21**, 13 (1968).
12. Anderson, P. W.: Physic. Rev. **181**, 21 (1969).
13. Kestner, N. R., Jortner, J., Cohen, M. H., Rice, S. A.: Physic. Rev. **140**, A 56 (1965).
14. Lippmann, B. A., Schwinger, J.: Physic. Rev. **79**, 469 (1950).

Dr. W. C. Mackrodt  
Central Instrument  
Research Laboratory  
Bozdown House  
Whitchurch Hill, Reading, Berkshire  
England



# Convenient Formulas for Evaluation of the Hybridized Valence States Involving the $s-p$ Hybrid Orbitals and Their Applications to the Atoms and the Ions of Carbon, Nitrogen, and Oxygen

Tosinobu Anno

Laboratory of Chemistry, College of General Education, Kyushu University  
Ropponmatsu, Fukuoka, 810 Japan

Received December 18, 1972

Formulas to calculate the energies of the hybridized valence states are given. The formulas cover any of the hybridized valence states, so far as the valence orbitals involved are  $s-p$  hybrids, and are useful in the sense that they give essentially the same results as those obtained with the modified Öpik method [1] quickly. The prescriptions and the numerical data for the actual evaluation of the hybridized valence-state energies are also given with particular reference to the atoms and the ions of carbon, nitrogen, and oxygen. In Appendix, addenda and corrigenda of the previous paper [1] are given.

*Key words:* Hybridized valence state energy formulas

## 1. Introduction

In a previous paper [1], it has been pointed out that off-diagonal terms, corresponding to interactions among multiplets of the same symmetry arising from different configurations participating in the hybridized valence state, must also be considered in addition to the diagonal terms considered in Öpik's method for evaluation of the hybridized valence-state energies [2], in order that Moffitt's [3] philosophy of defining the valence state be preserved even for the hybridized valence states. This modified Öpik method however is too complicated to be used. Therefore, formulas useful for the evaluation of the energies of hybridized valence states in the sense that they give essentially the same results as those obtained with the modified Öpik method quickly have been derived, although we have confined ourselves to those valence states which involve  $s-p$  hybrid AO's only. It is the purpose of the present paper to present such formulas and to give the prescriptions for the actual evaluation of the hybridized valence-state energies of the atoms and the ions of carbon, nitrogen, and oxygen.

## 2. Derivation of Formulas

Since we are confining ourselves to valence states involving  $s-p$  hybrid orbitals only, the atomic orbitals containing valence electrons may be expressed as

$$t_i = c_{si}s + c_{xi}x + c_{yi}y + c_{zi}z \quad (i = 1, 2, 3, 4) \quad (1)$$

without loss of generality. In Eq. (1),  $s$ ,  $x$ ,  $y$ , and  $z$  represent the  $s$ ,  $p_x$ ,  $p_y$ , and the  $p_z$  AO, respectively, while  $c_{si}$ ,  $c_{xi}$ ,  $c_{yi}$ , and  $c_{zi}$  are numerical coefficients subject to the orthonormalization conditions of  $t_i$ 's. The formulas to be presented are then as follows:

$$E(t_1, V_1) - c_{s1}^2 E(s, V_1) - (1 - c_{s1}^2) E(x, V_1) = 0, \quad (2)$$

$$\begin{aligned} E(t_1 t_2, V_2) - (c_{s1}^2 + c_{s2}^2) E(sx, V_2) - (1 - c_{s1}^2 - c_{s2}^2) E(xy, V_2) \\ = (1/2) c_{s1}^2 c_{s2}^2 Q, \end{aligned} \quad (3)$$

$$E(t_1^2, V_0) - c_{s1}^2 E(s^2, V_0) - (1 - c_{s1}^2) E(x^2, V_0) = c_{s1}^2 (c_{s1}^2 - 1) Q, \quad (4)$$

$$\begin{aligned} E(t_1 t_2 t_3, V_3) - (1 - c_{s4}^2) E(sxy, V_3) - c_{s4}^2 E(xyz, V_3) \\ = (1/2) (c_{s1}^2 c_{s2}^2 + c_{s1}^2 c_{s3}^2 + c_{s2}^2 c_{s3}^2) Q, \end{aligned} \quad (5)$$

$$\begin{aligned} E(t_1^2 t_2, V_1) - (2c_{s1}^2 + c_{s2}^2 - 1) E(s^2 x, V_1) \\ - (2 - 2c_{s1}^2 - c_{s2}^2) E(sx^2, V_1) \\ = (c_{s1}^4 + c_{s1}^2 c_{s2}^2 - 2c_{s1}^2 - c_{s2}^2 + 1) Q \\ - 5(c_{s1}^2 + c_{s2}^2 - 1) R, \end{aligned} \quad (6)$$

$$E(t_1 t_2 t_3 t_4, V_4) - E(sxyz, V_4) = (1/4) \left( 1 - \sum_{i=1}^4 c_{si}^4 \right) Q, \quad (7)$$

$$\begin{aligned} E(t_1^2 t_2 t_3, V_2) - (c_{s1}^2 - c_{s4}^2) E(s^2 xy, V_2) - (1 - c_{s1}^2 + c_{s4}^2) E(sx^2 y, V_2) \\ = [c_{s4}^2 - c_{s1}^2 c_{s4}^2 + (1/2) c_{s2}^2 c_{s3}^2] Q + 5c_{s4}^2 R, \end{aligned} \quad (8)$$

$$\begin{aligned} E(t_1^2 t_2^2, V_0) - (c_{s1}^2 + c_{s2}^2) E(s^2 x^2, V_0) - (1 - c_{s1}^2 - c_{s2}^2) E(x^2 y^2, V_0) \\ = (c_{s1}^2 + c_{s2}^2) (c_{s1}^2 + c_{s2}^2 - 1) Q, \end{aligned} \quad (9)$$

$$\begin{aligned} E(t_1^2 t_2 t_3 t_4, V_3) - c_{s1}^2 E(s^2 xyz, V_3) - (1 - c_{s1}^2) E(sx^2 yz, V_3) \\ = (1/2) (c_{s2}^2 c_{s3}^2 + c_{s2}^2 c_{s4}^2 + c_{s3}^2 c_{s4}^2) Q, \end{aligned} \quad (10)$$

$$\begin{aligned} E(t_1^2 t_2^2 t_3, V_1) - (c_{s1}^2 + c_{s2}^2 - c_{s4}^2) E(s^2 x^2 y, V_1) \\ - (1 - c_{s1}^2 - c_{s2}^2 + c_{s4}^2) E(sx^2 y^2, V_1) \\ = c_{s4}^2 (1 - c_{s1}^2 - c_{s2}^2) Q + 5c_{s4}^2 R, \end{aligned} \quad (11)$$

$$\begin{aligned} E(t_1^2 t_2^2 t_3 t_4, V_2) - (1 - c_{s3}^2 - c_{s4}^2) E(s^2 x^2 yz, V_2) \\ - (c_{s3}^2 + c_{s4}^2) E(sx^2 y^2 z, V_2) = (1/2) c_{s3}^2 c_{s4}^2 Q, \end{aligned} \quad (12)$$

$$\begin{aligned} E(t_1^2 t_2^2 t_3^2, V_0) - (1 - c_{s4}^2) E(s^2 x^2 y^2, V_0) \\ - c_{s4}^2 E(x^2 y^2 z^2, V_0) = c_{s4}^2 (c_{s4}^2 - 1) Q, \end{aligned} \quad (13)$$

$$E(t_1^2 t_2^2 t_3^2 t_4, V_1) - (1 - c_{s4}^2) E(s^2 x^2 y^2 z, V_1) - c_{s4}^2 E(sx^2 y^2 z^2, V_1) = 0. \quad (14)$$

In Eqs. (2)–(14),  $Q$  and  $R$  are the following combinations of the usual electron repulsion integrals:

$$\begin{aligned} Q &= (ss|ss) + (xx|xx) - 2(ss|xx) - 4(sx|sx), \\ R &= (sx|sx) - (xy|xy). \end{aligned} \quad (15)$$

The idea underlying our formulas is to express the energy of a hybridized valence state with reference to an appropriate weighted mean of energies of a pair of unhybridized valence states, in such a way that the core energies which are difficult to estimate do not appear in the formulas. The choice of the weights and the reference unhybridized valence states is, however, not unique. Our choice is based on the requirements that the resulting formula is as compact as possible and that the reliable values of the reference unhybridized valence-state energies are easily available.

Formulas (2)–(14) may be proved in the following ways:

(i) Write the energy expressions of the hybridized valence states in terms of the one- and the two-electron integrals over hybrid AO's.

(ii) Expand these integrals in terms of integrals over unhybridized AO's, using Eq. (1). The energy expressions of the hybridized valence states in terms of integrals over unhybridized AO's will then be obtained.

(iii) Write the energy expressions of the unhybridized valence states appearing in the left-hand sides of Eqs. (2)–(14) in terms of integrals over unhybridized AO's.

(iv) Make the expressions of the left-hand sides of Eqs. (2)–(14), using the valence-state energy expressions obtained in (ii) and (iii) above. Equations (2)–(14) will then be obtained by using assumptions for the one- and the two-electron integrals, which are best described with reference to some examples. Let us take Eq. (10) as an example. If one looks at the expressions of the quantities

$$E(t_1^2 t_2 t_3 t_4, V_3), \quad (16)$$

$$E(s^2 xyz, V_3), \quad (17)$$

$$E(sx^2 yz, V_3), \quad (18)$$

obtained in (ii) and (iii) above, one will find that integrals such as  $H_{ss}$  (one-electron core integral over  $s$  AO) and  $(ss|zz)$  appear in the expressions of all of (16)–(18). We assume that the value of a given one of such integrals in (16) is equal to the weighted mean of the values of that integrals in (17) and (18) with weights  $c_{s1}^2$  and  $(1 - c_{s1}^2)$ , respectively. The second of our assumptions is concerned with those integrals which appear in not all of (16)–(18); we assume that the value of a given one of such integrals is independent of the electron configuration.

Equations (2)–(14) can also be obtained by using the modified Öpik method [1] for the hybridized valence states and Moffitt's method [3] for the unhybridized valence states, if the orbital approximation and the set of assumptions on the equalities among the integrals mentioned in the preceding paragraph are

adopted for the difference between the hybridized valence-state energy and the weighted mean of the energies of the pair of the unhybridized valence states, given as the left-hand side of each of Eqs. (2)–(14). It is to be noted that Eqs. (7), (8), and (10) have already been derived by the present author [4] for special cases where  $c_{s4} = 0$ .

### 3. Numerical Evaluation

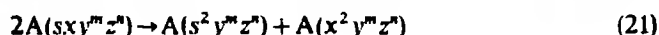
To evaluate the energies of hybridized valence states with Eqs. (2)–(14), those of unhybridized valence states must be determined first. These values are preferably determined directly from the observed term values as described by Moffitt [3]. Although Pritchard and Skinner [5] have already given such results, we have determined the energies of all the unhybridized valence states belonging to the configurations of  $1s^2 2s^m 2p^n$  ( $m = 0, 1, 2$ ;  $n = 0, 1, \dots, 6$ ) for the neutral atoms, the singly-negative ions, and the singly- and the doubly-positive ions of carbon, nitrogen, and oxygen with Moffitt's procedure. The results are given in Table 1. The observed term values have been taken from Moore's table [6] by averaging out the fine structure, each component of a particular term being given a weight of  $2J + 1$ . When no observed term values are available, the values obtained by extrapolation along isoelectronic series, have been used. In doing extrapolations, quadratic functions of atomic number have been used for most cases, but linear function had to be used for  $1s^2 2p^5 {}^2P$  for lack of data, while cubic functions have been used for  $1s^2 2p^6 {}^1S$ ,  $1s^2 2s^2 2p^5 {}^2P$ , and  $1s^2 2s^2 2p^4 {}^3P$ , because term values extrapolated for the negative ions using quadratic functions have turned out to be higher than those of the neutral atoms for these isoelectronic series; one would expect that the term value of a given term should decrease with decreasing (positive) ionic charge along isoelectronic series. For the  $1s^2 2p^4$  configuration, reliable term values are available only for  $O^{2+}$ , so that no inter- or extrapolation is possible for this isoelectronic series. The energies of the valence states of C and N<sup>+</sup> belonging to this configuration have therefore been determined from the semiempirical values of the average energy  $E_{av}$  of the configuration and of  $F^2(2p, 2p)$  given by Anno and Teruya [7].

Another data necessary for using Eqs. (2)–(14) are the values of the quantities  $Q$  and  $R$  defined by Eqs. (15). The values of  $(xy|xy)$  and  $(sx|sx)$  may be evaluated from  $F^2(2p, 2p)$  and  $G^1(2s, 2p)$ , respectively, since it holds that

$$(xy|xy) = (3/25) F^2(pp), \quad (19)$$

$$(sx|sx) = (1/3) G^1(sp). \quad (20)$$

The  $Q$  value on the other hand may be evaluated from the energy change  $\Delta E$  of the reaction



and the  $(sx|sx)$  value determined by Eq. (20), since it can be shown that

$$\Delta E = (ss|ss) + (xx|xx) - 2(ss|xx) + (sx|sx) \quad (22)$$

Table 1. Energies of valence states of atoms and ions of carbon, nitrogen, and oxygen as calculated with Moffitt's method (eV)<sup>a</sup>

Valence state	Energy	Valence state	Energy
$sx, V_2$	$C^{2+}$ 8.0392	$x^2y^2, V_0$	C 20.7225 <sup>b</sup>
$xy, V_2$	$C^{2+}$ 17.2946		$N^+$ 30.0113 <sup>b</sup>
$x^2, V_0$	$C^{2+}$ 19.5939		$O^{2+}$ 38.8301
$s^2x, V_1$	$C^+$ 0.0053	$s^2xyz, V_3$	$C^-$ (0.7243)
$(=s^2p, {}^2P)$	$N^{2+}$ 0.0144		N 1.1915
$sxy, V_3$	$C^+$ 8.4172		$O^+$ 1.6619
	$N^{2+}$ 11.2025	$s^2x^2y, V_1$	$C^-$ (1.8063)
$sx^2, V_1$	$C^+$ 10.1780		N 2.9787
	$N^{2+}$ 13.7599		$O^+$ 4.1696
$xyz, V_3$	$C^+$ 18.1258	$sx^2yz, V_3$	$C^-$ (9.1461)
	$N^{2+}$ 24.1612		N (14.1669)
$x^2y, V_1$	$C^+$ 19.7816		$O^+$ 19.1647
	$N^{2+}$ 26.8635	$sx^2y^2, V_1$	$C^-$ (10.2282)
$s^2xy, V_2$	C 0.3187		N (16.0406)
	$N^+$ 0.4828		$O^+$ 21.8010
	$O^{2+}$ 0.6474	$x^2y^2z, V_1$	$C^-$ (18.7542)
$x^2x^2, V_0$	C 1.7367	$(=p^5, {}^2P)$	N (29.0878)
	$N^+$ 2.6160	$s^2x^2yz, V_2$	$O^+$ (39.4215)
	$O^{2+}$ 3.4590		N (0.3398)
$sxyz, V_4$	C 8.2605	$s^2x^2y^2, V_0$	O 0.4989
	$N^+$ 11.9532		N (1.8503)
	$O^{2+}$ 15.3933		O 2.7072
$sx^2y, V_2$	C 9.8502	$sx^2y^2z, V_2$	$N^-$ (12.4735)
	$N^+$ 14.1812		O 17.6229
	$O^{2+}$ 18.3555	$x^2y^2z^2, V_0$	N (24.2436)
$x^2yz, V_2$	C 18.8124 <sup>b</sup>	$(=p^6, {}^1S)$	O (36.2761)
	$N^+$ 27.1765 <sup>b</sup>	$s^2x^2y^2z, V_1$	O (0.0061)
	$O^{2+}$ 35.6297	$(=s^2p^5, {}^2P)$	
		$sx^2y^2z^2, V_1$	O (14.9792)
		$(=sp^6, {}^2S)$	

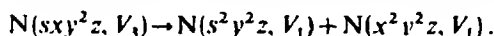
<sup>a</sup> The valence state energies given are referred to the ground states of the respective atoms or ions. The observed term values necessary for the evaluation of the valence-state energies have been taken from Moore [6] by averaging out the fine structure, each component of a particular term being given a weight of  $2J+1$ . If no observed term value is available, the value obtained by extrapolation along isoelectronic series has been used. The valence-state energies based on such extrapolated term values are enclosed in parentheses. See Section 3 of text for detail.

<sup>b</sup> For isoelectronic series atoms with  $1s^2 2p^4$  configuration, reliable term values are available only for  $O^{2+}$ , so that no inter- or extrapolation is possible for this isoelectronic series. The energies of the valence states of C and  $N^+$  belonging to this configuration have therefore been determined from the semiempirical values of the average energy  $E_{av}$  of the configuration and of  $F^2(2p, 2p)$ . As for  $F^2(2p, 2p)$  for this purpose, "corrected values" given in Table 2 of Ref. [7] have been used, while the  $E_{av}$  values have been obtained by the same method as described in footnote f to Table 1 of Ref. [7], except in that a quadratic function has been used for extrapolation.

for Reaction (21) within the usual orbital approximation. In either sides of Reaction (21), the two atoms concerned are supposed to be separated infinitely from each other. Moreover, the spins of electrons belonging to different orbitals of a given atom are supposed to be random. This means that the atoms are in valence states, although the valency number, which depends upon the  $m$  and the  $n$

values, is not shown. Thus, the  $\Delta E$  of Reaction (21) may easily be evaluated with the data of Table 1 if A is the atom or an ion of C, N, or O. It is to be noted that the Anno-Teruya values [7] of  $F^2$  and  $G^1$  have to be used for Eqs. (19) and (20), because some of the data of Table 1 are based on these values<sup>1</sup>.

Although we have described all the prescriptions and the data necessary for the application of our formulas derived in Section 2, a numerical example should facilitate the understanding of our prescriptions. For this purpose, a neutral nitrogen atom in its valence state  $tr_1^2 tr_2 tr_3 z, V_3$ , where  $tr_1$ ,  $tr_2$ , and  $tr_3$  are three equivalent  $sp^2$  hybrid AO's lying in the  $xy$  plane, will be considered, because this is the example adopted in a previous publication [1]. Now, if one would look at Table 1, remembering that  $x$ ,  $y$ , and  $z$  are equivalent with each other, it should not be difficult to find that Eq. (21) as applied to the present example is



Therefore, it is rather straightforward to obtain 9.2099 eV as the energy of this valence state above the ground state of the nitrogen atom from Eq. (10), by using the data of Table 1 and the  $G^1(2s, 2p)$  value taken from Table 3 of Ref. [7], since  $c_{s1}^2 = c_{s2}^2 = c_{s3}^2 = 1/3$  and  $c_{s4}^2 = 0$  in the present example. The value obtained for the same quantity with the modified Öpik method [1], by using the data which are used previously [1] and are the same as those used in the present work, is 9.2097 eV. This is very close to 9.2099 eV obtained above.

## Appendix

### Addenda and Corrigenda for Previous Work [1]

Since a valence state is an eigenstate neither of  $L^2$ ,  $S^2$ ,  $L_z$ , nor of  $S_z$  in general cases, more than one component of a given multiplet may be involved in an expansion of a valence-state wavefunction  $\Phi_V$ . This fact has been disregarded in Ref. [1]. Therefore, Eqs. (1) and (2) of Ref. [1] must now be written as

$$\tilde{\Phi}_V = \sum_{r=1}^N \sum_{i=1}^{f_r} c_{r,i} \tilde{\psi}_{r,i} \quad (\text{A.1})$$

$$\Phi_V = \sum_{r=1}^N \sum_{i=1}^{f_r} c_{r,i} \psi_{r,i} \quad (\text{A.2})$$

respectively, where  $\psi_{r,i}$  is the wavefunction of the  $i^{\text{th}}$  component of the  $r^{\text{th}}$  multiplet, which is supposed to be in an  $f_r$ -fold degeneracy if the spin-orbit

<sup>1</sup> As for the  $G^1(2s, 2p)$  value, it is inevitable to use that of the  $sp^3$  configurations, since the semi-empirical value of this parameter can be determined only for such type of configurations. As for the  $F^2(2p, 2p)$  value, it would be logical to use an appropriate weighted mean of values determined for different configurations of a given atom (or ion) if available. For example, the  $F^2(2p, 2p)$  value to be used for the calculation of the  $R$  value of Eq. (8), through Eqs. (15) and (19), would be the weighted mean of its values determined for the  $s^2p^2$  and the  $sp^3$  configurations with weights  $c_{s1}^2 - c_{s4}^2$  and  $1 - c_{s1}^2 + c_{s4}^2$ , respectively.

interaction is neglected and  $c_{r,i}$  is the expansion coefficient, the order notations being the same as those used in Ref. [1]. As a consequence, we have

$$\Phi_V = \sum_{r=1}^N \sum_{i=1}^{f_r} c_{r,i} \psi_{r,i} + \sum_{s=1}^f c_{s,i} \psi'_{s,i} + \sum_{t=1}^{f_t} c_{t,i} \psi'_{t,i} \quad (\text{A.3})$$

instead of Eq. (7) of Ref. [1] and similarly for Eqs. (4) and (6) of Ref. [1]. As in Ref. [1]  $s$  and  $t$  refer to the multiplets of the same symmetry by definition and  $\psi'_{s,i}$  and  $\psi'_{t,i}$  must correspond to the same  $M_L$  and the same  $M_S$  values in order that they interact to each other. Therefore, it holds that

$$f_s = f_t = f \quad (\text{A.4})$$

and that

$$\begin{aligned} E_V = & \sum_{r=1}^N \sum_{i=1}^{f_r} |c_{r,i}|^2 \langle \psi_{r,i} | \mathcal{H} | \psi_{r,i} \rangle \\ & + \sum_{i=1}^f |c_{s,i}|^2 \langle \psi'_{s,i} | \mathcal{H} | \psi'_{s,i} \rangle + \sum_{i=1}^f |c_{t,i}|^2 \langle \psi'_{t,i} | \mathcal{H} | \psi'_{t,i} \rangle \\ & + \sum_{i=1}^f (c_{s,i}^* c_{t,i} + c_{s,i} c_{t,i}^*) \langle \psi'_{s,i} | \mathcal{H} | \psi'_{t,i} \rangle. \end{aligned} \quad (\text{A.5})$$

If the spin-orbit interaction is neglected, the matrix elements involved in Eq. (A.5) are independent of  $i$ , so that this equation may be reduced to

$$\begin{aligned} E_V = & \sum_{r=1}^N \left( \sum_{i=1}^{f_r} |c_{r,i}|^2 \right) \langle \psi_r | \mathcal{H} | \psi_r \rangle \\ & + \left( \sum_{i=1}^f |c_{s,i}|^2 \right) \langle \psi'_s | \mathcal{H} | \psi'_s \rangle + \left( \sum_{i=1}^f |c_{t,i}|^2 \right) \langle \psi'_t | \mathcal{H} | \psi'_t \rangle \\ & + \left[ \sum_{i=1}^f (c_{s,i}^* c_{t,i} + c_{s,i} c_{t,i}^*) \right] \langle \psi'_s | \mathcal{H} | \psi'_t \rangle, \end{aligned} \quad (\text{A.6})$$

which shows that the following replacements are necessary in Eq. (8) of Ref. [1]:

$$\left. \begin{aligned} |c_r|^2 &\rightarrow \sum_{i=1}^{f_r} |c_{r,i}|^2 \\ |c_s|^2 &\rightarrow \sum_{i=1}^f |c_{s,i}|^2 \\ |c_t|^2 &\rightarrow \sum_{i=1}^f |c_{t,i}|^2 \\ c_s^* c_t + c_t^* c_s &\rightarrow \sum_{i=1}^f (c_{s,i}^* c_{t,i} + c_{s,i} c_{t,i}^*) \end{aligned} \right\}. \quad (\text{A.7})$$

This set of replacements is also necessary in Eqs. (3), (5), (13), (15), and (17) of Ref. [1]. Fortunately, however, the conclusions of Ref. [1], including the numerical value of  $E_V(I) - E_V(II)$  (see Eq. (26) of Ref. [1]), are unchanged with this modification. This is due to the fact that the set of replacements is necessary in Eqs. (13) and (15) of Ref. [1] at the same time.

*Acknowledgements.* This work has been motivated by the work which the present author has been doing in collaboration with Mr. Hirohide Teruya on the electronic structure of the nitrogen-containing heterocyclic molecules and the carbonyl-containing molecules. The author is grateful to him for this collaboration and for his help in the numerical calculations on the unhybridized valence state energies. He is also grateful to Dr. Uno Öpik of the Queen's University, Belfast. Dr. Öpik has been kind enough to read the manuscript of the present paper and to send unpublished details of his calculations, which have been very useful in confirming the results and the conclusions given in the present paper.

### References

1. Anno, T.: *Theoret. chim. Acta (Berl.)* **25**, 248 (1972).
2. Öpik, U.: *Mol. Phys.* **4**, 505 (1961).
3. Moffitt, W.: *Rept. Progr. Physics* **17**, 173 (1954).
4. Anno, T.: *J. chem. Phys.* **29**, 1161 (1958).
5. Pritchard, H. O., Skinner, H. A.: *Chem. Rev.* **55**, 745 (1955).
6. Moore, C. E.: *Atomic energy levels as derived from the analyses of optical spectra*. Vol. 1. Washington, D. C.: National Bureau of Standards (U.S.), Circular No. 467, 1949.
7. Anno, T., Teruya, H.: *Theoret. chim. Acta (Berl.)* **21**, 127 (1971).

Professor Dr. Tosinobu Anno  
Laboratory of Chemistry  
College of General Education  
Kyushu University  
Ropponmatsu, Fukuoka  
810 Japan



## Electron Redistribution in Disulfide Bonds under Torsion

Donald B. Boyd

The Lilly Research Laboratories, Indianapolis, USA

Received February 8, 1973

The origin of the conformational preference of acyclic disulfides is elucidated with population analyses and electron density maps of extended Hückel wave functions for HSSH and  $\text{H}_3\text{CSSCH}_3$ . Overlap population between the sulfurs is greatest when the dihedral angle about the S-S bond is near  $90^\circ$  because the negative contributions from the repulsive interactions of the lone-pair electrons are minimized in this conformation. Electron density maps are introduced to illustrate the rearrangement of the valence electrons in HSSH when the molecule is formed from the isolated atoms and the redistribution which occurs when the molecule is twisted about the S-S bond. A "C"-shaped distribution is found for the lone-pair clouds around each sulfur. The spacing between these clouds and the transfer of density away from the sulfurs toward the hydrogens are enhanced when the dihedral angle is near  $90^\circ$ .

**Key words:** Hydrogen persulfide Disulfides, conformation of

### Introduction

Recently, we have shown that the extended Hückel molecular orbital (EH MO) method can be used to explain the relation of the  $uv$  absorption spectra of organic disulfides to the dihedral angle about the S-S bond [1]. Computed transition energies and oscillator strengths varied in a manner qualitatively consistent with experiment for several of the long wavelength bands through the range of observed dihedral angles ( $\sim 0^\circ$  to  $\sim 120^\circ$ ). Since the EH MO's appear to give a satisfactory description of the electronic structure of the disulfide chromophore, we wish to bring them to bear on another aspect of disulfides, namely, the origin of the roughly  $90^\circ$  preference for the dihedral angle about the S-S bond. For instance, in HSSH the dihedral angle [2] is  $90.6^\circ$ , and in  $\text{H}_3\text{CSSCH}_3$ , the CSSC angle [3, 4] is about  $85^\circ$ . Of course, bulky substituents [1] can force the dihedral angle to open beyond  $90^\circ$ , and small rings or intramolecular hydrogen bonds [1] can impose dihedral angles considerably smaller than  $90^\circ$ .

Calculations by the EH method were carried out using previously published parameter values [5-7]. The usual Slater-type basis sets were employed, including the  $3d$  functions. Hydrogen persulfide, HSSH, and dimethyldisulfide,  $\text{H}_3\text{CSSCH}_3$ , were assigned dihedral angles from  $0^\circ$  (*cis*) to  $180^\circ$  (*trans*), including the experimental values near  $90^\circ$ . Bond lengths and angles were held fixed at the microwave determined values [2, 3]. For purposes of computing potential energy curves for internal rotation,  $0.5 \sum \epsilon_i$  was employed. This quantity has

Table 1 Calculations on the barriers to internal rotation in HSSH

Method	Preferred dihedral angle	<i>cis</i> barrier (kcal/mole)	<i>trans</i> barrier (kcal/mole)	Ref.
Simple LCAO-MO	90°	6.14	—	[18]
(NDO) with Sichel-Whitehead parameters	90	2.7	2.7	[19]
(NDO) with Santry-Segal parameters	95	3.4	0.8	[17]
<i>Ab initio</i> with Gaussian- type functions (Total energy 792.66 a.u.)	90-100	7.4	1.9	[15]
<i>Ab initio</i> with Gaussian- type functions (Total energy 793.97 a.u.)	98	7.7	2.2	[17]
<i>Ab initio</i> with Gaussian- type functions (Total energy 796.18 a.u.)	91	9.3	6.0	[16]
Present work	80-90	1.5	0.9	

been shown [8,9] to be more appropriate for evaluating total energies of molecules in EH theory than the simple sum of the eigenvalues of the occupied MO's over all valence electrons,  $\sum \epsilon_i$ .

The main purpose of this paper is to use electron density maps for extending our understanding of the disulfide rotational barriers and for visualizing the shape of the electron lone-pair clouds on sulfur. Electron density maps of EH MO's have been established as a highly useful technique in the study of molecular electronic structures [6,9-13]. Before presenting the illustrations, Mulliken [14] population analyses will be done on both HSSH and  $\text{H}_3\text{CSSCH}_3$ . Our population analysis results are presented in more detail than has been done by previous authors, so that all aspects of the variation of bond strengths and orbital populations can be traced as a function of dihedral angle. We will see that the essential features of the population analyses, which have been observed in *ab initio* calculations [15-17], are also displayed by our semi-empirical EH MO's. Hence the EH MO electron density maps should further elucidate the electron redistribution accompanying the conformational changes in the disulfide group. Electron density difference maps computed by standard procedures [13] will be presented for the smaller model compound HSSH.

### Barriers to Internal Rotation in HSSH and $\text{H}_3\text{CSSCH}_3$

As with numerous other quantum mechanical studies [15-19], our EH calculations give the correct general shape for the potential energy curve of HSSH (Table 1). But the EH barrier heights are obviously low compared to the *ab initio* values. Experimentally, the heights are not yet known precisely. The EH calculations do mimic the *ab initio* calculations [15-17] in regard to the S-S overlap population,  $n(\text{S-S})$ , being greatest when the dihedral angle is 90°. The value of  $n(\text{S-S})$  increases from 0.831 at a dihedral angle of 0° to 0.854 at 90°, and then drops to 0.844 at 180°. A significant property of  $n(\text{S-S})$  can be found by

breaking it down into  $\sigma$  and  $\pi$  components. Whereas the  $\sigma$  overlap population between the sulfurs increases monotonically as the dihedral angle is opened from 0–180°, the  $\pi$  value peaks near 90° at 0.178, compared to 0.162 at 0° and 180°. It follows that the interactions of valence AO's of  $\pi$  symmetry with respect to the S–S axis determine the preferred 90° conformation in disulfides. Furthermore, a repulsive interaction exists between the lone-pair electrons of each sulfur: the  $S_1 3p_x - S_2 3p_x$  contribution to the  $\pi$  component of  $n(\text{S-S})$  is negative. It is mainly due to the  $3p_x - 3d_x$  interactions that a net positive  $\pi$  component is obtained in our calculations. The  $S_1 3p_x - S_2 3p_x$  overlap contribution is least negative when the dihedral angle is near 90°, thus indicating that the repulsion between the lone-pair electrons is somewhat relieved in this conformation. The population analysis of the EH MO's also gives the smallest charge separation between S and H at this geometry: the net charge on sulfur,  $Q(\text{S})$ , is  $-0.098$  at 0°,  $-0.087$  at 90°, and  $-0.092$  at 180°.

Other quantities in the population analysis of HSSH did not show extrema at 90°. For instance, the S–H overlap population decreased marginally and monotonically from 0.761 at 0° to 0.756 at 180°. The only *ab initio* calculations [15] to report  $n(\text{S-H})$  give a shallow minimum near 90°. The total occupation of the 3d AO's on each sulfur increased steadily from 0.101 *e* at 0° to 0.115 *e* at 180°. Thus, the 3d AO's are not greatly occupied in the ground state of HSSH, and, in fact, the extent of occupation is almost the same as in the large basis set *ab initio* calculations [16]. At a dihedral angle of 90°, the rigorous dipole moment computed from all one- and two-center integrals [20] is 2.87 *D*. This contains a contribution of 0.79 *D* from the net atomic charges and a contribution of 3.88 *D* from each sulfur atomic dipole moment [13, 20]. The latter quantity reflects the large asymmetrical polarization of charge due to the lone-pair electrons as will be displayed later. A rather old experimental [21] dipole moment of 1.18 *D* for HSSH is bracketed by our rigorous and point charge values. The rigorous dipole moment of the hypothetical *cis* planar conformer of HSSH is 4.12 *D*.

In dimethyldisulfide  $\text{H}_3\text{CSSCH}_3$ , there are two S–C bonds and one S–S bond about which hindered rotation takes place. Calculations were done through the range of CSSC dihedral angles with three different methyl group arrangements as graphed in Fig. 1. The most stable geometry has a dihedral angle of about 90° and both methyls staggered. When the methyls are in their equilibrium conformation, the *cis* barrier for the S–S bond is 7.0 kcal/mole, and the *trans* barrier is 2.2 kcal/mole. The rotational barrier about the S–C bonds can be seen in Fig. 1 to be about 1.2 kcal/mole at those CSSC dihedral angles large enough to avoid steric hindrance between the methyl hydrogens. Thus, the predicted equilibrium conformation and the various barrier heights are in good agreement with experiment [3, 4, 18, 22]. Of the several previous calculations on the conformational energy of  $\text{H}_3\text{CSSCH}_3$ , the PCILIO method [23] yielded a preferred dihedral angle of 100°, a *cis* barrier of 2.9 kcal/mole, and a *trans* barrier of 1.3 kcal/mole. One point about the PCILIO calculations is that the molecule at a dihedral angle of 100° is predicted to be 1 kcal/mole more stable when both methyls are eclipsed than when both methyls are staggered. On the other hand, the EH calculations agree with

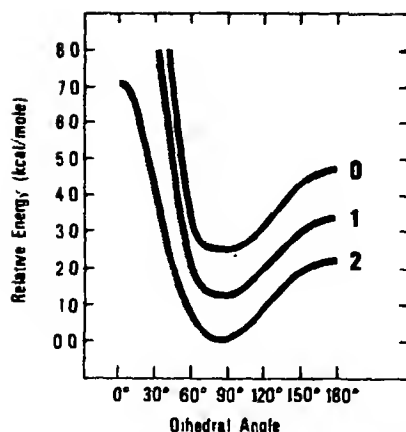


Fig 1 Conformational energies of  $\text{H}_3\text{CSSCH}_3$  with both methyls staggered (2), one methyl staggered and one eclipsed (1), and both methyls eclipsed (0) with respect to the S-S bond. The energy is relative to that for the most stable conformation. The top two curves extend off the graph at small dihedral angles because of steric hindrance between hydrogens of each methyl group

experiment [4] by favoring a staggered arrangement for the methyl groups. Perahia and Pullman [23] refer to some work [24] where an EH method failed to give the correct shape of the potential energy curve for  $\text{H}_3\text{CSSCH}_3$ . Instead of the near  $90^\circ$  dihedral angle, a  $180^\circ$  angle was predicted to be most stable. However, we encountered no difficulty in the implementation of our EH method. Other calculations on dimethyldisulfide used a ZDO-SCF method [25] and showed the total energy to be lower at  $90^\circ$  than at smaller dihedral angles, but the barrier heights of 45.9 kcal/mole (*cis*) and 14.5 kcal/mole (*trans*) seem much too high.

The Mulliken population analyses of the most stable conformers of  $\text{H}_3\text{CSSCH}_3$  yield conclusions similar to those for  $\text{HSSH}$ . The overlap population of the S-S bond maximizes at 0.952 and the charge on sulfur,  $Q(\text{S})$ , becomes least negative at  $-0.038$  when the CSSC dihedral angle is  $90^\circ$ . The overlap population of the S-C bonds reaches a peak of 0.675 and  $Q(\text{C})$  becomes most negative ( $-0.119$ ) when the dihedral angle is around  $60^\circ$ . The rigorous dipole moment of  $\text{H}_3\text{CSSCH}_3$  with both methyls staggered decreases monotonically from 5.70 D in the *cis* conformation to zero in the *trans*. At a dihedral angle of  $90^\circ$ , our rigorous dipole moment of 3.91 D and point charge value of 0.82 D again bracket the experimental value [3] of 1.985 D.

### Electron Density Maps of HSSH

We did not have the benefit of a plotter in the preparation of the electron density maps seen in Figs. 2-10. Hence our figures are made by photographing printed output from the computer (IBM 360/65). Our computer program can take a two-dimensional array of numbers, such as electron densities, and find specified contours of equal density. The resolution of the printout is limited by the size and ratio of height to width of the type characters. However, any area

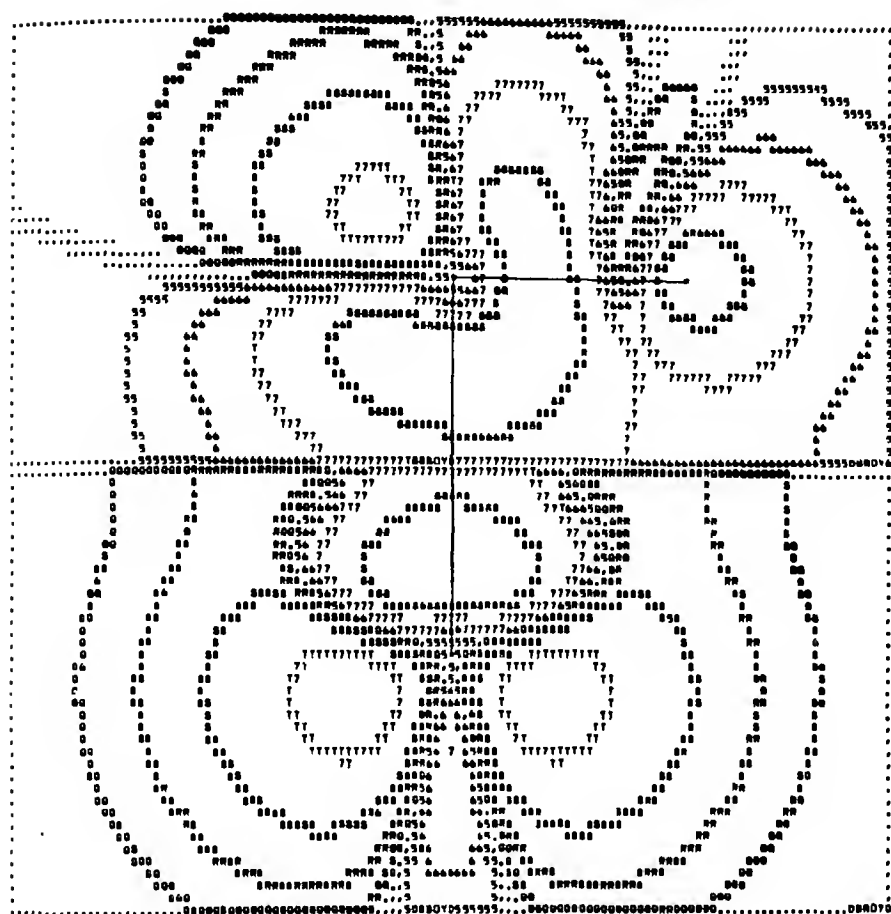


Fig. 2. Electron density in the  $0^\circ$  conformer of HSSH. The difference between the molecular and the spherically symmetric, ground state atomic densities is plotted in two mutually perpendicular planes through the S-S bond; the upper half shows the density in the plane of the S-S-H atoms; the lower half shows the density perpendicular to the S-S-H plane at the other end of the molecule. Each half of the figure, which splits the molecule at the midpoint of the S-S bond, covers  $5 \times 2.5 \text{ \AA}$ . Because of the  $C_{2v}$  symmetry of the *cis* conformer, both halves of the molecule are equivalent.

of the molecule may be magnified as much as necessary by having many maps each covering a small portion. The scale used in our figures was selected on the basis of giving maximum magnification of the molecule while still allowing the contour characters to be legible. Numerical characters correspond to negative density differences, i.e., a deficiency of electrons, and alphabetic characters correspond to positive density differences, i.e., an excess of electrons. Magnitudes of the density corresponding to each character are  $0.00024 e/\text{bohr}^3$  for 5 or Q,  $0.00112$  for 6 or R,  $0.0056$  for 7 or S,  $0.0280$  for 8 or T, and  $0.1400$  for 9 or U. Nodes occur in the middle of the dotted (.) contours. Some contours appear to be discontinuous in areas of steep changes in density because of the limited resolution. Internuclear axes between bonded atoms are drawn by solid lines if the atoms

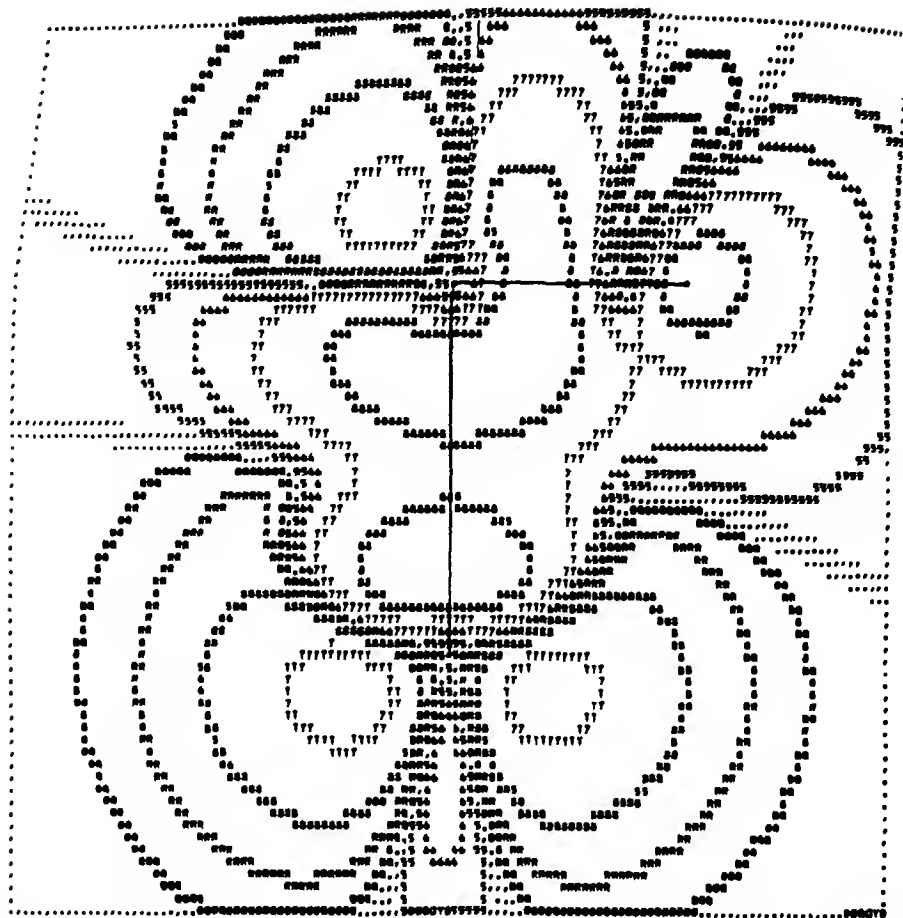


Fig. 3. Electron density in the 90° conformer of HSSH. The map covers  $5 \times 5 \text{ \AA}$  and shows the difference in molecular and atomic densities in the S-S-H plane

lie in the plane of calculation and by dashed lines otherwise. Density maps of the *trans* planar conformer of HSSH show no interesting differences from those for the *cis* planar conformer, except for the flip at one end of the molecule. Consequently, in order to conserve journal space, only plots of the conformers with dihedral angles of 0° and 90° are included here.

By mentally assembling the various slices through the molecule (Figs. 2-7), one ascertains that the regions occupied by the lone-pair electrons near each sulfur are roughly "C"-shaped. The plane of the "C" is perpendicular to the S-S-H plane at each end of the molecule with the top and bottom of the "C" above and below the sulfur nucleus. There is more electron density near the ends of the "C" than in the mid-section, which means that the lone-pair regions are intermediate between the directed valence implied by  $sp^3$  hybrid orbitals and a uniform, quasi-spherical distribution. Imagining that the "C" is hinged on the sulfur, one observes that the "C" is swiveled away from the other sulfur. This swiveling to behind the plane of Figs. 5-7 means that the effective distance

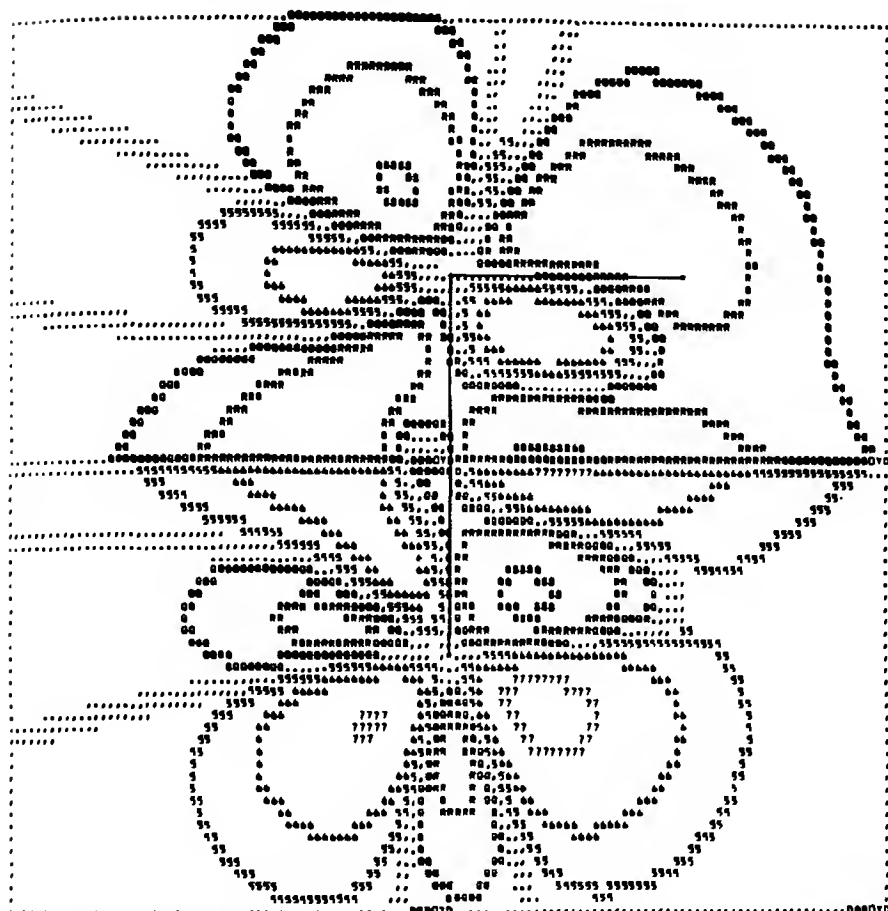


Fig. 4. Difference in the electron densities in the 90° conformer minus that in the 0° conformer. Each half shows the density in the half of the molecule where the atomic positions are fixed with respect to internal rotation, i.e., the two halves of Fig. 2 are subtracted from the upper and lower halves of Fig. 3. The features to observe are at the ends of the molecule near each S-H moiety because the redistributions along the S-S bond are partially masked by the tails of the AO's centered on the nuclei which change position

between the lone-pair clouds is increased relative to the situation in which the lone-pair regions are assumed to be pure  $3p_z$  or  $sp$  hybrid orbitals. Compensating for the build-up of density on the obtuse side of the S-S-H angle is a loss of electrons from the other sides of the sulfur atoms. In going from the 0° to the 90° conformation, the pattern of charge redistribution is complex. The bottom half of Fig. 4 shows that in the plane perpendicular to the S-S-H group, the electrons are shifted from behind the plane of Figs. 5-7 to the side between the sulfurs. But in the plane of the S-S-H group, the electrons are shifted into the vicinity of the hydrogen (Fig. 7) and toward the ends of the S-S axis (top of Fig. 4).

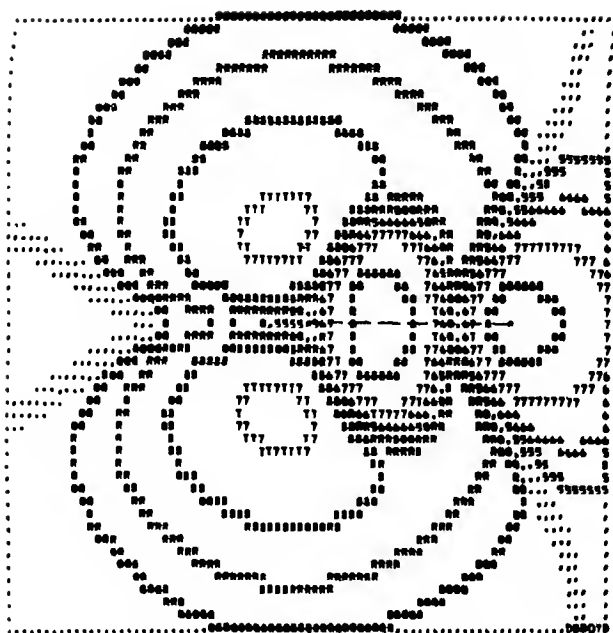


Fig. 5. Electron density in the 0° conformer of HSSH. The difference in molecular and atomic densities is computed in the plane passing through one sulfur perpendicularly to the S—S bond. Thus, one S—H bond axis lies slightly skew to this plane due to the S—S—H bond angle of  $\sim 91.5^\circ$ . The map covers  $4 \times 4 \text{ \AA}$ .

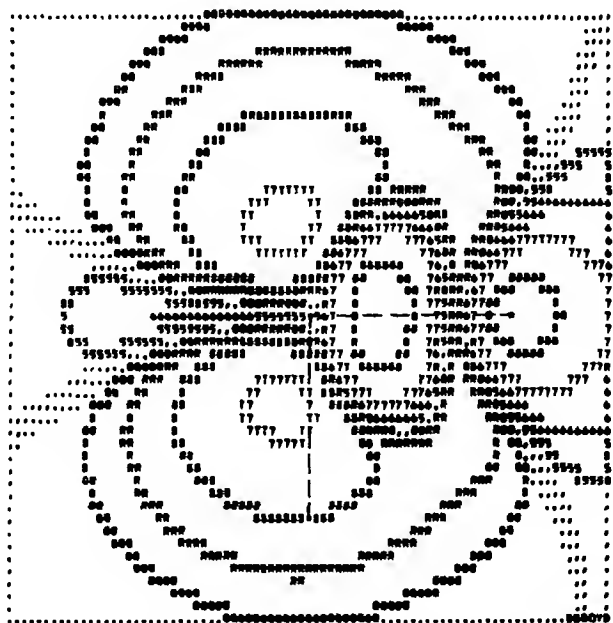


Fig. 6. Electron density in the 90° conformer of HSSH. The arrangement is like that in Fig. 5.



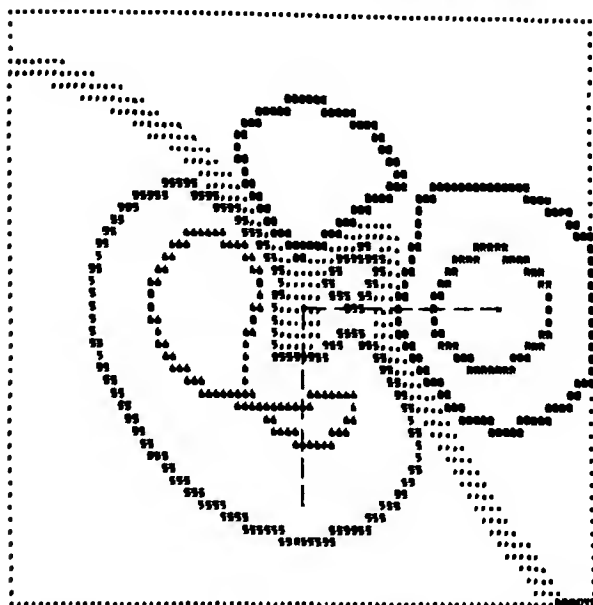


Fig. 7. Difference in the electron density in the 90° conformer of HSSH minus that in the 0° conformer. The density of Fig. 5 is subtracted from that in Fig. 6

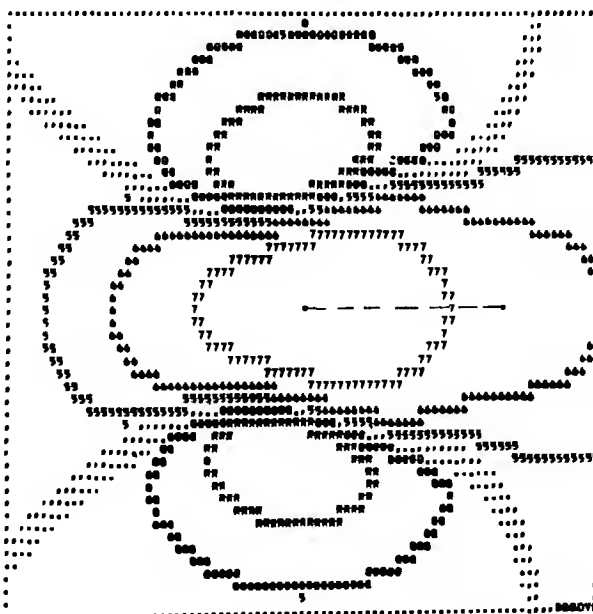


Fig. 8. Electron density in the 0° conformer of HSSH. The difference in molecular and atomic densities is shown in the plane bisecting the S-S bond perpendicularly. The map covers  $4 \times 4 \text{ \AA}$



Relative to the overlapping, but unperturbed, constituent atomic densities, the accumulation of electrons in the S-H bonds is rather small and strongly polarized away from the center of the molecule. In this respect, the S-H bond is similar to the O-H bond density obtained from all-electron wave functions [10]. Twisting the molecule from 0–90° increases the density near the hydrogens (Figs. 4 and 7). That the  $\sigma$  electron peak is higher in the 90° conformer is also apparent in Fig. 3 by the extra contour between sulfur and hydrogen.

The EH MO's give no density accumulation along the S-S bond expected for  $\sigma$  bonding (Figs. 2, 3, 8, 9). There does appear to be  $\pi$  bonding between the sulfurs as evidenced by the build-up of density between the sulfurs, but radially out from the S-S axis (Figs. 8 and 9). For instance, in the 90° conformer, there is a region of excess electrons (compared to the atomic densities) on the obtuse side of the dihedral angle. Comparison of the 90° and 0° conformers (Fig. 10) shows a roughly four-fold rearrangement. Visually estimating the contour sizes leads one to believe that there is a slight net increase in electron density at the midpoint of the S-S bond in the 90° conformer.

### Discussion

We begin this section by distilling from our population analysis results a qualitative, intuitive model for understanding the conformational preference of a disulfide moiety. Then this model will be refined on the basis of the more detailed description provided by the electron density maps. And, finally, our model will be discussed in relation to models proposed by other authors.

The population analysis yielded the fact that the S-S overlap population is greatest when the dihedral angle is near 90°. Thus, the S-S bond is strongest when the molecule is in its equilibrium conformation. However, we also saw that there are repulsive, antibonding interactions between the  $S3p_x$  AO's, which are highly occupied by the lone-pair electrons [1]. The S-S overlap population peaks at 90° where these repulsions are diminished. In addition, the negative net atomic charge on the sulfurs is lessened in the 90° conformation. This implies that electrons have moved away from the sulfurs toward the substituents.

The electron density maps show us exactly where the electrons are distributed around the nuclear skeleton without arbitrary partitioning of the density among the atoms or bonds. We saw that the regions occupied by the lone-pair electrons are "C"-shaped. In the 90° rotamer the effective distance between these regions is increased, and the interelectron repulsions are diminished. There also appears to be a slight increase in density halfway between the sulfurs as a result of twisting the dihedral angle from 0° or 180° to 90°. This migration would correlate with the increase in overlap population. Rearrangement of charge close to each sulfur nucleus is complex and difficult to interpret. On the other hand, the clear increase in density close to the hydrogen nuclei in the 90° conformer suggests a corresponding decrease in charge near the sulfurs and a more stable environment for the electrons remaining in the lone-pair clouds.

Various earlier models for understanding the conformational preference of disulfides are consistent with our calculations. Pauling [26, 27] proposed that

the repulsion of unshared electron pairs on adjacent atoms determines the orientation of the substituents about the single bond between those atoms. He assumed that the unshared electron pairs of each sulfur occupy orbitals orthogonal to each S-S-H plane, such as a  $3p_x$  AO or an  $sp$  hybrid orbital. Of course, in EH MO calculations no assumptions about the hybridization of the orbitals occupied by the lone-pair electrons need be made. The electron density maps show precisely how the MO's distribute the lone-pair electrons in "C"-shaped regions. The "C"-shaped clouds act effectively like  $3p_x$  or  $sp$  orbitals in that repulsive interactions between them are reduced at a dihedral angle of  $90^\circ$ . Another proposal for the conformational preference of disulfides is the hyperconjugation model [2]. In it,  $\pi$  bonding between the sulfurs is believed to be enhanced when the orbital of the unshared electron pair on one sulfur is in the same plane as the S-H bond of the other sulfur. Thus, in the  $90^\circ$  conformer, resonance structures of the type  $H^- S=S^+-H$  become important. Essentially equivalent to this model is one based on a stabilizing back donation of the lone-pair electrons on one sulfur into the antibonding S-H  $\sigma^*$  orbital at the other end of the molecule [28]. The consequences of hyperconjugation or back donation are that the S-S bond is strengthened and the density near the hydrogens is increased in the  $90^\circ$  conformation. As we have seen, the EH (and *ab initio*) population analyses and the EH electron density maps support this view.

Yet another model for molecules with lone-pair electrons on adjacent atoms has been expressed as the gauche effect [29-31]. Most such molecules adopt a conformation which allows the maximum number of gauche interactions between lone-pairs and/or polar bonds, although there are a few exceptions (e.g.,  $FCH_2OH$ ) which must be explained by additional rules and effects [28-32]. In order to rationalize the gauche effect [29-31], Wolfe *et al.*, employed Allen's repulsive-dominant, attractive-dominant scheme [33-35] for dissecting *ab initio* total energies [15, 17]. However, characterizations based on such dissections change depending on the basis set and on whether the molecular structure is allowed to relax in the transition state [36-39]. Hence this scheme does not seem to be a dependable approach to "understanding" rotational barriers. For convenience of counting gauche interactions, Wolfe *et al.*, treated the lone-pair electrons as if they occupied  $sp^3$ -like hybrid orbitals, although they emphasized that the computed potential energy curves for internal rotation in their example of  $FCH_2OH$  [29] suggested a quasi-spherical distribution of lone-pair electrons on oxygen. Our electron density maps of HSSH show the lone-pair regions on either side of the S-S-H planes to have higher density than in the plane, but there is still an appreciable amount in the plane. In other words, our findings indicate a small amount of directionality in the spatial distribution of the two electron pairs on a divalent atom. This result is consistent with *ab initio* electron density maps of  $H_2S$  [40], computed potential energy curves for internal rotation in  $CH_3OH$  [28, 29], computed potential energy curves for hydrogen bonded systems of water [41], and electrostatic potential energy calculations of oxirane and thiirane [42]. Published [43] electron density maps of  $FCH_2OH$  have not yet dealt with the question of whether a difference density map would show a directed valence around oxygen or a distribution which is quasi-spherical like the potential field it produces [28, 29].

In summary, we have seen that new insight into the origin of the preferred conformation of disulfides can be gained by the increasingly popular expedient of mapping the electron density of EH MO's. Both published and unpublished investigations in our laboratories on a variety of phosphorus compounds, hydrocarbons, and other organic molecules have established that many chemically significant features of the electronic structures of molecules are displayed by plots of EH MO's. One may recall that EH MO's were the orbitals instrumental (even if not essential) in the development of the famous Woodward-Hoffmann rules [44]. Our spectral study [1] and the similarities of the trends in the *ab initio* and EH population analyses of HSSH encourage us to think that the EH density maps may also exhibit the important aspects of the electron redistribution, especially in our situation where comparable wave functions for different rotamers are being compared. Nevertheless, it should be kept in mind that some discrepancies between *ab initio* and EH electron density maps can be expected not only because of the semiempirical nature [13] and neglect of the core electrons [8,40] in the EH wave functions, but also because of the different basis sets. The *ab initio* wave functions for HSSH which have been computed [15-17], but not yet published in full form, were expanded over Gaussian-type functions, whereas the EH MO's are linear combinations of Slater-type orbitals. Even different *ab initio* wave functions can yield density maps which display a modest to high dependence on the size and type of basis set [8, 40, 45-48]. Nevertheless, the very fact that several *ab initio* wave functions are available for HSSH makes our presentation of the EH results all the more worthwhile, so that at least a visual comparison can be made once the *ab initio* electron density maps are available.

*Acknowledgements.* Conversations with N. L. Allinger, W. A. Goddard, III, R. Hoffmann, W. N. Lipscomb, and M. M. Marsh were helpful to the development of some of the ideas in this paper.

## References

1. Boyd, D. B.: J. Am. Chem. Soc. **94**, 8799 (1972).
2. Winnewisser, G., Winnewisser, M., Gordy, W.: J. Chem. Phys. **49**, 3465 (1968).
3. Sutter, D., Dreizler, H., Rudolph, H. D.: Z. Naturforsch. **20**, 1676 (1965).
4. Beagley, B., McAloon, K. T.: Trans. Faraday Soc. **67**, 3216 (1971).
5. Boyd, D. B., Lipscomb, W. N.: J. Theoret. Biol. **25**, 403 (1969).
6. Hoffmann, R., Boyd, D. B., Goldberg, S. Z.: J. Am. Chem. Soc. **92**, 3929 (1970).
7. Boyd, D. B.: J. Am. Chem. Soc. **94**, 6513 (1972).
8. Boyd, D. B.: Theoret. Chim. Acta (Berl.) **20**, 273 (1971).
9. Boyd, D. B.: J. Am. Chem. Soc. **91**, 1200 (1969).
10. Boyd, D. B.: Theoret. Chim. Acta (Berl.) **18**, 184 (1970).
11. Boyd, D. B., Hoffmann, R.: J. Am. Chem. Soc. **93**, 1064 (1971).
12. Martensson, O.: Acta Chem. Scand. **25**, 3763 (1971).
13. Boyd, D. B.: J. Am. Chem. Soc. **94**, 64 (1972).
14. Mulliken, R. S.: J. Chem. Phys. **23**, 1833 (1955).
15. Schwartz, M. E.: J. Chem. Phys. **51**, 4182 (1969).
16. Veillard, A., Demuyneck, J.: Chem. Phys. Letters **4**, 476 (1970).
17. Hillier, I. H., Saunders, V. R., Wyatt, J. F.: Trans. Faraday Soc. **66**, 2665 (1970).
18. Bergson, G.: Ark. Kemi **12**, 233 (1958); **18**, 409 (1962).
19. Linderberg, J., Michl, J.: J. Am. Chem. Soc. **92**, 2619 (1970).

20. Boyd, D. B.: In: *The purines: theory and experiment*, Bergmann, E. D., Pullman, B. (Eds.), p. 48. Jerusalem: Israel Academy of Sciences and Humanities, 1972.
21. McClellan, A. L.: *Tables of experimental dipole moments*, p. 26. San Francisco, Calif.: W. H. Freeman and Co. 1963.
22. Fraser, R. R., Boussard, G., Saunders, J. K., Lambert, J. B., Mixan, C. E.: *J. Am. Chem. Soc.* **93**, 3822 (1971).
23. Perahia, D., Pullman, B.: *Biochem. Biophys. Res. Commun.* **43**, 65 (1971).
24. Ponnuswamy, P. K.: Thesis, University of Madras, India 1970.
25. Yamabe, H., Kato, H., Yonezawa, T.: *Bull. Chem. Soc. Japan* **44**, 604 (1971).
26. Pauling, L.: *Proc. Nat. Acad. Sci. U.S.* **35**, 495 (1949).
27. Pauling, L.: *Nature of the chemical bond*, p. 134. Ithaca, N.Y.: Cornell University Press, 1960.
28. Radom, L., Hehre, W. J., Pople, J. A.: *J. Am. Chem. Soc.* **94**, 2371 (1972).
29. Wolfe, S., Rauk, A., Tel, L. M., Csizmadia, I. G.: *J. Chem. Soc. B*, **1971**, 136.
30. Wolfe, S.: *Accounts Chem. Res.* **5**, 102 (1972).
31. Wolfe, S., Tel, L. M., Liang, J. H., Csizmadia, I. G.: *J. Am. Chem. Soc.* **94**, 1361 (1972).
32. Hine, J., Dalsin, P. D.: *J. Am. Chem. Soc.* **94**, 6998 (1972).
33. Fink, W. H., Allen, L. C.: *J. Chem. Phys.* **46**, 2261, 2276 (1967).
34. Allen, L. C.: *Chem. Phys. Letters* **2**, 597 (1968).
35. Jorgensen, W. L., Allen, L. C.: *J. Am. Chem. Soc.* **93**, 567 (1971).
36. Epstein, I. R., Lipscomb, W. N.: *J. Am. Chem. Soc.* **92**, 6094 (1970).
37. Veillard, A.: *Theoret. Chim. Acta (Berl.)* **18**, 21 (1970).
38. Clementi, E., Niessen, W. von: *J. Chem. Phys.* **54**, 521 (1971).
39. Lehn, J. M., Munsch, B.: *Mol. Phys.* **23**, 91 (1972).
40. Boyd, D. B.: *J. Chem. Phys.* **52**, 4846 (1970).
41. Del Bene, J. L.: *J. Chem. Phys.* **55**, 4633 (1971); **56**, 4923 (1972).
42. Bonaccorsi, R., Scrocco, E., Tomasi, J.: *J. Chem. Phys.* **52**, 5270 (1970).
43. Robb, M. A., Haines, W. J., Csizmadia, I. G.: *J. Am. Chem. Soc.* **95**, 42 (1973).
44. Woodward, R. B., Hoffmann, R.: *The conservation of orbital symmetry*. New York: Academic Press 1970.
45. Laws, F. A., Lipscomb, W. N.: *Israel J. Chem.* **10**, 77 (1972).
46. Kern, C. W., Karplus, M.: *J. Chem. Phys.* **40**, 1374 (1964).
47. Ransil, B. J., Sinai, J. J.: *J. Chem. Phys.* **46**, 4050 (1967).
48. Ransil, B. J., Sinai, J. J.: *J. Am. Chem. Soc.* **94**, 7268 (1972).

Dr. D. B. Boyd  
The Lilly Research Laboratories  
Eli Lilly and Company  
Indianapolis, Indiana 46206, USA

## The Protonation of Three-Membered Ring Molecules: The *ab initio* SCF versus the Electrostatic Picture of the Proton Approach

Caterina Ghio and Jacopo Tomasi

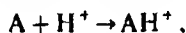
Laboratorio di Chimica Quantistica ed Energetica Molecolare del CNR, Via Risorgimento 35,  
56100 Pisa, Italy

Received January 22, 1973

The protonation processes for eight three-membered ring molecules have been investigated using the SCF LCAO MO method with Gaussian basis sets and the results are compared with those obtained at the first order approximation, i.e. the electrostatic approximation. The electrostatic results are linearly connected with the SCF ones and are sufficient to get an ordering of the protonation energies in different chemical sites and to obtain reliable representations of the proton approaching paths.

*Key words:* Protonation process · Three-membered ring

In the present paper it will be shown to what extent it is possible, in a given family of chemical compounds, to obtain from the wavefunction of molecule A only the essential information about the protonation process:






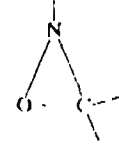


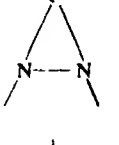
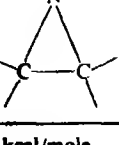
i.e. an ordering of the proton affinities (P.A.'s) along the family, and also more detailed information about the protonation paths and protonation sites.

Such a possibility arises from a first order treatment of the perturbation induced by the proton on molecule A. At the first order the interaction energy is given, at every stage of the proton approach process, by the value of the electrostatic potential  $V(r)$ <sup>1</sup> of molecule A, calculated at the point  $r$  where the proton is located. The electrostatic potential, already introduced [1], depends only on the charge distribution of the unperturbed A molecule, and from its spatial maps one can get the minima, i.e. the geometry of  $AH^+$  and the value of the protonation energy, and also the favoured paths leading to the minima, i.e. the protonation channels.

Such a simple electrostatic picture is as valid as the first order treatment. It is evident that the relatively great perturbation produced by the proton cannot be sufficiently represented by its first order approximation: the  $V(r)$  values are very far from the true P.A.'s. A typical example is given by  $NH_3$ : its experimental P.A. is about 200 kcal/mole, while the  $V(r)$  minimum, even with a good wavefunction, will hardly exceed 100 kcal/mole [2].

<sup>1</sup> Here-after we shall call  $V(r)$  both the electrostatic potential and the interaction energy with a + 1 point charge placed at position  $r$ .

Table 1. SCF energies for neutral molecules and numerical values of protonation energies in different approximations

Molecule		Neutral molecule SCF energy <sup>a</sup>	Protonation site	Protonation energy <sup>b</sup>		
				$\Delta E$ (SCF)	$V$	$\Delta E$ (pol)
Cyclopropane		-116.46366	C-C	-64.69	-15.13	-28.484
Cyclopropene		-115.26787	C-C	-62.239	-13.6	-27.197
			C=C	-76.930	-12.0	-22.321
Oxaziridine		-168.09006	O	-134.883	-43.3	-66.58
			N	-164.82	-65.1	-89.34
Oxirane		-152.17361	O	-141.039	-44.8	-70.705
1-Azirine		-131.16796	N	-163.787	-62.0	-96.270
Diaziridine, <i>cis</i> Diaziridine, <i>trans</i>		-148.31973	N	-178.59	-75.5	-101.27
		-148.33048	N	-174.94	-66.8	-91.15
Aziridine		-132.39751	N	-186.58	-76.9	-103.07
			C-C	-56.522	-10.1	-22.315

<sup>a</sup> = a.u.<sup>b</sup> = kcal/mole.



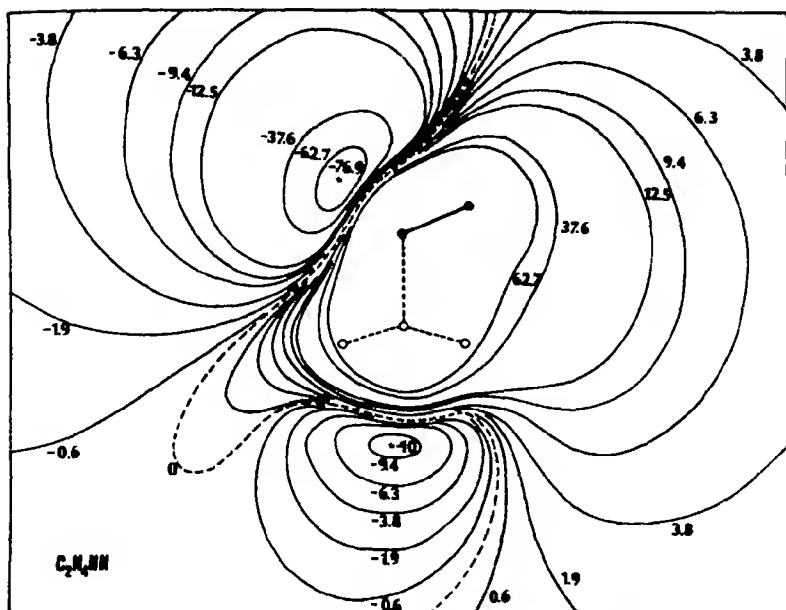


Fig. 1. Electrostatic potential energy map for the aziridine molecule in the plane perpendicular to the ring and containing the N-H nuclei. The energies are expressed in kcal/mole

Some effects not included in the first order treatment give in fact contributions to the interaction energy of the same order as the electrostatic one: polarization of the charge distribution of A and charge transfer to the proton. Other effects, such as exchange or overlap energy terms, which play an important role in other molecular interaction processes, give rise, in the present case, to contributions of lesser weight. Finally, the changes in geometry of A are surely important, but they depend extensively on the particular family of molecules considered; other comments on this point will be made later.

The main point is that effects like polarization, charge transfer and exchange, seem to be relatively constant at the  $V(r)$  minima in a given chemical family and that also their variations when the distance of  $H^+$  from the molecule is changed are not too different in passing from a molecule to another (of the same family).

The evidence of such empirical finding will be shown here by comparing the electrostatic potentials of some three-membered cyclic molecules (see Table 1) and the SCF protonation energies and protonation paths for the same molecules.

In all cases a gaussian basis set [3] ((7s, 3p/3s) contracted to [2s, 1p/1s]) was employed. SCF calculations have been performed with the IBMOL programme. SCF wavefunctions employing either gaussian basis sets (GTO) or Slater-type orbitals (STO) have been previously calculated for all the neutral molecules here considered [4-27] as well as for some protonated species [11, 12, 28-30]. The

energies obtained in the present calculations (reported in Table 1 for neutral species) range intermediately in accuracy among the above quoted results.

For all the molecules of Table 1 the electrostatic potential  $V(r)$  was calculated according to the procedure outlined in Ref. [31]. In every case the shape of  $V(r)$  is similar to that already found with STO wavefunctions [19, 20]. This is a gratifying finding, because it confirms once more that qualitative interpretations of chemical behaviour relying on the electrostatic potential do not depend too heavily on the wavefunction employed. The shape is similar, but the absolute values are not the same. An example may suffice: Fig. 1 reports the  $V(r)$  map for the aziridine molecule in a plane perpendicular to the ring and containing the N H nuclei, the same map is reported in Fig. 8 of Ref. [19] for the STO wavefunction. The outstanding features, the minima corresponding to the N lone pair and the C-C bent bond, are nearly in the same position, but the values are different ( $-92.6$  kcal/mole and  $-17.2$  kcal/mole respectively, for the w.f. of Ref. [19]). A good linear relation between STO and gaussian values of the potential minima in the overall set of molecules was found. For the molecules here considered the most probable protonation sites correspond to the heteroatom lone pairs and to the C-C bonds of the rings, each of these sites being characterized by a minimum for the electrostatic potential in a neighbouring position of the outer molecular space.

The SCF wavefunctions of protonated species were calculated keeping the geometry of A unaltered and placing the additional proton at one of the potential minima. The effect of changes in geometry has been in this way completely neglected. Some considerations must be made on this subject. It is well known that for almost all triatomic rings protonation is followed by ring opening, and that in some cases different opening channels leading to different molecular reorganization processes are possible (see, e.g. Ref. [30]). On the other hand a ring is a somewhat rigid structure, where deformations from the equilibrium position are not easy. A partial optimization of geometry for the loosest groups (e.g.  $-\text{NH}_2^+$ ) was however performed (the results are not reported here), but the corresponding changes in protonation energy have been found to be unessential with respect to the main topic of this paper. In conclusion, the difference  $\Delta E = E(\text{AH}^+) - E(\text{A})$  cannot be considered as an approximation of the proton affinity, which should be made at the true energy minimum, but can be considered to represent the interaction energy at the end of the primary protonation process, which may be eventually followed by a molecular reorganization process. The values of  $\Delta E$  (Table 1) are compared in Fig. 2 (curve a) with the corresponding  $V(r)$  values. A linear relationship is evident (the correlation value for regression line a is 0.985). The electrostatic potential seems to be sufficient to get a prediction of the ordering of the various protonation energies.

As a second point in the present investigation it has been controlled how realistic is the first order description of the reaction channels. It is evident that the electrostatic approximation will be better at the former stages of the interaction process, when the proton is at large distances from the molecule A. Polarization, charge transfer and the other terms discarded in the first order treatment will have a different  $R$ -dependence with respect to the electrostatic one.

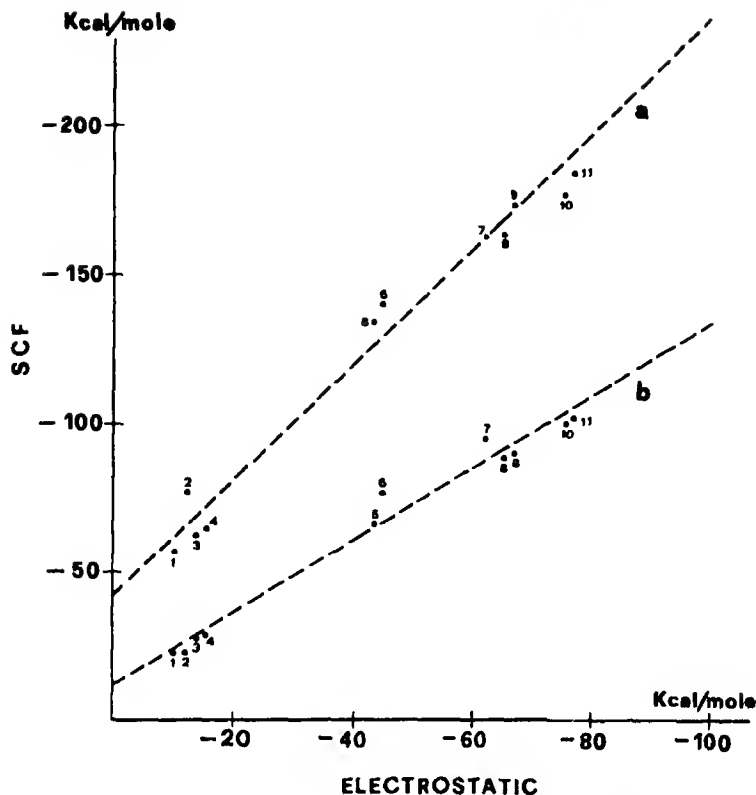


Fig. 2. Comparison between  $V(r)$  values in the minima and  $\Delta E$ . Curve *a* correlation with  $\Delta E$  *ab initio* SCF; curve *b* correlation with  $\Delta E$  electrostatic + polarization. The molecules considered and the protonation sites are respectively: 1 aziridine (C-C); 2 cyclopropene (C=C); 3 cyclopropene (C-C); 4 cyclopropane (C-C); 5 oxaziridine (O); 6 oxirane (O); 7 1-azirine (N); 8 oxaziridine (N); 9 *trans*-diaziridine (N); 10 *cis*-diaziridine (N); 11 aziridine (N)

Figure 3 depicts the situation for the favoured (on electrostatic grounds) approaching path of the proton to the N lone pair of aziridine (practically a straight line passing across the minimum of Fig. 1). Curve *a* gives the values of  $V(r)$ , curve *c* the SCF value of the interaction energy. At great distances the interaction is practically only electrostatic. As long as the proton approaches, the non-electrostatic terms become gradually of more weight, but it is important to point out that the minimum of the SCF curve lies at a  $R$ -value next to the electrostatic one (1.12 Å and 1.20 Å respectively).

When an approaching path is investigated, care must be taken to ensure the right convergency behaviour as well as to have sufficient flexibility in the basis to describe correctly the charge transfer to the proton. Some controls have been made, examining some characteristics of the wavefunction at large distances (populations, etc.) and repeating all the calculations without the constraint of

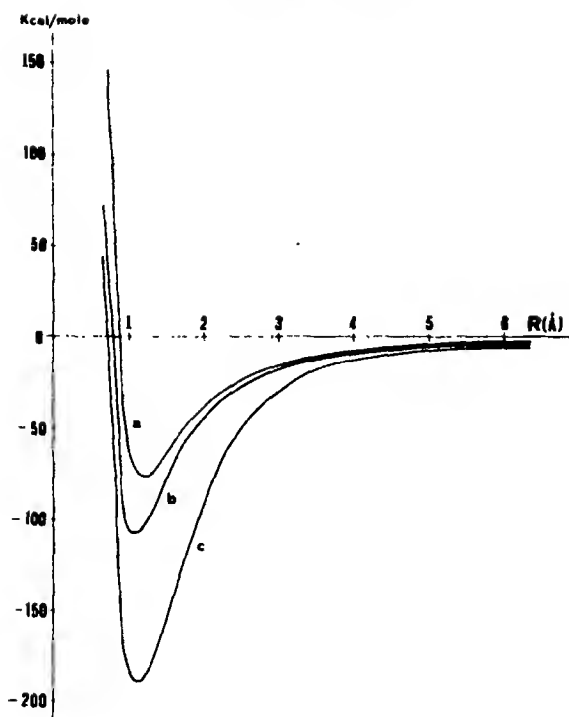


Fig. 3. The favoured approaching path of the proton to the N lone-pair of aziridine. Curve *a* gives the electrostatic term, curve *b* gives the electrostatic + polarization term, curve *c* gives the SCF value of the interaction energy

contraction on the three gaussian orbitals centered on the proton. The results are practically the same as those of Fig. 3 and are not reported here.

For obvious reasons of space, other comparisons between electrostatic and SCF previsions are not reported, but one may state that the example given in Fig. 3 is typical insofar as it concerns both other protonation sites and less favoured reaction paths.

A question concerning the practical application of simplified methods to calculate the energetics of the protonation process, may be posed at this point. Is it possible to add in a simple manner other terms to the first order ones and to improve the precision of the results? One of the first conceivable effects is the polarization one: it is the first in a logical sequence (the approaching proton is bare and produces a considerable field) and at the same time may be treated easily in a perturbative scheme.

We have calculated this effect, to all the orders, simply repeating the SCF calculations with the constraint that no basis functions are placed on the proton.

Some results are reported in Figs. 2 and 3. The straight line *b* of Fig. 2 shows that a linear relationship between  $V$  and the polarization is present. The

corresponding points relate the  $V(r)$  values at the minima to the values  $\Delta E_{\text{pol}} = W(\text{AH}^+) - E(\text{A})$  where  $W(\text{AH}^+)$  is the SCF energy (with the proton placed at the  $V$  minimum) obtained with the above introduced constraint.  $\Delta E_{\text{pol}}$  gives altogether the electrostatic and polarization terms as approximated by the minimal basis set employed in the present calculations.

Curve *b* of Fig. 3 reports the electrostatic plus polarization energy variation for the considered trajectory. The polarization terms (difference between curve *b* and curve *a*) are decidedly lower than the charge transfer and others (difference between curve *c* and curve *b*) and, in addition, the minimum of curve *b* differs from the SCF one by practically the same amount as the electrostatic curve. (For a similar analysis on CNDO wavefunctions see Ref. [32]).

Although the introduction of polarization, reduces the difference between approximate and SCF calculation, it does not improve the precision of the results substantially.

In conclusion linear relationships among electrostatic, polarization, and other terms have been found, at least near the end of the primary protonation process. The minima along the reaction paths are given reasonably well by the electrostatic approximation which on the whole gives a representation of the proton interaction hypersurface sufficient to permit the  $V(r)$  maps to be viewed as a useful tool for qualitative comparisons on the proton reactivity in different sites of chemically related molecules.

## References

1. Bonaccorsi, R., Petrongolo, C., Scrocco, E., Tomasi, J.: In: Quantum aspects of heterocyclic compounds in chemistry and biochemistry, Jerusalem Symposia Vol. II, 1970, 181.
2. Scrocco, E., Tomasi, J.: Fortschr. Chem. Forsch. to be published.
3. Clementi, E., André, J. M., André, M. C., Klint, D., Hahn, D.: IBM Technical Report: Study in the electronic structure of molecules. X. 1969.
4. Preuss, H., Dierksen, G.: Int. J. Quant. Chem. **1**, 361 (1967).
5. Preuss, H., Dierksen, G., Janoschek, R.: J. Mol. Struct. **3**, 423 (1969).
6. Veillard, A., Lehn, J. M., Munsch, B.: Theoret. chim. Acta (Berl.) **9**, 275 (1968).
7. Lehn, J. M., Munsch, B., Millie, P., Veillard, A.: Theoret. chim. Acta (Berl.) **13**, 313 (1969).
8. Kochanski, E., Lehn, J. M.: Theoret. chim. Acta (Berl.) **14**, 281 (1969).
9. Peyerimhoff, S. D., Buenker, R. J.: Theoret. chim. Acta (Berl.) **14**, 305 (1969).
10. Buenker, R. J., Peyerimhoff, S. D.: J. Phys. Chem. **73**, 1299 (1969).
11. Clark, D. T.: In: Quantum aspects of heterocyclic compounds in chemistry and biochemistry, Jerusalem Symposia Vol. II, 1970, 238.
12. Clark, D. T.: Theoret. chim. Acta (Berl.) **15**, 225 (1969).
13. Robb, M. A., Csizmadia, I. G.: J. Chem. Phys. **50**, 1819 (1969).
14. Robin, M. B., Basch, H., Kuebler, N. A., Wiberg, K. B., Ellison, G. B.: J. Chem. Phys. **51**, 45 (1969).
15. Basch, H., Robin, M. B., Kuebler, N. A., Baker, C., Turner, D. W.: J. Chem. Phys. **51**, 52 (1969).
16. Hayes, E. F.: J. Chem. Phys. **51**, 4787 (1969).
17. Snyder, L. C., Basch, H.: J. Am. Chem. Soc. **91**, 2189 (1969).
18. Siu, A. K. Q., St John, W. M., Hayes, E. F.: J. Am. Chem. Soc. **92**, 7249 (1970).
19. Bonaccorsi, R., Scrocco, E., Tomasi, J.: J. Chem. Phys. **52**, 5270 (1970).
20. Bonaccorsi, R., Scrocco, E., Tomasi, J.: Theoret. chim. Acta (Berl.) **21**, 17 (1971).
21. Hehre, W. J., Ditchfield, R., Radom, L., Pople, J. A.: J. Am. Chem. Soc. **92**, 4796 (1970).
22. Radom, L., Lathan, W. A., Hehre, W. J., Pople, J. A.: ibidem **93**, 5339 (1971).
23. Newton, M. D., Switkes, E., Lipscomb, W. N.: J. Chem. Phys. **53**, 2645 (1970).
24. Frost, A. A., Rouse, R. A.: J. Am. Chem. Soc. **90**, 1965 (1968).

25. Stevens, R. M., Switkes, E., Laws, E. A., Lipscomb, W. N.: *J. Am. Chem. Soc.* **93**, 2603 (1971).
26. Franchini, P. F., Zandomeneghi, M.: *Theoret. chim. Acta (Berl.)* **21**, 90 (1971).
27. Marzmann, H., Robert, J.-B., Van Wazer, J. R.: *Tetrahedron* **27**, 4377 (1971).
28. Petke, J. D., Whitten, J. L.: *J. Am. Chem. Soc.* **90**, 3338 (1968).
29. Peyerimhoff, S. D., Buenker, R. J.: *J. Chem. Phys.* **51**, 2528 (1969).
30. Radom, L., Pople, J. A., Buss, V., Schleyer, P. v. R.: *J. Am. Chem. Soc.* **93**, 1813 (1971).
31. Bonaccorsi, R., Pullman, A., Scrocco, E., Tomasi, J.: *Theoret. chim. Acta (Berl.)* **24**, 51 (1972).
32. Mély, B., Pullman, A.: *C. R. Acad. Sci. Paris* **274**, 1371 (1972).

Dr. J. Tomasi  
Laboratorio di Chimica  
Quantistica ed Energetica  
Molecolare del CNR  
Via Risorgimento 35  
I-56100 Pisa, Italy

# Electronic Structures of Organo-Transition-Metal Complexes

## I. Silver(I)-Olefin Complexes

Shigeyoshi Sakaki

Department of Hydrocarbon Chemistry, Faculty of Engineering, Kyoto University, Sakyo-ku, Kyoto

Received February 19, 1973

By using the closed-shell SCF-MO method with the CNDO type approximation for all valence electron systems, the electronic structures of some  $\text{Ag}^+$ -olefin complexes are investigated. The calculated values of  $-AH$  increase with the increasing number of methyl groups on the double bond and this trend agrees with the experimental result. Also calculation reproduces many experimental results, such as the infrared, Raman, and  $^{13}\text{C}$  NMR spectra. These experimental results are discussed on the basis of the calculated electronic structures of  $\text{Ag}^+$ -olefin complexes.

**Key words:**  $\text{Ag}^+$ -olefin complexes

### 1. Introduction

Many transition metal complexes catalyze certain reactions [1], such as isomerization, dimerization, polymerization, oxidation, hydrogenation of olefins and acetylenes. A number of organo-transition-metal complexes have been synthesized and investigated using various methods [2], because these complexes were interesting as models of the intermediates of such reactions.

The  $\text{Ag}^+$ -olefin complex [3] is one of the well known organo-transition-metal complexes, and its thermodynamic and spectroscopic studies have been carried out; heretofore equilibrium constants of the formation [4-7], enthalpies of formation [4, 6, 7], infrared [8, 9], Raman [9] and nuclear magnetic resonance (NMR) spectra [9-12] have been measured.

Since Dewar proposed the two-way donor acceptor bond in the silver-olefin complexes, some theoretical studies have been carried out on the natures of coordination bond in such complexes; the perturbation method has been applied for the estimation of the stability of  $\text{Ag}^+$ -olefin and  $\text{Ag}^+$ -aromatic compound complexes [8, 14-17] and molecular orbitals (MO) of  $\text{Ag}^+$ -ethylene have been obtained by the extended Hückel and *ab initio* MO methods [18, 19]. However there seems to have been no reports of systematic MO calculations on a series of  $\text{Ag}^+$ -olefin complexes, and theoretical interpretations of the experimental results, such as the infrared, Raman and NMR etc., are rather scarce. Thus, the author will calculate the MO's of six  $\text{Ag}^+$ -olefin complexes by the semi-empirical SCF-MO method, and present some discussions on the experimental results from the obtained MO's in this paper.

## 2. Calculation and Geometry

The SCF MO's are obtained by the CNDO type MO method, which has been applied to the MO calculations of  $\text{MnO}_4^-$ ,  $\text{CrO}_4^{2-}$ ,  $\text{PdX}_4^{2-}$  and  $\text{PdX}_6^{2-}$  (X = halogen) in a previous work [20].

All valence orbitals including 4d-atomic orbitals of the silver atom are considered explicitly. The zero-differential overlap approximation [21] is introduced into the Roothaan's SCF equation for the closed shell molecules [22]. Then the diagonal one-electron term  $H_{rr}$  in the Fock matrix element is evaluated according to the formula of Yonezawa *et al.* [23]<sup>1</sup>. The off-diagonal one-electron term  $H_{rs}$  ( $r \neq s$ ) is calculated by the Wolfsberg-Hermholz approximation [24],

$$H_{rs} = -kS_{rs}(I_r + I_s) \quad (1)^2$$

where the parameter  $k$  is taken as 0.55. The one-center Coulomb repulsion integrals of ligand atoms are obtained by the Pariser's approximation [25] and those of the silver atom are taken from the Oleari's report [26]. The two-center Coulomb repulsion integrals are computed according to the Ohno's formula [27]. The single Slater type orbital is used for all  $s$ - and  $p$ -orbitals, and the double- $\zeta$  form is used only for the 4d-orbitals of the silver atom. The values of the orbital exponents  $\zeta_r$ , ionization potentials  $I_r$ , and one-center Coulomb repulsion integrals ( $rr|rr$ ) are given in Table 1.

The core-repulsion energy  $E_{\text{nuc}}$  is approximated by:

$$E_{\text{nuc}} = \sum_A \sum_B \sum_r \sum_s \sum_{\text{on A}} \sum_{\text{on B}} N_r N_s (rr|ss). \quad (2)^2$$

<sup>1</sup> While the one-center exchange integrals are included in the formula of Yonezawa *et al.*, the author neglects them in this calculation.

<sup>2</sup> For the notations used in these formulas, see Ref. [23]

Table 1 Orbital exponents ( $\zeta_r$ ), valence state ionization potentials ( $I_r$ ) and one-center Coulomb repulsion integrals ( $rr|rr$ )

Atom	AO	$\zeta_r$	C*	$I_r$ (eV)	( $rr rr$ ) (eV)
H	1s	1.0000 [31]		13.60 [33]	12.85 [33]
C	2s	1.5679		21.07	12.10
	2p	1.5679		11.27	10.93
	4d	5.9830 [32]	0.5535 [32]	8.17 [24]	13.87 [24]
Ag		2.6130	0.6701		
	5s	2.1900		7.07	7.46
	5p	2.1900		3.30	6.22

\* The 4d-atomic orbital is represented by Basch *et al.* [32] as the linear combination of one 3d and two 4d Slater orbitals. In this work, the contribution of 3d Slater orbital is neglected and the 4d-atomic orbital is represented as the linear combination of two 4d Slater orbitals. Therefore strictly speaking, this 4d-atomic orbital is not normalized. However the contribution of the 3d Slater orbital is negligible small and the error induced by this approximation is very small, e.g., less than 0.2% in the case of the overlap integral between the silver atom and the carbon atom.



As the measure of the bond strength, the two atomic part of the total energy  $E_{AB}$  proposed by Pople *et al.* [22] is used and this term is expressed by Eq. (3), using the approximations described above.

$$E_{AB} = \sum_r \sum_s \begin{matrix} \text{on A} & \text{on B} \\ [2.0 P_{rs} H_{rs} - 0.5 P_{rs}^2 (rr|ss) + (P_{rr} - N_r)(P_{ss} - N_s)(rr|ss)] \end{matrix} \quad (3)^2$$

The distance between the silver atom and the center of the double bond of the olefin is fixed at  $2.39 \text{ \AA}$ <sup>3</sup> according to the work of Mathews *et al.* [28]. The olefin moieties in these complexes are supposed to be nonplanar in analogy with Zeise's salt [30], in which the four hydrogen atoms are pushed away from the platinum ion. However in this work, the assumption is made that the olefin moiety is planar and its bond lengths are the same as those of an uncomplexed olefin [29] due to the lack of information on the accurate configurations of these complexes. For the purpose of comparison, one nonplanar ethylene complex model has been calculated and its stability examined. Hereafter, the planar and the nonplanar ethylene complexes are named [A] and [B], respectively. These coordinate frames are shown in Fig. 1.

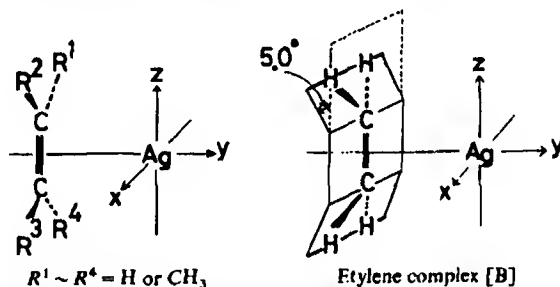


Fig. 1. Coordinate frame of  $\text{Ag}^+$ -olefin complex

### 3. Results and Discussions

**Enthalpies of Formation.** The calculated enthalpy of formation ( $\Delta H$ ) has been estimated from the difference between the total energy of the  $\text{Ag}^+$ -olefin complex and the sum of total energies of the silver (I) ion and of the olefin. The relative value of  $-\Delta H$  to that of  $\text{Ag}^+$ -ethylene [A] are shown in Table 2, together with the values of  $E_{\text{Ag}-\text{C}(\text{olefinic})}$  and  $E_{\text{Ag}-\text{C}(\text{allylic})}$ . The calculated values of  $-\Delta H$  increase with increasing number of methyl groups, which is good agreement with the experimental trend<sup>4</sup>. On the other hand, the absolute values of  $E_{\text{Ag}-\text{C}(\text{olefinic})}$  decrease with the increasing number of methyl groups. This suggests that the enthalpy of formation is decided not only by the interaction

<sup>3</sup> In  $\text{Ag}^+$ -cyclooctatetraene, the average  $\text{Ag}^+$ -olefinic carbon and  $\text{C}=\text{C}$  double lengths are estimated to be  $2.49 \text{ \AA}$  and  $1.37 \text{ \AA}$ , respectively [28]. From these values, the distance between the silver atom and the center of the  $\text{C}=\text{C}$  double bond is evaluated to be  $2.39 \text{ \AA}$ , assuming that the  $\text{C}=\text{C}$  double bond is perpendicular to its coordination bond.

<sup>4</sup> The calculated enthalpies of formation are compared not with the experimental values determined by the gas-chromatography technique [7] but with the ones estimated from the measurements of the dissociation pressures of these complexes [4, 6], because the value determined by the gas-chromatography should include the solvation energy of the olefin by the solvent in column packing of gas-chromatograph.

Table 2. Enthalpies of formation ( $\Delta H$ ) and  $E_{\text{Ag-C}}$  in  $\text{Ag}^+$ -olefin

Olefin	$-\Delta H$		$E_{\text{Ag-C(olefinic)}}$ <sup>c</sup>	$E_{\text{Ag-C(allylic)}}$ <sup>d</sup>
	Calculated <sup>a</sup> (in eV)	Experimental <sup>b</sup> (in kcal/mol)	(in eV)	(in eV)
Ethylene [A]	0.00	0.00	-4.57	—
[B]	0.04		-4.64	—
Propylene	0.30	0.029	-4.55	-1.10
<i>trans</i> -2-Butene	0.55	1.814	-4.44	-1.05
<i>cis</i> -2-Butene	0.57	1.950	-4.45	-1.04
2-Methyl-2-butene	0.80		-4.41	-1.06
2,3-Dimethyl-2-butene	1.00		-4.32	-1.06

<sup>a</sup> The relative value to the calculated value of  $-\Delta H$  of  $\text{Ag}^+$ -ethylene complex [A].

<sup>b</sup> The relative value to the experimental value of  $-\Delta H$  of  $\text{AgBF}_4 \cdot \text{C}_2\text{H}_4$  (Ref. [4]).

<sup>c</sup> The average value of two  $E_{\text{Ag-C(olefinic)}}$  in the olefin.

<sup>d</sup> The average value of all  $E_{\text{Ag-C(allylic)}}$  in the olefin.

between the silver atom and the olefinic carbon atom but also by the interaction between the silver atom and the other parts of olefin, which is supported by the bonding interaction between the allylic carbon atom and the silver atom, as shown in Table 2.

The calculated value of  $-\Delta H$  and the absolute value of  $E_{\text{Ag-C}}$  in the ethylene complex [B] are larger than those in the complex [A]. These facts suggest that the nonplanar model seems more likely for the structure of ethylene in the complex.

**Electron Distribution.** The electron densities on silver atoms are shown in Table 3, together with  $\pi$ -electron densities  $P_\pi$  of uncomplexed olefins and quantities of transferred electron  $\Delta Q$  from the olefin. The calculated results agree well with this configuration, while, compared with Basch's results ( $d^{9.94}s^{0.13}p^{0.07}$  in  $\text{Ag}^+$ -ethylene) [19], the  $5s$ - and  $5p$ -orbital electron densities obtained in this work seem to be too large. The  $5s$ - and  $5p$ -orbital electron densities and  $\Delta Q$  increase with the increasing number of methyl groups, whereas the  $4d$ -orbital

Table 3. Electron populations on silver atoms, quantities of the transferred electron ( $\Delta Q$ )<sup>a</sup> and  $\pi$ -electron densities of olefinic carbon atoms in uncomplexed olefin ( $P_\pi$ )

	Electron population on Ag			$\Delta Q$	$P_\pi$	
	4d	5s	5p			
Ethylene [A]	9.985	0.187	0.110	0.282	1.000	
[B]	9.985	0.189	0.111	0.285		
Propylene	9.985	0.195	0.122	0.303	0.929 <sup>b</sup>	1.113
<i>trans</i> -2-Butene	9.985	0.202	0.130	0.317	1.035	
<i>cis</i> -2-Butene	9.985	0.201	0.133	0.319	1.041	
2-Methyl-2-butene	9.986	0.206	0.140	0.331	0.968 <sup>b</sup>	1.141
2,3-Dimethyl-2-butene	9.986	0.210	0.146	0.341	1.068	

<sup>a</sup> The decrease in the electrons of olefin by the coordination to the silver ion.

<sup>b</sup> The  $\pi$ -electron density of the olefinic carbon atom which contains more methyl groups than the other.

electron density remains almost constant. A methyl group is known to increase the  $\pi$ -electron density not only by  $-I$  effect but also by hyperconjugation [34] and this seems to result in the increase of  $\Delta Q$  and the electron density on the silver atom.

In the ethylene complex [B], the  $5s$ - and  $5p$ -orbital electron densities and  $\Delta Q$  are slightly larger than those of the complex [A]. These facts suggest that the nonplanality increases the  $\pi$ -electron donation from ethylene to  $5s$ - and  $5p$ -atomic orbitals of the silver atom.

**Coordination of Olefin.** The calculated bond orders of the coordination bonds and the decrease in the  $\pi$ -bond orders of olefins are shown in Table 4. Apparently, bond orders of the  $\sigma$ -donor bond ( $d_\sigma - \pi$ ,  $s - \pi$ , and  $p_\sigma - \pi$  in Table 4) are much larger than those of the  $\pi$ -acceptor bond ( $d_\pi - \pi^*$ , and  $p_\pi - \pi^*$ ) in all complexes. Also as shown in Table 4, the decrease in the  $\pi$ -bond order by the  $\sigma$ -donor bond,  $(\Delta P_\pi)_\sigma$  is much larger than that by the  $\pi$ -acceptor bond,  $(\Delta P_\pi)_\pi$ . The largest contribution to the coordination bond is noticed in the interaction between the  $5s$ -atomic orbital of the silver atom and  $\pi$ -MO of the olefin, and the next largest

Table 4. The bond orders of the coordination bond in  $\text{Ag}^+$ -olefin complexes, and the changes in  $\text{C}=\text{C}$   $\pi$ -bond orders and  $E_{\text{C-H(olefinic)}}$  by the complex formation

in	Bond order of coordination bond					$(\Delta P_\pi)_\sigma^a$	$(\Delta P_\pi)_\pi^b$	$\Delta P_\pi^c$	$\Delta E_{\text{C-H}} $
	$\pi$ -acceptor		$\sigma$ -donor						
	$d_\pi - \pi^*$	$p_\pi - \pi^*$	$d_\sigma - \pi$	$s - \pi$	$p_\sigma - \sigma$				
	(in eV)	(in eV)	(in eV)	(in eV)	(in eV)				
ethylene [A]	0.146	0.0001	0.088	0.748	0.522	-0.122	-0.003	-0.125	-0.19
[B]*	0.148	0.001	0.090	0.751	0.526	-0.126	-0.003	-0.126	-0.19
ethylene	0.132	0.045	0.092	0.762	0.524	-0.133	-0.001	-0.134	-0.18
1,2-Butene	0.124	0.033	0.094	0.774	0.530	-0.130	-0.007	-0.137	-0.18
2-Butene	0.120	0.040	0.094	0.772	0.530	-0.130	-0.008	-0.138	-0.19
ethyl-2-butene	0.110	0.055	0.096	0.780	0.532	-0.134	-0.008	-0.142	-0.19
dimethyl-2-butene	0.102	0.064	0.096	0.786	0.534	-0.133	-0.009	-0.142	

<sup>a</sup> The decrease in the  $\pi$ -bond order due to the  $\pi$ -electron donation of the olefin to the silver atom defined as follows

$$(\Delta P_\pi)_\sigma = \left( 2 \sum_i^{\text{occ}} C_{i1p_\sigma} C_{i2p_\sigma} \right)_{\text{complexed}} - \left( 2 \sum_i^{\text{occ}} C_{i1p_\sigma} C_{i2p_\sigma} \right)_{\text{uncomplexed}},$$

where  $C_{i1p_\sigma}$  is the coefficient of the  $p_\sigma$  orbital of the carbon atom 1 in MO  $i$ , and the  $\text{C}=\text{C}$  double bond is formed by the carbon atom 1 and 2.

<sup>b</sup> The decrease in the  $\pi$ -bond order due to the  $d$ -electron acceptance of the olefin from the silver atom defined as follows

$$(\Delta P_\pi)_\pi = \left( 2 \sum_i^{\text{occ}} C_{i1p_\pi} C_{i2p_\pi} \right)_{\text{complexed}} - \left( 2 \sum_i^{\text{occ}} C_{i1p_\pi} C_{i2p_\pi} \right)_{\text{uncomplexed}},$$

where  $C_{i1p_\pi}$  is the coefficient of the  $p_\pi$  orbital of the carbon atom 1 in MO  $i$ .

<sup>c</sup>  $P_\pi = (\Delta P_\pi)_\sigma + (\Delta P_\pi)_\pi$ .

<sup>d</sup>  $E_{\text{C-H}} = (E_{\text{C-H}})_{\text{complexed}} - (E_{\text{C-H}})_{\text{uncomplexed}}$ , where  $E_{\text{C-H}}$  represents the  $E_{\text{AB}}$  value of the olefinic  $\text{C-H}$  bond. The ethylene complex [B],  $\pi$ -bond order ( $P_\pi$ ) is defined as follows:

$$P_\pi = 2 \sum_i^{\text{occ}} C_{i1p_y} C_{i2p_y},$$

where  $C_{i1p_y}$  is the coefficient of  $2p_y$  orbital of the carbon atom 1 in MO  $i$ .

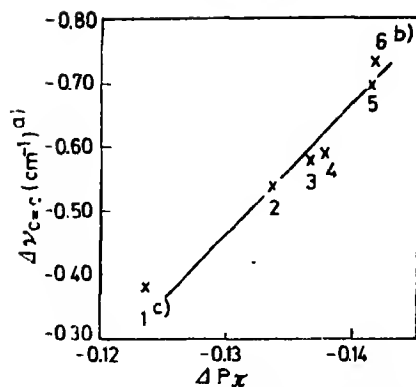


Fig. 2 The relation between  $\Delta P_\pi$  and  $\Delta \nu_{C=C}$ . 1 ethylene, 2 propylene, 3 *trans*-2-butene, 4 *cis*-2-butene, 5 2-methyl-2-butene, 6 2,3-dimethyl-2-butene. a These values are taken from  $\text{Ag(olefin)}_2\text{:BF}_4$  in solid (Ref. [9]). b This value is obtained from the measurement in solution (Ref. [9]). c This value is taken from the measurement for  $\text{Ag}^+\text{-C}_2\text{H}_4$  (Ref. [3b]), therefore the points 1 and 6 may deviate from the line

in that between the  $5p$ -atomic orbital of the silver atom and the  $\pi$ -MO of the olefin. These facts indicate that the coordination bond is mainly contributed by the  $\sigma$ -donor bond in which the olefin donates its  $\pi$ -electron to  $5s$ - and  $5p$ -atomic orbitals of the silver atom.

The coordination bond orders of the complex [B] are slightly larger than those of the complex [A], resulting in the larger absolute value of  $E_{\text{Ag-C}}$  in the complex [B]. Thus it is apparent that the interaction of ethylene with the silver atom in the complex [B] is stronger than that in the complex [A].

*The Electronic Structure of the Coordinated Olefin.* The coordination of an olefin to a transition metal results in a shift of  $\text{C}=\text{C}$  double bond stretching vibration ( $\nu_{C=C}$ ) to a lower frequency from that in the uncomplexed olefin by  $50\text{--}70\text{ cm}^{-1}$  for silver (I) [9] and about  $150\text{ cm}^{-1}$  for platinum (II) [35]. A shift of  $\nu_{C=C}$  ( $\Delta \nu_{C=C}$ ) is proportional to the change in the  $\text{C}=\text{C}$   $\pi$ -bond order ( $\Delta P_\pi$ ), as shown in Fig. 2. This linear relationship between  $\Delta \nu_{C=C}$  and  $\Delta P_\pi$  suggests that the shift to a lower frequency of  $\nu_{C=C}$  is mainly due to a decrease in the strength of the  $\text{C}=\text{C}$   $\pi$ -bond. The calculation also shows that the absolute values of  $E_{\text{C-H(olefin)}}$  decrease in the silver complex by ca.  $0.18\text{ eV}$  as shown in Table 4, which is in agreement with the experimentally observed shift to a lower frequency of the olefinic  $\text{C-H}$  bond stretching vibration [8].

The  $^{13}\text{C}$  NMR spectra of the cyclopentene and cyclohexene in aqueous silver nitrate solution reveal that the olefinic carbon resonances are shifted to higher fields, relative to those of uncomplexed cycloalkenes [13]. The most important term giving the shielding constant of  $^{13}\text{C}$  resonance is due to the paramagnetic susceptibility. This term  $\sigma_p$  is calculated<sup>5</sup> using the approximation formula proposed by Pople [36]. The obtained results are given in Table 5. The calculated olefinic carbon resonances are shifted to higher fields in  $\text{Ag}^+$ -olefin complexes.

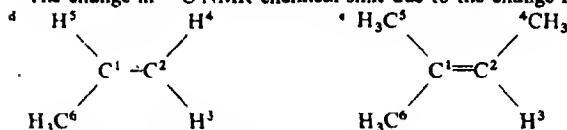
<sup>5</sup> This calculation is carried out on the assumption that the average transition energy is  $8\text{ eV}$  in all olefins and  $\text{Ag}^+$ -olefin complexes.

Table 5. The changes in  $^{13}\text{C}$  NMR chemical shifts by the complex formation

Unsaturated Carbon Olefin	$\Delta\delta^a$ (in ppm)	$\Delta\delta_{(AB)_{xx}}^b$ (in ppm)	$\Delta\delta_{\pi}^c$ (in ppm)
Ethylene [A]	+4.0	+12.0	+12.9
[B]	+3.7	+12.0	+12.9
Propylene <sup>d</sup> C <sup>1</sup>	+1.5	+11.9	+13.6
C <sup>2</sup>	+4.2	+12.0	+13.5
<i>trans</i> -2-Butene	+5.8	+11.9	+13.6
<i>cis</i> -2-Butene	+5.5	+11.9	+13.6
2-Methyl-2-butene <sup>e</sup> C <sup>1</sup>	+5.4	+11.7	+13.4
C <sup>2</sup>	+6.6	+11.6	+13.4
2,3-Dimethyl-2-butene	+6.9	+11.2	+13.0

Methyl Carbon Olefin	$\Delta\delta^a$ (in ppm)	Main contribution
Propylene	-3.1	$(Q_{AA})_{zz}^f (Q_{AB})_{zz}$
<i>trans</i> -2-Butene	-2.1	$(Q_{AA})_{yy} (Q_{AA})_{zz} (Q_{AB})_{zz}$
<i>cis</i> -2-Butene	-2.2	$(Q_{AA})_{yy} (Q_{AB})_{zz}$
2-Methyl-2-butene <sup>e</sup> C <sup>3</sup>	-0.1	$(Q_{AA})_{yy}$
C <sup>4</sup>	-2.1	$(Q_{AA})_{yy} (Q_{AB})_{zz}$
C <sup>5</sup>	-1.4	$(Q_{AA})_{yy} (Q_{AA})_{zz}$
2,3-Dimethyl-2-butene	-1.4	$(Q_{AA})_{yy} (Q_{AB})_{zz}$

<sup>a</sup>  $\Delta\delta = \delta_{\text{complex}} - \delta_{\text{free}}$ .<sup>b</sup> The change in  $^{13}\text{C}$  NMR chemical shift due to the change in the  $\sum_{B \neq A} (Q_{AB})_{xx}$ .<sup>c</sup> The change in  $^{13}\text{C}$  NMR chemical shift due to the change in the term,  $-2P_{AyBy}P_{AzBz}$ .<sup>f</sup> For these terms, see Ref. [36].

These shifts to higher fields ( $\Delta\delta$ ) are attributable to the increase in  $\delta_{\pi}$ <sup>6</sup> which is due to the term of  $P_{AyBy}P_{AzBz}$ , as shown in Table 5. Since the decrease in the  $\pi$ -bond order is reflected in the increase in  $\delta_{\pi}$ , and since the decrease in the  $\pi$ -bond order is mainly due to the  $\pi$ -electron donation from olefin as described before, the  $\pi$ -electron donation seems to be the main factor of these shifts to higher fields. On the other hand, the calculation reveals the downfield shifts for the  $^{13}\text{C}$  resonances of the  $sp^3$  carbon atoms in these  $\text{Ag}^+$ -olefin complexes, and these results agree with the experimental results [13]. These downfield shifts should be attributed not only to one term but also to two or three terms as shown in Table 5.

<sup>6</sup> The increase in the olefinic  $^{13}\text{C}$  resonance is mainly contributed by the term of  $(Q_{AB})_{xx}$ :  $(Q_{AB})_{xx} = -2P_{AyBy}P_{AzBz} + 2P_{AyBz}P_{AzBy}$  where A and B represent the olefinic carbon and the neighboring atoms, respectively. For the notations in the above formula, see Ref. [36]. The values of  $\Delta\delta_{\pi}$  represents the change in  $^{13}\text{C}$  NMR chemical shift due to the change in the value of  $P_{AyBy}P_{AzBz}$ . Since the  $P_{AzBz}$  is almost unchanged by the complex formation,  $\Delta\delta_{\pi}$  is mainly contributed by the change in  $P_{AyBy}$ .

Table 6  $\pi - \pi^*$  transition energies and energy differences between  $\pi$ - and  $\pi^*$ -MO's

Olefin	Transition energy		MO energy difference <sup>a</sup>	
	Uncomplexed (in eV)	Complexed (in eV)	Uncomplexed (in eV)	Complexed (in eV)
Ethylene [A]	8.87	9.19	14.89	14.88
[B]		9.19		13.99
Propylene	7.65	7.69	13.41	12.94
trans-2-Butene	6.78	6.62	12.35	11.65
cis-2-Butene	7.15	7.09	12.71	12.15
2-Methyl-2-butene	6.60	6.43	12.10	11.38

<sup>a</sup> MO energy difference between  $\pi$ - and  $\pi^*$ -MO's

**Transition Energy.** It is expected that the  $\pi - \pi^*$  transition energy should be changed and that the charge transfer band should appear at the formation of the transition metal complex. Unfortunately in the cases of the  $\text{Ag}^+$ -olefin complexes, the electronic spectra have not been reported except the charge transfer band of  $\text{Ag}^+$ -cyclohexene [8, 37]. The  $\pi - \pi^*$  transition energies of olefins and  $\text{Ag}^+$ -olefin complexes are calculated and shown in Table 6. While for ethylene and propylene the  $\pi - \pi^*$  transition energies are increased by the complex formation, for the other olefins it is decreased by the complex formation as in the case of Basch's results on  $\text{Ag}^+$ -ethylene<sup>7</sup>. It is yet unknown by an experiment whether the  $\pi - \pi^*$  transition band shifts to a lower frequency or to a higher one.

In  $\text{Ag}^+$ -cyclohexene, the charge transfer band has been observed at 5.51 eV [8, 37], which has been considered to have the mixed character of the charge transfer from the olefin to the silver ion and the Rydberg transition in the olefin moiety [8]. The charge transfer band from  $\pi$ -MO of ethylene to the 5s-orbital of the silver ion is calculated as 8.25 eV in  $\text{Ag}^+$ -ethylene complex [A]. This result is reasonable, since the  $\pi$ -MO energy of ethylene is lower than that of cyclohexene by ca. 1.5 eV. However more detail investigation of these transition energies will be carried out in the near future, since  $\pi - \pi^*$  transition bands in ethylene and propylene are increased by the complex formation, which is incompatible with the Basch's result.

Although there are a few unsolved problems about the transition energy, the calculated results in this work agree with the experimental results, such as the enthalpy of formation, infrared, Raman and NMR spectra. Thus, it is expected that this method can be satisfactorily applied in the MO calculations of other interesting organometal complexes.

The calculations have been carried out by the FACOM 230-60 Computer in the Data Processing Center at Kyoto University.

The author is grateful to Prof. Hiroshi Kato for very grateful discussion. He wishes to thank Prof. Kimio Tarama for his generous support to this work and also Dr. Hideyuki Konishi for his helping with the calculation.

The MO energy difference between  $\pi$  and  $\pi^*$  MO's of the olefin is decreased by the  $\text{Ag}^+$ -olefin complex formation. However the decreasing quantities are small in the cases of ethylene and propylene, since their  $\pi$ -MO's have the considerably low orbital energies compared with the other olefins. This may be one reason of the higher energy shift of the  $\pi - \pi^*$  transition in  $\text{Ag}^+$ -ethylene and propylene complexes.

## References

1. Bird, C.W.: Transition metal intermediates in organic synthesis. New York: Academic Press Inc. 1967.  
Transition metals in homogeneous catalysis, ed. by Schrauzer, G.N. New York: Marcel Dekker Inc. 1971.
2. Coates, G.E., Green, M.L.H., Wade, K.: Organometallic compounds, Vol. II. London: Methuen & Co. LTD. 1968.
- 3a. Winstein, S., Lucas, H.J.: J. Am. Chem. Soc. **60**, 836 (1938).
- 3b. Quinn, H.W., Tsai, J.H.: Advan. Inorg. Chem. Radiochem. **12**, 332 (1969).
4. Quinn, H.W., Glew, D.N.: Can. J. Chem. **40**, 1103 (1962).
5. Muhs, M.A., Weiss, F.T.: J. Am. Chem. Soc. **84**, 4697 (1962).
6. Tarama, K., Sano, M., Tatsuoka, K.: Bull. Chem. Soc. Japan **36**, 1366 (1963).
7. Cvetanovic, R.J., Ducan, F.J., Falconer, W.E., Invin, R.S.: J. Am. Chem. Soc. **87**, 1827 (1965).
8. Hosoya, H., Nagakura, S.: Bull. Chem. Soc. Japan **37**, 249 (1964).
9. Quinn, H.W., McIntyre, J.S., Perterson, D.J.: Can. J. Chem. **43**, 2896 (1965).
10. Powell, D.B., Sheppard, N.S.: J. Chem. Soc. **1960**, 2519.
11. Schug, J.S., Martin, R.J.: J. Phys. Chem. **66**, 1554 (1962).
12. Parker, R.G., Roberts, J.D.: J. Am. Chem. Soc. **92**, 743 (1970).
13. Dewar, M.J.: Bull. Soc. Chim. France **18**, 679 (1951).
14. Fukui, K., Imamura, A., Yonezawa, T., Nagata, C.: Bull. Chem. Soc. Japan **34**, 1076 (1961).
15. Fueno, T., Okuyama, T., Deguchi, T., Furukawa, J.: J. Am. Chem. Soc. **87**, 170 (1965).
16. Fueno, T., Okuyama, T., Furukawa, J.: Bull. Chem. Soc. Japan **39**, 2094 (1966).
17. Prichard, W.H., Orville-Thomas, W.J.: Theoret. chim. Acta (Berl.) **3**, 426 (1965).
18. Buch, R.D., Henneke, H.F.: J. Am. Chem. Soc. **92**, 5589 (1970).
19. Basch, H.: J. Chem. Phys. **56**, 441 (1972).
20. Sakaki, S., Kato, H.: To be published.
21. Roothaan, C.C.J.: Rev. Mod. Phys. **56**, 441 (1951).
22. Pople, J.A., Santry, D.P., Segal, G.A.: J. Chem. Phys. **43**, 129 (1965).
23. Yonezawa, T., Yamaguchi, K., Kato, T.: Bull. Chem. Soc. Japan **40**, 536 (1967).
24. Wolfsberg, M., Hermholz, L.: J. Chem. Phys. **20**, 837 (1952).
25. Pariser, R.: J. Chem. Phys. **21**, 568 (1953).
26. Di Sipio, L., Tondello, E., De Michelis, G., Oleari, L.: Chem. Phys. Letters **11**, 287 (1971).
27. Ohno, K.: Theoret. chim. Acta (Berl.) **2**, 219 (1964).
28. Mathews, F.S., Lipscomb, W.N.: J. Phys. Chem. **63**, 845 (1959).
29. Tables of interatomic distances and configurations in molecules and ions. London: The Chemical Society 1965.
30. Manojlović-Muir, L., Muir, K.W., Ibers, J.A.: Discussions Faraday Soc. **47**, 84 (1969).
31. Clementi, E., Raimondi, D.L.: J. Chem. Phys. **38**, 2686 (1963).
32. Basch, H., Gray, H.B.: Theoret. chim. Acta (Berl.) **4**, 367 (1966).
33. Hinze, J., Jaffé, H.H.: J. Am. Chem. Soc. **84**, 540 (1961).
34. Coulson, C.A.: Valence, p. 356. New York: Oxford Univ. Press 1961.
35. Hartly, F.R.: Chem. Rev. **69**, 799 (1969).
36. Pople, J.A.: Mol. Phys. **7**, 301 (1964).
37. Murrell, J.M., Carter, S.: J. Chem. Soc. **1964**, 6185.

Dr. S. Sakaki  
Department of Hydrocarbon Chemistry  
Kyoto University  
Kyoto, Japan





# Natural Spin Orbital Analysis of Diatomic Molecular Wave Functions in Terms of Generalized Diatomic Orbitals

## I. Outline of the Method. Results for the Ground State of $H_2$

Klaus Helfrich

Institute of Theoretical Chemistry, University of Frankfurt, Germany

Received January 31, 1973

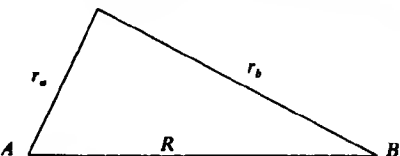
The method of linear combinations of generalized diatomic orbitals (LCGDO) is combined with the method of configuration interaction (CI). CI wave functions obtained in this way are finally submitted to a natural spin orbital analysis; the resulting natural spin orbitals are expansions in terms of generalized diatomic orbitals.

For the ground state of  $H_2$ , a one-determinantal-approach with a single completely optimized one-electron basis function nearly reproduces the Hartree-Fock-result. The two-determinantal approach with two optimized basis functions of type  $\sigma_g$  and  $\sigma_u$  nearly gives the optimized double configuration SCF result.

**Key words:** Natural spin orbitals · Generalized diatomic orbitals · LCGDO- and LCGDO-methods.

### A. Introduction

Generalized diatomic orbitals (GDOs) are the exact solutions of the one-particle Schrödinger equation

$$\left\{ -\frac{\Delta}{2} - \frac{Z_a}{r_a} - \frac{Z_b}{r_b} - \frac{Q}{r_a \cdot r_b} \right\} \chi = \varepsilon \chi \quad (1)$$


belonging to negative energy eigenvalues  $\varepsilon$ . The solutions of (1), which have been studied in three former papers [1–3], are chosen to be eigenfunctions of the  $z$ -component of angular momentum and will be denoted by

$$\chi = (nl\gamma_s; Z_a, Z_b, Q) \quad (2)$$

where  $n$  and  $l$  are united-atom quantum numbers,  $\gamma$  is an irreducible representation of  $C_{\infty v}$  (or  $D_{\infty h}$  if  $Z_a = Z_b$ ), and  $s$  is the sign of the eigenvalue  $m\hbar$  of the  $z$ -component of angular momentum.

Attempts to construct approximate solutions of the Schrödinger equation for diatomic molecules with several electrons in terms of antisymmetrized spin orbital products using orbitals of class (2) are very old. Hylleraas [4] suggested, for the ground and excited states of  $H_2$ , the use of the following approximations:

$$\Psi = \frac{1}{\sqrt{2}} \left[ |\chi_1 \bar{\chi}_2| \pm |\bar{\chi}_1 \chi_2| \right]$$

with

$$\chi_1 = |1s\sigma_g; 1, 1, 0\rangle, \quad \chi_2 = |nl\gamma(D_{\pi,h}); \frac{1}{2}, \frac{1}{2}, 0\rangle. \quad (4)$$

As  $\chi_1$  is an  $H_2^+$ -ground state function and  $\chi_2$  a "demi"- $H_2^+$ -function, this suggestion anticipates Mulliken's demi- $H_2^+$  model [5].

Hylleraas, however, used highly truncated expansions for the "diatomic orbitals"  $\chi_1$  and  $\chi_2$  in his numerical calculations. These calculations were later improved by Wallis [6]. Cooley [7] finally performed complete configuration interaction calculations on  $H_2$ , using up to 6 basis functions of the general type

$$\chi_k = |n_k l_k \gamma_k(D_{\pi,h}); Z_k, Z_k, 0\rangle \quad (5)$$

each depending on a variational parameter  $Z_k$  and being an exact solution of (1). Optimizing also these nonlinear parameters  $Z_k$ , he found: The use of a relatively few diatomic orbitals (5) whose symmetry  $\gamma_k(D_{\pi,h})$  permits the three major types of electron correlation gives approximately the same energy as the rank- and symmetry-equivalent truncated natural spin orbital expansion of very accurate  $H_2$  wave functions.

We were able to reproduce Cooley's results and concentrated on some questions such as:

- i) How can the results for the one- and two-determinantal treatment of  $H_2$  be improved which are inferior to the ones given by the LCAO-method?
- ii) Which basis is appropriate for the ground and excited states of  $HeH^+$ ?
- iii) Can diatomic molecules with more than two electrons be treated successfully?

This paper outlines the methods applied in all cases. Besides it gives the answer to question i), thus especially illustrating the use of symmetry-adapted linear combinations of generalized diatomic orbitals as one-electron basis functions.

## B. Method of Linear Combinations of Generalized Diatomic Orbitals

In case of molecular symmetry  $D_{\pi,h}$ , a symmetry-adapted linear combination of two generalized diatomic orbitals LCGDO is defined as the sum or difference

$$\begin{aligned} & |nl\gamma(D_{\pi,h}); Z_a, Z_b, Q\rangle \\ &= N_{\pm} \{ |nl\gamma(C_{\infty,v}); Z_a, Z_b, Q\rangle \pm |nl\gamma(C_{\infty,v}); Z_b, Z_a, Q\rangle \} \end{aligned} \quad (6)$$

where  $N_{\pm}$  is a normalizing factor. Just as the generalized diatomic orbital (2), the linear combination (6) is a product of three functions depending on the spheroidal coordinates  $\mu, \nu, \varphi$  respectively and behaves like a single basis function with regard to the computation of one- and two-electron-integrals.

The well-known most simple LCAO-approximation

$$\begin{aligned} & |10\sigma_g; Z, 0, 0\rangle \\ &= N \{ |10\sigma; Z, 0, 0\rangle + |10\sigma; 0, Z, 0\rangle \} \end{aligned} \quad (7)$$

for a  $\sigma_g$ -type molecular orbital in  $H_2^+$  or  $H_2$  evidently is a special case of (6).

In case of molecular symmetry  $C_{\infty,\infty}$  we start from a set of generalized diatomic orbitals (2) as basis functions. Combining orthogonalized basis functions of type

(2) or (6) with spin factors  $\alpha$  and  $\beta$ , a set of spin orbitals is generated. All linearly independent antisymmetrized products (Slater determinants) of these spin orbitals are then used within the frame of a full configuration interaction calculation. The final many-electron wave function obtained in this way is then submitted to a natural spin orbital analysis according to Löwdin's proposal. The resulting natural spin orbitals are expansions in terms of generalized diatomic spin orbitals (2) or symmetry-adapted linear combinations of generalized diatomic spin orbitals (6). Evidently natural spin orbitals appear as linear combinations of generalized diatomic spin orbitals. They are classified according to theorems proved by Bingel and Kutzelnigg [9] which are generalizations of the Delbrück-Roothaan-theorems [10] for Hartree-Fock-orbitals. All these operations are performed by means of two computer programs (CI 11 ( $C_{\alpha,\nu}$ ) and CI 04 ( $D_{\alpha,h}$ )) which also optimize non-linear parameters  $Z_{a_k}$ ,  $Z_{b_k}$ ,  $Q_k$ .

Further details on the computational steps may be taken from [11]. Some details on the calculation of two-electron integrals between LCDOs are contained in the Appendix.

### C. Ground State of $H_2$ in Single Configuration Approximation

Four types of single configuration calculations have been performed for various values of the internuclear distance  $R$  and will now be compared with the SCF results obtained by Kolos and Roothaan [12], especially for the internuclear distance  $R = 1.4a_0$  (Fig. 2 and Table 1).

I. In an MO-DO type of calculation, we used a single diatomic orbital  $\psi_1 = |1s\sigma_g; Z, Z, 0\rangle$  [Eq. (5)] and optimized its effective charge  $Z$ , reproducing Cooley's result [7] for the special internuclear distance  $R = 1.4a_0$ .

II. In an MO-LCAO type of calculation, a  $\sigma_g$ -type linear combination  $\psi_{II}$  of two atomic  $1s$ -functions centred at the two nuclei was used [Eq. (7)]; again the single parameter  $Z$  was optimized.

Table 1.  $H_2$  1 configuration  $\sigma_g^2$

I. MO-DO			II. MO-LCAO		III. MO-LCDO		
$R$	$Z = Z_a = Z_b(Q=0)$	$-E_{\text{tot}}$	$Z(Q=0)$	$-E_{\text{tot}}$	$Z_a$	$Z_b(Q=0)$	$-E_{\text{tot}}$
0.6	0.808	0.72266	1.449	0.72455	1.364	0.132	0.72482
0.8	0.797	0.97417	1.370	0.97560	1.253	0.211	0.97670
1.0	0.789	1.07873	1.301	1.07993	1.187	0.243	1.08189
1.4	0.779	1.12647	1.189	1.12819	1.103	0.264	1.13132
1.5	0.777	1.12389	1.166	1.12591	1.088	0.265	1.12921
2.0	0.778	1.08223	1.072	1.08631	1.025	0.264	1.08988
2.6	0.795	1.01709	0.995	1.02355	0.971	0.262	1.02681
3.2	0.821	0.95950	0.942	0.96698	0.934	0.264	0.96978
IV. MO-LCGDO							
$R = 1.4$	$Z_a = 0.793$	$Z_b = -0.196$	$Q = 0.513$	$-E_{\text{tot}} = 1.13342 e^2/a_0$			
$R = 1.4a_0$	SCF [12]			$-E_{\text{tot}} = 1.13363 e^2/a_0$			

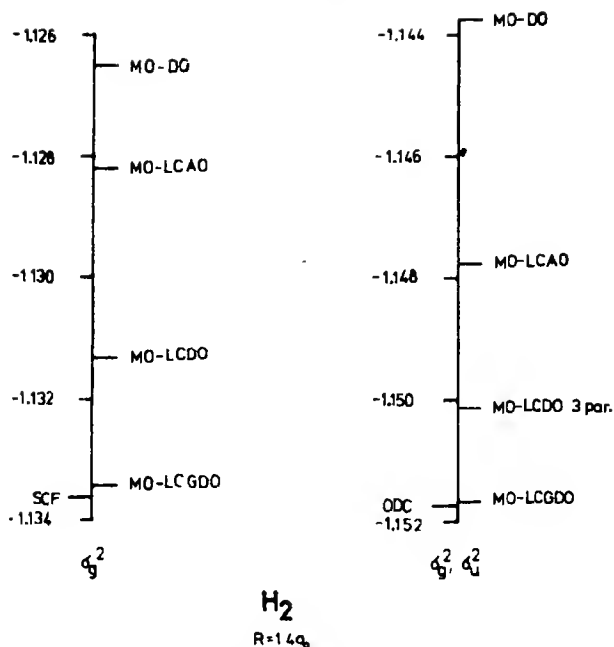


Fig. 1. Ground state of  $H_2$  at equilibrium distance. A comparison of several single and double configuration model calculations

III. In an MO-LCDO type of calculation, the molecular orbital  $\sigma_g$  was approximated by a linear combination of two diatomic orbitals, the charges of which were exchanged according to Eq. (6):

$$\psi_{III} = |1s\sigma_g; Z_a, Z_b, 0\rangle \quad (8)$$

The two parameters  $Z_a$  and  $Z_b$  were optimized.

IV. In an MO-LCGDO type of calculation, a linear combination of two generalized diatomic orbitals was formed, the parameters  $Z_a$  and  $Z_b$  of which being exchanged according to Eq. (6):

$$\psi_{IV} = |1s\sigma_g; Z_a, Z_b, Q\rangle \quad (9)$$

The three parameters  $Z_a$ ,  $Z_b$ , and  $Q$  were optimized. As the MO-LCDO method III (two variational parameters) contains methods I and II as special cases, it is superior to both of them (Fig. 1). The approximation  $\psi_{III}$  (Eq. (8)) is able to reflect the polarization of the electron charge clouds centred at the protons. In an MO-LCAO-SCF treatment, atomic  $2p_0$ -functions centred at the protons would have to be included in the basis to achieve this polarization effect.

The MO-LCGDO method IV is per definitionem (three parameters) superior to the MO-LCDO method. Nevertheless it is surprising how closely the SCF value obtained by Kolos and Roothaan [12] is approached (Fig. 1).

If the distance  $R$  is varied, the order of the results given by the four methods remains the same (Table 1). This may also be taken from Fig. 2, in which the differences  $H - E_{SCF}$  of the four types of calculations – as compared with the self-consistent values  $E_{SCF}$  – are shown for various values of  $R$ .

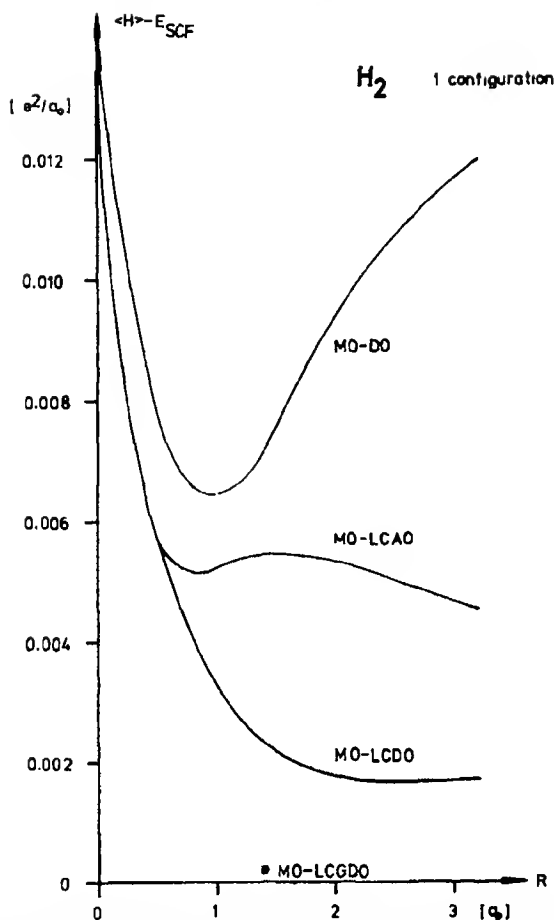


Fig. 2. Ground state of  $H_2$ . Deviations of single configuration model calculations from Hartree-Fock results

#### D. Ground State of $H_2$ in Double Configuration Approximation

A double configuration approximation based on two configurations  $\sigma_g^2$  and  $\sigma_u^2$  takes left-right correlation into account and ensures correct dissociation into two  $1s$ -hydrogen atoms when the internuclear distance  $R$  is increased.

Four types of double configuration calculations have been performed for various values of the internuclear distance  $R$  and will now be compared with the optimized double configuration (ODC) result obtained by Das and Wahl [13], especially for  $R = 1.4 a_0$ . (Fig. 1 and Table 2).

I. In an MO-DO type of calculation,  $\sigma_g$  and  $\sigma_u$  were approximated by  $1s\sigma_g$  and  $2p\sigma_u$  [Eq. (5)], and the two effective nuclear charges for  $\sigma_g$  and  $\sigma_u$  were optimized. Cooley's result was again reproduced.

II. In an MO-LCAO-double  $\zeta$  type of calculation,  $\sigma_g$  and  $\sigma_u$  were approximated by two functions of kind (7), and  $Z_g$  (for  $\sigma_g$ ) and  $Z_u$  (for  $\sigma_u$ ) were optimized.

Table 2.  $H_2$  2 configurations  $\sigma_g^2, \sigma_u^2$ 

I. MO-DO				II. MO-LCAO-double $\zeta$		
$R$	$Z(1s\sigma_g)$	$Z(2p\sigma_u)$	$-E_{tot}$	$Z(\sigma_g)$	$Z(\sigma_u)$	$-E_{tot}$
0.5	0.817	1.915	0.48770	1.495	1.314	0.48906
1.0	0.796	1.544	1.09167	1.308	1.249	1.09371
1.4	0.786	1.353	1.14376	1.201	1.189	1.14778
1.5	0.790	1.314	1.14244	1.179	1.179	1.14719
2.0	0.803	1.203	1.10865	1.095	1.120	1.11773
3.0	0.877	1.059	1.03106	1.012	1.045	1.04710

IIIa. MO-LCDO 2 par.				IIIb. MO-LCDO 3 par.			
$R$	$Z_a$	$Z_b$	$E_{tot}$	$\sigma_g$ $Z_a$	$Z_b$	$2p\sigma_u$ $Z$	$-E_{tot}$
0.5	1.476	0.027	0.48884	1.469	0.039	1.923	0.49018
1.0	1.210	0.210	1.09515	1.208	0.217	1.532	1.09571
1.4	1.131	0.220	1.14997	1.130	0.227	1.354	1.15031
1.5	1.117	0.218	1.14943	1.116	0.224	1.319	1.14974
2.0	1.062	0.200	1.11970	1.062	0.204	1.183	1.11995
3.0	1.009	0.150	1.04774	1.007	0.148	1.048	1.04795

IV. MO-LCGDO  $R = 1.4 a_0$ 

$1s\sigma_u$   $Z_a = 0.793$   $Z_b = 0.196$   $Q = 0.513$  (frozen)

$2p\sigma_u$   $Z_a = 1.316$   $Z_b = 1.371$  ( $Q = 0$ )

$E_{tot} = 1.15168 a_0^{-1}$

Das and Wahl [13]  $E_{ODC} = 1.15175$

III. a) In a first MO-LCDO type of calculation,  $\sigma_g$  was approximated by the linear combination  $\psi_{III}$  [Eq. (8)].  $\sigma_u$  was approximated by a linear combination  $|10\sigma_u; Z_a, Z_b, 0\rangle$  of the same diatomic orbitals  $|1s\sigma; Z_a, Z_b, 0\rangle$  and  $|1s\sigma; Z_b, Z_a, 0\rangle$ , the two effective charges of which were optimized.

This procedure is equivalent to using these two diatomic orbitals as a one-electron basis for a full configuration interaction.

b) In a second MO-LCDO type of calculation,  $\sigma_g$  was approximated by  $\psi_{III}$  [Eq. (8)].  $\sigma_u$  was approximated by an  $H_2^+$ -type diatomic orbital  $2p\sigma_u$  [Eq. (5)]. The three effective charges  $Z_a$ ,  $Z_b(\sigma_g)$  and  $Z(\sigma_u)$  were optimized.

IV. Finally, in an MO-LCGDO type of calculation,  $\sigma_g$  was approximated by  $\psi_{IV}$  [Eq. (9)], determined in the one-configuration approximation and frozen.  $\sigma_u$  was approximated by  $|21\sigma_u; Z_a, Z_b, 0\rangle$  [Eq. (6)]. The two parameters  $Z_a$  and  $Z_b$  of  $\sigma_u$  were optimized. (Starting from a Coulson-type ground state one-configuration approximation [14], Callen [15] determined a  $\sigma_u$ -type orbital in quite a similar way.)

As can be seen from Fig. 1, each of the methods II, III, and IV is superior to any of the preceding ones. The MO-LCGDO result nearly equals the ODC-value obtained by Das and Wahl [13].

Again the internuclear distance was varied (Table 2). The differences between the four calculations and the optimized double configuration result  $E_{ODC}$  are presented in Fig. 3.

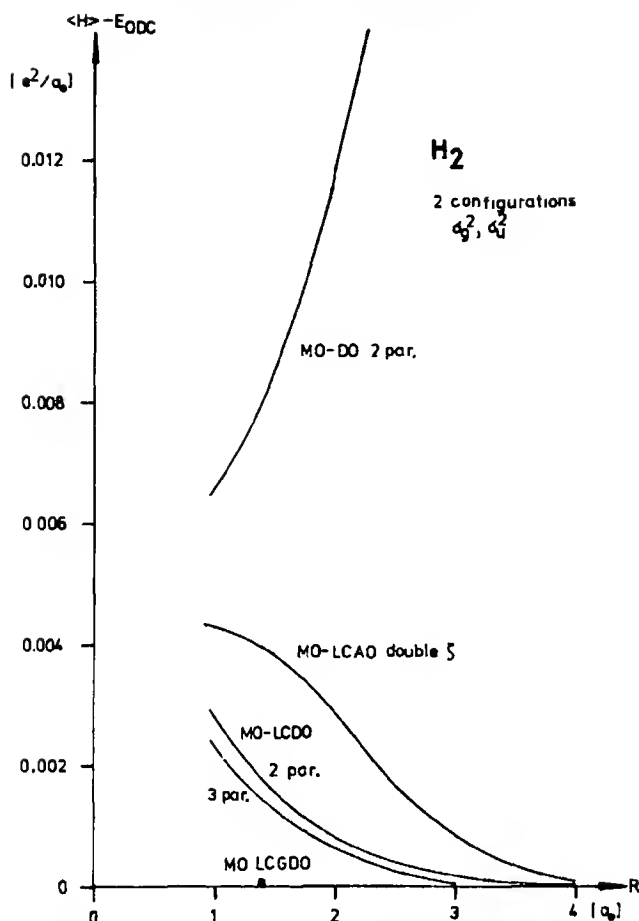


Fig. 3. Ground state of  $H_2$ . Deviations of double configuration model calculations from optimized double configuration SCF results

### E. Appendix: Transformation Properties of Two-Electron Two-Center Integrals

Be

$$\chi'_i(r) = \sum_{p=1}^{N_{\text{base}}} C_{pi} \chi_p(r) \quad (i = 1(1)N_{\text{orb}}) \quad (10)$$

a linear combination of  $K_{\text{base}}$  basis functions  $\chi_p(r)$ . For the CI calculation, all two-electron integrals  $[\chi'_i \chi'_j | \chi'_k \chi'_l]$  between these linear combinations are required.

Instead of transforming the set of two-electron integrals  $[\chi_p \chi_q | \chi_r \chi_s]$  into the required set, we proceed as follows:

According to Ruedenberg's ideas [16], all integrals between linear combinations are decoupled:

$$[\chi'_i \chi'_j | \chi'_k \chi'_l] = \int_1^\infty \sum_L G_L^{i,j}(\mu) G_L^{k,l}(\mu) d\mu. \quad (11)$$

Here

$$G_L^{i,j}(\mu) = \int \gamma_L^M(\mu, r') \chi_i'^*(r') \chi_j'(r') dV' \quad (12)$$

may be considered as an integral transform of the mixed density  $\chi_i'^* \chi_j'$  with the kernel  $\gamma_L^M(\mu, r')$  [11]. The integral transforms  $G_L^{i,j}(\mu)$  may be regarded as the elements of a second order tensor  $G_L'(\mu)$  ( $L$  fixed). It transforms under a change of basis (10) described by the matrix  $C$  like

$$G_L'(\mu) = C^+ G_L(\mu) C, \quad (13)$$

as the component  $G_L^{p,q}(\mu)$  of  $G_L(\mu)$  is defined by

$$G_L^{p,q}(\mu) = \int \gamma_L^M(\mu, r') \chi_p^*(r') \chi_q(r') dV'. \quad (14)$$

So the transformation of a tensor of fourth order  $[\chi_p \chi_q | \chi_r \chi_s]$  may be replaced by the transformation (13) of the tensors  $G_L(\mu)$  which are only of order two. Only the tensors  $G_L'(\mu)$  must be held in core to perform the integrations (11).

*Acknowledgment.* The author highly appreciates financial support by the Deutsche Forschungsgemeinschaft covering computer time used on the TR 440 of Deutsches Rechenzentrum Darmstadt.

## References

1. Helfrich, K., Hartmann, H.: Theoret. chim. Acta (Berl.) **16**, 263 (1970).
2. Kehl, S., Helfrich, K., Hartmann, H.: Theoret. chim. Acta (Berl.) **21**, 44 (1971).
3. Helfrich, K.: Theoret. chim. Acta (Berl.) **21**, 381 (1971).
4. Hylleraas, E. A.: Z. Physik **71**, 739 (1931).
5. Mulliken, R. S.: J. Amer. chem. Soc. **91**, 4615 (1969).
6. Wallis, R. F., Hulburt, H. M.: J. chem. Physics **22**, 774 (1954).
7. Cooley, J. W.: (a) On the use of diatomic orbitals in the calculation of electronic wave functions of diatomic molecules, AEC Research and Development Report No. NYO 104 23, AEC Computing and Applied Mathematics Center, Courant Institute of Mathematical Sciences, New York University, New York: 1962. (b) Hydrogen molecule wave functions in terms of diatomic orbitals, IBM Research Report RC-920, Thomas J. Watson Research Center, New York: 1963.
8. Löwdin, D. O.: Physic. Rev. **97**, 1474 (1955).
9. Bingel, W. A., Kutzelnigg, W.: Advances in quant. Chemistry, vol. 5, 201 (1969).
10. Bingel, W. A.: Theoret. chim. Acta (Berl.) **16**, 319 (1970).
11. Delbrück, M.: Proc. Roy. Soc. (London) A **129**, 686 (1930).
12. Roothaan, C. C. J.: Rev. mod. Physics **23**, 69 (1951).
13. Roothaan, C. C. J.: Rev. mod. Physics **32**, 179 (1960).
14. Helfrich, K.: Entwicklung natürlicher Spinorbitale kleiner zweiatomiger Moleküle nach verallgemeinerten Zweizentren-Funktionen, Habilitationsschrift Frankfurt 1971.
15. Kolos, W., Roothaan, C. C. J.: Rev. mod. Physics **32**, 219 (1960).
16. Das, G., Wahl, A. C.: J. chem. Physics **44**, 87 (1966).
17. Coulson, C. A.: Proc. Cambridge Phil. Soc. **34**, 204 (1938).
18. Callen, E.: J. chem. Physics **23**, 360 (1955).
19. Ruedenberg, K.: In Molecular orbitals in chemistry, physics, and biology, Löwdin, P., Pullmann, B. (Ed.), p. 215. New York: Academic Press 1964.

Priv. Doz. Dr. Klaus Helfrich  
 Institut für Theoretische Chemie der  
 Universität  
 D-6000 Frankfurt a. M., Robert Mayer-Str. 11  
 Federal Republic of Germany



## Correlation Effects in the Neutral and Ionized Ground States of Acetylene<sup>\*</sup>

Anthony J. Duben<sup>\*\*</sup> and Lionel Goodman

School of Chemistry, Rutgers University, New Brunswick, New Jersey 08903

H. Önder Pamuk<sup>\*\*\*</sup> and Oktay Sinanoğlu

Sterling Chemistry Laboratory, Yale University, New Haven, Connecticut 06520

Received August 21, 1972/February 26, 1973

Correlation energies were calculated by "Effective Pair Correlation Energy" (EPCE) and minimal basis set configuration interaction (CI) methods for pairs of electrons in the occupied molecular orbitals for the ( $\pi_g^4$ ) neutral ground state, ( $\pi_g^3$ ) ground state of the positive ion, and ( $\pi_g^4 \pi_u$ ) ground state of the hypothetical negative ion of acetylene.

The EPCE values allow detailed breakdown of the ionization potential and electron affinity (for the unstable negative ion). It is seen that the SCF values for the former can be modified by the EPCE values to give estimates close to the experimental quantity.

The EPCE values are compared against the pair-wise correlation energies obtained by minimal basis set CI and the percentages of the latter as compared to the former are interpreted by considering the form of the available excited configurations used in constructing the correlated functions. The MBSCI calculation accounts for only 20–30% of the EPCE correlation energy.

**Key words:** Pair correlation – Acetylene – Ionic States – Configuration interaction

### 1. Introduction

If an electron is added to or removed from a molecule, there is little doubt concerning the importance of the electron or hole to the stability of the molecule. To see how the energy of a molecule changes in detail upon electron loss or capture, it is necessary to analyze the effects of correlation and reorganization among all the electrons of the system. It is possible to estimate the correlation energy in the various shells of a molecule as well as the correlations between different shells (which may be as large as the intrashell energies) using recent work of two of the authors [1] in the theory of electron correlation [2–5].

Separate developments [6] have indicated the importance of  $\sigma$  and  $\pi$  reorganization effects in the SCF wavefunctions of  $\pi$ -electron systems. It is interesting to compare correlation and charge reorganization effects on the energetics of electron loss and capture.

<sup>\*</sup>Supported by National Science Foundation Grant 31496X.

<sup>\*\*</sup>Present address: Chemistry Department, St. Olaf College, Northfield, Minnesota 55057.

<sup>\*\*\*</sup>Present address: Middle-Eastern Technical University Ankara, Turkey.

Such an analysis is carried out, in this paper, for the neutral ground state, ( $\Sigma_u$ ) ( $\pi_u^4$ ), the lowest energy positive ion ( $\Sigma_g$ ) ( $\pi_u^3$ ), and the lowest energy negative ion ( $\Sigma_g$ ) ( $\pi_u^4 \pi_g$ ) of acetylene. The  $\Sigma$  configuration has identical occupancy for each species; the subscripts indicate that the  $\sigma$  electrons reorganize. The correlation energy is obtained by the semiempirical effective pair correlation energy (EPCE) [4, 5] and *ab initio* minimal basis set configuration interaction methods. More sophisticated calculations using an extended basis set may substantially revise the results presented here for the *ab initio* calculations. This calculation, partially completed 5 years ago [7], is an initial attempt to explore the correlation contributions to ionized states of a simple unsaturated molecule by partitioning the correlation energy into  $\Sigma$ ,  $\pi$ , and  $\Sigma-\pi$  contributions. Recently accurate calculations on  $H_2O$  and  $H_2O^+$  have been carried out by Meyer [8], and on the neutral ground state of acetylene by Moskowitz [8a]. An important goal of this paper is a critical comparison of the EPCE and CI methods.

## 2. Correlation Energies from the Effective Pair Correlation Energy Method

In the EPCE method, the total correlation energy of a molecule is approximately given by

$$E_{\text{corr}} = \sum_{k=1}^n \sum_{l=1}^m \bar{e}_{kl} \quad (1)$$

where  $n$  and  $m$  are the numbers of the molecular orbitals which are occupied by the electrons with  $\alpha$  and  $\beta$  spins respectively;  $\bar{e}_{kl}$  is the effective molecular pair correlation energy which is the sum of the  $\alpha-\beta$  and  $\alpha-\alpha$  molecular pair correlation energies.

The effective molecular pair correlation energies, in turn, are given in terms of  $\bar{e}_{pAqB}$ 's, the effective atomic pair correlation energies,  $N_k$  and  $N_l$ , the numbers of the electrons occupying the molecular orbitals  $k$  and  $l$ ,  $Q_{pA}^k$  and  $Q_{qB}^l$ , the partial gross atomic populations [9]:

$$\bar{e}_{kl} = \sum_A \sum_B \sum_p \sum_q (Q_{pA}^k / N_k) (Q_{qB}^l / N_l) \bar{e}_{pAqB} \quad (2)$$

Summations over A and B are taken over atoms, and  $p$  and  $q$  are over atomic orbitals on each atom. Generally, a limited basis set containing H atom 1s orbitals and first row atom 1s, 2s, and 2p orbitals is used in EPCE calculations. The atomic EPCE terms used in these calculations are the set C of Ref. [5].

The total correlation energy of a molecule containing  $\pi$  electrons can be separated into three parts by properly summing over the molecular orbitals:

$$E_{\text{corr}} = E_{\text{corr}}^{\sigma} + E_{\text{corr}}^{\sigma-\pi} + E_{\text{corr}}^{\pi} \quad (3)$$

where  $E_{\text{corr}}^{\sigma}$ ,  $E_{\text{corr}}^{\sigma-\pi}$  and  $E_{\text{corr}}^{\pi}$  are the correlation energies coming from the  $\sigma$  electrons only, interactions between the  $\sigma$  and  $\pi$  electrons, and  $\pi$  electrons only, respectively.

In the nonclosed shell many electron theory of the atomic systems, the total correlation energy is separated into three parts [3]: (i) transferable all-

external correlation energy, (ii) nontransferable semi-internal correlation energy, (iii) nontransferable internal energy<sup>1</sup>. Molecules frequently are closed shell states. Therefore molecular correlation energy is expected to be mainly transferable. However the states of atoms in molecules can only be represented by taking the linear combination of their valence states instead of the ground states. Thus, if the molecular correlation energy is obtained from atomic correlation energies, part of the former will consist of nontransferable portions of atomic correlation energy introduced by the need to consider open-shell valence states for the atoms. It was assumed that internal and semi-internal correlation energies may be attributed to  $2s-2s$ , and to  $2s-2p$  pairs, respectively [5].

Effective molecular pair correlation energies are given in Table 1. From this table, correlation energies between an electron in one of the inner orbitals ( $1\sigma_g$  or  $1\sigma_u$ ) and an electron in any other orbital are small corresponding to physical intuition that the innermost molecular orbitals originating in the C  $1s$  atomic orbitals do not interact significantly with the molecular orbitals for the valence electrons. The physical intuition that the valence molecular orbitals should have significant interorbital, as well, as *intra*-orbital correlation energies is also maintained.

The correlation energies among the molecular orbitals are collected into groups composed of  $\sigma$  and  $\pi$  electrons alone, and into terms involving both types in Table 2. All-external, semi-internal and internal parts of each term are also given in the same table. The  $\sigma$  term is largest as is to be expected from the number of the  $\sigma$  electrons. The  $\sigma-\pi$  term is also sizeable. Upon increasing the number of  $\pi$  electrons, both  $\pi$  and  $\sigma-\pi$  terms increase because of the increased  $\pi$  population, whereas the  $\sigma$  term decreases. The  $\sigma$  term decrease is apparently mainly due to the decrease in the internal and the semi-internal parts of the atomic correlation parameters arising from the decrease in  $\bar{\epsilon}_{2s}^2$ , and  $\bar{\epsilon}_{2s,2p}$  with the increasing population of  $2p$  electrons [5]. The  $\pi$  term contains only all-external parts because of the beginning hypothesis in obtaining the effective pair correlation energies. The partitioning of the all-external correlation energies may be realistic, but that of the nontransferable parts is subject to question. However these parts are usually less than 15% of the total correlation energy.

A breakdown of the terms entering the energetics of vertical ionization or vertical electron capture is given in Table 3. The terms are defined in Fig. 1 and in the subsequent paragraph. The ionization energy is given by

$$\Delta E(\text{total})^{n \rightarrow c} = \Delta E(K)^{n \rightarrow c} + \Delta E(\text{reorg})^{n \rightarrow c} + \Delta E(\text{corr})^{n \rightarrow c} + \Delta^2 E(\text{SCF})^{n \rightarrow c}. \quad (4)$$

The first term in Eq. (4) is the "approximate" Koopmans' Theorem [10] ionization energy where neither correlation nor reorganization effects are taken

<sup>1</sup> "Internal correlation" is the term applied to the portion of the correlation which is described by configurations constructed by exciting two electrons from occupied orbitals to unoccupied orbitals while still remaining within the Hartree-Fock manifold of orbitals. "Semi-internal correlation" is described by configurations constructed by placing one excited electron in an orbital within the Hartree-Fock manifold and the other in an orbital outside the manifold (e.g. a  $3s$  orbital for a first row atom). "External correlation" is described by configurations constructed by placing both excited electrons into orbitals outside the manifold. Transferable means that the value of the correlation energy is the same for different states of a given configuration of that system.

Table 1. Effective molecular pair correlation energies<sup>a</sup>

$k, l^b$	Neutral	Cation	Anion
$1\sigma_g, 1\sigma_g$	-0.614	-0.613	-0.614
$2\sigma_g$	-0.054	-0.058	-0.051
$3\sigma_g$	-0.044	-0.047	-0.042
$1\sigma_u$	-0.614	-0.613	-0.614
$2\sigma_u$	-0.035	-0.039	-0.032
$\pi_u'$	0.053	-0.054	-0.053
$\pi_u$	-0.053	-0.054	-0.053
$\pi_g$	---	---	-0.053
$2\sigma_g, 2\sigma_g$	-0.326	-0.435	-0.254
$3\sigma_g$	0.429	-0.469	-0.394
$1\sigma_u$	0.054	-0.058	-0.051
$2\sigma_u$	-0.361	-0.402	-0.303
$\pi_u'$	-0.380	-0.423	-0.337
$\pi_u$	0.380	-0.423	-0.337
$\pi_g$	---	---	-0.337
$3\sigma_u, 3\sigma_u$	0.477	-0.480	-0.476
$1\sigma_u$	-0.044	-0.046	-0.042
$2\sigma_u$	-0.448	-0.460	-0.439
$\pi_u'$	-0.232	-0.249	-0.222
$\pi_u$	-0.232	-0.249	-0.222
$\pi_g$	---	---	-0.222
$1\sigma_u, 1\sigma_u$	0.614	-0.613	-0.614
$2\sigma_u$	0.035	-0.039	-0.032
$\pi_u'$	-0.053	-0.054	-0.053
$\pi_u$	0.053	-0.054	-0.053
$\pi_g$	---	---	-0.053
$2\sigma_u, 2\sigma_u$	-0.400	-0.420	-0.390
$\pi_u'$	-0.222	-0.261	-0.194
$\pi_u$	-0.222	-0.261	-0.194
$\pi_g$	---	---	-0.194
$\pi_u', \pi_u'$	-0.849	-0.849	-0.849
$\pi_u, \pi_u$	0.378	-0.378	-0.378
$\pi_g$	---	---	-0.849
$\pi_u, \pi_u$	-0.849	---	-0.849
$\pi_g$	---	---	-0.378

<sup>a</sup>All energies are in eV.<sup>b</sup>Since  $\bar{\epsilon}_{kl} = \bar{\epsilon}_{lk}$ , only those pairs satisfying  $k \leq l$  relation are given.

into account. This has been computed to be 10.01 eV, about 1.4 eV lower than the experimental energy, using the minimal basis set SCF wavefunctions utilized in Table 1. An "exact" Koopmans' Theorem would replace the ground state SCF wavefunction by its Hartree-Fock counterpart. The sum of  $\Delta E(K)^{n-c}$  and  $\Delta E(\text{reorg})^{n-c}$  is defined as  $\Delta E(\text{SCF})^{n-c}$  and includes the reorganization effect.

This quantity is seen from Table 3 to be an additional 0.7 eV lower than the Koopmans' value, and hence 2.0 eV lower than the experimental quantity. Inclusion of the correlation terms should increase the ionization energy because of the decrease in correlation energy in going to the positive ion. In fact, the

Table 2. Correlation terms in acetylene<sup>a</sup>

State	Parts <sup>b</sup>	$E_{\text{corr}}^a$	$E_{\text{corr}}^{a-\pi}$	$E_{\text{corr}}^{\pi}$	$E_{\text{corr}}$
Positive ion <sup>c</sup>	A	-5.97	-2.39	-1.23	-9.59
	S	-0.43	-0.68	-	-1.11
	I	-0.62	-0.05	-	-0.67
	T	-7.02	-3.12	-1.23	-11.37
Neutral	A	-5.95	-3.02	-2.45	-11.42
	S	-0.34	-0.70	-	-1.04
	I	-0.37	-0.04	-	-0.41
	T	-6.66	-3.76	-2.45	-12.87
Negative ion <sup>c</sup>	A	-5.94	-3.62	-3.68	-13.24
	S	-0.21	-0.65	-	-0.86
	I	-0.20	-0.03	-	-0.23
	T	-6.35	-4.30	-3.68	-14.33

<sup>a</sup> Energies are given in eV.<sup>b</sup> Here A stands for "all-external", S stands for "semi-internal", I stands for "internal" and T stands for "total".<sup>c</sup> Calculated using the reorganized wave functions of Ref. [6].Table 3. Energy terms involved in formation of acetylene ions<sup>a</sup>

Term		$\Sigma$	$\Pi$	$\Sigma - \Pi$	Total
$\Delta E(\text{corr})^{n-\pi c}$	b	-0.36	1.22	0.64	1.52
$\Delta E(\text{reorg})^{n-\pi c}$	c	-4.01	-11.88	-15.23	-0.66
$\Delta E(\text{SCF})^f$	f	-	-	-	4.12
$\Delta^2 E(\text{SCF})^{n-\pi c}$	g	-	-	-	0.67
$\Delta E(K)^{n-\pi c}$	c	-	-	-	10.01
$\Delta E(\text{SCF})^{n-\pi c}$	c	-	-	-	9.44
$\Delta E(\text{SCF} + \text{corr})^{n-\pi c}$	-	-	-	-	10.96
$\Delta E(\text{EXP})^{n-\pi c}$	d	-	-	-	11.40
$\Delta E(\text{corr})^{n-\pi a}$	b	0.31	-1.23	-0.54	-1.46
$\Delta E(\text{reorg})^{n-\pi a}$	c	3.56	27.90	-33.50	-2.04
$\Delta E(G)^{n-\pi a}$	c	-	-	-	9.14
$\Delta E(\text{SCF})^{n-\pi a}$	c	-	-	-	7.10
$\Delta E(\text{SCF} + \text{corr})^{n-\pi a}$	-	-	-	-	5.64
$\Delta E(\text{SCF})^a$	e	-	-	-	4.79
$E(\text{HF})^a(\text{ab initio})$	e	-	-	-	-2091.20
$E(\text{HF})^a(\text{predicted})$	-	-	-	-	-2091.48
$E(\text{HF})^f(\text{predicted})$	f	-	-	-	-2081.32

<sup>a</sup> In eV. See Fig. 1 for definition of terms. Also  $\Delta E(\text{corr})^{n-\pi c} = E_{\text{corr}}^c - E_{\text{corr}}^{a-\pi c}$ ,  $\Delta^2 E(\text{SCF})^{n-\pi c} = \Delta E(\text{SCF})^f - \Delta E(\text{SCF})^a$ , etc.<sup>b</sup> From Tab. 2.<sup>c</sup> From Ref. [6]. The values differ slightly from those given in Table 6 of Ref. [6] because  $\zeta_{\text{H}(1s)} = 1.00$  there, and 1.20 here.<sup>d</sup> Dibeler, V.H., Reese, R.M.: J. Chem. Phys. 40, 2034 (1964). The zero point energy correction is neglected.<sup>e</sup> From Ref. [10].<sup>f</sup> Calculated from Eq. (7).<sup>g</sup> Calculated from Eq. (8).

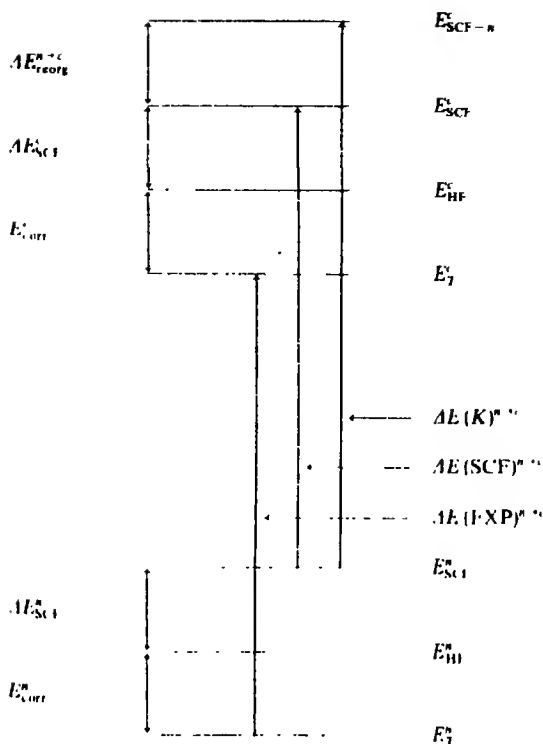


Fig. 1. Energy relationships in ionization.  $\Delta E(K)^{a \rightarrow c}$  refers to Koopmans' theorem  $E_{\text{SCF}-n}^a$  the energy of the ionized state calculated from the ground state SCF function.  $E(\text{true})^a$  and  $E(\text{true})^c$  are the true energy of the ground and ionized states respectively. A similar diagram holds for electron capture.

calculated decrease  $\Delta E(\text{corr})^{a \rightarrow c}$  is greater than the calculated reorganization energy term,  $\Delta E(\text{reorg})^{a \rightarrow c}$ . Thus the calculated correlation effects actually do account for most of the discrepancy between  $\Delta E(\text{SCF})^{a \rightarrow c}$  and  $\Delta E(\text{EXP})^{a \rightarrow c}$ .

Besides correlation and reorganization effects, the degree of goodness of the restricted basis set SCF solutions with respect to exact Hartree-Fock solutions can be considered. This quantity,  $\Delta^2 E(\text{SCF})^{a \rightarrow c}$  in Eq. (4), is

$$\begin{aligned} \Delta^2 E(\text{SCF})^{a \rightarrow c} = \Delta E(\text{SCF})^c - \Delta E(\text{SCF})^a = [E(\text{HF})^c - E(\text{SCF})^c] \\ - [E(\text{HF})^a - E(\text{SCF})^a]. \end{aligned} \quad (5)$$

We know that

$$E(\text{HF})^c = E(\text{true})^c + \Delta E(\text{EXP})^{a \rightarrow c} - E_{\text{corr}}^c. \quad (6)$$

Since  $E(\text{true})^a = E(\text{HF})^a + E_{\text{corr}}^a$ , then

$$E(\text{HF})^c = E(\text{HF})^a - \Delta E(\text{corr})^{a \rightarrow c} + \Delta E(\text{EXP})^{a \rightarrow c}. \quad (7)$$

Eq. (7) allows "empirical" Hartree-Fock positive ion energies to be obtained analogous to "empirical" Hartree-Fock ground state energies [13].

$E(\text{HF})^c$  is estimated to be  $-2081.32$  eV using McLean and Yoshimine's [11] Hartree-Fock energy for the acetylene neutral ground state.  $\Delta^2 E(\text{SCF})^{n \rightarrow c}$  can be computed from the observed ionization energy,

$$\Delta^2 E(\text{SCF})^{n \rightarrow c} = \Delta E(\text{EXP})^{n \rightarrow c} - \Delta E(\text{SCF})^{n \rightarrow c} - \Delta E(\text{corr})^{n \rightarrow c}. \quad (8)$$

Utilizing the quantities in Table 3 and the experimental ionization energy,  $\Delta^2 E(\text{SCF})^{n \rightarrow c}$  is calculated from Eq. (8) to be  $0.44$  eV, much less than either  $\Delta E^c(\text{SCF})$  or  $\Delta E^n(\text{SCF})$  using the minimal basis set, optimized atomic exponent SCF functions. This means that for this type of function the ionized state of acetylene is described about as well as the ground state (referring to the Hartree-Fock functions as the standard of comparison), and also that in considering the ionization energy the correlation and reorganization effects are as important as extending the basis set to approach the Hartree-Fock limit.

If the  $c$  superscripts in Eq. (4) are replaced by  $a$ , then  $\Delta E(\text{total})^{n \rightarrow a}$  is the electron affinity. There is no analog to Koopmans' Theorem for electron affinities. Since the reorganization,  $\Delta E(\text{reorg})^{n \rightarrow a}$ , and correlation,  $\Delta E(\text{corr})^{n \rightarrow a}$ , are additive, the first term in the negative ion version of Eq. (4) should not give good electron affinities. The calculated sum of the reorganization and correlation energies is  $-3.50$  eV for acetylene, and the magnitude of the terms themselves exceed all measured molecular electron affinities. Although it is clear that neglect of reorganization and correlation effects will lead to much too repulsive electron affinities, the final sum,  $\Delta E(\text{SCF})^{n \rightarrow a} + \Delta E(\text{corr})^{n \rightarrow a}$  is still very large predicting an unstable acetylene negative ion.

The EPCE method can be used to estimate the Hartree-Fock energy of acetylene. The experimental binding energy of acetylene is  $17.53$  eV [5a]. Adding this quantity to the estimated energy for the separated atoms (found by adding together twice the sum of the Hartree-Fock energy of carbon  $-1025.51$  eV; the estimated correlation energy of carbon  $-4.30$  eV [12] and the energy of hydrogen  $-13.60$  eV) estimates the total energy of acetylene. Subtracting the EPCE value for the correlation energy,  $-12.87$  eV gives the Hartree-Fock energy of acetylene,  $-2091.48$  eV. This is  $0.28$  eV lower than McLean and Yoshimine's *ab initio* Hartree-Fock energy consistent with the suggestion that given a minimal basis set calculation, an experimentally determined binding energy, and the parameters of the EPCE method, one can predict a good guess for the Hartree-Fock energy [13].

### 3. Correlation Energies from Minimal Basis Set Configuration

Minimal basis set configuration interaction calculations were performed based on the SCF orbitals [6]<sup>2</sup>. In the following discussion, the term "unreorganized" refers to wavefunctions constructed from molecular orbitals determined for the neutral ground state molecule. "Reorganized" wavefunctions have both the linear coefficients which weight the basis functions and the exponents of the basis functions optimized for the ionized states.

<sup>2</sup>  $\zeta = 1.0$  for H 1s AO in these calculations rather than  $\zeta = 1.2$  reported for the fully optimized functions in Ref. [6]. Comparison of integrals for the two sets of functions shows that only a slight error is incurred.

The quantities obtained from this calculation are listed in Table 4. The orbital combinations on the left side of the table indicate the particular orbital combinations from which electrons were excited in constructing excited configurations. A total of 108 configurations composed of all possible single and double excitations, were constructed for the neutral ground state and were treated all at once.

For the anion and the cation 300–400 configurations can be constructed because for a particular hole-particle combination there are three or five configurations from the satisfaction of spin statistics in the ions, where one or two configurations in the ground state suffice. Due to the size of the program, it is necessary to calculate the configuration interaction serially for the ions. The criterion by which configurations are selected or rejected is based on energy contributions of each configuration to the eigenvalue calculated. In particular, if  $\psi$  is the CI wavefunction and  $A_i$  the  $i^{\text{th}}$  SCF configuration in

$$\psi = \sum_i c_i A_i \quad (9)$$

then,

$$\begin{aligned} E &= \langle \psi | H | \psi \rangle = \sum_i \sum_j c_i c_j \langle A_i | H | A_j \rangle = \sum_i \sum_j c_i c_j H_{ij} \\ &= H_{11} + \sum_{i=2} [c_i^2 (H_{ii} - H_{11}) + 2c_1 c_i H_{1i} + \sum_{j \neq i, j \neq 1} c_i c_j H_{ij}]. \end{aligned} \quad (10)$$

If the magnitude of either  $c_i^2 (H_{ii} - H_{11})$  (the diagonal contribution), or  $2c_1 c_i H_{1i} + \sum_j c_i c_j H_{ij}$  (the off-diagonal contribution) is greater than  $10^{-5}$  Hartrees, the term is kept to be used in the final calculation for the species. According to this criterion, 100 configurations survived for the positive ion, and 109 configurations for the negative ion. (Four additional configurations are kept for the negative ion since they were the only ones which attempt to describe the  $\pi_g^+ \pi_u^-$  correlation). The 100 and 113 configurations were obtained for both the reorganized and unreorganized wavefunctions<sup>3</sup> so that an analysis of the reorganization vs the correlation problem could be made.

The correlation energies given in Table 4 are pair-wise correlation energies corresponding to the pair-wise correlation energies in Table 1 so that the entries in both tables can be compared in a direct manner.

**II Correlation.** The partitioning technique allows determination of the correlation energy of pairs of electrons and assignment to each configuration a partial energy lowering due to its presence. Each excited configuration, is constructed by replacing one or two of the occupied orbitals in the SCF configuration with one or two virtual orbitals. The correlation between two electrons in the  $\pi_u^+$  molecular orbital (denoted by  $\pi_u^{+2}$  in Table 4) is described by all configurations in which the  $\pi_u^+$  orbitals of the SCF determinant are replaced by virtual orbitals and the correlation energy associated with the two

<sup>3</sup> The SCF energies calculated for the neutral ground state and the unreorganized molecular orbital calculations on the cation and anion are 0.06 eV higher than the values reported in Ref. [6]. The SCF energies reported for the reorganized molecular orbital calculations on the cation and anion are 0.37 eV and 0.12 eV, respectively, more positive than the values in Ref. [6]. We ascribe the discrepancy to accumulated round-off errors in the calculation of the two-electron integrals over molecular orbitals from those over atomic basis functions due to transferring of integrals over the basis set and the coefficients in the molecular orbitals from print-out to cards.



Table 4. Types of correlations and their contributions to the correlation energy

Correlations <sup>a</sup>	Neutral	Cation (reorg)	Cation (unreorg)	Anion (reorg)	Anion (unreorg)
$(\pi_u^+)^2$	— 5.530 E-1	— 6.20 E-1	— 5.88 E-1	— 4.95 E-1	— 5.66 E-1
$\pi_u^+ \pi_u^-$	— 3.54 E-1	— 2.67 E-1	— 2.35 E-1	— 1.98 E-1	— 2.32 E-1
$\pi_g^+ \pi_g^-$	0.0	0.0	0.0	— 9.92 E-6	— 3.16 E-8
Total $\pi$	— 1.812E-0	— 1.208E-0	— 1.058E-0	— 8.93 E-1	— 1.029E-0
$\pi_u^3 \sigma_g$	— 8.30 E-2	— 7.48 E-2	— 7.91 E-2	— 6.16 E-2	— 6.06 E-2
$\pi_u^2 \sigma_u$	— 4.25 E-2	— 3.78 E-2	— 3.30 E-2	— 2.73 E-2	— 3.28 E-2
$\pi_u^2 \sigma_g$	— 1.35 E-1	— 1.20 E-1	— 9.86 E-2	— 8.78 E-2	— 1.09 E-1
$\pi_u^1 \sigma_u$	— 1.52 E-4	— 1.37 E-4	— 1.08 E-4	— 7.21 E-5	— 7.36 E-5
$\pi_u^1 \sigma_g$	— 1.01 E-3	— 9.94 E-4	— 8.10 E-4	— 5.98 E-4	— 8.15 E-4
Total $\sigma - \pi$	— 1.045E-0	— 9.36 E-1	— 8.46 E-1	— 7.10 E-1	— 8.14 E-1
$(3\sigma_g)^2$	— 1.70 E-1	— 1.62 E-1	— 1.63 E-1	— 1.97 E-1	— 1.51 E-1
$3\sigma_g^2 \sigma_u$	— 1.84 E-1	— 2.08 E-1	— 1.84 E-1	— 1.72 E-1	— 1.48 E-1
$3\sigma_g^2 \sigma_g$	— 1.15 E-1	— 7.95 E-2	— 1.15 E-1	— 1.46 E-1	— 1.19 E-1
$3\sigma_g^1 \sigma_u$	— 1.54 E-4	— 1.59 E-4	— 1.15 E-4	— 1.12 E-4	— 9.05 E-5
$3\sigma_g^1 \sigma_g$	— 6.05 E-4	— 6.65 E-3	— 6.15 E-4	— 5.00 E-4	— 5.15 E-4
$(2\sigma_u)^2$	— 1.88 E-1	— 1.84 E-1	— 1.75 E-1	— 1.96 E-1	— 1.72 E-1
$2\sigma_u^2 \sigma_g$	— 3.86 E-2	— 3.60 E-2	— 4.35 E-2	— 4.15 E-2	— 3.31 E-2
$2\sigma_u^1 \sigma_u$	— 3.55 E-4	— 3.69 E-4	— 3.64 E-4	— 3.33 E-4	— 3.27 E-4
$2\sigma_u^1 \sigma_g$	— 5.90 E-4	— 5.85 E-4	— 5.60 E-4	— 5.40 E-4	— 5.55 E-4
$(2\sigma_g)^2$	— 3.64 E-1	— 4.14 E-1	— 3.59 E-1	— 3.40 E-1	— 3.70 E-1
$2\sigma_g^1 \sigma_u$	— 7.00 E-4	— 5.55 E-4	— 5.75 E-4	— 7.10 E-4	— 7.35 E-4
$2\sigma_g^1 \sigma_g$	— 7.20 E-4	— 5.50 E-4	— 5.05 E-3	— 6.35 E-4	— 6.55 E-4
$(1\sigma_u)^2$	— 3.59 E-3	— 3.70 E-3	— 3.46 E-3	— 3.51 E-3	— 3.73 E-3
$1\sigma_u^1 \sigma_u$	— 1.05 E-3	— 9.25 E-4	— 9.00 E-4	— 1.12 E-3	— 1.17 E-3
$(1\sigma_g)^2$	— 3.48 E-3	— 3.59 E-3	— 3.34 E-3	— 3.43 E-3	— 3.65 E-3
$3\sigma_g$	— 8.65 E-3	— 1.97 E-2	— 1.29 E-1	— 1.00 E-2	— 3.27 E-1
$2\sigma_u$	— 1.43 E-2	— 3.85 E-2	— 1.50 E-1	— 5.65 E-2	— 2.57 E-1
$2\sigma_g$	— 6.86 E-3	— 1.59 E-2	— 1.15 E-2	— 1.31 E-2	— 2.14 E-2
$1\sigma_u$	— 3.38 E-5	— 1.32 E-4	— 1.01 E-4	— 2.45 E-4	— 7.20 E-4
$1\sigma_g$	— 5.75 E-7	0.0	0.0	— 7.60 E-5	— 2.57 E-4
Total $\sigma$	— 1.472E-0	— 1.575E-0	— 1.975E-0	— 1.624E-0	— 2.522E-0
Total $E(\text{corr})$	— 4.33 E-0	— 3.72 E-0	— 3.88 E-0	— 3.23 E-0	— 4.36 E-0
$E(\text{SCF})^b$	—2085.54	—2075.41	—2074.82	—2079.22	—2077.16
$E(\text{CI})^c$	—2089.86	—2079.14	—2078.71	—2082.46	—2081.54
$\Delta E(\text{SCF})^b$	—	10.12	10.72	6.31	8.38
$\Delta E(\text{CI})^c$	—	10.72	11.16	7.40	8.33
$\Delta E(\text{reorg})^d$	—	6.10 E-1	—	2.07 E-0	—
$\Delta E(\text{corr})\text{adj.}^e$	—	—	3.27 E-0	—	2.29 E-0
$\%E(\Sigma)^f$	22.1	22.4	—	25.6	—
$\%E(\Sigma\pi)^f$	73.9	98.1	—	24.3	—
$\%E(\pi)^f$	27.8	30.0	—	16.5	—
$\%E(\text{corr})^f$	33.6	32.7	28.8	22.5	16.0

<sup>a</sup> The contributions are in eV. They are written in E-format, e.g.  $1.23 \text{ E} - 5 = 1.23 \times 10^{-5}$ .<sup>b</sup> The difference  $E(\text{SCF})^{\text{reorg}} - E(\text{SCF})^{\text{unreorg}}$ .<sup>c</sup> The difference  $E(\text{CI})^{\text{reorg}} - E(\text{SCF})^{\text{unreorg}}$ .<sup>d</sup> The difference  $E(\text{SCF})^{\text{reorg}} - E(\text{SCF})^{\text{unreorg}}$  (reorganized) - (unreorganized).<sup>e</sup> The difference  $E(\text{corr})^{\text{reorg}} - E(\text{corr})^{\text{unreorg}}$ .<sup>f</sup> Calculated with respect to the quantities in Tab. 2.<sup>g</sup> The notation lists only the holes, e.g.  $(\pi_u^+)^2$  represents the sum of the effects of all configurations of the correct symmetry, spin, and angular momentum eigenvalues constructed by the excitation  $(\pi_u^+)^2 \rightarrow$ .

electrons in the  $\pi_u^+$  orbital is the sum of the partial energy contributions of all those configurations in which  $\pi_u^+$  orbitals have been replaced in pairs, since configurations which are formed by replacing orbitals *a* and *b* in the SCF determinant describe the correlation between electrons in these orbitals.

In the  $\pi_u^+ \pi_u^-$  hole state, the fact that we have fewer electrons correlating helps explain why the contribution is less for the cation than for the neutral molecule. In the case of the anion, configurations constructed to describe correlating electrons in the  $\pi_u^+ \pi_u^-$  molecular orbital pair possess two electrons in the  $\pi_g^+$  orbital. The presence of the two electrons in the  $\pi_g^+$  orbital destabilizes the configurations. The destabilizing influence of this pair is evidenced by the presence of small coefficients for these configurations as compared to similar coefficients for configurations of the same hole-particle designation in the cation and neutral molecule calculations where the configurations do not have two electrons in the  $\pi_g^+$  orbital. In this manner, the partitioned energy for this hole pair in the anion will be reduced. The minimal basis set does not allow the construction of additional configurations to alleviate the effects of the pair of electrons in the  $\pi_g^+$  orbital. In an extended basis set calculation, compensation for this pair of electrons should be possible<sup>4</sup>.

$\Sigma - \Pi$  Correlations. The argument used in the case of  $\pi_u^+ \pi_u^-$  correlation for the anion is probably also valid in explaining the small  $\sigma\pi_u$  correlation energy contributions in that species. Further there is no way to obtain  $\sigma\pi_u$  correlation energies in the anion since the minimal basis set does not leave any virtual orbital which can be used and preserve the symmetry<sup>5</sup>.

$\Sigma$  Correlation. Despite having essentially the same sort of hole-particle combinations to describe  $\Sigma$  correlation in the neutral ground state and in the ions, more configurations are available for a particular hole-particle combination in the ions than in the neutral ground state. The increased number of configurations (and, hence, increased flexibility) appear to be the means by which more  $\Sigma$  correlation is obtained for the ions than for the neutral ground state.

#### 4. Reorganized vs. Unreorganized Descriptions

The immediately noticeable difference between the reorganized and unreorganized CI calculations for an ion is in the contributions of the singly excited configurations. In the reorganized calculations, the single excitations should enter in by means of couplings with the doubly excited configurations, since by Brillouin's Theorem, the singly excited configurations, do not interact with the ground configuration. Brillouin's Theorem does not hold however, for the unreorganized wavefunctions; the unreorganized one-electron orbitals are not eigenfunctions of the Fock-operators for the  $(n+1)$ - and  $(n-1)$ -electron

<sup>4</sup> Another quantity which should be improved in an extended basis set calculation is the  $\pi_g^+ \pi_u^-$  correlation in the anion. In the minimal basis set, we could only use hole-particle combinations of the form  $\pi_g^+ \pi_u^- \rightarrow \sigma_u \sigma_g$ , which were inadequate to the task.

<sup>5</sup> Although there are fewer  $\pi$  electrons in the cation than in the neutral molecule, we obtain  $\Sigma - \Pi$  correlation energies which are numerically close to the correlation energies for the same hole pairs in the neutral molecule. In the neutral molecule, no matter which  $\pi - \sigma$  electron pair is correlated, there is either a  $\pi_u^+ \pi_u^-$  or  $\pi_u^+ \pi_u^-$  pair present in the excited configuration. However, two-thirds of the cation configuration lack this correlation which reduces destabilizing effects and encourages better convergence.

Table 5. Singly excited configuration energy contributions<sup>a</sup>

Species	Type of Calc.	E (SCF) "Singles"
Cation	Reorg.	-2075.56
Cation	Unreorg.	-2075.40
Anion	Reorg.	-2079.38
Anion	Unreorg.	-2078.37

<sup>a</sup> Energies in eV.; based on Table 3

ions and direct coupling exists between the single excitations and the ground configuration.

The effect of the single excitations returns some of the electron density to regions close to the molecular framework which are removed from these regions by the dispersive double excitations [14]. The effects of the single excitations using unreorganized wavefunctions show this effect plus the effects of reorganization [15]. Adding together the effects of the single excitations in Table 4 (see Table 5) for both the reorganized and unreorganized wavefunctions, gives a closer correspondence for the cation values than for the anion. Since this value is a guess to the energy of the configuration constructed from the first natural orbitals [16], then it would seem that the first natural orbitals for the  $\Sigma$  system of the cation by either method would be very similar. They would be less similar for the anion. The cation has the advantage of being a relatively well-described bound state and the anion the disadvantage of being a not-too-well-described nonbound state. Concerning the effects of single excitations on the  $\Pi$  system nothing much can be said except that they could be sizable given the significance of reorganization.

In any event, the single excitations are important, even for the reorganized wavefunctions where they contribute 5 to 10% of the  $\Sigma$  correlation energy<sup>6</sup>.

### 5. Comparison of the EPCE and Minimal Basis Set Calculations

Comparison of Tables 1 and 4<sup>7</sup> indicates that the minimal basis set pair correlation energies do not well approximate the EPCE pair correlation energies except for the  $\pi_u$  and  $(2\sigma_g)^2$  pairs for which minimal basis set calculations

<sup>6</sup> The minimal basis set calculation is useful as a guide to what should be done in an extended basis set configuration interaction calculation. Configurations such as single excitations in the  $\pi$  system, and better treatment of the hole combinations in the  $\pi$  system and in the  $\Sigma - \Pi$  correlations are desirable.

Secondly, only the valence electrons need be included. As mentioned earlier,  $1\sigma_g$  and  $1\sigma_u$  orbitals are practically carbon 1s orbitals. It is necessary to include at least 35 configurations for Hc like ions and 45 configurations for Li like ions if it is desired to obtain over 90% of the total correlation energy [17]. Therefore  $1\sigma_g$  and  $1\sigma_u$  orbitals may as well be deleted in more extensive calculations.

<sup>7</sup> The details of the atomic contributions in terms of internal, semi-internal, and external correlation are not significant to the total molecular correlation energy. However, incorrect conclusions may be inferred with respect to what one may expect from ab initio calculations by separating  $\Sigma$ ,  $\Pi$ , and  $\Sigma - \Pi$  correlation energies from the total correlation energy and then further breaking down this partition into contributions due to external, internal, and semi-internal correlation.

are from 50–100% of EPCE values. Why are these particular pairs singled-out for possession of large amounts of the possible pair correlation energies?

In the description of correlation in the  $\pi_u$  pairs, configurations which have the most significant effect are very low-lying ones which contain  $\pi_g$  orbitals substituted for  $\pi_u$ . The effect exercised by these configurations is the introduction of left-right correlation to the  $\pi$  electron system because of the nodal plane perpendicular to the molecular axis in the  $\pi_g$  orbitals, a quite desirable feature. These configurations are probably sufficiently low-lying to account for a very substantial part of the pair correlation energy.

The  $(2\sigma_g)^2$  pair is unusual in being the only correlated electron pair among the  $\sigma$  electrons to reproduce the EPCE method result to any large extent. What is unique about this pair as compared to other  $\sigma$  electron pairs?

The  $1\sigma_g$  and  $1\sigma_u$  orbitals are primarily the inner shell C 1s orbitals, hence, the small minimal basis set correlation energies [6] compared to the EPCE results for such pairs.

The  $3\sigma_g$  bonding orbital is essentially the bonding orbital between the carbons and the hydrogens. The portion of the  $(3\sigma_g)^2$  correlation energy predicted by the minimal basis set is  $\sim 1/3$  the EPCE value. This is a significant portion, but it is not as large as one would like for a pair of valence electrons. The correlation which one is trying to describe is between two electrons which can be considered localizable in the C–H  $\sigma$  bonds. In a minimal basis set calculation only the virtual orbitals of  $\sigma$  symmetry can introduce the nodal behavior and localization that is necessary to modify the electron distribution as determined by the  $3\sigma_g$  orbital. In an extended basis set calculation in which some  $\pi$ -type basis functions are present on the hydrogens, the density in the C–H bond region should be additionally modifiable. Thus, the poor agreement with the EPCE value is ascribed to the inability of the minimal basis set calculation to modify the C–H bond to any large extent because of lack of  $\pi$ -type functions on the H atoms.

Pairs of  $\sigma$  electrons in which one of the orbitals, or both, is  $2\sigma_u$  or  $2\sigma_g$  contain at least one orbital in which there is a significant contribution from the valence atomic orbitals on the carbons. These molecular orbitals represent primarily the bonding region between the two carbons, although  $2\sigma_u$  contains appreciable H 1s. Unlike the  $3\sigma_g$  case, the use of configurations in which  $2\sigma_g$  and  $2\sigma_u$  are replaced by  $\pi_g$  is an effective way of dealing with correlation since these configurations deal effectively with the C–C bonding region.

The  $(2\sigma_g)^2$  pair is exceptional; a possible reason may be found in comparison of the  $(2\sigma_u)^2$  and the  $(2\sigma_g)^2$  pair correlations. For a pair of electrons in the  $2\sigma_u$  orbital, some left-right correlation is present by the nodal behavior of the orbital. Excited configurations in which this orbital has been replaced by other functions of  $u$  symmetry serve merely to modify the details of the  $2\sigma_u$  orbital. The effects of such configurations can be reasonably expected to be slowly convergent. The introduction of configurations involving  $g$  symmetry orbitals can modify the density in the C–C bonding region by the lack of node and by the high density probability of  $g$  type orbitals in this region. This should significantly modify the left-right correlation. There is however, only one possible configuration involving a  $g$  symmetry orbital, that with  $4\sigma_g$  replacing

$2\sigma_u$  in the  $(2\sigma_g)^2$  pair. Compare the  $(2\sigma_g)^2$  correlation: there is only one slowly convergent configuration, that constructed by replacing  $2\sigma_g$  by  $4\sigma_g$ . The other configurations formed by the substitution of  $3\sigma_g$  and  $4\sigma_u$  will introduce left-right correlation into the  $(2\sigma_g)^2$  distribution, and thus even at the minimal basis set level the  $(2\sigma_g)^2$  pair correlation can be highly effective. The effectiveness of the interaction of configurations in which  $\pi_u$  has replaced  $2\sigma_u$  or  $2\sigma_g$  is also expected to depend on whether the node in  $\pi_u$  perpendicular to the molecular axis will cause important modification of the probability density or not; according to the foregoing discussion, it should be much more important in the latter case than in the former.

Moskowitz [8a], from an extended Gaussian basis set (EGBS) calculation, calculates as an upper limit for the neutral acetylene correlation energy,  $-15.02$  eV, significantly higher than the EPCE value in Table 2. This correction must contain some portion of the Hartree-Fock energy, since Moskowitz's SCF energy differs from the recently obtained HF energy [11] by  $3.05$  eV. By utilizing Moskowitz's EGBS estimate for the difference between the SCF and HF limit for  $C_2$  ( $1.22$  eV), a revised EGBS correlation energy is  $-15.02 + 3.05 - 1.22 = -13.19$  eV close to the EPCE value of  $-12.87$  eV.

Compared to CI calculations, the EPCE technique has the merit to reflect intuitions concerning molecular behavior using only atomic quantities as parameters in the molecular problem, a small computation time requirement, and apparent numerical reliability superior to minimal basis set CI.

## 6. Validity of $\Pi$ -Electron Approximation in Acetylene

The entries in Table 4 are correlation energies for the hole (occupied MO spin-orbital) pairs given on the left. The particle (virtual, unoccupied MO spin-orbitals) pairs created in order to describe this correlation which conserve the number of  $\sigma$  and  $\pi$  electrons can be considered to be proper configurations within the restrictions of the  $\Pi$ -electron approximation [18]. Those configurations which do not conserve the numbers of  $\sigma$  and  $\pi$  electrons give the error inherent in the wavefunctions constructed in the  $\Pi$ -electron approximation in the same way that excited configurations give the error in the SCF method. These contributions to the hole pair correlation energies are nowhere larger than  $10^{-8}$  eV. Apparently, then, acetylene in the neutral and charged states satisfies the conservation of electron type requirement of the  $\Pi$ -electron approximation.

*Acknowledgement.* The authors thank the referee for carefully reading and criticizing the manuscript.

## References

1. Fueno, T.: *Ann. Rev. Phys. Chem.* **12**, 303 (1961).
2. Sinanoğlu, O.: *Proc. Nat. Acad. Sci. U.S.* **47**, 1217 (1961); *J. Chem. Phys.* **36**, 706 (1962); *Advan. Chem. Phys.* **6**, 315 (1964).
3. Öksüz, I., Sinanoğlu, O.: *Phys. Rev.* **181**, 42, 54 (1969).
4. Sinanoğlu, O., Pamuk, H. Ö.: *Theoret. Chim. Acta (Berl.)* **27**, 289 (1972).

5. Pamuk, H. Ö.: *Theoret. Chim. Acta (Berl.)* **28**, 85 (1972).
- 5a. Pamuk, H. Ö., Sinanoglu, O.: Submitted to *J. Am. Chem. Soc.*
6. Griffith, M. G., Goodman, L.: *J. Chem. Phys.* **47**, 4494 (1967).
7. A brief summary is given in L. Goodman: *Photochem. and Photobiol.* **7**, 545 (1968).
8. Meyer, W.: *Intern. J. Quant. Chem.* **5S**, 341 (1971).
- 8a. Moskowitz, J. W.: *J. Chem. Phys.* **43**, 60 (1965).
9. Mulliken, R. S.: *J. Chem. Phys.* **23**, 1833, 1841, 2338, 2343 (1955).
10. Koopmans, T.: *Physica* **1**, 109 (1933).
11. McLean, A. D., Yoshimine, M.: Tables of linear molecule functions. A supplement to the paper "Computation of molecular properties and structure". In: *IBM J. Res. Develop.* November (1967).
12. Clementi, E.: *J. Chem. Phys.* **38**, 2248 (1963).
13. Hollister, C., Sinanoglu, O.: *J. Am. Chem. Soc.* **88**, 13 (1966).
14. Duben, A. J., Lowe, J. P.: *J. Chem. Phys.* **55**, 4276 (1971).
15. Sinanoglu, O.: *Rev. Mod. Phys.* **35**, 517 (1963).
16. Davidson, E. R., Jones, L. L.: *J. Chem. Phys.* **37**, 2966 (1962).
17. Weiss, A. W.: *Phys. Rev.* **122**, 1826 (1961).
18. Lykos, P. G., Parr, R. G.: *J. Chem. Phys.* **24**, 1166 (1956).

Prof Dr. L. Goodman  
School of Chemistry  
Rutgers University  
New Brunswick, New Jersey 08903  
USA

## Exchange Interaction between Two Different Atoms at Large Distances

E. A. Andreev

Institute of Chemical Physics, Academy of Sciences, Moscow, USSR

Received December 4, 1972

Different cases of the exchange interaction in the system  $(A + e + C^+)$  are considered and corresponding expressions for this interaction are obtained. A suitable representation for the electron-atom interaction is also discussed.

**Key words:** Exchange interaction    Electron-atom interaction    Negative ions

### 1.

The main purpose of the present paper is to obtain the expressions for the exchange interaction between two atoms (A and C) with considerably different ionization potentials  $I_A = \alpha_0^2/2$  and  $I_C = \gamma_0^2/2$ <sup>1</sup> ( $\alpha_0 > \gamma_0$ ). One-electron approximation will be used for the wave function of the loosely bound valence electron of the atom C. We shall consider the case when the projection of the orbital angular momentum of this electron on the interatomic axis is equal to zero and the effective range  $\rho$  of the interaction  $V_A(r)$  between the electron and perturbing atom A is small compared with the interatomic distance  $R$ .

The general expressions for the different cases of the exchange interaction are derived in Sections 2, 3, 4 and 5. In Section 6 the results of other works are discussed and in Section 7 we consider the suitable analytical representation for the potential  $V_A(r)$ .

### 2.

Let  $I_C > 1/R$ . Then the perturbing atom A is in the classically forbidden region (for the valence electron). We shall determine the energy level shift of the atom C caused by the exchange interaction between two atoms. The corresponding Schrödinger equations are

$$(\frac{1}{2}\Delta = V_C + E_0)\psi_0 = 0, \quad E_0 = -I_C; \quad (\frac{1}{2}\Delta - V_C - V_A + E)\psi = 0. \quad (1)$$

Multiplying the first equation by  $\psi$  (the wave functions are assumed to be real) and the second one by  $\psi_0$  and integrating over the space  $\Omega$  with the boundary surface  $S$  we obtain (Green's theorem is used)

$$E - E_0 \left[ \frac{1}{2} \oint_S (\psi \nabla \psi_0 - \psi_0 \nabla \psi) ds + \int_{\Omega} \psi_0 V_A \psi dr \right] / \left( \int_{\Omega} \psi \cdot \psi_0 dr \right). \quad (2)$$

<sup>1</sup> Atomic units are used.

Taking  $\Omega_e$  (that is the entire space with the exception of the sphere volume  $\tilde{\Omega}_e$  of the radius  $\varrho$  around the atom A) as  $\Omega$  we obtain ( $\psi \simeq \psi_0$  in  $\Omega_e$  and  $\int_{\Omega} \psi \cdot \psi_0 \, dr \simeq 1$ )

$$E - E_0 = \frac{1}{2} \oint_{S_e} (\psi \nabla \psi_0 - \psi_0 \nabla \psi) \, ds. \quad (3)$$

In  $\tilde{\Omega}_e$

$$\psi_0(\mathbf{R} + \mathbf{r}) \simeq \psi_0(\mathbf{R}) \exp(\gamma \cdot \mathbf{r} \cdot \cos \theta) = \psi_0(\mathbf{R}) \frac{1}{\gamma r} \sum_{l=0} (2l+1) P_l(\cos \theta) i_l(\gamma r) \quad (4)$$

where  $\gamma^2/2 = I_C - 1/R$  (here  $1/R$  is the first term of the expansion of  $V_C$ );  $r$  and  $\theta$  are the coordinates of the electron with respect to the atom A (the polar axis is directed from A to C);  $i_l$  (and further  $k_l, j_l, n_l$ ) are modified spherical Bessel functions multiplied by their arguments. The general form of the axially symmetrical solution of the Schrödinger equation is [1]

$$\psi(\mathbf{R} + \mathbf{r}) = \psi_0(\mathbf{R}) \cdot \frac{1}{\gamma r} \sum_{l=0} (2l+1) \cdot P_l(\cos \theta) \cdot \varphi_l(r) \quad (5)$$

where  $\varphi_l$  is the solution of the corresponding radial equation. If  $\varrho \leq r \ll R$  this function has the following form

$$\varphi_l = a_l i_l(\gamma r) + b_l k_l(\gamma r) \quad (6)$$

At large  $r$   $\psi$  must coincide with  $\psi_0$ . Then one obtains from (3)

$$E - E_0 = -\psi_0^2(\mathbf{R}) \frac{\pi^2}{\gamma} \sum_l (2l+1) \cdot b_l/a_l. \quad (7)$$

### 3.

In deriving (7) we have used the tacit assumption that there was no bound state A with the energy  $-\gamma^2/2$  (otherwise the corresponding coefficient  $a_l$  becomes zero).

Consider now the following process

$$\text{When } R \rightarrow \infty \text{ we have} \quad A^- + C^+ = A + C. \quad (8)$$

$$(-\frac{1}{2} \Delta + V_A) \psi_a = E_a \psi_a; \quad (-\frac{1}{2} \Delta + V_C) \psi_c = E_c \psi_c \quad (9)$$

where  $\psi_a$  and  $\psi_c$  describe ionic and covalent states.

The solution of the ordinary secular equation gives the following expression for the splitting between the adiabatic terms at the crossing point  $R_0$  of ionic ( $U_a = E_a + V_c^{aa}$ ) and covalent ( $U_c = E_c + V_A^{cc}$ ) terms [ $U_a(R_0) = U_c(R_0)$ , or  $I_C \simeq \beta^2/2 + 1/R_0$ ;  $\beta^2/2$  is the electron affinity of atom A;  $V_K^{nm} = \langle n | V_K | m \rangle$ ;  $S_{ac} = \langle a | c \rangle$ ]

$$\Delta E = 2 \cdot \Delta U / (1 - S_{ac}^2); \quad \Delta U = |V_C^{aa} S_{ac} - V_C^{cc}|. \quad (10)$$

By means of some simple transformations one can obtain

$$\Delta U = \frac{1}{2} \left| \oint_{S_e} (\psi_c \nabla \psi_a - \psi_a \nabla \psi_c) \, ds \right|. \quad (11)$$

We put (when  $r \geq \varrho$ )

$$\psi_a = \frac{A_L}{r} k_L(\beta r) P_L(\cos \theta) \quad (12)$$



and use (4) for  $\psi_c$ . Then

$$\Delta U_L = \pi^2 |A_L \psi_c(R_0)|. \quad (13)$$

For the case  $L = 0$  we have

$$\psi_a = \sqrt{\frac{\beta}{2\pi}} \frac{B}{r} \exp(-\beta r), r \geq \varrho; \quad \Delta U = \sqrt{2\pi\beta} |B \cdot \psi_c(R_0)|. \quad (14)$$

Note that  $B = 1$  for the short-range ( $\delta$ -function) potential.

#### 4.

Consider the case when the perturbing atom A is in the inner region of the atom C ( $1/R - I_C = k^2/2 > 0$ ). In  $\hat{\Omega}_\varrho$  we take the unperturbed wave function in the following form

$$\psi_0(\mathbf{R} + \mathbf{r}) = \psi_0(\mathbf{R}) \cdot \cos(kr \cdot \cos\theta) + \psi_1(\mathbf{R}) \cdot \sin(kr \cdot \cos\theta). \quad (15)$$

To obtain the perturbed wave function  $\psi$  we use the analogy of electron-atom scattering theory. We find a stationary solution which meets the definite demands of symmetry relatively to the substitution  $\theta \rightarrow \pi - \theta$ . Then one can obtain the following correspondence between the terms of  $\psi_0$  and  $\psi$  (when  $\varrho \leq r \ll R$ )

$$\cos(kr \cdot \cos\theta) \rightarrow \cos(kr \cdot \cos\theta) + \frac{1}{r} f'_1(\theta) \cdot \cos(kr) - f'_2(\theta) \cdot \sin(kr), \quad (16)$$

$$\sin(kr \cdot \cos\theta) \rightarrow \sin(kr \cdot \cos\theta) + \frac{1}{r} f'_2(\theta) \cdot \cos(kr) + f'_1(\theta) \cdot \sin(kr), \quad (17)$$

where  $f_1$  and  $f_2$  are real and imaginary parts of the scattering amplitude,  $f'_m$  and  $f''_m$  are symmetric and antisymmetric parts of  $f_m$ . Expressing  $f$  through the scattering phases ( $\delta_l$ ) and using the formulas (16), (17), (15) and (3) we obtain

$$E - E_0 = -\frac{\pi}{k} \left[ \psi_0^2(\mathbf{R}) \sum_l (4l+1) \sin(2\delta_{2l}) + \psi_1^2(\mathbf{R}) \sum_l (4l+3) \sin(2\delta_{2l+1}) \right]. \quad (18)$$

#### 5.

Let there exist a quasi-stationary state when the electron with the orbital moment  $L$  is scattered by the atom A. Then one can establish (modifying the results of Ref. [1]) the following correspondence

$$\sin(2\delta_L) \rightarrow \sin(2\delta_L^0) + \Gamma \cos(2\delta_L^0) \left/ \left[ k_n \left( I_C + \varepsilon_0 + \frac{\Gamma}{2} \cdot \frac{\gamma_0}{k_n} \right) \right] \right. \quad (19)$$

where  $\Gamma$  is the width,  $E_n = k_n^2/2$  is the resonance energy,  $\delta_L^0$  is the "potential" scattering phase,  $\varepsilon_0 \approx E_n - 1/R$ . Thus the function  $E(R)$  has a pole (as in the case considered in the Sections 2 and 3). This pole corresponds to the pseudo-crossing of the covalent term with the term of the ionic state which becomes stable at  $R < R_*$  ( $R_* \approx 1/E_n$ ).

For the ionic state we use the wave function (see for example [2]) which is normalized to unity in  $\tilde{\Omega}_q$  and has the following form at  $r \geq q$

$$\psi_a = \sqrt{\frac{\tilde{r}}{k_n}} \frac{1}{r} [\sin \delta_L^0 j_L(kr) + \cos \delta_L^0 n_L(kr)] Y_{L0}(\cos \Theta). \quad (20)$$

The splitting of the adiabatic terms at the curve crossing point is given by (10), (11)

$$\Delta U = \sqrt{\pi(2L+1)} \tilde{r}/k_n |\cos \delta_L^0| \begin{cases} |\psi_0(R_0)| & \text{if } L \text{ is even} \\ |\psi_1(R_0)| & \text{if } L \text{ is odd} \end{cases} \quad (21)$$

## 6.

We have obtained all the results using the assumptions that  $q \ll R$  and that the functions  $\gamma$  and  $k$  were the slowly varying functions in the interval  $(R-q, R+q)$ , that is

$$\frac{q^2}{\kappa R^2} \ll \min(1, \kappa q) \quad (22)$$

where  $\kappa$  stands for  $\gamma$  or  $k$ . Note if  $\kappa q > 1$  then the condition (22) allows to use the quasi-classical description of  $\psi_0$  in  $\tilde{\Omega}_q$ . If  $\kappa q \ll 1$  (and  $\psi_0$  is slowly varying function in  $\tilde{\Omega}_q$ ) then formulas (7) and (8) give the result of Ovchinnikova [3]

$$E - E_0 = 2\pi L_s \psi_0^2(R) \quad (23)$$

where  $L_s$  is the scattering length.

The particular cases of exchange interaction have been previously investigated by other authors. The result analogous to (7) has been obtained by Smirnov [4] who used the more rigid (than  $q \ll R$ ) assumption ( $R \gg l/\gamma, q$ ) which is broken at large  $l$  and small  $\gamma$ . Komarov [5] has investigated the splitting of the hydrogen atom terms at large distances ( $1/R \ll \beta^2/2, \gamma_0^2/2$ ) in the  $\delta$ -potential field. Formulas (14) and (10) give the exact expression (in the case of  $\delta$ -potential) for  $\Delta U$ . Smirnov [6] and Janev and Salin [7] have attempted to consider a more general (than in [5]) case. However their approach is incorrect and their results do not turn into the result of Komarov (see the formulas (20) and (21) from [7]).

## 7.

To determine the coefficients  $b_l/a_l$ ,  $B$ ,  $\delta_l$  in the equations above it is necessary to solve the Schrödinger equation with the concrete potential  $V_A(r)$ . Following the ideas of Hellman [8, 9] one may suppose that  $V_A$  behaves as  $-\alpha/2r^4$  at  $r > r_A$  ( $\alpha$  and  $r_A$  are the polarizability and the characteristic size of the atom A) and as  $\frac{\partial T}{\partial n}$  at  $r < r_A$  ( $T$  is the electron kinetic energy density and  $n$  is the electron density

in A). The theory of Thomas-Fermi (TF) gives  $\frac{\partial T}{\partial n} = \varphi(r)$ , where  $\varphi(r)$  is the TF potential for A. Thus  $V_A(r)$  has a strongly repulsive character at small  $r$ .

Note that considering the elastic electron-inert atom scattering Holtsmark [10] and a number of other authors (see the book [11]) took  $V_A = -\varphi(r)$  at small  $r$

(the approximation of static field). This potential is strongly attractive. Although the theory-experiment agreement was quite satisfactory at high energies (when Born approximation is valid and the scattering parameters do not depend on sign of the interaction) there was considerable discrepancy at low energies. Besides there are bound states  $A^-$  in this attractive potential. This fact is in contradiction with the experimental results (see for example Ref. [12]) that there do not exist negative ions of inert gas atoms in their ground states.

Let the potential  $V_A(r)$  have the following form

$$V_A = -\alpha/2r^4, \quad r > r_0; \quad V_A = \infty, \quad r \leq r_0 \quad (24)$$

which reproduces the main properties of the electron-atom interaction. (Solving the Schrödinger equation with the potential (24) numerically one can obtain the Ramsauer effect.) The Schrödinger equation with the potential  $\sim r^{-4}$  has been considered in Ref. [13]. Supposing  $E=0$  and demanding  $\psi(r_0)=0$  we can obtain an exact expression for the scattering length  $L_s$  and express  $L_s$  through  $r_0$

$$L_s = \sqrt{\alpha} \operatorname{ctg}(\sqrt{\alpha}/r_0); \quad r_0 = \sqrt{\alpha}/[N\pi + \operatorname{arccotg}(L_s/\sqrt{\alpha})] \quad (25)$$

where  $N$  is a number of bound states in the potential (24) and the condition of the existence of the bound state is  $\sqrt{\alpha}/r_0 > \pi$ .

To obtain suitable analytical results we shall use (instead of  $V_A$  from (24)) a modified potential  $W_A$  which equals to zero if  $|V_A| < |E|$  and to  $V_A + E$  if  $|V_A| > |E|$ . Then  $q = (\alpha/2|E|)^{1/4}$ . If there is only one bound state  $A^-$  with  $L=0$  than using  $W_A$  we obtain the following relations between  $\alpha$ ,  $L_s$ ,  $r_0$  and  $\beta$ :

$$r_0 = \frac{\sqrt{\alpha}}{\lambda + \pi - \operatorname{arctg}[\lambda/(1+\lambda)]}; \quad L_s = \sqrt{\alpha} \operatorname{ctg}\left(\lambda - \operatorname{arctg}\frac{\lambda}{1+\lambda}\right); \quad \lambda = \beta^{1/2} \cdot \alpha^{1/4}. \quad (26)$$

For the system  $e-H$  ( $\alpha=4.5$ ;  $\beta=0.236$  [12]) one can obtain  $L_s=6.55$ . Variational calculation with 1156 parameters [14] gives  $L_s=5.96$ .

For the coefficient  $B$  (14) we obtain

$$B = e^{\lambda} \cdot f(\lambda) = \left\{ 2\sqrt{(1+\lambda)^2 + \lambda^2} \int_{x_0}^1 x^2 \sin^2 \left[ \frac{\lambda(x_0 - x)}{x_0 \cdot x} \right] dx + 1 \right\}^{-1/2} \quad (27)$$

$x_0 = r_0 \beta^{1/2} \alpha^{-1/4}$ ;  $f(\lambda)$  is given in Table 1. Note that  $f^2$  gives the part of the electron density in the region  $r > q$ . For the ion  $H^-$  we obtain  $B=1.66$ ; variational calculations give 1.63 and 1.68 [12].

Then the splitting between the ionic term ( $H^+ + H^-$ ) and different covalent ones ( $H(1s) + H(nl)$ ;  $n=2$ ,  $R_0=11.1$ ;  $n=3$ ,  $R_0=35.6$  [15]) was calculated and compared with the variational calculation [15] (see Table 2 where  $\Delta E_{nl}$  are given in eV).

Note that by averaging (18) over different places of the perturbing atom A one can obtain the shift of the spectral line of the perturbed atom C (compare with the result of Alekseev and Sobelman [16]).

The author is indebted to Prof. E. E. Nikitin for the discussion of the present work.

Table 1

$\lambda$	$f$
0	1
0.25	0.956
0.5	0.881
0.75	0.815
1	0.763
1.25	0.722
1.5	0.690
1.75	0.665
2	0.644
2.25	0.627
2.5	0.612
3	0.589
3.5	0.571
4	0.558

Table 2

$(n, l)$	(2, 0)	(2, 1)	(3, 0)	(3, 1)	(3, 2)
Work [15]	0.333	0.407	$4.91_{10} - 3$	$6.40_{10} - 3$	$4.58_{10} - 3$
Present work	0.381	0.461	$5.83_{10} - 3$	$7.43_{10} - 3$	$5.43_{10} - 3$

### References

1. Landau, L. D., Lifshitz, E. M.: Quantum mechanics. Moscow: Fizmatgiz 1963, in Russian.
2. Baz, A. I., Zeldovitch, Ja. B., Perelomov, A. M.: Scattering, reactions and decays in nonrelativistic quantum mechanics. Moscow: Fizmatgiz 1966, in Russian.
3. Ovchinnikova, M. Ja.: JETP **49**, 275 (1965).
4. Smirnov, B. M.: JETP **51**, 466 (1966).
5. Komarov, I. V.: Thesis (LGU, 1968), in Russian.
6. Smirnov, B. M.: Dokl Akad. Nauk SSSR **161**, 92 (1965).
7. Janev, R. K., Salin, A.: J. Phys. B **5**, 177 (1972).
8. Hellman, H.: J. Chem. Phys. **3**, 61 (1935).
9. Hellman, H., Kassatotschkin, W.: J. Chem. Phys. **4**, 324 (1936).
10. Holtsmark, J.: Z. Physik **55**, 437 (1929).
11. Mott, N. F., Massey, H. S. W.: The theory of atomic collisions. Oxford: 1965.
12. Smirnov, B. M.: Atomic collisions and elementary processes in plasma. Moscow: Atomizdat 1968.
13. O'Malley, T. F., Spruch, L., Rosenberg, T. J.: J. Math. Phys. **2**, 491 (1961).
14. Schwartz, C.: Phys. Rev. **124**, 1468 (1968).
15. Bates, D. R., Lewis, J. T.: Proc. Phys. Soc. (London) A **68**, 173 (1955).
16. Alekseev, V. A., Sobelman, I. I.: JETP **49**, 1274 (1965).

E. A. Andreev  
Institute of Chemical Physics  
Academy of Sciences  
Moscow V-334, USSR

## Relationes

# Calculations of the Isotropic Hyperfine Coupling Constants in Free Radicals

G. M. Zhidomirov and N. D. Chuvylkin

Institute of Organic Chemistry, USSR Academy of Sciences, Moscow, USSR

Received October 6, 1972

For a number of free radicals the results of non-empirical (*ab initio*) and semi-empirical (INDO, DEPA, CNDO/SP) calculations of the isotropic hyperfine coupling constants are compared.

**Key words:** Radicals Spin-density distribution – Hyperfine coupling constants – Electron spin resonance

In the last few years there has been considerable interest in semi-empirical calculations of the hyperfine coupling constants (hfc) in free radicals. Several methods have been suggested for this purpose. Here, for a number of free radicals the calculations of isotropic hfc were carried out by some of these methods using the same values of geometrical parameters. It allows the adequacy of various semi-empirical methods to be analysed on the basis of comparison with the results of experiment as well as available *ab initio* calculations.

(I). *Ab initio* UHF method [1–10] followed by annihilation of the contaminating quartet spin state after energy minimization (UHF/AA method [2–7]) was used for most radicals presented in Table 1.

(II). INDO method [11] is a semi-empirical SCF LCAO MO one with special selection of the most adequate parameters reproducing the wavefunctions obtained by a more sophisticated calculation of some simple “standard” molecules. By comparison with the results of *ab initio* consideration of more complex molecules it was demonstrated [12–16] that INDO may be a sufficiently effective approach to the problem of calculating the molecular properties. To our knowledge, nothing similar has been done in the case of free radicals.

It is worth mentioning at this point that in the INDO calculations of hfc the spin populations of the AO's are taken to be equal to differences in the  $\alpha$ - and  $\beta$ -electron populations

$$q_{\mu\nu} = P_{\mu\nu}^{\alpha} - P_{\mu\nu}^{\beta}, \quad (1)$$

$$P_{\mu\nu}^{\alpha} = \sum_i^{\text{occ}} c_{i\mu}^{\alpha} \cdot c_{i\nu}^{\alpha}, \quad P_{\mu\nu}^{\beta} = \sum_i^{\text{occ}} c_{i\mu}^{\beta} \cdot c_{i\nu}^{\beta}, \quad (2)$$

where  $c_{i\mu}^{\alpha}$ ,  $c_{i\mu}^{\beta}$  are the coefficients of the AO  $\varphi_{\mu}$  in the MO's expressions ( $\Psi_i^{\alpha}$  and  $\Psi_i^{\beta}$ ) obtained within the scope of the UHF method.

(III). DEPA method is also a semi-empirical SCF LCAO MO scheme [17]. In this method the spin populations are similarly defined with the help of Eqs. (1) and (2). However, as distinct from INDO, the MO's  $\Psi_i^{\alpha}$  and  $\Psi_i^{\beta}$  are

Table 1. Isotropic hyperfine coupling constants (in G)

Radical (1)		<i>ab initio</i> (2)	INDO (3)	DEPAC (4)	CNDO/SP (5)	Expt. (6)
1. CH <sub>3</sub>	H	- 18.0	- 20.6	71.5	- 23.1	(-) 23.0[30] 38.3[31]
	C	31.7	43.1	- 72.7	60.4	
2. C≡CH	H		34.6	106.5	31.6	16.1[32] —
	C		287.4	252.6	282.3	
	C		7.0	- 16.2	7.2	
3. HC≡CH <sub>2</sub> ( $\theta \approx 135^\circ$ )	H	- 1.3	10.7	70.1	13.4	13.4[30] 37.0[30] 65.9[30] 107.6[31] (-) 8.6[31]
	H	42.8	33.8	87.3	37.9	
	H	62.4	74.0	113.5	73.6	
	C	139.3	127.7	107.8	125.4	
	C	- 16.4	- 14.9	- 23.4	- 2.4	
4. C <sub>6</sub> H <sub>5</sub>	H		18.7	59.1	17.6	17.4[33] 5.9[33] 1.9[33]
	H		6.7	42.8	5.6	
	H		3.7	40.3	5.5	
	C		149.7	83.2	143.4	
	C		- 3.9	- 8.5	1.2	
	C		9.9	8.0	10.5	
	C		- 1.8	- 5.9	- 1.1	
5. C≡N	C	339.2	149.4	151.6	191.8	210.0[34] ( ) 4.5[34]
	N	6.2	4.1	12.4	8.6	
6. HC≡N	H	140.3	148.9	170.3	147.7	137.5[35] 74.3[35] 6.5[35]
	C	74.4	156.1	165.8	140.7	
	N	4.9	3.1	1.5	4.1	
7. H <sub>2</sub> C≡N	H	84.8	56.1	111.5	63.5	92.1[36] 9.5[36]
	C	- 18.7	22.6	28.0	- 6.6	
	N	7.2	8.2	2.9	8.5	
8. HCO	H	112.5	112.7	151.2	115.5	127.0[37] 131.0[37]
	C	148.4	146.7	146.6	138.6	
	O	1.0	5.2	- 3.2	- 14.2	
9. CH <sub>3</sub> CO	H	4.9	5.4	62.6	3.4	5.1[38] 125.5[38] 47.5[38]
	C	153.2	128.2	101.8	129.0	
	C	39.9	17.6	6.6	23.6	
	O	- 9.4	- 5.8	- 1.5	- 15.8	
10. FCO	F		326.2	262.2	344.8	325.5[39] 288.7[39]
	C		199.6	205.2	179.8	
	O		- 0.7	- 0.8	- 14.9	
11. CO <sub>2</sub>	C		170.2	165.0	140.3	166.7[40] (-) 32.1[40]
	O		- 5.5	- 3.9	- 15.7	
12. NH <sub>2</sub>	H	- 22.3	- 17.3	105.9	- 20.6	(-) 23.9[41] 10.3[41]
	N	8.2	12.9	6.8	14.5	
13. NH <sub>3</sub> <sup>+</sup>	H	- 15.8	- 21.2	89.4	- 23.8	(-) 25.9[42] 19.5[42]
	N	14.8	19.2	- 36.7	21.1	
14. H <sub>2</sub> NO	H	- 8.8	12.9	93.6	15.1	11.9[43] 11.9[43] —
	N	11.2	10.4	22.0	12.5	
	O		- 10.9	- 11.2	- 28.4	
15. NO <sub>2</sub>	N		31.3	29.3	21.3	54.8[44] (-) 16.3[44]
	O		0.9	1.5	- 12.7	

Table 1 (continued)

Radical		<i>ab initio</i> (2)	INDO (3)	DEPAC (4)	CNDO/SP (5)	Expt. (6)
5. NH	H	- 56.7	- 30.4	113.8	- 40.6	
	N	11.6	12.9	6.1	16.6	
7. OH	H	- 41.4	- 16.9	148.9	- 22.4	(-) 229[45]
	O	(-)34.1	- 13.2	- 14.4	- 38.2	-
3. H <sub>3</sub> O	H		150.9	183.0	135.2	[46]
	O		-249.7	-233.5	-398.0	
9. HBO <sup>-</sup>	H	91.6	87.7	104.0	74.5	94.0 [47]
	B	123.0	212.2	223.2	191.9	101.0 [47]
	O	- 4.1	- 4.2	- 1.0	- 8.6	-
. BH <sub>3</sub>	H	- 17.2	- 16.9	42.3	- 19.4	(-) 16.5 [47]
	B	13.6	34.6	- 42.1	44.1	25.0 [47]
. BF <sub>2</sub>	B		336.5	355.3	288.2	295.0 [48]
	F		359.4	403.5	181.1	190.0 [48]

cepted as being those of the anion and cation with closed shells formed by addition or "subtraction" of one electron from the open electron shell of the responding free radical, i.e. the spin populations of the radical AO's are compared to semi-differences in the electron populations of the anion and cation (DEPAC).

With the use of this method the proton hfc in benzyl, allyl and some other conjugated radicals have been calculated within the framework of  $\pi$ -electron approach [17, 18]. For the former the para/ortho ratio greater than unity was readily reproduced with its standard geometry while a more refined consideration proved to be necessary in the usual open-shell methods (cf. INDO 18-20). Another example is the HCO  $\sigma$ -radical for which the all-valence-electron DEPAC method led to a satisfactory quantitative description of the carbon and hydrogen isotropic constants as well as principal components of the anisotropic hyperfine interaction [21].

Nevertheless it seems to be desirable to carry out systematic calculations of various free radicals by the DEPAC method in order to feel sure that this approach is either effective or unfit. DEPAC values of the isotropic hyperfine coupling constants are summarized in Table 1. They were obtained from consideration of the corresponding anions and cations within the scope of INDO, i.e. with the use of exactly the same approximations for the matrix elements of the Hartree-Fock operator as in the preceding section.

(IV). CNDO/SP method [22] may be considered as the consistent extension of the McLachlan procedure to the case of all-valence-electron calculations of the spin density distributions in free radicals. This method is based on the use of the effective hamiltonian for the open-shell electronic states [23] as well as the CNDO/2 approximations [24] within the framework of the restricted Hartree-Fock (RHF) approach.

Table 2 CNDO,SP delocalization and polarization contributions (in G)

Radical (1)		$a^0$ (2)	$a^{SP}$ (3)	$a^{SP}$ (4)
1. $\text{CH}_3$	H	0	0	-23.1
	C	0	0	-60.4
2. $\text{C}^+-\text{CH}$	H	36.3	-0.6	-4.1
	C	272.8	-1.9	11.4
	C	21.3	-5.7	-8.4
3. $\text{HC}^+-\text{CH}_2$	H	29.7	-5.2	-11.1
	H	39.7	0.9	-2.7
	H	75.4	1.7	-3.5
	C	91.9	-3.3	36.8
	C	4.1	-1.9	-4.6
4. $\text{C}_6\text{H}_5$	H	20.0	0.2	-2.6
	H	7.5	-0.3	-1.6
	H	5.6	0.1	-0.2
	C	117.6	-4.4	30.2
	C	5.1	-1.4	2.5
	C	9.5	-0.4	1.4
	C	0.1	-0.2	-1.0
5. $\text{C}^+-\text{N}$	C	185.3	-2.3	8.8
	N	6.8	-1.1	2.9
6. $\text{HC}^+\text{N}$	H	153.1	1.1	-6.5
	C	140.5	0.4	-0.2
	N	0.1	-0.2	4.2
7. $\text{H}_2\text{CN}$	H	64.7	-1.0	-0.2
	C	0	-1.6	-5.0
	N	0	0	8.5
8. $\text{HCO}$	H	125.6	-0.9	-9.2
	C	131.8	-0.8	7.6
	O	0.4	0.5	-14.3
9. $\text{CH}_3\text{CO}$	H	7.2	-0.1	-3.7
	C	117.7	1.4	12.7
	C	21.5	-0.7	2.8
	O	-0.3	2.6	-18.1
10. $\text{FCO}$	F	284.3	-31.3	91.8
	C	174.7	0.4	4.7
	O	-0.6	1.2	-15.5
11. $\text{CO}_2$	C	127.5	-2.6	15.4
	O	-6.3	1.3	-10.7
12. $\text{NH}_2$	H	0	0	-20.6
	N	0	0	14.5
13. $\text{NH}_3$	H	0	0	-23.8
	N	0	0	21.1
14. $\text{H}_2\text{NO}$	H	20.6	-0.6	-4.9
	N	11.3	-0.4	1.6
	O	-0.3	2.2	-30.3
15. $\text{NO}_2$	N	17.2	-0.6	4.7
	O	-0.4	1.0	-13.3



Table 2 (Continued)

Radical (1)		$a^0$ (2)	$a^{sp}$ (3)	$a^{vp}$ (4)
16. NH	H	0	0	-40.6
	N	0	0	16.6
17. OH	H	0	0	-22.4
	O	0	0	-38.2
18. H <sub>3</sub> O	H	146.8	2.9	-14.5
	O	-398.0	0	0
19. HBO	H	86.3	-0.8	-11.0
	B	187.8	0.8	3.3
	O	-0.8	1.0	-8.8
20. BH <sub>3</sub> <sup>-</sup>	H	0	0	-19.4
	B	0	0	44.1
21. BF <sub>2</sub>	B	288.4	0.5	-0.7
	F	234.3	-21.5	-31.7

According to CNDO/SP the spin density matrix may be presented as a sum of three constituents namely

- 1) the one electron (delocalization) term  $\hat{\rho}^0$
- 2) the spin-polarization term  $\hat{\rho}^{sp}$  and
- 3) the exchange ( $\sigma - \pi$ ) spin-polarization term  $\hat{\rho}^{vp}$ .

The delocalization contribution  $\rho_{\mu\mu}^0$  to the spin population of the AO  $\phi_\mu$  is accepted as being the square of the coefficient by this AO in the unpaired electron MO expression. The other two contributions to the spin population, arising from the unpaired electron polarization of paired electrons in doubly occupied MO's are calculated by a perturbation theory with the help of "atom-atom" mutual polarizabilities ( $\pi_{\mu\nu}$ ) of Coulson [25] and the values of the atomic electron repulsion ( $\gamma_{\mu\nu}$ ) and exchange ( $\kappa_{\sigma\nu}$ ) integrals

$$\rho_{\mu\mu}^{sp} = -\frac{1}{2} \cdot \lambda_{sp} \cdot \sum_{\nu} \pi_{\mu\nu} \cdot \gamma_{\nu\nu} \cdot \rho_{\nu\nu}^0, \quad (3)$$

$$\rho_{\mu\mu}^{vp} = -\frac{1}{2} \cdot \lambda_{vp} \cdot \sum_{\nu} \pi_{\mu\nu} \cdot \sum_{\sigma} \kappa_{\sigma\nu} \cdot (\rho_{\sigma\sigma}^0 + \rho_{\sigma\sigma}^{sp}). \quad (4)$$

Here, as in the McLachlan method, the semi-empirical parameters are introduced whose magnitudes  $\lambda_{sp}=0.1$  and  $\lambda_{vp}=2.35$  have been found from comparison with experiment.

The contributions to isotropic hfc are summarized in Table 2. CNDO/SP calculations of hfc were carried out with the semi-empirical quantities

$$\delta_N = \frac{4}{3} \cdot \pi \cdot g_e \cdot \beta_e \cdot \gamma_N \cdot \hbar \cdot \langle S_Z \rangle^{-1} \cdot |S(0)|^2 \quad (5)$$

presented in Table 3 together with those obtained [26] by least-squares fitting for INDO. The Hartree-Fock values [27] are also given in this table for comparison.

INDO as well as DEPAC and CNDO/SP calculations were performed for the same geometrical structure of any free radical in Table 1. In most cases the

Table 3.  $\delta_N$ -parameters for magnetic nuclei (in G)

Nucleus	HF	INDO	CNDO/SP
$^1\text{H}$	508	539.86	600
$^{11}\text{B}$	725	(725)	700
$^{13}\text{C}$	1130	820.10	850
$^{14}\text{N}$	552	379.34	300
$^{17}\text{O}$	1660	— 888.68	— 1500
$^{19}\text{F}$	17200	44829.20	36500

values of bond lengths and angles were estimated as those recommended for molecules [28] or taken from experiment if possible. Note that in *ab initio* calculations [1-10] the radical geometry was either similar or it was varied.

The results, summarized in Table 1, suggest the following conclusions:

1. Most of the experimental trends for the isotropic hfc in free radicals are well reproduced by the INDO method. The difference between the *ab initio* and INDO results is small as a rule in spite of the proper variation of parameters in *ab initio* calculations [2-7, 9]. This may partly justify some applications of the INDO method for semi-quantitative hfc predictions. On the other hand, INDO is rather simple and more economical and therefore practically preferable in the case of complex paramagnetic species. At present it can be considered as the best among the semi-empirical methods for hfc calculations [26].

2. As distinct from INDO, the DEPAC method is generally unable to reproduce the experimental hfc data reliably. Moreover DEPAC leads to unreasonable qualitative results when  $a''^p$  is the only contribution to the isotropic hfc (cf. Table 2). Thus DEPAC is unfit for the all-valence-electron calculations of  $\pi$ -electron free radicals. However, it is of interest to note that for some  $\sigma$ -electron radicals ( $\text{C}\equiv\text{N}$ ,  $\text{HCN}$ ,  $\text{H}_2\text{CN}$ ,  $\text{HCO}$ ,  $\text{CO}_2^-$ ,  $\text{NO}_2$ ,  $\text{H}_3\text{O}$ ,  $\text{HBO}$ ) there is a good qualitative accordance between the hfc magnitudes obtained by DEPAC and INDO. Nevertheless, for the  $\sigma$ -electron radicals such as  $\text{C}\equiv\text{CH}$ ,  $\text{HC}=\text{CH}_2$ ,  $\text{C}_6\text{H}_5$ ,  $\text{CH}_3\text{CO}$  the DEPAC method again proves to be unsatisfactory.

3. CNDO/SP method is the most economical and simple among those presented in Table 1. At the same time the results indicate that CNDO/SP is sufficiently effective as it leads to a satisfactory quantitative description of hfc. As distinct from INDO, the CNDO/SP approach facilitates the qualitative interpretation of the experimental data substantially as it allows the spin density matrix to be presented as a sum of the one electron and spin-polarization constituents and also makes possible the direct comparison with the results of simpler methods [29]. This approach is very attractive for the practical calculations due to the opportunity of estimating the one electron contribution reliably and obtaining a small spin-polarization correction by a perturbation theory.

Rather large values of the exchange spin-polarization terms  $a''^p$  for  $\sigma$ -electron radicals are worth mentioning at this point. They may be compared with similar INDO-magnitudes  $a''^p$  which are the UHF-differences in the isotropic hyperfine

Table 4. Isotropic hyperfine coupling constants and exchange spin-polarization contributions (in G)

Method <i>hfc</i>		INDO <i>a</i>	CNDO/2 <i>a</i>	INDO <i>a<sup>SP</sup></i>	CNDO/SP <i>a<sup>SP</sup></i>
HC=CH <sub>2</sub>	H	10.7	29.2	-18.5	-11.1
	H	33.8	37.3	-3.5	-2.7
	H	74.0	73.4	0.6	-3.5
	C	127.7	91.0	36.7	36.8
	C	-14.9	-9.1	-5.8	-4.6
C≡CH	H	34.6	30.3	4.3	-4.1
	C	7.0	9.4	-2.4	-8.4
	C	287.4	274.0	13.4	11.4
HCN <sup>-</sup>	H	148.9	155.0	-6.1	-6.5
	C	156.1	126.8	29.3	-0.2
	N	3.1	-0.3	3.4	4.2
HCO	H	112.7	128.0	-15.3	-9.2
	C	146.7	108.7	38.0	7.6
	O	-5.2	0.4	-5.6	-14.3
HBO	H	87.7	92.1	-4.4	-11.0
	B	212.2	181.0	31.2	3.3
	O	-4.2	0.2	-4.4	-8.8

coupling constants calculated within the scope of INDO and CNDO/2, as the latter neglects the atomic exchange integrals  $\kappa_{\sigma\sigma}$ . These differences for some  $\sigma$ -electron radicals are summarized in the last but one column of Table 4. In most cases they are much the same or greater than those obtained by the CNDO/SP method.

A good quantitative agreement with the experimental and INDO results shows a strong evidence for the efficiency of CNDO/SP in qualitative analyses of the isotropic *hfc*.

### References

1. Cook, D. B., Hinchliffe, A., Palmieri, P.: *Chem. Physics Letters* **3**, 223 (1969).
2. Claxton, T. A.: *Trans. Faraday Soc.* **66**, 1537, 1540 (1970).
3. Claxton, T. A., McWilliams, D., Smith, N. A.: *Chem. Physics Letters* **4**, 505 (1970).
4. Claxton, T. A.: *Int. J. quant. Chemistry* **4**, 337 (1970).
5. Claxton, T. A.: *Chem. Physics Letters* **4**, 469 (1969).
6. Claxton, T. A.: *Trans. Faraday Soc.* **67**, 897 (1971).
7. Claxton, T. A., Smith, N. A.: *Trans. Faraday Soc.* **67**, 1859 (1971).
8. Veillard, H., Rees, B.: *Chem. Physics Letters* **8**, 267 (1971).
9. Salotto, A. W., Burnelle, L.: *J. chem. Physics* **53**, 333 (1970).
10. Meyer, W.: *J. chem. Physics* **51**, 5149 (1969).
11. Pople, J. A., Beveridge, D. L., Dobosh, P. A.: *J. chem. Physics* **47**, 2026 (1967).
12. Gordon, M. S., Pople, J. A.: *J. chem. Physics* **49**, 4643 (1968).
13. Newton, M. D., Lathan, W. A., Hehre, W. J., Pople, J. A.: *J. chem. Physics* **52**, 4064 (1970).
14. Hehre, W. J., Ditchfield, R., Pople, J. A.: *J. chem. Physics* **53**, 932 (1970).
15. Lathan, W. A., Hehre, W. J., Pople, J. A.: *J. Amer. chem. Soc.* **93**, 808 (1971).
16. Pople, J. A.: *Accounts Chem. Res.* **3**, 217 (1970).
17. Adam, F. C., Laidlaw, W. G.: *Austral. J. Chem.* **19**, 897 (1966).

18. Benson, H. G., Hudson, A.: *Molecular Physics* **20**, 185 (1971).
19. Chuvylkin, N. D., Zhidomirov, G. M.: *Zh. Strukt. Khim.* **13**, 236 (1972).
20. Beveridge, D. L., Guth, E.: *J. chem. Physics* **55**, 458 (1971).
21. Chuvylkin, N. D., Zhidomirov, G. M., Schastnev, P. V.: *Zh. Strukt. Khim.* **13**, 602 (1972).
22. Zhidomirov, G. M., Chuvylkin, N. D.: *Chem. Physics Letters* **14**, 52 (1972).
23. Longuet-Higgins, H. C., Pople, J. A.: *Proc. phys. Soc. (London) A* **68**, 591 (1955).
24. Pople, J. A., Segal, G. A.: *J. chem. Physics* **44**, 3289 (1966).
25. Coulson, C. A., Longuet-Higgins, H. C.: *Proc. Roy. Soc. (London) A* **191**, 39 (1947).
26. Pople, J. A., Beveridge, D. L., Dobosh, P. A.: *J. Amer. chem. Soc.* **90**, 4201 (1968).
27. Atkins, P. W., Symons, M. C. R.: *The structure of inorganic radicals*. Amsterdam 1967.
28. Pople, J. A., Gordon, M.: *J. Amer. chem. Soc.* **89**, 4253 (1967).
29. Chuvylkin, N. D., Zhidomirov, G. M.: *Zh. Strukt. Khim.* **12**, 347 (1971).
30. Fessenden, R. W., Schuler, R. H.: *J. chem. Physics* **39**, 2147 (1963).
31. Fessenden, R. W.: *J. physic. Chem.* **71**, 74 (1967).
32. Cochran, E. L., Adrian, F. J., Bowers, V. A.: *J. chem. Physics* **40**, 213 (1964).
33. Kasai, P. H., Hedaya, E., Whippe, E. B.: *J. Amer. chem. Soc.* **91**, 4364 (1969).
34. Fasley, W. C., Weltner, W.: *J. chem. Physics* **52**, 197 (1970).
35. Root, K. D. J., Symons, M. C. R., Weatherley, B. C.: *Molecular Physics* **11**, 161 (1966).
36. Symons, M. C. R.: *J. chem. Physics* **55**, 1493 (1971).
37. Holmberg, R. W.: *J. chem. Physics* **51**, 3255 (1969).
38. Bennett, J. I., Mile, B.: *Trans. Faraday Soc.* **67**, 1587 (1971).
39. Cochran, E. L., Adrian, F. J., Bowers, V. A.: *J. chem. Physics* **44**, 4626 (1966).
40. Schlick, S., Silver, B. L., Luz, Z.: *J. chem. Physics* **54**, 867 (1971).
41. Foner, S., Cochran, E., Bowers, V., Jen, C.: *Physic. Rev. Letters* **1**, 91 (1958).
42. Cole, I.: *J. chem. Physics* **35**, 1169 (1961).
43. Adams, J. Q., Nickse, S. W., Thomas, J. R.: *J. chem. Physics* **45**, 654 (1966).
44. Luz, Z., Reuveni, A., Holmberg, R. W., Silver, B. L.: *J. chem. Physics* **51**, 4017 (1969).
45. Toriyama, K., Iwasaki, M.: *J. chem. Physics* **55**, 1890 (1971).
46. INDO does not support the discovery of  $H_2O$ , by: Martin, T. W., Swift, L. L.: *J. Amer. chem. Soc.* **93**, 2788 (1971), cf. Chuvylkin, N. D., Zhidomirov, G. M.: *Chem. Physics Letters* **14**, 70 (1972).
47. Catton, C. R., Symons, M. C. R., Wardale, H. W.: *J. chem. Soc. A* **1969**, 2622.
48. Nelson, W., Gordy, W.: *J. chem. Physics* **51**, 4710 (1969).

Dr. G. M. Zhidomirov  
 N. D. Zelinsky Institute of Organic Chemistry  
 Academy of Sciences of the USSR  
 Leninsky prospect, 47  
 Moscow, B-334, USSR

# Theory of Spin Triplet Ground States in $d^6$ Transition Metal Compounds and the Effect of High-Energy States on the Nature of the Ground State

E. König and R. Schnakig

Institut für Physikalische Chemie II, Universität Erlangen-Nürnberg, D-8520 Erlangen, Germany

Received February 12, 1973

The formation of spin triplet, quintet, and singlet ground states within the  $3d^6$  electron configuration is investigated in  $D_{4h}$  and  $D_{3d}$  symmetries employing irreducible tensor operator methods. Significant differences in the possible ground states are encountered between a complete CI and spin-orbit interaction treatment and an approximate calculation within the cubic  ${}^5T_2$ ,  ${}^1A_1$ ,  ${}^3T_1$ , and  ${}^3T_2$  parents.

**Key words:**  $d^n$  configuration    Ligand Field Theory

The stabilization of spin triplet ground states in compounds of the electronic configuration  $d^6$  has been a matter of considerable interest and of some speculation in recent years. On the basis of experimental investigations,  $S=1$  ground states are definitely established in the planar iron(II) phthalocyanine [1], in certain distorted octahedral bis(diimine) iron(II) complexes, a representative example being  $\text{Fe(phen)}_2\text{ox} \cdot 5\text{H}_2\text{O}$  [2–4], and in the planar bis(biuretato) cobalt(III) complexes [5, 6]. Triplet ground states are likewise formed on reduction from iron(III) to iron(II) under high pressure in biological compounds like hemin, hematin, and imidazole protohemichrome [7]. Finally, the apparent function of a triplet state in the biologically essential oxygenation of hemoglobin should not be overlooked [8].

At the beginning, the results of physical measurements (e.g. the effective magnetic moments) have not been understood, since, within the parent octahedral symmetry, only  ${}^5T_{2g}(t_{2g}^4 e_g^2)$  and  ${}^1A_{1g}(t_{2g}^6)$  ground states are formed. Under the same conditions, the lowest triplet state  ${}^3T_{1g}(t_{2g}^5 e_g)$  is at least  $5000\text{ cm}^{-1}$  higher in energy [9]. However, if tetragonal ( $D_{4h}$ ) or trigonal ( $D_{3d}$ ) symmetry is assumed, ligand field calculations based on a limited set of basis functions demonstrate that spin triplet states as well as various spin-mixed states may be stabilized in addition [10]. Recently, completely computerized methods have been developed which use the irreducible tensor operators of Racah in several different coupling schemes [11]. These methods may be applied in a straightforward way to any incompletely filled  $p^n$ ,  $d^n$  or  $f^n$  configuration and to any symmetry. On the basis of this method, complete configuration interaction calculations were performed within the  $d^6$  configuration in  $D_{4h}$  and  $D_{3d}$  symmetries both without and with spin-orbit coupling included. A subsequent search program determined the boundaries for the various electronic ground states in

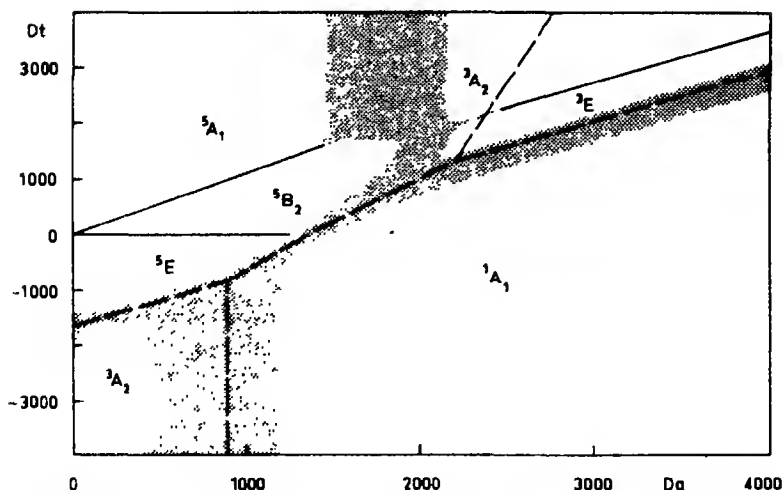


Fig. 1. Ground state boundary regions for the  $d^6$  configuration in  $D_{4h}$  symmetry including complete CI and spin-orbit coupling ( $B = 730 \text{ cm}^{-1}$ ,  $C = 4B$ ,  $\zeta = 420 \text{ cm}^{-1}$ ) assuming  $\kappa = Ds/Dt = 1.0$ . Results of a limited calculation are indicated by broken lines

parameter space. The results have interesting consequences with respect to the effect of high-energy levels in general.

Figure 1 shows the ground states which result from a complete configuration interaction calculation within a space spanned by the parameters [12]  $Dq$  of the parent octahedral ( $O_h$ ) field and  $Dt$  of the tetragonal ( $D_{4h}$ ) field, whereas  $Ds$  has been fixed by the requirement  $\kappa = Ds/Dt = 1.0$ . In addition, the Racah parameters of interelectronic repulsion have been taken as  $B = 730 \text{ cm}^{-1}$  and  $C = 4B$  and the spin-orbit coupling constant  $\zeta = 420 \text{ cm}^{-1}$ . When spin-orbit interaction is taken into account, there may be non-zero contributions of various spin multiplicities to each state in question. In addition to (almost) pure spin singlet, triplet, and quintet ground states, substantially spin-mixed ground states are expected. For the purpose of demonstration, we arbitrarily define a pure spin ground state as one having less than 2% admixture of any other spin multiplicity (blank areas in Fig. 1 separated by full lines) and all other ground states are considered as spin-mixed (shaded areas in Fig. 1). For comparison, the results obtained from a limited basis set calculation comprising the four lowest energy multiplets of the octahedral field, i.e.  $^5T_{2g}(t_{2g}^4 e_g^2)$ ,  $^1A_{1g}(t_{2g}^6)$ ,  $^3T_{1g}(t_{2g}^5 e_g)$  and  $^3T_{2g}(t_{2g}^5 e_g)$ , are shown by a broken line [10]. These states are all which occur up to an energy of at least  $10000 \text{ cm}^{-1}$ . The approximation is reasonable for  $Dt < 0$  and for small positive  $Dt$  in conjunction with reasonably large  $Dq$ . On the other hand, significant differences are clearly evident for large and positive values of both  $Dt$  and  $Dq$ . In particular, a new  $^3A_2$  ground state arises for large  $Dq$  and a new  $^5A_1$  ground state for small  $Dq$ , both at  $Dt > 0$ . A large spin-mixed area separates the two states. Additional differences comprise a broadening of all spin-mixed state areas in the complete CI calculation as compared to the limited calculation including spin-orbit coupling. In addition, the spin-mixed regions are larger in tetragonal symmetry than if the symmetry is  $O_h$ , viz.  $Dt = 0$ .

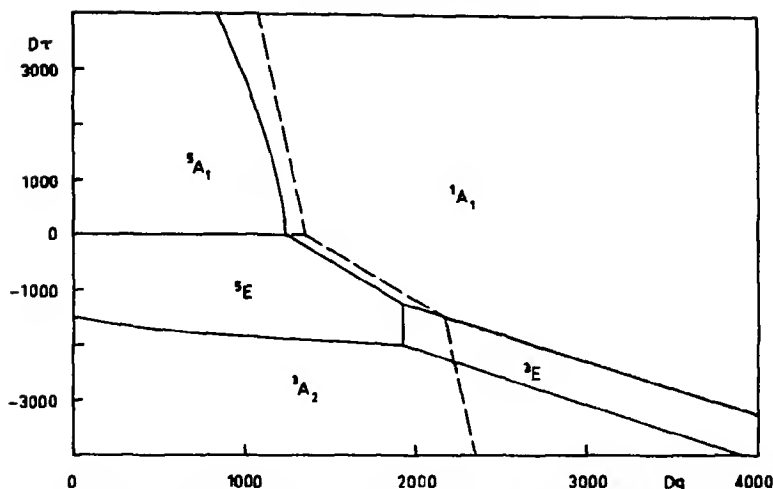


Fig. 2. Ground state boundary regions for the  $d^6$  configuration in  $D_{3d}$  symmetry including complete CI and spin-orbit coupling ( $B = 730 \text{ cm}^{-1}$ ,  $C = 4B$ ,  $\zeta = 420 \text{ cm}^{-1}$ ) assuming  $\kappa = D\sigma/D\tau = 1.0$ . Results of a limited calculation are indicated by broken lines

$Dq \sim 1400 \text{ cm}^{-1}$  in Fig. 1. These areas on both sides of the actual cross-over are important in that various physical properties are determined by the actual distribution of low-lying levels and by their mixing [13].

In a separate study, we investigated the origin of the  $^3A_2$  ground state at high and positive values of  $Dt$  and  $Dq$ . It is well known that, in an  $O_h$  field, altogether seven different excited  $^3T_{1g}$  states exist [14]. All of these states could be parents to the  $^3A_2$  state in question since, in a  $D_{4h}$  field,  $^3T_1 \rightarrow ^3A_2 + ^3E$ , whereas  $^3A_2(O_h) \rightarrow ^3B_1(D_{4h})$ . The investigation shows the  $^3A_2$  state to consist of  $\sim 50\%$  contribution from the parent  $^3T_1[t_2^4(^3T_1)e^2(^1A_1)]$  which is known to occur at an energy  $> 30000 \text{ cm}^{-1}$  and  $\sim 40\%$  contribution from  $^3T_1[t_2^4(^3T_1)e^2(^1E)]$  at an energy  $> 21000 \text{ cm}^{-1}$ . Neither one of the two states can become ground state alone, and no effect of the remaining  $^3A_2(^3T_1)$  states on the ground state is apparent.

Figure 2 shows the ground states resulting from a complete CI calculation within a space spanned by the parameters [12]  $Dq$  of  $O_h$  and  $D\tau$  of trigonal ( $D_{3d}$ ) symmetry in the limit of zero spin-orbit interaction. The parameter  $D\sigma$  is fixed by  $\kappa = D\sigma/D\tau = 1.0$ . Again, the results of a limited basis set calculation employing the same multiplets as above have been indicated by a broken line. It is evident that the approximation is applicable for  $D\tau > 0$  and if  $D\tau$  assumes negative though small values. As in  $D_{4h}$  symmetry, a  $^3A_2$  ground state is formed if  $D\tau < -1500 \text{ cm}^{-1}$  or less. It should be observed that, in  $D_{3d}$  symmetry,  $^3T_1 \rightarrow ^3A_2 + ^3E$ , whereas the  $^3A_2$  is not changed. A detailed study shows that the  $^3A_2$  ground state encountered is composed of  $\sim 70\%$   $^3T_1[t_2^4(^1T_2)e^2(^3A_2)]$  (at  $> 25000 \text{ cm}^{-1}$ ) and  $\sim 20\%$   $^3A_2[t_2^4(^1A_1)e^2(^3A_2)]$  (at  $> 30000 \text{ cm}^{-1}$ ) parents. Additional contributions ( $\sim 5\%$  each) derive from  $^3A_2[t_2^3(^2E)e^3]$  and  $^3T_1[t_2^3(^2T_2)e^3]$ , these states occurring normally at an energy above  $30000$  and  $45000 \text{ cm}^{-1}$ , respectively. For small values of  $Dq$  and  $D\sigma = D\tau < -1500 \text{ cm}^{-1}$ ,

another  ${}^3A_2$  state is formed, its parent being almost exclusively (to  $\sim 95\%$ )  ${}^3T_1(t_2^2e^4)$ . The accurate boundaries between the two  ${}^3A_2$  states were not studied.

Complications similar to those discussed above are encountered if values different from  $\kappa = Ds/Dt = 1.0$  are investigated. Thus, if  $\kappa = 3.0$  and  $D_{4h}$  symmetry are assumed,  ${}^3B_2$ ,  ${}^3A_2$ , and  ${}^3E$  ground states arise for  $Dt > 0$  in the region of the  ${}^3A_2$  and  ${}^3E$  states of Fig. 1. Compared to a limited basis set study, the additional terms  ${}^3A_2$ ,  ${}^3E$ , and  ${}^5A_1$  are formed. If  $\kappa = -3.0$ , the ground state boundaries are similar in both the limited and the complete CI calculation, while the  ${}^3B_2$  state region is replaced by that of the  ${}^3E$  state. Turning our attention to  $D_{3d}$  symmetry and assuming  $\kappa = 3.0$ , the CI calculation differs from the limited study [10] in that an additional region of  ${}^3A_2$  state stabilization is formed for  $D\tau < -1500 \text{ cm}^{-1}$  and  $Dq < 2500 \text{ cm}^{-1}$ . Finally, if  $\kappa = -3.0$ , a  ${}^3E$  ground state arises in the CI treatment for  $D\tau < -1500 \text{ cm}^{-1}$  and  $Dq < 1500 \text{ cm}^{-1}$ , whereas no such state is formed within the limited approach.

In conclusion, limited basis set calculations comprising the low-energy octahedral terms  ${}^5T_2$ ,  ${}^1A_1$ ,  ${}^3T_1$ , and  ${}^3T_2$  reasonably describe the electronic ground state in  $D_{4h}$  and  $D_{3d}$  symmetries close to  $O_h$  within large regions of parameter space ( $Dt$ ,  $Ds$  or  $D\tau$ ,  $D\sigma$  and  $Dq$ ). However, if significant departures from octahedral symmetry are considered, *an incorrect ground state may result*. The possible conclusions concerning the excited states are even more restrictive. Therefore, great caution should be exercised in applications of any limited basis set treatment in ligand field theory.

*Acknowledgements.* The authors appreciate financial support by the Deutsche Forschungsgemeinschaft, the Fonds der Chemischen Industrie, and the Stiftung Volkswagenwerk.

## References

1. Dale, R. W., Williams, R. J. P., Johnson, C. E., Thorp, T. L.: J. Chem. Physics **49**, 3441 (1968).
2. König, E., Madeja, K.: Inorg. Chemistry **7**, 1848 (1968).
3. König, E., Kanellakopoulos, B.: Chem. Physics Letters **12**, 485 (1972).
4. König, E., Ritter, G., Kanellakopoulos, B.: J. chem. Physics **58**, (1973), in press.
5. Bour, J. J., Beurskens, P. T., Steggerda, J. J.: J. chem. Soc. Chem. Commun. **1972**, 221.
6. Birker, P. J. M. W. L., Bour, J. J., Steggerda, J. J.: in press.
7. Grenoble, D. C., Frank, C. W., Barger, C. B., Drickamer, H. G.: J. chem. Physics **55**, 1633 (1971).
8. Trautwein, A., Schretzmann, P.: Proc. Int. Conf. Hyperfine Interactions, Israel 1970.
9. König, E., Kremer, S.: J. phys. Chem. in press.
10. König, E., Schnakig, R.: Inorg. chim. Acta, in the press.
11. König, E., Kremer, S.: To be published.
12. Ballhausen, C. J.: Introduction to ligand field theory. New York: McGraw-Hill, 1962.
13. König, E.: Ber. Bunsenges. Phys. Chem. **76**, 975 (1972).
14. McClure, D. S.: Solid state physics **9**, 399 (1959).

Dr. E. König  
Institut für Physikalische Chemie II  
Universität Erlangen-Nürnberg  
D-8520 Erlangen  
Egerlandstraße 3  
Federal Republic of Germany



## *Commentationes*

# The Use of Average Natural Orbitals for Configuration Interaction Calculations on the Boron Hydride Molecule

S. A. Houlden\* and I. G. Csizmadia\*\*

Department of Chemistry, University of Toronto, Toronto, Ontario, Canada, M5S 1A1

Received July 24, 1972/January 29, 1973

The use of average natural orbitals is compared to some better known methods of performing limited and restricted CI calculations. It is found that a moderately extensive restricted valence shell CI computation using a subset of these orbitals is an efficient and accurate method for the calculation of state wavefunctions. Total and electronic excitation energies have been calculated for the BH molecule.

Die Verwendung von gemittelten natürlichen Orbitalen wird mit einigen besser bekannten Methoden beschränkter CI-Rechnungen verglichen. Man findet, daß eine eingeschränkte Valenzschalen-CI-Rechnung von mäßigem Umfang mit einer Untermenge der genannten Orbitale eine leistungsfähige und genaue Methode zur Berechnung der Wellenfunktion eines Zustandes darstellt. Die Gesamtenergien und elektronische Anregungsenergien wurden für das BH-Molekül berechnet.

**Key words:** Average natural orbitals    Excitation energies of BH

## Introduction

The computation of accurate electron excitation energies can be an expensive task since it usually requires extensive calculations to be repeated for each state of interest. Efficiency is therefore a more important criterion for such calculations than for those in which properties of only one state are determined. This paper illustrates a method which combines accuracy with efficiency and compares the results obtained for BH with those obtained from some well known CI methods.

## Results and Discussion

### *Choice of Atomic Orbitals*

Since most sets of atomic orbitals quoted in the literature have been optimized for ground state wave functions only, our set of orbitals includes additional ones chosen for the more diffuse excited states. The core of this set of atomic orbitals for BH is a so-called "double zeta" set of contracted gaussian orbitals. These orbitals (Boron  $s_1, s_2, s_3, s_4, p_1, p_2$  and Hydrogen  $s_1$  plus the first gaussian orbital of  $s_2$ , shown in Table 1) are taken from published works.

\* Taken in part from a Ph. D. thesis submitted to the University of Toronto in 1971.

\*\* Person to whom correspondence should be addressed.

Table 1 Contracted gaussian function basis set for BH

Atom	Type	Exponent	Coefficient
Boron	s <sub>1</sub>	10411.559	0.00602874
		1576.1919	0.03414955
		361.66537	0.21343952
		98.726437	0.81532002
	s <sub>2</sub>	31.781408	0.14008659
		10.842225	0.32796748
		4.9774725	0.43910393
		1.5888265	0.21500160
	s <sub>3</sub>	2.8590772	0.10128056
		0.35556953	0.50247350
		0.14972248	0.56801575
	s <sub>4</sub>	0.07433206	0.91758759
		0.03701718	0.08939910
	s <sub>5</sub>	0.1	1.0
	s <sub>6</sub>	0.0556	0.82613835
		0.0185	0.20653459
	p <sub>1</sub>	26.8281	0.00918291
		5.81572	0.06903735
	p <sub>2</sub>	1.63092	0.29193173
		0.54881	0.74403225
		0.204009	0.61097738
		0.0822550	0.40114602
		0.0356435	0.06767884
	p <sub>3</sub>	0.2415	1.0
Hydrogen	s <sub>1</sub>	19.24060	0.32828011
		2.89915	0.23120807
		0.65341	0.81723826
	s <sub>2</sub>	0.17758	0.92065144
		0.05	0.10229460
	s <sub>3</sub>	0.1	1.0
	p <sub>1</sub>	0.5	1.0

The orbitals centred on the Boron nucleus are those of Huzinaga [1] while those on Hydrogen are from Basch *et al.* [2].

These orbitals are augmented with orbitals which increase electron density in the bonding region of the molecule rather than with orbitals optimized for improved ground state energy. This latter approach invariably leads to orbitals highly localized on the atomic nucleus; i.e. to better representation of the Boron 1s cusp. The maximum density of the radial part of a gaussian orbital is related to the value of the exponent,  $\alpha$ , by the relationship

$$\alpha = \frac{n-1}{2r^2}$$

For an s-type gaussian orbital ( $n=1$ ) the maximum is always at  $r=0$  and so exponents were selected which came between those of the two most diffuse orbitals in the double zeta set. For p-type gaussian orbitals ( $n=2$ ) on Boron the value of  $r$  in the above expression was set at the position of the second maximum of the numerical Hartree-Fock 2s orbital [3]. This value ( $r=1.439$  bohr) yields an ex-

ponent of 0.2415. An exponent of 0.5 was arbitrarily chosen for the  $p$ -type gaussian orbital on H atom which places the maximum density at  $r = 1$  bohr from the H nucleus or slightly less than the mid-point of the BH axis. The full set of atomic orbitals used consists of 21 contracted gaussian orbitals; 6  $s$ -type and 3 sets of  $p$ -type orbitals on Boron and 3  $s$ -type and 1 set of  $p$ -type orbitals on Hydrogen (Table 1).

### SCF Calculations

An SCF calculation was performed on BH using the above set of atomic orbitals for a nuclear separation of 2.3291 bohr. This calculation may be compared with two published ones. Cade and Huo [4] using a large set of Slater orbitals obtained an energy of  $-25.1314$  hartree. This energy is taken to be the Hartree-Fock limit for BH. Kaufman and Burnelle [5] using a large set of gaussian orbitals obtained  $-25.1298$  hartree. In spite of the fact that the augmenting orbitals used in this work were not chosen on an energy lowering criterion, quite a good energy is obtained. This energy,  $-25.1196$  hartree, is only 0.0118 hartree above the Hartree-Fock limit.

Just as the ground state wavefunction may be approximated by a single configuration, the excited state wavefunctions may be also. These configurations are constructed by replacing one of the occupied orbitals in the SCF ground state wavefunction with one of the virtual orbitals. First, however, it must be pointed out that since BH belongs to the  $C_{\infty v}$  space point group, the SCF ground state wavefunction has the form

$$\sigma_1(1) \sigma_1(2) \sigma_2(3) \sigma_2(4) \sigma_3(5) \sigma_3(6)$$

(where  $\sigma_1$  is an orbital which transforms according to the  $\Sigma^+$  irreducible representation). The SCF calculation involves only atomic orbitals of  $\sigma$  symmetry and so results in SCF orbitals of  $\sigma$  symmetry only. Orbitals of  $\pi$  symmetry were formed by symmetrically orthonormalizing [6] atomic orbitals of  $\pi$  symmetry. Thus the  $A^1\pi$  single configuration wavefunction formed by replacing one of the  $\sigma$  orbitals by a  $\pi$  virtual orbital which is an orthonormalized symmetry adapted orbital is too poor to be used for the calculation of transition energy.

The  $B^1\Sigma^+ \leftarrow X^1\Sigma^+$  transition energy is calculated to be 0.246 hartree compared to an experimental value of 0.238 hartree [7]. The observed  $C^1\Sigma^+$  state wavefunction cannot be approximated by the virtual orbital technique since it has no single principle configuration but rather a combination of two configurations involving double substitutions by orbitals of  $\pi$  symmetry.

### CI Calculations

All CI calculations were performed by making substitutions for the orbitals of the valence electrons only. We are calling this a *valence shell* CI. The calculation is a *full* valence shell CI when all possible substitutions of the valence orbitals by all combinations of virtual orbitals are included in the wavefunction. We refer to a full *double* valence shell CI when only the configurations formed by single and double replacements of the four valence orbitals are included in

the wavefunction. The term *restricted* valence shell CI refers to a calculation where all possible substitutions of the valence orbitals are made from a subset of the virtual orbitals. Finally a *limited* valence shell CI is one in which a subset of the configurations of a full valence shell CI are used. (The full double valence shell CI and the restricted valence shell CI are particular examples of a limited valence shell CI).

The partitioning of the CI calculation into *core* and *valence shell* is after Miller and Ruedenberg [8] and is based on the postulate that the core electrons are relatively unaffected by the molecular environment. The core correlation energy can therefore be treated as a constant quantity and attention confined to the valence electrons only. They calculate the total correlation energy and the core correlation energy of BH to be 0.152 hartree and 0.039 hartree respectively, leaving a valence shell correlation energy of 0.113 hartree.

### *Full Double Valence Shell CI Calculations*

A full double valence shell CI calculation was performed for each of the five lowest singlet electronic states of BH at a separation of 2.3291 bohr. The  $^1\Sigma^+$  wavefunctions included 253 configurations while the  $^1\Pi$  wavefunction included 376 configurations. Only the  $X^1\Sigma^+$  and the  $A^1\Pi$  states are represented accurately since higher state wavefunctions have important terms which involve higher than double replacement. The energies obtained were  $-25.1706$  hartree and  $-25.0503$  hartree respectively, yielding a transition energy of 0.1202 hartree (experimental, 0.105 hartree [7]). The ground state energy represents an improvement of 0.0510 hartree over the SCF result. This corresponds to a recovery of 45% of the valence shell correlation energy.

These wavefunctions cannot be improved simply by performing a full valence shell CI calculation since this would involve 3526  $^1\Sigma^+$  and 3410  $^1\Pi$  configurations. A working maximum for the present computer program is 2500 configurations; hence we turned our attention to several forms of restricted and limited valence shell CI methods.

### *Restricted Valence Shell CI Calculations*

The first attempt was to restrict the substituting orbitals to a subset of the virtual orbitals choosing those with lowest orbital energy<sup>1</sup>. This subset included 5 virtual orbitals of  $\sigma$  symmetry and 4 of  $\pi$  symmetry. The ground state wavefunction includes 622 configurations and yields an energy of  $-25.1443$  hartree. This corresponds to a lowering of only 0.0247 hartree or 22% of the valence shell correlation energy. In addition, a similar calculation for the  $A^1\Pi$  state (588 configurations) leads to a predicted  $A^1\Pi \leftarrow X^1\Sigma^+$  transition energy of 0.210 hartree!

<sup>1</sup> Strictly speaking the term "orbital energy" applies only to the SCF orbitals. In the case of the orthonormalized symmetry orbitals, the value calculated in the same manner as an orbital energy is used; i.e. the term orbital energy is used for the diagonal Lagrangian multiplier of any orbital when substituted into the SCF equation. This is reasonable in the sense that increasing orbital energies are obtained as the number of nodes in the orbital increases, as found for SCF orbitals.

It is obvious that this is an extremely poor method of extending a calculation. This conclusion is extremely relevant considering that restriction of substituting orbitals in this way is a relatively common practice.

### Limited Valence Shell CI Calculations

The next procedures that were considered limit the configurations rather than restricting the orbitals. In the first case, the sums of the orbital energies of the orbitals in each configuration were listed and those with the lowest sums selected. It is felt that this is justified on the grounds that this would rank the configurations in a similar manner to total energy.

Two limited valence shell CI calculations were made, one for the  $X^1\Sigma^+$  state and one for the  $A^1\Pi$  state, both at 2.3291 bohr and both limited to 2000 configurations. The energies obtained were  $-25.1828$  hartree and  $-25.0700$  hartree respectively. The  $A^1\Pi \leftarrow X^1\Sigma^+$  transition energy is predicted almost exactly equal to experimental while the ground state energy represents a lowering of  $0.0632$  hartree or  $56\%$  of the valence shell correlation energy.

Since this size of calculation is unsuitable for a series of calculations, the number of configurations was further limited to 700 by the same method and new calculations performed. The ground state energy,  $-25.1765$  hartree, is only slightly below that for the full double valence shell CI calculation. The transition energy between the two states,  $0.1215$  hartree, is also similar to the full double valence shell CI calculation. This demonstrates the limitation of this simple procedure.

The use of Perturbation Theory for limiting configurations has already been described [9]. This theory was applied to the two sets of 2000 configurations discussed above in order to limit the wavefunctions to the most significant 748  $^1\Sigma^+$

Table 2. Molecular state energies of BH

Calculation	Energy (hartree)		
	$X^1\Sigma^+$	$A^1\Pi$	$\Delta E$
Full double valence shell CI <sup>a</sup>	$-25.1706$	$-25.0503$	$0.1202$
Restricted valence shell CI <sup>b</sup>	$-25.1443$	$-24.9341$	$0.2102$
Limited valence shell <sup>c</sup>			
A	$-25.1828$	$-25.0700$	$0.1127$
B	$-25.1765$	$-25.0549$	$0.1215$
C	$-25.1824$	$-25.0695$	$0.1128$
Experimental transition energy [7]			$0.105$

<sup>a</sup> 253  $^1\Sigma^+$  and 376  $^1\Pi$  configurations.

<sup>b</sup> Basis orbitals restricted to 12 virtual orbitals with lowest orbital energy; 622  $^1\Sigma^+$  and 588  $^1\Pi$  configurations.

<sup>c</sup> Full valence shell CI restricted as follows:

A. 2000 configurations of each symmetry selected on sum of orbital energies of orbitals in each configuration.

B. 700 configurations selected as for A.

C. 748  $^1\Sigma^+$  and 740  $^1\Pi$  configurations selected by perturbation theory.

and 740  $^1H$  configurations. The energies obtained,  $-25.1824$  hartree and  $-25.0695$  hartree for the  $X^1\Sigma^+$  and  $A^1H$  states respectively, are virtually identical to the calculations with 2000 configurations. This is a significant demonstration of the applicability of perturbation theory for this type of problem.

The various energies obtained in the above calculations are summarized in Table 2.

### Natural Orbital Calculations

The full double valence shell CI wavefunctions discussed above were analyzed in terms of their natural orbitals. When the NO are put in order of increasing occupation number, the first twelve include 8 of  $\sigma$  and 4 of  $\pi$  symmetry as for the 12 orbitals ranked by orbital energy previously. These 12 NO were selected for restricted valence shell CI calculations. The results of these calculations as given in columns 1 and 3 of Table 3, are essentially the same as for the 2000 configuration calculation described above. In fact, the slight difference in the  $A^1H$  energy is such that the transition energy agrees better with the experimental value. The calculations involved 622  $^1\Sigma^+$  and 588  $^1H$  configurations respectively.

Table 3. Total and transition energies<sup>a</sup> for states of BII calculated with NO and ANO<sup>b</sup>

Quantity	$X^1\Sigma^+(\text{NO})$	$X^1\Sigma^+(\text{ANO})$	$A^1H(\text{NO})$	$A^1H(\text{ANO})$	$B^1\Sigma^+(\text{ANO})$	$C^1\Sigma^+(\text{ANO})$
Total energy	-25.1827	-25.1802	-25.0710	-24.9534	-24.9600	-24.917
Transition energy	—	—	0.1083	0.2268	0.2203	0.261
Experimental transition energy [11]			0.105	0.211	0.238	0.257

<sup>a</sup> In hartree

<sup>b</sup> Restricted valence shell CI using 12 NO or ANO from full double valence shell CI wavefunctions. The N ANO with highest occupancy numbers were chosen resulting in 622  $^1\Sigma^+$  and 588  $^1H$  configurations.

### Average Natural Orbital Calculations

The use of NO also requires separate calculations to be performed for each state of interest. Therefore, in order to look at values predicted for several states, the use of average natural orbitals (ANO) was investigated. The ANO are calculated in the same manner as NO except that the one particle density matrices of the wavefunctions in question are first averaged and then the resultant matrix is diagonalized.

Each state has a one particle density matrix  $P_i^{(0)}$  which may be diagonalized to give the NO  $\{\chi^i\}$ :

$$\begin{array}{ccccccc}
 P_1^{(0)} & P_1^{(1)} & P_1^{(2)} & \dots & P_1^{(n)} \\
 \downarrow & \downarrow & \downarrow & & \downarrow \\
 \{\chi^0\} & \{\chi^1\} & \{\chi^2\} & \dots & \{\chi^n\}
 \end{array}$$

Each set of NO  $\{\chi^i\}$  is an orthonormal set but the sets are not orthogonal to each other. Since the individual density matrices,  $P_1^{(i)}$  are all hermitian, their average  $P_1^A$ , where

$$P_1^A = \frac{P_1^{(0)} + P_1^{(1)} + P_1^{(2)} \dots P_1^{(n)}}{n+1}$$

must also be hermitian and can be diagonalized. The diagonalization of  $P_1^A$  yields  $\{\bar{\chi}\}$  the "average" NO or ANO.

The ANO resulting from the averaged density matrix of the full double valence shell CI wavefunctions of each of five singlet states of BH (three  $^1\Sigma^+$  and two components of the  $C^1\Delta$  state) were formed. The restricted valence shell CI calculation using the 12 ANO with highest occupation numbers was then performed. These 12 ANO also include eight of  $\sigma$  and four of  $\pi$  symmetry and so yield 622 configurations of  $^1\Sigma$  symmetry and 588 of  $^1\Pi$  symmetry. The wavefunctions for five states together with total energy were obtained from this calculation. These results are included in columns 2, 4, 5 and 6 of Table 3. The ground state energy is only 0.0025 hartree higher than from the NO calculation indicating that the loss in absolute accuracy is very slight. The electronic transition energies are all close to experimental values. The energies of the  $C^1\Delta$  and  $B^1\Sigma^+$  are calculated very close together and occur intermediate to the experimental values for the two states. More extensive calculations, to be published separately, have indicated that the reason for this is that configurations involving substitutions by orbitals of  $\delta$  symmetry are important for accurate representation of these two states. There were no orbitals of this symmetry resulting from our atomic orbital basis.

### Conclusion

The use of a subset of ANO formed by averaging the density matrices of a set wavefunctions resulting from intermediate calculations (in this case limiting the configuration to double substitutions) as basis orbitals for a more extensive calculation (restricted valence shell CI) yielding several state wavefunctions at one time has been found to yield results comparable in accuracy other sophisticated CI procedures. The intrinsic efficiency of this method, however, suggests that it is more suitable for the calculations of multiple state wavefunction of molecules.

*Acknowledgements.* The financial support of the National Research Council of Canada are gratefully acknowledged. One of us (SAH) would like to thank the Province of Ontario and the National Research Council of Canada for Graduate Fellowships

### References

1. Huzinaga, S., Sakai, Y.: J. Chem. Physics **50**, 1371 (1969).
2. Basch, H., Robin, M. B., Kuebler, N. A.: J. chem. Physics **47**, 1201 (1967).
3. Herman, F., Skillman, S.: Atomic structure calculation. Englewood Cliffs N.J.: Prentice-Hall Inc. 1963.

4. Cade, P.E., Huo, W.M.: *J. chem. Physics* **47**, 614 (1967).
5. Kaufman, J.J., Burnelle, T.A.: RIAS Technical report **1967**, 65.
6. Löwdin, P.O.: *J. chem. Physics* **18**, 365 (1950)
7. Johns, J.W.C., Crum, F.A., Porter, R.F.: *J. molecular Spectroscopy* **22**, 435 (1967).
8. Miller, K.J., Ruedenberg, K.: *J. chem. Physics* **48**, 34, 4 (1968).
9. Gershgorin, Z., Shavitt, I.: *Int. J. quant. Chemistry* **2**, 751 (1968).
10. Löwdin, P.O.: *Physic. Rev.* **97**, 1474 (1955).

• Dr. J. G. Csizmadia  
Associate Professor  
Lash Miller Chemical Laboratories  
80 St. George Street  
Toronto M5A 1I1, Canada



# Non Radiative Transition Probabilities in the Statistical Limit

Abraham Nitzan and Joshua Jortner

Department of Chemistry, Tel-Aviv University, Tel-Aviv, Israel

Received October 20, 1972

In this paper we derive a general computational scheme for the calculation of the non radiative decay probability of a polyatomic molecule in the statistical limit. Within the framework of the Harmonic Approximation the relaxation rate of any polyatomic molecule can be expressed in terms of an infinite sum where each term consists of a medium distribution function and an intramolecular term. In the statistical limit the medium induced vibrational relaxation widths do not affect the non radiative decay characteristics. Numerical calculations are reported for the  $T_1 \rightarrow S_0$  intersystem crossing in the benzene molecule.

**Key words:** Radiationless transitions    Electronic relaxation    Energy transfer

## 1. Introduction

This paper is concerned with some features of the electronic relaxation of a large molecule in a dense inert medium. Adopting the definition of the inert medium presented in previous work [1, 2] the non radiative decay characteristics of a statistical large molecule can be affected by the medium as follows:

- (a) The medium may provide accepting modes for the electronic relaxation.
- (b) The medium provides a mechanism for vibrational relaxation in the final intramolecular quasicontinuum.
- (c) The medium provides a loss mechanism for vibrational relaxation in the initial electronic manifold.

The coupling between electronic and vibrational relaxation in large molecules has been recently considered by us [3]. We were able to demonstrate that when the vibrational relaxation is slow relative to electronic relaxation (as is the case for some ultrafast processes) the non radiative decay involves the initially excited level, while in the limit of fast vibrational relaxation a Boltzman averaged (over the initial states) non radiative transition probability is obtained. Thus the implications of the vibrational relaxation in the initial electronic manifold [effect (C)] were elucidated. It was pointed out [1, 4] (but not proved) that vibrational relaxation in the final electronic manifold of a statistical molecule is unaffected by vibrational relaxation in the final manifold.

The purpose of this paper is twofold:

- (a) From the point of view of general methodology we shall demonstrate that for a molecule which corresponds to the statistical limit the vibrational relaxation in the final vibronic manifold does not affect the non radiative decay characteristics, and does not modify the expressions previously derived [1] which did not include this effect.

(b) From the technical point of view we shall provide a computational scheme for the evaluation of the non radiative decay probability of a statistical molecule by the generating functions method. This method was briefly outlined and applied by us [5]. In view of recent criticism of our approach [6] we would like to provide a complete justification for this technique.

## 2. Non Radiative Decay Probability

We shall consider the model two electronic level system previously described [1] and invoke the following simplifying assumptions: (a) The medium does not provide accepting modes, and its effect can be subsumed to add a vibrational relaxation width  $\Gamma$  so that the generating function is modified by an exponential damping term [2]. Thus we consider the decay of a zero phonon molecular line. This restriction will be relaxed in Section 3. (b) We consider the fast vibrational relaxation limit whereupon in the low temperature limit the non radiative decay probability corresponds to the relaxation of the vibrationless level in the initial electronic manifold.

The non radiative decay probability of a molecule in a Shpolskii matrix can be expressed in the form

$$W_{\nu\nu} = \frac{1}{2\hbar^2} \sum_{\kappa} |C_{\nu}^{\kappa}|^2 I_{\kappa} \quad (2.1)$$

where  $C_{\nu}^{\kappa}$  is the electronic coupling matrix element between the two electronic states induced by the promoting mode  $\kappa$ . In the Harmonic molecular model the vibrational integral  $I_{\kappa}$  is determined [1, 5, 7, 8] in terms of a Fourier transform of a function  $F(\beta_{\mu}, A_{\mu}, \exp(i\omega_{\mu}t))$  of the molecular frequencies  $\omega_{\mu}$ , the origin displacements of the normal modes  $A_{\mu}$  and the frequency ratios  $\beta_{\mu}$  between the two electronic states

$$I_{\kappa} = \int_{-\infty}^{\infty} dt \exp[-i\Delta E_{\kappa}t/\hbar - \Gamma|t|/2\hbar] F(\beta_{\mu}, A_{\mu}, \exp(i\omega_{\mu}t)) \quad (2.2)$$

where  $\Delta E_{\kappa} = AE - \hbar\omega_{\kappa}$  is the effective energy gap and where  $\Gamma$  is the (average) width of the level in the quasicontinuum manifold [2]. In the simple model of displaced identical energy surfaces

$$F(\beta_{\mu}, A_{\mu}, \exp(i\omega_{\mu}t)) = \exp\left(-\frac{1}{2} \sum_{\mu} A_{\mu}^2\right) \exp\left[\frac{1}{2} \sum_{\mu} A_{\mu}^2 \exp(i\omega_{\mu}t)\right] \quad (2.3)$$

while in the case of displaced potential surfaces involving frequency changes

$$\begin{aligned} F = & \left[ \prod_{\mu} (\beta_{\mu})^{-1} \right] \left\{ 1 + \frac{(1-\beta_{\kappa})^2}{4\beta_{\kappa}} [1 - \exp(2i\omega_{\kappa}t)] \right\}^{-1} \\ & \times \prod_{\mu} \left\{ 1 + \frac{(1-\beta_{\mu})^2}{4\beta_{\mu}} [1 - \exp(2i\omega_{\mu}t)] \right\}^{-1} \\ & \times \exp \left\{ - \sum_{\mu} \frac{\beta_{\mu} A_{\mu}^2 [1 - \exp(i\omega_{\mu}t)]}{1 + \beta_{\mu} + (\beta_{\mu} - 1) \exp(i\omega_{\mu}t)} \right\}. \end{aligned} \quad (2.4)$$

The mathematical problem is thus reduced to the evaluation of the integrals  $I_k$ . Several attempts have been reported to perform these integrations by the saddle point method [1-7] (assuming that  $\Delta E$  is sufficiently large). This procedure is valid for the statistical limit only in the case of displaced identical potential surfaces. When frequency changes as well as unharmonicity are included it was found necessary to perform a power expansion in the exponential function of (2.4), in order to apply the saddle point integration [1, 7-9]. It can be demonstrated (see Appendix A) that this expansion method, retaining low order terms is unjustified. This conclusion was also supported by numerical calculations performed by us. Thus when more complicated (and more realistic) physical models are introduced the saddle point method is inapplicable. Furthermore, the saddle point method cannot be applied when the exponential damping term  $\exp(-\Gamma|t|)$  is present in the Fourier integral (2.2). Thus we conclude that alternative numerical procedures are required for the evaluation of the non radiative decay probability.

We shall now introduce a normalizing frequency,  $\omega_N$ , so that the numbers

$$\tilde{\omega}_\mu = \omega_\mu / \omega_N \quad (2.5)$$

are integers for all  $\mu$ . It should be noted that the definition of  $\omega_N$  is not unique. In particular it is important to notice that for the set  $\{\omega_\mu\}$  (expressed as integers in arbitrary units and given for any available experimental accuracy) we can define the largest common integer divider  $\omega_N^{\max}$ . We shall also define the reduced quantities

$$\epsilon_\kappa = \Delta E_\kappa / \hbar \omega_N \quad (2.6)$$

$$\gamma = \Gamma / \hbar \omega_N \quad (2.7)$$

and

$$x = \omega_N t. \quad (2.8)$$

Eq. (2.2) may be recast in the form

$$I_\kappa = \frac{1}{\omega_N} \int_{-\infty}^{\infty} dx \exp(-i\epsilon_\kappa x - \gamma|x|/2) F(\beta_\mu, A_\mu, \exp(i\tilde{\omega}_\mu x)). \quad (2.9)$$

Making use of the relation

$$\exp(-\gamma|x|/2) = \frac{1}{2\pi} \int_{-\infty}^{\infty} dy \exp(-iyx) \frac{\gamma}{y^2 + (\gamma/2)^2}. \quad (2.10)$$

Eq. (2.9) may be rewritten in the form

$$I_\kappa = \frac{1}{2\pi\omega_N} \int_{-\infty}^{\infty} dy \frac{\gamma}{y^2 + (\gamma/2)^2} \int_{-\infty}^{\infty} dx \exp[-i(\epsilon_\kappa + y)x] F(\beta_\mu, A_\mu, e^{i\tilde{\omega}_\mu x}). \quad (2.11)$$

As the numbers  $\tilde{\omega}_\mu$  are integers it is easy to perform the integration over  $x$ , which yields (Appendix B)

$$\frac{1}{\omega_N} \int_{-\infty}^{\infty} dx \exp[-i(\epsilon_\kappa + y)x] F(\beta_\mu, A_\mu, \exp(i\tilde{\omega}_\mu x)) = I_0(\epsilon_\kappa + y) \sum_{s=-\infty}^{\infty} \delta(\epsilon_\kappa + y - s) \quad (2.12)$$

where

$$I_0(z) = \frac{1}{\omega_N} \int_0^{2\pi} dx \exp(-izx) F(\beta_\mu, A_\mu, \exp(i\tilde{\omega}_\mu x)). \quad (2.13)$$

Inserting Eqs. (2.12) and (2.13) into Eq. (2.11) and performing integration over  $y$  we obtain

$$I_x = \frac{1}{2\pi} \sum_{s=-x}^x I_0(s) \frac{\gamma}{(\epsilon_x - s)^2 + (\gamma/2)^2}. \quad (2.14)$$

Thus the non radiative decay probability of a zero phonon line can be expressed in terms of the infinite sum (2.14) where each term involves a medium induced Lorentzian distribution and a (finite) integral of the intramolecular generating function. This result is general, being valid both for the statistical limit and for the small molecule case.

### 3. The Statistical Limit

Within the framework of the present theoretical scheme the statistical limit is characterized by the inequality

$$I' \gg \omega_N^{\max} \quad (3.1)$$

where  $\omega_N^{\max}$  is the largest common integer divider of the frequencies. Eq. (3.1) is equivalent<sup>1</sup> to the more physically transparent inequality

$$I' \gg \varrho^{-1} \quad (3.2)$$

in which  $\varrho$  is the density of non-degenerate levels in the final manifold. The last inequality is easily recognized to be the condition for the smoothness of the non-radiative line-shape function (with  $I_1 = I'$ ) which is the Freed-Jortner definition [4] of the statistical limit.

If  $\Delta E \gg I'$  which is always the case we now have

$$\epsilon_x \gg \gamma \gg 1. \quad (3.3)$$

Eq. (3.3) implies that the summation in Eq. (2.14) may be replaced by an integration, so that

$$I_x = \frac{1}{2\pi} \int_{-\infty}^{\infty} ds I_0(s) \frac{\gamma}{(\epsilon_x - s)^2 + (\gamma/2)^2}. \quad (3.4)$$

Now, if  $I_0(s)$  does not change appreciably within the Lorentzian width  $\gamma$  we may take it outside the integral at the point  $s = \epsilon_x$ , getting just  $I_x = I_0(\epsilon_x)$ . The condition for the slow variation of  $I_0(\epsilon_x)$  is

$$\left( \frac{1}{I_0} \frac{dI_0}{ds} \right)_{s=\epsilon_x} \gamma \ll 1. \quad (3.5)$$

<sup>1</sup> Provided that the energy gap  $\Delta E$  is large enough. (The necessary condition may be shown to be  $\Delta E/\hbar\omega_M \gg \omega_M/\bar{\Delta\omega}$  where  $\omega_M$  is the largest molecular frequency and  $\bar{\Delta\omega}$  is the average difference between the molecular frequencies.)

For the sake of an order of magnitude estimate we invoke the approximate result of Engleman, Freed and Jortner [1] for  $I_0$

$$I_0(\epsilon_x) \propto \exp(-\epsilon_x/\hbar\tilde{\omega}_M) \quad (3.6)$$

where  $\tilde{\omega}_M$  is the totally symmetric mode of maximum frequency, the condition (3.5) leads to

$$\Gamma/\hbar\omega_M \ll 1. \quad (3.7)$$

It may thus be concluded that under the conditions [Eqs. (3.3) and (3.5)]

$$\hbar\omega_N^{\max} \ll \Gamma \ll \hbar\omega_M \ll \Delta E \quad (3.8)$$

the non-radiative decay rate of an excited electronic state in the statistical limit may be computed by expressing the integral (2.2) in the form

$$I_x = I_0(\epsilon_x) = \frac{1}{\omega_N} \int_0^{2\pi} dx \exp(-i\epsilon_x x) F(\beta_\mu, \Delta_\mu, \exp(i\tilde{\omega}_\mu x)). \quad (3.9)$$

It is important to notice that Eq. (3.9) clearly demonstrates that the non-radiative decay rate in the statistical limit is independent of the width  $\Gamma$  of the levels in the dissipative  $\{|j\rangle\}$  intramolecular manifold. Such assumption has been silently invoked in many previous works which dealt with non-radiative transitions in large molecules embedded in an inert medium [1, 5-9].

So far we have been focusing attention on the non-radiative decay of a zero phonon line of a statistical molecule in a matrix. Our conclusion concerning the independence of the non-radiative decay rate on the vibrational relaxation width pertains only to a large molecule in a Shpolskii matrix. We have stated in Section 1 that direct coupling to medium modes is of minor importance in the statistical limit, where the decay rate is dominated by the larger molecular frequencies [1]. This argument may be presented in a more quantitative manner by considering the decay rate of an initial  $|sim_s\rangle$  level (where  $i$  and  $m_s$  denote molecular vibrational state and medium vibrational state, respectively). We assume that the medium provides only promoting modes, so that the non-radiative decay probability is now

$$W_{sim_s} = \frac{1}{2\hbar^2} \sum_x |C_{si}^x|^2 \sum_{j, m_l} |V_{sim_s, ljm_l}|^2 \times \delta(\Delta E_x + E_i - E_j + E_{m_s} - E_{m_l}) \quad (3.10)$$

where  $E_i$  and  $E_j$  are the vibrational energies of the molecule in the  $s$  and in the  $l$  electronic states, respectively, while  $E_{m_s}$  and  $E_{m_l}$  denote medium vibrational energies.  $|V_{sim_s, ljm_l}|^2$  is the appropriate Franck Condon (FC) factor which may be factorized into a product of a molecular (FC) factor and a medium (FC) factor.

$$|V_{sim_s, ljm_l}|^2 = |V_{si, lj}|^2 |V_{m_s, m_l}|^2. \quad (3.11)$$

Eq. (3.10) may now be recast a convolution

$$W_{sim_s} = \frac{1}{2\hbar^2} \sum_x |C_{si}^x|^2 \int dE F(\Delta E_x - E) G(E). \quad (3.12)$$

The functions  $F(E)$  and  $G(E)$  are easily recognized as the vibronic line-shape functions which correspond to the intramolecular and the medium modes, respectively.

$$F(\Delta E_x - E) = \sum_j |V_{si, tj}|^2 \delta(\Delta E_x - E + E_i - E_j) \quad (3.13a)$$

$$G(E) = \sum_{m_l} |V_{m_s, m_l}|^2 \delta(E + E_{m_s} - E_{m_l}). \quad (3.13b)$$

In a Shpolskii matrix  $G(E) = \delta(E)$  and we regain the former result (Section 2). Now, also in a non-Shpolskii matrix and even in the strong medium-molecule coupling limit [2]  $G(E)$  is a narrow function of  $E$  around  $E=0$  relative to  $F(E)$ . The characteristic width of  $G(E)$  is about  $< 1000 \text{ cm}^{-1}$  while  $F(E)$  is nearly constant (around  $E = \Delta E_x$ ) within this range. We thus may take  $F(\Delta E_x - E)$  out of the integral in Eq. (3.12) at the point  $E=0$ , obtaining

$$W_{si, m_s} = W_{si} \sum_{m_l} |V_{m_s, m_l}|^2 = W_{si} \sum_{m_l} |\langle m_s | m_l \rangle|^2 = W_{si}, \quad (3.14)$$

where  $W_{si}$  is the decay rate of the vibronic level  $si$  in a Shpolskii matrix, or rather in an isolated molecule.

We have thus demonstrated that a direct coupling to the medium degrees of freedom does not modify the decay rate of a statistical molecule.

#### 4. Numerical Procedures

We proceed to discuss some mathematical manipulations of the non-radiative decay rate, which in the statistical limit can be expressed in terms of the integral (3.9). When the functional form of  $F(\beta_\mu, A_\mu, e^{i\tilde{\omega}_\mu t})$  allows the application of the saddle point method, Eq. (3.9) provides the mathematical justification for taking the contribution of only one saddle point of the integrand in Eq. (2.2) or (2.9) (where  $I' = 0$ ). To exhibit the difficulty encountered in the original approach we may consider the zero temperature limit of the non-radiative decay rate in the displaced potential surfaces model, where Eq. (2.9) takes the form [neglecting the factor  $\exp(-\gamma|x|/2)$ ]

$$I_x = \frac{1}{\omega_N} \int_{-\infty}^{\infty} dx \exp \left[ -i v_x x + \sum_\mu \frac{1}{2} A_\mu^2 \exp(i\tilde{\omega}_\mu x) \right] \quad (4.1)$$

where now  $v_x = (1E - \hbar\omega_N)/\hbar\omega_N$ . The saddle point approximation up to first order yields

$$\int \exp(zf(x)) dx = \sum_n \exp(zf(x_n)) \left[ \frac{2\pi}{-zf''(x_n)} \right]^{1/2} \quad (4.2)$$

where  $f(x)$  is an oscillating function of  $z \gg 1$  and where  $x_n$  are the saddle points of  $f(x)$ . In Eq. (4.1) we have

$$z = v_x; \quad f(x) = -ix + \frac{1}{\omega_N} \sum_\mu \frac{1}{2} A_\mu^2 \exp(i\tilde{\omega}_\mu x) \quad (4.3)$$

so that the equation for the saddle points is [1]

$$\frac{1}{2} \sum_{\mu} A_{\mu}^2 \tilde{\omega}_N \exp(i \tilde{\omega}_{\mu} x) = \varepsilon_x. \quad (4.4)$$

Provided that  $x_0$  is a solution of Eq. (4.4) then every  $x_n$  which satisfies

$$x_n = x_0 + 2\pi n; \quad n = 0, \pm 1, \pm 2, \dots \quad (4.5)$$

is also a solution of this equation. If the normalizing frequency  $\omega_N$  will be taken as the largest possible one,  $\omega_N^{\max}$ , then Eq. (4.5) spans all the solutions of Eq. (4.4). Any interval of the length  $2\pi$  on the real  $x$  axis corresponds to one and only one solution  $x_n$  whose real part lies in this interval. The solution which corresponds, say, to the interval  $(0, 2\pi)$  was obtained by Freed and Jortner [1]. Denoting this solution by  $x_0$  and its contribution to the sum in Eq. (4.2) by  $I_0(\varepsilon_x)$ , it is easy to show that

$$I_x = I_0(\varepsilon_x) \sum_{n=-\infty}^{\infty} \exp(-2\pi i n \varepsilon_x) = I_0(\varepsilon_x) \sum_{s=-\infty}^{\infty} \delta(\varepsilon_x - s) \quad (4.5)$$

which is equivalent to Eq. (2.12). The justification to replacing Eq. (4.5) by the equality  $I = I_0(\varepsilon_x)$  is provided by Eqs. (3.1-3.9).

Eq. (3.9) constitutes a convenient starting point for numerical computation of the non-radiative decay probability. It is easy to see that as  $\varepsilon_x$  in Eq. (3.9) is an integer (as energy conservation is expected<sup>2</sup>), Eq. (3.9) is independent of the chosen normalizing frequency  $\omega_N$ . This fact suggests the following approximate numerical procedure:

1)  $\Delta E_x$  and  $\{\omega_{\mu}\}$  will be approximated by integers chosen so that they all have a large common integer divider.

2) The largest common integer divider of  $\Delta E_x$  and of  $\{\omega_{\mu}\}$  will be applied for the calculation of the integral (3.9).

3) The integral in Eq. (3.9) will be computed numerically using any conventional numerical integration method. As, according to (1) and (2),  $\varepsilon_x$  and  $\{\tilde{\omega}_{\mu}\}$  are relatively small numbers, (for example, choosing  $\omega_N = 50 \text{ cm}^{-1}$  in calculating the intersystem crossing  $^3B_{1u} \rightarrow ^1A_{1g}$  rate in Benzene, performed in the next section, we have  $\varepsilon_x = 600$  and  $\{\omega_{\mu}\} = 10-60$ ) the integrand in Eq. (3.9) is not a strongly oscillating function [as, for example, the integrand in Eq. (2.2)] and the integral is easily evaluated by numerical methods.

It should be noted that the choice of a large value of  $\omega_N$  for the computation of the integral (3.9) should not be confused with the inequality (3.1), as this inequality has provided the ideological basis for deriving the result in the statistical limit [Eq. (3.9)] while now we are just engaged in approximate numerical calculation of the integral in this equation.

We shall now proceed to apply this technique to a real physical system.

<sup>2</sup> It may be shown, in fact, that if  $\varepsilon_x$  is not an integer,  $I_0(\varepsilon_x) = 0$ . This should not worry us as from Eq. (3.1) it is clear that  $\varepsilon_x$  should be taken as the integer closest to the real value of  $\Delta E_x / h\omega_N$ .

Table 1. Results of numerical integration of Eq. (4.2) for  $T_1 \rightarrow S_1$  crossing in benzene  $H_+$ .

$\omega_N = 500 \text{ cm}^{-1}$		$\omega_A = 50 \text{ cm}^{-1}$		$\omega_A = 10 \text{ cm}^{-1}$	
$\omega \text{ cm}^{-1}$	Promoting mode <sup>a</sup>	$\{\prod_i \beta_{N_i}\}^{-1} I_i \text{ (cm}^{-1})$	$\omega \text{ cm}^{-1}$	Promoting mode <sup>a</sup>	$\{\prod_i \beta_{N_i}\}^{-1} I_i \text{ (cm}^{-1})$
$\omega_A = 10 \text{ cm}^{-1}$					
28500	1	0	29550	1	29630
	2	$5.7 \times 10^{-16}$		2	
29000	1	$5.6 \times 10^{-16}$	29600	1	29640
	2	0		2	
29500	1	0	29650	1	29650
	2	$1.3 \times 10^{-16}$		2	
30000	1	$1.3 \times 10^{-16}$	29700	1	29660
	2	0		2	
30500	1	0	29750	1	29670
	2	$3.2 \times 10^{-17}$		2	

<sup>a</sup> 1 denotes the C stretching mode,  $\omega_1 = 1313 \text{ cm}^{-1}$ ; 2 denotes the H bending mode,  $\omega_2 = 1147 \text{ cm}^{-1}$ .



### 5. Intersystem Crossing ( $T_1 \rightarrow S_0$ ) in the Benzene Molecule

The procedure outlined in the previous section will now be utilized to compute the intersystem crossing rate from the vibrational level of the  $^3B_{1u}$  electronic state of the Benzene molecule to the ground electronic  $A_{1g}$  state, utilizing Eqs. (2.1), (2.2) and (2.4) for the non-radiative decay rate and making use of the molecular parameters given by Burland and Robinson [10]. This transition is characterized by two promoting modes (C stretching,  $\omega_1 = 1313 \text{ cm}^{-1}$  and H bending,  $\omega_2 = 1147 \text{ cm}^{-1}$  which are characterized by a  $b_{2u}$  symmetry); by two totally symmetric modes of non-vanishing origin displacements (C-H stretching,  $\omega = 3063 \text{ cm}^{-1}$ ,  $\Delta = 0.3$ , and C-C stretching,  $\omega = 990 \text{ cm}^{-1}$ ,  $\Delta = 1.1$ ), by the frequency changes tabulated by Burland and Robinson [10] and by an energy gap,  $\Delta E = 29650 \text{ cm}^{-1}$ .

Making use of the procedure outlined in Sections (2) and (3) the non-radiative decay probability is [1b]

$$W_{so} = \frac{1}{2\hbar^2} \sum_{\mu} |C_{si}|^2 \left[ \prod_{\mu} (\beta_{\mu})^{-1} \right] I_{\mu} \quad (5.1)$$

where

$$\begin{aligned} I_{\mu} = & \frac{1}{\omega_N} \int_0^{2\pi} dx \exp(-i\epsilon_{\mu} x) \left\{ 1 + \frac{(1-\beta_{\mu})^2}{4\beta_{\mu}} [1 - \exp(2i\tilde{\omega}_{\mu} x)] \right\}^{-1} \\ & \times \prod_{\mu} \left\{ 1 + \frac{(1-\beta_{\mu})^2}{4\beta_{\mu}} [1 - \exp(2i\tilde{\omega}_{\mu} x)] \right\}^{-1} \\ & \times \exp \left\{ - \sum_{\mu} \frac{\beta_{\mu} \Delta_{\mu}^2 [1 - \exp(i\tilde{\omega}_{\mu} x)]}{\beta_{\mu} + 1 + (\beta_{\mu} - 1) \exp(i\tilde{\omega}_{\mu} x)} \right\} \end{aligned} \quad (5.2)$$

where now

$$\epsilon_{\mu} = \frac{\Delta E + \hbar \sum_{\mu} \delta_{\mu}^{(-)}}{\hbar \omega_N} - \frac{\hbar \omega_{\mu}}{\hbar \omega_N} \quad (5.3)$$

in which  $\delta_{\mu}^{(-)}$  is the difference in frequencies between the two electronic states.

In order to check our numerical method we have chosen  $\omega_N = 500 \text{ cm}^{-1}$ ,  $50 \text{ cm}^{-1}$  and  $10 \text{ cm}^{-1}$ , modifying each time the molecular frequencies and the effective energy gap so that  $\epsilon_{\mu}$  and  $\{\tilde{\omega}_{\mu}\}$  are obtained as integers. As a rule,  $\epsilon_{\mu}$  and  $\{\tilde{\omega}_{\mu}\}$  were chosen to correspond to the integers closest to the values of  $(\Delta E - \hbar \sum_{\mu} \delta_{\mu}^{(-)} - \hbar \omega_{\mu})/\hbar \omega_N$  and of  $\{\omega_{\mu}/\omega_N\}$  respectively.

From the results summarized in Table 1 we may conclude that our mathematical approximation is valid. In particular, we note that the results are

Table 2. Average values for the integral  $I_{\mu}$  for  $C_6H_6$

$\omega_N \text{ cm}^{-1}$	500 <sup>a</sup>	50	10
Average result for mode 1 ( $\text{cm}^{-1}$ )	$1.7 \times 10^{-16}$	$7.0 \times 10^{-17}$	$7.3 \times 10^{-17}$
Average result for mode 2 ( $\text{cm}^{-1}$ )	$1.4 \times 10^{-16}$	$6.0 \times 10^{-17}$	$7.2 \times 10^{-17}$

<sup>a</sup> The relatively large average in the case of  $\omega_N = 500$  evolves from the contribution of the "low"  $28500 \text{ cm}^{-1}$  gap.

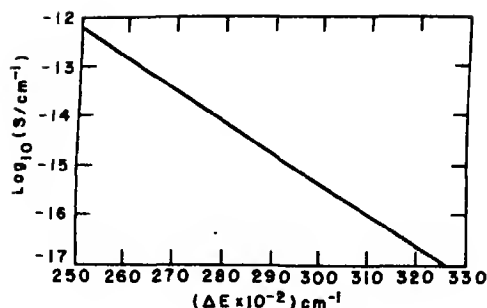


Fig. 1 The energy gap law in the low temperature limit of the  $T_1 \rightarrow S_0$  transition in the benzene molecule. These results were obtained by numerical integration of Eqs. (5.1) and (5.2) using the spectroscopic data of Burland and Robinson (Ref. [10]).

practically insensitive to the choice<sup>3</sup> of  $\omega_N$ . Taking for each  $\omega_N$  the average of the five results (displayed in Table 1) we obtain the final values summarized in Table 2. The physical implications of these numerical computations may be summarized as follows:

a) The inclusion of frequency changes is crucial for a semi-quantitative calculation of the non-radiative decay rate. The numerical results obtained from Eq. (4.2) with  $\beta_\mu$  taken as unity for every  $\mu$ , are three orders of magnitude lower than the results displayed in Table 1.

b) The energy gap law is retained (Fig. 1), but the decrease of the non-radiative decay rate as a function of increasing the energy gap is slightly modified when frequency changes are included. The energy gap law may be approximately represented by the relation

$$W_{10} \sim A \exp(-\gamma \Delta E / h \omega_M)$$

where from Fig. 1 we obtain  $\gamma \approx 4$ , while for the displaced undistorted potential surfaces model we have  $\gamma = 2$  [1]. This result is reasonable, as with the inclusion of frequency changes the contributions of low frequencies which are strongly modified in the electronic transition, becomes more important.

c) Following Fischer and Schneider [9b] we may add a displacement of  $\Delta = 0.9$  for the  $\nu_{2g}$  ( $1584 \text{ cm}^{-1}$ ) C-C stretching mode. This modification causes an increase by a numerical factor  $\sim 40$  in the calculated non-radiative decay rate<sup>4</sup>.

d) Repeating the calculation of Eq. (4.2) using Burland and Robinson's data [10] for the  $\text{C}_6\text{D}_6$  molecule we obtain  $\frac{1}{2} \prod_{\mu} \beta_{\mu}^{-1/2} I_1 = 9 \times 10^{-21} \text{ cm}^{-1}$ ;  $\frac{1}{2} \prod_{\mu} \beta_{\mu}^{-1/2} I_2 = 4 \times 10^{-21} \text{ cm}^{-1}$ . We may conclude that the non-radiative decay rate of  $\text{C}_6\text{D}_6$  is lower by about four orders of magnitude than that of the  $\text{C}_6\text{H}_6$  molecule.

e) Utilizing the results of Table 2 and taking  $C_{st} = 1.6 \times 10^{-1} \text{ cm}^{-1}$  [10] we may calculate  $W_{10}$  for the  $T_1 - S_0$  intersystem crossing in the benzene molecule.

<sup>3</sup> The fluctuations of the result as functions of  $\Delta E$  should not worry us as they just represent the non-uniform distribution of  $\{|I_i\rangle\}$  levels resulting from the "round off" approximation. This effect is most profound when we choose  $\omega_N \approx 500 \text{ cm}^{-1}$ .

<sup>4</sup> The increase is much more profound (about three orders of magnitude) in the case of deuterobenzene.

Table 3. Theoretical intersystem crossing rates in the benzene-H<sub>6</sub> and benzene-D<sub>6</sub> molecules

	C <sub>6</sub> H <sub>6</sub>	C <sub>6</sub> D <sub>6</sub>
Present work	$7.2 \times 10^{-7} \text{ sec}^{-1}$ ..... $2.6 \times 10^{-5} \text{ }^a$	$6.6 \times 10^{-11} \text{ sec}^{-1}$ ..... $1.2 \times 10^{-7} \text{ sec}^{-1} \text{ }^a$
Burland and Robinson [10]	$9.04 \times 10^{-5} \text{ sec}^{-1}$	$1.18 \times 10^{-10} \text{ sec}^{-1}$
Fischer and Schneider [9]	$7.4 \times 10^{-4} \text{ sec}^{-1}$	$3.1 \times 10^{-5} \text{ sec}^{-1}$
Experiment [10]	$2.4 \times 10^{-2} \text{ sec}^{-1}$	

<sup>a</sup> Using Fischer's and Schneider's data for the displacement of the  $e_{2g}$  deformation mode.

Our numerical results together with previously obtained results of Burland and Robinson [10] and of Fischer and Schneider [9b] are summarized in Table 3. The results of Burland and Robinson are based on an approximate level counting procedure. The results of Fischer and Schneider, which are obtained from a formalism equivalent to ours attempting to incorporate both frequency changes and unharmonicities are doubtful, as they are based on the unjustified expansion discussed in Appendix A.

The results presented in Table 3 should be compared with the experimental result [10]  $W_{s0} \approx 2.4 \times 10^{-2} \text{ sec}^{-1}$ . The difference of about three to four orders of magnitude is probably caused by the neglect of unharmonicities [13, 10].

We have obtained the worst agreement reported up to date between theory and experiment for the  $T_1 \rightarrow S_0$  non-radiative decay probability in the benzene molecule. However, we feel that the numerical results presented herein provide the first correct calculation of the non-radiative decay probability of a harmonic molecule. It is not surprising that the neglect of unharmonicities yields a rather serious underestimate of the decay rate. At present no systematic valid procedure is available for the incorporation of unharmonicities. (The Fischer Schneider procedure [9] is unfortunately invalid in view of unjustified expansions of the generating function.) People interested in this field should attempt to derive the density matrix (i.e., the Green's function [11]) for an unharmonic oscillator and use this result for the evaluation of the generating function.

The goal of theoretical chemistry is not to reproduce experimental results but rather to provide general relations and correlations. In this context, the general formulation of the non-radiative decay of a model harmonic molecule in the statistical limit is of considerable interest.

#### Appendix A: A Comment on the Convergence Problem

Lin and Berson [8], Freed and Jortner [1b], Fischer [7] and others [6,9] have used expansions of the form

$$F(\xi \exp(i\omega t)) = 1 + a\xi e^{i\omega t} + b\xi^2 e^{2i\omega t} + \dots \quad (\text{A.1})$$

where  $F$  is some function and  $\xi \ll 1$  is a small parameter, in order to simplify the generating function obtained in the theory of radiationless transitions in the statistical limit. Most of the available expressions [1, 6–8] for the non radiative decay rate of a large molecule characterized by displaced and modified potential surfaces and also Fischer's attempt to include unharmonicities in the theory [9] utilize such expansions and neglect high order terms before evaluating the necessary Fourier transform of the generating function. We now wish to demonstrate that such an approximation which neglects the higher order terms is unfortunately justified. To this end we shall compare the contributions of the low order terms which are usually retained in the approximate expression and of a higher order term which is usually neglected. Suppose, for example, that  $E/\omega$  is an even integer and we want to compare  $\int_{-\infty}^{\infty} dt \exp[-iEt + \xi \exp(i\omega t)]$  and  $\int_{-\infty}^{\infty} dt \exp[-iEt + \xi^2 \exp(2i\omega t)]$ . Expanding the integrand in the form

$$\exp[\xi \exp(i\omega t)] = \sum_{n=0}^{\infty} \frac{\xi^n}{n!} \exp(in\omega t) \quad (\text{A.2})$$

it is easy to get

$$\int_{-\infty}^{\infty} dt \exp[-iEt + \xi \exp(i\omega t)] = 2\pi \sum_{n=0}^{\infty} \frac{\xi^n}{n!} \delta(E - n\omega). \quad (\text{A.3})$$

In the statistical limit it may be shown that  $\delta(E - n\omega)$  may be replaced by  $\delta_{E, n\omega}$ . This may be proved by utilizing the same procedure which leads to Eq. (3.9) and noting that

$$\int_0^{2\pi} dt \exp[-iEt + \xi \exp(i\omega t)] = 2\pi \frac{\xi^n}{n!} \delta_{E, n\omega}. \quad (\text{A.4})$$

Thus we get  $2\pi \frac{\xi^{E/\omega}}{(E/\omega)!}$  where  $\xi$  will be an average over the contributions from many modes.

In the same way, we get

$$\int_{-\infty}^{\infty} dt \exp[-iEt + \xi^2 \exp(2i\omega t)] = 2\pi \frac{(\xi^2)^{E/2\omega}}{(E/2\omega)!} \quad (\text{A.5})$$

which is greater than the first result for every  $\xi$ . Of course, higher order terms  $O(\xi^n)$  with  $n \gg 2$  lead to vanishingly small contributions. Thus one cannot get away by neglecting terms of the order of  $O(\xi^2)$  in the expansion (A.1), and one has to retain the terms up to  $m = (E/\omega)$ . This conclusion is supported by numerical calculations performed by us on Eq. (4.1).

## Appendix B: Verification of the Identity [11.12]

Starting from

$$I = \int_{-\infty}^{\infty} dx \exp(-iax) F(x) \quad (\text{B.1})$$

where  $F(x)$  is a periodic function of  $x$ , characterized by a period of  $2\pi$ , we proceed as follows [12]:

$$I = \sum_{n=-\infty}^{\infty} \int_{2\pi n}^{2\pi(n+1)} dx \exp(-iax) F(x) \quad (\text{B.2})$$

$$= \sum_{n=-\infty}^{\infty} \exp(2\pi i n a) \int_0^{2\pi} dx \exp(-iax) F(x)$$

where in each integral we have replaced  $x$  by  $x - 2n\pi$ . Relation (2.12) is now easily verified by utilizing the identity

$$\sum_{n=-\infty}^{\infty} \exp(2\pi i n a) = \sum_{s=-\infty}^{\infty} \delta(s - a). \quad (\text{B.3})$$

### References

- 1a. Engelman, R., Jortner, J.: *Mol. Phys.* **18**, 145 (1970).
- 1b. Freed, K. F., Jortner, J.: *J. Chem. Phys.* **52**, 6272 (1970).
2. Nitzan, A., Jortner, J.: Electronic relaxation in small molecules in a medium, submitted to *Theoret. Chim. Acta (Berl.)*.
3. Nitzan, A., Jortner, J.: The effects of vibrational relaxation on electronic transition. *J. Chem. Phys.* (in press).
4. Freed, K. F., Jortner, J.: *J. Chem. Phys.* **50**, 2916 (1969).
- 5a. Nitzan, A., Jortner, J.: *J. Chem. Phys.* **55**, 1355 (1971).
- 5b. Nitzan, A., Jortner, J.: *J. Chem. Phys.* **56**, 2079 (1972).
6. Heller, D. F., Freed, K. F., Gelbart, W.: *J. Chem. Phys.* **56**, 2309 (1972).
7. Fischer, S.: *J. Chem. Phys.* **53**, 3195 (1970).
8. Lin, S. H., Bersohn, R.: *J. Chem. Phys.* **48**, 2732 (1968).
- 9a. Fischer, S.: *Chem. Phys. Letters* **11**, 577 (1971).
- 9b. Fischer, S., Schneider, S.: *Chem. Phys. Letters* **10**, 392 (1971).
10. Burland, D., Robinson, G. W.: *J. Chem. Phys.* **51**, 4548 (1969).
11. Vetchinkin, S. I., Bachrach, V. L.: *Int. J. Quantum Chem.* **6**, 143 (1972).
12. Lax, M.: *J. Chem. Phys.* **20**, 1752 (1952).
13. Siebrand, W.: *J. Chem. Phys.* **54**, 363 (1971).

Prof. Dr. J. Jortner  
Department of Chemistry  
Tel-Aviv University  
Tel-Aviv, Israel



# Semiempirical Extended Hartree-Fock Theory

Karl Jug\*

Institut für Theoretische Chemie der Universität Stuttgart

Received September 18, 1972

A truncated multi-configuration SCF formalism is presented which is particularly suited to describe correlation effects in semiempirical molecular orbital methods. The orbital energies reflect a correlated, SCF-like description of the situation of electrons in molecules. On the basis of symmetrically orthogonalized atomic orbitals approximations are introduced which lead to CNDO and INDO like methods. Consistency requirements lead to a new formula for the  $\beta$  integral. The method can be parametrized so as to yield good ground state potential surfaces. The orbital part is demonstrated in the simple case of  $H_2$ .

*Key words:* Semiempirical MO theory - Multiconfiguration SCF formalism

## 1. Introduction

Semiempirical molecular orbital methods have a great deal of attraction among chemists these days. However, to our knowledge, there exists presently no semiempirical method which includes correlation effects in a theoretically satisfactory and practically useful fashion. CNDO and INDO methods were designed by Pople and collaborators [1] to reproduce dipole moments and equilibrium geometries, but fail to predict binding energies and force constants [2]. Since the binding energies are in general too large, it would be meaningless to add a configuration interaction formalism to the existing scheme. Dewar and collaborators have designed a sequence of MINDO methods and managed after extensive use of adjustable empirical parameters to obtain both equilibrium distances and binding energies [3]. Both methods are based on the SCF formalism and thus unable to describe potential surfaces far from the equilibrium.

We propose here a procedure which allows with little empirical adjustment to retain the attractive features of both Pople's and Dewar's work, namely to be theoretically justifiable and practically useful. For this purpose we develop a modified and truncated multi-configuration SCF formalism. In this formalism we introduce systematic approximations by means of a symmetrically orthogonalized AO basis [4]. Various levels of ZDO assumptions lead to CNDO and INDO like methods. The consequences of the ZDO assumption are reflected in the representation of formulas of the remaining integrals. In particular, a new formula for the  $\beta$  integral is derived which reduces the number of adjustable parameters considerably.

\* Permanent address: Department of Chemistry, Saint Louis University, Saint Louis, Missouri 63156, USA.

The definition of a multi-configuration SCF operator after a CI step yields orbital energies which are physically more meaningful than SCF energies, in particular, at distances far from the equilibrium. This is demonstrated for the simple case of  $H_2$ . For polyatomics the use of a localization procedure is suggested to reduce the number of configurations for dissociation. The involved relation to the orbital picture is briefly discussed.

## 2. The Extended Hartree-Fock Method

In our discussion of correlation effects, we restrict ourselves to intra-shell pair correlation. The total wavefunction is approximated as a linear combination of the dominant Hartree-Fock configuration  $\Psi_0$  and doubly excited configurations  $\Psi_i$  of closed-shell or open-shell form.

$$\Psi = A_0 \Psi_0 + \sum_{i=1}^I A_i \Psi_i \quad (2.1)$$

with

$$\begin{aligned} \Psi_0 &= (\psi_1 \bar{\psi}_1 \psi_2 \bar{\psi}_2 \dots \psi_k \bar{\psi}_k \dots \psi_n \bar{\psi}_n), \\ \Psi_i &= \begin{cases} (\psi_1 \bar{\psi}_1 \psi_2 \bar{\psi}_2 \dots \psi_p \bar{\psi}_p \dots \psi_n \bar{\psi}_n) & \text{closed shell} \\ \frac{1}{\sqrt{2}} \{ (\psi_1 \bar{\psi}_1 \psi_2 \bar{\psi}_2 \dots \psi_p \bar{\psi}_q \dots \psi_n \bar{\psi}_n) & \text{open shell} \\ - (\psi_1 \bar{\psi}_1 \psi_2 \bar{\psi}_2 \dots \bar{\psi}_p \psi_q \dots \psi_n \bar{\psi}_n) \}, \end{cases} \\ &1 \leq k \leq n; p, q > n. \end{aligned}$$

For convenience, we use the abbreviation  $i$  for  $(k, p)$  or  $(kk, pq)$ . The set  $\Psi_0, \Psi_i (i = 1 \dots I)$  is orthonormal. Usually the multiconfiguration Hartree-Fock equations [5, 6] are derived by a variation of the following energy functional with respect to the MO's  $\psi$  subject to the orthogonality conditions.

$$E = \langle \Psi | H | \Psi \rangle / \langle \Psi | \Psi \rangle \quad (2.2)$$

$$= \left( A_0^2 H_{00} + 2 \sum_{i=1}^I A_0 A_i H_{0i} + \sum_{i,j} A_i A_j H_{ij} \right) / \left( A_0^2 + \sum_{i=1}^I A_i^2 \right)$$

with

$$H_{ij} = \langle \Psi_i | H | \Psi_j \rangle$$

The coefficients  $A$  are determined by a secular equation.

$$\sum_{j=0}^I A_j (H_{ij} - E \delta_{ij}) = 0, \quad i = 0, 1 \dots I \quad (2.3)$$

We suggest another way of arriving at (2.3). This will open the way to eigenvalue equations of an extended Hartree-Fock Hamiltonian which appears to be particularly useful in semiempirical methods. We shall show later that the resulting eigenvalues can be physically interpreted.



If we consider the exact eigenfunctions  $\Psi$  of the system's Hamiltonian  $H$ , the following equality holds

$$E = \langle \Psi_i | H | \Psi \rangle / \langle \Psi_i | \Psi \rangle, \quad i = 0, 1, \dots$$

With (2.1) the energy takes the form

$$E = H_{ii} + \sum_{j \neq i} a_j H_{ij}, \quad i = 0, 1, \dots \quad (2.4)$$

with

$$a_j = A_j / A_i.$$

Concerning the determination of coefficient  $A_i$  and energy  $E$ , (2.4) is equivalent to (2.3) also in a finite expansion. In particular the total energy of the ground state is represented as a sum of Hartree-Fock energy and correlation energy in a simple form.

$$E = H_{00} + \sum_{i=1} a_i H_{0i} \quad \text{with} \quad a_j = A_j / A_0. \quad (2.4a)$$

Such an expression has also been used by Öksüz and Sinanoglu [7]. The  $A_i$  are determined by (2.4). If the molecular orbitals  $\psi_i$  used in (2.2) and (2.4) are the same, the ground state energy values of (2.2) and (2.4a) will be the same. However, variation of (2.2) and (2.4a) with respect to the MO's  $\psi_i$  leads to different multi-configuration SCF operators, hence to different  $\psi_i$ . In general, (2.4) will yield less correlation energy than (2.2) at intermediate internuclear distances. Dissociation is, however, described properly. The advantage of this extended Hartree-Fock operator is the linear form of correlation energy in the  $A_i$  which makes the eigenvalues  $\epsilon_i$  of such an operator the straightforward generalization of the eigenvalues of an SCF operator. This is not the case for the multiconfiguration orbital energies of Das and Wahl [5] or Veillard and Clementi [6].

In the following, we shall demonstrate the derivation of a multi-configuration closed-shell case. A generalization to open-shells is straightforward. The total energy expressed in integrals over MO's  $i$  ( $\equiv \psi_i$ ) is

$$\begin{aligned} E &= 2 \sum_i^n H_{ii}^{\text{core}} + \sum_{i,j}^n 2J_{ij} - K_{ij} + \sum_{k,p} a_{kp} K_{kp} \\ H_{ii}^{\text{core}} &= \langle i | H_{\text{core}} | i \rangle \\ J_{ij} &= (ii|jj) \\ K_{ij} &= (ij|ij) \\ K_{kp} &= (kp|kp) \\ a_{kp} &= A_{kp} / A_0. \end{aligned} \quad (2.5)$$

MO's  $k, \bar{k}$  of  $\Psi_0$  are replaced by  $p, \bar{p}$  to form a representative doubly excited configuration. Variation of the energy subject to the MO orthogonality conditions

$$\delta \left( E + \sum_{i,j} \epsilon_{ij} \langle i | j \rangle \right) = 0$$

yields

$$F_i|i\rangle = \sum_j \varepsilon_{ij}|j\rangle, \quad i = 1 \dots n \quad (2.6)$$

with

$$F_i = F_i^{\text{SCF}} + W_i$$

$$W_i = \sum_{l>n} a_{il} W_{il}.$$

We obtain an explicit form for  $W_{il}$  in the following way. Since  $K_{kp}$  does not depend on  $\psi_i$  for  $i \neq k$ , it holds that

$$W_{il} = W_{kp} \delta_{ik} \delta_{lp}.$$

For  $i = k$   $K_{kp}$  can be rewritten as

$$K_{kp} = \frac{1}{2} \langle k(1) | V_{kp} + V_{kp}^\dagger | k(1) \rangle$$

with

$$V_{kp} = \left[ k(2) \left| -\frac{1}{r_{12}} \right| p(1)p(2) \right] \langle k(1) |$$

$$V_{kp}^\dagger = \left[ |k(1)\rangle \langle p(2)p(1) | -\frac{1}{r_{12}} \right] |k(2)\rangle$$

so that

$$W_{kp} = \frac{1}{2} (V_{kp} + V_{kp}^\dagger).$$

For the unoccupied SCF orbitals  $i = p$  the coupling operator  $W_{pk}$  is obtained by exchange of  $k$  and  $p$  in (2.7). Also  $a_{pk} = a_{kp}^{-1}$  holds. The coupling part of the Hamiltonian then takes the final form

$$W_i = \begin{cases} 0 & i = 1 \dots n, i \neq k, \\ \sum_p a_{kp} W_{kp} & \text{for } i = k, \\ \sum_k a_{kp}^{-1} W_{pk} & i = p, p > n. \end{cases} \quad (2.8)$$

Because of the difference between (2.2) and (2.4) the coupling operator  $W$  is only half of the one in Wahl's paper [5]. A similar form to (2.8) appears in Kutzelnigg's approximate natural orbital approach [8].

The non-diagonal Lagrangean multipliers  $\varepsilon_{ij}$  can be absorbed by the use of orthogonality relations [5]. The final equations then take the form

$$(F_i - R_i)|i\rangle = \varepsilon_i|i\rangle \quad (2.9)$$

$$R_i = \sum_{j \neq i} |j\rangle \langle j| F_i + F_i |j\rangle \langle j|.$$

In practice, one cycle of the following three steps will be sufficient to obtain an improved SCF-like description: 1) Solution of the SCF equations, 2) Determination of the CI coefficients  $A$  by means of (2.3), 3) Solution of the EHF equations (2.9). Repetition of this cycle will not lead to new aspects, but may involve

convergence problems, so we do not advocate it here. The energy can then be written in the following way

$$\begin{aligned}
 E &= \sum_i^n \langle i | H_{\text{core}} + F_i | i \rangle \\
 &= \sum_i^n \langle i | H_{\text{core}} + F_i^{\text{SCF}} + W_i | i \rangle \\
 &= \sum_i^n (e_i^{\text{core}} + \varepsilon_i).
 \end{aligned} \tag{2.10}$$

The orbital energies play here the same role as in SCF theory, but include correlation effects.

### 3. CNDO and INDO Forms

To relate the formalism of Section 2 to approximate molecular orbital methods, we expand the MO's in AO's and write the EHF equations in matrix form

$$\begin{aligned}
 (F_i - R_i)C_i &= \varepsilon_i C_i \quad i = 1 \dots n, \dots, p \dots \\
 F_i &= F_i^{\text{SCF}} + W_i \\
 R_i &= \sum_j (S C_j C_j^\dagger F_i + F_i C_j C_j^\dagger S).
 \end{aligned} \tag{3.1}$$

We concentrate now on the representative operator  $F_k$ . Its elements are

$$F_{\mu\nu} = F_{\mu\nu}^{\text{SCF}} + W_{\mu\nu}$$

with

$$\begin{aligned}
 F_{\mu\nu}^{\text{SCF}} &= H_{\mu\nu}^{\text{core}} + \sum_{\varrho, \sigma} P_{\varrho\sigma} [(\mu\nu|\varrho\sigma) - \frac{1}{2}(\mu\varrho|\nu\sigma)] \\
 W_{\mu\nu} &= \frac{1}{2} \sum_{\varrho, \sigma} \sum_{\tau, \omega} P'_{\varrho\sigma} P''_{\tau\omega} [(\mu\tau|\varrho\omega) S_{\sigma\nu} + (\nu\tau|\varrho\omega) S_{\sigma\mu}] \\
 P_{\varrho\sigma} &= 2 \sum_i^{\text{occ}} c_{i\varrho} c_{i\sigma} = 2 \sum_i^{\text{occ}} P_{\varrho\sigma}(i) \\
 P'_{\varrho\sigma} &= c_{k\varrho} c_{k\sigma} \\
 P''_{\tau\omega} &= \sum_p c_{p\tau} c_{p\omega} a_{kp}.
 \end{aligned} \tag{3.2}$$

In the following symmetrically orthogonalized AO's [4] will be assumed, which lead to further simplifications

$$\begin{aligned}
 R_i &= \sum_j C_j C_j^\dagger F_i + F_i C_j C_j^\dagger \\
 W_{\mu\nu} &= \frac{1}{2} \sum_{\varrho} \sum_{\tau, \omega} P''_{\tau\omega} [P'_{\varrho\nu} (\mu\tau|\varrho\omega) + P'_{\varrho\mu} (\nu\tau|\varrho\omega)].
 \end{aligned} \tag{3.3}$$

Various levels of approximation will be considered:

a) CNDO form

$$\begin{aligned}
 F_{\mu\mu}^{\text{SCF}} &= H_{\mu\mu}^{\text{core}} + \frac{1}{2} P_{\mu\mu}(\mu\mu|\mu\mu) + \sum_{\varrho \neq \mu} P_{\varrho\varrho}(\mu\mu|\varrho\varrho) \\
 F_{\mu\nu}^{\text{SCF}} &= H_{\mu\nu}^{\text{core}} - \frac{1}{2} P_{\mu\nu}(\mu\mu|\nu\nu) \\
 W_{\mu\mu} &= \sum_{\varrho} P'_{\varrho\mu} P''_{\varrho\mu}(\mu\mu|\varrho\varrho) \\
 W_{\mu\nu} &= \frac{1}{2} \sum_{\varrho} P'_{\varrho\nu} P''_{\varrho\mu}(\mu\mu|\varrho\varrho) + P'_{\varrho\mu} P''_{\varrho\nu}(\nu\nu|\varrho\varrho)
 \end{aligned} \tag{3.4}$$

so that

$$\begin{aligned}
 F_{\mu\mu} &= H_{\mu\mu}^{\text{core}} + \frac{1}{2} (P_{\mu\mu} + 2P'_{\mu\mu} P''_{\mu\mu})(\mu\mu|\mu\mu) \\
 &\quad + \sum_{\varrho \neq \mu} (P_{\varrho\varrho} + P'_{\varrho\mu} P''_{\varrho\mu})(\mu\mu|\varrho\varrho) \\
 F_{\mu\nu} &= H_{\mu\nu}^{\text{core}} - \frac{1}{2} [P_{\mu\nu} - (P'_{\mu\mu} + P'_{\nu\nu}) P''_{\mu\nu}](\mu\mu|\nu\nu) \\
 &\quad + \frac{1}{2} P'_{\mu\nu} (P''_{\mu\mu} + P''_{\nu\nu})(\mu\mu|\mu\mu) \\
 &\quad + \frac{1}{2} \sum_{\varrho \neq \mu, \nu} P'_{\varrho\nu} P''_{\varrho\mu}(\mu\mu|\varrho\varrho) + P'_{\varrho\mu} P''_{\varrho\nu}(\nu\nu|\varrho\varrho).
 \end{aligned} \tag{3.5}$$

It is widely believed that semiempirical SCF methods can account for correlation by empirical adjustment of parameters. How much of this is true will be shown in the following. We try to reduce the EHF equations (3.5) to an SCF form:

$$F_{\mu\mu} = H_{\mu\mu}^{\text{core}} + \frac{1}{2} P_{\mu\mu}(\mu\mu|\mu\mu)' + \sum_{\varrho \neq \mu} P_{\varrho\varrho}(\mu\mu|\varrho\varrho)'$$

with

$$(\mu\mu|\mu\mu)' = \left( 1 + 2 \frac{P'_{\mu\mu} P''_{\mu\mu}}{P_{\mu\mu}} \right) (\mu\mu|\mu\mu) \tag{3.6a}$$

$$(\mu\mu|\varrho\varrho)' = \left( 1 + \frac{P'_{\varrho\mu} P''_{\varrho\mu}}{P_{\mu\mu}} \right) (\mu\mu|\varrho\varrho)$$

$$F_{\mu\nu} = H_{\mu\nu}^{\text{core}} - \frac{1}{2} P_{\mu\nu}(\mu\mu|\nu\nu)' + A_{\mu\nu}$$

with

$$(\mu\mu|\nu\nu)' = \left( 1 - \frac{(P'_{\mu\mu} + P'_{\nu\nu}) P''_{\mu\nu}}{P_{\mu\nu}} \right) (\mu\mu|\nu\nu) \tag{3.6b}$$

$$\begin{aligned}
 A_{\mu\nu} &= \frac{1}{2} P'_{\mu\nu} (P''_{\mu\mu} + P''_{\nu\nu})(\mu\mu|\mu\mu) \\
 &\quad + \frac{1}{2} \sum_{\varrho \neq \mu, \nu} P'_{\varrho\nu} P''_{\varrho\mu}(\mu\mu|\varrho\varrho) + P'_{\varrho\mu} P''_{\varrho\nu}(\nu\nu|\varrho\varrho).
 \end{aligned}$$

From (3.6a) it appears that modified one- and two-center repulsion integrals could be introduced which would keep the SCF formalism intact. However, (3.6b) shows that the modifications to be introduced here are not consistent with those in (3.6a). Also a new term  $\Delta_{\mu\nu}$  appears which has no analogue in SCF theory. It is hard to conceive that the modifications for parametrization introduced in (3.6) would be satisfactory even under further simplifying assumptions in a particular class of molecules with fixed geometries. It is obvious from there that previous attempts of reparametrization had to fail [9, 10]. Caution was expressed already in Hansen's paper.

Equations (3.5) involve only four types of parameters

$$\alpha_\mu \equiv H_{\mu\mu}^{\text{core}}, \beta_{\mu\nu} \equiv H_{\mu\nu}^{\text{core}}, (\mu\mu|\mu\mu), (\mu\mu|\nu\nu),$$

whose evaluation will now be attempted. In the calculation of  $\alpha$  we follow Pople

$$\alpha_\mu = W_\mu - \sum_{B \neq A} U_{AB}$$

with

$$U_{AB} = \begin{cases} \int s_A^2(1) \frac{Z_B}{r_{AB}} d\tau, & \text{CNDO/1} \\ Z_B \gamma_{AB} & \text{CNDO/2.} \end{cases} \quad (3.7)$$

It should be noticed here that in the choice of  $W_\mu$  ( $W_s \neq W_p$ ) Pople does not (!) follow his invariance requirements. He drops the invariance under hybridization. But this is not serious, since recent work shows [11, 12] that invariance under hybridization is not a necessary, but sufficient condition for the invariance of the SCF equations.

To evaluate  $\beta$ , we use our own studies. We have shown that in polyatomics [13, 14]

$$\bar{\beta}_{\mu\nu} = \frac{1}{2} S_{\mu\nu} [(\bar{\alpha}_\mu + \bar{\alpha}_\nu) + \kappa_{\mu\nu}(\bar{\alpha}_\mu - \bar{\alpha}_\nu)] + \frac{1 - S_{\mu\nu}^2}{\bar{R}_{\mu\nu}} \frac{dS_{\mu\nu}}{d\bar{R}_{\mu\nu}} \quad (3.8)$$

and in diatomics [15]

$$\beta_{\mu\nu} = \frac{1}{1 - S_{\mu\nu}^2} \left[ \bar{\beta}_{\mu\nu} - \frac{1}{2} S_{\mu\nu} (\bar{\alpha}_\mu + \bar{\alpha}_\nu) \right] \quad (3.9)$$

holds.

The simplest approximation for the two-center integral  $\beta_{ab}$  better than Linderberg's [16], which was proven to be unreliable [13], would then be

$$\begin{aligned} \beta_{ab} &\approx \frac{1}{2} S_{ab} [(\bar{\alpha}'_a + \bar{\alpha}'_b) + \kappa_{ab}(\bar{\alpha}'_a - \bar{\alpha}'_b)] + \frac{1}{R} \frac{dS_{ab}}{dR} - \frac{1}{2} S_{ab}(\bar{\alpha}_a + \bar{\alpha}_b) \\ &= \frac{1}{2} S_{ab} [(\Delta\bar{\alpha}_a + \Delta\bar{\alpha}_b) + \kappa_{ab}(\bar{\alpha}_a - \bar{\alpha}_b + \Delta\bar{\alpha}_a - \Delta\bar{\alpha}_b)] + \frac{1}{R} \frac{dS_{ab}}{dR}. \end{aligned} \quad (3.10)$$

In the spirit of the CNDO method we put

$$\Delta\bar{\alpha}_a + \Delta\bar{\alpha}_b = -\Delta Z \gamma_{AB} \quad (3.11)$$

with

$$\Delta Z = Z'_A - Z_A + Z'_B - Z_B.$$

$\Delta Z$  can be used as an adjustable parameter, e.g. to adjust the binding energy.

Since it is well known that the electronic Coulomb integrals over orthogonalized orbitals do not differ considerably from their non-orthogonal counterparts, we again follow Pople to put

$$\begin{aligned} \gamma_{AA} &= (\mu_A \mu_A | \mu_A \mu_A) = (\mu_A \mu_A | \nu_A \nu_A) = (s_A s_A | s_A s_A) \\ \gamma_{AB} &= (\mu_A \mu_A | \sigma_B \sigma_B) = (s_A s_A | s_B s_B). \end{aligned} \quad (3.12)$$

The total energy including nuclear repulsion can be separated in "atomic" and "interatomic" parts.

$$\begin{aligned} E &= \sum_A (E_A^{\text{SCF}} + E_A^{\text{corr}}) + \sum_{A < B} (E_{AB}^{\text{SCF}} + E_{AB}^{\text{corr}}) \\ E_A^{\text{SCF}} &= \sum_\mu^\Lambda P_{\mu\mu} W_\mu + \frac{1}{2} \sum_{\mu, \nu}^\Lambda (P_{\mu\mu} P_{\nu\nu} - \frac{1}{2} P_{\mu\nu}^2) \gamma_{AA} \\ E_{AB}^{\text{SCF}} &= \sum_\mu^\Lambda \sum_\nu^B (2P_{\mu\nu} \beta_{\mu\nu} - \frac{1}{2} P_{\mu\nu}^2 \gamma_{AB}) \\ &\quad + Z_A Z_B R_{AB}^{-1} - P_{AA} U_{AB} - P_{BB} U_{BA} + P_{AA} P_{BB} \gamma_{AB} \\ E_A^{\text{corr}} &= [\frac{1}{2} \sum_k \sum_\mu^\Lambda \sum_\nu \sum_q^\Lambda P_{\mu\nu}(k) P'_{\nu\nu}(k) P''_{\nu\mu}(k)] \gamma_{AA} \\ E_{AB}^{\text{corr}} &= [\sum_k \sum_\mu^\Lambda \sum_\nu \sum_q^B P_{\mu\nu}(k) P'_{\nu\nu}(k) P''_{\nu\mu}(k)] \gamma_{AB}. \end{aligned} \quad (3.13)$$

b) INDO forms

$$\begin{aligned} F_{\mu\mu}^{\text{SCF}} &= F_{\mu\mu}^{\text{SCF, CNDO}} - \frac{1}{2} \sum_{q \neq \mu}^\Lambda P_{qq} (\mu\varrho | \mu\varrho) \\ F_{\mu\nu}^{\text{SCF}} &= F_{\mu\nu}^{\text{SCF, CNDO}} - \frac{3}{2} P_{\mu\nu} (\mu\nu | \mu\nu) \delta_{\Lambda_\mu \Lambda_\nu} \\ W_{\mu\mu} &= W_{\mu\mu}^{\text{CNDO}} + \sum_{q \neq \mu}^\Lambda (P'_{\mu\mu} P''_{qq} + P'_{\nu\nu} P''_{\mu\mu}) (\mu\varrho | \mu\varrho) \\ W_{\mu\nu} &= W_{\mu\nu}^{\text{CNDO}} + \frac{1}{2} \sum_q^\Lambda (P'_{\mu\nu} P''_{qq} + P'_{\nu\mu} P''_{\mu\mu}) (\mu\varrho | \mu\varrho) \\ &\quad + \frac{1}{2} \sum_q^{\Lambda_\nu} (P'_{\mu\nu} P''_{qq} + P'_{\nu\mu} P''_{\nu\nu}) (\nu\varrho | \nu\varrho) \end{aligned} \quad (3.14)$$

so that

$$\begin{aligned}
 F_{\mu\mu} &= F_{\mu\mu}^{\text{CNDO}} + \sum_{\varrho \neq \mu} \Lambda_{\mu} (P'_{\mu\mu} P''_{\varrho\varrho} + P'_{\varrho\mu} P''_{\mu\varrho} - \frac{1}{2} P_{\varrho\varrho}) (\mu\varrho | \mu\varrho) \\
 F_{\mu\nu} &= F_{\mu\nu}^{\text{CNDO}} - \frac{1}{2} P_{\mu\nu} (\mu\nu | \mu\nu) \delta_{\Lambda_{\mu}\Lambda_{\nu}} \\
 &\quad + \frac{1}{2} \sum_{\varrho \neq \mu} \Lambda_{\mu} (P'_{\mu\nu} P''_{\varrho\varrho} + P'_{\varrho\nu} P''_{\mu\varrho}) (\mu\varrho | \mu\varrho) \\
 &\quad + \frac{1}{2} \sum_{\varrho \neq \nu} \Lambda_{\nu} (P'_{\mu\nu} P''_{\varrho\varrho} + P'_{\varrho\mu} P''_{\nu\varrho}) (\nu\varrho | \nu\varrho).
 \end{aligned} \tag{3.15}$$

In addition to the CNDO parameters, exchange integrals appear. For the same reasons as in the CNDO part, all two-electron integrals are evaluated over non-orthogonal orbitals according to Pople's procedure. Differences arise in the evaluation of  $\alpha_{\mu} \equiv H_{\mu\mu}^{\text{core}}$  and  $\beta_{\mu\nu} \equiv H_{\mu\nu}^{\text{core}}$ . We have shown previously [15] that in diatomics

$$\alpha_{\mu} = \frac{1}{1 - S_{\mu\nu}^2} \left[ \bar{\alpha}_{\mu} - \frac{1}{2} (1 - \sqrt{1 - S_{\mu\nu}^2}) (\bar{\alpha}_{\mu} - \bar{\alpha}_{\nu}) - S_{\mu\nu} \bar{\beta}_{\mu\nu} \right] \tag{3.16}$$

holds. A combination of (3.16) with (3.8) yields

$$\alpha_a = \bar{\alpha}_a - \frac{1}{2} \frac{(1 - \sqrt{1 - S_{ab}^2}) - (1 - \chi_{ab}^2)}{1 - S_{ab}^2} (\bar{\alpha}_a - \bar{\alpha}_b) - \frac{S_{ab}}{R} \frac{dS_{ab}}{dR}. \tag{3.17}$$

In the CNDO method Pople neglected the second and third term in (3.17) and we followed in (3.7) to keep in line with the CNDO invariance assumptions. In the INDO method however, the neglect of these terms cannot be justified.

To obtain a valid formula for  $\beta_{ab}$ , we use again (3.10), but replace (3.11) by

$$A\bar{\alpha}_a = K_a \bar{\alpha}_a. \tag{3.18}$$

$K$  is considered as an adjustment parameter. The total energy is again separated in atomic and interatomic, SCF and correlation part

$$E = \sum_A (E_A^{\text{SCF}} + E_A^{\text{corr}}) + \sum_{A < B} (E_{AB}^{\text{SCF}} + E_{AB}^{\text{corr}}). \tag{3.19}$$

For reasons of convenience, we do not list the detailed expressions, they can be obtained similarly to the CNDO approach. Differences will not only arise through the appearance of exchange integrals, but also through modification of  $\alpha$ 's and  $\beta$ 's.

#### 4. Orbital Description of the Ground State of $H_2$

To demonstrate the consequences of the foregoing sections, we choose the simple example of the ground state of  $H_2$ . Let us take, for convenience, a double configuration wavefunction which allows for proper dissociation.

$$\Psi = A_0 \Psi_0 + A_1 \Psi_1 \tag{4.1}$$

with

$$\Psi_0 = 1s\sigma_g(1)1s\sigma_g(2)$$

$$\Psi_1 = 1s\sigma_\mu(1)1s\sigma_\mu(2).$$

The first term represents the Hartree-Fock part, the second the correlation part. We now approximate the MO's as a linear combination of symmetrically orthogonalized AO's  $a, b$

$$\begin{aligned} 1s\sigma_g &= \frac{1}{\sqrt{2}}(a+b) \\ 1s\sigma_\mu &= \frac{1}{\sqrt{2}}(a-b). \end{aligned} \quad (4.2)$$

Under neglect of differential overlap the elements of the EHF operator take the form

$$\begin{aligned} F_{aa}^{\text{EHF}} &= \alpha_a + \frac{1}{2} \left( 1 + \frac{1}{2} \frac{A_1}{A_0} \right) (aa|aa) + \left( 1 - \frac{1}{4} \frac{A_1}{A_0} \right) (aa|bb) \\ F_{ab}^{\text{EHF}} &= \beta_{ab} + \frac{1}{4} \frac{A_1}{A_0} (aa|aa) - \frac{1}{2} \left( 1 + \frac{1}{2} \frac{A_1}{A_0} \right) (aa|bb) \end{aligned} \quad (4.3)$$

For  $A_1 = 0$  we obtain the well-known Hartree-Fock elements

$$\begin{aligned} F_{aa}^{\text{SCF}} &= \alpha_a + \frac{1}{2} (aa|aa) + (aa|bb) \\ F_{ab}^{\text{SCF}} &= \beta_{ab} - \frac{1}{2} (aa|bb). \end{aligned} \quad (4.4)$$

If we wish to reduce the diagonal part of the EHF operator to SCF form, we can put

$$\begin{aligned} (aa|aa)' &= \left( 1 + \frac{1}{2} \frac{A_1}{A_0} \right) (aa|aa) \\ (aa|bb)' &= \left( 1 - \frac{1}{4} \frac{A_1}{A_0} \right) (aa|bb). \end{aligned}$$

$A_1/A_0$  is negative, as can be seen from the secular equation

$$\begin{aligned} \frac{A_1}{A_0} &= - \frac{H_{00} - E}{H_{01}} \\ H_{00} &> E, \quad H_{01} > 0. \end{aligned} \quad (4.5)$$

This implies that the single-center repulsion integral is decreased, whereas the two-center integral is increased. The maximum change occurs for large inter-nuclear distances where  $A_1/A_0 \rightarrow -1$  and amounts to 50% decrease for the single-center integral and 25% increase for the two-center integral. Unfortunately, this parametrization cannot be applied to  $F_{ab}^{\text{EHF}}$ . Here,  $(aa|bb)'$  must equal  $\left( 1 + \frac{1}{2} \frac{A_1}{A_0} \right)$  and an entirely new term  $(aa|aa)$  appears. We conclude that it is impossible to define modified one- and two-center integrals consistently for both diagonal and non-diagonal elements of the EHF operator.



We now proceed to the orbital eigenvalues. From symmetry reason, the MO's  $\sigma_g$  and  $\sigma_u$  are orthogonal. So the orthogonalization operator  $R$  can be dropped. Since the AO's are also orthogonal, we obtain

$$\begin{aligned} \epsilon_+^{\text{EHF}} &= F_{aa}^{\text{EHF}} + F_{ab}^{\text{EHF}} \\ &= \alpha_a + \beta_{ab} + \frac{1}{2} \left( 1 + \frac{A_1}{A_0} \right) (aa|aa) + \frac{1}{2} \left( 1 - \frac{A_1}{A_0} \right) (aa|bb) \end{aligned} \quad (4.6)$$

whereas the Hartree-Fock energy would be

$$\epsilon_+^{\text{SCF}} = \alpha_a + \beta_{ab} + \frac{1}{2} (aa|aa) + \frac{1}{2} (aa|bb). \quad (4.7)$$

The total energy is in both cases

$$E = \epsilon_+^{\text{core}} + \epsilon_+$$

so that

$$\begin{aligned} E^{\text{EHF}} &= 2(\alpha_a + \beta_{ab}) + \frac{1}{2} \left( 1 + \frac{A_1}{A_0} \right) (aa|aa) + \frac{1}{2} \left( 1 - \frac{A_1}{A_0} \right) (aa|bb) \\ E^{\text{SCF}} &= 2(\alpha_a + \beta_{ab}) + \frac{1}{2} (aa|aa) + \frac{1}{2} (aa|bb). \end{aligned} \quad (4.8)$$

For large internuclear distances as  $R \rightarrow \infty$ ,  $A_1 \rightarrow -A_0$ , the set of formulas appears as follows

$$\begin{aligned} F_{aa}^{\text{EHF}} &= \alpha_a + \frac{1}{4} (aa|aa) \\ F_{ab}^{\text{EHF}} &= -\frac{1}{4} (aa|aa) \\ \epsilon_+^{\text{EHF}} &= \alpha_a \\ E^{\text{EHF}} &= 2\alpha_a, \end{aligned} \quad (4.9)$$

$$\begin{aligned} F_{aa}^{\text{SCF}} &= \alpha_a + \frac{1}{2} (aa|aa) \\ F_{ab}^{\text{SCF}} &= 0 \\ \epsilon_+^{\text{SCF}} &= \alpha_a + \frac{1}{2} (aa|aa) \\ E^{\text{SCF}} &= 2\alpha_a + \frac{1}{2} (aa|aa). \end{aligned} \quad (4.10)$$

Most noticeable is that the EHF formalism does not only yield the correct total energy  $E$  but also the correct orbital energy  $\epsilon$ . An earlier paper on  $\text{H}_2$  by Hansen [9] used a CI formalism and did not give this insight. Finally, Wahl's formalism with a twice as large coupling operator would lead to  $\epsilon_+ \rightarrow \alpha_a - \frac{1}{2} (aa|aa)$  for  $R \rightarrow \infty$ . So Wahl's orbital energies do not reflect the physical situation.

## 5. Discussion and Conclusion

In this paper, we have developed an Extended Hartree-Fock formalism suitable for semiempirical molecular orbital methods. The advantage of the fact that the correlation energy is represented linearly in the coefficients  $A$  in Eq. (2.4) leads to an SCF like orbital approach reflected in Eq. (2.10) for the total energy. In the case of  $\text{H}_2$  we demonstrated that the eigenvalues of the EHF operator have physically interpretable characteristics, in particular they follow dissociation properly. To treat polyatomics efficiently, further assumptions about

the MO's would be necessary. Work now in progress will use Boys' localization procedure [17] to keep the number of configurations in polyatomics as small as possible. This is not only easier, but supported by recent results for  $\text{CH}_4$  [18] that, contrary to conclusions by Sinanoglu [19], *intra-pair* correlation in localized orbitals is dominant. There are some questions with the orbital picture when the CI part is based on localized orbitals. The following steps would be necessary to keep as close as possible to the delocalized SCF part: 1) Solution of the SCF equations, 2) Localization of the MO's, 3) Solution of the secular equation, 4) Definition of an EHF operator based on localized MO's, 5) Solution of the EHF equations. In general, this last step will partially delocalize the MO's so that the orbital energies  $\epsilon$  will be physically descriptive. In CNDO and INDO like forms with minimal basis sets, left-right and angular correlation can be partially accounted for. But there is no way to include in-out correlation.

We have already applied the new parametrization of  $\beta$  integrals in the CNDO and INDO forms of the theory. Most encouraging results for potential curves and force constants will be published elsewhere [20].

*Acknowledgement* I appreciate the hospitality of Prof. H. Preuss during my stay in his institute. I thank Dr. W. Meyer for a discussion about some aspects of the correlation problem.

## References

1. Pople, J. A., Santry, D. P., Segal, G. A.: J. Chem. Phys. **43**, S 129 (1965) Pople, J. A., Segal, G. A.: J. Chem. Phys. **43**, S 136 (1965). Pople, J. A., Beveridge, D. L., Dobosh, P. A.: J. Chem. Phys. **47**, 2026 (1967)
2. Pople, J. A., Beveridge, D. L.: Approximate molecular orbital theory, p. 89. New York-London: McGraw-Hill 1970
3. Dewar, M. J. S., Haselbach, E.: J. Am. Chem. Soc. **92**, 590 (1970)
4. Löwdin, P. O.: J. Chem. Phys. **18**, 365 (1950)
5. Das, G., Wahl, A. C.: J. Chem. Phys. **47**, 2934 (1967)
6. Veillard, A., Clementi, E.: Theoret. Chim. Acta (Berl.) **7**, 133 (1967)
7. Öksüz, I., Sinanoglu, O.: Phys. Rev. **181**, 42 (1969)
8. Kutzelnigg, W.: Theoret. Chim. Acta (Berl.) **1**, 327 (1963); Ahlrichs, R., Kutzelnigg, W., Bingel, W. A.: Theoret. Chim. Acta (Berl.) **5**, 289 (1966)
9. Hansen, A. E.: Theoret. Chim. Acta (Berl.) **7**, 230 (1967)
10. Brown, R. D., Roby, K. R.: Theoret. Chim. Acta (Berl.) **16**, 291 (1970)
11. Jug, K.: Internat. J. Quant. Chem. **3S**, 241 (1969)
12. Fischer, H., Kollmar, H.: Theoret. Chim. Acta (Berl.) **12**, 345 (1968)
13. Jug, K.: Theoret. Chim. Acta (Berl.) **23**, 183 (1971)
14. Jug, K.: Theoret. Chim. Acta (Berl.) **26**, 231 (1972)
15. Jug, K.: Theoret. Chim. Acta (Berl.) **16**, 95 (1970)
16. Linderberg, J.: Chem. Phys. Letters **1**, 39 (1967)
17. Boys, S. F.: Quantum theory of atoms, molecules and the solid state, ed. by Löwdin, P. O., p. 253. New York: Academic Press 1966
18. Meyer, W.: Private communication
19. Sinanoglu, O., Skutnik, H.: Chem. Phys. Letters **1**, 399 (1968)
20. Coffey, P., Jug, K.: J. Am. Chem. Soc., to be published

Prof. Dr. K. Jug  
Department of Chemistry  
Saint Louis University  
Saint Louis, Missouri 63156, USA

# L'utilisation d'orbitales localisées dans l'étude théorique des molécules

## I. Les hydrocarbures Saturés

Ph. Degand, G. Leroy et D. Peeters

Laboratoire de Chimie Quantique, Louvain, Belgique

Reçu le 8 février 1973

### *Use of Localized Orbitals in the Theoretical Study of Molecules. 1. Saturated Hydrocarbons*

The five simplest alkanes have been studied in terms of localized orbitals. The transferability of the Fock matrix elements in this basis allows us to elaborate a simple parametric procedure adapted for saturated hydrocarbons. Some original applications of this procedure are performed.

**Key words:** Localized orbitals    Saturated hydrocarbons

### Introduction

Les orbitales canoniques obtenues en méthode LCAO-SCF-MO sont délocalisées. Grâce à une transformation unitaire appropriée on peut les localiser dans différents domaines moléculaires conformément à l'intuition chimique. On obtient ainsi des orbitales localisées au niveau des coeurs d'atomes, des liaisons chimiques et des paires libres.

Il existe différents procédés de localisation [1-5] dont les résultats sont généralement comparables.

L'utilisation des orbitales localisées en chimie quantique continue à faire l'objet de nombreuses recherches [6-7].

Ainsi, certains auteurs modifient l'hamiltonien monoélectronique de manière à obtenir directement des orbitales localisées [8-10]. D'autres [11-14] utilisent une base de fonctions localisées dans des calculs *ab initio*.

De son côté, Rothenberg [15] a démontré clairement le caractère transférable des orbitales localisées C-H obtenues par la méthode d'Edmiston-Ruedenberg [2] [E.-R.].

Dans ce travail, nous étudions de façon approfondie les propriétés des orbitales localisées obtenues par le procédé de Magnasco-Perico [4] [M.-P.]. Celui-ci consiste essentiellement à rechercher la matrice de transformation qui rend maximum une fonction de localisation définie en termes de populations locales de coeurs, de liaisons et de paires libres. Nous avons choisi ce procédé à cause de la simplicité des calculs qu'il requiert et de la similitude que présentent ses résultats avec ceux de la méthode E.-R. Nous avons tout d'abord localisé les résultats *ab initio* obtenus dans une série d'hydrocarbures saturés, grâce au procédé M.-P.

Les résultats de la localisation sont présentés dans le premier paragraphe. Les détails techniques et la description du programme de calcul écrit pour un ordinateur IBM 370/155 seront publiés ultérieurement [16].

Dans le second paragraphe, nous proposons une méthode paramétrique exploitant la transférabilité des orbitales localisées et de leurs propriétés.

Cette méthode, préalablement testée sur des molécules déjà étudiées, est également appliquée à quelques nouveaux systèmes.

Les calculs décrits dans ce paragraphe ont été effectués sur un ordinateur IBM 1130 ce qui illustre la simplicité de la méthode.

### Résultats et discussion

Nous avons localisé les résultats des calculs *ab initio* effectués précédemment [18] sur le méthane, l'éthane, le propane, le butane normal et l'isobutane.

Les coefficients LCAO-SCF-LO supérieurs à 0,05, préalablement recalculés en utilisant un système d'axes de référence unique, sont repris dans les tableaux 1, 2 et 3. Nous y donnons également le degré de localisation de chaque orbitale localisée ainsi que le pourcentage  $s$  des différentes liaisons.

Le degré de localisation est apprécié en calculant l'écart entre l'orbitale considérée et une orbitale strictement localisée  $\theta^{ST}$ . Par définition  $\theta^{ST}$  ne contient que les orbitales correspondant au coeur ou à la liaison considérée affectées de coefficients renormalisés.

L'écart quadratique est calculé par la formule (1):

$$Q_i = \frac{1}{2} \int (\theta_i - \theta_i^{ST})^2 d\tau \quad (1)$$

que l'on peut développer comme suit:

$$Q_i = 1 - \frac{1}{2} \sum_p \sum_q C_{pi} C_{qi}^{ST} S_{pq} \quad (2)$$

$S_{pq}$  est une intégrale de recouvrement dans la base atomique;  $C_{pi}$  et  $C_{qi}^{ST}$  désignent respectivement les coefficients LCAO des orbitales localisées et strictement localisées.

Quant au pourcentage  $s$  d'une liaison, on l'obtient grace à la relation (3):

$$s_{AB} = \frac{C_{2sA}^2 + C_{2sB}^2}{\sum_n (C_{2nA}^2 + C_{2nB}^2)} \quad \text{avec } n = s, p_x, p_y, p_z \quad (3)$$

Les résultats repris dans les tableaux 1, 2 et 3 illustrent le caractère transférable des différents types de liaison.

En particulier, les coefficients importants sont peu modifiés d'un composé à l'autre.

On notera aussi que les orbitales de coeur sont plus localisées que les orbitales de liaison.

Celles-ci renferment en effet, des termes non négligeables provenant des atomes voisins.

Tableau 1. Caractéristiques des orbitales de coeur

Orbitale <sup>a</sup>	Composé	Ecart quadratique	% s	Coefficients LCAO-LO
1s (4)	CH <sub>4</sub>	0,007	—	1,0228(1s) — 0,0805(2s)
1s (3)	C <sub>2</sub> H <sub>6</sub>	0,007	—	1,0223(1s) — 0,0774(2s)
1s (3)	C <sub>3</sub> H <sub>8</sub>	0,007	—	1,0224(1s) — 0,0770(2s)
1s (2)	C <sub>3</sub> H <sub>8</sub>	0,007	—	1,0220(1s) — 0,0740(2s)
1s (1)	i C <sub>4</sub> H <sub>10</sub>	0,007	—	1,0216(1s) — 0,0719(2s)

<sup>a</sup> Le chiffre entre parenthèses indique le nombre d'atomes d'hydrogène liés au carbone.

Tableau 2. Caractéristiques des orbitales localisées C-H

Orbitale <sup>a</sup>	Système	Ecart quadratique	% s	Coefficients LCAO-LO <sup>b</sup>
C-H (4)	CH <sub>4</sub>	0,012	28,6	- 0,0651(1s) + 0,3413(2s) + 0,5388(p) + 0,4809(H) - 0,0656(H)(3x)
C-H (3)	C <sub>2</sub> H <sub>6</sub>	0,015	28,0	- 0,0647(1s) + 0,3388(2s) + 0,5439(p) + 0,4870(H) - 0,0677(H)(2x) + 0,0616(H)*
C-H (3)	C <sub>3</sub> H <sub>8</sub>	0,015	27,3	- 0,0641(1s) + 0,3358(2s) + 0,5479(p) + 0,4857(H) - 0,0690(H)(2x) + 0,0607(H)*
CH (2)	C <sub>3</sub> H <sub>8</sub>	0,018	26,2	- 0,0635(1s) + 0,3316(2s) + 0,5567(p) + 0,4888(H) + 0,0741(H) + 0,0636(H)* (2x)
CH (1)	C <sub>4</sub> H <sub>10</sub>	0,020	26,3	- 0,0640(1s) + 0,3337(2s) + 0,5582(p) + 0,4908(H) + 0,0608(H)* (3x)

<sup>a</sup> Le chiffre entre parenthèses indique le nombre d'atomes d'hydrogène liés au carbone.

<sup>b</sup> L'astérisque \* note un atome d'hydrogène en position «conjuguée» par rapport à la liaison

Tableau 3. Caractéristiques des orbitales localisées C'-C'

Orbitale <sup>a</sup>	Système	Ecart quadratique	% s	Coefficients LCAO-LO <sup>b</sup>
C(3)-C'(3)	C <sub>2</sub> H <sub>6</sub>	0,020	27,8	- 0,0651(1s) + 0,3081(2s) — 0,4967(2p) — 0,0651(1s') + 0,3081(2s') + 0,4967(2p') — 0,0575(H)(6x)
C(3)-C'(2)	C <sub>3</sub> H <sub>8</sub>	0,023	28,1	- 0,0676(1s) + 0,3147(2s) — 0,4941(2p) — 0,0653(1s') + 0,3077(2s') + 0,5010(2p') — 0,0558(H)(3x) - 0,0591(H)(2x) + 0,0544(H)* (1x)
C(2)-C'(2)	C <sub>4</sub> H <sub>10</sub> n	0,025	28,2	- 0,0667(1s) + 0,3135(2s) — 0,5006(2p) — 0,0667(1s') + 0,3135(2s') + 0,5006(2p') — 0,0585(H)(4x) + 0,0529(H)* (2x)
C(3)-C'(1)	C <sub>4</sub> H <sub>10</sub> i	0,026	27,4	- 0,0643(1s) + 0,3046(2s) — 0,5110(2p) — 0,0679(1s') + 0,3150(2s') + 0,4981(2p') — 0,0578(H)(3x) - 0,0633(H)(1x) + 0,0539(H)* (2x)

<sup>a</sup> Les chiffres entre parenthèses indiquent les nombres d'atomes d'hydrogène liés aux carbones.

<sup>b</sup> L'astérisque \* note un atome d'hydrogène en position «conjuguée» par rapport à la liaison.

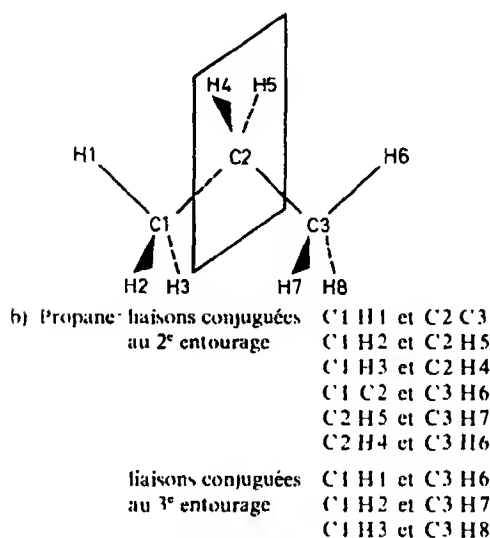
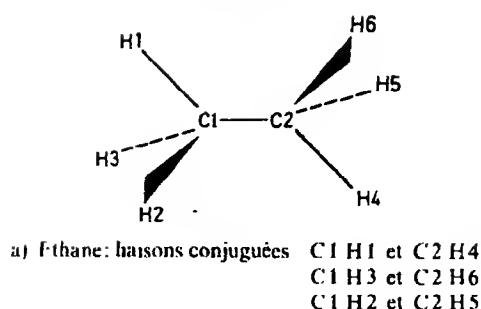


Fig. 1. Liaisons «conjuguées» dans l'éthane et le propane

L'analyse de ces termes conduit à introduire la notion de «position conjuguée» illustrée dans la Fig. 1.

Deux liaisons, séparées par une ou plusieurs autres liaisons, sont dites conjuguées si elles sont disposées, dans un même plan, symétriquement par rapport à un centre ou un plan de symétrie.

Il est intéressant de constater que les orbitales atomiques excédentaires des liaisons C-H proviennent d'une part des atomes d'hydrogène voisins et d'autre part des atomes d'hydrogène en «position conjuguée».

Les coefficients LCAO-LO relatifs aux hydrogènes conjugués ont toujours le même signe que le coefficient de l'atome d'hydrogène de la liaison considérée et un signe contraire à celui des coefficients des hydrogènes immédiatement voisins de la liaison.

Des conclusions similaires peuvent être tirées de l'analyse des orbitales localisées C-C.

Nous réunissons dans le tableau 4 les contributions de chaque orbitale localisée aux populations totales des atomes, dans les trois premiers composés étudiés.

Tableau 4. Contribution des orbitales localisées aux populations totales des atomes

$\text{CH}_4$	O.L. Atome	1s	C1H1	C1H2(3x)
	C1	2	1,20	1,20
	H1	0	0,85	-0,02

$\text{C}_2\text{H}_6$	O.L. Atome	1sC1	1sC2	C1C2	C1H1	C1H2(2x)	C2H4(3x)
	C1	2	0	1,04	1,20	1,20	-0,02
	H1	0	0	-0,01	0,86	-0,02	0

$\text{C}_3\text{H}_8$	O.L. Atome	1sC1	1sC2	1sC3	C1C2	C2C3	C1H1	C1H2(2x)	C2H4	C2H5	C3H1
	C1	2	0	0	1,05	-0,02	1,20	1,20	-0,02	-0,02	0
	C2	0	2	0	1,05	1,05	-0,02	-0,02	1,20	1,20	-0,02
	H1	0	0	0	-0,01	0	0,86	-0,02	0	0	0
	H4	0	0	0	-0,01	-0,01	0	0	0,86	-0,02	0

Tableau 5. Matrice de Fock du méthane dans une base d'orbitales localisées (u.a.)

	1sC	C1H1	CH2	C'H3	C'H4
C	-11,2112				
H1	-0,6447	-0,7383			
H2	-0,6447	-0,1383	-0,7383		
H3	-0,6447	-0,1383	-0,1383	-0,7383	
H4	-0,6447	-0,1383	-0,1383	-0,1383	-0,7383

Tableau 6. Matrice de Fock de l'éthane dans une base d'orbitales localisées (u.a.)

	1sC1	1sC2	C1C2	C1H1	C1H2	C1H3	C2H4	C2H5	C
C1	-11,2233								
C2	+0,0177	-11,2233							
C2	-0,6112	-0,6112	-0,8361						
H1	-0,6407	+0,0540	-0,1344	-0,7346					
H2	-0,6407	+0,0540	-0,1344	-0,1361	-0,7346				
H3	-0,6407	+0,0540	-0,1344	-0,1361	-0,1360	-0,7346			
H4	+0,0540	-0,6407	-0,1344	+0,0428	-0,0137	-0,0137	-0,7346		
H5	+0,0540	-0,6407	-0,1344	-0,0137	+0,0428	-0,0137	-0,1361	-0,7346	
H6	+0,0540	-0,6407	-0,1344	-0,0137	-0,0137	+0,0428	-0,1361	-0,1361	-C

A nouveau, ces contributions présentent un caractère transférable évident.

Les matrices de Fock des trois premiers alcanes, calculées en base localisée, sont reprises dans les tableaux 5, 6 et 7. Elles ont été obtenues grâce à la relation (4):

$$H^{\text{O.L.}} = \tilde{T} \epsilon T \quad (4)$$

dans laquelle  $T$  est la matrice de transformation des orbitales moléculaires en orbitales localisées et  $\epsilon$ , la matrice des énergies des orbitales moléculaires.

L'examen des tableaux 5, 6 et 7 permet de faire quelques observations intéressantes.

Tableau 7 Matrice de Fock du propane dans une base d'orbitales localisées (u.a.)

1sC1	1sC2	1sC3	C1C2	C2C3	C1H1	C1H2	C1H3	C2H4	C2H5	C3H6	C3H7	C3H8
-11,2192												
+ 0,0192	-11,2375											
- 0,0042	+ 0,0192	-11,2192										
- 0,6237	- 0,6178	+ 0,0525	-0,8527									
+ 0,0525	- 0,6178	- 0,6237	-0,1284	-0,8527								
- 0,6374	+ 0,0555	- 0,0222	-0,1317	+ 0,0419	-0,7372							
- 0,6358	+ 0,0550	+ 0,0054	-0,1343	-0,0124	-0,1370	-0,7376						
- 0,6358	+ 0,0550	+ 0,0054	-0,1343	-0,0124	-0,1370	-0,7376	-0,7392					
+ 0,0523	- 0,6305	+ 0,0523	-0,1335	-0,1335	-0,0144	-0,0145	+ 0,0425	-0,7392				
+ 0,0523	- 0,6305	+ 0,0523	-0,1335	-0,1335	-0,0144	+ 0,0425	-0,0145	-0,1376	-0,7392			
- 0,0222	+ 0,0555	- 0,6374	+ 0,0420	-0,1317	-0,0088	-0,0040	+ 0,0040	-0,0144	-0,0144	-0,7372		
+ 0,0054	+ 0,0550	- 0,6374	-0,0124	-0,1343	+ 0,0040	-0,0105	-0,0019	-0,0145	+ 0,0425	-0,1370	-0,7375	
+ 0,0054	+ 0,0550	- 0,6374	-0,0124	-0,1343	+ 0,0046	-0,0019	-0,0105	+ 0,0425	-0,0145	-0,1370	-0,1370	-0,7375

Tableau 8 Valeurs extrêmes et moyennes de quelques éléments de Fock localisés

Élément	Valeur maximum	Système	Valeur minimum	Système	Valeur moyenne
$h_{CH}$	-0,7415	$i$ C <sub>4</sub> H <sub>10</sub>	-0,7331	$n$ C <sub>4</sub> H <sub>10</sub>	-0,735
$h_{CC}$	-0,8527	C <sub>3</sub> H <sub>8</sub>	-0,8361	C <sub>2</sub> H <sub>6</sub>	-0,840
$(h_{CH}-CH)_0$	-0,1430	C <sub>4</sub> H <sub>10</sub>	-0,1360	C <sub>2</sub> H <sub>6</sub>	-0,136
$(h_{CH}-CC)_0$	-0,1355	$i$ C <sub>4</sub> H <sub>10</sub>	-0,1305	$n$ C <sub>4</sub> H <sub>10</sub>	-0,134
$(h_{CH}-1sC)_0$	-0,6447	CH <sub>4</sub>	-0,6305	C <sub>3</sub> H <sub>8</sub>	-0,640
$(h_{CC}-1sC)_0$	-0,6237	C <sub>3</sub> H <sub>8</sub>	-0,6071	$i$ C <sub>4</sub> H <sub>10</sub>	-0,615
$(h_{CC}-CC)_0$	-0,1285	$i$ C <sub>4</sub> H <sub>10</sub>	-0,1266	$n$ C <sub>4</sub> H <sub>10</sub>	-0,128
$(h_{CH}-CH)_1$	-0,0145	$n$ C <sub>4</sub> H <sub>10</sub>	-0,0137	$n$ C <sub>4</sub> H <sub>10</sub>	-0,014
$(h_{CH}-CH)_1$	+0,0415	C <sub>4</sub> H <sub>10</sub>	+0,0425	C <sub>3</sub> H <sub>8</sub>	+0,042



1. Pour un type donné de liaison ou de terme d'interaction entre liaisons, l'élément de matrice garde une valeur approximativement constante d'un composé à l'autre.

2. La valeur absolue des éléments de matrice décroît avec la distance entre les orbitales, dans l'ordre suivant:

$$h_{ii} > (h_{ij})_0 > (h_{ij}^*)_1 > (h_{ij})_1 > (h_{ij}^*)_2 > (h_{ij})_2 > (h_{ij})_3 \approx 10^{-3} \text{ u.a.}$$

Le chiffre placé en indice est égal au nombre de liaisons qui séparent les orbitales en interaction. La présence de l'astérisque indique que les orbitales considérées sont «en conjugaison».

3. Il s'ensuit logiquement que les valeurs des éléments non diagonaux dépendent intimement de la conformation de la molécule.

Le tableau 8 illustre le caractère transférable des éléments de Fock dans une base d'orbitales localisées.

Pour chaque élément repris dans le tableau, nous indiquons les valeurs extrêmes que nous avons relevées ainsi que la valeur moyenne calculée en tenant compte de l'ensemble des résultats obtenus. A ce stade du travail, nous pouvons déjà constater que les méthodes de localisation s'avèrent utiles non seulement pour préciser quantitativement les concepts traditionnels de liaison chimique et de paire libre mais encore à cause du caractère transférable que présentent les éléments de matrice de l'hamiltonien monoélectronique dans une base localisée. On prévoit dès lors la possibilité de construire a priori des matrices de Fock «synthétiques» de systèmes complexes en utilisant des paramètres obtenus dans l'étude de composés plus simples. Nous développerons cet aspect du problème dans le paragraphe suivant.

Signalons encore que les résultats que nous avons obtenus par le procédé de localisation de Boys ne présentent pas un caractère transférable comparable à celui des résultats de la méthode de Magnasco et Perico.

Nous retrouvons ainsi une conclusion déjà émise par Bonaccorsi *et al.* [17].

## Description et application d'un procédé LCLO-SCF-MO paramétrisé

### 1. Formalisme de la méthode

Les orbitales moléculaires  $\varphi_j$  doivent satisfaire l'équation monoélectronique:

$$h^{\text{SCF}} \varphi_j = \varphi_j \epsilon_j. \quad (5)$$

Développées en termes de fonctions localisées, les orbitales moléculaires s'écrivent:

$$\varphi_j = \sum_p \theta_p T_{pj}. \quad (6)$$

L'équation (6) devient alors:

$$\sum_p h^{\text{SCF}} \theta_p T_{pj} = \sum_p \theta_p T_{pj} \epsilon_j \quad (7)$$

soit encore, en langage matriciel:

$$H^{\text{O.L.}} T = A T \epsilon. \quad (8)$$

Tableau 9. Paramètres de base pour construire des matrices  $H^{O.L.}$  synthétiques

a) Eléments diagonaux						
Orbitale	(1sC) <sub>CH<sub>4</sub></sub>	(1sC) <sub>primaire</sub>	(1sC) <sub>sec</sub>	(1sC) <sub>ter</sub>	CH	CC
$h_{ii}(\text{u.a.})$	11,211	-11,220	-11,235	-11,250	-0,735	-0,840
b) Eléments non diagonaux*						
Elément	$h_{ij}(\text{u.a.})$	Elément	$h_{ij}(\text{u.a.})$	Elément	$h_{ij}(\text{u.a.})$	
(1sC-CH) <sub>0</sub>	0,640	(1sC-CC) <sub>0</sub>	-0,615	(1sC-1sC) <sub>1</sub>	+0,019	
(1sC-CH) <sub>1</sub>	+0,052	(1sC-CC) <sub>1</sub>	+0,050			
(CH-CH) <sub>0</sub>	0,136	(CH-CC) <sub>0</sub>	-0,134			
(CH-CH) <sub>1</sub>	-0,014	(CH-CC) <sub>1</sub>	-0,012			
(CH-CH) <sub>1</sub> <sup>*</sup>	+0,042	(CH-CC) <sub>1</sub> <sup>*</sup>	+0,040			
(CC-CH) <sub>0</sub>	0,134	(CC-CC) <sub>0</sub>	-0,128			
(CC-CH) <sub>1</sub>	0,012	(CC-CC) <sub>1</sub>	(-0,012)			
(CC-CH) <sub>1</sub> <sup>*</sup>	+0,040	(CC-CC) <sub>1</sub> <sup>*</sup>	+0,040			
(CH-CH) <sub>2</sub> <sup>*</sup>	0,011	(CH-CC) <sub>2</sub> <sup>*</sup>	-0,010			
(CC-CH) <sub>2</sub> <sup>*</sup>	-0,010	(CC-CC) <sub>2</sub> <sup>*</sup>	-0,010			

\* Les valeurs entre parenthèses ont été estimées.

Comme les orbitales localisées sont orthogonales par construction, l'équation (8) s'écrit enfin:

$$H^{O.L.} T = T \epsilon. \quad (9)$$

Dans le paragraphe précédent, nous avons mis en évidence le caractère transférable des éléments de la matrice  $H^{O.L.}$ .

Il est dès lors aisé de construire la matrice  $H^{O.L.}$  «synthétique» de n'importe quel hydrocarbure saturé.

Nous reprenons dans le tableau 9 les valeurs moyennes des éléments de Fock à utiliser dans ce but. Toutes celles qui étaient inférieures au seuil de  $10^{-2}$  u.a. ont été négligées.

Le procédé LCLO-SCF-MO paramétrisé comporte trois parties.

a) La construction de la matrice de Fock synthétique pour le composé considéré.

b) La diagonalisation de cette matrice en vue d'obtenir  $T$  et  $\epsilon$ .

c) Le calcul des grandeurs traditionnelles de la chimie quantique telles que les populations d'atomes et de liaisons.

Dans ce but il faut calculer les coefficients LCAO classiques en utilisant les développements transférables des fonctions localisées en termes d'orbitales atomiques.

On peut en effet écrire:

$$\theta = \chi C' \quad (10)$$

$$\varphi = \theta T \quad (11)$$

soit encore:

$$\varphi = \chi C' T. \quad (12)$$

Comme :

$$\varphi = \chi C, \quad (13)$$

on en déduit la relation :

$$C = C' T \quad (14)$$

où les coefficients LCAO-MO sont exprimés en fonction des coefficients LCAO-LO, dont nous avons reconnu le caractère transférable, et des éléments de la matrice de transformation obtenus dans la première partie du procédé.

## 2. Test de la méthode

Nous avons testé le procédé LCLO-SCF-MO décrit dans le paragraphe précédent en l'appliquant aux hydrocarbures saturés ayant déjà fait l'objet d'un calcul *ab initio*.

Nous nous sommes intéressés tout particulièrement à l'influence des différents types d'interaction sur les énergies d'orbitales. Nous donnons respectivement dans les tableaux 10, 11 et 12 les différentes matrices synthétiques du méthane, de l'éthane et du propane obtenues en limitant successivement les interactions au premier, deuxième et troisième entourage.

Les énergies d'orbitales résultant des diagonalisations de ces matrices sont chaque fois comparées aux valeurs obtenues dans le calcul *ab initio* correspondant.

Dans le cas du butane, nous nous contentons de donner les énergies d'orbitales calculées dans les différentes options. Ces résultats sont repris dans le tableau 13.

On constate que l'introduction des interactions au deuxième entourage est nécessaire pour lever certaines dégénérescences et retrouver des énergies d'orbitales voisines de celles du calcul *ab initio* complet.

Les résultats de la deuxième colonne du tableau 13 sont à rapprocher de ceux obtenus par Fukui [19] dans le cadre de l'approximation «H».

L'imperfection de ce modèle peut être levée, dans notre procédé grâce à l'introduction de termes d'interaction complémentaires dans la matrice  $H^{0,1}$ .

Tableau 10. Matrice synthétique et énergies d'orbitales du méthane

	1sC	CH1	CH2	CH3	CH4
1sC	- 11,210				
CH1	- 0,640	- 0,735			
CH2	- 0,640	- 0,136	- 0,735		
CH3	- 0,640	- 0,136	- 0,136	- 0,735	
CH4	- 0,640	- 0,136	- 0,136	- 0,136	- 0,735

$\epsilon$ (u.a.)	Calcul <i>ab initio</i>	Diagonalisation de $H^{0,1}$
1	- 11,3738	- 11,3702
2	- 0,9904	- 0,9828
3	- 0,6000	- 0,5990
4	- 0,6000	- 0,5990
5	- 0,6000	- 0,5990

Tableau 11. Matrices synthétiques et énergies d'orbitales de l'éthane<sup>a</sup>

	1sC1	1sC2	C1C2	C1H1	C1H2	C1H3	C2H4	C2H5
1sC1	-11,220							
1sC2	+ 0,019	-11,220						
C1C2	- 0,615	- 0,615	- 0,840					
C1H1	- 0,640	+ 0,052	- 0,134	- 0,735				
C1H2	- 0,640	+ 0,052	- 0,134	- 0,136	- 0,735			
C1H3	0,640	+ 0,052	- 0,134	- 0,136	- 0,136	- 0,735		
C2H4	+ 0,052	- 0,640	- 0,134	+ 0,042	- 0,014	- 0,014	- 0,735	
C2H5	+ 0,052	0,640	- 0,134	- 0,014	+ 0,042	- 0,014	- 0,136	- 0,735
C2H6	+ 0,052	0,640	- 0,134	- 0,014	- 0,014	+ 0,042	- 0,136	- 0,136

i (u.a)	Calcul ab initio	Diagonalisation de $H^{0,1}$	
		1 <sup>er</sup> entourage	2 <sup>e</sup> ent.
1	- 11,3812	- 11,4167	- 11,378
2	- 11,3808	- 11,3389	- 11,377
3	- 1,0767	- 1,0655	- 1,076
4	0,8821	- 0,8881	- 0,882
5	- 0,6510	- 0,5990	- 0,655
6	- 0,6510	- 0,5990	- 0,655
7	0,5752	- 0,5990	- 0,579
8	- 0,5419	- 0,5990	0,543
9	0,5419	- 0,5848	- 0,543

<sup>a</sup> Les valeurs encadrées correspondent aux interactions faisant intervenir le deuxième entourage.

Sauf dans les systèmes hautement symétriques comme le néopentane, il n'est généralement pas nécessaire de prendre en considération les interactions au troisième entourage pour obtenir des résultats satisfaisants.

Notons encore que les potentiels d'ionisation théoriques obtenus par notre procédé, dans le cadre de l'approximation de *Koopmans* [20] peuvent être corrélés aux valeurs expérimentales correspondantes par la relation linéaire:

$$I = -0.9674 \varepsilon - 2,737 \text{ (eV)}. \quad (15)$$

Celle-ci permet de prévoir le potentiel d'ionisation d'un alcane dont l'énergie de la dernière orbitale occupée a été préalablement déterminée par notre méthode (voir tableau 14).

### 3. Application de la méthode

Le procédé respectivement décrit et testé dans les paragraphes précédents a été appliqué aux six composés suivants: le pentane normal, l'isopentane, le néopentane, l'hexane normal, le cyclohexane dans sa forme chaise et l'heptane normal.

Certains éléments de matrice non repris dans la systématique précédemment établie ont été estimés sur la base d'analogies avec d'autres éléments connus.



Tableau 13. Energies d'orbitales du butane normal

$\epsilon$ (u.a.)	Calcul	Diagonalisation de $H^{(0)}$		
	<i>ab initio</i>	1 <sup>er</sup> entourage	2 <sup>e</sup> entourage	3 <sup>e</sup> entourage
1	- 11,3858	- 11,4502	- 11,3926	- 11,3925
2	11,3854	11,4053	- 11,3921	- 11,3920
3	11,3764	11,3566	- 11,3763	- 11,3733
4	11,3764	- 11,3240	- 11,3756	- 11,3756
5	1,1348	1,1141	- 1,1320	- 1,1375
6	1,0385	- 1,0296	- 1,0430	- 1,0344
7	0,9122	- 0,9199	- 0,9120	- 0,9081
8	0,8400	- 0,8280	- 0,8293	- 0,8392
9	0,6890	0,5990	- 0,6896	- 0,6996
10	0,6506	0,5990	- 0,6542	- 0,6506
11	0,6416	0,5990	0,6336	- 0,6365
12	0,6234	- 0,5990	- 0,6295	- 0,6240
13	0,5771	0,5990	- 0,5894	- 0,5810
14	0,5491	0,5990	- 0,5644	- 0,5544
15	0,5461	0,5876	0,5411	- 0,5371
16	0,5286	0,5859	- 0,5166	- 0,5225
17	0,5115	0,5843	- 0,5084	- 0,5179

Tableau 14. Potentiels d'ionisation calculés et observés (eV)

Composé	I(Th.)	I(Th.)	I(exp.) [21]
	Calcul <i>ab initio</i>	- 0,9674 $\epsilon$ - 2,737	
CH <sub>4</sub>	16,32	13,03	12,99
C <sub>2</sub> H <sub>6</sub>	14,74	11,55	11,65
C <sub>3</sub> H <sub>8</sub>	14,26	11,08	11,21
C <sub>4</sub> H <sub>10</sub> <i>n</i>	13,91	10,89	10,80
C <sub>4</sub> H <sub>10</sub> <i>t</i>	14,22	10,88	10,79
C <sub>4</sub> H <sub>12</sub> <i>n</i>		10,80	10,55
C <sub>4</sub> H <sub>12</sub> <i>t</i>		10,70	10,60
C <sub>4</sub> H <sub>12</sub> néo		10,61	10,29
C <sub>6</sub> H <sub>14</sub> <i>n</i>		10,74	10,48
C <sub>6</sub> H <sub>12</sub> cyclo		10,35	10,16
C <sub>7</sub> H <sub>16</sub> <i>n</i>		10,65	10,35

Ainsi, l'élément de cœur relatif à un atome de carbone quaternaire a été pris égal à - 11,265 u.a. Comme les composés envisagés n'ont pas encore fait l'objet d'un calcul *ab initio*, la qualité des résultats théoriques a été évaluée en comparant les potentiels d'ionisation calculés par la formule (15) aux valeurs expérimentales correspondantes.

Dans l'ensemble, on observe un très bon accord entre les deux séries de valeurs comme le montre le tableau 14.

Il faut noter que l'introduction des interactions au troisième ordre n'a été nécessaire que dans le cas du néopentane.

D'autre part, l'inversion dans l'ordre des potentiels d'ionisation constatée au niveau du pentane normal et de l'isopentane est peut-être imputable à une erreur

expérimentale car le potentiel d'ionisation d'un dérivé à chaîne normale est en général supérieur à celui de l'isomère «iso» correspondant.

Notre procédé paramétrisé dont les bases théoriques sont clairement établies fournit, avec un minimum de labeur, des résultats comparables à ceux des méthodes purement empiriques de Hall [22], Fueki [23], Lorquet [24] et d'autres auteurs dont les travaux ont fait l'objet d'une analyse critique détaillée dans un article de Herndon [25].

### Conclusion

Le caractère transférable de nombreuses grandeurs calculées dans une base d'orbitales localisées, par le procédé de Magnasco et Perico nous a permis d'élaborer un procédé quantique paramétrisé pour étudier les hydrocarbures saturés.

Ce procédé qui repose sur une systématique d'éléments de Fock établie en termes d'entourages successifs permet de calculer les différentes grandeurs généralement obtenues dans les calculs *ab initio*, à savoir les énergies d'orbitales et les coefficients LCAO-MO.

On peut également atteindre l'énergie totale en exploitant la transférabilité des termes cinétiques dans la base localisée et en utilisant le théorème du viriel [26].

L'obtention des orbitales virtuelles elles-mêmes n'est pas à exclure [3] mais leur intérêt est assez restreint.

Au total les résultats déjà obtenus sont suffisamment encourageants pour justifier la généralisation du procédé à tous les types de composés chimiques «localisables».

Nous envisageons également, comme amélioration possible de la méthode, l'emploi d'une base d'orbitales hybrides.

La localisation d'orbitales moléculaires développées en termes d'hybrides est en effet généralement bien meilleure et conduit à des grandeurs mieux transférables.

L'emploi des techniques de localisation présente ainsi de multiples avantages.

Il permet l'analyse des résultats *ab initio* en termes de liaisons chimiques et fournit la possibilité de définir quantitativement le concept de «liaisons semblables» qui joue un rôle essentiel en thermochimie.

Il débouche naturellement sur des procédés *ab initio* paramétrisés qui permettent d'étudier de façon satisfaisants des composés renfermant de nombreux atomes et fournissent en outre des coefficients LCAO-MO pouvant servir de vecteurs d'essai dans des méthodes *ab initio* plus élaborées [27].

*Remerciements.* L'un de nous (D. Peeters) exprime ses remerciements à «l'Institut pour l'Encouragement de la Recherche Scientifique dans l'Industrie et l'Agriculture» (I.R.S.I.A.), pour le mandat qui lui a été accordé.

### Bibliographie

1. Lennard-Jones, J.E., Pople, J.A.: Proc. Roy. Soc. (London) A **202**, 166 (1950).
2. Edmiston, C.E., Ruedenberg, K.: Rev. Mod. Phys. **35**, 457 (1963).
3. Boys, S.F.: Rev. Mod. Phys. **32**, 296 (1960). — Foster, J.M., Boys, S.F.: Rev. Mod. Phys. **32**, 300 (1960).
4. Magnasco, V., Perico, A.: J. Chem. Phys. **48**, 800 (1968).

5. Peters, D.: *J. Chem. Soc. (London)* **1963**, 2003.
6. Berthier, G., Meyer, A.Y., Praud, L.: *The Jerusalem symposia on quantum chemistry and biochemistry*, III, p. 174. Jerusalem: Israel Academy of Sciences and Humanities (1971).
7. Newton, M.D., Switkes, E.: *J. Chem. Phys.* **54**, 3179 (1971). — Lipscomb, W.: *J. Chem. Phys.* **53**, 2645 (1970).
8. Peters, D.: *J. Chem. Phys.* **51**, 1559 (1969).
9. Adams, W.H.: *J. Chem. Phys.* **34**, 89 (1961); **37**, 2009 (1962); **42**, 4030 (1965).
10. Gilbert, I. L.: *Molecular orbitals in chemistry physics and biology*, ed. by P. O. Lowdin, B. Pullman, p. 405. New York: Academic Press 1964.
11. Polak, R.: *Theoret. chim. Acta (Berl.)* **14**, 163 (1969).
12. Hoyland, I. R.: *J. Am. Chem. Soc.* **90**, 2227 (1968); **50**, 473 (1969).
13. Barthelat, J. C., Durand, Ph.: *Theoret. chim. Acta (Berl.)* **27**, 109 (1972).
14. Letcher, J. C., Dunning, T. H.: *J. Chem. Phys.* **48**, 4538 (1968). — Letcher, J. H.: *J. Chem. Phys.* **54**, 3215 (1971).
15. Rothenberg, S.: *J. Chem. Phys.* **51**, 3389 (1969).
16. Degand, Ph.: à publier
17. Bonaccorsi, R., Petrongolo, C., Scrocco, E., Tomasi, J.: *Theoret. chim. Acta (Berl.)* **15**, 332 (1969); — *J. Chem. Phys.* **48**, 1500 (1968).
18. André, J. M., Degand, Ph., Leroy, G.: *Bull. Soc. Chim. Belges* **80**, 585 (1971).
19. Fukui, K., Kato, H., Yonezawa, T.: *Bull. Chem. Soc. Japan* **33**, 1197, 1201 (1960).
20. Koopmans, T.: *Physica* **1** **1933**, 104.
21. Vedenev, V. I., Gurvich, I. V., Kondrat'yev, V. N., Medvedev, V. A., Frankevich, Ye. I.: *Bond energies, ionization potentials and electron affinities*. London: Edward Arnold 1966.
22. Hall, G. G.: *Proc. Roy. Soc. (London)* **A205**, 541 (1951).
23. Fues, K.: *J. Phys. Chem.* **68**, 2656 (1964).
24. Lorquet, J. C.: *Mol. Phys.* **9**, 101 (1965).
25. Herndon, W. C.: *Progress in physical organic chemistry*, Vol. 9, A. Streitwieser, jr., R. W. Taft, ed., p. 99. New York: Wiley Interscience 1972.
26. Allen, L. L., Shull, H.: *J. Chem. Phys.* **35**, 1644 (1961).
27. Letcher, J. C., Absar, G., van Wazer, J. R.: *Intern. J. Quantum Chem., Symposium n° 6*, **6**, 451 (1972).

Professeur G. Leroy  
 Laboratoire de Chimie Quantique  
 Celestijnenlaan, 200 G  
 B-3030 Heverlee  
 Louvain, Belgique



## Proton Magnetic Shielding in $\text{H}_2\text{O}$ and $(\text{H}_2\text{O})_2$

Michał Jaszuński and Andrzej J. Sadlej

Institute of Organic Chemistry, Polish Academy of Sciences, Warsaw 42, Poland

Received January 24, 1973

The proton magnetic shielding constants in the water molecule and its linear perpendicular dimer are computed from SCF-MO-LCGO wave functions by using the uncoupled Hartree-Fock variation-perturbation procedure due to Karplus and Kolker. The convergence of the calculated shielding constants as well as their gauge dependence is studied. The final results for 17-term polynomial variation function indicate that the best choice for the gauge origin corresponds to the molecular electronic centroid.

The calculated proton magnetic shielding constant in the water molecule is in remarkable agreement with experimental data and favourably compares with the best coupled Hartree-Fock results. It follows from the calculations for the water dimer that the H-bond NMR-shift amounts in this case  $-1.0$  ppm and qualitatively agrees with the experimental data for the liquid water.

*Key words:* Proton magnetic shielding · Hydrogen bond NMR shift of water molecule and dimer

### Introduction

Recently we have reported [1] the results of the uncoupled Hartree-Fock (UCHF) variation-perturbation calculations of the proton magnetic shielding constant in the water molecule. It was shown that the simplified UCHF scheme due to Karplus and Kolker [2, 3] is able to reproduce the results of the time-consuming and laborious coupled Hartree-Fock (CHF) procedure [4]. Moreover, the gauge non-invariance of the Karplus-Kolker scheme was considerably less pronounced than in the case of the limited basis set CHF calculations [5]. In this way the results for the water molecule confirmed our previous conclusions concerning the validity and applicability of the Karplus-Kolker UCHF method for the calculation of the second-order energies related to pure imaginary operators [6–8].

More recently we have applied the same approach to the calculation of the hydrogen-bond NMR shift in the water dimer [9]. The preliminary results for the hydrogen-bonded proton indicated a down-field shift of the corresponding shielding constant in comparison with the isolated water molecule. It should be pointed out that the paramagnetic effect of the hydrogen-bond formation has been obtained without introducing any empirical parameter and all the calculations have been performed using the Gaussian SCF-MO-wave functions computed recently by Diercksen [10].

In the present paper we report the results of more extensive study of magnetic properties of the linear water dimer. A particular attention is paid to

the influence of the hydrogen bonding on the proton magnetic shielding constant. We shall consider the hydrogen-bonded as well as the outer protons in the water dimer. The results for the water dimer will be compared with analogous calculations for the isolated water molecule. The influence of the choice of the origin for the magnetic field vector potential will also be discussed.

In comparison with previously reported calculations for the water molecule [1] and preliminary results for the water dimer [9] we have extended the polynomial representation of the variation functions. This extension leads to further improvement of the calculated proton shielding constant in the water molecule and lowers the shielding constant of the hydrogen-bonded proton in the water dimer.

### Computational Details

The method employed in the present study — so-called Karplus-Kolker UCHF variation-perturbation procedure — has been extensively described in the previous paper [1] and we refer to this publication for the notation and general discussion. For the sake of clarity we only remind that within the Karplus-Kolker method the first-order perturbed orbitals are approximated in the form

$$u_{i\mu}^{(1,0)} = f_{i\mu}^{(1,0)} u_i^{(0)} - \sum_{k=1}^n \langle u_k^{(0)} | f_{i\mu}^{(1,0)} u_i^{(0)} \rangle u_k^{(0)} \quad (1)$$

(cf. Eq. (7) of Ref. [1]), where  $f_{i\mu}^{(1,0)}$  is the variation function for the magnetic field perturbation in the  $\mu$ -th direction. A usual procedure for the determination of  $f_{i\mu}^{(1,0)}$  is to express it in a polynomial form

$$f_{i\mu}^{(1,0)} = \sum_p^L A_{p,i\mu} g_{p\mu} \quad (2)$$

where  $g_{p\mu}$  are the products of the electronic coordinates with appropriate symmetry. The linear variation parameters  $A_{p,i\mu}$  are then determined by extremizing the second-order energy functional of the Karplus-Kolker method [2, 3]. It should be mentioned that some additional problems arise when the calculated property is bilinear in external perturbations (e.g. the paramagnetic component of the magnetic shielding tensor) [1, 3, 11].

All the calculations presented in this paper were performed by using the method and formulae given in Ref. [1]. The ground state unperturbed wave functions for the isolated water molecule and water dimer are also the same as employed in our previous study [1, 9]. They were recently computed by Diercksen [10] and correspond to the experimental geometry and so-called "linear perpendicular" configuration of the water molecule and water dimer, respectively. The O...O distance in the water dimer equals 3 Å. A detailed description and discussion of the quality of these SCF-MO-LCGO-wave functions can be found in Diercksen's paper [10].

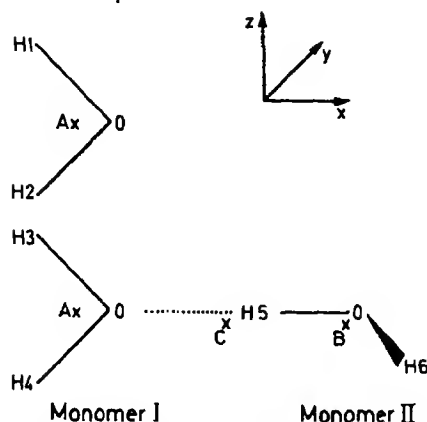


Fig. 1. The coordinate system for  $\text{H}_2\text{O}$  and  $(\text{H}_2\text{O})_2$ .  $A$ ,  $B$ ,  $C$  denote the gauge origins;  $B$  and  $C$  lie in front of the monomer I plane

The variation functions  $f_{i\lambda}^{(1,0)}$  were expressed in terms of the following  $g_{p\lambda}$  functions:

$$\begin{aligned} g_{p\lambda}: & x_\mu, x_\nu, x_\mu x_\nu, x_\lambda x_\nu, x_\lambda x_\mu, x_\mu^2, x_\nu^2; \\ & x_\mu x_\lambda^2, x_\mu x_\mu^2, x_\mu x_\nu^2, x_\nu x_\lambda^2, x_\nu x_\mu^2, x_\nu x_\nu^2; \\ & x_\lambda x_\mu x_\nu, x_\mu x_\nu x_\lambda^2, x_\mu x_\nu x_\mu^2, x_\mu x_\nu x_\nu^2; \end{aligned} \quad (3)$$

where  $(\lambda, \mu, \nu)$  form a cycle and refer to the corresponding Cartesian coordinates. The origin of the coordinate system has been chosen at the oxygen atom [water I in the case of  $(\text{H}_2\text{O})_2$ ]. The coordinate systems employed for the water molecule and its linear dimer are shown in Fig. 1.

In comparison with previously adopted  $g_{p\lambda}$  basis set [1, 9], the present one involves five additional functions and allows for a better representation of the first-order perturbed orbitals. However, it should be mentioned that also the present extension of the polynomial basis set does not remove the node-shift problems discussed in Ref. [1] and these can hardly be avoided within the Karplus-Kolker scheme [3, 12]. On the other hand, this should not significantly affect the results for non-linear molecules considered in this paper.

All the integrals which appear in the Karplus-Kolker functional for the second-order energy [2] as well as those arising in the calculation of the proton magnetic shielding constants were computed according to standard formulae [13, 14]. To evaluate the necessary  $F_m(t)$  functions [14] the analytical approximations of Schaad and Morrell [15] have been employed. The calculations were programmed in Algol and run on the ODRA 1204 computer.

## Results

For any approximate theory of the second-order magnetic properties the gauge dependence of final results is quite obvious and should be carefully examined. We have therefore repeated our calculations for several different ori-

Table 1 The convergence of the paramagnetic contribution to the proton magnetic shielding (in

$I^b$	Monomer <sup>a</sup>		Dimer <sup>a</sup>	
	H 1	H 2	H 3 = H 4	H 5
3	2.919		69.102	-151.294
5	2.919		69.136	-151.485
7	2.919		69.161	-151.502
10	3.341		71.392	-154.108
13	3.257		71.397	-156.558
14	3.480		71.742	-156.565
17	3.776		72.242	-157.246

<sup>a</sup> The gauge origin is taken at the molecular electronic centroid. For the numbering of at see Fig. 1.

<sup>b</sup> See Eqs (2), (3).

gins for the vector potential of the external magnetic field. In the case of isolated water molecule the calculations were carried out in the coordin system of the monomer *I* in the dimer (Fig. 1) and point *A* refers to the ga origin at the monomer electronic centroid. Additionally, the proton shield constant in the isolated monomer has also been computed for the gauge ori chosen at the shielded H atom.

As regards the gauge origin for the water dimer we tried the follow choices:

- (i) the electronic centroid of the monomer *I* in the dimer configur (point *A* in Fig. 1),
- (ii) the electronic centroid of the monomer *II* in the dimer configur (point *B* in Fig. 1), and
- (iii) the electronic centroid of the water dimer (point *C* in Fig. 1).

As will be explained in the next section, the gauge origins (i) (iii) correspc to some supposedly best choices of the origin for the external magnetic fi vector potential in monomers and in the dimer, respectively.

We studied the convergence of the calculated second-order energies using  $g_{PA}$  basis sets with first 3, 5, 7, 10, 13 and 14, and with all the terms appear in (3). It should be mentioned that some of these terms may not contribute to given component of the magnetic susceptibility or magnetic shielding tens. However, they were included in the basis set for symmetry reasons.

The second-order energies quadratic in the magnetic field or in the nucl magnetic moment (see Ref. [1]) exhibit a monotonous, convergent behav with respect to the number of variation parameters. No violation of the variat principle for the Karplus-Kolker approximate UCHF functional has be noticed. For the present study the most interesting is the convergence of calculated paramagnetic contribution ( $\sigma^p$ ) to the proton shielding constants a this is illustrated by the data of Table 1. The corresponding figures refer to gauge origin chosen at the electronic centroid of  $H_2O$  and  $(H_2O)_2$ , respective. For the other gauge origins the convergence of  $\sigma^p$  is quite similar and in w' follows we shall confine our considerations to the results obtained with richest, 17-term representation of variationally determined first-order perturb

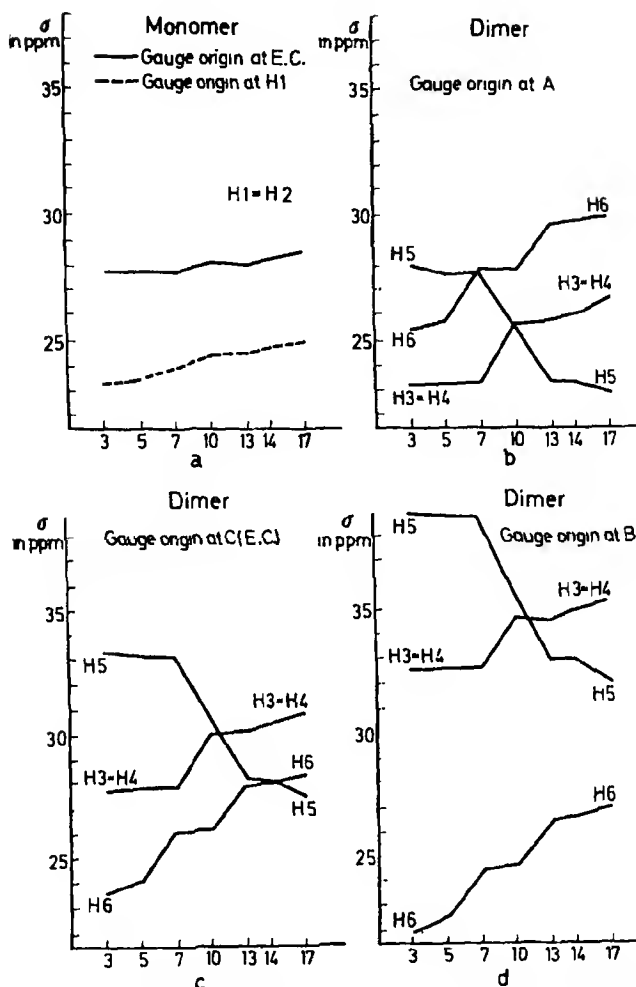


Fig. 2. A schematic plot of the convergence data for  $\sigma$  calculated with different gauge origins

orbitals. However, one can obtain some further information about the convergence of the total proton shielding constant for different gauge origins by looking at Fig. 2. Obviously Fig. 2 has only an illustrative meaning and the scale of the abscissa axis is quite arbitrary.

The final results for the proton magnetic shielding in the water molecule are shown in Table 2. For the gauge origin at the shielded H atom they are compared with the CHF results of Arrighini *et al.* [5] and with the experimental data [16]. Table 2 contains also our previous results obtained with a shorter variation function.

The corresponding results for the water dimer are given in Table 3. In this case we reported only the rotational average of the paramagnetic, diamagnetic

Table 2 Proton magnetic shielding in the water molecule (in ppm)

	Gauge origin	$\sigma_{xx}^p$	$-\sigma_{yy}^p$	$\sigma_{zz}^p$	$\sigma^p$	$\sigma$
This work	c.c.	4.42	6.26	0.65	3.78	28.
KK [1]	c.c.	3.66	6.26	0.65	3.52	28.
This work	H 1	-75.54	-117.07	-39.01	-77.21	25.
KK [1]	H 1	76.65	-118.44	-39.01	-78.03	24.
CH1- [5]	H 1	52.63	-79.18	-25.76	-52.52	50.
Exp. <sup>a</sup>	H 1	71.79	-107.04	-36.57	-71.80	30. $\pm 0.$

<sup>a</sup> Taken from Ref. [5]

Table 3 Proton magnetic shielding in the water dimer (in ppm)

Proton <sup>a</sup>	Gauge <sup>a</sup> origin	$\sigma^p$	$\sigma^d$	$\sigma$
H 3 H 4	A	-18.92	45.69	26.77
	C	72.24	-41.15	31.09
	B	162.93	-127.55	35.39
H 5	A	259.29	282.31	23.02
	C	157.24	184.80	27.56
	B	-55.73	87.80	32.08
H 6	A	80.47	-50.46	30.01
	C	29.43	-0.90	28.53
	B	-21.26	48.32	27.06

<sup>a</sup> See Fig. 1.Table 4. Magnetic susceptibility (in erg/mole gauss<sup>2</sup>)

	Monomer Gauge origin <sup>a</sup>		Dimer Gauge origin <sup>a</sup>		
	A (c.c.)	H 1	A	C (c.c.)	B
$\chi^p$	1119	25.854	269 906	134.414	268.9
$\chi$	-14.290	-13.252	-21.114	-26.256	-20.7

<sup>a</sup> See Fig. 1

and the total shielding constant. There are no experimental data and other theoretical results to be directly compared with our calculations.

On calculating the first-order perturbed orbitals  $\mu_\mu^{(1,0)}$  we obtained as a by-product the paramagnetic contribution ( $\chi^p$ ) to the magnetic susceptibility tensor of  $\text{H}_2\text{O}$  and  $(\text{H}_2\text{O})_2$ . The relevant results for  $\chi^p$  as well as the final values of the total magnetic susceptibility ( $\chi$ ) calculated for different gauge origins were shown in Table 4. It is worth attention that the theoretical value of  $\chi^p$  provides, according to Chan and Das [17], some criterion for the choice of the appropriate gauge origin in approximate calculations.

### Discussion

It is evident from the data of Table 1 that even the 17-term representation of variation functions does not allow to reach a complete convergence of the calculated values of  $\sigma^p$ . Unfortunately, a further extension of the polynomial basis set (3) goes beyond the ability of our computing facilities but owing to a monotonous behaviour of the calculated shielding constants (Fig. 2) we can draw out rather general conclusions.

The gauge-dependence of the Karplus-Kolker method is also evident but appears to be less pronounced than in the case of the finite basis set CHF calculations. This is illustrated by the data of Table 2. Shifting the gauge origin from the central atom of  $\text{H}_2\text{O}$  to the shielded proton Arrighini *et al.* [5] found in their CHF calculations the gauge dependence of +22.64 ppm. In the present case, shifting the gauge origin from the electronic centroid (e.c.) of the monomer to the shielded proton we obtain the gauge dependence of -3.43 ppm. It should be pointed out that in the water molecule the central atom and e.c. almost coincide.

In comparison with the experimental data the calculated proton shielding constant in  $\text{H}_2\text{O}$  is much better when computed with the gauge origin at e.c. Our value (28.55 ppm) compares favourably with the best CHF result (28.94 ppm) obtained in rather cumbersome calculations by Arrighini *et al.* [5].

The results for the monomer indicate some significance of e.c. as the gauge origin in the Karplus-Kolker method. According to Chan and Das [17] this choice leads to the lowest (positive) value of  $\chi^p$  (see also Table 4) and one can also expect that it minimizes the absolute error of the computed  $\chi^p$  and  $u_\mu^{(1,0)}$ . For this reason one can expect rather good results for  $\sigma^p$  calculated with the gauge origin at e.c. This qualitative reasoning is nicely supported by the corresponding numerical data [17, 1, 9]. Moreover, it is important that e.c. can be defined for any molecule while some other concepts, e.g. the origin at the central atom, are in general rather arbitrary.

According to the discussion presented in [1] we attribute more significance to the results obtained for the gauge origin at the molecular electronic centroid, especially when we compare the data for different molecules. Thus, comparing the proton shielding constants in  $\text{H}_2\text{O}$  and  $(\text{H}_2\text{O})_2$  (Tables 2 and 3) we find for the gauge origins at e.c. the H-bond NMR shift of -1.0 ppm. Additionally, examining Fig. 2c we observe that the calculated value provides a sort of the "upper bound" to the H-bond NMR shift in the water dimer and unambiguously indicates a decrease of  $\sigma$  for the H-bonded proton. Qualitatively the same effect is obtained for the gauge origin at A (Fig. 2) but at B the corresponding shielding constant unexpectedly increases in comparison with that in the monomer. To explain this rather peculiar result it is worth attention that for all the gauge origins considered in this paper an extension of the polynomial basis set, in general results in increase of  $\sigma$  for H 3 (= H 4) and H 6 while  $\sigma$  of H 5 simultaneously decreases. This also leads to rather systematic increase of  $\sigma$  in the monomer. Thus, on augmenting the basis set we should reach the desired sequence also for the gauge origin B.

For the monomer I in the dimer its protons should resemble to some extent those in the isolated molecule and it appears that  $\sigma(\text{H } 3) = \sigma(\text{H } 4)$  must not be

gher than  $\sigma(\text{H } 5)$ . On the other hand, in the liquid an average proton surrounding resembles rather that of H 5 and in this respect our calculation predicts a down-field shift of the corresponding NMR signal. It is worth mentioning that qualitative considerations [18] predict rather an up-field shift and agree with experiment [19].

Recently Guidotti *et al.* [20] reported the CHF calculations of several properties of the water molecule in an ice-like cluster. The surrounding molecules were taken into account by an appropriate perturbation-like modification of the SCF function of the isolated molecule. The calculated change in the proton shielding constant ( $-3.81$  ppm and  $-5.83$  for the gauge origins at O and H, respectively) is rather close to the observed association shift ( $-4.58$  ppm at  $0^\circ\text{C}$  [19]). However, the observed shift is strongly temperature-dependent [9]. The Boltzmann average of  $\sigma$  which is reported in [20] takes into account only the existence of several configurations of the cluster but does not include the influence of the O...O stretching motion. To our feeling the computed values must not be directly compared with the experimental data and only the direction of the chemical shift appears to be meaningful. In this respect the result of the Karplus-Kolker method agrees with that of Guidotti *et al.*

Guidotti *et al.* [20] calculated also the change of the magnetic susceptibility of  $\text{H}_2\text{O}$  upon the cluster formation but their result ( $-0.355$  erg/mole gauss<sup>2</sup>) differs in sign from the quoted experimental value ( $+0.45$  erg/mole gauss<sup>2</sup>) for the liquid. From the data of Table 4 we find  $+1.16$  erg/mole gauss<sup>2</sup> (per mole of  $\text{H}_2\text{O}$ ) for the change of  $\chi$  upon the hydrogen bond formation. We believe that the direction of the computed change of  $\chi$  can be compared with that in the liquid.

Summing up we want to stress that the method applied in this paper to the study of the H-bond induced changes in the magnetic properties of  $\text{H}_2\text{O}$  is much simpler than the CHF approach and does not offer any computational difficulties. Obviously, this method is approximate but it works quite well. In this respect we refer the reader to Tables 2 and 3 to recognize the order of magnitude of the computed dia- and paramagnetic contributions which result in their small final value of  $\sigma$ . These final results compare rather favourably with the corresponding CHF data. It should be also pointed out that in the case of all perturbing operators (e.g. electric polarizability calculations) some modification of the Karplus-Kolker scheme is necessary [6, 8].

*Acknowledgments.* The authors wish to thank Dr. G. H. P. Diercksen for the original computer inputs of the SCF-MO-1.CGO-functions and one-electron properties.

## References

1. Jaszuński, M., Sadlej, A.J.: *Theoret. chim. Acta* (Berl.) **27**, 135 (1972).
2. Karplus, M., Kolker, H.J.: *J. Chem. Phys.* **38**, 1263 (1963).
3. Kolker, H.J., Karplus, M.: *J. Chem. Phys.* **41**, 1259 (1964).
4. Stevens, R. M., Pitzer, R. M., Lipscomb, W. N.: *J. Chem. Phys.* **38**, 550 (1963).
5. Arrighini, G. P., Maestro, M., Moccia, R.: *J. Chem. Phys.* **52**, 6411 (1970).
6. Sadlej, A.J.: *Chem. Physics Letters* **8**, 100 (1971).
7. Sadlej, A.J.: *Molecular Physics* **21**, 145 (1971); **21**, 959 (1971).



8. Sadlej, A. J., Jaszuński, M.: *Mol. Phys.* **22**, 761 (1971).
9. Jaszuński, M., Sadlej, A. J.: *Chem. Physics Letters* **15**, 41 (1972).
10. Diercksen, G. H. F.: *Theoret. chim. Acta (Berl.)* **21**, 335 (1971).
11. Sadlej, A. J.: *Acta Phys. Polon. A* **41**, 173 (1972).
12. Okniński, A., Sadlej, A. J.: *Acta Phys. Polon. A* **42**, 709 (1972).
13. Taketa, H., Huzinaga, S., Oohata, K.: *J. Phys. Soc. Japan* **21**, 2314 (1966).
14. Kern, C. W., Karplus, M.: *J. Chem. Phys.* **43**, 415 (1965).
15. Schaad, L. J., Morrell, G. O.: *J. Chem. Phys.* **54**, 1965 (1971).
16. Arrighini, G. P., Maestro, M., Moccia, R.: *J. Chem. Phys.* **52**, 6411 (1970).
17. Chan, S. I., Das, T. P.: *J. Chem. Phys.* **37**, 1527 (1962).
18. Pople, J. A.: In: *Hydrogen bonding*, p. 71. London: Pergamon Press 1959.
19. Eisenberg, D., Kauzmann, W.: *The structure and properties of water*. Oxford: Clarendon Press 1966.
20. Guidotti, C., Lamanna, U., Maestro, M.: *Theoret. chim. Acta (Berl.)* **26**, 147 (1972).

Mr. Michał Jaszuński  
Dr. Andrzej J. Sadlej  
Institute of Organic Chemistry  
Polish Academy of Sciences  
Warsaw 42, Kuźprzaka 44, Poland



## Calculations on the $\pi \rightarrow {}^1\pi^*$ Transitions in Large Conjugated Carbonyl Compounds Using the Molecules-in-Molecules Method

T. G. Edwards\*

Department of Chemistry, The University, Sheffield S3 7HF, England

Received March 5, 1973

Assignments of the  $\pi \rightarrow {}^1\pi^*$  electronic transitions in large carbonyl compounds have been carried out using the molecules-in-molecules method.

**Key words:**  $\pi \rightarrow {}^1\pi^*$  transitions · Conjugated carbonyl compounds · Molecules-in-molecules methods

### Introduction

Sidman [1] observed that the electronic spectra of a large number of quinones [2] were similar, with three absorption regions in common —  $\pi \rightarrow \pi^*$ , weak  $\pi \rightarrow {}^1\pi^*$  and strong  $\pi \rightarrow {}^1\pi^*$ . He also observed that these spectra were more similar than were those of the parent hydrocarbons. He concluded that this similarity was the result of a common structural feature — the quinone group, and that the molecules could be regarded as vinyl-substituted *p*-benzoquinones. Confirmation was given in the case of 9:10-anthraquinone by the single crystal studies of Sidman [1] who showed that as with *p*-benzoquinone [3] both  $\pi \rightarrow {}^1\pi^*$  transitions were polarized perpendicularly to the C—O axis. As further evidence for a *p*-benzoquinone structure in the *p*-quinones he pointed out that unexcited resonance structures cannot be drawn in which the C—C bonds of the C—O carbon atom have double bond character, thus indicating a long bond as is known for *p*-benzoquinone [4]. An X-ray analysis of 9:10-anthraquinone by Sen [5] showed this bond-length to be 1.50 Å which is equal to that in *p*-benzoquinone. The model appeared to be well-founded and was used in interpreting the electronic spectrum of 9:10-anthraquinone [1]. However, in a later paper Sidman [6] drew attention to the X-ray work on *p*-benzoquinone of Brand and Goodwin [7] who had shown that the optical axes adopted by Sidman were *incorrect* and should be *reversed*. This gave an important difference between the spectra of *p*-benzoquinone and 9:10-anthraquinone (Sidman warned against his polarization analysis of 9:10-anthraquinone although there was no *a priori* reason why it should have been incorrect — it will be seen later that there was nothing at all wrong with it). The presence of the long C—C bonds in 9:10-anthraquinone cannot and need not be disputed. On examining the molecular dimensions of 9:10-anthraquinone more

\* Present address: The Royal Liberty School, Romford, Essex, England.

closely it is seen that the C-C bond-lengths in the two outer rings are in the range 1.38-1.40 Å, with the short C-C bond of the inner ring being 1.40 Å as compared to 1.31 Å in *p*-benzoquinone [4]. On the basis of geometry alone it is not only clear that Sidman's model of 9:10-anthraquinone was incorrect, but also that a more realistic model is that of a symmetric composition of two benzene rings and two carbonyl groups. It is concluded that similarity between the single crystal spectra of *p*-benzoquinone and 9:10-anthraquinone should not be anticipated, and that the observed similarity of the solution spectra is of no significance.

This model has previously been used in polarization excitation studies on 9:10-anthraquinone [8] and anthrone [8,9], the interpretation of the spectra being carried out in terms of interaction between the benzene rings and with the aid of Platt's spectroscopic moment theory [10]. This is a very simple approach, but, if the assignment of the anthrone spectrum due to Drott and Dearman [9] (hereinafter D-D) is adopted, nonetheless a successful one. In the present work a more detailed theory has been used for the following compounds, where the validity of the model in each case is judged on the extent of agreement between the calculated and experimental  $\pi \rightarrow \pi^*$  electronic transitions: 9:10-anthraquinone, methylene anthrone, 1:4-naphthoquinone, anthrone and fluorenone.

### Theory

The method used was the molecules-in-molecules (MIM) method of Longuet-Higgins and Murrell [11] where the states are described in terms of local excitation (LE) and charge transfer (CT) configurations. This method has been used previously in calculations on simple carbonyl compounds [12]. Except for the electron affinity of benzene [13] all the integrals and integral-values necessary for the present work are contained in the latter paper. Ionization from the C-O group is not included. Further description is unwarranted.

### Molecular Dimensions

9:10-anthraquinone. The dimensions used were essentially those determined by Sen [5], with the simplifications that all "benzene" C-C bond-lengths were taken as 1.39 Å and all bond-angles were assumed to be 120°. These changes are sure to have an insignificant effect on the results to be presented, and were made simply for easier calculation.

1:4-naphthoquinone. The dimensions used were taken from those used for 9:10-anthraquinone, with the short non-benzenoid C-C bond-length being taken from *p*-benzoquinone [4].

The dimensions for the above two molecules have been used in earlier calculations [14].

Anthrone and methylene anthrone. As with 1:4-naphthoquinone the dimensions were taken from those adopted for 9:10-anthraquinone, with the new C-C bond in the methode having the ethylene bond-distance [15].

Fluorenone. Iball [16] suggested that fluorene was non-planar, but in a later paper on an X-ray study Burns and Iball [17] concluded, "It is clear, therefore,

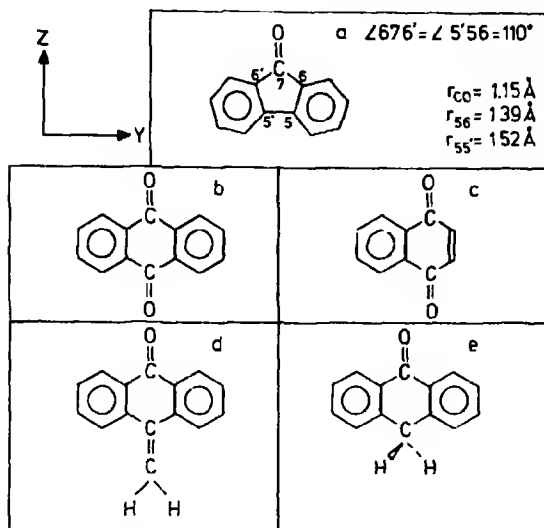


Fig. 1. Structures of investigated molecules: a) fluorenone, b) 9:10-anthraquinone, c) 1:4-naphthoquinone, d) methylene anthrone and e) anthrone

that the molecule is planar ...". Commenting on this second paper Gray *et al.* [18] said, "... X-ray studies suggest that they (fluorene and fluorenone — the latter was assumed to have essentially the same structure as the former) are distorted". From the published data there is no doubt as to the planarity of fluorene. It is assumed that fluorenone too is planar.

The dimensions adopted for fluorenone are given in Fig. 1 together with the other molecules being investigated.

### Results

In Tables I (i-v) the results of the MIM calculations are compared with experimental data. The configurations composing  $> 10\%$  of each state are given. The positive combinations benzene states are symmetric to a  $180^\circ$  rotation about the C—O axis.

### Discussion

Scott [23] and Singh *et al.* [24] used the CT and LE terminology in a qualitative interpretation of the electronic spectra of 1:4-naphthoquinone and 9:10-anthraquinone. It was hoped that their work would be complementary to that presented here, but, unfortunately, the impreciseness of the terms as used by these workers has made this impossible.

9:10-anthraquinone. Only the three lowest  $\pi \rightarrow {}^1\pi^*$  transition energies can be measured from the polarization spectrum [8] — these agree moderately well with the values taken from the solution spectrum [19]. They also agree with the MIM results and those of previous *P*-method calculations. D-D reported that there

were indications of a Z-polarized transition at higher energy, but they could not be absolutely certain because of the poor resolution in this region. Such a band is predicted from the MIM results (and from the *P*-method results for that matter). However, there is considerable doubt as to the value of the experimental energy. Poquet [19] reported an intense fourth band at 4.9 eV, whereas Kuboyama and Wada [20] reported an intense fourth band at 6.1 eV. The latter agrees exceedingly well with the calculated energy, but the 4.9 eV band is clearly the fourth and is, therefore, included in Table 1 (i).

Using Platt's spectroscopic moment theory D-D deduced the following order of transitions: A Y-polarized transition consisting of benzene  $\alpha$  states ( $\alpha_1 \sim \alpha_2$ ); a Z-polarized transition consisting essentially of benzene  $p$  states ( $p_1 + p_2$ ); a transition arising from the benzene  $\beta$  states — for Y-polarization this is

Table 1 Comparison of calculated and experimental  $\pi \rightarrow \pi^*$  transition energies (eV), *s* solution, *r* rigid medium oscillator strength,  $\epsilon_{\max}$  maximum of molar extinction coefficient, *M* transition dipole moment, *P* suffix results previous *P*-method calculations (14), *b* benzene

i) 9,10-anthraquinone

MIM	calculated			Experimental [19] <i>s</i>			Main configurations
	<i>M</i>	<i>E<sub>P</sub></i>	<i>f<sub>P</sub></i>	<i>E</i>	$\epsilon_{\max}$	Pol [8] <i>r</i>	
26	0.18(Y)	4.06	0.51(Y)	3.8	5,000	Y	0.63 ( $\alpha_1 \sim \alpha_2$ ), 0.39 ( $b \rightarrow C^+ O$ )
27	0	3.99	0				0.64 ( $\alpha_1 + \alpha_2$ ), 0.38 ( $b \rightarrow C^+ O$ )
88	0	4.28	0				0.43 ( $p_1 - p_2$ ), 0.62 ( $b \rightarrow C^+ O$ ), 0.36 ( $b \rightarrow b$ )
88 <sub>2</sub>	0.39(Z)	4.68	0.37(Z)	4.5	16,000	Z	0.42 ( $p_1 + p_2$ ), 0.66 ( $b \rightarrow C^+ O$ ), 0.38 ( $b \rightarrow b$ )
38	0.92(Y)	5.66	1.76(Y)	4.7	20,000	Y	0.46 ( $\beta_1 - \beta_2$ ), 0.61 ( $b \rightarrow C^+ O$ ), 0.35 ( $b \rightarrow b$ )
82	0	5.62	0				0.40 ( $\beta_1 + \beta_2$ ), 0.32 ( <i>LEC</i> $C^+ O$ ), 0.52 ( $b \rightarrow C^+ O$ ), 0.44 ( $b \rightarrow b$ )
84	0	5.75	0				0.36 ( $p_1 \sim p_2$ ), 0.42 ( $\beta'_1 - \beta'_2$ )
							0.54 ( $b \rightarrow C^+ O$ ), 0.32 ( $b \rightarrow b$ )
92	0.70(Z)	5.92	0.71(Z)	4.9	50,000	Z	0.33 ( $p_1 + p_2$ ), 0.37 ( $\beta'_1 + \beta'_2$ ), 0.58 ( $b \rightarrow C^+ O$ ), 0.41 ( $b \rightarrow b$ )
55							

ii) Methylene anthrone

MIM	calculated		Experimental [25] <i>r</i>		Main configurations
	<i>M</i>	<i>E<sub>MIM</sub></i> (9,10-anthraquinone)	<i>E</i>	Pol	
37	0.33(Z)	4.27			0.45 ( $\alpha_1 + \alpha_2$ ), 0.33 ( $b \rightarrow C^+ C$ ), 0.32 ( $b \rightarrow C^+ O$ ), 0.39 ( $C^+ C \rightarrow C^+ O$ )
22	0.10(Y)	4.26(Y)	3.6	Y	0.64 ( $\alpha_1 - \alpha_2$ )
38	0.09(Y)	4.88			0.47 ( $p_1 - p_2$ ), 0.41 ( $b \rightarrow C^+ C$ ), 0.40 ( $b \rightarrow C^+ C$ )
38	0.26(Z)	4.88 <sub>2</sub> (Z)	4.4	Z	0.40 ( $\alpha_1 + \alpha_2$ ), 0.22 ( $p_1 + p_2$ ), 0.32 ( <i>LEC</i> $C^+ C$ ), 0.43 ( $b \rightarrow C^+ C$ )
					0.42 ( $C^+ C \rightarrow b$ )
12	0.33(Z)	5.82			0.26 ( $\beta_1 + \beta_2$ ), 0.48 ( $b \rightarrow C^+ O$ ), 0.38 ( $b \rightarrow b$ ), 0.39 ( $C^+ C \rightarrow b$ )
34	0.93(Y)	5.38(Y)	5.2	Y	0.47 ( $\beta_1 - \beta_2$ ), 0.41 ( $b \rightarrow C^+ O$ ), 0.42 ( $C^+ C \rightarrow b$ )
50	0.15(Y)	6.55(Y)			0.44 ( $b \rightarrow C^+ C$ ), 0.62 ( $b \rightarrow b$ ), 0.57 ( $C^+ C \rightarrow b$ )
51	0.39(Z)	5.92(Z)			0.37 ( $p_1 + p_2$ ), 0.22 ( $\beta'_1 + \beta'_2$ ), 0.42 ( $b \rightarrow C^+ O$ ), 0.34 ( $C^+ C \rightarrow b$ )
51					

## iii) 1:4-naphthoquinone

MIM	calculated			Experimental $s$		Main configurations
	$ M $	$E_p$	$f_p$	$E$ [19]	$\epsilon_{\max}$ [19]	
20	0.13(Y)	3.88	0.003(Z)	3.7	3,000	0.86 $\alpha$ , 0.23 ( $b \rightarrow C^+C^-$ ), 0.43 ( $b \rightarrow C^+O$ )
62	0.28(Z)	3.97	0.25 (Y)	4.8	13,000	0.50 $p$ , 0.26 $\beta'$ , 0.47 ( $b \rightarrow C^+C^-$ ), 0.67 ( $b \rightarrow C^+O$ )
70	0.37(Z)	4.76	0.89 (Z)	4.9	24,000	0.48 ( $LE C^+C^-$ ), 0.39 ( $C^+C^- \rightarrow b$ ), 0.76 ( $C^+C^- \rightarrow C^+O$ )
45	0.50(Y)	5.57	0.40 (Y)	5.0	22,000	0.40 $\alpha$ , 0.51 $\beta$ , 0.44 ( $b \rightarrow C^+C^-$ ), 0.57 ( $b \rightarrow C^+O$ )
30	0.45(Z)	5.69	0.49 (Z)			0.68 $p$ , 0.48 $\beta'$ , 0.29 ( $b \rightarrow C^+C^-$ ), 0.47 ( $b \rightarrow C^+O$ )
46		6.43				

## iv) Anthrone

calculated		Experimental <i>r</i>			Benzophenone [21]			Main configurations
<i>um</i>	<i>M</i>	<i>E</i> [9]	Pol. [9]	<i>E</i>	Pol. [9]	<i>c</i> <sub>max</sub> <i>s</i> <i>f</i>		
47 <sub>n</sub>	0.09(Y)						0.66 ( <i>α</i> <sub>1</sub> − <i>α</i> <sub>2</sub> )	
47 <sub>i</sub>	0.10(Z)	4.0	Z	4.2 [9]	Z	1,900 0.007	0.67 ( <i>α</i> <sub>1</sub> + <i>α</i> <sub>2</sub> )	
16	0.47(Y)	4.5	Y	4.6 [9]	Y	18,500 0.42	0.43 ( <i>p</i> <sub>1</sub> − <i>p</i> <sub>2</sub> ), 0.24 ( <i>β</i> <sub>1</sub> − <i>β</i> <sub>2</sub> ), 0.55 ( <i>h</i> → C' O), 0.35 ( <i>h</i> → <i>h</i> )	
42	0.21(Z)	4.7	Z	4.9 [9]	Z		0.48 ( <i>p</i> <sub>1</sub> + <i>p</i> <sub>2</sub> ), 0.23 ( <i>LE</i> C' O), 0.52 ( <i>h</i> → C' O) 0.32 ( <i>h</i> → <i>h</i> )	
43	0.71(Y)			6.1		31,000 0.56	0.36 ( <i>β</i> <sub>1</sub> − <i>β</i> <sub>2</sub> ), 0.35 ( <i>β</i> <sub>1</sub> ' − <i>β</i> <sub>2</sub> '), 0.48 ( <i>h</i> → C' O) 0.38 ( <i>h</i> → <i>b</i> )	
3	0.61(Z)							
8	0.63(Y)							
41	0.36(Z)			6.6		56,000 1.14		
49	0.73(Y)							
41	0.41(Y)							

## v) Fluorenone

MIM	calculated		Experimental $s$		Main configurations
	$ M $		$E$ [22]	$\epsilon_{\max}$ [22]	
6	0.26 (Y)		4.2	3,700	0.48 ( $\alpha_1 - \alpha_2$ ), 0.50 ( $b \rightarrow C^+O$ ), 0.42 ( $b \rightarrow b$ )
1	0.012(Z)		3.3	260	0.65 ( $\alpha_1 + \alpha_2$ )
6	0.21 (Y)		4.4	2,800	0.37 ( $\alpha_1 - \alpha_2$ ), 0.36 ( $p_1 - p_2$ ), 0.35 ( $b \rightarrow C^+O$ ), 0.50 ( $b \rightarrow b$ )
9	0.91 (Y)		4.8	91,000	0.51 ( $\beta_1 - \beta_2$ ), 0.40 ( $b \rightarrow C^+O$ ), 0.57 ( $b \rightarrow b$ )
4	0.40 (Z)				0.41 ( $p_1 + p_2$ ), 0.50 ( $b \rightarrow C^+O$ ), 0.49 ( $b \rightarrow b$ )
3					

the negative combination. This analysis is wholly substantiated by the results of the MIM calculations, although there is considerable  $b \rightarrow C^+O$  in the third state.

Methylene anthrone. In Table I (ii) the states of methylene anthrone have been correlated with the 9:10-anthraquinone states of the same symmetry. The calculated results for these two molecules are similar, as are the polarization and absorption spectra [25]. The three observed polarized bands are assigned to the states shown; the corresponding states in 9:10-anthraquinone are those to which its experimental bands are assigned. Adopting the exciton interaction

treatment previously used for diphenyl, diphenylmethane and dibenzyl by McClure [28]. Smith and Dearman [25] predicted the following order of states:  $(\alpha_1 - \alpha_2)$ ,  $(\alpha_1 + \alpha_2) + (p_1 + p_2)$ ,  $(p_1 - p_2)$ . It is difficult to directly compare the results of this and the present method since the latter allows for a far greater interaction of configurations. However, the present results are essentially in accord with the assignments of Smith and Dearman, although it is felt that the third band will also contain a large proportion of the intense ground state to  $(\beta_1 - \beta_2)$  transition.

1:4-naphthoquinone. Of the five calculated transitions reported in Table I (iii) the polarizations and energies for the last three agree with those calculated previously using the *P*-method [14]. In this previous work the two lowest transition energies (3.38 and 3.97 eV) were both assigned to the first observed band — partially because of their near degeneracy and partially because the former was virtually forbidden; the other three experimental bands were assigned to the calculated energies in order. Thus, the bands were predicted to arise from transitions polarized *Y* (predominately), *Z*, *Y*, and *Z*, in order of increasing energy. But the MIM results indicate that the first two transitions are both very much allowed and 0.42 eV apart. Moreover, the more intense band from the MIM results is the virtually forbidden band from the *P*-method results. From the MIM method results the order of polarization is *Y*, *Z*, *Z* and *Y*. The same sequence could be obtained for the *P*-method results by "unpairing" and reversing the first two transitions. Unfortunately, while agreement is thus improved in one way it is worsened in another — the second experimental band should then arise from a virtually forbidden transition, which it certainly does not. This is not a happy state of affairs. Certainly, the polarization spectrum of this compound would help to clear matters up, but because of the weakness of its phosphorescence it has not, as yet, been observed [25].

Platt's spectroscopic moment theory predicts that the first band would arise from a *Y*-polarized transition essentially of  $\alpha$  character, with a second *Z*-polarized transition essentially of *p* character. This is in good agreement with the results of the calculation, although the amount of *p*-character is on the low side (25 %).

It is interesting to note the similarity of the MIM results for 1:4-naphthoquinone and benzaldehyde. The first band of benzaldehyde is generally considered to be essentially  $\alpha$  with the second to arise from *p* and/or *h*  $\rightarrow$  C—O [26, 27]. The third band was of too high an energy to occur in the polarization spectrum [9], but Walsh [26] regarded it as essentially  $\beta$ . These conclusions are consistent with previous MIM calculations [12] where the second band arises from *p* + *h*  $\rightarrow$  C—O and the third arises from  $\beta$  (also with considerable *h*  $\rightarrow$  C—O). From Table I (iii) it is clearly reasonable to compare the first three transitions of benzaldehyde with the first, second and fourth transitions, respectively, of 1:4-naphthoquinone. The third excited state of 1:4-naphthoquinone is composed almost entirely (95 %) of ethylene LE and CT from the ethylene group, and obviously has no place in the benzaldehyde spectrum.

Anthrone. The anthrone and benzophenone data taken from the spectra of Shimada and Goodman [9] are given in Table I (iv) and are in excellent agreement with the results of Smith and Dearman [25]. Shimada and Goodman attempted to correlate the two experimental bands of lowest energy with the  $^1A_1(\alpha_1 + \alpha_2)$



and  ${}^1B_1(\alpha_1 - \alpha_2)$  states which are Z- and Y-polarized, respectively. On estimating the energy separation using the exciton interaction treatment of McClure [28] they obtained a value of  $700\text{ cm}^{-1}$  (0.09 eV) with the  ${}^1A_1$  state at higher energy. The same ordering of states was obtained by these workers using the *P*-method, with the splitting being brought down from a high of 0.4 eV to a low of 0.025 eV by systematically increasing the complexity of the wavefunctions. The problem was left unsolved. From the present calculations it can be seen that the two lowest states are of  ${}^1A_1$  and  ${}^1B_1$  symmetry, with the former at a level only 0.005 eV higher than the latter. Since the states have different symmetries they could be made to interchange by judicious changes in the values of the semi-empirical parameters, but this is not a worthwhile exercise since no reasonable change in integral-values would give rise to the 0.5 eV splitting observed; this is also true of the *P*-method calculations of Shimada and Goodman. That the observed peak separation does not arise from the  ${}^1A_1 - {}^1B_1$  splitting has been very convincingly argued by D-D. They calculated the  $-\text{CHO}$  group substituent contribution to the oscillator strengths for these two transitions using the spectroscopic moments derived by Petruska [29]. It was found that  $f({}^1A_1)/f({}^1B_1) \sim 3$ . The spectroscopic moment of a  $-\text{CH}_3$  group is far smaller than that of a  $-\text{CHO}$  group, but giving the  $-\text{CH}_2$  group in anthrone the value derived for  $-\text{CH}_3$  in toluene results in a marked change in the ratio  $-\ f({}^1A_1)/f({}^1B_1) \sim 8$ . The very reasonable suggestion was then made that the two states are very close in energy with the  ${}^1A_1 \leftarrow A_1$  transition masking the  ${}^1B_1 \leftarrow A_1$  transition, thus giving the required polarization for the first band. This explanation is compatible with the results of the present calculation. It is true that the transition dipole moments are predicted to be of approximately the same magnitude, but in the calculation the  $-\text{CH}_2$  group was neglected, and, as shown above, its effect is to increase the value of  $f({}^1A_1)/f({}^1B_1)$ . The calculated separation of 0.7 eV is somewhat greater than the experimental value, but it is comforting to note that the state has a good deal of  $(p_1 - p_2)$  character, in agreement with the assignments suggested by D D.

In view of the similarity between the structures of benzophenone and anthrone and that between their spectra at long wavelengths ( $> 2500\text{ \AA}$ ) [9, 25, 30] similarity is expected between their spectra at shorter wavelengths. Certainly, the observed strong bands in the spectrum of benzophenone at 6.1 eV and 6.6 eV are consistent with the results calculated for anthrone.

Fluorenone. There is no doubt that the lowest energy band at 3.3 eV arises from a  $\pi \rightarrow {}^1\pi^*$  transition [22, 31] and not from an  $n \rightarrow {}^1\pi^*$  transition. The assignment suggested in Table I (v) is satisfactory as regards intensities, but this has caused the unhappy situation of having the 3.3 eV band assigned to a transition calculated to be 1.0 eV higher in energy. Kuboyama [22] has attempted the assignment using naïve Hückel theory. He deduced the polarizations to be Y, Y, Z and Z, which disagrees completely with the present results which are Z, Y, Y and Y. The polarization spectrum would be invaluable.

### Conclusion

For 9:10-anthraquinone, methylene anthrone and anthrone the results of the calculations offer a reasonable interpretation of their electronic spectra, and,

consequently, justify the molecular model adopted. For 1 : 4-naphthoquinone and fluorenone insufficient experimental data has resulted in the assignments being hardly more than guesses: Knowledge of the polarizations is essential.

*Acknowledgements.* The author is indebted to Professor H. H. Dearman for the provision of experimental and theoretical results prior to publication. A post-doctoral research fellowship from the Science Research Council is gratefully acknowledged

## References

1. Sidman, J. W. : *J. Am. Chem. Soc.* **78**, 4567 (1956).
2. Hartmann, H., Lorenz, E. : *Z. Naturforsch.* **7a**, 360 (1952).
3. Sidman, J. W. : *J. Am. Chem. Soc.* **78**, 2363 (1956).
4. Kimura, M., Shihata, S. : *Bull. Chem. Soc. Japan* **27**, 163 (1954).
5. Sen, S. N. : *Indian J. Phys.*, **22**, 347 (1948).
6. Sidman, J. W. : *J. chem. Phys.* **27**, 820 (1957).
7. Brand, J. C. D., Goodwin, I. H. : *Trans. Faraday Soc.* **53**, 295 (1957).
8. Drott, H. R., Dearman, H. H. : *J. Chem. Phys.* **47**, 1896 (1967).
9. Shimada, R., Goodman, I. : *J. Chem. Phys.* **43**, 2027 (1965).
10. Platt, J. R. : *J. Chem. Phys.* **19**, 263 (1951).
11. Longuet-Higgins, H. C., Murrell, J. N. : *Proc. Phys. Soc. A* **68**, 601 (1955).
12. Edwards, T. G., Grinter, R. : *Theoret. Chim. Acta (Berl.)* **12**, 387 (1968).
13. Grinter, R., Taylor, J. M. : to be published.
14. Edwards, T. G., Grinter, R. : *Mol. Phys.* **15**, 349, 357 (1968).
15. Tables of interatomic distances. London: The Chemical Society 1958.
16. Iball, J. : *Z. Krist.*, **94**, 397 (1936).
17. Burns, D. M., Iball, J. : *Nature* **173**, 635 (1954).
18. Gray, G. W., Hartley, J. B., Ibbotson, A., Jones, B. : *J. Chem. Soc. (London)* **1955**, 4359.
19. Poquet, B., quoted by Lethovici, C., Deschamps, J. : *Theoret. Chim. Acta (Berl.)* **4**, 321 (1966).
20. Kuboyama, A., Wada, K. : *Bull. Chem. Soc. Japan*, **39**, 1874 (1966).
21. McClure, D. S., Hanst, P. I. : *J. Chem. Phys.* **23**, 1772 (1955).
22. Kuboyama, A. : *Bull. Chem. Soc. Japan* **37**, 1540 (1964).
23. Scott, A. I. : *Interpretation of the ultraviolet spectra of natural products*. London: Pergamon 1964.
24. Singh, I., Ogata, R. I., Moore, R. F., Chang, C. W. J., Scheuer, P. J. : *Tetrahedron* **24**, 6053 (1968).
25. Smith, J. C., Dearman, H. H. : Private communication and unpublished results.
26. Walsh, A. D. : *Trans. Faraday Soc.* **42**, 62 (1946).
27. Nagakura, S., Tanaka, J. : *J. Chem. Phys.* **22**, 236 (1954).
28. McClure, D. S. : *Can. J. Chem.* **36**, 59 (1958).
29. Petruska, J. : *J. Chem. Phys.* **34**, 1120 (1961).
30. Jones, R. N. : *J. Am. Chem. Soc.* **67**, 2127 (1945).
31. Yoshihara, K., Kearns, D. R. : *J. Chem. Phys.* **45**, 1991 (1966).

Dr T. G. Edwards  
The Royal Liberty School  
Romford  
Essex, England

## *Relatio* An EHT Re-Examination of Acetylcholine

D. Ajò, M. Bossa, R. Fidenzi, S. Gigli, and G. Jeronimidis

Istituto Chimico dell'Università di Roma, Italia

A. Damiani and A. Lapicciarella

Istituto di Chimica delle Macromolecole, Nucleo di Roma

Received February 13, 1973

The results of EHT calculations on the most stable conformations of the neurotransmitter molecule acetylcholine (ACh) are reported. These results are compared with those obtained with other semiempirical quantum mechanical methods CNDO/2, INDO and PCILO, and with those obtained by the classical partitioning of the energy method (PEM). From this comparison it becomes evident a wide agreement between the results of PCILO, EHT and PEM, all these methods allowing accessibility to discrete regions in conformational space.

*Key words:* Acetylcholine, electronic structure of ~

The allowed conformations of the neurotransmitter molecule acetylcholine (ACh)  $(\text{CH}_3)_3\text{N}^+-\text{CH}_2-\text{CH}_2-\text{O}-\text{C}(=\text{O})\text{CH}_3$  has been the subject of extensive experimental [1–4] and theoretical [5–10] investigations.

At the present time there is a basic theoretical agreement on the flexibility of this substrate while the differences in the details of the results are critically examined in many laboratories.

A satisfactory agreement exists among a number of features [6, 9, 10] derived with the classical semiempirical procedures of the partition of the energy in physically relevant contributions (PEM) [11] and with the quantum mechanical procedure PCILO [12]. Notwithstanding the prediction of PCILO for a low barrier about the torsion angle  $\psi_2$  ( $\text{N}-\text{C}_\alpha-\text{C}_\beta-\text{O}$ ) (Fig. 1), a feature in common with the results [7–10] of INDO [13] and CNDO/2 [14] quantum mechanical procedures, the predictions about position and energy differences are in better agreement as derived with PCILO and PEM than with PCILO and INDO or CNDO/2 techniques.

Among the available theoretical investigations, that carried out with the EHT [15] procedure has been apparently less successful in predicting the allowed conformations as supported by the experimental data.

It turns out in fact from the analysis of Kier [5] on ACh with the EHT method that for the torsion angles  $\psi_1$  ( $\text{C}_\alpha-\text{C}_\beta-\text{O}-\text{C}$ ) and  $\psi_2$  only one conformation, later found experimentally, in solution [3] and in the crystal of the chloride [4], but not in that of the bromide [2], should be allowed on energy grounds.

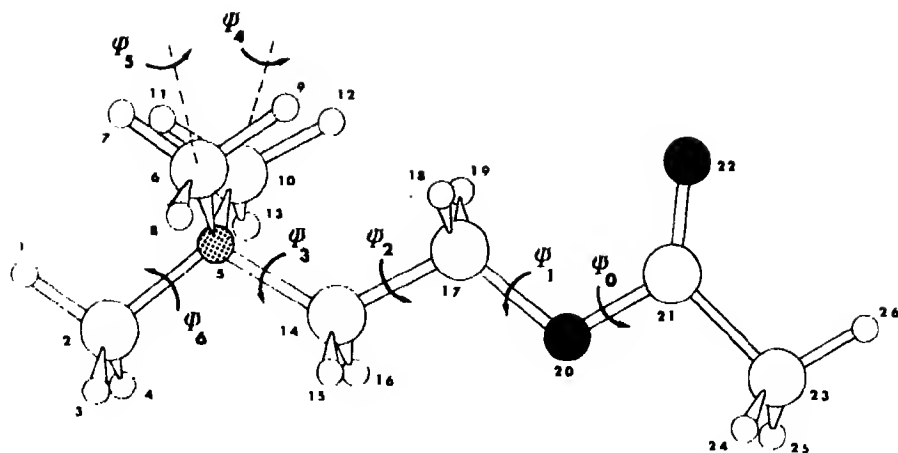


Fig. 1. Schematic view of the ACh molecule corresponding to the starting fully extended *TTTT* conformation. Labels for the conformation about the skeletal bonds are in the order from  $\psi_0$  to  $\psi_6$ . Torsions are measured from the antiplanar conformations and are positive for counterclockwise rotations,  $\psi_0(\text{C}_{17}-\text{O}_{20}-\text{C}_{21}-\text{C}_{23})$ ,  $\psi_1(\text{C}_{14}-\text{C}_{17}-\text{O}_{20}-\text{C}_{21})$ ,  $\psi_2(\text{N}_5-\text{C}_{14}-\text{C}_{17}-\text{O}_{20})$ ,  $\psi_3(\text{C}_2-\text{N}_5-\text{C}_{14}-\text{C}_{17})$ ,  $\psi_4(\text{H}_{13}-\text{C}_{10}-\text{N}_5-\text{C}_{14})$ ,  $\psi_5(\text{H}_{18}-\text{C}_6-\text{N}_5-\text{C}_{10})$ ,  $\psi_6(\text{H}_1-\text{C}_2-\text{N}_5-\text{C}_{14})$ .

But as Kier carried out the analysis by varying the torsional angles individually and with large increments a more complete analysis based on results derived at the same level of complexity of the other procedures has been considered to be appropriate.

This, as well as the successful computations on a number of charged molecules carried out with the EHT and PEM techniques [16, 17] prompted us to undertake a re-examination of the allowed conformations of the ACh molecule with the EHT procedure.

A comparison of a number of  $\text{C}_\alpha$ ,  $\text{C}_\beta$  unsubstituted derivatives of choline indicates that bond lengths and angles used in the previous PEM analysis [6] were accurate enough for the purpose of this investigation (Table 1), therefore we used them also in the present investigation, however a number of peculiarities derived there from refinements on a group of seven torsion angles have been incorporated in the starting conformation of ACh.

It was shown in that paper that by labelling with *T* an extended antiplanar and with *G* a folded ( $\sim 120^\circ$  of torsion from antiplanarity) synclinal conformation about a bond and by taking into consideration the sequence of the torsion angles from  $\psi_0$  to  $\psi_3$  (Fig. 1), four conformations corresponding to the *TTTT*, *TGTT*, *TTGT* and *TGGT* ones, turned out to be grouped in the rather narrow energy range of 0.8 kcal/mole. After refinement of these four conformations it was found for two of them (*TTTT* and *TGTT*) an almost exactly antiplanar conformation about  $\psi_3$  ( $\text{C}-\text{N}-\text{C}_\alpha-\text{C}_\beta$ ) but a deviation from antiplanarity of about  $-6^\circ$  for the other two (*TTGT* and *TGGT*)<sup>1</sup>. Furthermore the methyls on the onium

<sup>1</sup> It is interesting to remark that in the most refined structure of ACh chloride [4] the torsion about  $\psi_3$  as measured from the sequences  $\text{C}_2-\text{N}_5-\text{C}_{14}-\text{C}_{17}$ ,  $\text{C}_6-\text{N}_5-\text{C}_{14}-\text{C}_{17}$ ,  $\text{C}_{10}-\text{N}_5-\text{C}_{14}-\text{C}_{17}$  are respectively  $9^\circ$ ,  $-8^\circ$ ,  $-6^\circ$  degrees. The mean value of  $-7.5^\circ$  is therefore in good agreement with the theoretical predictions.

Table 1. Values for bond lengths and angles as derived from the crystal structure of a number of choline derivatives with unsubstituted  $-\text{CH}_2-\text{CH}_2-$  group

Bond	$\text{C}_2-\text{N}_5$	$\text{C}_6-\text{N}_5$	$\text{C}_{10}-\text{N}_5$	$\text{N}_5-\text{C}_{14}$	$\text{C}_{14}-\text{C}_{17}$	$\text{C}_{17}-\text{O}_{20}$	$\text{O}_{20}-\text{C}_{21}$	$\text{C}_{21}-\text{O}_{22}$	$\text{C}_{21}-\text{O}_{23}$
Mean values <sup>a</sup>	1.51	1.51	1.53	1.51	1.53	1.46	1.34	1.22	
ACH-Br <sup>b</sup>	1.50	1.52	1.52	1.54	1.52	1.50	1.32	1.25	1.55
This paper	1.52	1.52	1.52	1.54	1.52	1.50	1.32	1.25	1.55
Angles	$\text{C}_2-\text{N}_5-\text{C}_6$	$\text{C}_2-\text{N}_5-\text{C}_{10}$	$\text{C}_2-\text{N}_5-\text{C}_{14}$	$\text{C}_6-\text{N}_5-\text{C}_{10}$	$\text{C}_6-\text{N}_5-\text{C}_{14}$	$\text{C}_{10}-\text{N}_5-\text{C}_{14}$	$\text{N}_5-\text{C}_{14}-\text{C}_{17}$	$\text{C}_{14}-\text{C}_{17}-\text{O}_{20}$	$\text{C}_{17}-\text{O}_{20}-\text{C}_{21}$
Mean values <sup>a</sup>	109	109	111	109	109	110	117	108	114
ACH-Br <sup>b</sup>	106	—	111	109	—	109	118	113	115
This paper	109	109	110	109	110	110	114	113	115

<sup>a</sup> Mean values are derived from the data of Refs. [2, 4, 21, 22, 23, 29].<sup>b</sup> Values for acetylcholine bromide are derived from Ref. [2].

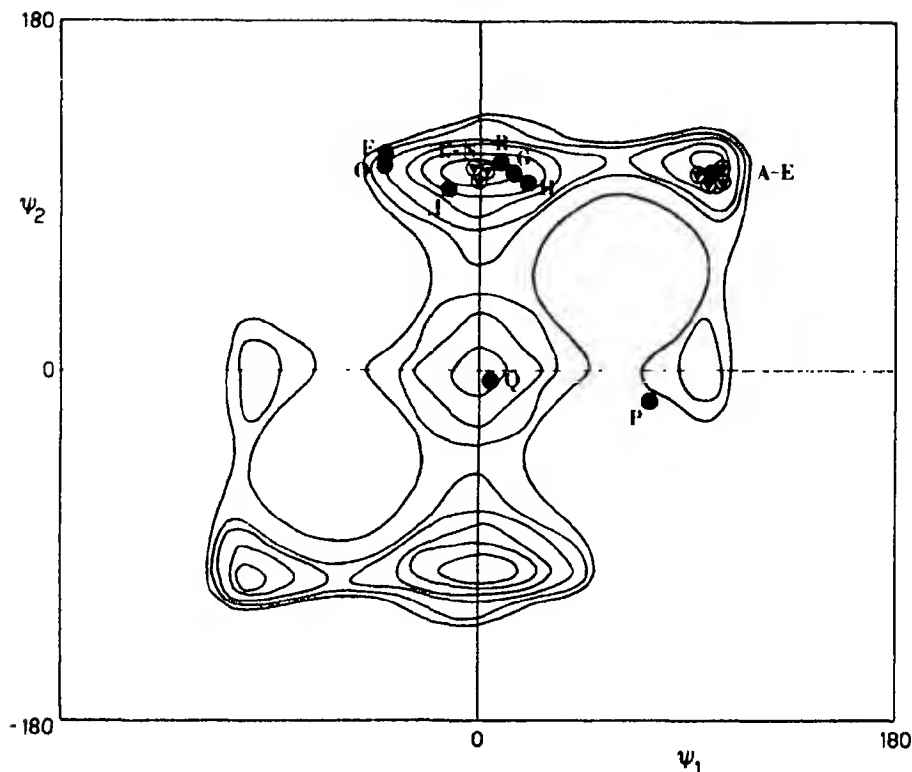


Fig. 2. EHT energy map of ACh in the undistorted  $\psi_3 = 0^\circ$  conformation. Energy contour lines at constant increments of 0.5 kcal/mole. ● rather accurately defined conformation ○ poorly defined conformation. Letters are in agreement with Table 3

group have been found rotated, almost independently from the rotations of the skeletal bonds, about  $-7$ ,  $7$  and  $0$  degrees around  $\psi_4$ ,  $\psi_5$  and  $\psi_6$  respectively (Fig. 1).

In the starting conformation of ACh  $\psi_4$ ,  $\psi_5$  and  $\psi_6$  have been therefore fixed at the above mentioned values, while due to the rigidity of the ester bond [2]  $\psi_0$  has been fixed to the antiplanar position.

To gain insight on the dependence of the quantum mechanical predictions from the torsion about  $\psi_3$ , two distinct sets of computations have been carried out, the first with  $\psi_3$  fixed at  $0^\circ$ , the second one with  $\psi_3$  at  $-5^\circ$ .

For the two cases the conformational energy has been derived as a function of the two parameters  $\psi_1$  and  $\psi_2$  increased at constant steps of  $20^\circ$  degrees, by using in the EHT procedure the parametrization of Hoffmann and Imamura [18], slightly different from the previous one of Kier [5]. The most symmetrical ( $\psi_3 = 0^\circ$ ) map is reported in Fig. 2, while in Table 2 are summarized the energy of the minima corresponding to both situations.

The lowest energy *TTGT* conformation already predicted by Kier is confirmed but the full set of the allowed conformations falls in a rather short energy range, well comparable with the PEM or PCIO ones, and therefore

Table 2. EHT energy differences (kcal/mole) for ACh for the undistorted  $\psi_3 = 0^\circ$  and for the distorted  $\psi_3 = -5^\circ$  model. Energies are computed from the global minimum *TTGT* at  $\psi_3 = -5^\circ$  fixed at zero

Conformation	Model	
	$\psi_3 = 0^\circ$	$\psi_3 = -5^\circ$
<i>TTTT</i>	1.6	1.6
<i>TGTT</i>	2.4	2.5
<i>TTGT</i>	0.4	0.0
<i>TGGT</i>	1.1	0.7
<i>TG*TT*</i>	2.4	2.1
<i>TTG*T</i>	0.4	1.1
<i>TG*G*T</i>	1.1	1.9

\* Starred symbols for negative rotations

further support is gained to the idea of flexibility of ACh and to the usefulness of the above schematization for the allowed conformations of ACh.

But finer details are likewise worthy of mention. The energy difference of about 0.8 kcal/mole computed for the conformations *TGGT* ( $\psi_3 = 0^\circ$ ) and *TG\*G\*T* ( $\psi_3 = -5^\circ$ ) (Table 2) is related to a variation of 0.06 Å (from 1.86–1.80 Å) of the interatomic distance between atoms H(9)...H(18) and to a like variation of 0.06 Å (from 2.53–2.47 Å) between atoms C(6)...H(19). Likewise the greatest energy variation computed for equivalent pair of conformations is that between *TGGT* ( $\psi_3 = -5^\circ$ ) and *TG\*G\*T* ( $\psi_3 = -5^\circ$ ). The value of 1.2 kcal/mole corresponds to a change in the interatomic distances of the mentioned pairs of about 0.14 Å. We are confident therefore that inaccuracy in bond lengths, of the order of those derived from crystal structures determination, that are from three to five times smaller, and of few degrees in the bond angles are likely to bear no significant role on the picture emerging from the present computations.

Further the energy barriers that have been found in some instances to be greater than the experimental ones [15] are in ACh for rotations about  $\psi_2$  in the  $-120^\circ < \psi_2 < 120^\circ$  region lower than those predictable from PEM computations. This result is in agreement with the INDO [7], PCILO [8] and CNDO/2 [10] predictions even if the last three mentioned procedures allow for greater flexibility about this torsion angle, clearly a point open to further investigation.

Anyhow in agreement with former observations the EHT computations allow for greater accessibility in conformational space [18], a feature in common to other quantum mechanical procedures [19].

The computed maps account for the distribution of the experimental points (Fig. 2) in a rather satisfactory way, to the conformation *TTGT* of the lowest energy minimum correspond, among the others, the observed conformations of ACh in the crystal of chloride [4] and in solution [3], the conformation of carbamylcholine<sup>2</sup> (Carbachol) in solution [20] and the conformation of

<sup>2</sup> The EHT and CNDO/2 conformational energy maps of Carbachol are quite similar to that of ACh. The ACh maps can be therefore profitably used to interpret the allowed conformations of the group of the carbamylcholine derivatives with unsubstituted  $C_\alpha$ - $C_\beta$  hydrogen atoms.

Table 3. Conformations of a number of choline derivatives. Capital letters are in agreement with those of Fig. 2

	$\Psi_1$	$\Psi_2$	Ref.
A Acetylcholine bromide	-101	-103	[24]
B Palmitylcholine iodide	G	G	[25]
C Stearylcholine iodide	G	G	[25]
D Stearylcholine bromide	G	G	[26]
E Laurylcholine iodide	G	G	[27]
I 1- $\alpha$ -glycerylphosphorylcholine I	42	-107	[28]
G Dimethyl-5,6-phenylcarbamylcholine bromide	17	99	[21]
H 1-lactoylcholine iodide	23	-95	[24]
I Acetylcholine chloride	13	95	[4]
I Acetylcholine	T	G	[3]
M Carbamylcholine	T	G	[20]
N 1- $\alpha$ -glycerylphosphorylcholine $\text{CdCl}_2 \cdot 3\text{H}_2\text{O}$	T	-130	[30]
O 1- $\alpha$ -glycerylphosphorylcholine II	-40	105	[28]
P Phenyl-4-carbamylcholine bromide	74	18	[23]
Q Carbamylcholine bromide	6	-2	[22]
R Methyl-4-carbamylcholine bromide	8	107	[29]

dimethyl-5,6-phenyl-Carbachol in the crystal of the bromide [21], the *TGGT* conformation 0.7 kcal higher has been found in the crystal of ACh bromide [2], the fully extended *TTTT* one 1.2 kcal higher in the crystal of Carbachol bromide [22] and finally the less favoured *TGTT* one in the crystal of phenyl-4-Carbachol bromide [23].

In conclusion the EHT predictions compare rather well with those of PEM and PCILO, and the useful schematization previously made [6] of four preferred regions is well supported.

Moreover, notwithstanding the differences in the relative order of the minima, the allowed conformations are always grouped in a range of about 2 kcal/mole and under varying field of forces any one of them can be easily preferred against the others.

This work has been carried out with financial support of the Consiglio Nazionale delle Ricerche.

### References

1. Canepa, F. G., Mooney, F. F.: *Nature* **207**, 78 (1965).
2. Canepa, F. G., Pauling, P., Sörm, H.: *Nature* **219**, 907 (1966).
3. Culvenor, C. C. J., Ham, N. S.: *Chem. Comm.* **15**, 537 (1966).
4. Herdktolz, J. K., Sass, R. L.: *Biochem. biophysic. Res. Commun.* **40**, 583 (1971).
5. Kier, L. B.: *Molecular Pharmacol.* **3**, 487 (1967).
6. Liquori, A. M., Damiani, A., De Coen, J. L.: *J. molecular Biol.* **33**, 445 (1968).
7. Beveridge, D. L., Radna, R. J.: *J. Amer. chem. Soc.* **93**, 3759 (1971).
8. Pullman, B., Courriere, P., Coubeils, J. L.: *Molecular Pharmacol.* **7**, 397 (1971).
9. Ajò, D., Bossa, M., Damiani, A., Fidenzi, R., Gigli, S., Lanzi, L., Lapicciarella, A.: *J. theoret. Biol.* **34**, 15 (1972).
10. Ajò, D., Bossa, M., Damiani, A., Fidenzi, R., Gigli, S., Lanzi, L., Scarponi, C.: submitted to *Gazz. Chim. It.*
11. Liquori, A. M., Damiani, A., Elefante, G.: *J. Mol. Biol.* **33**, 439 (1968) and references therein.



12. Diner, S., Malrieu, J. P., Jordan, F., Gilbert, M.: *Theoret. chim. Acta (Berl.)* **15**, 100 (1969) and references therein.
13. Pople, J. A., Beveridge, D. L., Dobosh, D. A.: *J. chem. Physics* **47**, 2076 (1967).
14. Pople, J. A., Segal, G. A.: *J. chem. Physics* **43**, S136 (1965).
15. Hoffmann, R.: *J. chem. Physics* **39**, 1397 (1963).
16. Bossa, M., Damiani, A., Fidenzi, R., Gigli, S., Leli, R., Ramunni, G.: *Theoret. chim. Acta (Berl.)* **20**, 299 (1971).
17. Bossa, M., Damiani, A., Fidenzi, R., Gigli, S., Lanzi, L., Leli, R., Ramunni, G.: submitted to *Gazz. Chim. It.*
18. Hoffmann, R., Imamura, A.: *Biopolymers* **7**, 207 (1969).
19. Pullman, B.: In: *Aspects de la chimie quantique contemporaine*, R. Daudel and A. Pullman, Ed. CNRS., p. 261. Paris, 1971 and references therein.
20. Conti, F., Damiani, A., Pietronero, C., Russo, N.: *Nature New Biology* **233**, 232 (1971).
21. Babeau, A., Barrans, Y.: *C. r. hebd. Séances Acad. Sci. Paris* **270**, 609 (1970).
22. Barrans, Y., Clastre, J.: *C. r. hebd. Séances Acad. Sci. Paris* **270**, 306 (1970).
23. Barrans, Y., Dangoumau, J.: *C. r. hebd. Séances Acad. Sci. Paris* **270**, 480 (1970).
24. Chothia, C., Pauling, P.: *Nature* **219**, 1156 (1968).
25. Stora, C.: *Bull. Soc. chim.* **199**, 867 (1949).
26. Stora, C.: *Bull. Soc. chim.* **200**, 874 (1949).
27. Stora, C.: *Bull. Soc. chim.* **213**, 883 (1950).
28. Ahrahamsson, S., Pascher, I.: *Acta Cryst.* **21**, 79 (1966).
29. Barrans, Y., Bidcau, J. P.: *C. r. hebd. Séances Acad. Sci. Paris* **270**, 994 (1970).
30. Sundaralingam, M.: *Nature* **217**, 35 (1968).

Prof. Dr. A. Damiani  
Istituto di Chimica Delle Macromolecole  
Nucleo di Roma  
Roma, Italy

## Recensio

F. A. Cotton, G. Wilkinson: *Advanced Inorganic Chemistry*, 3rd. Ed. 1170 pages, Chichester John Wiley & Sons Ltd. 1972. £ 6.50.

"Advanced Inorganic Chemistry" von F. A. Cotton und G. Wilkinson ist nun in seiner dritte Auflage bei John Wiley & Sons erschienen. Nicht ohne Grund fand das Werk auch im deutschsprachigen Raum die zweite Auflage wurde ins Deutsche übersetzt - eine weite Verbreitung.

Der fortgeschrittene Student findet neben einem breit gestreuten Tatsachenmaterial, wobei allerdings nach der persönlichen Meinung des Rezensenten die Chemie der Übergangsmetallkomplexe etwa im Verhältnis zur Chemie der Nichtmetalle etwas zu stark betont wird, vergleichende Betrachtungen auf der Basis theoretischer und rezeptartiger Vorstellungen. Zahlreiche Hinweise auf weiterführende Literatur geben dem Leser die Möglichkeit, sich schnell in ein spezielleres Gebiet einzuarbeiten zu können.

Daß gegenüber der zweiten Auflage das erste Kapitel über die Elektronenstruktur der Atome weitgehend weggefallen ist, mag insofern positiv zu beurteilen sein, als eine solch kurze Einführung ohnehin kaum zu einem Verständnis führen kann.

Umgekehrt, mehr das Grundsätzliche betreffende Anmerkungen seien noch gemacht:

Es ist einerseits zweifellos deutlich festzustellen, daß sich die Autoren des Modellcharakters der gebotenen Vorstellungen zur Theorie der chemischen Bindung durchaus bewußt sind; andererseits ist zu bezweifeln, daß dies den theoretisch weniger geschulten Lesern, welche wohl weit in der Überzahl sind, auch klar wird.

So kann das Kapitel über die Natur der chemischen Bindung einem solchen Leser in größere Passagen kaum verständlich sein. Die Erklärungen zur „Resonanzenergie“ sind ohne die Kenntniss des Variationsprinzips der Quantenmechanik nicht zu verstehen. Das Überlappungsintegral  $S$  in Formel 3. 15 bei der Plausibilitätsbetrachtung zur Resonanzstabilisierung zu vernachlässigen während es an anderen Stellen als Maß für die Stärke einer Bindung gewählt wird, erscheint nicht zwingend. Anders gesagt:

Entweder ist dem Leser das Variationsprinzip bereits bekannt, dann ist die gebotene „Pseudableitung“ überflüssig, oder es ist ihm nicht bekannt, und dann versteht er die Zusammenhänge auch nach der Lektüre des betreffenden Abschnittes nicht.

Ein anderes Beispiel sei noch herausgegriffen. Aussagen über die Bindungsverhältnisse im  $\text{SiF}_4$  wie: "It is probable that both ionic covalent resonance and multiple bonding contribute significantly", sind typisch für gewisse Argumentationsweisen: Man kann eine Meßgröße (Bindungsabstand) theoretisch auf einfachem Wege nicht verstehen und man erklärt einfach, daß da wohl mehrere „Gründe“ vorhanden sein müßten, obwohl es nur einen Grund gibt, nämlich eine bestimmte Lage des Energieminimums. Daß die Beschreibung der Elektronenzustände eines Moleküls besser wird, wenn man der eine Grenzformel repräsentierenden  $\psi$ -Funktion weitere beimischt, ist aufgrund des Variationsprinzips selbstverständlich. Die Tatsache, daß die realiter vorliegenden Bindungsverhältnisse im Valenzstrichschema nicht darstellbar sind, wird als Begründung dafür gewählt, daß verschiedene ihre „Existenz“ nur dem Näherungsverfahren nicht aber der Natur verdankende „Anteile“ überlagert werden.

Gerechterweise muß gesagt werden, daß die Autoren an einigen Stellen auf den jeweiligen Näherungscharakter der Methode hinweisen, aber diese Hinweise werden letztlich überlesen, wenn der Leser nicht erkennen kann, worin denn nun die Näherung besteht.

Beim  $\text{ClF}_3$ -Molekül wird gesagt, daß die Hückeltheorie einen  $\text{F}-\text{Cl}-\text{F}$  Winkel von ca.  $80^\circ$  nahegelegt, ein Wert, der mit dem Experiment halbquantitativ übereinstimme. Der Rezensent würde eine umgekehrte Argumentation bevorzugen, etwa: „Das Experiment ergibt einen bestimmten Winkel... ein Ergebnis, das sogar schon im Rahmen der erweiterten Hückeltheorie verständlich wird.“

Das Buch ist insgesamt durchaus empfehlenswert, aber nur für den, der aufgrund solider theoretischer Vorbildung zwischen Mythologie und Theorie zu unterscheiden weiß.

Karl Hensen

Received April 12, 1973

## Commentationes

# An ICSCF Investigation of Walsh's Rules

Larilyn Zeller Stenkamp and Ernest R. Davidson

Chemistry Department BG-10, University of Washington, Seattle, Washington 98195 USA

Received March 27, 1973

The ICSCF method is applied to the calculation of orbital energies as a function of bond angle for several  $AH_2$  molecules. The resulting orbital energy diagrams are quite similar in appearance to the canonical SCF results even though the sum of the ICSCF energies is the SCF energy. The method is also applied to  $Li_2O$ ,  $CO_2$ ,  $HCN$  and a few  $AlH_3$  molecules with similar results. The sum of the ICSCF valence orbital energies generally correlates better with the equilibrium bond angle than does the similar sum of canonical orbital energies.

*Key words:* Walsh's rules · Orbital energies

## Introduction

Rules for predicting the geometry and spectra of triatomic molecules have been formulated by Walsh [1] and Mulliken [2] in the molecular orbital language. Implicit in Walsh's formulation is a set of "binding energies", associated with the orbitals, having the property that changes in total energy are given approximately by changes in the sum of the orbital energies. Thus, in discussing geometry, Walsh assumed that the minimum total energy occurred where the sum of the orbital energies was minimum. Also, in discussing spectra, differences of orbital energies were used to predict the relative positions of excited states.

Within this context Walsh estimated in detail how the energy of each molecular orbital would vary with angle in various triatomic molecules. These estimates have proven to be fairly accurate although certain ones of them were significantly in error. Based on his detailed estimates, Walsh was able to correctly predict the geometry of most triatomic molecules.

Since these original papers, there have appeared innumerable articles attempting to formulate in a rigorous manner these superficially simple results. No attempt will be made to review these articles here since a review paper has recently been written by Buenker and Peyerimhoff [3]. Clearly the orbital energies as used by Walsh have many of the properties associated with orbital energies in the Hückel empirical interpolation schemes. Extended Hückel theory results do generally parallel the predictions of Walsh's rules (even when they are wrong) [4].

Within the Hartree-Fock framework the situation is more difficult. Let

$$h = -\frac{1}{2}V^2 - \sum_A Z_A r_A^{-1} \quad (1)$$

$$F = h + 2J - K \quad (2)$$

be the one-electron and Fock operators respectively, and let

$$F\psi_i = \epsilon_i \psi_i \quad (3)$$

and

$$h_{ii} = \langle \psi_i | h | \psi_i \rangle \quad (4)$$

define the canonical Hartree-Fock orbitals  $\psi_i$  with orbital energy  $\epsilon_i$  and one-electron energy  $h_{ii}$ . Then the energy of a closed-shell molecule is given by

$$E = \sum_{i=1}^{N/2} (2\epsilon_i + h_{ii}) + V_N \quad (5)$$

where

$$V_N = \sum_{A, B} Z_A Z_B R_{AB}^{-1}. \quad (6)$$

Alternatively,

$$E = \sum_i 2\epsilon_i + V_N - V_e \quad (7)$$

where

$$V_e = \sum_{i=1}^{N/2} (2\epsilon_i - h_{ii}) \quad (8)$$

is the electron-electron repulsion energy. Coulson and Neilson [5] proposed that the quantity  $1/2(\epsilon_i + h_{ii})$  be associated with the orbital binding energy of Walsh. While this works to some extent for  $AH_2$  molecules where  $V_N$  does not change much with angle, it leads to quite erroneous results for  $AB_2$  molecules such as  $OF_2$  [6].

For many molecules the SCF orbital energy,  $\epsilon_i$ , seems to work fairly well. Since the charge distribution tends to follow the nuclei,  $V_N - V_e$  changes slowly with angle for non-ionic molecules. Peyerimhoff, Buenker and Allen [7] have shown that the sum of the valence orbital  $\epsilon_i$  parallels the true energy dependence on angle for some  $AH_2$  and non-ionic  $AB_2$  molecules. Two well-known exceptions are  $Li_2O$  in which Walsh's formulation and the sum of the SCF orbital energies both fail to predict the linear geometry [6] and  $HCN$  for which the Walsh formulation makes a correct prediction, but the sum of the  $\epsilon_i$  does not [3]. Curiously, the fact that the water molecule,  $H_2O$ , is also exceptional seems to have been overlooked. For water, the sum of the valence orbital energies decreases with decreasing bond angle so that the sum does predict that  $H_2O$  is non-linear, but this sum still has not reached a minimum at a  $45^\circ$  bond angle [8] so it can hardly be regarded as a reliable prediction of geometry.

In a previous paper [9] a generalized form of the self-consistent-field equation was derived. One special case of this generalization is the internally consistent SCF equation. This may be arrived at by noticing that, if the hamiltonian is partitioned into one and two body operators as

$$H = \sum_{i=1}^N [h(i) + (N-1)\alpha(i)] + \sum_{i<j}^N [g(i,j) - \alpha(i) - \alpha(j)], \quad (9)$$

$$h(i) = \frac{1}{2} \nabla^2 - \sum_A Z_A r_{Ai}^{-1}, \quad (10)$$

$$g(i,j) = r_{ij}^{-1}. \quad (11)$$

Table 13 The  $1a_1^2 2a_1^2 1b_2^2 3a_1^1 B_1$  state of  $\text{CH}_2$ 

	90	110	120	140	160	180	$\alpha_e$
ICSCF							
$1a_1$	-12.3409	-12.3391	-12.3377	-12.3346	-12.3325	-12.3316	
$2a_1$	-2.6113	-2.5980	-2.5936	-2.5877	-2.5844	-2.5836	
$3a_1$	-2.2507	-2.2203	-2.2032	-2.1680	-2.1371	-2.1233	
$1b_1$	2.1183	2.1207	-2.1213	-2.1221	-2.1229	-2.1233	
$1b_2$	2.2758	2.3224	-2.3410	-2.3704	-2.3894	-2.3964	
$\Sigma_{\text{val}}$	14.1432	-14.1818	-14.1937	14.2063	-14.2076	-14.2066	161
$L$	38.8250	38.8600	38.8692	38.8755	-38.8726	-38.8698	143
Canonical							
$1a_1$	11.2562	11.2510	-11.2487	-11.2443	-11.2411	-11.2397	
$2a_1$	0.8874	0.8675	0.8603	-0.8500	-0.8440	-0.8424	
$3a_1$	0.5085	-0.4752	-0.4576	-0.4221	0.3911	-0.3771	
$1b_1$	0.3842	0.3818	-0.3807	-0.3789	0.3776	-0.3771	
$1b_2$	0.5170	-0.5591	0.5765	0.6043	-0.6219	-0.6284	
$\Sigma_{\text{val}}$	3.7015	-3.7102	-3.7119	-3.7096	3.7005	-3.6958	123
$\Sigma_{\text{all}}$	26.2139	26.2122	26.2093	26.1982	-26.1827	-26.1752	< 90

Table 14 The  $1a_1^2 2a_1^2 1b_2^2 1b_1^1 A_1$  state of  $\text{CH}_2$ 

	90	110	120	140	160	180	$\alpha_e$
ICSCF							
$1a_1$	-12.3728	-12.3688	-12.3659	-12.3614	-12.3585	-12.3574	
$2a_1$	-2.6073	-2.5977	-2.5948	-2.5911	-2.5891	-2.5885	
$3a_1$	-2.1252	-2.0980	-2.0836	-2.0558	-2.0345	-2.0262	
$1b_1$	-2.0580	-2.0588	-2.0584	-2.0573	-2.0564	-2.0560	
$1b_2$	-2.2849	-2.3312	-2.3494	-2.3773	-2.3940	-2.3996	
$\Sigma_{\text{val}}$	-13.9004	-13.9754	-14.0052	-14.0514	-14.0790	-14.0882	180
$L$	-38.6459	-38.7119	-38.7369	-38.7742	-38.7960	-38.8033	180
Canonical							
$1a_1$	11.2824	-11.2766	-11.2742	-11.2704	-11.2682	-11.2674	
$2a_1$	-0.8849	-0.8698	-0.8648	-0.8580	-0.8542	-0.8531	
$3a_1$	-0.0459	-0.0161	-0.0011	0.0273	0.0491	0.0575	
$1b_1$	0.3195	-0.3175	-0.3166	-0.3152	-0.3143	-0.3141	
$1b_2$	-0.5270	-0.5702	-0.5880	-0.6161	-0.6331	-0.6391	
$\Sigma_{\text{val}}$	-3.4628	-3.5150	-3.5388	-3.5786	-3.6032	-3.6126	180
$\Sigma_{\text{all}}$	-26.0276	-26.0682	-26.0872	-26.1194	-26.1396	-26.1474	180

For the 2, 4, and 6 valence electron molecules (lowest singlet state),  $\text{BeH}_2$ ,  $\text{BH}_2^+$ ,  $\text{BH}_2^-$ , it was claimed [7] that the sum of the valence orbital  $\epsilon_i$  correlated correctly with the geometry. The present results agree with the claim except that the orbital energy sum seems to predict too small a bond angle. Also as in that study [7], this correlation of geometry and the sum of the  $\epsilon_i$  was not found to hold for the 6 electron system  $^1A_1 \text{NH}_2^+$ . Examination of the 25  $\text{AH}_2$  results

Table 15. The  $1a_1^2 2a_1^2 1b_1^2 3a_1^2 1b_1^2 B_1$  state of  $\text{CH}_2$ 

	90	110	120	140	160	180	$\alpha_e$
ICSCF							
$1a_1$	-12.1394	-12.1404	-12.1406	-12.1411	-12.1418	-12.1419	
$2a_1$	-2.3931	-2.3746	-2.3671	-2.3536	-2.3424	-2.3377	
$3a_1$	-1.8800	-1.8615	-1.8518	-1.8345	-1.8237	-1.8203	
$1b_1$	-1.8801	-1.8817	-1.8819	-1.8820	-1.8818	-1.8817	
$1b_2$	-2.0500	-2.0915	-2.1075	-2.1318	-2.1464	-2.1513	
$\Sigma_{\text{val}} E$	-14.5263	-14.5369	-14.5347	-14.5218	-14.5068	-14.5003	110
$E$	-38.8051	-38.8177	-38.8161	-38.8041	-38.7901	-38.7842	112
Canonical							
$1a_1$	-10.8920	-10.8893	-10.8888	-10.8887	-10.8895	-10.8898	
$2a_1$	-0.5805	-0.5563	-0.5468	-0.5310	-0.5190	-0.5142	
$3a_1$	-0.0373	-0.0116	0.0005	0.0210	0.0338	0.0378	
$1b_1$	-0.0339	-0.0309	-0.0300	-0.0290	-0.0287	-0.0286	
$1b_2$	-0.1909	-0.2323	-0.2492	-0.2758	-0.2923	-0.2981	
$\Sigma_{\text{val}} E$	-1.6513	-1.6313	-1.6210	-1.6006	-1.5837	-1.5776	< 90
$\Sigma_{\text{all}} E$	-23.4353	-23.4099	-23.3986	-23.3780	-23.3627	-23.3572	< 90

Table 16. The  $1a_1^2 2a_1^2 1b_1^2 3a_1 1b_1^2 A_1$  state of  $\text{CH}_2$ 

	90	110	120	140	160	180	$\alpha_e$
ICSCF							
$1a_1$	-12.1463	-12.1446	-12.1437	-12.1421	-12.1418	-12.1419	
$2a_1$	-2.3676	-2.3542	-2.3497	-2.3432	-2.3391	-2.3377	
$3a_1$	-2.0011	-1.9719	-1.9556	-1.9224	-1.8940	-1.8817	
$1b_1$	-1.8168	-1.8194	-1.8199	-1.8203	-1.8203	-1.8203	
$1b_2$	-2.0405	-2.0840	-2.1013	-2.1282	-2.1452	-2.1513	
$\Sigma_{\text{val}} E$	-14.4509	-14.4871	-14.4974	-14.5062	-14.5032	-14.5003	145
$E$	-38.7432	-38.7762	-38.7846	-37.7901	-38.7869	-38.7842	143
Canonical							
$1a_1$	-10.9004	-10.8943	-10.8922	-10.8898	-10.8895	-10.8898	
$2a_1$	-0.5585	-0.5375	-0.5303	-0.5205	-0.5154	-0.5142	
$3a_1$	-0.1659	-0.1297	-0.1111	-0.0742	0.0426	0.0286	
$1b_1$	0.0321	0.0356	0.0367	0.0379	0.0380	0.0378	
$1b_2$	-0.1864	-0.2279	-0.2452	-0.2731	-0.2913	-0.2981	
$\Sigma_{\text{val}} E$	-1.5915	-1.5893	-1.5889	-1.5856	-1.5800	-1.5776	< 90
$\Sigma_{\text{all}} E$	-23.3923	-23.3779	-23.3733	-23.3652	-23.3590	-23.3572	< 90

presented here show that in seven cases the sum of the valence orbital  $\epsilon_i$  correctly predicted the linear geometry, and in one case it satisfactorily predicted the non-linear geometry. In three cases it predicted the molecule to be linear when it wasn't. But the most consistent trend was shown in 14 out of the 25 cases where the predicted bond angle was significantly less than that shown by  $E_{\text{SCF}}$ . This error was not due to the effect of the core orbitals since inclusion of them in the sum only made the quantitative predictions worse.

Table 17. The  $1a_1^2 2a_1^2 1b_2^2 3a_1^2 {}^1A_1$  state of  $\text{NH}_2^+$ 

	90	110	120	140	160	180	$\alpha_e$
ICSCF							
$1a_1$	-17.5004	17.4975	-17.4946	17.4873	-17.4809	-17.4782	
$2a_1$	3.7312	3.7142	3.7075	-3.6965	-3.6881	-3.6849	
$3a_1$	3.0756	3.0537	3.0432	-3.0251	-3.0137	-3.0100	
$1b_1$	2.9910	2.9957	2.9975	-3.0001	-3.0020	-3.0025	
$1b_2$	3.2291	3.2814	-3.3026	-3.3364	3.3578	-3.3653	
$\Sigma_{\text{calc}}$	20.0718	20.0986	-20.1066	-20.1160	-20.1192	-20.1204	180
$E$	55.0726	-55.0935	55.0958	-55.0905	-55.0811	-55.0767	116
Canonical							
$1a_1$	16.1329	16.1208	16.1133	-16.0972	16.0836	-16.0783	
$2a_1$	1.5835	1.5564	1.5439	1.5215	-1.5040	-1.4974	
$3a_1$	0.9448	0.9179	0.9047	-0.8816	0.8660	-0.8607	
$1b_1$	0.3734	0.3689	0.3661	0.3605	0.3557	-0.3538	
$1b_2$	1.0614	1.0981	1.1125	-1.1344	-1.1464	1.1504	
$\Sigma_{\text{calc}}$	7.1794	7.1448	7.1222	-7.0750	7.0328	-7.0170	< 90
$\Sigma_{\text{all}}$	-39.4452	39.3864	-39.3488	39.2694	-39.2000	-39.1736	< 90

Table 18. The  $1a_1^2 2a_1^2 1b_2^2 3a_1^2 1b_1^2 {}^1B_1$  state of  $\text{NH}_2^+$ 

	90	110	120	140	160	180	$\alpha_e$
ICSCF							
$1a_1$	-17.4585	17.4584	-17.4572	-17.4531	17.4491	-17.4472	
$2a_1$	-3.6999	-3.6874	3.6835	-3.6786	-3.6766	-3.6764	
$3a_1$	3.2364	-3.2008	-3.1820	3.1448	-3.1142	-3.1013	
$1b_1$	3.0906	-3.0947	-3.0961	-3.0984	-3.1004	-3.1013	
$1b_2$	-3.2235	-3.2747	-3.2956	-3.3291	-3.3509	-3.3589	
$\Sigma_{\text{calc}}$	20.1738	-20.2197	-20.2363	20.2586	-20.2696	-20.2732	180
$E$	-55.0908	55.1367	55.1505	-55.1648	-55.1679	-55.1676	168
Canonical							
$1a_1$	16.0787	16.0732	-16.0694	-16.0609	-16.0524	-16.0486	
$2a_1$	-1.5345	-1.5159	1.5086	-1.4969	-1.4889	-1.4863	
$3a_1$	-1.0772	-1.0419	-1.0235	-0.9884	-0.9596	-0.9476	
$1b_1$	0.9622	-0.9597	-0.9579	-0.9537	-0.9495	-0.9476	
$1b_2$	-1.0344	-1.0751	-1.0918	-1.1182	-1.1337	-1.1390	
$\Sigma_{\text{calc}}$	-7.1772	-7.1836	-7.1822	-7.1723	-7.1543	-7.1470	110
$\Sigma_{\text{all}}$	39.3346	-39.3300	-39.3210	-39.2941	-39.2591	-39.2442	< 90

From the limited data shown here, it would appear possible in some of these 14 cases that the sum of the  $\epsilon_i$  might show a minimum, and therefore better correlation with the total energy, if calculations were done at some angles between  $90^\circ$  and  $110^\circ$ . However, other work by Krauss [11] reports decreases in the sum of the  $\epsilon_i$  at  $5^\circ$  intervals over parts of this range for  ${}^1A_1 \text{CH}_2$ ,  ${}^2B_1 \text{NH}_2$ , and  ${}^2B_1 \text{H}_2\text{O}^+$  which seem to be linear with respect to decrease in angle.

Table 19. The  $1a_1^2 2a_1^2 1b_2^2 1b_1^2 {}^1A_1$  state of  $\text{NH}_2$ 

	90	110	120	140	160	180	$\alpha_e$
ICSCF							
$1a_1$	-17.4819	-17.4825	-17.4819	-17.4802	17.4788	-17.4782	
$2a_1$	-3.7056	-3.6956	-3.6923	-3.6880	-3.6856	-3.6849	
$3a_1$	-3.1020	-3.0722	-3.0574	-3.0299	-3.0100	-3.0025	
$1b_1$	-3.0089	-3.0107	-3.0109	-3.0105	-3.0102	-3.0100	
$1b_2$	-3.2441	-3.2927	-3.3118	-3.3414	-3.3592	-3.3653	
$\Sigma_{\text{val}} E$	-19.9172	-19.9966	-20.0300	-20.0798	-20.1100	-20.1204	180
$E$	-54.8810	-54.9627	-54.9939	-55.0402	-55.0676	-55.0767	180
Canonical							
$1a_1$	-16.0832	-16.0824	-16.0816	-16.0800	-16.0787	-16.0783	
$2a_1$	-1.5263	-1.5137	-1.5090	-1.5026	-1.4986	-1.4974	
$3a_1$	-0.4793	-0.4422	-0.4239	-0.3899	-0.3638	-0.3538	
$1b_1$	-0.8617	-0.8620	-0.8618	-0.8613	-0.8608	-0.8607	
$1b_2$	-1.0374	-1.0804	-1.0982	-1.1270	-1.1443	-1.1504	
$\Sigma_{\text{val}} E$	-6.8508	-6.9122	-6.9380	-6.9818	-7.0048	-7.0170	180
$\Sigma_{\text{all}} E$	-39.0172	-39.0770	-39.1012	-39.1418	-39.1622	-39.1736	180

Table 20. The  $1a_1^2 2a_1^2 1b_2^2 3a_1^2 1b_1^2 {}^2B_1$  state of  $\text{NH}_2$ 

	90	110	120	140	160	180	$\alpha_e$
ICSCF							
$1a_1$	-17.1816	-17.1801	-17.1783	-17.1733	-17.1688	-17.1668	
$2a_1$	-3.4327	-3.4159	-3.4092	-3.3979	-3.3887	-3.3850	
$3a_1$	-2.7931	-2.7678	-2.7553	-2.7334	-2.7191	-2.7143	
$1b_1$	-2.7910	-2.7944	-2.7957	-2.7979	-2.7996	-2.8003	
$1b_2$	-2.9492	-2.9993	-3.0192	-3.0507	-3.0704	-3.0773	
$\Sigma_{\text{val}} E$	-21.1410	-21.1604	-21.1631	-21.1619	-21.1560	-21.1535	127
$E$	-55.5043	-55.5204	-55.5198	-55.5083	-55.4936	-55.4872	114
Canonical							
$1a_1$	-15.5763	-15.5684	-15.5634	-15.5526	-15.5433	-15.5395	
$2a_1$	-1.1295	-1.1059	-1.0954	-1.0765	-1.0613	-1.0553	
$3a_1$	-0.4805	-0.4502	-0.4356	-0.4099	-0.3928	-0.3871	
$1b_1$	-0.5004	-0.4953	-0.4922	-0.4857	-0.4801	-0.4778	
$1b_2$	-0.6019	-0.6424	-0.6584	-0.6829	-0.6969	-0.7017	
$\Sigma_{\text{val}} E$	-4.9242	-4.8923	-4.8710	-4.8243	-4.7821	-4.7660	< 90
$\Sigma_{\text{all}} E$	-36.0768	-36.0291	-35.9978	-35.9295	-35.8687	-35.8450	< 90

This tendency to produce bond angles systematically too small can be predicted from Eq. (7). If the hydrogens carry any net positive charge,  $V_N - V_H$  will tend to increase as the bond angle is decreased and the charges are brought closer together. Hence  $\Sigma 2\epsilon_i$  must be systematically wrong in just the opposite direction so the 0 quantities will give  $E_{\text{SCF}}$  when added together. The few cases where the bond



Table 21. The  $1a_1^2 2a_1^2 1b_2^2 3a_1 1b_1^2 {}^2A_1$  state of  $\text{NH}_2$ 

	90	110	120	140	160	180	$\alpha_c$
ICSCF							
$1a_1$	- 17.1777	- 17.1767	- 17.1753	- 17.1717	17.1684	- 17.1668	
$2a_1$	-- 3.4102	-- 3.3980	-- 3.3939	-- 3.3885	-- 3.3856	-- 3.3850	
$3a_1$	2.9394	-- 2.9031	-- 2.8839	-- 2.8459	-- 2.8040	-- 2.8003	
$1b_1$	2.7051	2.7086	2.7098	2.7118	2.7135	- 2.7143	
$1b_2$	2.9476	2.9974	- 3.0174	- 3.0492	- 3.0698	- 3.0773	
$\Sigma_{\text{val}}^i$	21.0652	21.1043	21.1261	- 21.1449	- 21.1518	- 21.1535	180
$E_c$	55.4204	55.4644	- 55.4769	- 55.4884	- 55.4887	- 55.4872	153
Canonical							
$1a_1$	15.5654	15.5594	- 15.5561	- 15.5489	- 15.5424	- 15.5395	
$2a_1$	1.0993	1.0815	- 1.0747	-- 1.0643	- 1.0575	- 1.0553	
$3a_1$	0.6195	- 0.5804	-- 0.5607	0.5226	- 0.4911	- 0.4778	
$1b_1$	0.3993	- 0.3965	- 0.3949	-- 0.3916	- 0.3885	- 0.3871	
$1b_2$	-- 0.5928	- 0.6349	0.6521	0.6795	- 0.6960	- 0.7017	
$\Sigma_{\text{val}}^i$	4.8023	4.8062	4.8041	4.7934	4.7751	- 4.7660	110
$\Sigma_{\text{all}}^i$	35.9331	35.9250	35.9163	35.8913	- 35.8599	35.8450	< 90

Table 22. The  $1a_1^2 2a_1^2 1b_2^2 3a_1^2 1b_1^2 {}^1A_1$  state of  $\text{NH}_2$ 

	90	110	120	140	160	180	$\alpha_c$
ICSCF							
$1a_1$	16.9322	16.9319	-- 16.9312	- 16.9289	- 16.9269	16.9259	
$2a_1$	3.1503	3.1335	3.1270	3.1150	- 3.1052	- 3.1010	
$3a_1$	2.5212	2.4951	2.4819	2.4581	2.4420	- 2.4366	
$1b_1$	2.4294	2.4323	2.4333	-- 2.4350	-- 2.4362	- 2.4366	
$1b_2$	2.6845	- 2.7310	- 2.7494	- 2.7779	-- 2.7957	- 2.8019	
$\Sigma_{\text{val}}^i$	21.5708	21.5838	21.5832	21.5720	21.5582	- 21.5522	115
$E_c$	- 55.4353	- 55.4478	- 55.4452	- 55.4298	- 55.4118	- 55.4040	110
Canonical							
$1a_1$	-- 15.1475	- 15.1409	- 15.1376	- 15.1308	- 15.1251	- 15.1227	
$2a_1$	0.7380	0.7144	- 0.7046	- 0.6871	- 0.6729	- 0.6670	
$3a_1$	- 0.0865	- 0.0528	- 0.0370	- 0.0092	0.0093	0.0155	
$1b_1$	- 0.0033	0.0019	0.0044	0.0093	0.0136	0.0155	
$1b_2$	- 0.2095	- 0.2511	- 0.2677	- 0.2933	- 0.3082	- 0.3131	
$\Sigma_{\text{val}}^i$	- 2.0746	- 2.0404	- 2.0274	- 1.9978	- 2.0080	- 2.0222	< 90, 180
$\Sigma_{\text{all}}^i$	- 32.3696	- 32.3222	- 32.3010	- 32.2594	- 32.2582	- 32.2676	< 90

angle was overestimated were the cases where one would expect the hydrogens to carry a net negative charge, and the bulk of the cases such as  $\text{H}_2\text{O}$  where the bond angle was underestimated were just those cases where the hydrogens were expected to carry a net positive charge.

Table 23. The  $1a_1^2 2a_1^2 1b_2^2 3a_1^2 1b_1^2 B_1$   $H_2O^+$ 

	90	110	120	140	160	180	$\alpha_c$
ICSCF							
$1a_1$	-23.1359	-23.1329	-23.1300	-23.1226	-23.1159	-23.1131	
$2a_1$	-4.7054	-4.6913	-4.6857	-4.6766	-4.6703	-4.6679	
$3a_1$	-3.9189	-3.8909	-3.8780	-3.8558	-3.8410	-3.8360	
$1b_1$	-3.9352	-3.9401	-3.9422	-3.9458	-3.9484	-3.9495	
$1b_2$	-4.0531	-4.1071	-4.1290	-4.1637	-4.1856	-4.1932	
$\Sigma_{val}E$	-29.2900	-29.3187	-29.3276	-29.3380	-29.3422	-29.3437	180
$E$	-75.5617	-75.5844	-75.5875	-75.5832	-75.5741	-75.5698	119
Canonical							
$1a_1$	-21.1317	-21.1184	-21.1101	-21.0919	-21.0764	-21.0702	
$2a_1$	-1.8651	-1.8412	-1.8296	-1.8080	-1.7914	-1.7850	
$3a_1$	-1.0931	-1.0615	-1.0460	-1.0185	-0.9996	-0.9929	
$1b_1$	-1.1444	-1.1366	-1.1316	-1.1210	-1.1120	-1.1084	
$1b_2$	-1.1850	-1.2213	-1.2354	-1.2561	-1.2674	-1.2708	
$\Sigma_{val}E$	-9.4308	-9.3846	-9.3536	-9.2862	-9.2288	-9.2058	< 90
$\Sigma_{all}E$	-51.6942	-51.6214	-51.5738	-51.4700	-51.3816	-51.3462	< 90

Table 24. The  $1a_1^2 2a_1^2 1b_2^2 3a_1^2 1b_1^2 A_1$  state of  $H_2O^+$ 

	90	110	120	140	160	180	$\alpha_c$
ICSCF							
$1a_1$	-23.1235	-23.1237	-23.1226	-23.1190	-23.1149	-23.1131	
$2a_1$	-4.6880	-4.6778	-4.6744	-4.6700	-4.6683	-4.6679	
$3a_1$	-4.0868	-4.0472	-4.0274	-3.9903	-3.9611	-3.9495	
$1b_1$	-3.8232	-3.8278	-3.8296	-3.8326	-3.8350	-3.8360	
$1b_2$	-4.0572	-4.1092	-4.1305	-4.1640	-4.1856	-4.1932	
$\Sigma_{val}E$	-29.2236	-29.2768	-29.2964	-29.3235	-29.3389	-29.3437	180
$E$	-75.4704	-75.5243	-75.5416	-75.5615	-75.5685	-75.5698	180
Canonical							
$1a_1$	-21.1034	-21.0977	-21.0935	-21.0837	-21.0743	-21.0702	
$2a_1$	-1.8293	-1.8141	-1.8074	-1.7958	-1.7879	-1.7850	
$3a_1$	-1.2402	-1.2019	-1.1827	-1.1469	-1.1193	-1.1084	
$1b_1$	-1.0096	-1.0070	-1.0049	-1.0000	-0.9950	-0.9929	
$1b_2$	-1.1694	-1.2097	-1.2261	-1.2514	-1.2661	-1.2708	
$\Sigma_{val}E$	-9.2568	-9.2635	-9.2595	-9.2413	-9.2173	-9.2058	110
$\Sigma_{all}E$	-51.4636	-51.4589	-51.4465	-51.3817	-51.3659	-51.3462	< 90

The ICSCF results are somewhat superior to the canonical results. The  $1a_1$  ICSCF orbital energy changes with angle, on the average, only half as much as does the RHF  $e_i$  (but notice later that wherever the ICSCF makes the wrong prediction, it is, by definition, due to the change of the  $1a_1$  energy). Except for

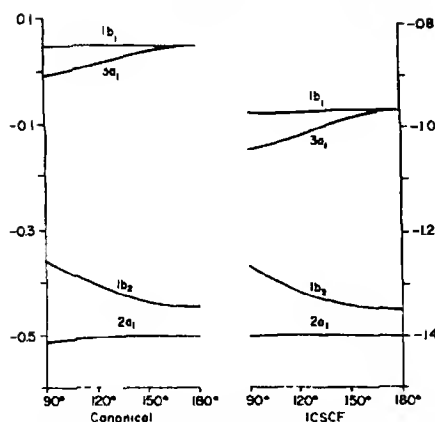
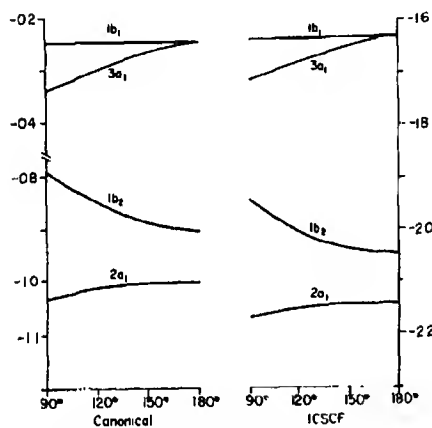
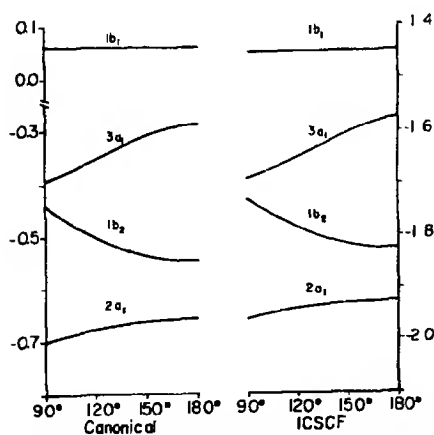
Table 25. The  $1a_1^2 2a_1^2 1b_2^2 3a_1^2 1b_1^2 {}^1A_1$  state of  $H_2O$ 

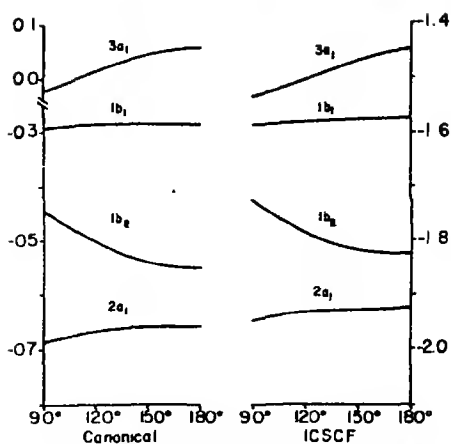
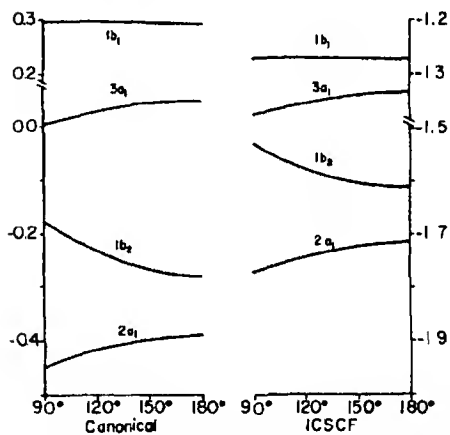
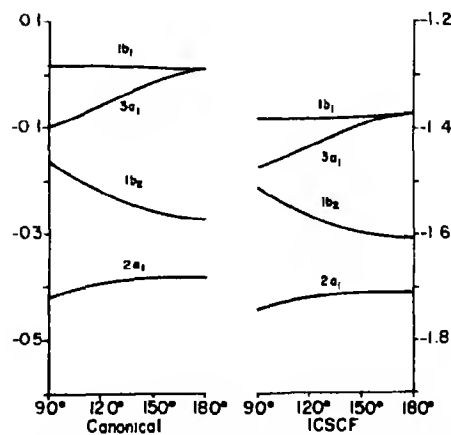
	90	110	120	140	160	180	$\alpha_c$
ICSCF							
$1a_1$	22.8025	- 22.8010	- 22.7975	- 22.7911	- 22.7849	- 22.7823	
$2a_1$	4.3688	- 4.3548	- 4.3493	- 4.3400	- 4.3330	- 4.3301	
$3a_1$	- 3.5968	- 3.5648	- 3.5497	- 3.5230	- 3.5048	- 3.4985	
$1b_1$	3.4855	3.4896	3.4914	3.4948	3.4974	3.4985	
$1b_2$	- 3.7358	- 3.7887	- 3.8098	- 3.8429	- 3.8638	- 3.8711	
$\Sigma_{val}^I$	30.3738	- 30.3958	- 30.4004	- 30.4014	- 30.3980	- 30.3964	135
$E$	75.9787	75.9959	- 75.9954	- 75.9835	- 75.9678	- 75.9608	115
Canonical							
$1a_1$	20.5650	20.5548	- 20.5481	- 20.5332	- 20.5199	- 20.5144	
$2a_1$	1.3761	- 1.3552	- 1.3452	1.3262	1.3110	- 1.3048	
$3a_1$	0.5928	0.5576	0.5405	0.5102	- 0.4894	- 0.4821	
$1b_1$	0.5117	0.5055	0.5016	0.4930	0.4853	- 0.4821	
$1b_2$	0.6891	0.7291	0.7447	0.7677	0.7803	- 0.7843	
$\Sigma_{val}^I$	6.3394	6.2948	6.2640	6.1942	- 6.1320	- 6.1066	< 90
$\Sigma_{all}^I$	47.4694	47.4044	47.3602	47.2606	47.1718	- 47.1354	< 90

BeH<sub>2</sub>,  $\epsilon_{1a}$  changes less than 15 kcal (and usually only half that amount) as the bond angle varies from 90-180°. The other orbital energy curves are generally similar to the RHF results. The  $2a_1$  orbital energy still has a positive slope, but perhaps a little less steep. The  $1b_2$  and  $3a_1$  orbital energy curves are nearly identical in shape to the canonical result. The  $1b_1$  curves are generally even flatter than the canonical curves in closer agreement with Walsh's assumptions. The dependence of the orbital energy on whether the orbital is occupied or vacant is less pronounced than for the canonical orbitals but still sufficient to cause the orbital energy plots to vary in appearance from molecule to molecule rather more than Walsh assumed.

By definition, the sum of the ICSCF orbital energies is the SCF energy, so the only relevant question is whether the sum over only the valence orbital correlates with the geometry. In the 25 examples considered here, the correlation was satisfactory for all 8 of the linear cases and 8 of the non-linear cases. In the remaining 9 non-linear cases, the bond angle was significantly overestimated. In these latter cases, however, this occurred because the energy curve was quite flat so that a small error in the energy caused a large deviation in the bond angle. On the whole, the ICSCF results are right about twice as often as the canonical results. There is no apparent qualitative difference between the cases where the ICSCF valence energy sum works and those where it does not. In almost every case the  $1a_1$  orbital energy has a small positive slope so that omitting it leads systematically to too large a bond angle.

Because the results for AH<sub>2</sub> molecules tend to be too good [3], it is of interest to consider three other molecules: CO<sub>2</sub>, Li<sub>2</sub>O, and HCN. Carbon dioxide is

Fig. 1. Orbital energies for the  $1a_1^2 2a_1^2 1b_2^2 1A_1$  state of  $\text{BeH}_2$ Fig. 2. Orbital energies for the  $1a_1^2 2a_1^2 1b_2^2 1A_1$  state of  $\text{BH}_2$ Fig. 3. Orbital energies for the  $1a_1^2 2a_1^2 1b_2^2 3a_1 2A_1$  state of  $\text{BH}_2$

Fig. 4. Orbital energies for the  $1a_1^2 2a_1^2 1b_2^2 1b_1^2 B_1$  state of  $BH_2$ Fig. 5. Orbital energies for the  $1a_1^2 2a_1^2 1b_2^2 3a_1^1 A_1$  state of  $BH_2$ Fig. 6. Orbital energies for the  $1a_1^2 2a_1^2 1b_2^2 3a_1 1b_1^3 B_1$  state of  $BH_2$

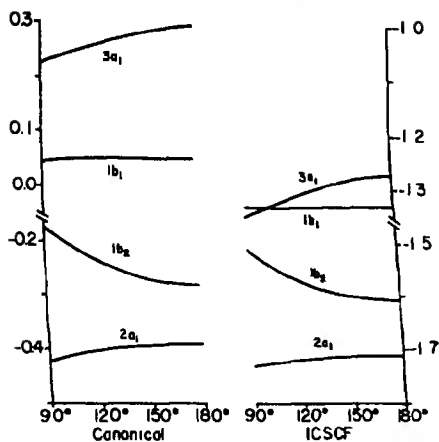


Fig. 7. Orbital energies for the  $1a_1^2 2a_1^2 1b_2^2 1b_1^2 {}^1A_1$  state of  $BH_2$

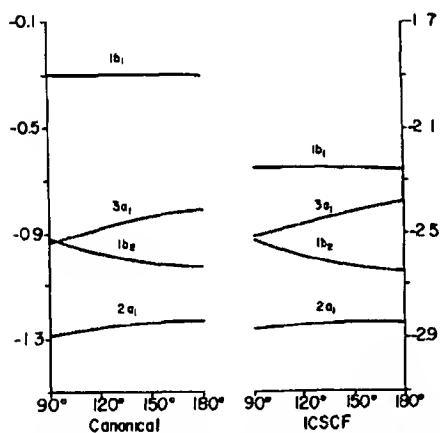


Fig. 8. Orbital energies for the  $1a_1^2 2a_1^2 1b_2^2 3a_1 {}^2A_1$  state of  $CH_2^+$

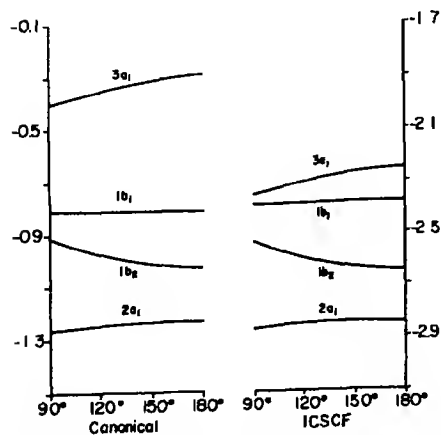
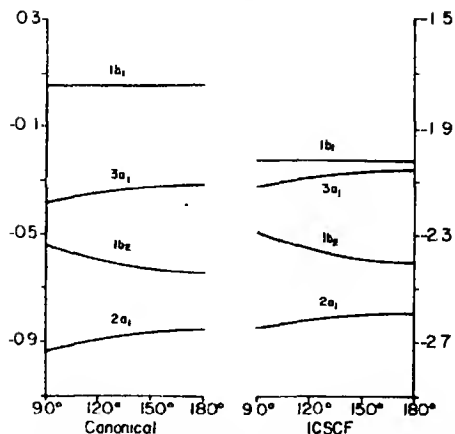
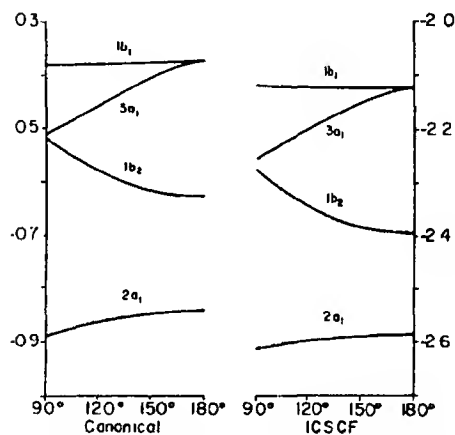
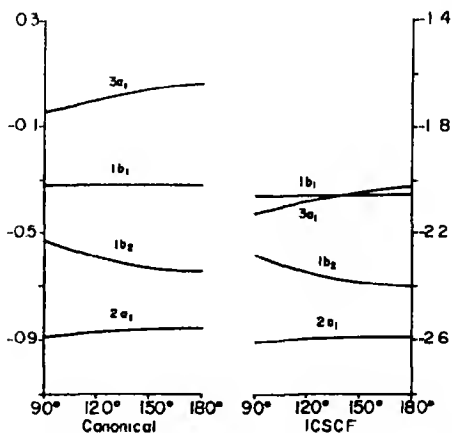


Fig. 9. Orbital energies for the  $1a_1^2 2a_1^2 1b_2^2 1b_1 {}^2B_1$  state of  $CH_2^+$

Fig. 10. Orbital energies for the  $1a_1^2 2a_1^2 1b_2^2 3a_1^2 {}^1A_1$  state of  $\text{CH}_2$ Fig. 11. Orbital energies for the  $1a_1^2 2a_1^2 1b_2^2 3a_1 1b_1 {}^1B_1$  state of  $\text{CH}_2$ Fig. 12. Orbital energies for the  $1a_1^2 2a_1^2 1b_2^2 1b_1^2 {}^1A_1$  state of  $\text{CH}_2$

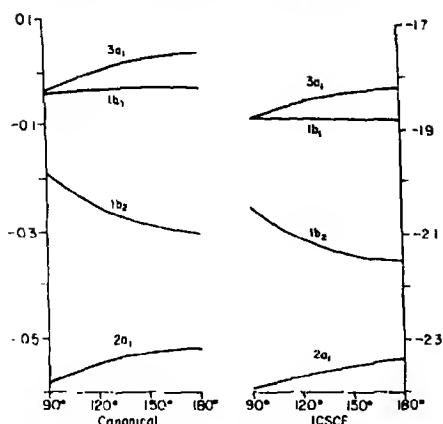


Fig. 13. Orbital energies for the  $1a_1^2 2a_1^2 1b_2^2 3a_1^1 1b_1^1 {}^2B_1$  state of  $\text{CH}_2$

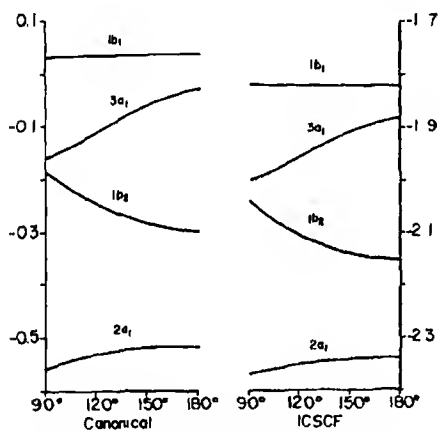


Fig. 14. Orbital energies for the  $1a_1^2 2a_1^2 1b_2^2 3a_1^1 1b_1^2 {}^2A_1$  state of  $\text{CH}_2$

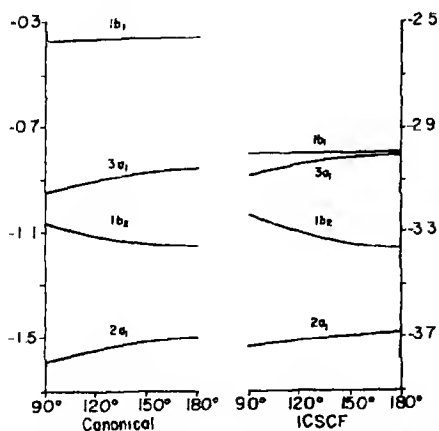
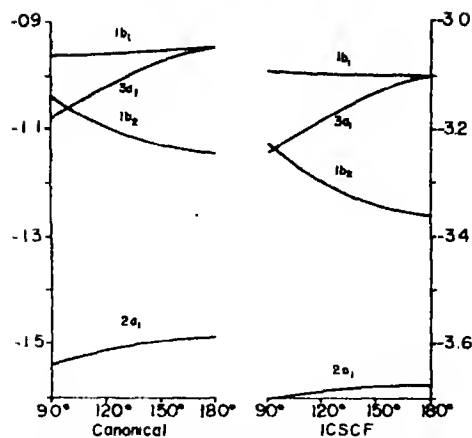
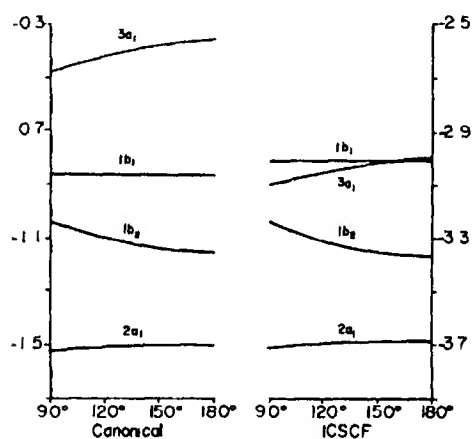
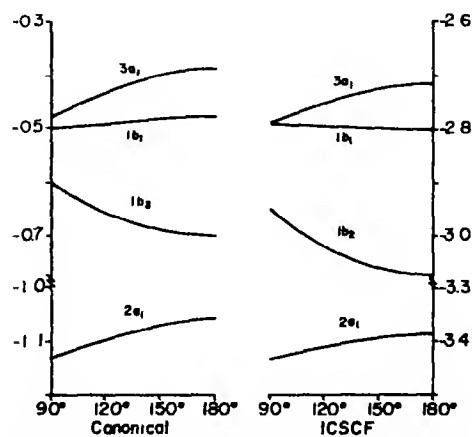
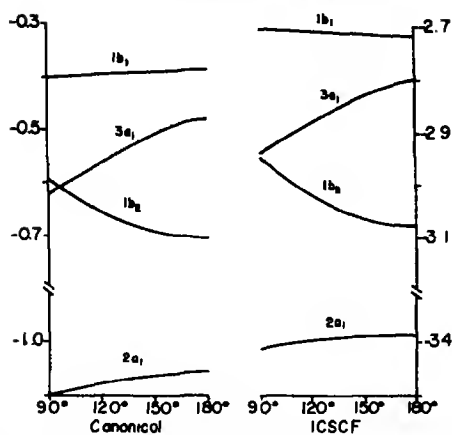
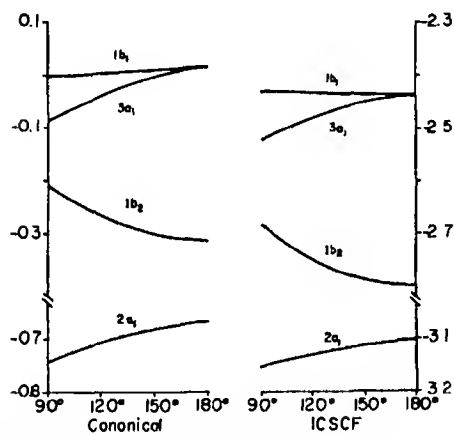
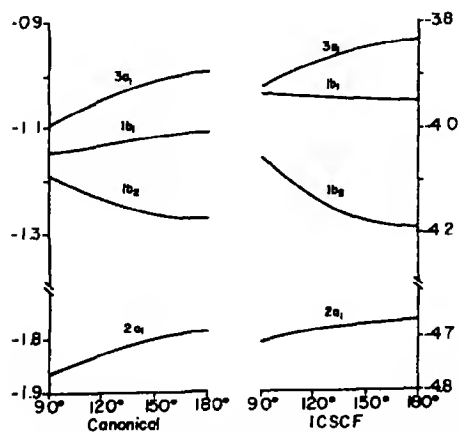


Fig. 15. Orbital energies for the  $1a_1^2 2a_1^2 1b_2^2 3a_1^2 {}^1A_1$  state of  $\text{NH}_2$



Fig. 16. Orbital energies for the  $1a_1^2 2a_1^2 1b_2^2 3a_1 1b_1$   $^3B_1$  state of  $\text{NH}_2^+$ Fig. 17. Orbital energies for the  $1a_1^2 2a_1^2 1b_2^2 1b_1^2$   $^1A_1$  state of  $\text{NH}_2^+$ Fig. 18. Orbital energies for the  $1a_1^2 2a_1^2 1b_2^2 3a_1 1b_1$   $^2B_1$  state of  $\text{NH}_2^+$

Fig. 19. Orbital energies for the  $1a_1^2 2a_1^2 1b_2^2 3a_1 1b_1^2 {}^2A_1$  state of  $\text{NH}_2$ .Fig. 20. Orbital energies for the  $1a_1^2 2a_1^2 1b_2^2 3a_1 1b_1^2 {}^1A_1$  state of  $\text{NH}_2$ .Fig. 21. Orbital energies for the  $1a_1^2 2a_1^2 1b_2^2 3a_1 1b_1^2 {}^2B_1$  state of  $\text{OH}_2$ .

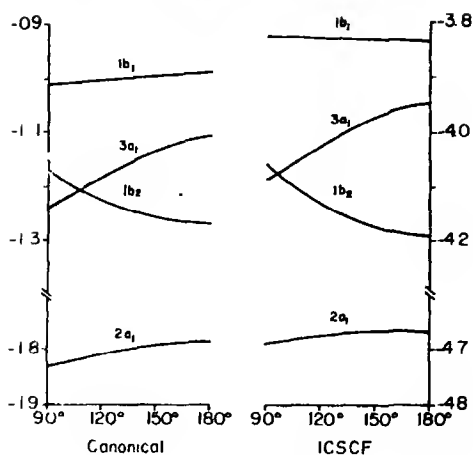


Fig. 22. Orbital energies for the  $1a_1^2 2a_1^2 1b_2^2 3a_1 1b_1^2 A_1$  state of  $\text{OH}_1^+$

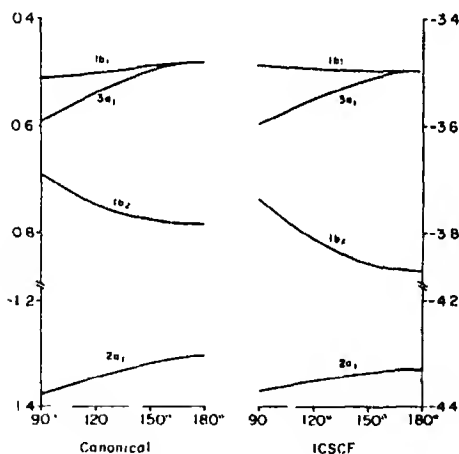


Fig. 23. Orbital energies for the  $1a_1^2 2a_1^2 1b_2^2 3a_1 1b_1^2 A_1$  state of  $\text{OH}_2$

good example of an  $\text{AB}_2$  system for which all theories work. Walsh's diagram, the canonical energies (Fig. 24a), and the ICSCF energies (Fig. 24b) are quite similar, and all predict a linear molecule. When considered in detail, it is seen that the  $3a_1$  and  $2b_2$  orbitals change with energy more than Walsh imagined, but their sum is nearly constant. The  $4a_1$  orbital (analogous to the  $2a_1$  orbital for  $\text{AH}_2$ ) has a slight positive slope rather than the large negative slope predicted by Walsh. The  $1b_1$  and  $5a_1$  orbital energies are nearly constant in agreement with Walsh, but the slope of the  $5a_1$  orbital has the opposite sign from his prediction. The  $3b_2$  orbital is in the right place, and the slope has the predicted sign but a rather smaller magnitude. The  $1a_2$ ,  $4b_2$ , and the ICSCF  $6a_1$  and  $2b_1$  are just as Walsh

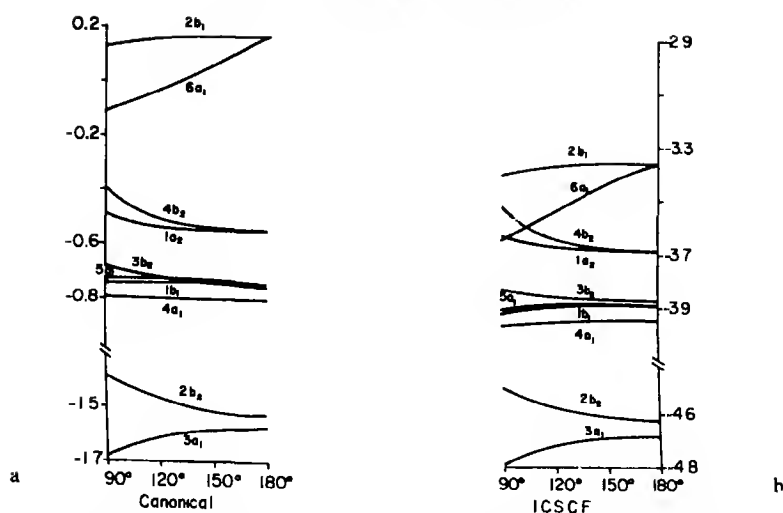


Fig. 24. a Canonical energies for the  $1a_1^2 2a_1^2 1b_2^2 3a_1^2 2b_2^2 4a_1^2 1b_1^2 5a_1^2 3b_2^2 1a_2^2 4b_2^2 1A_1$  state of  $\text{CO}_2$ . b ICSCF energies for the  $1a_1^2 2a_1^2 1b_2^2 3a_1^2 2b_2^2 4a_1^2 1b_1^2 5a_1^2 3b_2^2 1a_2^2 4b_2^2 1A_1$  state of  $\text{CO}_2$ .

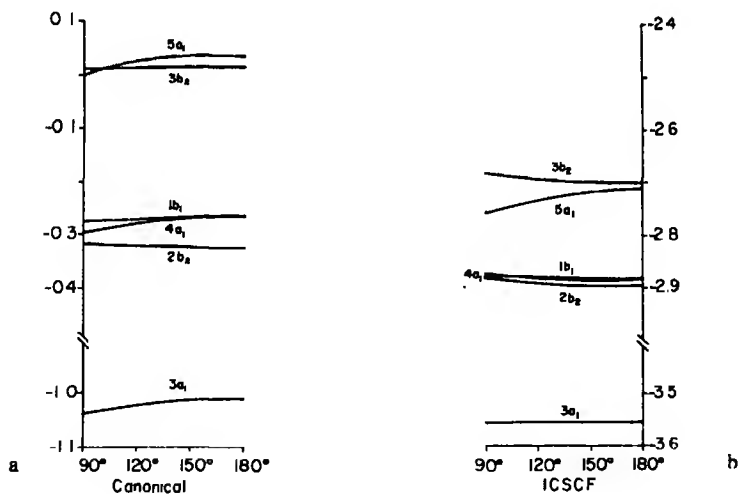


Fig. 25. a Canonical energies for the  $1a_1^2 2a_1^2 1b_2^2 3a_1^2 2b_2^2 4a_1^2 1b_1^2 1A_1$  state of  $\text{Li}_2\text{O}$ . b ICSCF energies for the  $1a_1^2 2a_1^2 1b_2^2 3a_1^2 2b_2^2 4a_1^2 1b_1^2 1A_1$  state of  $\text{Li}_2\text{O}$ .

predicted. The molecule in this model is linear largely because of the  $4h_2$  non-bonding  $\pi$  electrons.

The  $\text{Li}_2\text{O}$  molecule is formally similar to  $\text{H}_2\text{O}$  in its valence electron structure and hence should be bent in the Walsh model. The canonical orbital energy plot (Fig. 25a) resembles that for  $\text{H}_2\text{O}$  although the slope of the curves is much

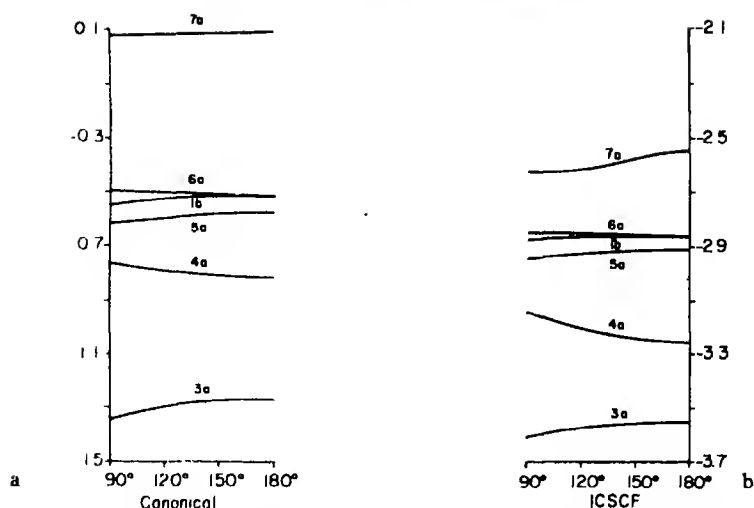


Fig. 26. a Canonical energies for the  $1a^2 2a^2 3a^2 4a^2 5a^2 1b^2 6a^2 1A_1$  state of HCN. b ICSCF energies for the  $1a^2 2a^2 3a^2 4a^2 5a^2 1b^2 6a^2 1A_1$  state of HCN

Table 26. The ground state of  $\text{CO}_2$

	90	120	150	180	$\alpha_r$
ICSCF					
$1a_1$	-23.4706	23.5096	23.5211	-23.5225	
$2a_1$	-14.5107	14.4714	-14.4601	-14.4582	
$3a_1$	-4.7893	-4.7194	-4.6903	-4.6826	
$4a_1$	-3.9730	-3.9572	-3.9499	-3.9472	
$5a_1$	-3.9166	-3.8954	-3.8891	-3.8896	
$1b_2$	-23.4708	-23.5097	23.5212	-23.5225	
$2b_2$	-4.4999	-4.5743	-4.6116	-4.6238	
$3b_2$	-3.8376	-3.8623	-3.8718	-3.8738	
$4b_2$	-3.5327	-3.6464	-3.6793	-3.6836	
$1b_1$	-3.9183	-3.8968	-3.8901	-3.8896	
$1a_2$	-3.6401	-3.6737	-3.6826	-3.6836	
$\Sigma_{vib}^r$	-64.3150	-64.4510	-64.5294	-64.5476	180
$E$	-187.1190	-187.4328	-187.5342	-187.5541	180
Canonical					
$1a_1$	-20.6163	-20.6601	-20.6763	-20.6767	
$2a_1$	-11.5110	-11.5027	-11.5076	-11.5079	
$3a_1$	-1.6834	-1.6130	-1.5839	-1.5733	
$4a_1$	-0.7964	-0.8017	-0.8021	-0.7982	
$5a_1$	-0.7278	-0.7237	-0.7349	-0.7390	
$1b_2$	-20.6164	-20.6602	-20.6764	-20.6767	
$2b_2$	-1.3730	-1.4659	-1.5134	-1.5262	
$3b_2$	-0.6793	-0.7203	-0.7387	-0.7404	
$4b_2$	-0.3932	-0.5063	-0.5410	-0.5456	
$1b_1$	-0.7440	-0.7376	-0.7398	-0.7390	
$1a_2$	-0.4923	-0.5325	-0.5459	-0.5456	
$\Sigma_{vib}^c$	-13.7788	-14.2020	-14.3994	-14.4146	180
$\Sigma_{all}^c$	-119.2662	-119.8480	-120.1200	-120.1372	180

Table 27. The ground state of  $\text{Li}_2\text{O}$ 

	90	120	150	180	$\alpha_e$
ICSCF					
$1a_1$	-22.3983	-22.4000	-22.3981	-22.3975	
$2a_1$	-5.1373	-5.1332	-5.1333	-5.1340	
$3a_1$	-3.5546	-3.5569	-3.5567	-3.5562	
$4a_1$	-2.8754	-2.8819	-2.8831	-2.8829	
$1b_2$	-5.1355	-5.1328	-5.1332	-5.1340	
$2b_2$	-2.8798	-2.8892	-2.8939	-2.8953	
$1b_1$	-2.8782	-2.8813	-2.8828	-2.8829	
$\Sigma_{\text{val}}^e$	-24.3760	-24.4186	-24.4330	-24.4346	180
$E$	-89.7184	-89.7507	-89.7624	-89.7654	180
Canonical					
$1a_1$	-20.3532	-20.3408	-20.3312	-20.3281	
$2a_1$	-2.4081	-2.3806	-2.3686	-2.3652	
$3a_1$	-1.0338	-1.0200	-1.0106	-1.0070	
$4a_1$	-0.2966	-0.2776	-0.2661	-0.2618	
$1b_2$	-2.4062	-2.3801	-2.3686	-2.3651	
$2b_2$	-0.3163	-0.3191	-0.3219	-0.3227	
$1b_1$	-0.2751	-0.2695	-0.2641	-0.2618	
$\Sigma_{\text{val}}^e$	-3.8436	-3.7724	-3.7254	-3.7066	< 90
$\Sigma_{\text{all}}^e$	-54.1786	-53.9754	-53.8622	-53.8234	< 90

less steep. As discussed previously, for a molecule like  $\text{H}_2\text{O}$  or  $\text{Li}_2\text{O}$  where the H or Li carries a net positive charge, the sum of the canonical valence orbital energies gives too small a bond angle. In the case of  $\text{Li}_2\text{O}$  which is linear, this sum behaves just as it did for  $\text{H}_2\text{O}$  and shows no minimum above  $90^\circ$ . In the ICSCF model, the slope of each of the orbital energy curves (Fig. 25b) is slightly negative so the sum of the valence energies correctly predicts a linear molecule.

In the Walsh model, a molecule such as  $\text{HCN}$  is intermediate between  $\text{AH}_2$  and  $\text{AB}_2$ . The  $1a$  and  $2a$  orbitals are  $1s$  cores. The  $3a$  orbital is supposedly analogous to  $3a_1$  and  $2b_2$ , in the  $\text{AB}_2$  system and was predicted by Walsh to not vary with angle. The  $4a$  and  $5a$  orbitals are the sigma bonds (analogous to  $2a_1$ ,  $1b_2$  in  $\text{AH}_2$  or  $4a_1$ ,  $3b_2$  in  $\text{AB}_2$ ). Walsh predicted both would have negative slopes in analogy to his predictions for  $\text{AH}_2$  and  $\text{AB}_2$  systems. Finally, the  $1b$  and  $6a$  orbitals are the  $\pi$  orbitals (analogous to  $1b_1$ ,  $3a_1$  in  $\text{AH}_2$  or  $1b_1$ ,  $5a_1$  in  $\text{AB}_2$ ). The  $1b$  remains a  $\pi$  orbital in the bent molecule and was predicted to be independent of angle, while the  $6a$  orbital energy was predicted to have a small negative slope. Based on this model, Walsh correctly predicted that  $\text{HCN}$  should be linear. The sum of the canonical valence orbital energies, on the other hand, incorrectly predicts that  $\text{HCN}$  is bent (the sum is still decreasing down to  $90^\circ$ ). This is largely due to the positive slopes of the  $3a$  and  $5a$  orbitals (Fig. 26a). The ICSCF orbital energy picture (Fig. 26b) is qualitatively similar to the canonical energies with only slight changes in the magnitude of the slopes (particularly of the  $4a$  orbital).

Table 28. The ground state of HCN

	90	120	150	180	$\alpha_e$
ICSCF					
1a	-17.5783	-17.5734	-17.5672	-17.5651	
2a	-13.3603	-13.3761	-13.3854	-13.3881	
3a	-3.6057	-3.5707	-3.5559	-3.5520	
4a	-3.1404	-3.2057	-3.2433	-3.2555	
5a	-2.9428	-2.9248	-2.9148	-2.9114	
6a	-2.8485	-2.8574	-2.8649	-2.8642	
1b	2.8724	2.8675	2.8627	2.8643	
$\Sigma_{val}^+$	30.8196	30.8522	30.8832	30.8948	180
$E$	-92.6970	-92.7512	-92.7884	-92.8009	180
Canonical					
1a	15.6741	-15.6533	-15.6420	15.6388	
2a	-11.3286	-11.3316	-11.3367	-11.3387	
3a	1.3381	1.2895	1.2714	1.2673	
4a	0.7627	0.7901	0.8083	0.8144	
5a	0.6162	0.5906	0.5808	0.5782	
6a	0.4941	0.5030	0.5106	0.5130	
1b	0.5480	0.5248	0.5154	0.5131	
$\Sigma_{val}^+$	7.5022	7.3960	7.3730	7.3720	< 90
$\Sigma_{all}^+$	61.5076	61.3658	61.3304	61.3270	< 90

Table 29. The  $1a_1^2 2a_1^2 1e^4 3d_1$  state of BH<sub>3</sub>

	90	100	110	120	$\alpha_e$
ICSCF					
1a <sub>1</sub>	-8.2158	-8.2094	-8.2022	-8.1949	
2a <sub>1</sub>	-1.8189	-1.8080	-1.8004	-1.7953	
1e	-1.5404	-1.5622	-1.5806	-1.5962	
3d <sub>1</sub>	1.3629	1.3459	1.3241	1.2983	
$\Sigma_{val}^+$	-9.7994	-9.8648	-9.9232	-9.9754	120
$E$	-26.2309	-26.2835	-26.3278	-26.3651	120
Canonical					
1a <sub>1</sub>	-7.6331	-7.6284	-7.6245	-7.6209	
2a <sub>1</sub>	-0.7417	-0.7252	-0.7139	-0.7063	
1e	-0.4399	-0.4605	-0.4795	-0.4963	
3d <sub>1</sub>	-0.0023	0.0155	0.0359	0.0591	
$\Sigma_{val}^+$	-3.2430	-3.2924	-3.3458	-3.3978	120
$\Sigma_{all}^+$	-18.5092	-18.5492	-18.5948	-18.6396	120

Yet these small quantitative changes are sufficient so that the ICSCF valence orbital energies correctly predict the molecule to be linear.

Calculations have also been carried out on some AH<sub>3</sub> molecules with less satisfactory results. For these molecules it takes a rather sophisticated ba-

Table 30. The  $1a_1^2 2a_1^2 1e^4 {}^1A_1$  state of  $\text{CH}_3^+$ 

	90	100	110	120	$\alpha_v$
ICSCF					
$1a_1$	-12.3907	-12.3891	-12.3863	-12.3829	
$2a_1$	-2.6436	-2.6308	-2.6210	-2.6135	
$1e$	-2.2384	-2.2630	-2.2838	-2.3015	
$3a_1$	-2.0767	-2.0590	-2.0375	-2.0131	
$\Sigma_{\text{val}} \epsilon$	-14.2408	-14.3136	-14.3772	-14.4330	120
$E$	-39.0221	-39.0916	-39.1499	-39.1989	120
Canonical					
$1a_1$	-11.6892	-11.6867	-11.6849	-11.6833	
$2a_1$	-1.3125	-1.2943	-1.2806	-1.2702	
$1e$	-0.8885	-0.9093	-0.9287	-0.9462	
$3a_1$	-0.3643	-0.3405	-0.3143	-0.2853	
$\Sigma_{\text{val}} \epsilon$	-6.1790	-6.2258	-6.2760	-6.3250	120
$\Sigma_{\text{all}} \epsilon$	-29.5664	-29.5992	-29.6458	-29.6916	120

Table 31. The  $1a_1^2 2a_1^2 1e^4 3a_1 {}^2A_1$  state of  $\text{CH}_3^+$ 

	90	100	110	120	$\alpha_v$
ICSCF					
$1a_1$	-12.1692	-12.1685	-12.1671	-12.1655	
$2a_1$	-2.4545	-2.4391	-2.4271	-2.4179	
$1e$	-2.0467	-2.0718	-2.0937	-2.1134	
$3a_1$	-2.0015	-1.9764	-1.9442	-1.9022	
$\Sigma_{\text{val}} \epsilon$	-15.0973	-15.1418	-15.1732	-15.1916	120
$E$	-39.4355	-39.4787	-39.5074	-39.5227	120
Canonical					
$1a_1$	-11.2286	-11.2233	-11.2186	-11.2146	
$2a_1$	-0.9488	-0.9250	-0.9062	-0.8912	
$1e$	-0.5081	-0.5268	-0.5443	-0.5605	
$3a_1$	-0.4766	-0.4477	-0.4134	-0.3699	
$\Sigma_{\text{val}} \epsilon$	-4.4066	-4.4049	-4.4030	-4.3943	< 90
$\Sigma_{\text{all}} \epsilon$	-26.8638	-26.8515	-26.8402	-26.8235	< 90

set to get the geometry reliably (rather than accidentally) correct at the SCF level. For  $\text{BH}_3$ ,  $\text{CH}_3^+$ ,  $\text{CH}_3$ ,  $\text{OH}_3^+$  and  $\text{NH}_3^+$  the basis set of the quality used here gives the presumably correct planar geometry as judged by other calculations and experimental evidence. But this basis set also gives planar geometry for  $\text{NH}_3$ . With this difficulty in mind, the RHF and ICSCF results can be compared. For



Table 32. The  $1a_1^2 2a_1^2 e^4 3a_1^2 A_1$  state of  $\text{NH}_3^+$ 

	90	100	110	120	$\alpha_r$
ICSCF					
$1a_1$	-17.1841	-17.1846	-17.1832	-17.1801	
$2a_1$	-3.4483	-3.4339	-3.4228	-3.4147	
$1e$	-2.8954	-2.9232	-2.9480	-2.9706	
$3a_1$	-2.8857	-2.8574	-2.8225	-2.7790	
$\Sigma_{val} E$	-21.3642	-21.4180	-21.4601	-21.4908	120
$E$	-55.7320	-55.7871	-55.8262	-55.8511	120
Canonical					
$1a_1$	-16.0118	-16.0048	-15.9971	-15.9875	
$2a_1$	-1.5793	-1.5559	-1.5361	-1.5189	
$1e$	-1.0044	-1.0218	-1.0375	-1.0511	
$3a_1$	-1.0248	-0.9935	-0.9581	-0.9158	
$\Sigma_{val} E$	-8.2010	-8.1925	-8.1803	-8.1581	< 90
$\Sigma_{all} E$	-40.2246	-40.2021	-40.1745	-40.1331	< 90

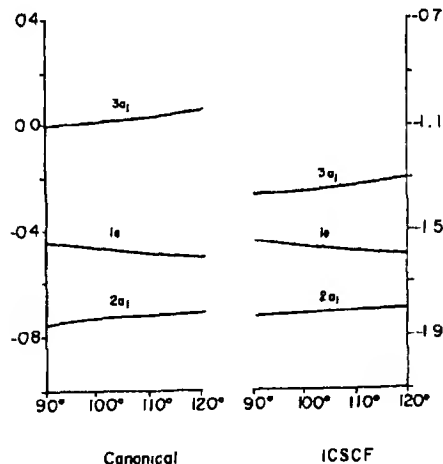
Table 33. The  $1a_1^2 2a_1^2 e^4 3a_1^2 A_1$  state of  $\text{NH}_3$ 

	90	100	110	120	$\alpha_r$
ICSCF					
$1a_1$	-16.9616	-16.9608	-16.9582	-16.9542	
$2a_1$	-3.2370	-3.2174	-3.1991	-3.1804	
$1e$	-2.6772	-2.7036	-2.7265	-2.7462	
$3a_1$	-2.4978	-2.4819	-2.4661	-2.4526	
$\Sigma_{val} E$	-22.1784	-22.2110	-22.2364	-22.2508	120
$E$	-56.1014	-56.1346	-56.1527	-56.1589	120
Canonical					
$1a_1$	-15.5449	-15.5356	-15.5247	-15.5122	
$2a_1$	-1.1917	-1.1624	-1.1340	-1.1047	
$1e$	-0.5929	-0.6084	-0.6212	-0.6308	
$3a_1$	-0.4444	-0.4213	-0.3991	-0.3794	
$\Sigma_{val} E$	-5.6438	-5.6010	-5.5510	-5.4914	< 90
$\Sigma_{all} E$	-36.7336	-36.6722	-36.6004	-36.5158	< 90

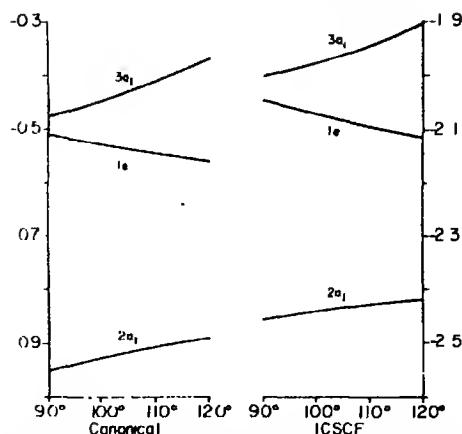
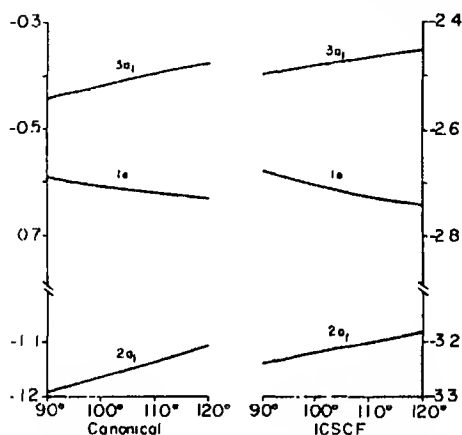
all these molecules the ICSCF valence orbital energy sum predicted a planar geometry in agreement with  $E_{\text{SCF}}$ . But the slope of  $e_{1r}$  is large enough to make this sum continue to predict a planar geometry even for better basis sets for  $\text{NH}_3$ . The sum of the RHF valence energies is still worse, however, since it would predict that  $\text{CH}_3$ ,  $\text{NH}_3^+$ ,  $\text{NH}_3$ , and  $\text{OH}_3^+$  were all bent to a HAH angle of less

Table 34. The  $1a_1^2 2a_1^2 e^4 3a_1^2 A_1$  state of  $H_3O^+$ 

	90	100	110	120	$\alpha_e$
ICSCF					
$1a_1$	-22.7984	-22.7965	-22.7922	-22.7860	
$2a_1$	-4.4104	-4.3933	-4.3773	-4.3615	
$1e$	-3.6841	-3.7126	-3.7375	-3.7593	
$3a_1$	-3.5233	-3.5057	-3.4887	-3.4735	
$\Sigma_{val} \epsilon$	-30.6038	-30.6484	-30.6820	-30.7072	120
$E$	-76.2004	-76.2411	-76.2663	-76.2793	120
Canonical					
$1a_1$	-21.0404	-21.0254	-21.0084	-20.9894	
$2a_1$	-1.8963	-1.8657	-1.8356	-1.8049	
$1e$	-1.1422	-1.1537	-1.1628	-1.1692	
$3a_1$	-1.0246	-0.9986	-0.9738	-0.9511	
$\Sigma_{val} \epsilon$	-10.4106	-10.3434	-10.2700	-10.1888	< 90
$\Sigma_{all} \epsilon$	-52.4915	-52.3942	-52.2868	-52.1676	< 90

Fig. 27. Orbital energies for the  $1a_1^2 2a_1^2 e^4 A_1$  state of  $BH_3$ 

than  $90^\circ$ . The orbital energy versus bond angle diagrams (Fig. 27-29) for all these molecules for both the canonical and ICSCF results are similar to those predicted by Walsh and previously reported [7].

Fig. 28. Orbital energies for the  $1a_1^2 2a_1^2 1e^4 3a_1^{-2} A_1$  state of  $CH_4$ .Fig. 29. Orbital energies for the  $1a_1^2 2a_1^2 1e^4 3a_1^{-1} A_1$  state of  $NH_3$ .

*Acknowledgement.* The authors wish to acknowledge the financial support of the National Science Foundation.

## References

1. Mulliken, R. S.: *Rev. Mod. Phys.* **14**, 204 (1942)
2. Walsh, A. D.: *J. Chem. Soc. (London)* **2260**, 1953
3. Peyerimhoff, S. D., Buenker, R. J.: To be published. The authors wish to thank Dr. Peyerimhoff for providing us with an advance copy of this manuscript
4. Allen, L. C.: *Theoret. Chim. Acta (Berl.)* **24**, 117 (1972)
5. Coulson, C. A., Neilson, A. H.: *Discussions Faraday Soc.* **35**, 71 (1963)
6. Buenker, R. J., Peyerimhoff, S. D.: *J. Chem. Phys.* **45**, 3682 (1966)
7. Peyerimhoff, S. D., Buenker, R. J., Allen, L. C.: *J. Chem. Phys.* **45**, 734 (1966)
8. Moskowitz, J. W., Harrison, M. C.: *J. Chem. Phys.* **43**, 3550 (1965)
9. Davidson, E. R.: *J. Chem. Phys.* **57**, 1999 (1972)
10. Whitten, J. L.: *J. Chem. Phys.* **44**, 359 (1966)
11. Krauss, M.: *J. Res. Nat. Bur. Std.* **68 A**, 635 (1964)

Prof. Dr. E. R. Davidson, —chemistry Department BG-10  
University of Washington, Seattle, Washington 98195, USA

## *Ab-initio* Calculations on Small Hydrides Including Electron Correlation

### XI. Equilibrium Geometries and Other Properties of $\text{CH}_3$ , $\text{CH}_3^+$ , and $\text{CH}_3^-$ , and Inversion Barrier of $\text{CH}_3^-$

Frank Driessler, Reinhart Ahlrichs, Volker Staemmler, Werner Kutzelnigg

Institut für Physikalische Chemie und Elektrochemie der Universität Karlsruhe

Received April 3, 1973

The ground state energies of  $\text{CH}_3^+$ ,  $\text{CH}_3$ , and  $\text{CH}_3^-$  are calculated both in the SCF (near Hartree-Fock) approximation and in the 11:PA-PNO scheme including correlation energy. Due to a more appropriate choice of the basis, our SCF-values for  $\text{CH}_3^-$  are substantially better than previously published ones. Both  $\text{CH}_3^+$  and  $\text{CH}_3$  are planar whereas the equilibrium bond angles in  $\text{CH}_3^-$  are nearly tetrahedral. The inversion barrier of  $\text{CH}_3^-$  is  $\sim 2$  kcal/mol. The force constants of the out-of-plane bending modes are changed by correlation in the case of  $\text{CH}_3$  from 0.03–1.8 mdyn/Å. The localized MO's that correspond to the C-H-bonds are "bent" in the non-equilibrium geometries. The dependence of the different pair correlation contributions on the angle  $\gamma$  that describes out-of-plane deformation is analyzed. The electron affinity of  $\text{CH}_3$  is  $\sim 0.3$  eV. Finally the Pariser-Parr disproportionation reaction is analyzed in the light of the present results. Changes in correlation energy for this reaction amount to less than 1 eV.

**Key words:** Correlation energy · Negative ions · Inversion barrier · Hyperfine coupling constants · Electron affinity

#### 1. Introduction

Many SCF calculations on  $\text{CH}_3^+$ ,  $\text{CH}_3$ , and  $\text{CH}_3^-$  have been published so far (for an up-to-date review see [1]), the most refined ones being those of Millie and Berthier [2] and the recent ones [5, 6] of a series of calculations [3–6] by Kari and Csizmadia. To our knowledge quantum chemical treatments of these molecules that take electron correlation into account are virtually non-existing, only a CI calculation of  $\text{CH}_3^-$  that accounts for about 45% of the estimated correlation energy has to be mentioned [5].

The main concern of the present paper is a study of the correlation energy in  $\text{CH}_3^+$ ,  $\text{CH}_3$ , and  $\text{CH}_3^-$  and its influence on the properties of these molecules. We also found, however, that the previous SCF calculations on  $\text{CH}_3^-$  (not  $\text{CH}_3^+$  and  $\text{CH}_3$ ) were performed with inappropriate basis sets. With an improved basis set one not only gets a lower total SCF-energy, but also quite a different inversion barrier.

It is generally accepted that  $\text{CH}_3^+$  has a planar equilibrium structure with  $D_{3h}$  symmetry, but less definite information has been obtained so far concerning the equilibrium structures of  $\text{CH}_3$  and  $\text{CH}_3^-$ . By analogy with the isoelectronic species  $\text{NH}_3$  one should expect a  $C_{3v}$  structure for  $\text{CH}_3^-$  and an inversion barrier of the same order of magnitude, i. e. of a few kcal/mol.

## 2. The Method

The method used, abbreviated as IEPA-PNO, is the same as in the recent papers in this series (see e. g. [7, 8]). We start from a molecular Hartree-Fock calculation with a basis of gaussian lobes, the doubly occupied orbitals are then transformed to localized ones. For each doubly occupied localized orbital the intrapair correlation energy  $\epsilon_i$  and for each pair of orbitals the interpair correlation energy  $\epsilon_{ij}$  (a sum of the singlet and triplet contributions  $^1\epsilon_{ij}$  and  $^3\epsilon_{ij}$ ) is calculated "in the field of the other electrons". The total correlation energy is approximated as the sum of the different pair contributions. For open shell states like  $\text{CH}_3$  the situation is somewhat more complicated, since also correlation contributions involving the singly occupied orbitals have to be included. For details and the general theory the reader is referred to Ref. [9].

## 3. The Gaussian Basis

For carbon we started from the 10s/6p basis of Huzinaga [10] in the contraction [5,1,1,1,1,1] for *s* and [3,1,1,1] for *p* and augmented this basis by a set of *p*-functions<sup>1</sup> with the small exponential factor  $\eta = 0.021$  and a set of *d*-functions with  $\eta = 0.65771$ . The  $\eta$ -value of the additional *p*-functions is the result of an energy minimization, whereas variation of the  $\eta$  of the *d*-functions between 0.5 and 1.0 did not affect the energy much, so for convenience the  $\eta$ -value of the most important *p*-function was used for the *d*-functions as well. For hydrogen the 5s-1-Huzinaga basis in the contraction [3,1,1] was augmented by a *p*-set with  $\eta = 0.65$ .

For the calculation of the correlation energy a second incomplete *d*-set ( $d_{xz}, d_{yz}, d_{z^2}$ ) on carbon was included with  $\eta = 0.2$ , this  $\eta$ -value was the result of an optimization of the intrapair correlation energy of the lone pair in  $\text{CH}_3^-$ . In test calculations the effect of a 8<sup>th</sup> *p*-set with  $\eta = 0.005$  was found to improve the energy by only 0.0002 a.u., so it was not included, although it had a coefficient of  $\sim 0.075$  in the  $1a_2''$  MO.

Our basis set differs from those of previous large calculations [2, 5, 6] mainly in the presence of as many as 5 sets of *p* groups one of which is very "diffuse" ( $\eta = 0.021$ ). Kari et Csizmadia [5] used 2 sets of *p* groups, Millie and Berthier [2] 4 sets. It ought to be obvious that for a negative ion diffuse basis functions have to be included. Taking into account that in planar  $\text{CH}_3^-$  the orbital energy of the highest ( $1a_2''$ ) MO is  $\epsilon = -0.0065$  the appropriate STO for describing its tail behaviour should be [11]  $re^{-\alpha r} \cos \delta$  with  $\alpha = \sqrt{-2\epsilon} \approx 0.12$ , such an STO has its maximum radial charge density for  $r = \frac{n}{\alpha} \approx 16a_0$ . A gaussian with the maximum

at the same distance has  $\eta = \frac{n}{2r^2} = -\frac{\epsilon}{n} \approx 0.003$ . This estimate is, of course, somewhat crude but indicates that unusually small  $\eta$ -values have to be included for negative ions that have orbital energies close to the ionization limit.

<sup>1</sup> *p*- and *d*-functions were constructed from lobes.

#### 4. Discussion of the SCF Results

We calculated the SCF energy of  $\text{CH}_3^-$  for the planar and different pyramidal configurations (characterized by the angle  $\gamma$  which indicates the simultaneous out-of-plane deformation of the three CH-bonds with respect to a plane perpendicular to the threefold axis) and optimized the CH distance for each value of  $\gamma$ . These equilibrium distances  $r_e$  are given in Table 1 together with the orbital energies and the total SCF energy. For  $\gamma=0$  we find  $r_e=2.033 a_0 \cong 1.075 \text{ \AA}$ , for  $\gamma=18.5^\circ$  (which corresponds to  $\text{HCH}$  angles of  $110.4^\circ$ ) we find  $r_e=2.069 a_0 \cong 1.095 \text{ \AA}$ . This increase in bond length agrees with the picture that in the planar configuration carbon is  $sp^2$ - and in the tetrahedral configuration  $sp^3$ -hybridized. The lowest energy of  $\text{CH}_3^-$  is obtained for  $\gamma=18.5^\circ$ , and i.e. for practically tetrahedral bond angles. Our SCF energy of  $-39.51995 \text{ a.u.}$  is substantially lower than the claimed "near-Hartree-Fock energy" ( $-39.51292 \text{ a.u.}$  for  $\gamma=23.5^\circ$  and  $r=2.090 a_0$ ) of Ref. [5] or the very similar value ( $-39.5125 \text{ a.u.}$  for  $\gamma=22^\circ$  and  $r_e=2.040 a_0$ ) of Ref. [2]. That the previous results for  $\text{CH}_3^-$  were unsatisfactory could have been concluded from the orbital energy. In the planar configuration the orbital energy of the lone pair was found positive both in Ref. [5] and [2], whereas we obtain a negative orbital energy<sup>2</sup>.

The omission of a set of "diffuse"  $p$ -AO's is more serious for the planar configuration than for the equilibrium geometry of  $\text{CH}_3^-$  (where even the previous calculations gave negative orbital energies for the lone pair), so with a poor basis one gets a spurious destabilization of the planar configuration and too high an inversion barrier. We are therefore confident that our SCF-value of  $2.0 \text{ kcal/mol}$  for the inversion barrier of  $\text{CH}_3^-$  is more reliable than the previous values of  $5.2$  [2] or  $5.46$  [5] kcal/mol.

Table 1. CH-distances  $r_e$  (in  $a_0$ ), orbital energies and SCF energy of  $\text{CH}_3^-$  and SCF energies of  $\text{CH}_3^-$  and  $\text{CH}_3^-$  as functions of the out-of-plane deformation angle  $\gamma$

$\gamma$	$r_e$	$\text{CH}_3^-$					$\text{CH}_3^-$	
		$D_{3h}$	$1a_1'$	$2a_1'$	$e'$	$1a_2''$	$E_{\text{SCF}}$	$E_{\text{SCF}}$
		$C_{3v}$	$1a_1$	$2a_1$	$e$	$3a_1$		
$0^\circ$	2.033		-10.9642	-0.6466	-0.3196	-0.0065	-39.51675	-39.57055
$5^\circ$	2.037		-10.9626	-0.6449	-0.3161	-0.0075	-39.51719	-39.57051
$10^\circ$	2.044		-10.9573	-0.6413	-0.3069	-0.0107	-39.51841	-39.56965
$20^\circ$	2.075		-10.9431	-0.6306	-0.2745	-0.0245	-39.51987	-39.55995
$30^\circ$	2.115		-10.9336	-0.6266	-0.2351	-0.0492	-39.51293	-39.51973
$40^\circ$	2.163		-10.9356	-0.6356	-0.1963	-0.0843	-39.48716	

<sup>2</sup> In fact, (discrete) positive eigenvalues for occupied orbitals of the Hartree-Fock operator of a singly negative ion are perfectly meaningless and can only be an artefact of the chosen basis, irrespective of whether or not the considered state is physically bound. For such ions the potential  $V(r)$  in the Fock operator fulfils the condition

$$\lim_{r \rightarrow \infty} |r|^{1/2} V(r) = 0$$

and this condition is, as Kato [24] has shown, sufficient for the existence of only negative discrete eigenvalues. Positive eigenvalues are hence only possible in a truncated matrix representation and can always be reduced to zero (for continuum states) or below zero (for bound states) by extension of the basis.

Table 2 Coefficient of  $r_e^2\gamma^2$  and  $r_e^4\gamma^4$  in the expansion of  $E(\gamma)$  for  $\text{CH}_3^+$ ,  $\text{CH}_3$ ,  $\text{CH}_3^-$  with and without correlation (values in a.u.)

Molecule	SCF		With correlation	
	$c(r_e^2\gamma^2)$	$c(r_e^4\gamma^4)$	$c(r_e^2\gamma^2)$	$c(r_e^4\gamma^4)$
$\text{CH}_3^+$	0.1021	-0.0019	0.0930	-0.0046
$\text{CH}_3$	0.0026	0.0336	0.0171	0.0158
$\text{CH}_3^-$	-0.0141	0.0167	-0.0127	0.0172

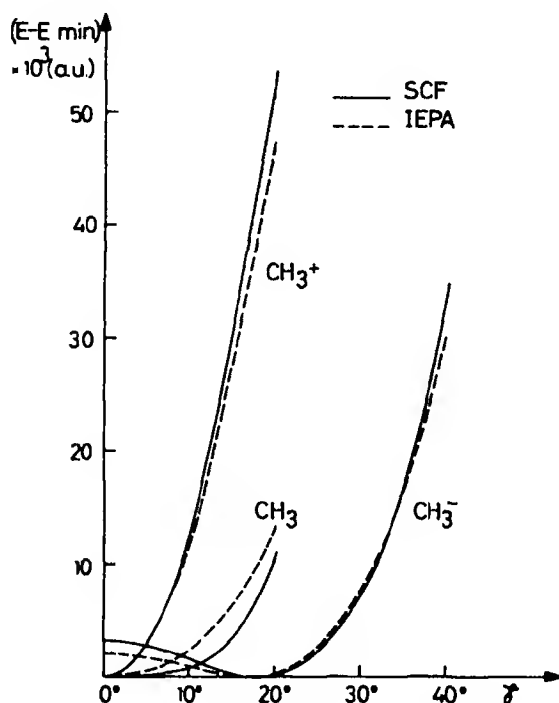


Fig. 1

We performed the SCF calculations for  $\text{CH}_3$  and  $\text{CH}_3^+$  as functions of  $\gamma$  for those CH-distances  $r_e$  that were optimum for  $\text{CH}_3^-$ . A new optimization of  $r_e$  would not have changed the energy appreciably and was not regarded as worthwhile since the absolute minimum of the energy was found for the planar structure both for  $\text{CH}_3$  and  $\text{CH}_3^+$ . We have then optimized the CH-distance only for  $\gamma = 0^\circ$  and found  $r_e = 2.026 a_0$  for  $\text{CH}_3$  and  $r_e = 2.044 a_0$  for  $\text{CH}_3^+$  (compared to  $2.033 a_0$  for  $\text{CH}_3^-$ ).

Our SCF energies  $-39.57055$  a.u. ( $r_e = 2.026 a_0$ ) and  $-39.24471$  a.u. ( $r_e = 2.044 a_0$ ) for  $\text{CH}_3$  and  $\text{CH}_3^+$  respectively may be compared with  $-39.57148$  a.u. ( $r = 2.040 a_0$ ) and  $-39.24592$  a.u. ( $r = 2.040 a_0$ ) of Ref. [2] and  $-39.57028$  a.u. ( $r = 2.038$ ) and  $-39.24216$  a.u. ( $r = 2.038 a_0$ ) of Ref. [5, 6]. The slightly lower

values of Ref. [2] for  $\text{CH}_3$  and  $\text{CH}_3^+$  (not  $\text{CH}_3^-$ ) are due to the use of two  $d$ -sets on carbon in Ref. [2].

In Table 2 the coefficients of  $r_e^2\gamma^2$  and  $r_e^4\gamma^4$  in the expansion of the energy are given. This table confirms what one concludes pictorially from Fig. 1, namely that in SCF-approximation  $\text{CH}_3^+$  has a "normal" parabolic dependence on  $\gamma$ , whereas the minimum for  $\text{CH}_3$  is extremely flat and practically of the fourth order in  $\gamma$ . The harmonic force constant of  $\text{CH}_3$  almost vanishes. In  $\text{CH}_3^-$ , finally, the coefficient of the  $\gamma^2$  term is negative and the pyramidal configuration is more stable.

### 5. The Localized Orbitals in $\text{CH}_3^+$ , $\text{CH}_3$ , and $\text{CH}_3^-$

We transformed the doubly occupied orbitals of all the molecules to localized ones according to the criterion of Boys [12]. Each localized orbital can be characterized by the distance  $d$  of its centroid to the carbon atom and by the angle  $\alpha$  that the line connecting the centroid and the atoms forms with a plane perpendicular to the threefold axis. For the localized orbitals corresponding to CH bonds  $d$  and  $\alpha$  and for the lone orbital just  $d$  are given in Table 3 as functions of the bond angle  $\gamma$ .

The angles  $\alpha$  do not coincide exactly with the bond angles  $\gamma$ . One may interpret these deviations by saying that the Boys-localized orbitals represent bent bonds. Even if one admits that this may be an artefact of the Boys criterion (which keeps the centroids as far from each other as possible) one realizes that in  $\text{CH}_3^+$  and  $\text{CH}_3$  the angles  $\alpha$  are always smaller than the respective  $\gamma$ 's (the molecules want to keep  $sp^2$  hybridized carbon and planar structure), but that  $\alpha$  is larger than  $\gamma$  for  $\text{CH}_3^-$  (the carbon wants to have  $sp^3$  hybridization and tetrahedral arrangement). It is interesting to note that at equilibrium geometry the angles  $\alpha$  and  $\gamma$  almost coincide for any of the three molecules. A similar result, though in a slightly different context was found by Klessinger [25] for  $\text{H}_2\text{O}$ . The fact that the localized orbitals do not point towards the H-atoms causes some troubles for  $\text{CH}_3^-$  in the planar or near-planar configuration. For  $\gamma=0$  we obtain  $\alpha=0$  by the Boys-procedure (unlike to what one finds for  $\text{OH}_3^+$  [13]), but the transition from

Table 3. Direction ( $\alpha$ ) and distance ( $d$  in  $a_0$ ) of the centroids of the localized orbitals referred to the C-atom, for different out-of-plane angles  $\gamma$

$\gamma$	$\alpha(\text{CH})$			$d(\text{CH})$			$d(\text{lone orbital, pair})$	
	$\text{CH}_3^+$	$\text{CH}_3$	$\text{CH}_3^-$	$\text{CH}_3^+$	$\text{CH}_3$	$\text{CH}_3$	$\text{CH}_3$	$\text{CH}_3$
0°	0°	0°	0°	1.28	1.38	1.42		0.00
2°			5°			1.42		0.29
5°		4°20'	9°		1.38	1.41	0.18	0.49
10°	7°10'	8°30'	13°50'	1.28	1.39	1.43	0.33	0.66
20°	14°	16°30'	21°40'	1.28	1.40	1.47	0.52	0.84
30°			29°			1.47		0.91
40°			36°20'			1.54		0.88



$\gamma \neq 0$  to  $\gamma = 0$  does not seem to be continuous. This has an unpleasant consequence for the calculation of the correlation energy as a function of  $\gamma$  in  $\text{CH}_3^-$  (but not in  $\text{CH}_3^+$  and  $\text{CH}_3$ ).

## 6. The Correlation Energy and Its Effects

The correlation contributions and their sums are collected in Table 4.

A comparison of the intrapair correlation energy  $\epsilon_{bb}$  of a CH-bond and the interpair correlation energy  $\epsilon_{bb'}$  between two CH-bonds in the series  $\text{CH}_3^+$ ,  $\text{CH}_3$ , and  $\text{CH}_3^-$  shows nicely the effect of the different "availability" of the  $p_z$ -AO of carbon for correlation. In  $\text{CH}_3^+$  where this AO is "fully available"  $|\epsilon_{bb}|$  and  $|\epsilon_{bb'}|$  are larger than in  $\text{CH}_3$  and in  $\text{CH}_3^-$ . Both  $|\epsilon_{bb}|$  and  $|\epsilon_{bb'}|$  increase with  $\gamma$ , for  $|\epsilon_{bb'}|$  this increase is due to the fact that in the pyramidal structure the CH-bonds get closer to each other.

The total correlation energy for  $\text{CH}_3^+$  (to which only  $\epsilon_{bb}$  and  $\epsilon_{bb'}$  contribute) increases therefore in absolute value with  $\gamma$ , it lowers the energy more for large than for small  $\gamma$ , i.e. it makes the potential curve of Fig. 1 somewhat flatter. Inclusion of correlation reduces the out-of-plane force constant of  $\text{CH}_3^+$  somewhat (see Table 5). A similar effect has been found for the isoelectronic molecule  $\text{BH}_3$  [8].

In neutral  $\text{CH}_3$  the contributions to the correlation energy that involve the singly occupied "lone" orbital ( $\epsilon_{bn}$ ) decrease in absolute value with increasing  $\gamma$ . This decrease overcompensates the increase of  $|\epsilon_{bb}|$  and  $|\epsilon_{bb'}|$ , so that the  $|E_{\text{corr}}|$  of  $\text{CH}_3$  decreases with  $\gamma$ . The decrease of  $|\epsilon_{bn}|$  with  $\gamma$  is understandable because the more the molecule is bent the more is the lone orbital localized and distant from the CH-bonds.

In  $\text{CH}_3^-$  inclusion of correlation makes the potential curve of Fig. 1 somewhat steeper (unlike in  $\text{CH}_3^+$ ). The harmonic out-of-plane force constant of  $\text{CH}_3^-$  which was only 0.034 mdyne/Å in the SCF approximation becomes 0.175 mdyne/Å when correlation is taken into account. Experimental values of 0.159 mdyne/Å (gaseous  $\text{CH}_3^-$  [18]) and 0.253 mdyne/Å (in argon matrix [14]) have been reported, neither of which is "harmonic", i.e. corrected for unharmonicity effects. Our computed force constant should rather be compared to the first value. In view of the experimental difficulties and the (computed) high anharmonicity of the potential one cannot say whether either the experimental or the theoretical value is most reliable. Millié and Berthier [2] have already pointed out that the computed value of this force constant is highly sensitive to changes in the basis, they found 0.175 mdyne/Å in an SCF calculation without polarization functions ( $d$  on C and  $p$  on H) and 0.014 when they include polarization functions. Inclusion of polarization functions and of correlation have an opposite effect on this force constant.

As to the correlation energy of  $\text{CH}_3^-$  and its dependence on the out-of-plane angle  $\gamma$  the situation is somewhat less straightforward. The sum of the intra- and inter-pair contributions of the CH-bonds is very close to the respective one for  $\text{CH}_3$ , except for  $\gamma = 0^\circ$  where (as we already mentioned in Section 5) the result of the Boys-localization seems to depend discontinuously on  $\gamma$ . Similarly the intrapair correlation energy  $\epsilon_{nn}$  of the lone pair decreases in absolute value with decreasing angle, but jumps when coming to  $\gamma = 0^\circ$ . We have therefore decided to extrapolate the values for  $\gamma \geq 10^\circ$  to  $\gamma = 0^\circ$  and to take the extrapolated

Table 4. Correlation energy contributions and their sums for  $\text{CH}_3^+$ ,  $\text{CH}_3$ ,  $\text{CH}_3^-$  as function of the out-of-plane  $\gamma$

$\text{CH}_3^+$				
	0°/2.033	10°/2.044	20°/2.075	
$-E_{bb}$	0.03238	0.03254	0.03316	
$-^1E_{bb'}$	0.00739	0.00750	0.00786	
$-^3E_{bb'}$	0.00966	0.00979	0.01024	
$E_{\text{corr}}$	0.14829	0.14949	0.15378	

$\text{CH}_3$				
	0°/2.033	5°/2.037	10°/2.044	20°/2.075
$-E_{bb}$	0.02964	0.02966	0.02973	0.02995
$-^1E_{bb'}$	0.00531	0.00534	0.00543	0.00575
$-^3E_{bb'}$	0.00886	0.00889	0.00900	0.00945
Sum of CH-bond contributions	0.13143	0.13167	0.13248	0.13545
$-^1E_{bn}$	0.00890	0.00875	0.00836	0.00752
$-^3E_{bn}$	0.00861	0.00851	0.00830	0.00776
Sum of CH-bond-lone electron interaction	0.05256	0.05178	0.04998	0.04584
$E_{\text{corr}}$	0.18399	0.18345	0.18246	0.18129

$\text{CH}_3^-$							
	(calc.)		(extrap.)	(calc.)			
	[0°/2.033]	[5°/2.037] <sup>a</sup>	0°/2.033	10°/2.044	20°/2.075	30°/2.115	40°/2.163
$-E_{bb}$	0.02916	0.02915		0.02930	0.02969	0.02989	0.02978
$-^1E_{bb'}$	0.00517	0.00559		0.00582	0.00604	0.00634	0.00707
$-^3E_{bb'}$	0.00854	0.00912		0.00951	0.01014	0.01085	0.01198
Sum of CH-bond contributions	0.12861	0.13158	0.1328	0.13389	0.13761	0.14124	0.14649
$-^1E_{bn}$	0.01183	0.01093		0.01037	0.00957	0.00909	0.00898
$-^3E_{bn}$	0.01727	0.01620		0.01575	0.01491	0.01394	0.01327
Sum of C'H-bond-lone pair interaction	0.08730	0.08139	0.0806	0.07836	0.07344	0.06909	0.06675
$-E_{nn}$	0.02850	0.02640	0.0264	0.02711	0.02764	0.02786	0.02812
$E_{\text{corr}}$	0.24441	0.23937	0.2398	0.23936	0.23869	0.23819	0.24136

<sup>a</sup> Due to the localization discontinuity (see Section 6) even the values for 5°/2.037 are unreliable.

correlation energy as reference for the discussion of the  $\gamma$ -dependence of  $E_{\text{corr}}$  in  $\text{CH}_3^-$ . With this correction we get the potential curves in Fig. 1 and the force constants in Table 5. The extrapolation procedure is not very accurate and may be in error by as much as 1 kcal/mol. We therefore do not put much stress on the change of the inversion barrier from 2 kcal/mol in SCF approximation to

Table 5. Force constants (in mdyn/Å) for the out-of-plane bending vibration

	$\text{CH}_3^+$	$\text{CH}_3$	$\text{CH}_3^-$
SCF	1.06	0.034	0.265
With correlation	0.96	0.175	0.235
exp.		0.159 [18] 0.253 [14]	---

1.5 kcal/mol with correlation. We rather think that for  $\text{CH}_3^-$  the total correlation is — within the limits of the method — invariant with respect to changes of  $\gamma$ , and that, therefore, the SCF value for the barrier is a good approximation to the true one. This statement cannot be checked for  $\text{CH}_3$ , because an experimental barrier is not known, but the analogous claim for the isoelectronic  $\text{NH}_3$  [15] is generally accepted.

The extrapolation problem is irrelevant for the  $\text{CH}_3^-$  near its equilibrium geometry. Inclusion of correlation changes the optimum  $\gamma$  slightly to  $18^\circ$  (corresponding to a HCH angle of  $111^\circ$ ) where the total energy is  $-39.7588$  a.u.

From the experience with similar basis sets for comparable molecules we can assume that we have accounted for about 90% of the valence shell correlation energy. By extrapolating to 100% and adding the estimates (0.057 in  $\text{CH}_3^+$ , 0.059 in  $\text{CH}_3$ , 0.061 in  $\text{CH}_3^-$ )<sup>3</sup> for the contributions involving the *K*-shell of carbon we get the following estimated (absolute values of the) correlation energies in the equilibrium geometries:

$$\text{CH}_3^+ 0.220 \text{ a.u.}, \quad \text{CH}_3 0.262 \text{ a.u.}, \quad \text{CH}_3^- 0.325 \text{ a.u.}$$

### 7. Binding Energy, Ionization Potential and Electron Affinity of $\text{CH}_3$

The computed total energy of  $\text{CH}_3$  is  $-39.7545$  a.u. If we subtract the energy of the carbon ground state ( $^3P$ ) calculated with a comparable basis [16] of  $-37.7783$  a.u. and of three H-atoms ( $3 \times 0.49986 = 1.49958$ ) we get the binding energy

$$\Delta E_e = -0.4767 \text{ a.u.} \approx 300 \text{ kcal/mol.}$$

If we correct for the zero-point energy of  $-6000 \text{ cm}^{-1} \approx 17 \text{ kcal/mol}$  we get  $\Delta E \approx 283 \text{ kcal/mol}$  which may be compared with the "recommended" experimental binding energy of  $\text{CH}_3$  of  $291 \text{ kcal/mol}$  [17].

The difference of the total energies (including correlation) of  $\text{CH}_3$  ( $-39.7545$  a.u.) and  $\text{CH}_3^+$  ( $-39.3930$  a.u.), namely  $0.3615$  a.u.  $\approx 9.83$  eV gives us the vertical ionization potential. In SCF approximation we find  $8.86$  eV, whereas the experimental ionization potential is  $9.84$  eV [18] in agreement with the calculated value including correlation. The Koopmans theorem gives  $10.3$  eV.

We obtain the (adiabatic) electron affinity *A* of  $\text{CH}_3$  as the difference between the total energies of  $\text{CH}_3$  ( $-39.7545$  a.u.) and  $\text{CH}_3^-$  ( $-39.7586$  a.u.). While in SCF

<sup>3</sup> 0.045 for  $\epsilon_{KK}$  and 0.004 for any  $\epsilon_{KL}$ .

approximation  $\text{CH}_3^-$  is not stable with respect to  $\text{CH}_3$  ( $A = -1.38$  eV) our calculation that include correlation gives  $A = 0.11$  eV for the adiabatic electron affinity. If we use the estimated correlation energies given at the end of Section 5 rather than the computed ones we get  $A = 0.33$  eV<sup>4</sup>. So we conclude that the correct electron affinity of  $\text{CH}_3$  is  $0.3 \pm 0.1$  eV. We think that this value is more reliable than the experimental one of 1.1 eV [19]. The experiment on which it is based (magnetron techniques) is so complicated and so subject to errors that it may easily be wrong by 1 eV or more.

### 8. The Pariser-Parr "Disproportionation Reaction" and the Correlation Energy of a Doubly Occupied $\pi$ -AO

In the semiempirical  $\pi$ -electron theory the so-called Pariser-Parr disproportionation reaction [20] played a central role. Let us formulate it for  $\text{CH}_3$  rather than for C in the  $\text{tr}^3\pi$  valence state. The exact reaction energy of the hypothetical reaction



(keeping all three molecules in the same, planar geometry) is, of course, equal to the difference between vertical ionization potential  $I$  and electron affinity  $A$  of  $\text{CH}_3$  (the vertical and adiabatic  $A$  of  $\text{CH}_3$  differ by only 2 kcal/mol  $\sim 0.1$  eV, namely by the inversion barrier). We have therefore

$$\Delta E = I - A_{\text{ad}} = 9.8 \text{ eV} - 0.2 \text{ eV} = 9.6 \text{ eV}.$$

In the Hartree-Fock approximation one gets

$$\Delta E_{\text{HF}} = I_{\text{HF}} - A_{\text{ad, HF}} = 8.9 \text{ eV} + 1.4 = 10.3 \text{ eV}.$$

The correlation contribution to this disproportionation is hence roughly 0.7 eV.

Let us now assume tentatively that the occupied MO's in  $\text{CH}_3^+$ ,  $\text{CH}_3$ , and  $\text{CH}_3^-$  are the same and equal to the correct ones for  $\text{CH}_3$ . We have calculated the energies of both  $\text{CH}_3^+$  and  $\text{CH}_3^-$  in the planar configuration with the MO's of  $\text{CH}_3$ . The "non-relaxed" Hartree-Fock energies of  $\text{CH}_3^+$  and  $\text{CH}_3^-$  are respectively 1.3 and 2.7 eV. above the correct Hartree-Fock energies, which leads to

$$\Delta E_{\text{nonrelaxed}} = I_{\text{n.r.}} - A_{\text{n.r.}} = 10.2 \text{ eV} + 4.1 \text{ eV} = 14.3 \text{ eV}.$$

On the other hand this "reaction energy" of 14.3 eV is equal to the self-repulsive energy

$$(\pi\pi|\pi\pi) = 14.3 \text{ eV}$$

of the lone  $\pi$ -orbital in  $\text{CH}_3^-$ . The crudest possible approach to  $\Delta E$  would consist in approximating this  $\pi$ -MO by a simple STO according to Slater's rules. It is well known [20] that one then gets  $\sim 17$  eV for  $(\pi\pi|\pi\pi)$  and hence for  $\Delta E$ . In analyzing the different contributions that reduce  $\Delta E$  from  $\sim 17$  to eventually  $\sim 10$  eV (for a discussion of previous work on this topic see [21]) one realizes that a reduction by  $\sim 3$  eV is achieved if one replaces the  $2p_z$ -STO by the Hartree-

<sup>4</sup> The analogous correction would only have a small influence on  $\Delta E$ , ( $= 287$  kcal/mol) and  $I$  (10.0 eV).

Fock AO of  $\text{CH}_3$ . An additional reduction by 4 eV is obtained if one allows for a relaxation of the orbitals from  $\text{CH}_3$  to the ions, mainly for a change of the  $\pi$ -AO from  $\text{CH}_3$  to  $\text{CH}_3^-$ . The final decrease by 0.7 eV due to inclusion of correlation is almost negligible. This is in strong contrast to Pariser and Parr's original hypothesis that the reduction of the  $(\pi\pi|\pi\pi)$  integral from  $\sim 17$  to  $\sim 10$  eV is mainly a correlation effect.

Nevertheless we also like to know which pair correlation energies are responsible for these  $\sim 0.7$  eV of change in correlation energy. We first note that the only new term in  $\text{CH}_3^+ + \text{CH}_3^-$  compared to  $2\text{CH}_3$  is the intrapair correlation energy of the lone  $(\pi)$ -pair  $\varepsilon_{nn}$  in  $\text{CH}_3^-$ . This was calculated to be  $\sim 0.026$  a.u.  $\cong 0.7$  eV, so it is actually equal to the difference in correlation energy. A more careful analysis shows, however, that the other contributions (which are present for all three or two of the species) change as well and that it is rather accidental that the change in correlation energy equals one particular (new) pair contribution.

### 9. Spin Densities and Hyperfine Coupling Constants in $\text{CH}_3$

$\text{CH}_3$  is the simplest  $\pi$ -radical and has as such vanishing spin density in restricted-Hartree-Fock approximation both at the C and the H nuclei. A wavefunction like ours that accounts for the intergroup correlation between the lone orbital and the CH-bonds should also be able to furnish good spin densities. Rather than to compute the spin density from the complete wavefunction we have only calculated the bulk contribution to it, the so-called spin-polarization terms which are the only ones linear in the expansion coefficients of substituted configurations. Let the restricted HF-wavefunction be

$$\varphi = |b_1 \bar{b}_1 b_2 \bar{b}_2 b_3 \bar{b}_3 n|,$$

then one of the three equivalent spin polarization configurations is

$$\psi_{sp}^{(1)} = \frac{1}{\sqrt{6}} \{ -|b_1 \bar{p}_1 b_2 \bar{b}_2 b_3 \bar{b}_3 n| + |p_1 \bar{b}_1 b_2 \bar{b}_2 b_3 \bar{b}_3 n| + 2|b_1 p_1 b_2 \bar{b}_2 b_3 \bar{b}_3 n| \}$$

with the spin-polarization orbital  $p_1$  determined such that it minimizes the energy of the two-configuration function

$$\Psi = c_0 \varphi + c_1 \psi_{sp}^{(1)}.$$

The spin density

$$\varrho(\mathbf{R}) = \frac{1}{M_s} \int \psi^* \sum_k 2S_{Zk} \delta(\mathbf{R} - \mathbf{r}_k) \psi d\tau$$

is then first order in  $c_1$  given by

$$\varrho(\mathbf{R}) = \frac{1}{M_s} \left\{ c_0^2 [n(\mathbf{R})]^2 + \frac{4}{\sqrt{6}} \sum_{i=1}^3 c_0 c_i p_i(\mathbf{R}) b_i(\mathbf{R}) \right\}.$$

With the values

$$\begin{array}{llll} c_0 & = & 0.959 & c_1 & = & -0.0574 \\ b_1(\mathbf{R}_{H1}) & = & 0.4573 & p_1(\mathbf{R}_{H1}) & = & 0.4296 \\ b_1(\mathbf{R}_{H2}) & = & -0.0338 & p_1(\mathbf{R}_{H2}) & = & 0.1622 \\ b_1(\mathbf{R}_C) & = & -0.5778 & p_1(\mathbf{R}_C) & = & 0.8299 \end{array}$$

we get

$$\begin{array}{ll} \varrho(\mathbf{R}_C) & = & 0.259 \\ \varrho(\mathbf{R}_H) & = & -0.035 \end{array}$$

and the hyperfine coupling constants

$$\frac{a}{h} = \frac{4\pi}{3h} g g_N \beta \beta_N \varrho(\mathbf{R}_N)$$

$$a(C) = 145.4 \text{ MHz} = 52 \text{ Gauss},$$

$$a(H) = -74.5 \text{ MHz} = -26.6 \text{ Gauss}.$$

The experimental values are 41 and  $-23$  Gauss, respectively [23].

Perfect agreement with experiment cannot be expected for several reasons.

1. With gaussian basis functions the values of the wavefunction at the nuclei are somewhat too small. This can be corrected with a trick proposed by Meyer [22] which we have not used.

2. Other terms than the spin-polarization function contribute to the spin density as well, though probably to much less extent.

3. The experimental coupling constants are averages over the zero-point vibrations. For the out-of-plane bending mode large amplitudes are expected and for pyramidal arrangement the restricted Hartree-Fock value is different from zero.

We postpone a comparison with previous theoretical values [22, 26, 27] to a forthcoming paper, where we study these additional effects in detail.

*Acknowledgement.* The work reported has been sponsored in part by Deutsche Forschungsgemeinschaft and Fonds der Chemie. One of the authors (F.D.) benefices of a stipend of Studienstiftung des Deutschen Volkes. Preliminary studies to the present investigation have been performed with the assistance of José Pujol from Bahía Blanca, Argentina.

## References

1. Radom, L., Pople, J.A.: In: MTP internat. rev. science. Sec. 1, 1, 71 (1972)
2. Millié, P., Berthier, G.: Intern. J. Quant. Chem. **2**, 67 (1968)
3. Kari, R.E., Csizmadia, I.G.: J. Chem. Phys. **46**, 1817, 4585 (1967)
4. Kari, R.E., Csizmadia, I.G.: J. Chem. Phys. **50**, 1443 (1969)
5. Kari, R.E., Csizmadia, I.G.: J. Chem. Phys. **56**, 4337 (1972)
6. Kari, R.E., Csizmadia, I.G.: Intern. J. Quant. Chem. **6**, 401 (1972)
7. Jungen, M., Ahlrichs, R.: Theoret. Chim. Acta (Berl.) **17**, 339 (1970)
8. Gelus, M., Kutzelnigg, W.: Theoret. Chim. Acta (Berl.) **28**, 103 (1973) (In this paper there are some typographical errors, in the formulae namely a factor  $R_0^2(R_0)$  missing in the definition of  $F_2, F_4(F_{34})$  and  $2\pi v$  has always to be replaced by  $(2\pi v)^2$ .)
9. Staemmler, V., Jungen, M.: to be published
10. Huzinaga, S.: J. Chem. Phys. **42**, 1293 (1965)

11. Ahlrichs, R.: Chem. Phys. Letters **15**, 609 (1972), **18**, 512 (1973)
12. Boys, S.F.: Rev. Mod. Phys. **32**, 296 (1960)
13. Lischka, H., Dyczmons, V.: to be published
14. Andrews, L., Pimentel, G.C.: J. Chem. Phys. **47**, 3637 (1965)
15. Rauk, A., Allen, L.C., Clementi, E.: J. Chem. Phys. **52**, 4133 (1970)
16. Staemmler, V.: to be published
17. Gaydon, A.G.: Dissociation energies and spectra of diatomic molecules. London: Chapman and Hall, 1968
18. Herzberg, G.: Electronic spectra and electronic structure of polyatomic molecules. New York: D. Van Nostrand, 1966
19. Page, P.M., Goode, P.C.: Negative ions and the magnetron. London: Wiley Interscience 1969
20. Pariser, R.: J. Chem. Phys. **21**, 568 (1953). Pariser, R., Parr, R.G.: J. Chem. Phys. **21**, 466, 767 (1953)
21. Kutzelnigg, W., Del Re, G., Berthier, G.: Fortschr. Chem. Forsch. **22**, 1 (1971)
22. Meyer, W.: J. Chem. Phys. **51**, 5149 (1969)
23. Carrington, A., McLachlan, A.D.: Introduction to magnetic resonance. Harper International Ed 1969
24. Kato, T.: Comm. Pure Appl. Math. **12**, 403 (1959). Kato, T.: J. Phys. Soc. Japan **14**, 382 (1959)
25. Klessinger, M.: J. Chem. Phys. **43**, S 117 (1965)
26. Milhè, P., Levy, B., Berthier, G.: Intern. J. Quant. Chem. **6**, 155 (1972)
27. Chang, S.V., Davidson, E.R., Vincow, G.: J. Chem. Phys. **52**, 1740 (1972)

Prof. Dr. W. Kutzelnigg  
Lehrstuhl f. Theoretische Chemie  
Ruhr-Universität, Bochum  
D-4630 Bochum  
Federal Republic of Germany

## An MO-Theoretical Calculation of Solvent Effect upon the $\text{NH}_3 + \text{HF} = \text{NH}_4\text{F}$ Reaction

Shinichi Yamabe, Shigeki Kato, Hiroshi Fujimoto and Kenichi Fukui  
Faculty of Engineering, Kyoto University, Sakyo-ku, Kyoto, Japan

Received March 1, 1973

An *ab initio* molecular orbital calculation was done as to a reacting system,  $\text{NH}_3 + \text{HF} \rightarrow \text{NH}_4\text{F}$ , with the inclusion of the solvent effect as the origin of dipolar field. The reactants were assumed to stay in dimers,  $(\text{NH}_3)_2$  and  $(\text{HF})_2$ , in advance to the reaction, and the respective partners of two reactants were regarded as point dipoles. The system was stabilized to some extent by two dipoles adopted. A study of *configuration analysis* on this system was made with and without the dipoles. Their effect was found to be favorable for proceeding of the reaction.

**Key words:** Reactivity – Solvent effect

### 1. Introduction

Solvent effect upon reaction rates and mechanisms has been of long-standing interest to both physical and organic chemists [1]. And the effect in the course of the liquid-phase reaction is microscopically understood as the interactions between reactants and solvent molecules, called *solvation*. Then the interactions have been interpreted in the theoretical word by partitioning them into several terms, such as Van der Waals force, hydrogen bonding, electrostatic force, and charge-transfer effect. Of course, which plays the major role in the reaction process among them is dependent upon the type of reactions. For example in the case of the Menschutkin reaction between alkyl halides and amines, the electrostatic term was pointed out to be of considerable importance [2].

Thus in order to clarify the manner in which the solvent effect operates, it is indispensable to seek the nature of the *interactions* systematically and elaborately.

Then it seems an attractive problem for theoretical investigations, especially in terms of the Molecular Orbital (MO) method, to analyze how the interactions in the solvation process affect the reactivity of a reagent and a substrate [3].

Here among the above mentioned several terms of the interactions between the solvent molecules and reactants, we tentatively take up only the electrostatic operation of the *polar* solvent upon the reactants by simplifying it as the origin of the dipolar field. As seen easily, this simplification holds several questionable points for grasping the whole feature of the solvent effect in consideration of the complexity of the phenomenon caused by the solvent. But at least as long as the dipole moment is the one measure of the *polar* solvent, the effect originated from the moment can be by no means neglected.



So in this work, as a first step to consider the interactions between the solvent molecules and the reactants, we focus our attention on the subject how the ability of the dipolar potential in the *polar* solvent can change the electronic structure and the reactivity of the reactants in the frame of MO method.

In the next section we will describe the way of the treatment of this additive effect on MO's. Then with and without this external field the numerical details about the MO calculation will be displayed for a model reaction,  $\text{NH}_3 + \text{HF} = \text{NH}_4\text{F}$ .

Finally in the light of these results, we discuss how the deformation of MO's in  $\text{NH}_3$  and  $\text{HF}$  is brought about and how the orbital overlap interaction, which is the one criterion of the easiness of reactions, is changed by the influence.

## 2. Description of Method

For closed-shell molecules, the well known Roothaan's equation [4] is derived as Eq. (1).

$$\sum_s F_{rs} c_s^i = e_i \sum_s S_{rs} c_s^i. \quad (1)$$

Here  $S_{rs}$  is the element of the overlap matrix and  $F_{rs}$  is that of the Fock matrix given as follows:

$$F_{rs} = H_{rs}^{\text{core}} + \sum_{t,u} P_{tu} [(rs|tu) - 1/2(rt|su)], \quad (2)$$

where  $P_{tu}$  is the element of the bond order density matrix.

$$P_{tu} = 2 \sum_i^{\text{occ}} c_t^i c_u^i. \quad (3)$$

$H_{rs}^{\text{core}}$  is that of the core Hamiltonian (kinetic plus potential energy in the field of fixed nuclei), and  $(rs|tu)$  is the electronic repulsion integral;

$$(rs|tu) = \int \int \chi_r(2) \chi_s(2) e^2 / r_{12} \chi_t(1) \chi_u(1) d\tau_1 d\tau_2. \quad (4)$$

The LCAO (Linear Combination of Atomic Orbitals) coefficient,  $c_s^i$ , can be obtained by the usual iterative procedure.

Here the basis functions,  $\chi_r$  and  $\chi_s$ , are Slater Type Orbitals (STO) expanded in three Gaussian Type Orbitals (GTO)<sup>1</sup> for the easiness of calculation [7, 8]. Namely we adopt STO-3G (minimal) basis set for the evaluation of the integrals,  $H_{rs}^{\text{core}}$ ,  $S_{rs}$  and  $(rs|tu)$ . Then we define a new matrix element,  $F'_{rs}$ ,

$$F'_{rs} = F_{rs} + V_{rs}, \quad (5)$$

where  $V_{rs}$  is the matrix element of any one electronic operator,  $\hat{V}(1)$ .

$$V_{rs} = \int \chi_r(1) \hat{V}(1) \chi_s(1) d\tau_1. \quad (6)$$

<sup>1</sup> The Gaussian  $\alpha$  exponents and the coefficients are taken from the least-squares fitting by Stewart [5].

At the same time we have used the standard Slater  $\zeta$  exponents by Pople *et al.* [6].

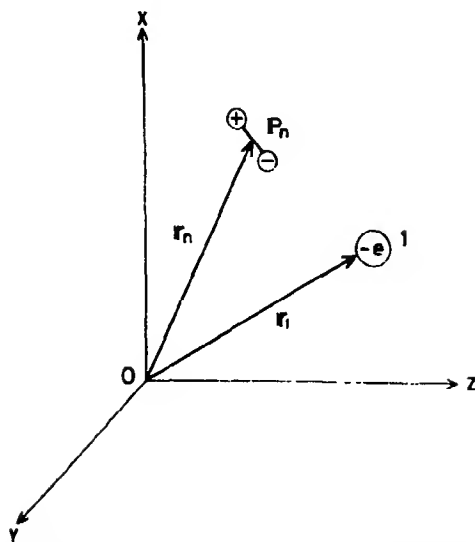


Fig. 1. The vector representation of the position of a point dipole  $P_n$  and an electron, 1

This operator is used so as to represent the additive external field. Of course  $V_{rs}$  will change the variational condition concerning  $F_{rs}$  and we can not predict whether Self-Consistent-Field (SCF) is obtained with respect to the new matrix element,  $F'_{rs}$ . But if the absolute value of  $V_{rs}$  is so small as to be regarded as a *perturbation*, in other words the external field is sufficiently weak, we may expect the convergence will be still gained. Here we give the following concrete formula to  $\hat{V}(1)$ .

$$\hat{V}(1) = \sum_n \frac{-P_n(r_n - r_1)}{|r_n - r_1|^3} \quad (7)$$

As well known, Eq. (7) indicates the scalar potential for one electron, 1, by the dipole moment,  $P_n$  ( $n = 1, 2, \dots, j$ ) [9]. There,  $r_n$  is the vector from the origin,  $O$ , to a dipole  $P_n$ .  $r_1$  is the same with respect to electron 1 (see Fig. 1). Although  $P_n$  should be identified as a point dipole in a strict sense, the positive and the negative centers of it are divided distinctly in the representation of Fig. 1 for reader's understanding. The way to evaluate the element of  $V_{rs}$  is the same Gaussian expansion method [10] as mentioned above. Following the literature [10],  $V_{rs}$  is termed *Field Integral* (FI).

The use of Eq. (7) means that the solvent molecules are simply looked upon as the source of the dipolar field to change the electronic structure, i.e. MO's. On this point some discussion will be held later.

As for the procedure to deal with the orbital overlap interaction between two reactants, we have derived the equation in another paper [11] available here, so we hope readers would refer to it about the details.

Briefly speaking of the method, the state of the whole reacting system expressed by  $\Psi$  is divided into some states with various types of orbital interactions

as shown below:

$$\begin{aligned} \Psi = & C_0 \Psi_0 + \sum_i \sum_l^{\text{occ uno}} C_{i \rightarrow l} \Psi_{i \rightarrow l} + \sum_k \sum_j^{\text{occ uno}} C_{k \rightarrow j} \Psi_{k \rightarrow j} \\ & + \sum_i \sum_j^{\text{occ uno}} C_{i \rightarrow j} \Psi_{i \rightarrow j} + \sum_k \sum_l^{\text{occ uno}} C_{k \rightarrow l} \Psi_{k \rightarrow l} + \dots \end{aligned} \quad (8)$$

There,  $\Psi_0$  is the adiabatic interacting state without any jumping of electrons, and  $\Psi_{i \rightarrow l}$  means a charge-transferred state from the  $i$ -th occupied MO to the  $l$ -th unoccupied one, and the others are similar charge-transferred or excited states. Furthermore the coefficients,  $C_0$ ,  $C_{i \rightarrow l}$  and  $C_{k \rightarrow j}$ , ..., can be obtained by the usual configuration analysis [11-13].

In this work these quantities play an important role for our discussion.

### 3. Numerical Results of Calculation

A few years ago Clementi presented an extensive *ab initio* calculation [14, 15] for a reacting system,  $\text{NH}_3 + \text{HCl} = \text{NH}_4\text{Cl}$ , and then he detected the stabilization energy and the charge transferred in a variety of distances between the nitrogen atom in  $\text{NH}_3$  and the hydrogen atom in  $\text{HCl}$ . We here adopt a similar reaction model,  $\text{NH}_3 + \text{HF} = \text{NH}_4\text{F}$ .

Then we must mention the motive for this adoption; the respective reactants,  $\text{NH}_3$  and  $\text{HF}$ , can not exist solely before the reaction occurs, and they are thought to form the complexes, called *hydrogen bonding* such as the dimer of ammonia [16] and the zigzag polymer of hydrogen fluoride [17].

With respect to the molecules taken here, Kollman and Allen looked for the reasonable geometries of  $(\text{NH}_3)_2$  and  $(\text{HF})_2$  [18, 19] to predict both dimers gain their stableness in the *linear* structure (see Fig. 2).



Fig. 2. The most stable linear structure of  $(\text{NH}_3)_2$  and  $(\text{HF})_2$  by Kollman and Allen [18, 19]

As a result of taking circumstances into consideration, the reactants in the reaction,  $\text{NH}_3 + \text{HF} = \text{NH}_4\text{F}$ , will accept the influence by their partners, provided that the reactants had no associates in the original state except the *partners*.

Hereupon the reasons for the employment of the system,  $\text{NH}_3 + \text{HF} = \text{NH}_4\text{F}$ , are summarized in the following:

1. The system has a reaction path clearly grasped by the information from above mentioned Clementi's result [14, 15] or the overlap and orientation principle by Mulliken [20].

2. By assuming the reactant has only one *fellow* respectively at the beginning of the reaction, we can take into account the effect of their partners as the origin of scalar potential of two dipoles in a first approximation, reflecting that  $(\text{NH}_3)_2$  and  $(\text{HF})_2$  are not so strongly bound [18, 19].

In Fig. 3 the reacting model is sketched.

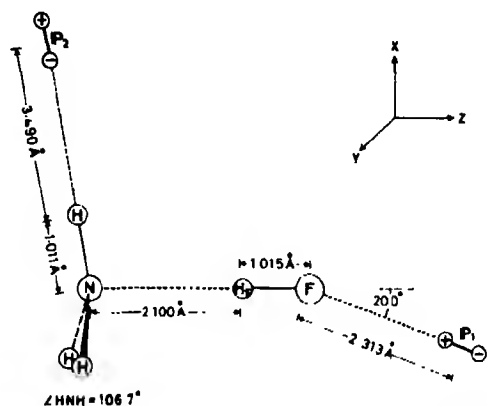


Fig. 3. The reacting model taken in this calculation. The position of  $P_1$  and  $P_2$  was taught by the work of Kollman and Allen.  $P_1$  corresponds to  $\text{HF}$  and  $P_2$  to  $\text{NH}_3$  in Fig. 2

We used the experimental values for the moment ( $|P_1| = 1.82$  debye [21],  $|P_2| = 1.48$  debye [22]).

The geometry of ammonia is taken also from the experimental result [23]. The distance,  $R(\text{N}-\text{F})$ , is arbitrarily taken  $3.115 \text{ \AA}$ , and  $R(\text{N}-\text{H}_F)$  is determined by the optimization with respect to the whole system in CNDO/2 method [24] excluding the two dipoles.

This system involving dipoles has a  $C_s$  symmetry as to  $x-z$  plane, while it has  $C_{3v}$  symmetry when they are absent.

In Table I the results of MO calculation are given. Here we show the difference by  $F'_{rs}$  and  $F_{rs}$  according to whether  $V_{rs}$  is contained or not.  $E_k$  and  $E_t$  mean kinetic and total energy in atomic units (a.u.). In the evaluation of MO's by  $F'_{rs}$  they always undergo the two dipoles simultaneously. But actually the other partners of the reactants, that is  $P_1$  for  $\text{NH}_3$  and  $P_2$  for  $\text{HF}$ , give no serious effect upon MO's owing to the remarkable sensitivity to the distance,  $|r_n - r_1|$ , of  $V(1)$  in Eq. (7).

Then the comparison of (I) with (II) in Table I indicates the effect by  $P_1$  to prompt the tendency of the charge redistribution ( $\text{H}^{\delta+} - \text{F}^{\delta-}$ ). This is because the nearer cationic center of  $P_1$  to fluorine atom attracts the charge density of  $\text{HF}$  (see Fig. 3).

As for the lowest unoccupied (LU) MO of  $\text{HF}$ , having a node along the direction of the sigma bond, the spatial extension on the contrary increases on the side of the hydrogen atom ( $\text{H}_F$ ). At the same time  $\text{HF}$  molecule is a little stabilized thanks to the operation of the nearer cationic center of  $P_1$ . On the other hand

Table 1 The results of MO calculation

No	System	Dipoles?	Atom population	$E_T$ (a.u.)	$(-E_K/E_T)$
(I)	HF	$I_\alpha$	H 0.8407    F 9.1593	- 98.5540	0.9940
(II)	HI	$I'_\alpha$	H 0.8199    I 9.1801	- 98.5672	
(III)	NH <sub>3</sub>	$F_\alpha$	H 0.8501 N 7.4498 H H	- 55.4450	0.9969
(IV)	NH <sub>3</sub>	$F'_\alpha$	H 0.8336 N 7.4589 H H 0.8537	- 55.4808	
(V)	NH <sub>4</sub> F	$F_\alpha$	H 0.8343 7.4595 N    H 0.8143    F 9.2110 H H	- 154.0094	0.9957
(VI)	NH <sub>4</sub> F	$F'_\alpha$	0.8211 H 7.4693 N    H 0.7956    F 9.2318 0.8411 H H	- 154.0601	

NH<sub>3</sub> in (III) experiences the migration of charge density from the hydrogen in  $x$ - $z$  plane to both nitrogen atom and the residual two hydrogens by virtue of  $P_2$  as shown in (IV). And the highest occupied (HO) MO of NH<sub>3</sub>, which is mainly composed of the lone pair on the nitrogen, undergoes a destabilization and the growth of the lone pair to a minor extent.

At a glance the more stabilized total energy in (IV) than in (III) may seem strange, reflecting that NH<sub>3</sub> is linked to the nearer anionic center in  $P_2$  and that electronic repulsion energy may increase. However the *classical* attractive energy between the anionic center of  $P_2$  and the positive nuclear charge on the hydrogen atom in  $x$ - $z$  plane mainly overcomes the above painful condition. As a whole a small stabilization is gained also in NH<sub>3</sub>.

From the inspection of these deviations of the quantities by the external field, we can expect the growth of the overlapping between HOMO of NH<sub>3</sub> and LUMO of HF, as will be shown directly by the coefficients in Eq. (8) later.

We can obtain the similar information from the comparison in (V) and (VI) both on the calculation in terms of the whole reacting system, the latter more stabilized.

Referring to (III) and (V), we should notice the decrease of the charge density on the three hydrogens of  $\text{NH}_3$  part as a new bond ( $\text{N} \cdots \text{H}_\text{F}$ ) is formed. It is meaningful that toward the product,  $\text{NH}_4^+ \text{F}^-$ , the cationic component on  $\text{NH}_3$  is first redistributed on three hydrogen atoms, shown also by Kollman and Allen [18]. The stabilization energy ( $\Delta E$ ) of the system in Fig. 3,  $\Delta E = E_\text{T}(\text{NH}_3) + E_\text{T}(\text{HF}) - E_\text{T}(\text{NH}_4\text{F})$ , are 6.5 kcal/mole in  $F_\text{rs}$  and 7.6 kcal/mole in  $F'_\text{rs}$  respectively, compared with 11.7 kcal/mole in their most stable geometry of  $\text{NH}_4\text{F}$  by Kollman and Allen.

#### 4. The Interaction Mode of MO's

By applying the solution in Eq. (1) to a variety of the systems in Table I, the CI (Configuration Interaction) representation of the reacting system in the form of Eq. (8) is achieved, shown below:

$$\begin{aligned} F_\text{rs} : \Psi &= 0.9787 \Psi_0 + 0.0976 \Psi_{\text{HO} \rightarrow \text{LU}} + 0.0048 \Psi_{\text{HO} \rightarrow \text{LU}}^{\sigma \rightarrow \sigma^*} + 0.0242 \Psi_{\sigma \rightarrow \sigma^*}^{\sigma \rightarrow \sigma^*} + \cdots \\ F'_\text{rs} : \Psi' &= 0.9772 \Psi'_0 + 0.1029 \Psi'_{\text{HO} \rightarrow \text{LU}} + 0.0054 \Psi'_{\text{HO} \rightarrow \text{LU}}^{\sigma \rightarrow \sigma^*} + 0.0238 \Psi_{\sigma \rightarrow \sigma^*}^{\sigma \rightarrow \sigma^*} + \cdots \end{aligned} \quad (9)$$

where  $F'_\text{rs}$  or  $F_\text{rs}$  corresponds to the presence or the absence of two dipoles. In this paper we use the prime for the caution of the existence of them.

$\Psi_0$  and  $\Psi'_0$  denote the adiabatic interacting state without inclusion of any configurations different from the original one.

The coefficients attached to  $\Psi_0$  and  $\Psi'_0$ , the overwhelming values compared with others, show that at the reacting point adopted here the original configuration without any jumping of electrons retains its majority yet. The comparison of these two coefficients gives us the knowledge of the effective operation of two point dipoles to decrease the weight of this state and to make electrons active in favor for the progress of the reaction.

Furthermore  $\Psi_{\text{HO} \rightarrow \text{LU}}$  and  $\Psi_{\text{HO} \rightarrow \text{LU}}^{\sigma \rightarrow \sigma^*}$  stand for one- and two-electron transferred states from HOMO of  $\text{NH}_3$  to LUMO of HF. These configurations do their part in increasing the weight of the ionic character of the reacting system and accelerating the formation of a new bond [25].

Here the existence of two dipoles is found to support these *invasions* of electrons into the unoccupied MO's of the other reactant.  $\Psi_{\sigma \rightarrow \sigma^*}^{\sigma \rightarrow \sigma^*}$  means one electron excited state from the third occupied MO ( $3\sigma$ ) (in order of increasing orbital energies) to the LUMO ( $1\sigma^*$ ) in HF. The reason for the reduction of the coefficients ( $0.0242 \rightarrow 0.0238$ ) is as follows; namely two dipoles act more remarkably on the isolated reactant, HF, than the reacting whole system, with the result of the proper charge redistribution beforehand because of the dipolar field. Therefore the contribution of the excited state to polarize electronic densities is not so necessary as in the case without dipoles.

Other states, such as tri-transferred and di-excited ones, are omitted in the above expression owing to their negligible smallness. Viewing these results as to  $\Psi$  and  $\Psi'$ , we may say the two dipoles play their role to prompt the tendency to decrease the contribution of the original state,  $\Psi_0$ , along the reaction path.

Here from another standpoint this insistence will be understood more clearly. That is, as displayed in Table 2, the configuration analysis presents some vivid feature<sup>2</sup> in the sense of organic chemistry.

Table 2. The weights of some electronic structures

Structures	$F_{rs}$ (in %)	$F'_{rs}$ (in %)
$(\text{NH}_3 \cdot \text{HF})$	97.3540	97.1504
$(\text{NH}_3^+ \cdot \text{HF}^-)$	0.0071	0.0054
$(\text{NH}_3^- \cdot \text{HF}^+)$	2.4705	2.6742
$(\text{NH}_3 \cdot \text{HF}^*)$	0.0901	0.0873
$(\text{NH}_3^+ \cdot \text{HF}^-)$	0.0141	0.0163
$(\text{NH}_3^- \cdot \text{HF}^+)$	0.0000	0.0000
$(\text{NH}_3^+ \cdot \text{HF}^-)$	0.0836	0.0969
$(\text{NH}_3^- \cdot \text{HF}^+)$	0.0001	0.0000
$(\text{NH}_3^+ \cdot \text{HF}^*)$	0.0000	0.0000
Total	99.9487	99.9434

There the evaluation by the use of the method was done as to both models with and without two dipoles, denoted by  $F'_{rs}$  and  $F_{rs}$  in the same way as before. Hereupon  $(\text{NH}_3 \cdot \text{HF})$  means the covalent structure,  $(\text{NH}_3^+ \cdot \text{HF}^-)$  is an ionic structure with one electron moving from  $\text{NH}_3$  to  $\text{HF}$ , and  $(\text{NH}_3^- \cdot \text{HF}^+)$  holds the reverse relation.  $(\text{NH}_3^+ \cdot \text{HF})$  is the one electron excited state in  $\text{NH}_3$ , and  $(\text{NH}_3 \cdot \text{HF}^*)$  is the same in  $\text{HF}$ .  $(\text{NH}_3^+ \cdot \text{HF}^-)$  means two electron transferred ionic structure mutually between two entities. For other structures in Table 2, the analogy is available. From the tabulated results the favorable effect of dipoles upon the proceeding of the reaction can be observed, particularly in that the weight of  $(\text{NH}_3^+ \cdot \text{HF}^-)$  and  $(\text{NH}_3^- \cdot \text{HF}^+)$  is made larger.  $(\text{NH}_3 \cdot \text{HF}^*)$  contains the above mentioned  $\Psi_{\sigma \rightarrow \sigma^*}$  state. Summing up the tabulated values with respect to the two cases,  $F_{rs}$  and  $F'_{rs}$ , we can get the totals which are almost 100% in both cases, indicated in the bottom of the Table. This gives the ground for demonstrating the adequacy regarding the employment of only the tabulated electronic structures in representing the whole state,  $\Psi$  and  $\Psi'$ .

Next in Table 3, the overlap bond population between the nitrogen atom in  $\text{NH}_3$  and the hydrogen atom in  $\text{HF}$  ( $\text{H}_F$ ) is given in the partitioned form as regards to four different types of the orbital interaction. There, "Exchange type" corresponds to the population produced by the overlap between both occupied orbitals of the two reactants in their beginning, and this term yields antibonding population as shown in the table. However this tendency is weakened by the inclusion

<sup>2</sup> The involvement of overlap integrals makes somewhat intricate the actual calculation. The derivation of the equation used here will be noted elsewhere by one of the authors (S.K.).

Table 3. The atomic bond population between N and H<sub>F</sub>

Types	$F_{rs}$	$F'_{rs}$
Exchange type	- 0.0225	- 0.0216
CT type	0.0365	0.0387
Back CT type	- 0.0002	- 0.0001
Both unocc	- 0.0000	- 0.0000
Total	0.0138	0.0169

of dipoles to some extent. "CT type" is the population originated from the charge transfer interaction between the occupied orbitals in  $\text{NH}_3$  and the unoccupied ones in HF.

This mode presents the considerable quantity to the bond formation with the larger value in  $F'_{rs}$  than  $F_{rs}$ . Thus the importance of the charge transfer interaction can be confirmed in the standpoint of the analysis of the new bond formation [26].

Other types, "Back CT type" which means the donation from HF to  $\text{NH}_3$  and "Both unocc" which denotes the orbital interaction between both unoccupied ones of two, are found to play a minor role in the bond formation.

As a whole the dipolar field helps to form a new bond also. Configuration analysis offers another interesting quantity termed *Occupancy of MO's* [11]. When the interaction between two molecules is absent, their MO's are filled with two electrons respectively. But the occurrence of the electron migration or the excitation by the interaction somewhat changes this number, that is, the *old* occupied orbitals lose the portion of the number, and the *old* unoccupied ones gain the electronic density a little.

Table 4. Occupancy of MO's in the interacting state

$1\sigma^*$	0.0264	0.0285
$\bar{\pi}$	2.0000	2.0000
$\pi$	2.0000	2.0000
$3\sigma$	1.9988	1.9989
$2\sigma$	2.0000	2.0000
$1\sigma$	2.0000	2.0000
MO's of HF	$F_{rs}$	$F'_{rs}$
$2e_2$	0.0001	0.0001
$2e_1$	0.0001	0.0001
$4a_1$	0.0001	0.0001
$3a_1$	1.9749	1.9729
$1e_2$	1.9999	1.9999
$1e_1$	1.9999	1.9999
$2a_1$	1.9997	1.9997
$1a_1$	2.0000	2.0000
MO's of $\text{NH}_3$	$F_{rs}$	$F'_{rs}$



Table 4 displays these rearrangements in MO's owing to the active electrons, where these notations of the respective MO's are defined in the case without two dipoles ( $F_{rs}$ )<sup>3</sup>.

There the notable change can be found in  $1\sigma^*$  of HF and  $3a_1$  in  $\text{NH}_3$ . These are both, in a greater part, due to the particular orbital interactions, that is,  $\Psi_{\text{HO} \rightarrow \text{L.U.}}$  and  $\Psi_{\text{HO} \rightarrow \text{L.U.}}$ . The decrease in  $3\sigma$  of HF is mainly owing to the appearance of  $\Psi_{\sigma \rightarrow \sigma^*}$  in Eq. (9). Comparison of  $F_{rs}$  with  $F'_{rs}$  again demonstrates the efficient operation of the two dipoles upon the inclination to change the original occupancy more and more.

### 5. Conclusive Discussion

In this report we have described a method to inform the MO's of the solvent effect as if it could be reduced to that of some dipole moments. We have here only two dipoles tentatively as the source of the potential which are the partners of two reactants. And the two dipoles,  $P_1$  and  $P_2$ , in Fig. 3 are the simplified products in  $(\text{HF})_2$  and  $(\text{NH}_3)_2$  by the use of the result by Kollman and Allen. Of course if we had no knowledge about the report, we could not determine the position and the direction of  $P_1$  and  $P_2$ , i.e. the *partners* after the simplification. In other words, it is a too crude abstraction to take only the dipole-electron interaction into account in the dimer systems in Fig. 2. That is, even if the reactants had only one fellow to interact with each other, more detailed informations are necessary for the description of the *interaction*. Then the first step to improve the condition in the frame of this method seems to adopt the operator  $\hat{V}(1)$  in Eq. (6) of another type as well as the dipolar potential, already set forth in this work. In this respect the circumstances are not so troublesome for us, and now with the utilization of other operators a new calculation is in progress concerning a typical  $\text{SN}_2$  reaction. But in spite of these improvements the enough accuracy will not be gained yet as far as the *static* treatment for many solvent molecules is not considered. This procedure will be included in the future.

Viewing the above mentioned weak point of this calculation on  $\text{NH}_3 + \text{HF} = \text{NH}_4\text{F}$  in a quantative sense, here again we would like to insist our situation that we do not intend to seek *accurate* properties as to the interacting mode from the energetic standpoint, but to show the analytical and concrete representation about the phenomenon of the interactions, called *solvation*.

Lastly the results of this work are summarized as follows; *if the two reactants in a reaction,  $\text{NH}_3 + \text{HF} = \text{NH}_4\text{F}$ , originally exist in their dimers,  $(\text{NH}_3)_2$  and  $(\text{HF})_2$ , and furthermore the influence of the respective partners of the reactants are sufficiently weak to be regarded as if it could be simply approximated to that of the dipolar field, the effect of the partners works favorably for proceeding of the reaction.*

*Acknowledgement.* One of the authors (S.Y.) is grateful to Mr. Kazuhiro Ishida for his helpful advice in making the FORTRAN program of MO calculation. The authors wish to express their appreciation to the Data Processing Center of Kyoto University for generous use of the FACOM 230-60 computer.

<sup>3</sup> The two dipoles lower the symmetry of the whole system from  $C_{3v}$  to  $C_s$  with respect to  $x-z$  plane, mentioned before (see Fig. 3). Therefore as for the state including them ( $F'_{rs}$ ), these notations can not be applied. But the deviation is so small that a new notation for  $C_s$  symmetry is not prepared in Table 4.

### References

1. See for instance; Amis, E. S.: Solvent effects on reaction rates and mechanisms New York and London: Academic Press, 1966
2. Glasstone, S., Laidler, K. J., Eyring, H.: The theory of rate processes, p. 419. New York: McGraw-Hill Book Co. 1941
3. Cremaschi, P., Gamba, A., Simonetta, M.: Theoret. chim. Acta (Berl.) **25**, 237 (1972)
4. Roothaan, C. C. J.: Rev. Mod. Phys. **23**, 69 (1951)
5. Stewart, R. F.: J. Chem. Phys. **52**, 431 (1970)
6. Hehre, W. J., Stewart, R. F., Pople, J. A.: J. Chem. Phys. **51**, 2657 (1969)
7. O-ohata, K., Taketa, H., Hujinaga, S.: J. Phys. Soc. Japan **21**, 2306 (1966)
8. Taketa, H., Hujinaga, S., O-ohata, K.: J. Phys. Soc. Japan **21**, 2313 (1966)
9. Ray, S.: Chem. Phys. Letters **11**, 573 (1971)
10. Matsuoka, O.: Intern. J. Quant. Chem. **5**, 1 (1971)
11. Fujimoto, H., Kato, S., Yamabe, S., Fukui, K.: J. Chem. Phys. in press
12. Baba, H., Suzuki, S., Takemura, T.: J. Chem. Phys. **50**, 2078 (1969)
13. Morita, H., Nagakura, S.: Theoret. chim. Acta (Berl.) **27**, 325 (1972)
14. Clementi, E.: J. Chem. Phys. **46**, 3851 (1967)
15. Clementi, E.: J. Chem. Phys. **47**, 2323 (1967)
16. Pimentel, G. C., Bulatin, M. O., Tiel, M. V.: J. Chem. Phys. **36**, 500 (1962)
17. Hamilton, W., Ibers, J. A.: Hydrogen bonding in solids, p. 154. New York: W. A. Benjamin, 1968
18. Kollman, P. A., Allen, L. C.: J. Am. Chem. Soc. **93**, 4991 (1971)
19. Kollman, P. A., Allen, L. C.: J. Chem. Phys. **52**, 5085 (1970)
20. Mulliken, R. S.: Rec. trav. Chim. **75**, 845 (1956)
21. Nelson, R. D., Lide, D. R., Maryott, A. A.: Selected values of electric dipole moment for molecules in the gas phase, NSRDSNBS 10, Washington, D. C. U. S. Government Printing Office 1967
22. Regnier, J. F., Daum, A.: Commun. Res. Acad. Sci. Paris **255**, 2417 (1960)
23. Swalen, J. D., Ibers, J. A.: J. Chem. Phys. **36**, 1914 (1962)
24. Pople, J. A., Beveridge, D. L.: Approximate molecular orbital theory. New York: McGraw-Hill 1970
25. Fukui, K., Fujimoto, H., Yamabe, S.: J. Phys. Chem. **76**, 232 (1972)
26. Fujimoto, H., Yamabe, S., Fukui, K.: Tetrahedron Letters **1971**, 443

Dr. S. Yamabe  
Department of Hydrocarbon Chemistry  
Faculty of Engineering  
Kyoto University  
Kyoto, Japan



## A Calculation of the Rotatory Strengths of the Electron-Transfer Transitions of the *Tris*-(1,10-phenanthroline)iron(II) Ion

M. Král\*, A. Moscowitz\*\*, and C. J. Ballhausen

Department of Physical Chemistry, H. C. Ørsted Institute, University of Copenhagen, Denmark

Received April 5, 1973

The rotatory strengths of the metal-to-ligand transitions observed in the spectrum of the complex ion  $(-)\text{-Fe(phen)}_3^{2+}$  have been calculated theoretically. The excited electronic states were characterized using a coupled chromophore model. The calculated rotatory strengths are higher than the corresponding experimental values by a factor of about four.

**Key words:** Rotary strengths of inorganic complexes *Tris*-(1,10-phenanthroline) iron (II) ion  
Electron-transfer transitions in inorganic chelates

### Introduction

Many papers dealing with the optical rotatory dispersion (ORD spectra) and circular dichroism (CD spectra) of complex ions have appeared in the last ten years. The quantity which can be extracted from these measurements is the rotatory strength, defined for a transition from state *A* to state *B* by the relation [1]

$$R_{A \rightarrow B} = \text{Im} \{ \langle A | \mu_e | B \rangle \cdot \langle B | \mu_m | A \rangle \}, \quad (1)$$

where  $\mu_e$  and  $\mu_m$  are the electric and magnetic dipole operators respectively.

The reported calculations of the optical activities of complex compounds of metal ions with bidentate ligands forming an octahedral coordination of donor atoms of  $D_3$  symmetry have used either an ionic [2–8] or a molecular orbital approach [9–13]. Such models are quite useful for studies of the circular dichroism of the *d-d* bands but are impractical when used to account for optically active metal-to-ligand  $\pi^*$  orbital transitions. To analyse this type of transition we have used the "coupled chromophore" model proposed by Longuet-Higgins and Murrell [14] for studies of conjugated  $\pi$ -electronic systems and utilized for the investigation of the optical activities of organic compounds by Moscowitz and Hansen [15, 16]. As an example we shall treat the complex ion  $(-)\text{-Fe(phen)}_3^{2+}$  (phen = 1,10-phenanthroline). Hanazaki and Nagakura [17] have previously studied the same ion using similar methods. However, their results are in doubt because of shortcomings in the wave functions they used.

\* Present address: Vysoká škola chemicko-technologická, Praha, Czechoslovakia.

\*\* Present address: Department of Chemistry, University of Minnesota, Minnesota, U.S.A.

### Theory

With

$$\mu_e = e \sum_i r_i, \quad (2)$$

$$\mu_m = \frac{e}{2mc} \sum_i r_i \times p_i = \frac{eh}{2mci} \sum_i r_i \times \nabla_i, \quad (3)$$

and upon changing the matrix element of the operator  $\mu_e$  to a dipole velocity representation [18], (1) can be expressed as

$$R_{A \rightarrow B} = \frac{e^2 h^2}{4\pi m^2 c^2 \sigma_{A \rightarrow B}} \langle A | \nabla | B \rangle \cdot \langle B | r \times \nabla | A \rangle, \quad (4)$$

where the symbols  $e$ ,  $h$ ,  $m$  and  $c$  have their usual meaning and where  $\sigma_{A \rightarrow B}$  is the energy difference between states  $A$  and  $B$  measured in  $\text{cm}^{-1}$ . State  $A$  is taken as the ground state and state  $B$  as a single-electron excited state. The electronic states are represented in the coupled chromophore model by linear combinations of functions of the form

$$|X\rangle = \prod_g |C_g^x\rangle, \quad (5)$$

$|C_g^x\rangle$  being the wave function which describes the  $i^{\text{th}}$  electronic state of the  $g^{\text{th}}$  chromophore. We assume that the wave functions associated with a single chromophore are orthogonal to each other, viz:

$$\langle C_g^x | C_g^y \rangle = \delta_{xy}. \quad (6)$$

The ground state, having  $n$  groups of ligands, is then given by the function

$$|A, I, S\rangle = |M^0\rangle \prod_{g=1}^n |L^0(g)\rangle, \quad (7)$$

where  $I$  designates the symmetry classification of the function,  $S$  is the total spin,  $|M^0\rangle$  is the function which describes the electronic ground state of the metal ion and where  $|L^0(g)\rangle$  stands for the electronic ground state of the  $g^{\text{th}}$  ligand.

State  $B$  in Eq. (4) is a one-electron excited state in which a  $d$ -electron from the central metal ion has been excited into a  $\pi$ -antibonding orbital located on a ligand. As a  $d$ -electron goes into  $\pi$ -antibonding orbitals on the first, second, ...,  $n^{\text{th}}$  ligands, this state is described by the function

$$|ET, I, S\rangle = \sqrt{\frac{1}{j}} \sum_j \sum_{h=1}^n D_h^{I, j} \left| \begin{smallmatrix} L(h)_r \\ M_j \end{smallmatrix} \right\rangle \prod_{g=1}^n |L^0(g)\rangle, \quad (8)$$

where  $D_h^{I, j}$  are the group transformation coefficients and where  $\left| \begin{smallmatrix} L(h)_r \\ M_j \end{smallmatrix} \right\rangle$  stands for the single determinantal function of the configuration arising from the promotion of a  $d$ -electron from the state described by the spin-orbital function  $|M_j\rangle$  into the  $r^{\text{th}}$  antibonding state of the  $h^{\text{th}}$  ligand described by the spin-orbital function  $|L(h)_r\rangle$ . Now, if we introduce (7) and (8) into the expression for the matrix

elements of the operator  $\mathcal{V}$ , we get

$$\langle A, \Gamma S | \sum_i \mathcal{V}_i | E T, \Gamma_i S \rangle = \sqrt{\frac{1}{j}} \sum_j \sum_h D_h^{f_1} \langle M^0 | \sum_i \mathcal{V}_i \left| \begin{smallmatrix} L(h)_r \\ M_j \end{smallmatrix} \right\rangle. \quad (9)$$

Similarly, for the matrix element of the operator  $(\mathbf{r} \times \mathcal{V})$  we get

$$\langle E T, \Gamma_i S | \sum_i \mathbf{r}_i \times \mathcal{V}_i | A, \Gamma S \rangle = \sqrt{\frac{1}{j}} \sum_j \sum_h D_h^{f_1} \left\langle \begin{smallmatrix} L(h)_r \\ M_j \end{smallmatrix} \right| \sum_i \mathbf{r}_i \times \mathcal{V}_i | M^0 \rangle. \quad (10)$$

Since  $\mathcal{V}_i$  and  $(\mathbf{r}_i \times \mathcal{V}_i)$  are one-electron operators, the matrix elements of these operators can be reduced to

$$\langle M^0 | \sum_i \mathcal{V}_i \left| \begin{smallmatrix} L(h)_r \\ M_j \end{smallmatrix} \right\rangle = \langle M_j | \mathcal{V} | L(h)_r \rangle \quad (11)$$

and

$$\left\langle \begin{smallmatrix} L(h)_r \\ M_j \end{smallmatrix} \right| \sum_i \mathbf{r}_i \times \mathcal{V}_i | M^0 \rangle = \langle L(h)_r | \mathbf{r} \times \mathcal{V} | M_j \rangle. \quad (12)$$

We do not consider spin-orbit coupling so we can write an arbitrary spin orbital as

$$|C_i\rangle = |c_i\rangle |\gamma_i\rangle \quad (13)$$

where  $|c_i\rangle$  is the orbital part and  $|\gamma_i\rangle$  is the spin part of the wave function. Hence

$$\langle M_j | \mathcal{V} | L(h)_r \rangle = \langle m_j | \mathcal{V} | l(h)_r \rangle \quad (14)$$

and

$$\langle L(h)_r | \mathbf{r} \times \mathcal{V} | M_j \rangle = \langle l(h)_r | \mathbf{r} \times \mathcal{V} | m_j \rangle. \quad (15)$$

Substituting (14) and (15) into the Eqs. (9) and (10) we obtain, after summing over all orbital states,

$$\langle A, \Gamma, S | \sum_i \mathcal{V}_i | E T, \Gamma_i S \rangle = \sqrt{\frac{1}{k}} \sum_k \sum_h D_h^{f_1} \langle m_k | \mathcal{V} | l(h)_r \rangle \quad (16)$$

and

$$\langle E T, \Gamma_i S | \sum_i \mathbf{r}_i \times \mathcal{V}_i | A, \Gamma S \rangle = \sqrt{\frac{1}{k}} \sum_k \sum_h D_h^{f_1} \langle l(h)_r | \mathbf{r} \times \mathcal{V} | m_k \rangle. \quad (17)$$

We can therefore rewrite expression (4) in the form

$$R_{I \rightarrow I_1} = -\frac{e^2 \hbar^2}{4\pi m^2 c^2 \sigma_{I \rightarrow I_1}} \frac{1}{k} \sum_k \sum_h (D_h^{f_1})^2 \langle m_k | \mathcal{V} | l(h)_r \rangle \cdot \langle l(h)_r | \mathbf{r} \times \mathcal{V} | m_k \rangle. \quad (18)$$

### Matrix Elements of the Operators $\vec{\mathcal{V}}$ and $(\vec{r} \times \vec{\mathcal{V}})$

The molecular orbitals  $|m_k\rangle$  and  $|l(h)_r\rangle$  are expressed as linear combinations of real atomic  $d$ -orbitals and ligand orbitals

$$|m_k\rangle = \sum_m b_{km} d_m \quad (19)$$

and

$$|l(h)_r\rangle = \sum_s c_{rs} p_{zs}^{(h)}, \quad (20)$$

where  $p_{zs}^{(h)}$  is a  $p_z$ -orbital on the  $h^{\text{th}}$  ligand localized on the  $s^{\text{th}}$  centre.

Table 1. Matrix elements  $\langle n_m l_m m_m^u | V | 2p_z \rangle$ 

Matrix Element	<i>i</i>	<i>j</i>	<i>k</i>
$\langle 3d_{3/2}   V   2p_z \rangle$	0	0	0
$\langle 3d_{5/2}   V   2p_z \rangle$	$\langle 3d_{3/2}   \frac{\partial}{\partial x}   2p_z \rangle$	0	0
$\langle 3d_{3/2}   V   2p_x \rangle$	0	$\langle 3d_{3/2}   \frac{\partial}{\partial y}   2p_z \rangle$	0
$\langle 3d_{3/2}   V   2p_y \rangle$	0	0	$\langle 3d_{3/2}   \frac{\partial}{\partial z}   2p_z \rangle$
$\langle 3d_{5/2}   V   2p_x \rangle$	0	0	$\langle 3d_{5/2}   \frac{\partial}{\partial z}   2p_z \rangle$

Table 2. Matrix elements  $\langle 2p_z | r \times V | n_m l_m m_m^u \rangle$ 

Matrix Element	<i>i</i>	<i>j</i>
$\langle 2p_z   r \times V   3d_{3/2} \rangle$	0	$\langle 2p_z   3d_{3/2} \rangle$
$\langle 2p_z   r \times V   3d_{5/2} \rangle$	0	0
$\langle 2p_z   r \times V   3d_{3/2} \rangle$	0	0
$\langle 2p_z   r \times V   3d_{5/2} \rangle$	$\frac{1}{3} \langle 3d_{3/2}   2p_z \rangle$	0
$\langle 2p_z   r \times V   3d_{3/2} \rangle$	$\frac{1}{3} \langle 2p_z   3d_{3/2} \rangle$	0

The matrix elements  $\langle m_k | V | l(h)_r \rangle$  and  $\langle l(h)_r | r \times V | m_k \rangle$  are therefore given by a sum of two-center integrals taken over normalized Slater orbitals:

$$\langle n_m l_m m_m^u | V | n_l l_m m_l^u \rangle \quad (2)$$

and

$$\langle n_l l_m m_l^u | r \times V | n_m l_m m_m^u \rangle. \quad (2')$$

The non-vanishing matrix elements of the operator  $V$  can be found by standard group-theoretical methods [19, 20]. Their components are given in Table 1. In addition the matrix elements of the operator  $(r \times V)$  may be expressed as overlap integrals [15], and their non-zero components are given in Table 2.

### Calculation of $R_{A \rightarrow B}$ for $(\text{---})\text{Fe(phen)}_3^{+2}$

The complex is schematically illustrated in Fig. 1. For simplification only the donor atoms are indicated and the bidentate ligands are replaced by thick line. The symmetry of the entire complex ion is taken as  $D_3$ . In Fig. 1 the unit vectors used to describe the positions of the ligands are shown. These have been chosen in such a way that for ligand 1 all the vectors are positive. Referred to this choice the positions of ligands 2 and 3 are given as follows:

$$\begin{array}{ccc} L(1) & L(2) & L(3) \\ i & k & -j \\ j & -i & -k \\ k & -j & i \end{array} \quad (2'')$$

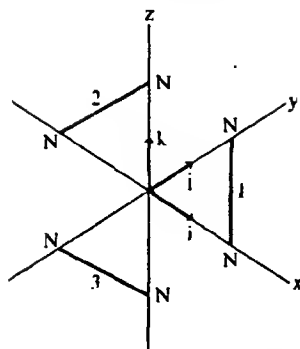


Fig. 1. Unit vectors describing the ligand positions

The distances of the carbon and nitrogen atoms from the central metal ion are given in Table 3. Of these values only the bond distance Fe-N has been experimentally determined [21].

Studies of the magnetic properties of the complex ion  $(-)\text{-Fe(phen)}_3^{+2}$  have shown that the ground state is a magnetic singlet state [22], i.e. the function  $|M^0\rangle$  in the expressions (7), (9) and (10) can be written

$$|M^0\rangle = |m_1\alpha, m_1\beta, m_2\alpha, m_2\beta, m_3\alpha, m_3\beta|, \quad (24)$$

where  $m_k$  are the atomic orbitals of the metal [23],

$$\begin{aligned} m_1 &= \sqrt{\frac{2}{3}}(x^2 - y^2) - \sqrt{\frac{1}{3}}(xz), \\ m_2 &= \sqrt{\frac{2}{3}}(xy) + \sqrt{\frac{1}{3}}(yz) \end{aligned} \quad (25)$$

and

$$m_3 = (z^2),$$

the expressions in brackets, e.g.  $(x^2 - y^2)$ , being the real  $d$  orbitals.

We now turn to the electron transfer states. The optically active transitions can easily be identified because these are the electronic transitions possessing mutually dissymmetrically oriented transition moments [24]. In  $D_3$  symmetry the transitions localized on the metal atom are polarized either parallel or per-

Table 3. Interatomic distances in  $\text{Fe(phen)}_3^{+2}$ 

$M-X$	Bond length in Å	$M-X$	Bond length in Å
Fe-N <sub>1</sub>	1.97	Fe-C <sub>5</sub>	5.10
Fe-N <sub>10</sub>		Fe-C <sub>6</sub>	
Fe-C <sub>2</sub>	3.12	Fe-C <sub>11</sub>	2.68
Fe-C <sub>9</sub>		Fe-C <sub>12</sub>	
Fe-C <sub>3</sub>	4.36	Fe-C <sub>13</sub>	4.07
Fe-C <sub>8</sub>		Fe-C <sub>14</sub>	
Fe-C <sub>4</sub>	4.73		
Fe-C <sub>7</sub>			



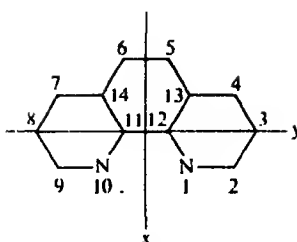


Fig. 2. Numbering and coordinate axis used for o-phenanthroline

pendicular to the  $C_2$  axis. In an o-phenanthroline molecule the electronic transitions are polarized either along the long axis ( $y$ ) or along the short axis ( $x$ ) (see Fig. 2). In the molecular geometry of the complex the transitions polarized along the short ( $x$ ) axis are parallel to the molecular  $C_2$  axis. The transition moments of the  $d-d$ -transitions have the same orientations; it follows that the charge transfer transitions are optically inactive. On the other hand the ligand transitions polarized along the long ( $y$ ) axis yield a dis-symmetric transition moment mirrored by the transition moments of the  $d-d$ -transitions. Hence these bands will be optically active.

A study of the electronic spectra of 1,10-phenanthroline has revealed that the transitions polarized along the long axis originate from the excitation of an electron in the highest filled  $\pi$  orbital to the second empty  $\pi$ -antibonding orbital [25]. This is therefore the molecular orbital into which we excite a  $d$ -electron.

### Numerical Calculations

The carbon and nitrogen atomic functions were taken in mono- $\zeta$  form with the values  $\zeta_C = 1.5679$  and  $\zeta_N = 1.9170$  [26]. The atomic iron function used had a double zeta form [27]:

$$[\text{Fe(II)}, 3dm^u] = 0.5661 [\text{Fe(II)}, 3dm^u\zeta_1] + 0.5860 [\text{Fe(II)}, 3dm^u\zeta_2]$$

with

$$\zeta_1 = 5.35 \quad \text{and} \quad \zeta_2 = 2.20.$$

In addition the SCF molecular orbitals given for o-phen by Ito *et al.* [28] were used. The rotatory strengths of the transitions  ${}^1A_1 \rightarrow {}^1A_2$  and  ${}^1A_1 \rightarrow {}^1E$  were then calculated, and the results are compared with the corresponding experimental values for these transitions in Table 4. The experimental figures were calculated from data published in the literature [29, 30].

The theoretical and the experimental values of the oscillator strengths of these transitions are also given in Table 4.

Table 4. Calculated and experimental results

Transition	$R$ in cgs	$R^{\text{exp}}$ in cgs	Oscillator strengths $f$	$f^{\text{exp}}$
${}^1A_1 \rightarrow {}^1A_2$	$+5.80 \cdot 10^{-38}$	$+1.38 \cdot 10^{-38}$	$6.78 \cdot 10^{-3}$	$8.7 \cdot 10^{-2}$
${}^1A_1 \rightarrow {}^1E$	$-7.21 \cdot 10^{-38}$	$-1.62 \cdot 10^{-38}$	$7.30 \cdot 10^{-3}$	$1.03 \cdot 10^{-1}$

### Discussion

In order that the calculated and experimental rotatory strength of a certain transition might be compared it is, of course, necessary to make a spectral identification. For the electron transfer transitions found in the complex  $(-)\text{-Fe(phen)}_3^{2+}$  we have assigned the  $21400\text{cm}^{-1}$  band as due to the transition  $^1A_1 \rightarrow ^1A_2$  and the  $19600\text{cm}^{-1}$  band as due to the transition  $^1A_1 \rightarrow ^1E$ . This means that the negative component of the CD curve was assigned to the long wavelength transition while its positive component was assigned to the short wavelength transition. This identification is in agreement with the proposal of Orgel [31], and yields reasonable agreement with the experimental results.

If we compare the theoretical values of the rotatory strengths with the corresponding experimental data (Table 4) we see that for both types of transition  $R(\text{theoretical})$  is greater than  $R(\text{experimental})$  by a factor of about four. Presumably this means that the electron transfer state is not the pure state described by the wave function (8), but is mixed with mono-excited states localized on the ligands. Such mixing may lower the rotatory strengths of both transitions since the rotatory strengths of the transitions localized on the ligands can differ in sign. Presumably the oscillator strengths of the pertinent transitions, which are about ten times lower than the experimental values, would be increased at the same time.

*Acknowledgements.* M.K. thanks the Czechoslovak Ministry of Education for the grant which enabled him to spend the Spring of 1968 in Denmark. We express our gratitude to Dr. Aage E. Hansen for clarifying discussions.

### References

1. Condon, E. U.: *Rev. Mod. Phys.* **9**, 432 (1937)
2. Moffitt, W.: *J. Chem. Phys.* **25**, 1189 (1956)
3. Hamer, N. K.: *Mol. Phys.* **5**, 339 (1962)
4. Piper, T. S., Karipides, A.: *Mol. Phys.* **5**, 475 (1962)
5. Piper, T. S.: *J. Chem. Phys.* **36**, 2224 (1962)
6. Poulet, H.: *J. Chem. Phys.* **59**, 584 (1962)
7. Sugano, S.: *J. Chem. Phys.* **33**, 1883 (1960)
8. Shinada, M.: *J. Phys. Soc. Japan* **19**, 1607 (1964)
9. Liehr, A. D.: *J. Phys. Chem.* **68**, 665 (1964)
10. Liehr, A. D.: *J. Phys. Chem.* **68**, 3629 (1964)
11. Liehr, A. D.: *Transition metal chemistry*, ed. by Carlin, R., p. 165. New York: Marcel Dekker 1966
12. Karipides, A., Piper, T. S.: *J. Chem. Phys.* **40**, 674 (1964)
13. Schäffer, C. E.: *Proc. Roy. Soc. (London), Ser. A* **297**, 96 (1967)
14. Longuet-Higgins, H. C., Murrell, J. N.: *Proc. Phys. Soc. (London) A* **68**, 601 (1955)
15. Moscovitz, A. J., Hansen, Aa. E., Forster, L. S., Rosenheck, K.: *Biopolymers, Symp. No. 1*, 75 (1964)
16. Hansen, Aa. E.: Thesis. University of Copenhagen, Copenhagen 1964
17. Hanazaki, I., Nagakura, S.: *Inorg. Chem.* **8**, 654 (1969)
18. Seaton, M. J.: *Quantum theory*, ed. by Bates, D. R., Vol. 2, p. 81. New York: Academic Press 1962
19. Tinkham, M.: *Group theory and quantum mechanics*, p. 41. New York: McGraw-Hill 1964
20. Král, M.: *Collection Czech. Chem. Commun.* **35**, 1939 (1970)
21. Templeton, D. H., Zalkin, A., Ueki, T.: *Acta Cryst. (Supplement)* **21**, A 154 (1966)
22. Williams, R. J. P.: *J. Chem. Soc.* **137**, (1955)
23. Balhhausen, C. J.: *Introduction to the ligand field theory*, p. 68. New York: McGraw-Hill 1962
24. Fyring, E., Liu, Han-Chung, Caldwell, D.: *Chem. Rev.* **68**, 525 (1968)
25. McCaffery, A. J., Mason, S. F., Norman, B. J.: *J. Chem. Soc. A* **1428** (1969)

- 26 Clementi, E., Raimondi, D. F.: *J. Chem. Phys.* **38**, 2686 (1963)
- 27 Richardson, J. W., Nieuwpoort, W. C., Powell, R. R., Fdgett, W. F.: *J. Chem. Phys.* **36**, 1057 (1962)
- 28 Ito, T., Tanaka, N., Hanazaki, I., Nagakura, S.: *Bull. Chem. Soc. Japan* **42**, 702 (1969)
- 29 Moscovitz, A.: *Optical rotatory dispersion*, ed. by Djerassi, C., p. 155, 165. New York: McGraw-Hill 1960
- 30 Mason, S. F.: *Inorg. Chim. Acta Rev.* **2**, 89 (1968)
- 31 Orgel, L. E.: *J. Chem. Soc.* 3683 (1961)

Prof. Dr. C. J. Ballhausen  
Department of Physical Chemistry  
H. C. Ørsted Institute  
University of Copenhagen  
København Ø, Universitetsparken 5  
Denmark

## Relatio

# Examination of Charge Alternation in $\text{CH}_4$ and $\text{CH}_3\text{F}$ from *ab initio* LCAO SCF MO Wavefunctions and Their Localized Bond Orbitals

Conrad A. Naleway and Maurice E. Schwartz

Department of Chemistry and the Radiation Laboratory\*,  
University of Notre Dame, Notre Dame, Indiana

Received April 28, 1972/April 2, 1973

The question of whether or not fluorine substitution produces charge alternation is examined for  $\text{CH}_4$  and  $\text{CH}_3\text{F}$ . Two sets of *ab initio* LCAO SCF MO wavefunctions (one a 3 G STO based one, the other a double zeta based one) are analyzed *via* charge density, localized C-H bond moment, and population analysis calculations. Although both sets of wavefunctions show a slightly more negative H region in  $\text{CH}_3\text{F}$  relative to  $\text{CH}_4$ , in qualitative agreement with earlier work by Pople *et al.*, the differences are small, and their sources are not clear. For example, in the 3 G calculations the C-H localized orbital is the essential source of the increased density in  $\text{CH}_3\text{F}$ , while for the double zeta calculations the increased density is due to the tail of an F lone-pair orbital *trans* to the C-H bond. Consideration of details of these studies as well as those from large STO based SCF MO wavefunctions by Arrighini *et al.*, suggests that one will need very accurate wavefunctions to resolve the problem unambiguously.

**Key words:** Charge density Atomic charge Inductive effect Localized orbitals

## Introduction

In an early application of the CNDO semi-empirical self-consistent field molecular orbital (SCF MO) method, Pople and Gordon [1] studied substituent effects and dipole moments in a series of simple organic molecules. They found the rather surprising result that fluorine substitution in a saturated hydrocarbon gives rise to a charge alternation effect, instead of inducing a positive character which diminishes down the chain (as suggested by older concepts of the inductive effect). For example, the hydrogens in  $\text{CH}_3\text{F}$  were predicted to be more negative than those in  $\text{CH}_4$ . The consequences of this charge alternation were discussed and shown to be consistent with dipole moment data. However, Schwartz, Coulson, and Allen [2] later analyzed the Mulliken population charge distribution from *ab initio* SCF MO wavefunctions (based on atomic SCF orbitals) for the fluorinated methanes and obtained the opposite results – to charge alternation. But later, Hehre and Pople [3] utilized their optimized minimum Slater orbital basis set approach to find *ab initio* SCF MO population analysis results in essential agreement with the earlier CNDO ones. In the present paper we consider this

\* The Radiation Laboratory is operated under contract with the U.S. Atomic Energy Commission. This is AEC document no. COO-38-847.

problem in a more detailed way, to try answer the question of whether charge alternation does or does not occur.

Let us briefly outline why we believe the previous investigations are inconclusive, and then our own approach to the problem. Firstly, the charge distributions of the preceding work were taken from Mulliken population analyses [4] of the wavefunction, which do not correspond to direct examination of the electronic distributions, and which are sensitive to basis set composition. Secondly, since CNDO is a calibrated semi-empirical theory and the *ab initio* SCF MO results were based on modest basis sets, there are possible ambiguities in the previously considered wavefunctions, irrespective of how they might be analyzed. We eliminate the first of these ambiguities by direct examination of the electronic density. This is done not only for the total density but also, for further elucidation, by a partitioning of the density into contributions from the chemically appealing localized molecular orbitals [5] (LMO's). In this connection we also examine average values of some electronic position operators for the LMO's. The basis set question is considered by examination of two different sets of *ab initio* LCAO SCF MO wavefunctions we have determined - one with a modest basis set, and the other with a more extended, more flexible basis set. In this paper we consider just the two molecules  $\text{CH}_4$  and  $\text{CH}_3\text{F}$ , which are the simplest appropriate molecules. Although charge alternation is not as large here as in other molecules [1] it does exist, and, of course, the systems are small enough for careful examination.

Examination of the electronic densities throughout the entire 3-dimensional regions of the molecules is unreasonable, and we employ the simpler approach of investigating densities along the CH internuclear lines. This is clearly sufficient for  $\text{CH}_4$ , because the tetrahedral symmetry forces the CH regional density to be concentrated about this line. In  $\text{CH}_3\text{F}$  there is no rigorous *a priori* reason to anticipate this, although chemical intuition suggests it. But as we shall observe later, our analysis will substantiate this approach.

## Results and Discussion

For direct comparison with previous work, we have first repeated the 3 G optimized STO basis calculations of Hehre and Pople. [3] Figure 1 displays the resultant total electronic densities along the CH lines. It shows that indeed there is more density in the proton region in  $\text{CH}_3\text{F}$  than in  $\text{CH}_4$ , in accord with the earlier population analysis results [3] for the same wavefunctions. This more negative character of the  $\text{CH}_3\text{F}$  protons can be further probed with the LMO's. Table I shows the total densities in  $\text{CH}_4$  and  $\text{CH}_3\text{F}$  as well as the contributions from the appropriate CH bond LMO. After the large density region near the carbon atoms is passed, the total densities are almost entirely due to the CH LMO's. Paralleling the total densities in the CH regions of the molecules, the CH LMO of  $\text{CH}_3\text{F}$  has a greater density than that in  $\text{CH}_4$ . The total density differences and CH LMO density differences are not precisely the same, of course, since no orbital is entirely localized, and the "tails" of other orbitals can contribute to the density in the CH region. But for this minimum basis set

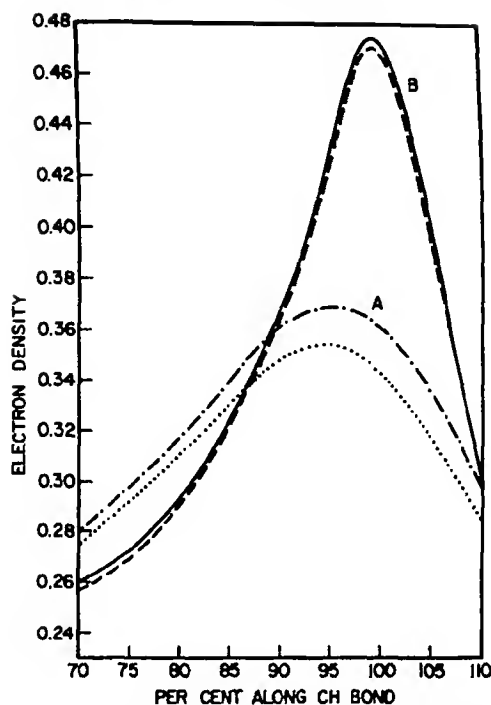


Fig. 1. Total electron densities along the C-H line in  $\text{CH}_4$  and  $\text{CH}_3\text{F}$ . Set A presents the 3G STO results; set B, the double zeta results. In both cases the  $\text{CH}_3\text{F}$  density is the upper curve

Table I Total and CH LMO density for both  $\text{CH}_3\text{F}$  and  $\text{CH}_4$  with minimum basis set

% R(C H)	$\text{CH}_3\text{F}$		$\text{CH}_4$	
	Total density	Density due to CH LMO	Total Density	Density due to CH LMO
24.6	0.58276	0.22194	0.57362	0.21449
58.7	0.26478	0.26455	0.26105	0.26085
77.9	0.30850	0.30546	0.30216	0.30041
87.8	0.35392	0.34690	0.34245	0.33877
97.4	0.36648	0.35626	0.35117	0.34587
100.0	0.36018	0.34963	0.34471	0.33919
107.3	0.31300	0.30278	0.29885	0.29361

calculation the essential source of the more negative proton region in  $\text{CH}_3\text{F}$  is the difference between the CH localized bond orbitals. Further illustration comes from the electronic bond moments of the CH LMO's:  $\langle r \rangle = 1.4399$  a.u. in  $\text{CH}_3\text{F}$  and 1.4263 a.u. in  $\text{CH}_4$ . That is, the average CH electronic positions are nearer the proton in  $\text{CH}_3\text{F}$ . The average CH bond moment in  $\text{CH}_3\text{F}$  does not lie precisely on the CH internuclear line (as it must by symmetry in  $\text{CH}_4$ ), but lies only 17.6°

Table 2. Total and CH LMO density for both  $\text{CH}_3\text{F}$  and  $\text{CH}_4$  with double zeta basis set

%R (C-H)	$\text{CH}_3\text{F}$		$\text{CH}_4$	
	Total density	Density due to CH LMO	Total density	Density due to CH LMO
50.0%	0.27284	0.27097	0.26236	0.25993
80.0%	0.29236	0.29059	0.29061	0.29041
90.0%	0.36714	0.36292	0.36522	0.36415
97.0%	0.45992	0.45296	0.45656	0.45438
100.0%	0.47379	0.46605	0.47001	0.46747
110.0%	0.29710	0.29129	0.29718	0.29502

by this average CH moment, comparison with  $\text{CH}_4$  yields the same conclusion as before—a more negative proton region, due to the CH LMO.

To acquire a more realistic density description we determined a second set of wavefunctions by employing a "double zeta" quality basis set [6] derived from gaussian expansions of atomic SCF orbitals (essentially the same basis set used by Basch, Robin, and Brundle in their recent examination of the fluoromethanes [7]). Experimental molecular geometries were taken from the summary of Gordon and Pople [8]. The resulting data are summarized in Fig. 1 and Table 2. The calculated CH LMO moments were found to be  $\langle r \rangle = 1.3910$  in  $\text{CH}_3\text{F}$  and 1.3719 in  $\text{CH}_4$ , and the average CH moment in  $\text{CH}_3\text{F}$  lies only 18.4° outside the CH internuclear line. The proton region is again calculated to be more negative in  $\text{CH}_3\text{F}$  than in  $\text{CH}_4$ , but the difference is smaller than for the 3 G STO wavefunctions.

Notice, however (Table 2), that for this more extended basis set the density near the hydrogen due to the CH LMO in  $\text{CH}_4$  is greater than in  $\text{CH}_3\text{F}$ : here the CH localized orbital alone does not account for the total density difference in the two molecules. When the density due to the CH LMO plus nearest neighboring LMO's are compared for both molecules, it is found that all of these LMO's collectively cannot account for the more negative character of the protons in  $\text{CH}_3\text{F}$ . The next highest contributing component comes from the fluorine lone pair LMO which is pointing in a *trans* manner away from the proton. (F lone pair LMO's are staggered with respect to CH LMO's). The tail of this orbital is thus directed back at the proton and contributes to its electronic density. Thus, the total density difference might be attributed to the fluorine's contribution, of which the *trans* orientated fluorine lone pair is the principal donor. This donation in part, at least, is due to electronic rearrangement caused by molecular formation and not to a "spilling over" of density from the fluorine atom. This is substantiated by calculations showing that the density contributed by either a fluorine atom or fluorine negative ion (when examined at distances comparable to those in  $\text{CH}_3\text{F}$ ) is an order of magnitude smaller than that contributed by the center while in the molecular environment.

Notice by examination of Fig. 1 that the calculated charge density near the protons with the extended basis set is considerably greater than that in the minimum basis set. Calculations of the gross atomic population by use of

Table 3. Summary of population analysis

	Double zeta basis		3G STO basis	
	$\text{CH}_3\text{F}$	$\text{CH}_4$	$\text{CH}_3\text{F}$	$\text{CH}_4$
Carbon	6.1294	6.7507	5.8316	6.0758
Hydrogen	0.8287	0.8123	1.0044	0.9811
Fluorine	9.3846	—	9.1552	—

Mulliken's analysis for both molecules are summarized in Table 3. In a qualitative way the population analysis seems more closely to coincide with the CH bond moments than it does with the charge density at the hydrogens. Neither bond dipole moment nor population analysis makes apparent the substantial change in charge density at the hydrogen as a function of basis set shown in the figure. Both predict a greater charge density further out along the CH bond in  $\text{CH}_3\text{F}$ , but neither reflects the greater density spike in the extended basis set as compared to the minimum basis set in the region of the proton. Thus it appears that qualitative comparison by use of Mulliken's analysis is limited to similar molecules with comparable basis sets.

### Conclusions

Both the minute size of the determined charge alternation as well as its inconclusive source lead us to be wary of establishing a definite view on this problem. Furthermore, interpretation of the work on  $\text{CH}_4$  and  $\text{CH}_3\text{F}$  by Arrighini *et al.* [9] with a still more extensive basis set suggests a further diminished charge alternation effect. They found by use of a large STO basis set that the CH LMO [10] moments for  $\text{CH}_3\text{F}$  and  $\text{CH}_4$  were nearly equal [ $\langle r \rangle = 1.390$  for  $\text{CH}_3\text{F}$  and  $\langle r \rangle = 1.386$  for  $\text{CH}_4$ ]. Perhaps such small effects as charge alternation cannot be unambiguously resolved short of essentially solving the problem exactly.

*Acknowledgements.* All calculations described here were done with the MOLE quantum chemistry system, [11] the many contributors to which we thank. A grant from the Research Corporation has furnished partial support for our LMO work.

### References

1. Pople, J. A., Gordon, M.: *J. Am. Chem. Soc.* **89**, 4253 (1967).
2. Schwartz, M. E., Coulson, C. A., Allen, L. C.: *J. Am. Chem. Soc.* **92**, 447 (1970).
3. Hehre, W. J., Pople, J. A.: *J. Am. Chem. Soc.* **92**, 2191 (1970).
4. Mulliken, R. S.: *J. Chem. Phys.* **23**, 1833, 1841, 2338, 2343 (1955); **36**, 3428 (1962).
5. Obtained via the minimum exchange energy criterion of Edmiston, C., Ruedenberg, K.: *Rev. Mod. Phys.* **35**, 457 (1963). Here only the valence MO's are transformed, the C and F 1S MO's being fixed as they come from the canonical SCF calculation.



# THEORETICA CHIMICA ACTA

edenda curat

**Hermann Hartmann**

adiuvantibus

**C. J. Ballhausen, København**

**R. D. Brown, Clayton**

**E. Hellbronner, Basel**

**J. Jortner, Tel-Aviv**

**M. Kotani, Tokyo**

**J. Koutecký, Praha**

**J. W. Linnett, Cambridge**

**E. E. Nikitin, Moskva**

**R. G. Pearson, Evanston**

**B. Pullman, Paris**

**K. Ruedenberg, Ames**

**C. Sandorfy, Montreal**

**M. Simonetta, Milano**

**O. Sinanoğlu, New Haven**



**Vol. 27, 1972**

**Springer-Verlag · Berlin · Heidelberg · New York**

## Recensio

**Chemieunterricht heute (Chemistry today).** Ein Handbuch für Lehrer, herausgegeben von der OECD (Organization for Economic Cooperation and Development). Frankfurt am Main-Berlin-München: Verlag Moritz Diesterweg, 1972, 392 S., 38,— DM.

Das vorliegende Werk ist dem Chemieunterricht gewidmet, ein Gebiet auf dem in der deutschsprachigen Literatur zweifellos ein Nachholbedarf besteht. Achtzehn Beiträge von Wissenschaftlern verschiedener Nationalität sind in dem Band, einer Übersetzung aus dem Englischen, gesammelt.

Den Theoretiker interessiert, inwieweit die theoretische Behandlung chemischer Probleme in einer solchen Sammlung berücksichtigt worden ist. Die Betonung der physikalischen und allgemeinen Chemie in der Themenauswahl ist bemerkenswert. Für die Besprechung an diesem Ort seien die Kapitel 4 und 5 von E. Cartmell und H. Fromherz herausgegriffen, die sich mit der Theorie der Elektronenhülle beschäftigen. Es ist klar, daß gerade bei der Behandlung dieses Stoffes eine hohe Anordnung an das didaktische Geschick gestellt wird, darf doch selbst bei einer knappen Darstellung mit minimalen Voraussetzungen an die Vorkenntnisse des Lesers die wissenschaftliche Exaktheit der Aussage nicht geopfert werden. Bei den beredeten Artikeln ist dies nach Auffassung des Rezensenten unterschiedlich geglückt. Während der Artikel von E. Cartmell über den Atomhauf das Thema inwandfrei abhandelt, stimmen Redewendungen in dem Artikel von H. Fromherz über die Natur der chemischen Bindung bedenklich. Dort ist von „Verzahnung von ungepaarten Elektronen“ und „Vervollständigung der Achterschale“ die Rede; der mesomere Zustand wird mit einem Maulesel und einem Rhinoceros verglichen. Derartige Wendungen verschleiern den Charakter der abzuhandelnden Modelle mehr als daß sie dem Interessierten weiterhelfen. In einem Handbuch für Lehrer wäre eine präzisere Ausdrucksweise und eine anspruchsvollere Behandlung durchaus angebracht gewesen. - Auf die Darstellung in den anderen Kapiteln kann nicht weiter eingegangen werden.

Horst Heydtmann

Eingegangen am 21. Mai 1973

Accession number

38968

24.4.73  
Hf